Towards Artificial Metalloenzymes: Synthesis of Novel Non-Natural Amino Acids

By

Ana Isabel Oliveira Almeida

A thesis submitted to the University of Birmingham
for the degree of DOCTOR OF PHILOSOPHY

School of Chemistry
college of Engineering and Physical Sciences
University of Birmingham

November 2020

Abstract

Enzymes are Nature's catalysts known for their high selectivity, turnover rates, stereocontrol, low catalyst loading and water solubility. For years researchers have striven to bring some of these features into small molecule catalysis. Chemoenzymatic synthesis is a growing field that utilizes natural proteins to perform organic transformations. However, use of natural proteins is not straightforward due to their high sensitivity to pH and temperature changes, which together with their specificity does limit substrate scope. Recent efforts combine synthetic peptide scaffolds with non-biological transition metals to prepare artificial enzymes. One can expect that a structured peptide could provide a chemo- and stereoselective environment, capable of behaving in an enzyme-like manner.

The amino acid toolbox available to nature is restricted to twenty commonly available side chains, which are limited regarding their transition metal coordination abilities. In order to move towards artificial enzymes and expand the potential of metal coordination onto peptides, novel non–natural amino acids containing ligand side chains are required

In this work, amino acid feedstocks were successfully converted into imidazolium and phosphorous ligands for transition metals. Gold and palladium metals complexes bearing amino acid side chains were synthesized and the catalytic activity of the gold complexes was tested in the regioselective hydration of alkynes and cycloisomerization of enynes reactions. These amino acids have been successfully used in solid phase peptide synthesis including in the preparation of structured peptides.

Acknowledgements

Firstly, I would like to thank my supervisors Dr Anna Peacock and Dr Paul Davies for the opportunity to work on this project and all their support and guidance. To Anna – thank you for always having an open door, positivity and supportive words. To Paul – thank you for all the support and for always pushing me to become a better organic chemist. I have learned a lot from you and you have been a true mentor.

I would like to thank the School of Chemistry of the University of Birmingham for funding and providing the facilities that made this work possible.

To all the present and past members of the Peacock and Davies groups – thank you for all the support, encouragement and companionship. To Sarah, Josh and Mat thank you for having the patience to train me and help me in the beginning. To Ale, Paige, Peter and Laura thank you for making the lab a more fun and exciting place to work and providing all the motivation to keep me going. A special thanks to Mat, Elsa and Louise which started as colleagues four years ago and became my friends, being there for me at some of my most important life events.

I would like to thank everyone in the analytical facility of the school, this work would not have been possible without you. To Lianne, Louise, Allen, Ian, Chris, Bridget and Peter a big thank you for all your patience and help. To Cécile and Chi a big thank you for all your help but most of all your friendship.

To Thomas, Roger, Sandro and Prof. Artur – thank you for always believing in me, teaching me the tools I needed to start this journey and support.

To my family- família for your unconditional love and support throughout my endeavours. You are like stars, no matter how many kilometres stand between us you are always here for me, no matter what.

Finally, but certainly not the least to Oliver – there are no words to thank you enough. You have been there in the brightest of days and the darkest of nights. Without your unconditional support and help I would have not been where I am today.

List of Abbreviations

$[\alpha]_D$	Specific rotation at 25 °C using 589 nm light
°	degree (s)
δ	ppm
Δ	Heating
ν	wavenumber
Å	Angstrom (s)
Ala, A	Alanine
All	Allyl
app	Apparent
Arg, R	Arginine
Asn, N	Asparagine
Asp, D	Aspartic acid
Ar	Aryl
arom.	Aromatic
Bn	Benzyl
Boc	tert-butyloxycarbonyl
C	Celsius
Cbz	Benzyloxycarbonyl
CD	Circular dichroism
Cys, C	Cysteine

d	Doublet
dd	Doublet of doublets
DIEA	*N,N'*-Diisopropylethylamine
DMF	*N,N'*- Dimethylformamide
ee	Enantiomeric excess
ESI	Electrospray ionisation
eq.	Equivalents
Fmoc	Fluorenylmethyloxycarbonyl
Fmoc-OSuc	N-(9-Fluorenylmethoxycarbonyloxy)succinimide,
g	Gram (s)
Gln, Q	Glutamine
Glu, E	Glutamic acid
Gly, G	Glycine
h	Hour (s)
HATU	1-[Bis(dimethylamino)methylene]-1H-1,2,3-triazolo[4,5-b]pyridinium 3-oxide hexafluorophosphate
HBTU	*N,N,N',N'*-Tetramethyl-O-(1H-benzotriazol-1-yl)uronium hexafluorophosphate
HEPES	2-(4-(2-Hydroxyethyl)piperazin-1-yl)ethanesulfonic acid
His, H	Histidine
HOBt	1-Hydroxybenzotriazol
HPLC	High performance liquid chromatography

HRMS	High resolution mass spectrometry
Hz	Hertz
Ile, I	Isoleucine
IMes	1,3-Bis(2,4,6-trimethylphenyl)imidazole-2-ylidene
IPr	1,3-Bis(2,6-diidopropylphenyl)imidazole-2-ylidene
IR	Infrared
J	Coupling constant
Leu,L	Leucine
Lys,K	Lysine
m	Multiplet
M	Molar
m/z	Mass/charge
Mes	Mesityl
Met, M	Methionine
mmol	Millimol
Mp.	Melting point
MS	Mass spectrometry
ms	Molecular sieves
NHC	Nucleophilic heterocyclic carbene
NMR	Nuclear magnetic resonance
PDB	Protein data bank
PG	Protecting group

Phe, F	Phenylalanine
ppm	Parts per million
Pro,P	Proline
Py	Pyridine
PyBOP	Benzotriazol-1-yl-oxytripyrrolidinophosphonium hexafluorophosphate
q	Quartet
rac	Racemic
rpm	Rotations per minute
RT	Room temperature
s	Singulet
SPPS	Solid-phase peptide synthesis
t	Triplet
^{t}Bu	tert-Butyl
TFA	Trifluoroacetic acid
TIPS	Triisopropylsilane
TMS	Trimethylsilyl
TLC	Thin layer chromatography
Trp, W	Tryptophan
Trt	Triphenylmethyl (trityl)
Tyr, Y	Tyrosine
UV-vis	Ultraviolet-visible spectroscopy

Table of Contents

Chapter 1:

1.Introduction

1.1 - Catalysis, Enzymes and Artificial Metalloenzymes

Catalysis is a process by which a chemical reaction is promoted or accelerated by a species which reduces the activation energy necessary. This decrease in activation energy is achieved by an interaction between the catalyst and the starting material, which can lead to polarization of bonds or formation of reactive intermediates that cannot otherwise be formed. From the synthesis of materials such as polymers, fertilizers and drugs to making cars more sustainable, catalysis is heavily involved in our day-today life (Figure 1). Even though many people are unaware of the importance of catalysis, it is estimated that over 80% of all manufactured products involve a catalytic step.[1, 2] The continuously expanding demand for new materials, commodities and pharmaceuticals continue to drive the discovery of new reactions and processes for which new catalysts are required.

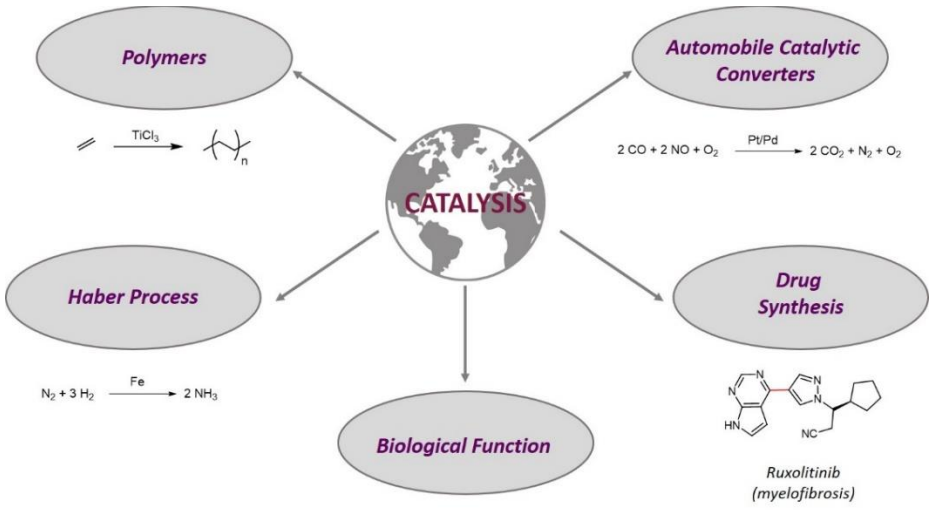

Figure 1: *A selection of some of the chemistry that shapes the world and for which catalytic processes are involved.*

Enzymes are biological molecules, typically proteins, that catalyse chemical transformations in nature. As nature's catalysts, they are vital for life, allowing the synthesis of important biomolecules as well as mediating key metabolic pathways. They are known for their high selectivity, high turnover rates, exquisite stereocontrol, low catalyst loading and water solubility. Approximately 50% of all proteins contain a metal, many of those proteins have catalytic function and therefore constitute what are called metalloenzymes.[3]

Synthetic organic chemistry is a key tool to access molecules that are responsible for impacting human heath, quality of life, available materials and the global economy. Drug molecules, dyes and pigments, skincare, electronics and materials are amongst the many applications of synthetic organic chemistry. However, one of the main challenges in organic synthesis lies in the synthesis and functionalization of molecules in a chemo- and stereoselective manner. Traditional small molecule transition metal catalysts are not recyclable, and most reactions are performed in toxic solvents. Thus, there is a need for catalysts capable of performing novel transformations and achieving better selectivity whilst being more sustainable.

Enzymes have some of the most desirable properties of a catalyst as such they have received a large amount of interest from the research community for solving synthetic problems. Chemoenzymatic synthesis is a growing field that utilizes natural proteins to perform organic transformations.[2, 4,5] However, manipulation of natural proteins is not always straightforward due to their high sensitivity to pH and temperature changes, which together with their exacting specificity limits their application.[6]

In an attempt to create a catalyst that combines enzymatic characteristics with the reactivity and versatility of small molecule catalysts, the concept of artificial metalloenzymes was born.[7] Artificial metalloenzymes are catalysts comprised of a peptide/protein ligand that was designed or modified to bind a on biological relevant transition metal in order to achieve novel catalytic activity. In this type of catalyst, the superstructure of the peptide/protein provides a complex ligand sphere that could protect the metal centre from degradation, as well as provide selectivity and stabilize transition states and reactive intermediates. The metal centre can be used to activate otherwise unreactive functional groups, achieving high reactivity.[7]

Transition metals are capable of catalysing some of the most versatile chemical transformations, such as carbon-carbon bond formation and C-H bond activation.[8, 9] Some of the most used metals in organometallic catalysis such as palladium, rhodium, gold and ruthenium are not found in enzymes. Incorporating these metals in peptide/protein scaffolds could expand upon nature's toolbox.

In the late 1970's, the first reports of artificial metalloenzymes used the modification of native proteins to induce new catalytic activity.[10, 11] Since then the field has had tremendous growth with developments on the fields of organometallic chemistry and protein engineering.[12] Modification of native proteins to form artificial metalloenzymes can be achieved in four complementary ways: metal replacement, supramolecular interactions; covalent bonding and dative interactions (Figure 2).[12]

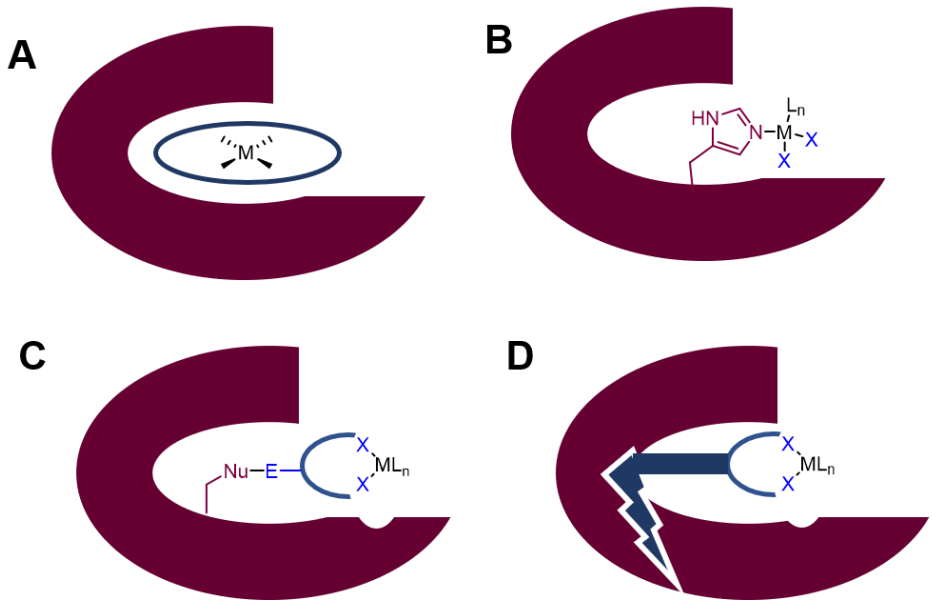

Figure 2: *Strategies for introducing metal cofactors in proteins. The burgundy loop represents the protein scaffold. A- metal replacing; B- dative bond formation between metal and amino acid residue; C-covalent anchoring and D supramolecular anchoring via non-covalent interactions.*

Metal replacement is a strategy in which a metalloprotein is expressed without the native metal ion and a different metal ion is inserted using dialysis. This approach is limited to metals such as copper and zinc that can have their coordination sphere accessed using natural amino acid side chains (Figure 2 A). The supramolecular approach (Figure 2 D) takes advantage of anchoring non-covalent binding cofactors or inhibitors to which a metal moiety is attached. Two of the risks with this strategy is that the covalent modification of the cofactor can diminish it's binding affinity, or that the linker is so long that the active site is no longer taking advantage of the protein ligand sphere. Covalent linking of a metal cofactor to an amino acid side chain has been explored (Figure 2 C).[13] The most common processes involve nucleophilic attack of cysteine residues, disulfide bridge formation or click type chemistry on previously expressed azide or alkyne amino acids.[7, 12, 13] Large proteins tend to have several repeats of the same amino acids which can lead to over and uncontrolled functionalization of the protein with

the metal cofactor.[14] Another widely used approach is the anchoring of a metal centre to a nucleophilic amino acid such as histidine or cysteine to complete a metal ligand sphere (Figure 2 B). Once again this is limited to the naturally occurring amino acids. Using these types of artificial metalloenzymes, transformation such as olefin metathesis, Suzuki cross couplings, sulfoxidation, epoxidation and C-H oxidation have been successfully performed.[12, 15]

Unfortunately, all of these approaches suffer from difficulties with synthesis and purification of complex proteins, solubility and stability issues. In order to implement these types of catalysts in a conventional organic laboratory, protein expression, and engineering facilities knowledge are required. Thus, the synthesis of an artificial enzyme with more simplified and tuneable properties is desirable. There is a particular interest in the study of artificially synthesized metallopeptides, which can provide a well-defined secondary, tertiary or quaternary structure without introducing the complex architecture of native proteins. In the past five years the modification of the metalloproteins has been extensively reviewed.[7, 12] The inclusion of different metal binding sites in different protein scaffolds for various applications was extensively reviewed by Pecoraro and co-workers.[16] This review will focus on the use of synthetic metallopeptides in catalysis applications.[1, 12]

1.2 – Peptide Scaffolds for Artificial Metallopeptides

In this discussion we will focus on peptides which are between two and one hundred amino acids. Small peptides can still form complex superstructures creating good three-dimensional mimics for enzymes. Molecular self-assembly into three-dimensional structures is a fantastic tool yet complex to produce new

materials and properties which are not present in the linear forms.[17] *De novo* design of peptides involves considering a sequence of amino acids, in which each amino acid is deliberately used and positioned to access specific properties and three-dimensional conformations. Helical assemblies and bundles are some of the most widely used scaffolds due to the well understood design principles, however examples of β-turns and sheets can also be found.[18-20] Synthesis of non-natural amino acids and β-amino acids allows for the access to an even larger variety of supramolecular assemblies such as sheets, twisted linear fibres, spheres and tubes.[21, 22]

Solid-phase peptide synthesis (SPPS) methodologies allows access to synthetic peptides, which can lead to rapid library construction to establish structure activity relationships. Synthetic peptides are ideal scaffolds for catalyst design due to their reduced size, simple folds and potential inclusion of different motifs.[23] Advances in SPPS by increasing its efficiency, number of amino acids coupled and green chemistry approaches will make peptides even more accessible and cost-efective.[24] Non-natural amino acids also allow for incorporation of functionality that is not present in nature which can lead to new function.[25, 26] Amino acids and peptides have also been successfully used in metal-free catalysis or organocatalysis, as described in the reviews by Miller and Korendovych.[17, 27]

In a similar fashion to the modification of native proteins there are several approaches to prepare a catalytic metallopeptide. Natural binding sites can be introduced in artificial scaffolds in order to create an enzyme mimic and cofactors such as hemes can also be used.[28-30] Non-natural amino acids can be incorporated for binding metal ions to form catalytic active peptides.[25]

1.3 - Proteogenic Amino Acids in Metallopeptides

Nature utilizes the natural amino acid toolbox to create coordinating sphere for metal ions. Proteogenic amino acids offer nitrogen donors (histidine, lysine, asparagine, tryptophan and glutamine), sulfur donors (methionine and cysteine) and oxygen donors (tyrosine, serine, threonine, glutamate and aspartate) which can bind metals such as copper, zinc, cobalt and iron (Figure 3).

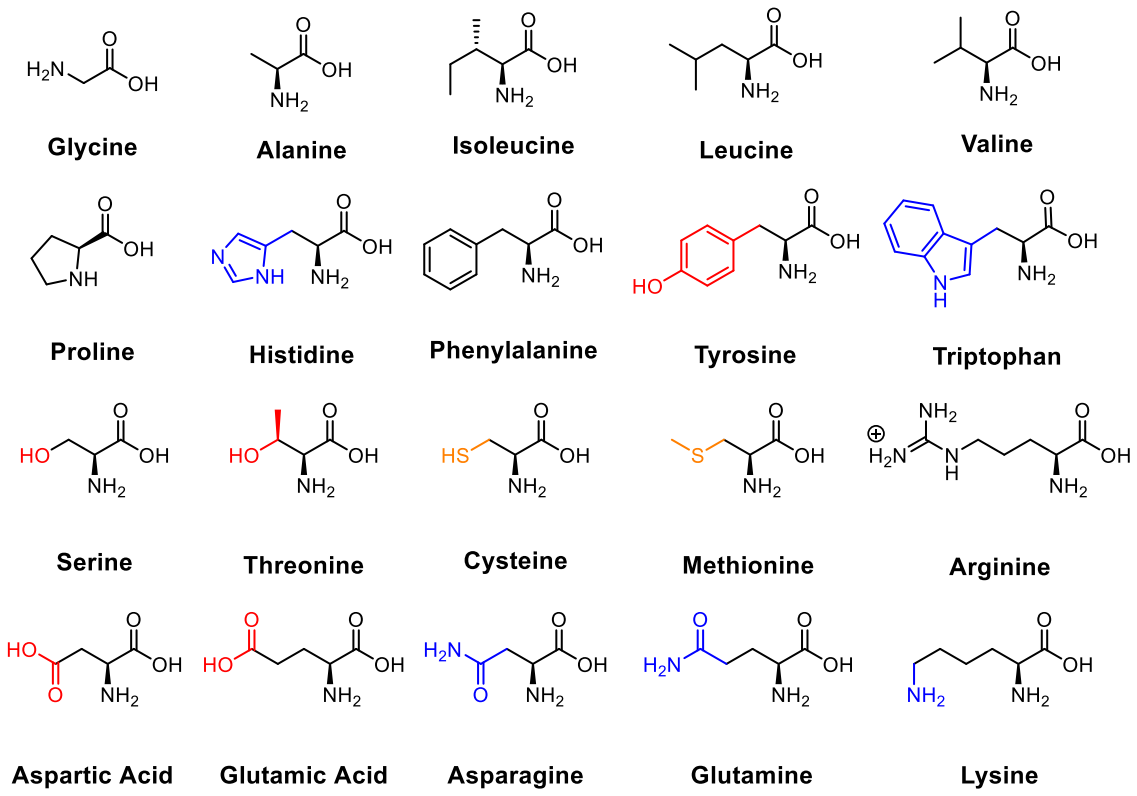

Figure 3: *Natural amino acid structures with oxygen donors side chains highlighted in red, nitrogen donors in blue and sulfur donors in yellow.*

Many enzyme mimetic constructs make use of natural occurring metal binding sites and introduce them to simpler scaffolds. A widely explored example is the use of histidine residues to bind copper, zinc or nickel.[31-33] In the following section the use of histidine binding sites in peptides to yield catalytic activity will be discussed.

Short peptides can self-assemble to form amyloid-like structures.[34] This assembly can be triggered by metal ions such as zinc and these constructs have been reported to have hydrolytic and redox catalytic activity.[17, 35, 36] Due to their insolubility in aqueous media these fibrils can act as heterogeneous catalysts which demonstrate the versatility of building peptide superstructures for homogeneous and heterogeneous catalyst design. Zinc binding amyloids have been used in the hydrolysis of *para*-nitrophenyl acetate and activated amino acid esters.[37, 38] Lengyel *et al*. reported the use of copper (II) binding short peptides in the hydrolysis of a highly toxic pesticide Paraoxon (Figure 4).[34] The peptide sequence (Ac-IHIHIYI-NH_2) was comprised of a total of seven amino acids of which three were histidine residues. These short peptides formed amyloid-like fibrils which acted as a heterogeneous catalyst. The fibrils were deposited on a filter, which allowed the use of a simplified syringe flow-like catalytic system. This demonstrated the potential of using these systems as purification flow columns, however, the immobilized fibrils showed lower activity than the free suspension.

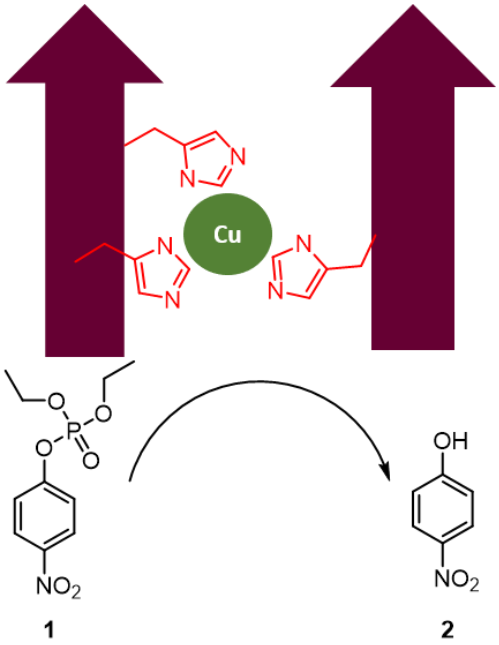

Figure 4: *Schematic representation of the copper binding amyloid fibrils in which the burgundy arrows represent the fibrils. Histidine residues in two of the fibrils bind copper ions in the exterior surface. These fibrils catalysed the hydrolysis reaction of Paraoxon* ***1****.*

Combining lauryl chains with the peptide VVAGHH-CO_2NH in the presence of Cu(II) yielded self-assembled nanofibers which were capable of catalysing azide-alkyne cycloaddition reactions under physiological conditions.[39]

Coiled coils and helical bundles are supramolecular assemblies of peptide helices which have been used to coordinate metals for enzyme mimetics.[16, 31] A three histidine residue zinc binding sites in peptides has been used to model hydrolase activity however, these models are still far from achieving the catalytic efficiency of the native enzymes.[23, 37, 40-42] Carbonic anhydrase is a hydrolase enzyme which facilitates the dissolution of carbon dioxide by reacting it with water to form carbonic acid.[43] A trimeric coiled coil was employed as one of the most competitive mimics of carbonic anhydrase by Zastrow *et al.*[31] This de novo coiled coil uses three histidine residues to bind zinc as an active site and then a mercury binding site composed of three cysteine residues for structural stability (Figure 5). This good mimetic scaffold, while exhibiting activity, is still far from achieving the

same catalytic activity as nature's hydrolase (500 fold less than native enzyme). Recent studies employed a multi-stage computational enzyme design approach to improve activity of carbonic anhydrase mimics. Despite the promising results once again the catalytic efficiencies fell 500 fold short of the ones nature achieves.[23]

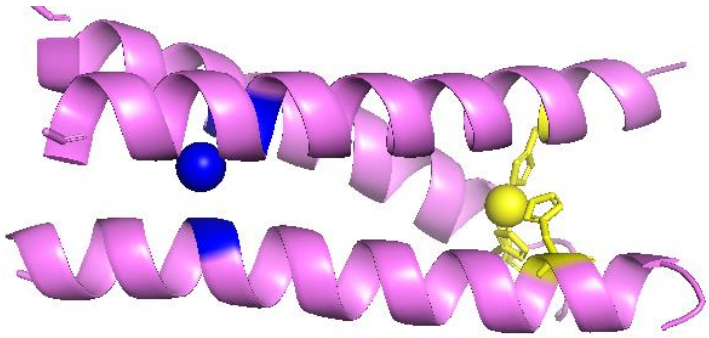

Figure 5: *Representation of the trimeric coiled coil reported by Zastrow et al. from the PDB structure (3PBJ). Sequence (Pen = penicillamine, sequence Ac-E WEALEKK PenAALESK LQALEKK HEALEHG-NH_2). In yellow the zinc ion and the histidine side chains and in blue the mercury ion responsible for structural stability.*

In 2002, DeGrado and co-workers reported the use of a heterotetrameric coiled coil capable of binding two Fe(II) ions using glutamate and histidine residues. This helical bundle was capable of catalysing the oxidation of 4-aminophenol (Figure 6, A).[44, 45] Later in 2012, DeGrado *et al.* designed a different *de novo* coiled coil capable of binding two iron atoms, but this time a trimeric assembly with a histidine binding site. The 3His-G4DFsc is capable of catalysing the *N*-hydroxylation of *p*-anisidine (Figure 6, B).[46] This peptide was reprogrammed to catalyse this synthetic transformation by remodelling the substrate access cavity. Replacement of alanine residues with glycine allowed the opening of channel to the iron active site, and addition of a His residue ligand stabilised the transition state in the active site. This biomimetic approach gave a perspective of key structural features in biological duo ferri proteins.

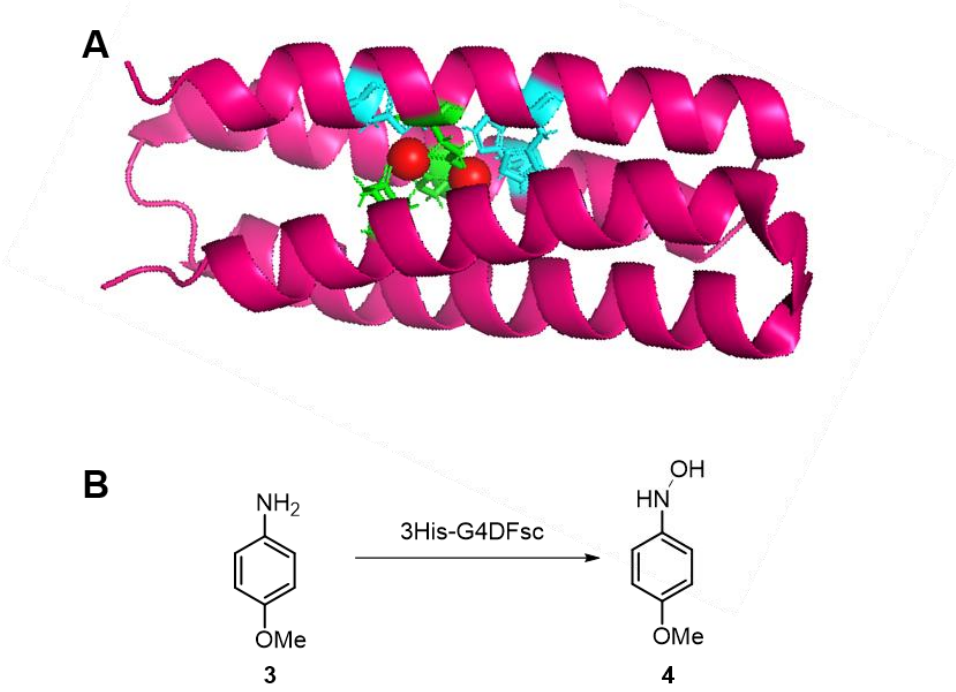

Figure 6: *A) Schematic representation of a duo-ferri mimic using a helical bundle (PDB 2LFD), sequence MDE LRELLKA EQQGIKI LKEVLKK AKEGDE QELARLN QEIVKAEK QGVKVYK EAAEKARN PEKRQVI DKILEDE EKHIEWHK AASKQGNA EQFASLV QQHLQDE QRHVEEI EKKN. The histidine side chains are shown in cyan, the glutamate side chains shown in green and the iron ions in red. B) The reaction of N-hydroxylation of -para-anisidine catalysed by the 3His-G4DFsc trimeric variant is shown.*

Tri-histidine binding sites have been engineered in three stranded coiled coils to bind copper ions.[32, 47] Such coiled coils have been used to create nitrite reductase mimics, which despite showing similar reactivity, had activity seven orders of magnitude smaller than the native enzymes.[32] Replacing the Leucine residue in the layer above the histidine binding site with a less bulky alanine led to seventy-five-fold increase in activity.[47] This highlights the potential of modifying second sphere interactions in a peptide motif which can directly impact activity in a way that is not always possible with small molecule catalysts or large proteins.

The tripeptide GGH is known as ATCUN- amino terminal Cu(II) and Ni(II) binding motif and has been widely used in metallodrugs.[48] The metal is bound to the imidazole nitrogen of a histidine residue and the three α-amino groups of the two glycine residues and the histidine residue (Scheme 1).[49] Yu *et al.* took

advantage of the ATCUN binding motif to synthesize an artificial metallopeptide capable of cleaving a glycosidic bond of a fucose residue attached to other sugars.[50] The metallopeptide analysed were compose of a copper (II) binding motif GGH which was then bound to a fucoside binding sequence (YASPKCFRYPNGVLACT or KCFRYPNGVLACT). This artificial enzyme had a broader substrate scope than natural fucosidase enzymes and overcame issues of incomplete cleavage of glycosidic bond. The reaction was performed under physiological conditions and allowed for the modification of H2 blood antigen into the rarer antigen of Bombay blood type. The binding domain was structurally characterized to adopt a β-turn conformation, however, the impact of the of the addition of the copper binding domain was not studied.[51]

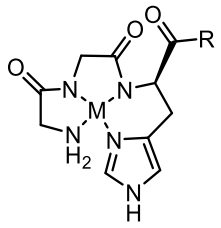

M = Cu, Co or Ni

Scheme 1: *Amino terminal Cu(II) and Ni(II) binding motif (ATCUN) coordinated to copper and cobalt.*

The same tripeptide GGH was used to coordinate cobalt for electrocatalyst applications in the selective six-electron, eight-proton reduction of nitrite to ammonium. The cobalt metallopeptide complex was able to mimic the activity of nitrogenase enzymes which to date was a challenge with molecular catalysts (Scheme 1).[52]

Natural amino acid side chains can be utilized to create binding sites for ions not present in biological systems such as transition metals ions or lanthanide ions. [53, 54] Ball and co-workers have taken advantage of well-known dirhodium

carboxylate interactions to create artificial metallopeptides with catalytic activity.[54-56] De novo helical peptides were synthesized with glutamate side chains which were used to bind a dirhodium metal centre by ligand exchange of trifluoroacetate by the carboxylates of the glutamate residues.[57] The dirhodium complex was also shown to chemoselectively bind carboxylate side chains versus terminal carboxylamides or guanidine groups.[57] The use of two complementary peptides, E3 and K3, which dimerize in solution to form a coiled coil, allowed the analysis of the impact of dirhodium complex coordination on the secondary structure (Figure 7). The mixture of E3 with K3 bound to the dirhodium tetracarboxylate complex exhibited no evidence of coiled coil formation. The complex causes a bridging in the peptide that disrupts association with E3 to form a coiled coil. Thus the binding of the dirhodium complex can be used to inhibit the assembly of peptides into higher complexity secondary structures.[57] This study also reinforces the need to structurally analyse the impact of metal ion binding, because metal complex formation can drastically alter the superstructure of the peptide.

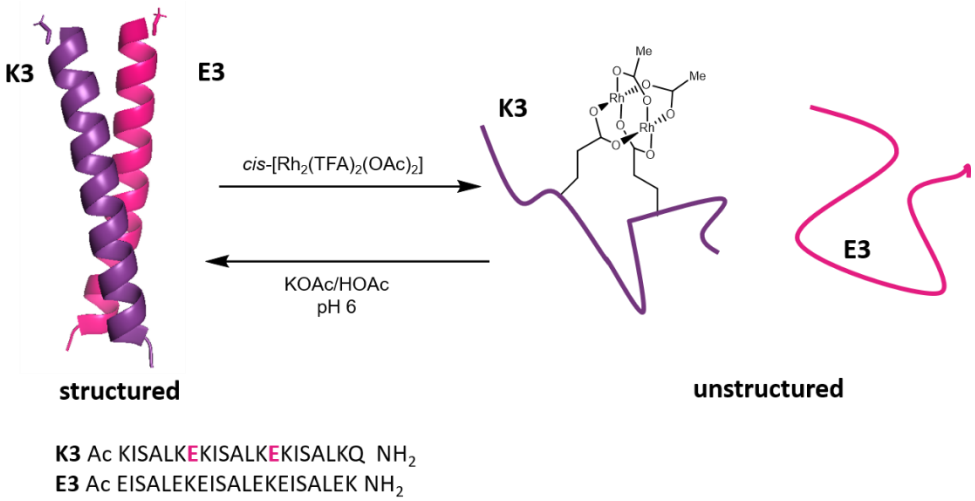

Figure 7: *Reversible control of coiled coil heterodimerization using rhodium coordination. Sequences displayed in the figure and glutamate residues involved in rhodium coordination highlighted in pink.*

The dirhodium-peptides were used in the target-selective modification of protein residues in which coiled coil sequences in the metallopeptides were used as recognition sites for specific protein sequences.[56] The choice of coiled coil motifs was due to their biological use in protein-protein interactions in nature, being a natural contender for molecular recognition motifs.[55] Selective C-H insertion on glutamine, asparagine and phenylalanine residues was achieved with the novel rhodium metallopeptides. Chemical modification of usually unreactive tyrosine and phenylalanine residues was performed in the presence of a more reactive tryptophan.[55] One of the ground-breaking aspects of this work is that the selectivity of the catalyst relies on molecular shape and site recognition, rather than functional group selectivity.[54, 56] This observation highlights the potential of peptide scaffolds to achieve selectivity using strategies that are not possible for small molecule catalysts.

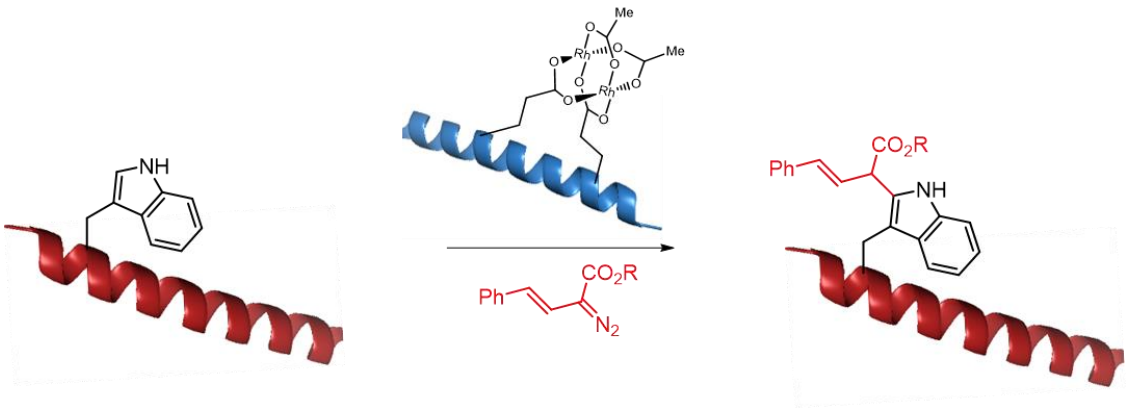

Figure 8: *Functionalization of tryptophan residues using a coiled coil rhodium catalyst. Peptide sequence used was KISALKQ KESALEQ KISALKQ in which rhodium coordination occurs in the i+4 glutamates.*

The dirhodium carboxylate peptide systems were also employed in the asymmetric insertion of diazoacetates into a Si-H bond, being the only example of non-biological use of these systems (Figure 9). Using a polypeptide ligand bound to a chiral dirhodium catalytic centre, ten diazo starting materials (**5**)

provided access to the corresponding allylsilanes (**6**) with relatively reasonable yields and high enantioselectivity (up to 99% *ee)*. This work also demonstrated the potential of SPPS for the preparation of catalyst libraries, as the first catalyst had a moderate 45% *ee* which was rapidly improved through parallel SPPS.[54]

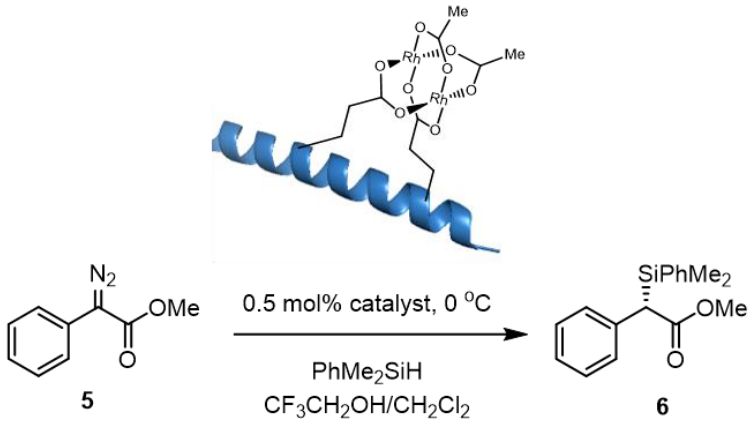

Figure 9*: Rhodium peptide catalysts in the asymmetric insertion of diazoacetates into a Si-H bond.*

Ruthenium is widely used in the catalytic activation of C-H bonds, redox chemistry and even in polymer synthesis.[58, 59] *N*-Boc protected dipeptides were used as ligands for ruthenium and the corresponding organometallic complexes (**7** and **8**) where shown to catalyse the asymmetric transfer hydrogenation of aryl alkyl ketones.[60] Commercially available amino acids were coupled to 1,2-amino alcohols and then coordinated to ruthenium (Figure 10). These catalysts achieved high enantioselectivity (*ee* of 96%) in the transfer hydrogenation of thirteen different aromatic ketones. This work demonstrates that even small peptides can be used to successfully access enantioselective catalysts.

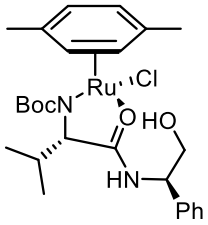

7

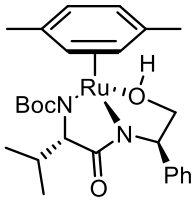

8

Figure 10: *Example of two of the ruthenium peptide catalysts developed by Pastor et al.*[60]

In 2019, Dolan *et al.* reported the use of proline containing dipeptides as ligands for IrCp* to provide enantioselective transfer hydrogenation of ketones in over 90% *ee* exhibiting excellent conversion (Figure 11).[61] This study took advantage of the reported proline performance in enantioselective catalysis. A library of NH_2-Pro-X-$CONH_2$ peptides was created and screened in transfer hydrogenation reactions.[61] Side chains capable of binding transition metals such as histidine, cystine and methionine provided low yields and low enantioselectivity, whilst leucine was found to be the best substituent. The maximum enantioselectivity was achieved when the amino acids had opposite stereochemical configuration. Thus, a mixture of a D and a L amino acid was used. In order to try an improve the dipeptide catalyst performance, long chain hydrocarbons were attached to the C terminus of NH_2Pro-Leu$CONH_2$, which lead to a three-fold improvement in enantioselectivity. This was due to the self-assembly of the peptide metal complexes in a micellar fashion. The best results were achieved for a C16 side chain bound to a D-Pro and L-Leucine, which had a turnover number of at least 3500. In order to obtain the opposite enantiomer it was just a matter of swapping the chirality of the proline and leucine residues. A study using a common transfer hydrogenation catalyst in a micellar system did not cause improvement of the enantioselectivity. Thus, showing that the high

enantioselectivity is not only due to the micelle effects but also heavily influenced by the peptide ligand.

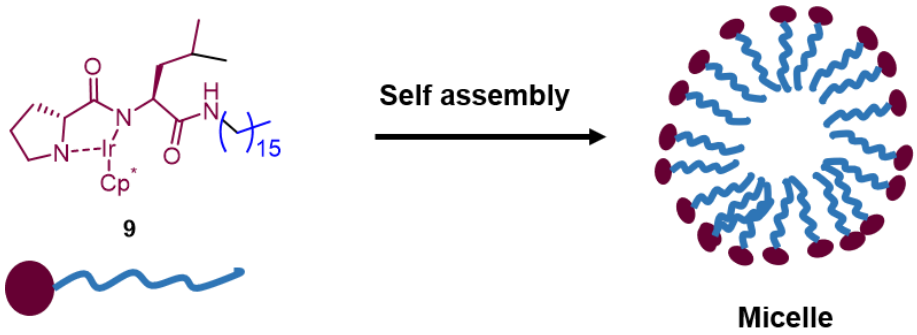

***Figure 11**: Dipeptide iridium complex with large hydrophobic chains self-assembles into micellar catalytic systems.*

1.4 - Non-natural Amino Acids in Metallopeptides

In this section, the use of non-natural ligands in peptide structures for catalytic applications will be explored. The ligands can be part of side chains of amino acids or can be covalently bound non-amino acid groups at the termini of a peptide.

In 1992, Inoue and co-workers reported novel titanium metallopeptides to catalyse asymmetric epoxidation of allylic alcohols.[62] The dipeptides were capped with two different phenolic derived imines (10 and 11) instead of the tartrates used by Sharpless (Figure 12).[63] Although asymmetric catalysis was achieved, these ligands were no improvements on the Sharpless conditions. The same peptide-titanium complexes were also employed in the synthesis of optically active cyanohydrins.[64, 65]

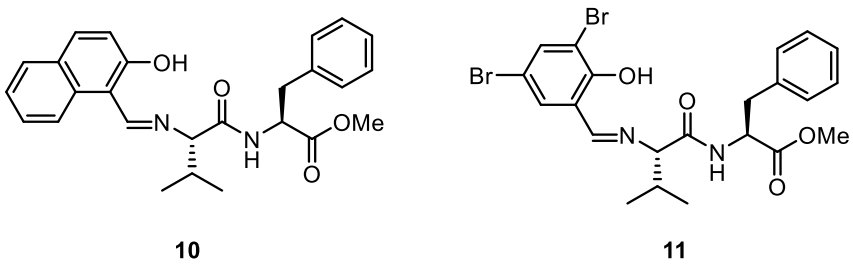

10 **11**

Figure 12: *Representative examples of the imine-peptide ligands used by Inoue and co-workers.*

In 1999, Francis *et al*. reported a combinatorial library of metallopeptides for use as catalysts for alkene epoxidation.[66] Different peptide core structures, containing five amino acid residues with electron donor side chains, were combined with 12 end caps which were chosen due to their metal binding properties (Figure 13). This method generated a total of 192 ligands attached to a polystyrene-based solid support. These ligands were then exposed to a set of thirty metal ions sources to create up to 5760 different complexes. Epoxidation of methylstyrene was used as a test reaction. Libraries containing Fe (II) centres were the most active, however the highest *ee* was only 20%. This can be explained by the fact that the peptides employed were flexible and did not have a well-defined superstructure. Even though this approach showed enormous potential in the generation of large numbers of metal catalysts by combinatorial approach, this type of work has not been further developed.

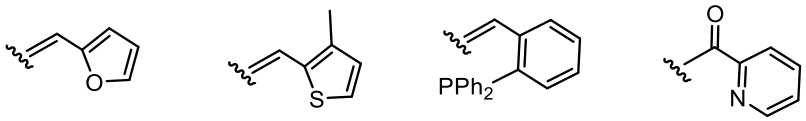

12 **13** **14** **15**

Figure 13: *Selected examples of the end caps used in the combinatorial library by Francis et al.*

Lewis *et al.* described the synthesis of non-natural amino acids with metal complex bearing side chains (Figure 14).[67] The peptide based catalyst prepared provided enantioselectivity and site selectivity in a range of organic transformations. Palladium, iridium and ruthenium were the metals used in the formation of the organometallic amino acid complexes (**16** to **18**, Figure 14). A small peptide with a β-turn proved to be catalytically active in an imidate rearrangement, in a 70% yield but provided no enantioselectivity. [67] The control reaction showed that the catalysis was induced by the organometallic complex, and not by the apo amino acids.

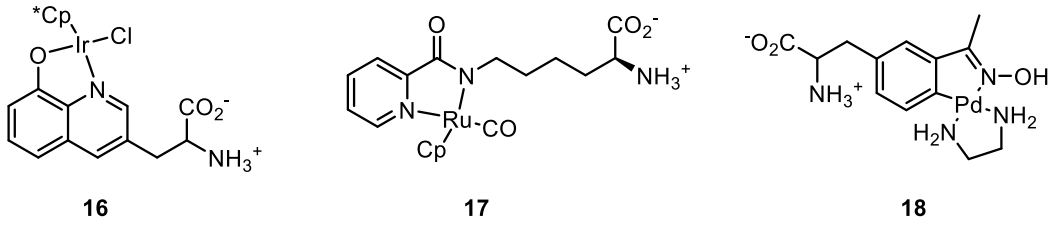

16 **17** **18**

Figure 14: *Selected examples of the metal complexes synthesized by Lewis et al.*

In 2017, Costas and co-workers described the synthesis of supramolecular systems in which a β-turn peptide design was used as a carboxylic donor ligand to a chiral iron coordination complex. The complex was tested in the enantioselective epoxidation of styrene derivatives (Figure 15).[68, 69] The carboxylic acid moiety of the peptide was shown to help the activation of hydrogen peroxide, while the three-dimensional structure of the peptide was crucial for the high enantioselectivity (84 to 92% *ee*). The reactions were performed in acetonitrile with the addition of aqueous hydrogen peroxide. It was Peptides with a flexible backbone provided inferior enantioselectivities and no degradation of the peptide scaffolds was observed. This study tested simple

substrates which are unlikely to interact with the peptide scaffold, thus the selectivity might simply be due to sterics. In that case simpler bulky scaffolds might be able to be used instead of the complex peptide motifs.

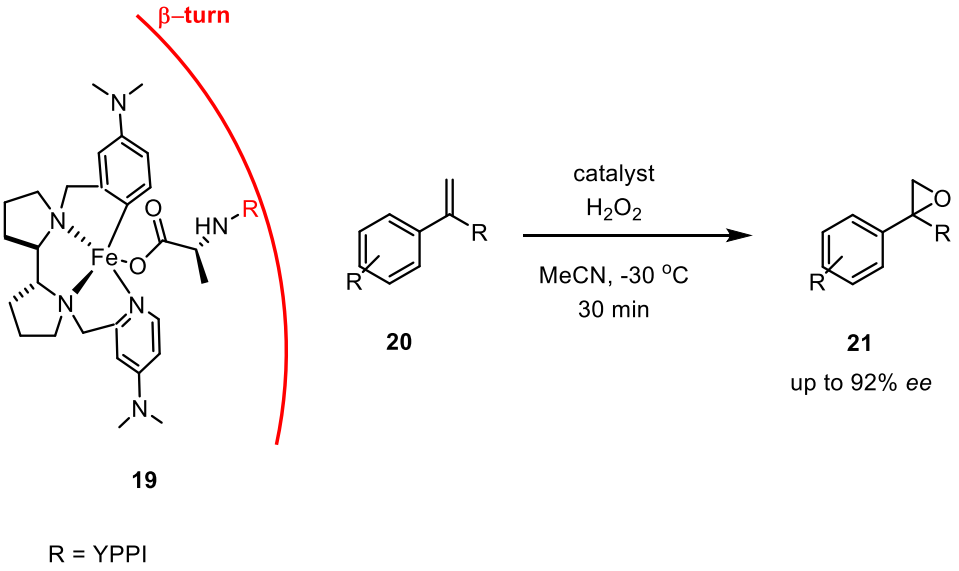

Figure 15: *Schematic representation of the interaction between the metal catalyst and the peptide secondary structure and the enantioselective epoxidation of styrene derivatives reaction used to test the catalyst library.*

Pyridine based motifs are known to be good ligands for transition metals such as copper, palladium, ruthenium and iridium and thus is not surprising that they have been included in peptide scaffolds.[70] Escuder and co-workers have reported the use of peptides containing pyridine moieties to bind palladium and form gel structures. These superstructures were capable of catalysing the oxidation of benzylic alcohol (50% yield).[71] Meldal and co-workers utilized bipyridine and phenanthroline non-natural amino acids in SPPS to prepare different peptides that showed selective proteolytic activity (Figure 16).[72] Metals such as Fe, Zn and Cu were used and the library of peptide ligands was screened to assess their proteolytic activity. Known peptide-peptide interactions were used to design the sequence around the metal centre. These interactions allowed for

allowed for selective cleavage of the amide bond between specific amino acids. This library of catalysts has not been explored for other applications such as small molecule homogeneous catalysis.

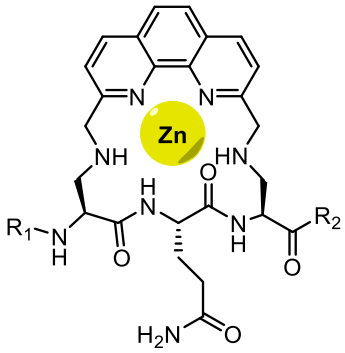

R_1, R_2 = natural amino acid strand

22

Figure 16: *Representation of the zinc binding in a phenanthroline bearing peptide.*

Karimiavargani *et al.* incorporated three non-natural amino acids containing bipyridyl residues into a peptide sequence which lead to the self-assembly of a derivative of tris(bypyridine)rutheninum complex upon the coordination of the ruthenium ion (Figure 17).[73] The residues were incorporated via SPPS in different sequences (up to sixteen amino acids). The electrochemical study of these peptides demonstrated that they could potentially be used in redox catalysis, but no specific reactions were tested.

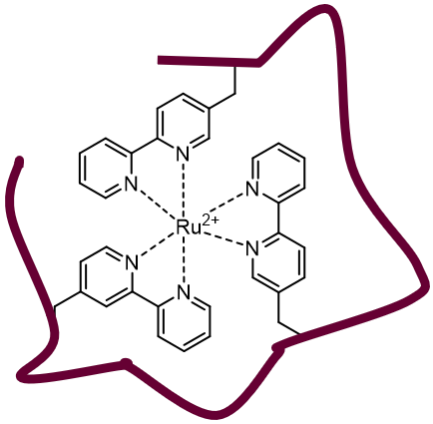

Figure 17: *Representation of the assembly of a ruthenium bipyridyl complex within a peptide strand. The bipyridyl residues were incorporated in the peptide sequence by SPPS and upon Ruthenium coordination folds to form a hexpyridyl metal complex.*

1.4.1 - Phosphorous Functionalized Amino Acids

Phosphorous ligands are ubiquitous in transition metal catalysis, their diverse chemistry and versatility in binding different metals makes them appealing for use in peptide scaffolds.[74] By including phosphine ligands in peptide scaffolds a large variety of non-biological reactions can potentially be accessed and benefit from enzyme-like activity. In this section, the precedent for the synthesis of amino acids bearing phosphorous ligand moieties and their use in peptides for catalysis will be discussed.

Gilbertson and co-workers have reported extensive work on the inclusion of phosphorous ligands in peptide scaffolds.[25, 75-82] In 1994, the first incorporation of a phosphine containing amino acid into a peptide sequence using SPPS was reported.[76] The serine derived alkyldiaryl phosphine readily oxidized under SPPS conditions and thus a sulfur protecting group strategy was employed. The phosphine was converted to the phosphine sulfide **27** which could be regenerated using the harsh Raney nickel reagent. Achiral acrylic acid **23** reacted with diphenylphosphine in the presence of tetramethyl ammonium and subsequently

sodium thiosulfate to form the phosphine sulfide **24** (Scheme 2). Evan's chiral oxazolidinone chemistry was then used to asymmetrically introduce the amine in the alpha position. However, two diastereomers of the azide were obtained, which required chromatographic separation (**26**, Scheme 2). The Fmoc group was then installed after reduction of the azide to the amine with tin(II) chloride (Scheme 2). The amino acid **27** was then included by SPPS in a helical sequence in two positions, separated by three residues to be able to bind one metal ion between them. The sequence was composed of non-reactive residues such as alanine and valine which tolerated the Raney nickel conditions (Figure 18). The helical structure of this peptide and derivatives were characterized by X-ray crystallography and NMR spectroscopy structural studies.[79]

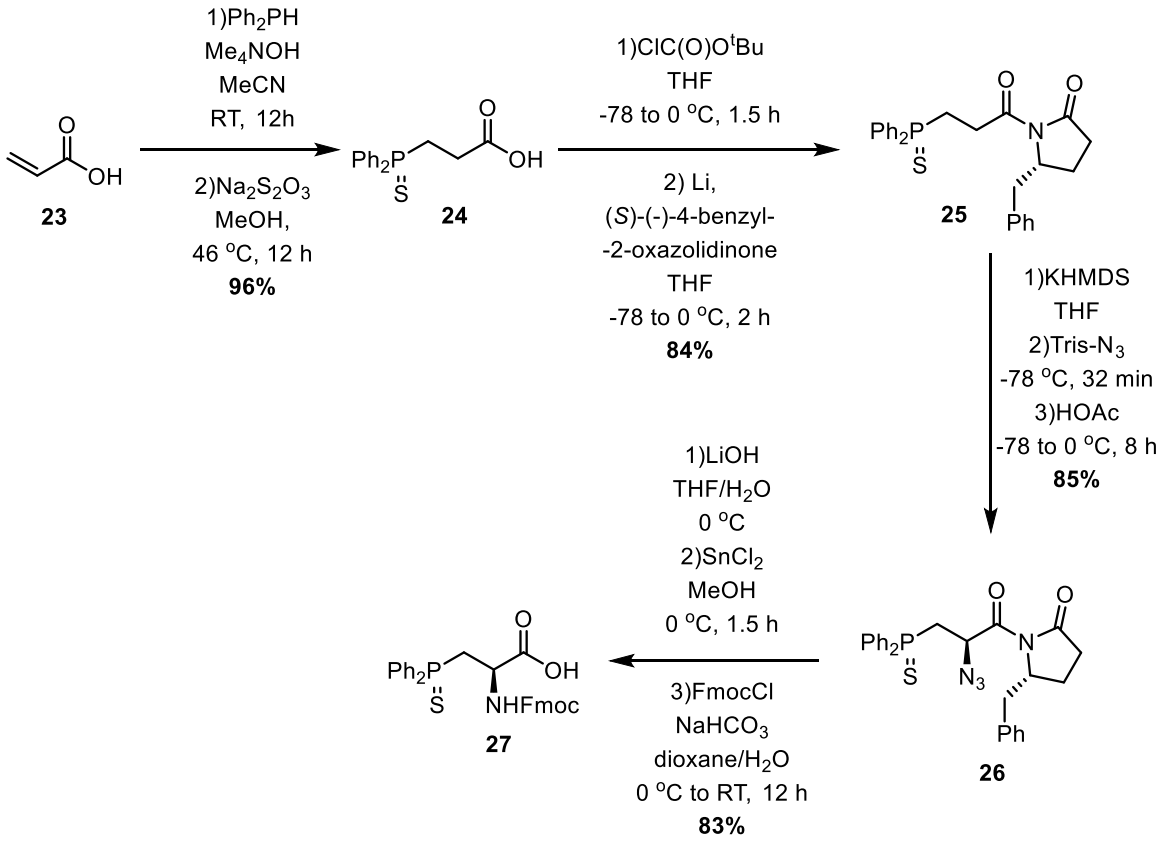

Scheme 2: *Synthesis of diphenylphosphine sulfide amino acid reported by Gilbertson and co-workers.*

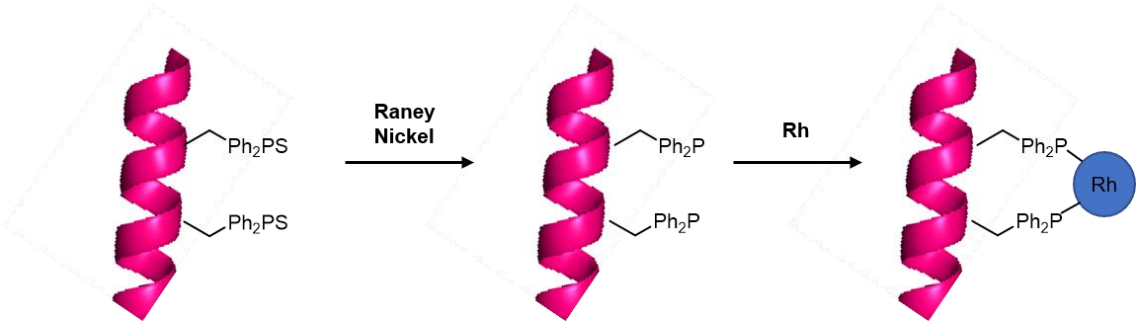

Figure 18: *Formation of rhodium peptide complexes via reduction of phosphine sulfides.*

The same group reported the ability to reduce the phosphine sulfide to the phosphine and subsequent rhodium coordination on resin using milder conditions.[75] Reaction of the phosphine sulfide with methyl trifluoromethanesulfonate yielded the phosphonium salt which was further reacted with tris(dimethylamino)phosphine to yield the phosphine. Even though these conditions are milder than Raney nickel, and allow for the use of solid-phase advantages it is still a harsh and time-consuming process. Coordination to rhodium on resin was achieved yielding a peptide metal complex on a solid support.

A similar phosphine sulfide amino acid was reported bearing two cyclohexyl groups bound to the phosphorous and used in a similar helical sequence.[77] The peptide contained a diphenyl phosphine and a dicyclohexyl phosphine three residues further in the sequence and was able to bind rhodium. The complex demonstrated the ability to catalyse the hydrogenation of methyl-2-acetamidoacrylate in high yield but a poor 8% *ee.* The two reported phosphine sulfide amino acids were then used in the combinatorial synthesis of sixty-three rhodium-peptide catalysts. The library was screened for the asymmetric hydrogenation of an enamide.[78] The percentage of conversion ranged from 1% to 100%, and the *ee* from 0% to 17%. The amino acid included in the sequences

possess unreactive side chains with exception of a histidine in some of the catalysts which had no visible impact.

The synthesis of phosphine sulfide amino acids was optimized by starting from chiral amino acids instead of achiral precursors.[83] Serine was converted to its iodoalanine counterpart **28** which was then activated with zinc. The zinc iodide amino acid was then coupled directly with the desired phosphorochloridite and protected with sulfur to yield a library of phosphorous bearing amino acids (**30**) (Scheme 3). The coupling was performed in the Boc protected methyl ester iodoalanine which cannot be used directly in standard Fmoc-based SPPS. Conversion of tyrosine derived residues **31** to the correspondent triflates **32**, allowed for the coupling of diphenylphosphine onto the phenyl ring which was then protected with sulfur to yield the corresponding triphenyl phosphine sulfides **33** (Scheme 3). This procedure was not carried out in Fmoc- protected amino acids.

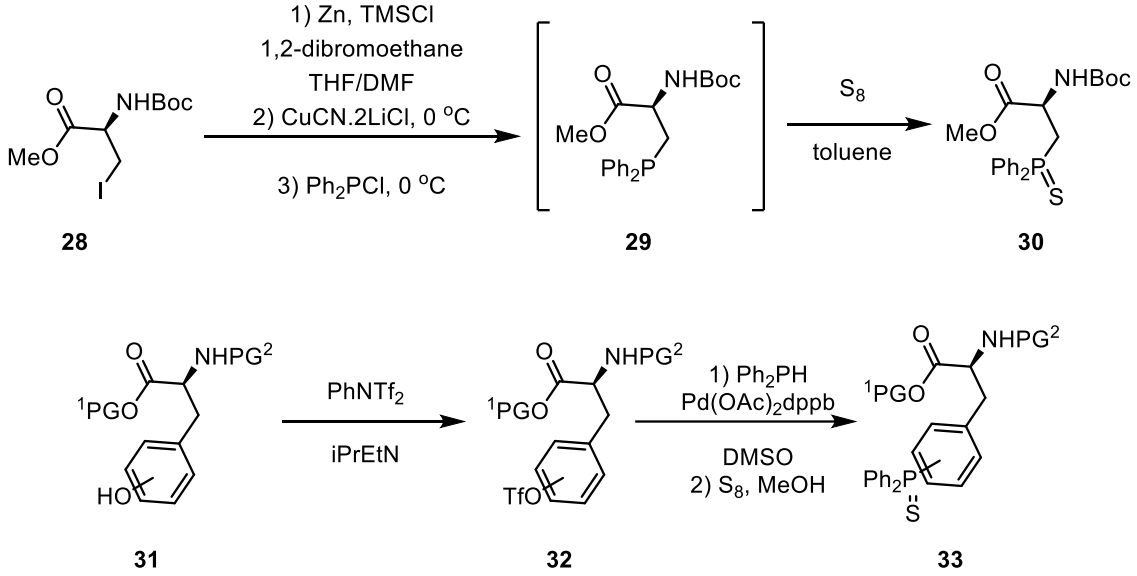

Scheme 3: *Synthesis routes to phosphine sulfide containing amino acids.*

Gilbertson and co-workers included their phosphine sulfide amino acids in β-turn inducing sequences which were used to bind rhodium and palladium. Proline derivatives bearing phosphine sulfide functionality were reported (Figure 19, A).[82] In the synthesis of these derivatives, chiral hydroxyproline was the starting material which set the stereochemistry of the amino acid from the start. The 9-step synthesis of proline derived diphenylphosphine sulfide (**34** and **35**) involved the diphenyphosphinide nucleophilic substitution on the mesylate and oxidation of the primary hydroxyl group to the carboxylic acid. The phosphorous containing proline residue **35** and diphenylphosphine sulfide residue **30** were included in a β-turn inducing peptide sequence and coordinated to rhodium.

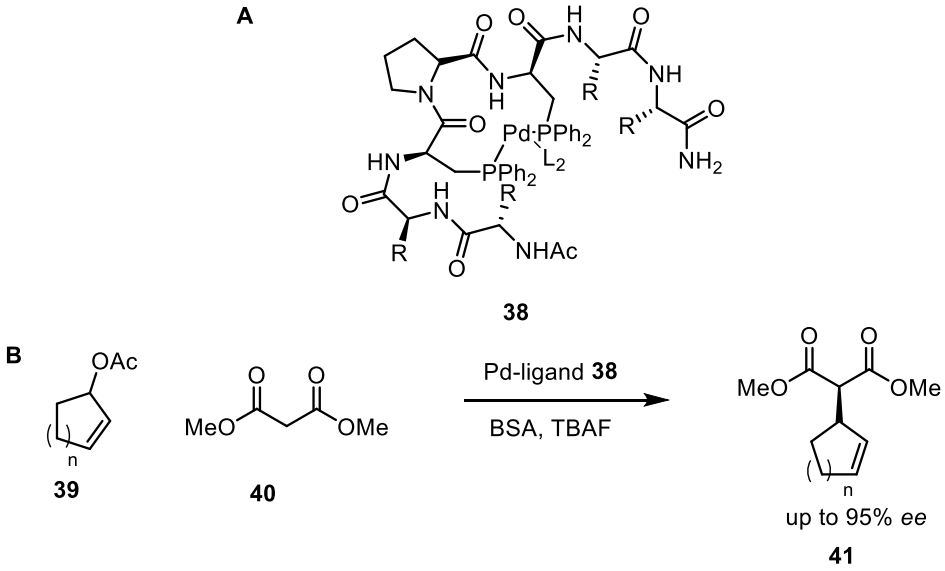

Figure 19: A) *Example of palladium peptide catalysts used by Gilbertson and co-workers.* ***B)*** *Addition of dimethylmalonate to cyclic acetates using the novel palladium catalysts.*

A series of proline-based P,N and P,O ligands were synthesized and their palladium and iridium complexes used in asymmetric catalysis, however, these systems were not incorporated in peptide systems (Figure 20, B).[***8***4-86]

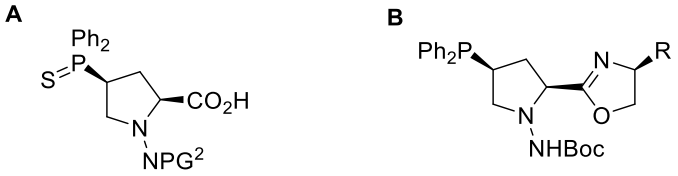

34 PG^2 = Boc
35 PG^2 = Fmoc

36 R= Ph
37 R = ^{t}Bu

Figure 20: A) *Examples of proline derived phosphine sulfide amino acids.* ***B)*** *Example of P,N proline derived ligands for transition metals.*

Hoveyda and co-workers reported the condensation of (diphenylphosphino)benzaldehyde with the terminal amine of a dipeptides to form an imine bond between the phosphine and the peptides (Figure 21). These peptide systems were then used in the asymmetric copper conjugated addition to cyclic enones and the titanium catalysed Strecker reaction with high enantioselectivity.[87, 88]

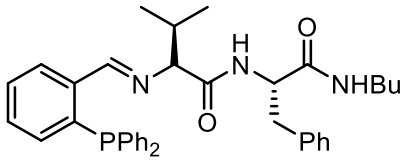

42

Figure 21: *Example of ligands developed by Hoveyda and co-workers.*

Breit and co-workers coupled ortho-diphenylphosphinebenzoic acid to valine, divaline and trialanine methyl ester to create a library of ligands. This library was used in the enantioselective copper conjugated addition of diethylzinc to cycloalkenones with *ee* up to 97% (Figure 22).[89]

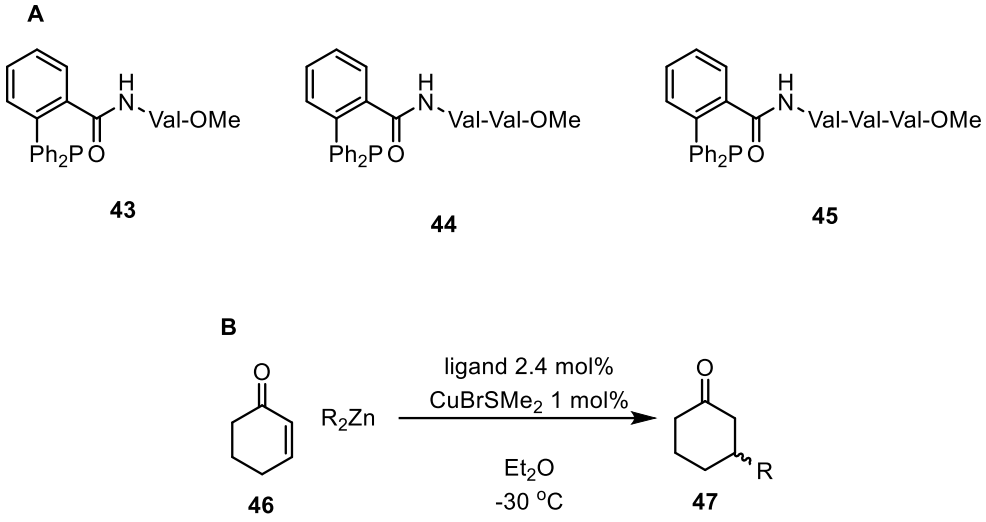

Figure 22: A) *Ligands reported by Breit and co-workers.* ***B)*** *Asymmetric copper conjugated addition to cyclic enones.*

Five years later the same group reported more complex peptide-phosphine systems with a β-sheet like structure.[90] In this case meta-diphenylphosphinebenzoic acid and 6-diphenyl-phosphanyl-2-aminopyridine were coupled to the N and C terminus respectively of a series of β-sheet inducing peptide sequences. The ligands were coordinated to both platinum and rhodium. The rhodium catalysts were tested in the hydroformylation of styrene with excellent yield and regioselectivity, albeit modest enantioselectivity (38% *ee,* Figure 23 B).***[90]*** Breit and co-workers reported shortly after an improved system which made use of similar triphenylphosphine based peptide systems combined with binolphosphite peptide ligands which catalysed rhodium asymmetric hydrogenation with up to 99% *ee* (Figure 23).***[91]***

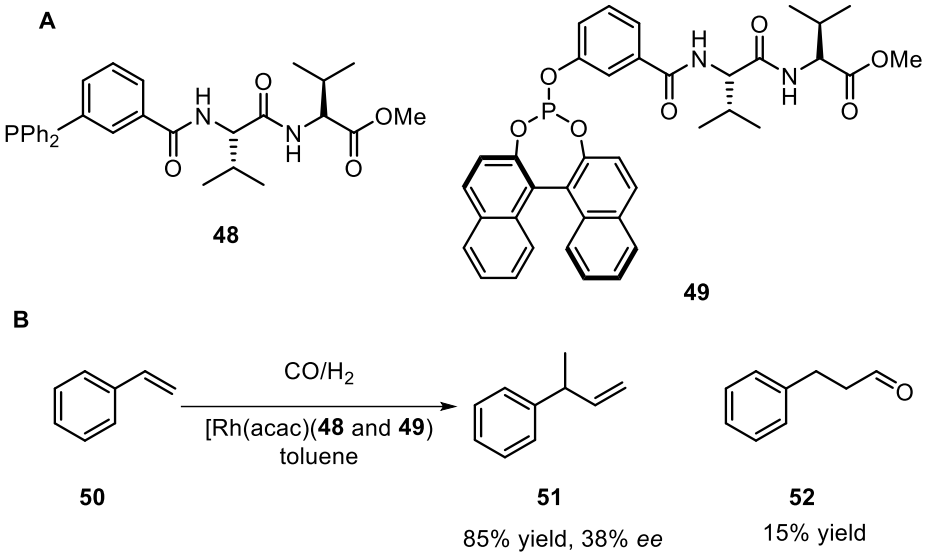

Figure 23: A) *Ligand systems described by Breit and co-workers;* ***B)*** *example of one of the test reactions of rhodium catalysed asymmetric hydrogenation.*

Meldal and co-workers reported a method to synthesize peptide derived phosphine-palladium complexes without the need to protect and deprotect the phosphine moiety.[92] In their approach the phosphine moiety was introduced by phosphinomethylation of the free amines which were immediately coordinated to palladium. However, the synthesis of the peptide substrate for selective amine phosphinomethylation are laborious. The activity of the palladium allyl complexes (**53**) was tested in asymmetric allylic substitution with high yields but moderate *ee* (21%) (Figure 24). By placing a cysteine derivatives adjacent to the phosphine a series of P,S-peptide ligands were accessed and their palladium complexes (**54**) showed a higher enantioselectivity than the P,P-ligand systems in the allylic substitution reaction (Figure 24).[93]

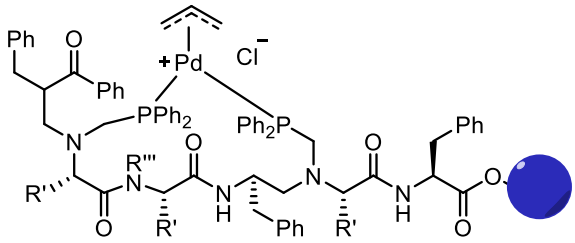

53

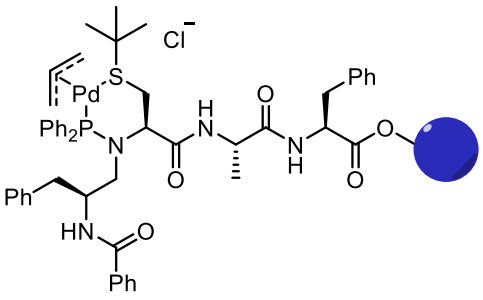

54

Figure 24: *Solid supported palladium metallopeptides containing phosphorous based ligands.*

Hydrogenases are enzymes which catalyse the reversible reduction of protons to molecular hydrogen. Jones and co-workers utilized phosphine sulfide amino acids in the synthesis of peptide enzyme mimics for hydrogenases (Figure 25).[94] The phosphorous containing peptide was reacted with diiron nonacarbonyl to yield the diiron reactive centre which performed electrocatalysis in mixed aqueous-organic solutions.

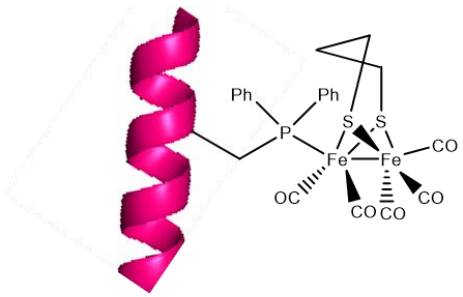

Figure 25: *Schematic representation of the hydrogenase mimic reported by Jones and co-workers.*

Phosphine amino acids have been synthesized and incorporated in peptides via Fmoc-based SPPS. However, the synthesis routes are lengthy and do not include direct modification of Fmoc amino acids which adds two synthetic steps of deprotection and protection with Fmoc groups. The peptide sequences in which such amino acids were included do not possess many or any complex amino acid side chains and there is little variety in the superstructures formed (simple single helical systems and β-turns). Catalytic activity was only evaluated for copper, rhodium and palladium complexes. There is still a need to explore better synthetic access to Fmoc based building blocks and study their tolerance to more complicated structures as well as the coordination of different transition metals and their use in catalysis.

1.4.2 – Imidazolium salts and Metal-NHC in Metallopeptides

Nucleophilic heterocyclic carbenes (NHC) are electron-rich nucleophilic species which can act as organocatalysts or ligands for transition metals and main group elements.[95-97] The corresponding organometallic complexes are known for their air, light and moisture stability which facilitates their handeling.[98-100] The NHC backbone is modular and it can be modified to create a library of derivatives which is useful when considering structure-activity relationships. Several NHC metal complexes have shown potential antimicrobial and anticancer activity, therefore they have been used as metal based drugs.[101-103] Their versatility as both organo and metal catalysts combined with their reported biological activity makes them interesting building blocks to include in the design of metallopeptides for catalysis and medicinal applications.[103, 104] In this section

the introduction of imidazolium salts and their metal complexes in peptide structures will be discussed.

1.4.2.1 - Inclusion of Imidazolium salts and NHC in Metallopeptides for Catalysis

Artificial metalloenzymes have been constructed by covalently anchoring NHC complexes into native proteins, utilizing linkers such as maleimide[105] and biotin-streptavidin.[13] The catalytic activity of these artificial metalloenzymes was studied in a range of reactions from hydrogenation of ketones to aqueous olefin metathesis.[106] However, this type of covalent anchoring will not be discussed in detail, since it has been widely reviewed elsewhere.[15, 107-110]

As a result of their chirality, amino acids and peptides have been conjugated to different catalytically active complexes in an attempt to achieve asymmetric catalysis. In order to improve activity and stereoselectivity of ruthenium based olefin metathesis catalysts, complexes bearing an amino acid as a chiral anionic ligand were synthesized and tested.[***111***] Silver carboxylate salts of Boc-protected amino acids were utilized to perform ligand exchange of the two chloride atoms in the commercially available Hoveyda-Grubbs second generation complex. The amino acids glycine, alanine, phenylalanine and leucine were used as exchange ligands and the activity of the resulting complexes tested in asymmetric ring closing metathesis and asymmetric ring opening cross-metathesis (Figure 26). The complexes demonstrated high conversions but poor enantioselectivity.

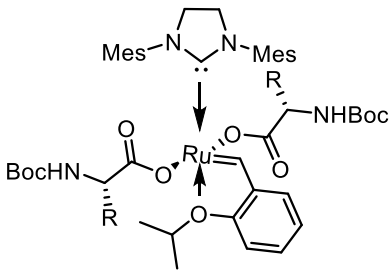

55 R = H
56 R = Me
57 R = CH_2Ph

Figure 26: *Selected example of the ruthenium amino acid complexes used by Lemcoff and co-workers for ring closing metathesis.*

An imidazolium salt with a carboxylic acid functionality was coupled to a cell penetrating peptide labelled with a fluorescent probe.[112] Subsequent coordination on resin using BEMP and $PdCl_2COD$ gave access to the palladium complex that was then cleaved of the resin using 95% TFA in water. The palladium complex was catalytically active in cell lysate in the depropargylation of a rhodamine derived dye (Figure 27). The peptide/NHCPd conjugate showed a higher cellular uptake than palladium acetate and showed no cytotoxicity even at 200 µM. This showcased the potential for conjugation of homogeneous NHC catalysts and molecular recognition peptides to achieve selective transformations in target cells.

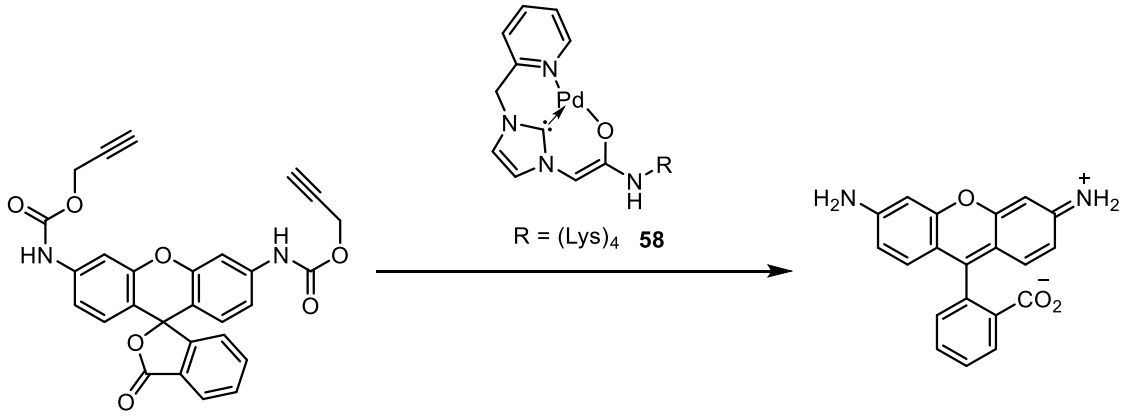

59 **60**

Figure 27: *Palladium NHC peptide catalyst in the depropargylation of rhodamine derived dye inside living cells.*

Later on, Dohi *et al.* reported the synthesis of benzoimidazolium tethered into an amino acid chain to act as chiral ligands for copper-catalysed asymmetric conjugated addition of acyclic enones in high yields and high enantioselectivities (up to 88% *ee*).[113]

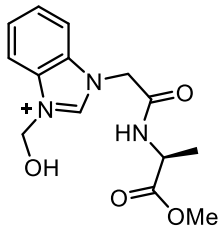

61

Figure 28: *Selected example of the benzoimidazolium ligand reported by Dohi et al.*[113]

1.4.2.2 - Amino Acids Bearing Imidazolium salts and NHC Functionality

Amino acids bearing imidazolium and metal-NHC functionality have not been widely incorporated in complex peptide sequences or used in SPPS. Their catalytic activity has only been explored in a limited capacity. Nevertheless, these building blocks could potentially be used in the design and synthesis of artificial metalloenzymes and thus their synthesis and applications could provide valuable insights.

NHCs can be synthesised through the deprotonation of an imidazolium salt to generate a free carbene, this carbene can then react with metal sources to form a metal-carbene.[114] Therefore, the synthesis of imidazolium salts allows for access to NHC functionality. Imidazolium salts can be synthesized through the alkylation of imidazole.[115] Histidine is a proteogenic amino acid with an imidazole side chain thus being an obvious precursor for the synthesis of amino acids bearing imidazolium functionality. In 1996, the first amino acid bearing imidazolium salt functionality was reported as an intermediate in the synthesis of

folylpolyglutamate synthetase inhibitors.[116] Mono alkylated Boc-histidine derivative **62** was further alkylated with ethylbromoacetate, after DCC activation of the nitrogen of the imidazole (Scheme 4). The imidazolium salt **63** was then deprotected to form a mono alkylated histidine derivative, which was further coupled to Pteroic acid derivatives.

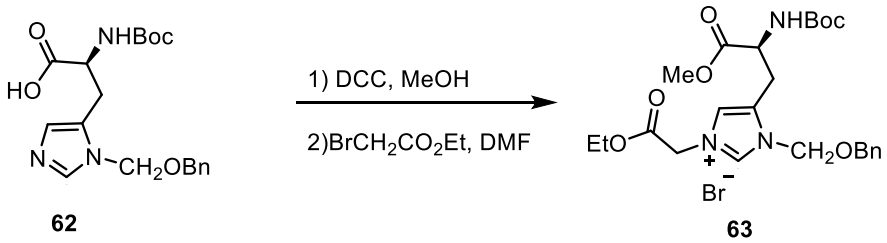

Scheme 4: *Synthesis of imidazolium salt* ***63.***

In the same year bis-allyl imidazolium salts of Boc protected histidine were synthesised as intermediates in the synthesis of both regioisomers of allyl histidine N(π)-allyl and N(τ)-allyl-histidine.[117] Allyl bromide was used as the alkylating agent in the presence of sodium bicarbonate as a base and refluxed in acetonitrile for three days (Scheme 5).

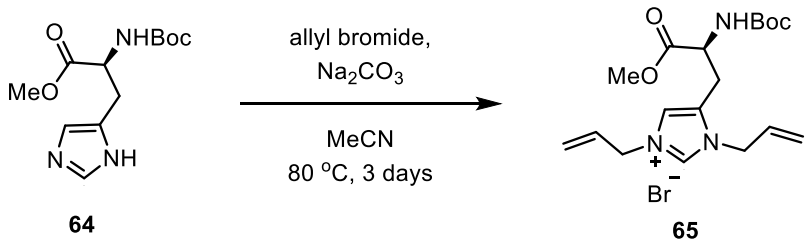

Scheme 5: *Synthesis of the double allyl imidazolium salt* ***65.***

The first report of an Fmoc-bearing imidazolium amino acid was in 2001 when Juliano and co-workers synthesized the dimethyl imidazolium salt (Scheme 6).[118] *N*-benzoylhistidine **66** was treated with a mixture of methyl sulfate and potassium carbonate mixture under anhydrous conditions. Subsequent

hydrolysis of the benzoyl group and protection with Fmoc succinimide yielded the amino acid **69**. No yield was provided for any of the synthetic steps. The amino acid was further included in a peptide of sequence GFSPF-X-SSRPQ via automated SPPS. The peptide was a substrate for the study of the activity of a peptidase enzymes.[118] This amino acid was also used in other enzymatic studies.[119]

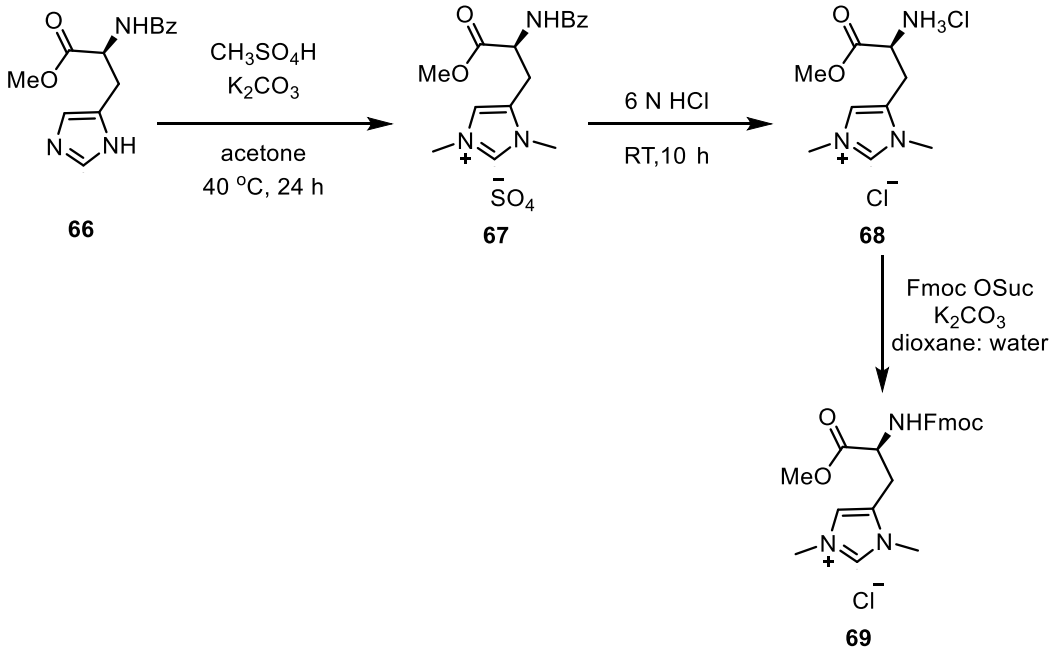

Scheme 6: *Synthetic route to access Fmoc bearing amino acid **69** reported by Juliano and co-workers. No yields were provided for the reactions.*

Imidazolium alkyl salts tend to have a low melting point and therefore find use as ionic liquids. In an attempt to synthesize chiral ionic liquids Hannig *et al.* prepared different histidine based imidazolium salts.[120] After protecting both the carboxylic acid (methyl, ethyl esters) and the amine (benzoyl and Boc amides) the imidazole was double alkylated with three different alkyl substituents. Alkylation with tetrafluoroborate caused racemisation and also alkylated the oxygen of the benzyl amide. Optimization of the procedure using the alkyl halides in acetonitrile with sodium bicarbonate as a base yielded the corresponding salts

with no racemization and very good yields. The salts were then used to coordinate to palladium and rhodium via silver transmetallation (Figure 29). Despite no inclusion in peptides or manipulation of protecting groups, this methodology demonstrated the potential of modification of histidine for accessing different amino acid imidazolium salts.

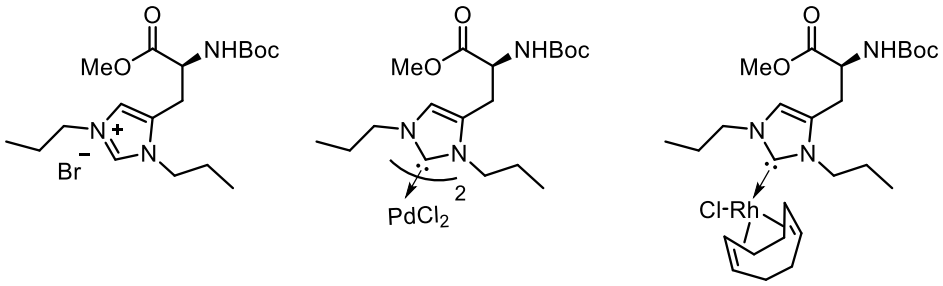

70 **71** **72**

Figure 29: *Selected examples of the compounds synthesized by Hannig et al.*

Guillen *et al.* described the unsymmetrical alkylation of histidine through a carbonyldiimidazole intermediate (Scheme 7).[121] This intermediate should prevent both racemization and double methylation. After the first methylation the carbonyldiimidazole was hydrolysed under basic conditions, and the methyl-histidine was further alkylated with a butyl group. Counterion exchange facilitated the handling, as replacing halides with triflates or hexafluorophosphate anions reduced hygroscopicity. The Boc protected imidazolium salt was successfully deprotected and subsequently coupled in solution to an alanine residue. Even though no metal coordination was achieved, this particular synthesis strategy would be further employed by other groups to obtain imidazolium salts with different N-substituents.

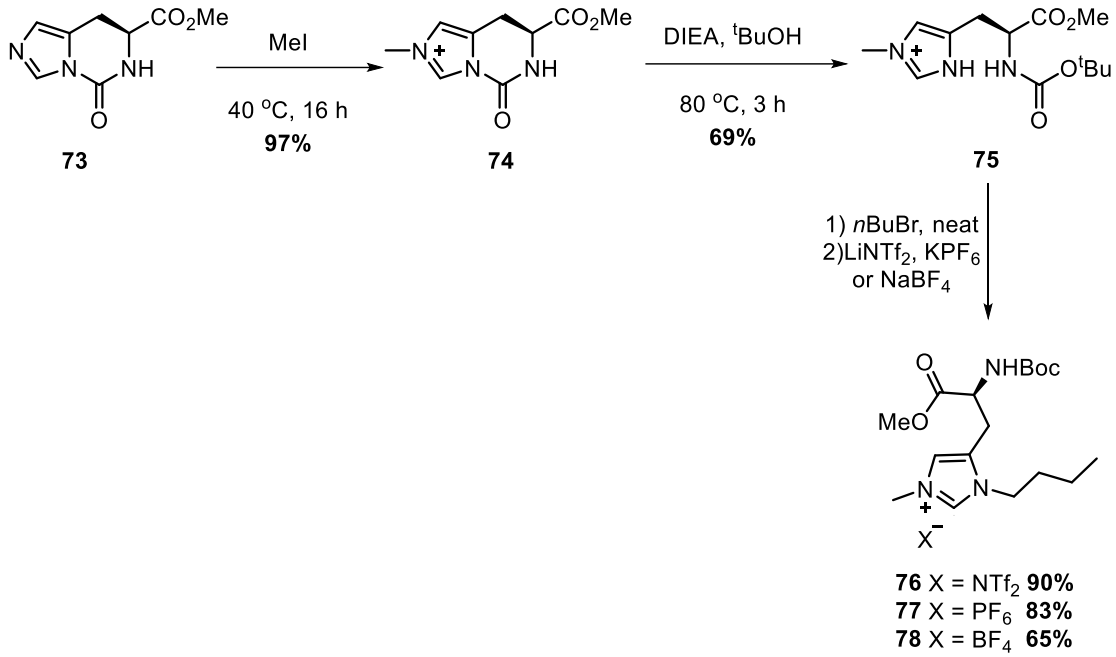

Scheme 7: *Synthesis of histidine derived imidazolium salts through a carbonyldiimidazole intermediate.*

Five years later, the Albrecht group released a series of publications with the synthesis and use of imidazolium bearing amino acids.[122, 123] Starting from N-acetyl-His-methyl ester solubility problems occurred in subsequent transformations and therefore the methyl ester was replaced by a butyl group.[122] Using the double methylation conditions from Hannig *et al*., racemization was observed. However, the racemic product was carried forward to the formation formation of the ruthenium complex (Figure 30). The preliminary studies in transfer hydrogenation did not show improvement from the amino acid catalyst (**79** and **80**) when compared to the non-amino acid derivative (**81** and **82**). Nevertheless, the NMR spectra of the reaction mixture showed potential effects of the backbone in the catalysis which would be further explored.

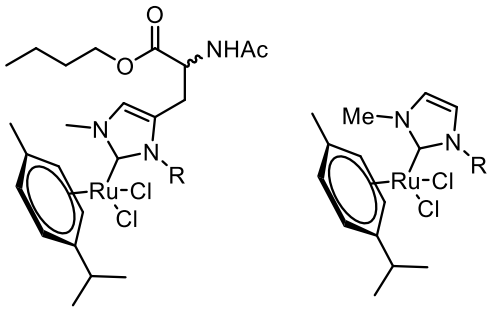

79 R = Me
80 R = *i*-Pr

81 R = Me
82 R = *i*-Pr

Figure 30: *Examples of ruthenium complexes prepared by the Albrech group.*

The same group later reported a stereospecific synthesis of the same family of imidazolium amino acid. Utilizing the previously described carbonyldiimidazole intermediate, a stepwise methylation followed by metal coordination provided the desired organometallic complexes. This time an iridium complex was also obtained. Racemization occurred during the silver complexation hypothesized to result from basicity of silver oxide, which can deprotonate the α-carbon. The rhodium complex was tested in the hydroxylation of ketones but no chirality was induced.[123] The same amino acids were used in a peptide containing a methionine residue in which interaction between the sulfur and metal ion was observed (Scheme 8). The peptide rhodium catalysts displayed activity in hydrosilylation reactions and showcased the potential of using neighbouring coordinating amino acid residues to influence catalytic activity.[124, 125] The Boc amino acid was incorporated in the peptides via solution phase coupling, thus there is no information about the tolerance of this residue to SPPS.

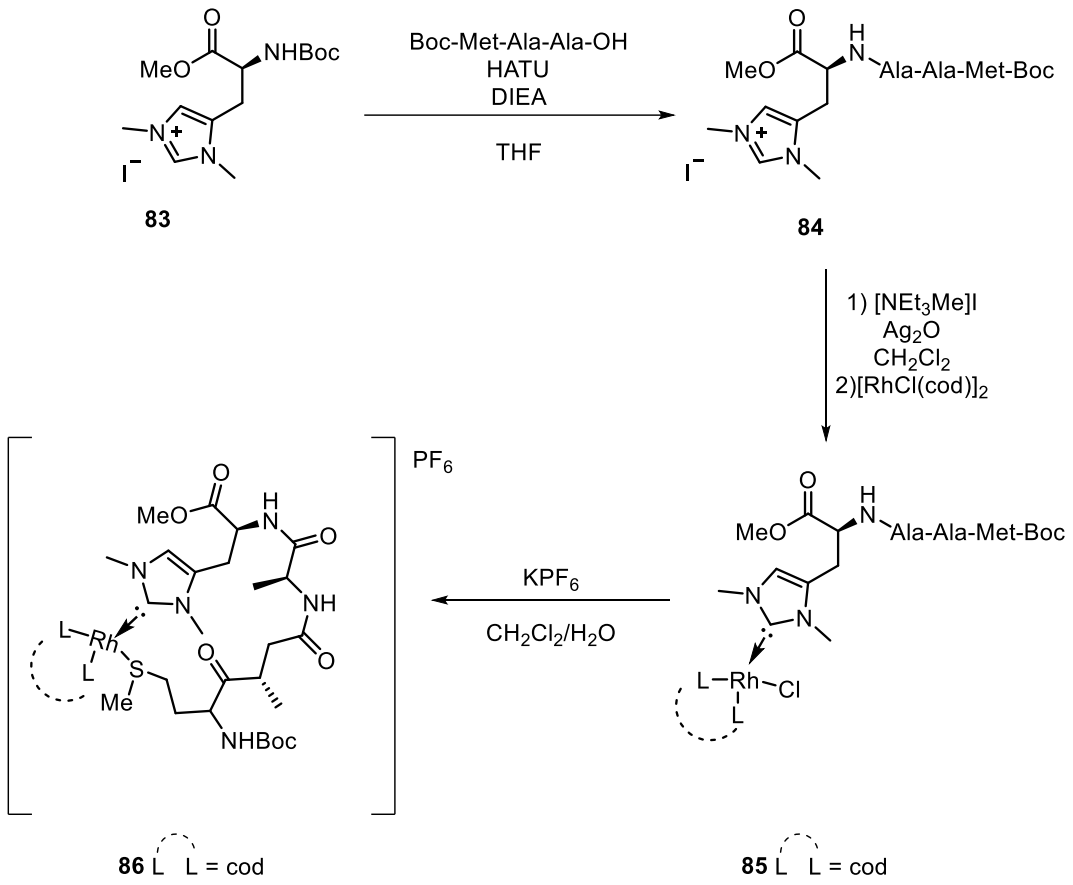

Scheme 8: *Synthesis of a rhodium metallopeptide using an imidazolium bearing amino acid.* ***86*** *is a representation of the proposed conformation induced by the methionine sulfide interaction with the metal centre.*

The reported *N,N'*-dimethyl NHCRu amino acid **87** and the novel corresponding gold and platinum complexes (**88** and **89**) were tested for use as anticancer drugs in seven cancer cell lines (Figure 31).[126] The histidine derived metal complexes displayed higher anticancer activity than their imidazole derived counterparts, highlighting the importance of the amino acid backbone. The platinum complex **88** was highly cytotoxic against cisplatin resistant HT-29 cell line. Mueller and co-workers hypothesize that the histidine base ligand acts as a transmembrane carrier and initiates DNA degradation. Reithofer and co-workers reported the use of the same NHCAu amino acid **89** to stabilize gold nanoparticles demonstrating that the versatility of this building block transcend catalysis and medical applications.[127]

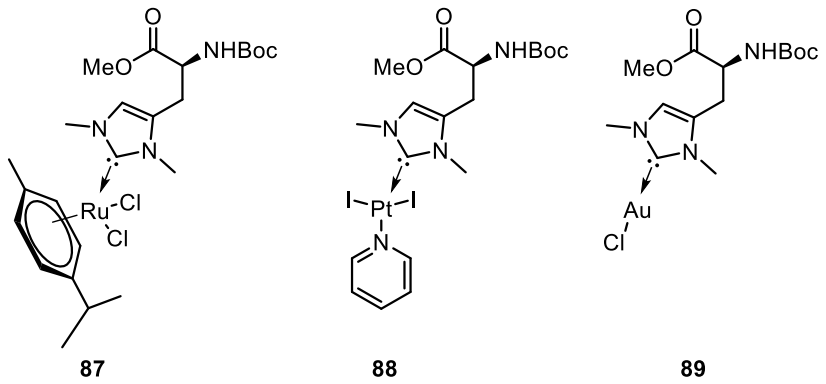

Figure 31: *Histidine derived metal complexes tested for anticancer therapies.*

Drost and co-workers synthesized a library of allyl-palladium histidine derived NHCs, which were able to catalyse Z-selective transfer semihydrogenation of alkynes (Figure 32).[128] The ligands displayed varied substitution of the nitrogens of the imidazolium including pyridine derivatives. The substitution pattern of the ligand has significant effects on the reactivity of these compounds, with the presence of a mesityl substituent on the increasing conversion up to 99% and diminishing the reaction time from twenty-wight to eighteen hours.

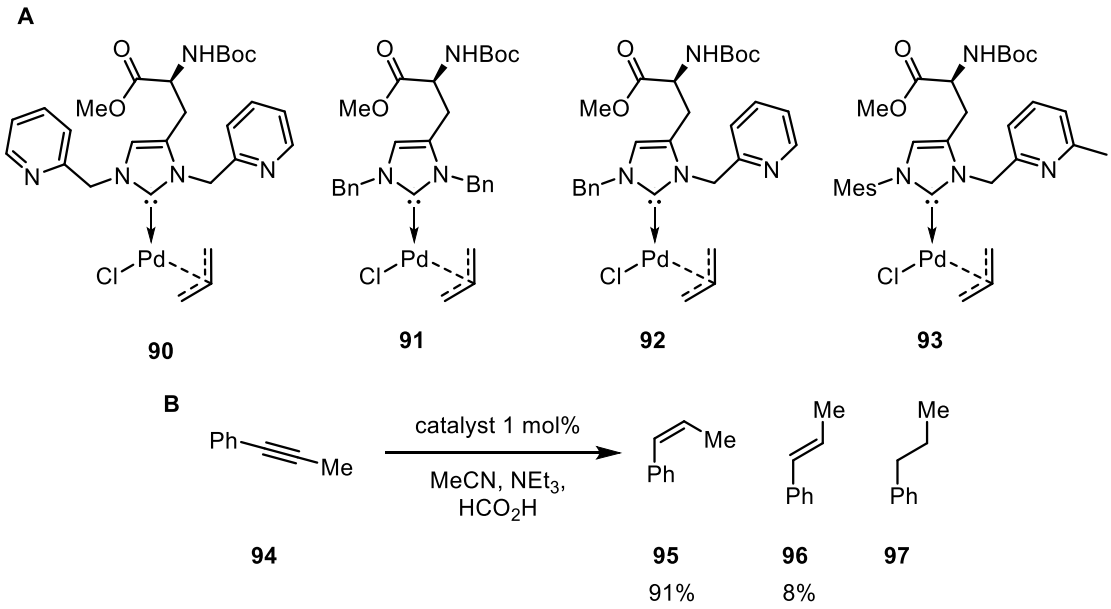

Figure 32: A) *library of palladium allyl complexes synthesized by Drost et al;* ***B)*** *Test reaction of Z-selective transfer semihydrogenation of 1-phenyl-1-propyne, yields provided for catalyst* ***90.***

DesMarteu and co-workers reported the trifluoroethylation of the nitrogens of histidine methyl ester using iodonium salts (Scheme 9).[129] The imidazolium salt **99** was synthesised in 91% yield with a trifluoroethyl protecting group at the α-amine. The tolerance of this synthesis methodology to carbamates such as Boc or Fmoc was not explored, and thus the viability of this building block for SPPS is unknown.

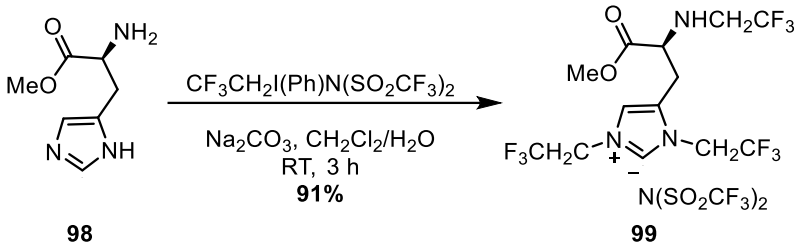

98 **99**

Scheme 9: *N,N',N''-Trifluoroethylation of L-histidine methyl ester by an iodonium salt.*

Bang and co-workers alkylated Fmoc-histidine methyl ester with long hydrophobic carbon chains (up to fourteen carbon units) to create a library of peptides for screening as antimicrobial drugs (Figure 33). The imidazolium amino acids were incorporated in peptides using Fmoc-based SPPS. No metal coordination or catalytic activity was tested for these types of scaffolds but it is a positive precedent for the incorporation of these ligands in peptides.[130]

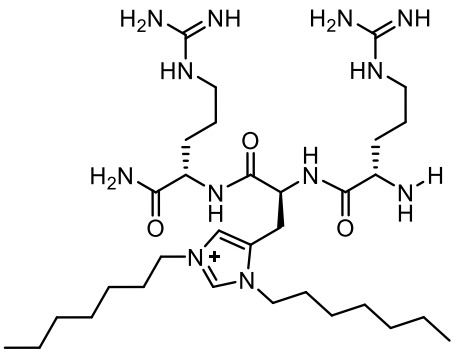

100

Figure 33: *Selected example of an imidazolium salt containing peptide prepared by Shin and co-workers for antimicrobial testing.*

Alkylation of histidine is not the only method to access imidazolium and NHC bearing amino acids. Gilbertson and co-workers used cross-coupling reactions to introduce a bis-aryl imidazolium salt onto an alanine backbone. The known derivative iodoalanine***131*** was utilized in a Negishi type coupling with several imidazolium salts containing an aryl iodide (Scheme 10). The amino acids were successfully coordinate to rhodium and ruthenium via silver transmetallation. In order to utilize these amino acids in standard SPPS synthesis procedures, the Boc group was replaced by an Fmoc protecting group on the amine and the methyl ester hydrolysed in one of the imidazolium derivatives. The same compound was coupled to a tripeptide containing isoleucine, proline and alanine, that was then cleaved from the resin using 2% TFA in dichloromethane. After cleavage the peptide was coordinated to silver in THF, followed by transmetallation to ruthenium. No catalytic or medicinal applications of this system were reported.[132]

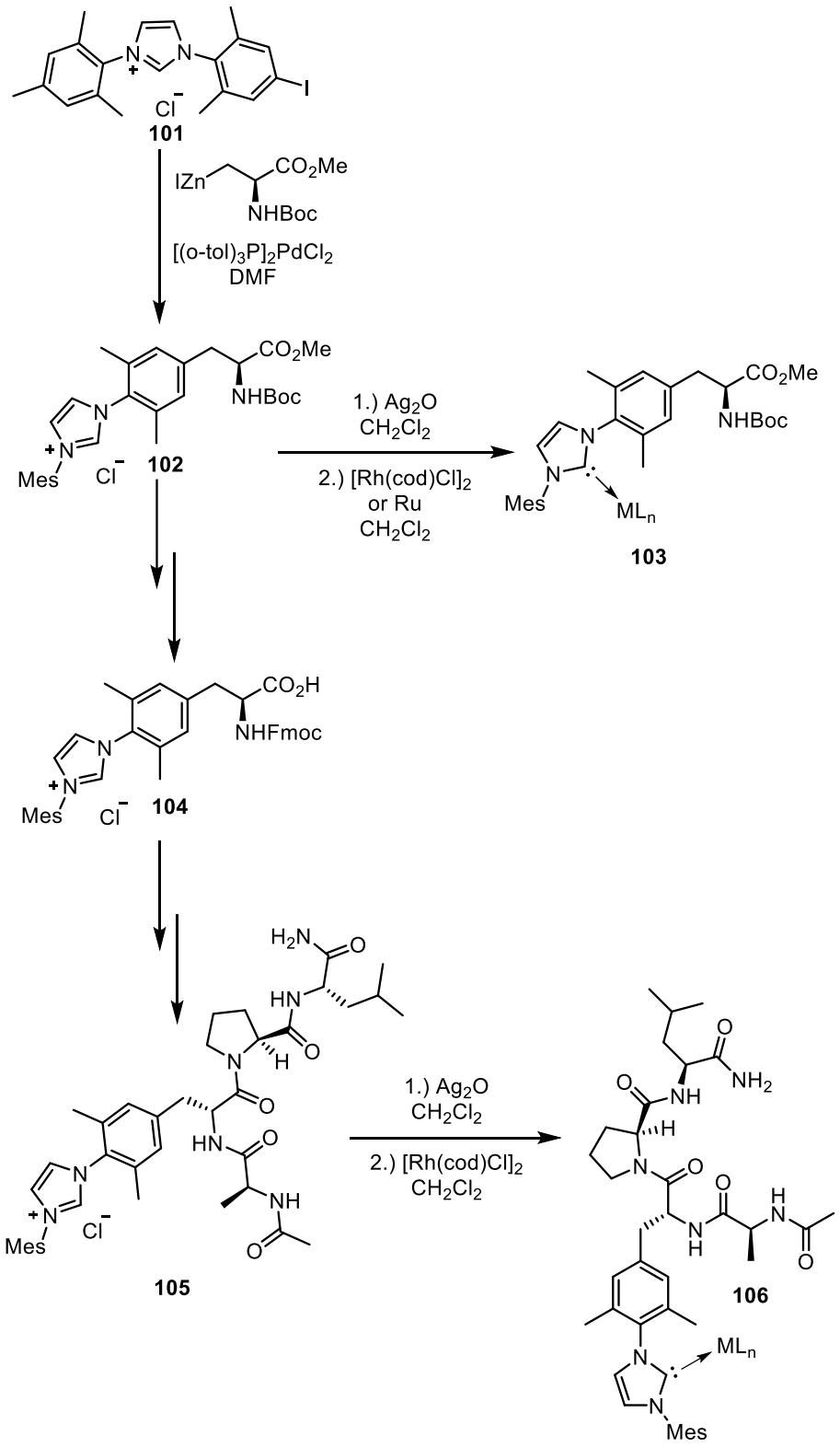

Scheme 10: *Gilbertson and co-worker's synthesis of NHC bearing amino acids and peptides and corresponding metal complexes.*

Using a similar cross coupling approach Meldal and co-workers coupled an imidazole with an N-substituent bearing a carboxylic acid to an alkyl iodide

bearing an α azide yielding an imidazolium salt.[26] The azide was further reduced to the free amine which was subsequently used in SPPS. This allowed for the synthesis of imidazolium bearing peptides. The palladium complex of the peptides displayed an interaction between the palladium ion and the oxygen of the carbonyl adjacent to the NHC. This result lead to the design of bidentate ligands by incorporation of two imidazolium units in peptides containing proline residues to induce a turn motif. Further work from the group optimized the library of peptides by incorporating pyridine functionality adjacent to the two imidazolium units to create a chelate systems for palladium (Figure 34, B).[133] The library of on resin complexes was studied in the catalysis of Sonogoshira and Suzuki cross-coupling reactions with high yields. Recycled heterogeneous palladium catalyst showed no loss in yield after 8 reaction cycles. This work demonstrated the potential of recyclability of on resin metallopeptide catalysts.

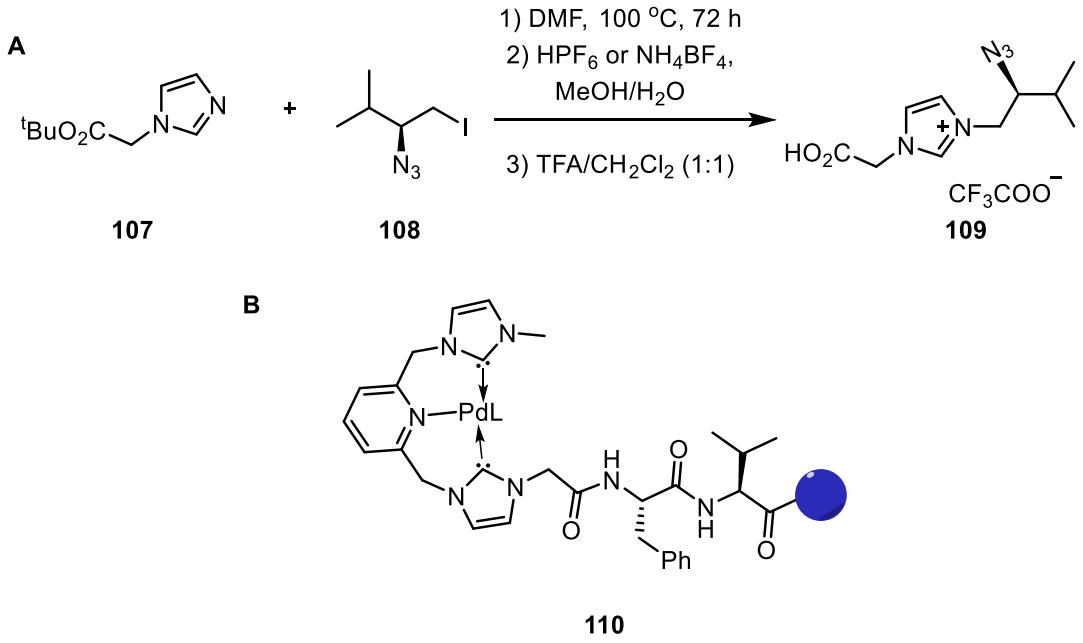

Figure 34: A) *Synthesis of imidazolium bearing amino acid precursor;* ***B)*** *selected example of palladium metallopeptide on resin prepared by Meldal and co-workers.*

Proline is known to induce turns in secondary structures of proteins. Thus, proline derivatives containing NHCs were described. Hydroxyproline **111** was

converted to the triflate **112** and used in a C-N bond formation with N-mesitylimidazolium to give access to the amino acid derived NHC salt **113** (Scheme 11). Several protecting group transformations were carried out successfully including hydrogenation of the Cbz group on the proline amine and subsequent Fmoc protection. The imidazolium amino acid derivative was coupled to an alanine residue in solution. Rhodium complexation was achieved for the individual amino acid and the peptides.[134]

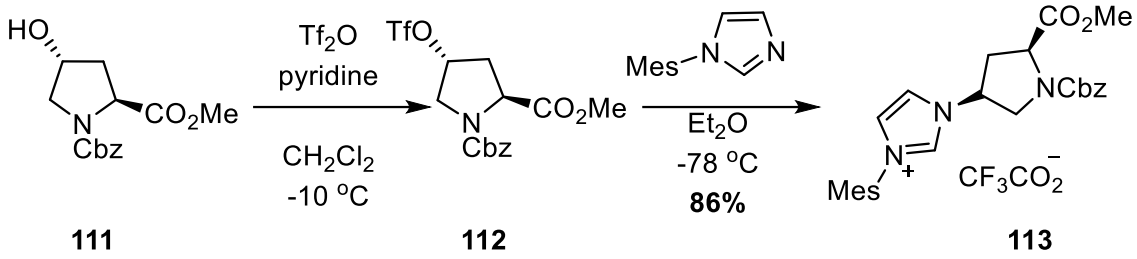

Scheme 11: *Synthesis of proline derived imidazolium salts*

In 2008 the first example of an NHC containing an amino acid backbone as a substituent in the nitrogen atom the imidazolium ring was reported. Utilizing a previously reported chiral Ni(II) complex, a dehydroalanine derivative was accessed. Subsequent addition of an imidazole to the olefin, followed by alkylation with iodomethane gave access to an NHC salt **117** (Scheme 12). Treatment with hydrochloric acid at reflux caused hydrolysis of the Ni(II) complex and released the amino acid moiety with no protecting groups. Protection with Boc and treatment with silver oxide gave access to the silver complex. This synthesis route is expensive and not very atom economical when compared to the simpler alkylation routes. No applications were described.[135]

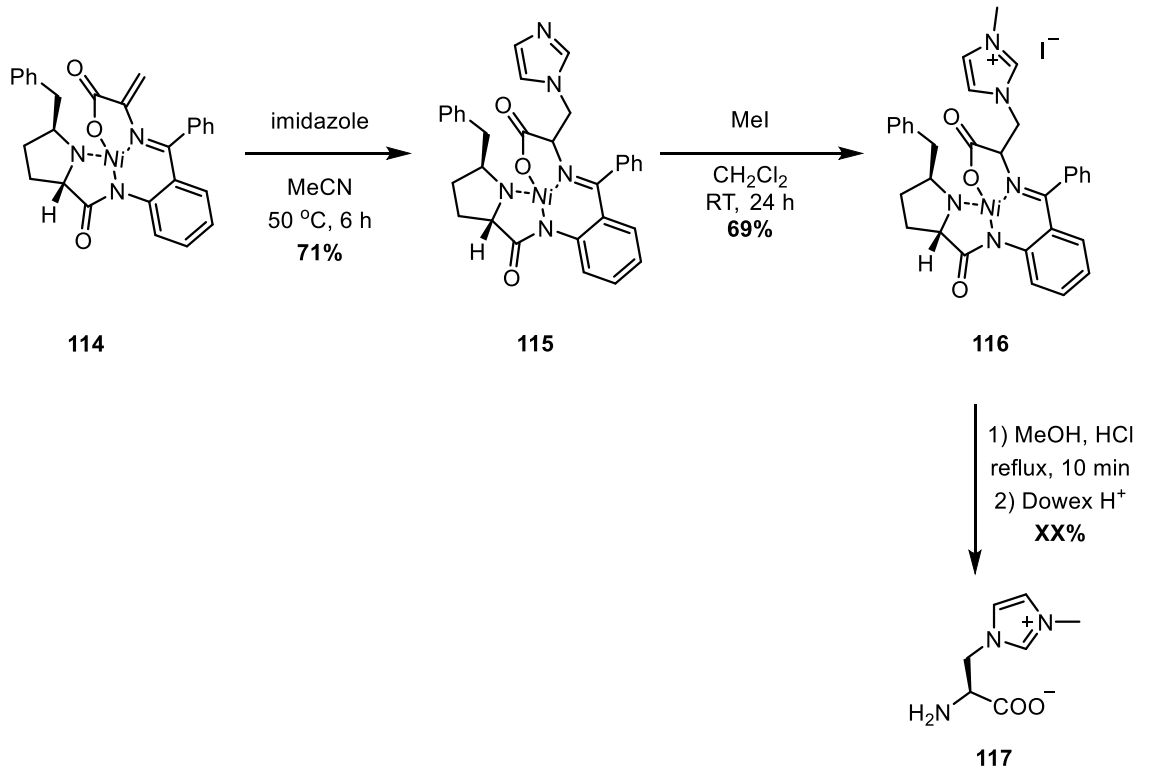

Scheme 12: *Synthesis of histidine derived imidazolium salt* ***117*** *via a nickel templating.*

Ukaji and co-workers synthesized pyridine containing imidazolium salts derived from amino acids which showed promising activity in the copper-catalysed asymmetric alkylation of N-tosylimines.[136] The α-carboxylic acid of the amino acids (**118** and **119**) were reduced with lithium aluminium hydride to the primary alcohols which were treated with phosphorus tribromide to yield the corresponding alkyl bromides (**120** and **121**, Scheme 12). The alkyl bromides were then used as an alkylating agent in the alkylation of pyridinoimidazole yielding the imidazolium salts (**125** and **126**, Scheme 12). The valine derived amino acid yielded the best enantioselectivity in the alkylation of phenyltosyl imine. This synthesis methodology could provide a route to modify the C-terminus of a peptide with an imidazolium salt. However, it would not tolerate residues with a carboxylic acid side chain such as glutamates and aspartates.

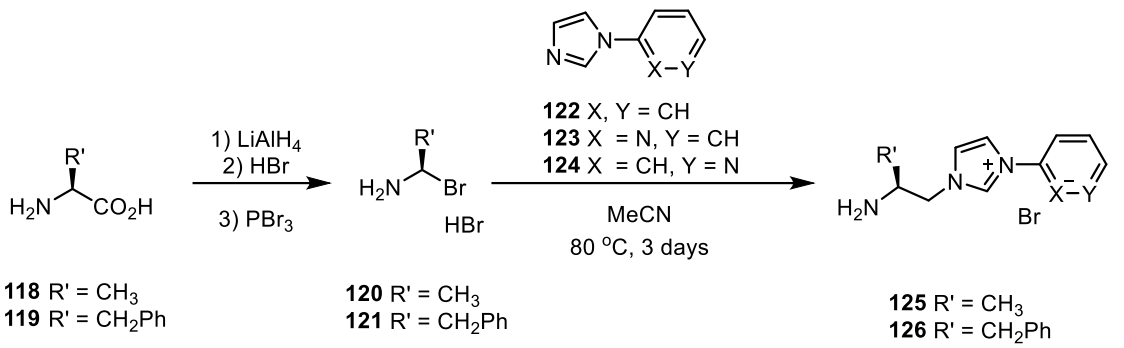

Scheme 13: *Synthesis route to access imidazolium salt bearing amino acids reported by Ukaji and co-workers.*

The common approach of late-stage metal complexation leads to the re-designing of the ligand requiring new synthesis routes. In attempt to overcome this problem, Chardon *et al.* proposed the use of click chemistry as a post-metallation functionalization tool. An alkyne containing NHC platinum complex was conjugated to a lysine amino acid and phenylalanine via ruthenium catalysed cycloaddition with the corresponding azide derivatives (Scheme 14). The lysine derivative containing NHC platinum complex **127** was tested as an antiproliferative agent against several lines of tumour cells. This compound showed particular activity towards colon cancer cells.[137]

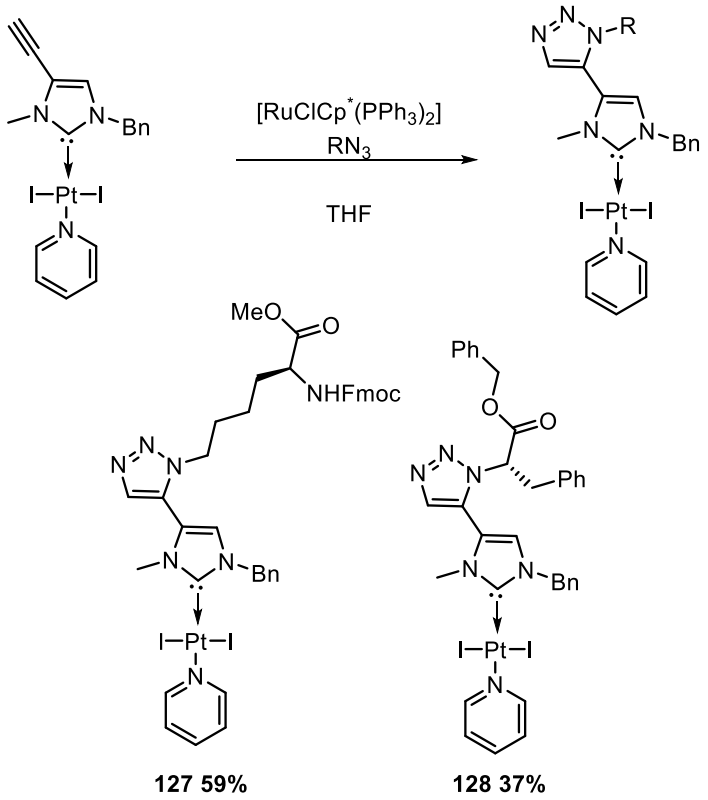

Scheme 14: *Synthesis of amino acid bearing NHC-platinum complexes via ruthenium catalysed azide-alkyne cycloaddition.*

The literature reports show viable routes to access imidazolium and NHC bearing peptides and amino acids. Moreover, the limited use of such scaffolds in SPPS procedures gives an encouraging precedent for the incorporation of NHC derived building blocks in combinatorial synthesis of peptide catalysts. However, the atom economical access to a library of Fmoc-based imidazolium and metal NHC containing amino acids has not been explored. Coordination of different scaffolds to metals such as gold has not been widely explored and many of the metal complexes reported have not been tested in catalytic reactions.

1.5 – Aims and Objectives

This thesis describes my efforts towards the synthesis of artificial metalloenzymes using synthetic peptide scaffolds and novel non-natural amino acids bearing ligand and metal complexes as side chains (*Error! Reference s ource not found.*). Currently, there is a lack of late-stage transition metal ligands within protein scaffolds. Late transition metal ligands are ubiquitous in organic synthesis and allow access to reactivity that is not present in nature. Therefore, in order to explore the activity of late-stage transition metals in designed artificial enzymes, non-natural amino acids able to bind these metals are required.

Herein, the design and synthesis of non-natural amino acids building blocks capable of binding transition metals will be explored. The designed building blocks will need to be tested for their compatibility with SPPS procedures and transition metal coordination.

A strategy for artificial metalloenzyme design uses peptide scaffolds which self-assemble into complex three-dimensional structures. The hypothesis is that three-dimensional structure provides the catalysts with a chiral environment as well as potentially protecting the metal centre from degradation pathways. The current literature lacks examples of incorporation ligand building blocks in larger, synthetically accessed structured peptides. Thus, the tolerance of the designed building blocks to be included in three-dimensional peptide structures needs to be studied.

Chapter 2:

2.Synthesis and Exploration of Amino Acids Bearing Imidazolium and Thiazolium Functionalities

2.1 - Introduction

In an effort to prepare an artificial metalloenzyme utilizing a synthetic peptide scaffold, an amino acid capable of binding metal ions with a defined set of properties is required. In order to understand which are the desirable properties of an amino acid for peptide synthesis, the procedure of SPPS must be considered. Since the first reports by Merrifield in 1963, the field of SPPS has had tremendous growth.[138, 139] The principle, however has remained the same, a solid support covalently binds the first amino acid (Figure 35,a)), followed by a selective deprotection which exposes the next reactive point (usually the amine; Figure 35, b)) to which the subsequent amino acid is coupled (Figure 35, c)). This step-by-step deprotection/coupling sequence leads to the synthesis of a peptide which is covalently bound to a solid support, whilst side products and excess reagents from each step can conveniently be washed away. After the last amino acid is incorporated the desired peptide is released by selective cleavage of the resin-amino acid bond (Figure 35, d)). The success of this technique relies on orthogonal deprotection strategies between the resin amino acid bond, side chain protecting groups and amine or carboxylic acid protecting groups.

Throughout the past fifty years several protocols for SPPS have been described with the most used being the Boc and the Fmoc-based approaches. The Fmoc-based solid phase procedure has been widely used since 1993 when a comparative evaluation concluded that it provided milder reaction conditions than its Boc counterpart.[139] The use of large quantities of trifluoroacetic acid as a deprotecting agent, combined with the use of hydrofluoric acid as a resin cleavage agent, has made the Boc-based SPPS method undesirable. The standard Fmoc based procedures combine acid labile resins and amino acid side chains protecting groups with a piperidine based Fmoc removal. The fluorene ring in Fmoc is capable of absorbing UV light, which allows for coupling and deprotection reactions to be monitored by UV-vis spectroscopy, providing a valuable glimpse into the reaction.[140, 141] Nowadays automated peptide synthesizers make use of microwave-assisted peptide synthesis and allow for the synthesis of complex peptide sequences up to 100 amino acids in length.[142] Therefore, a versatile building block amino acid for SPPS would have an Fmoc carbamate protected amine and a free carboxylic acid. It would also be desirable to have tolerance of microwave radiation, high quantities of trifluoroacetic acid and mixtures of 20% piperidine in DMF, THF or dichloromethane.

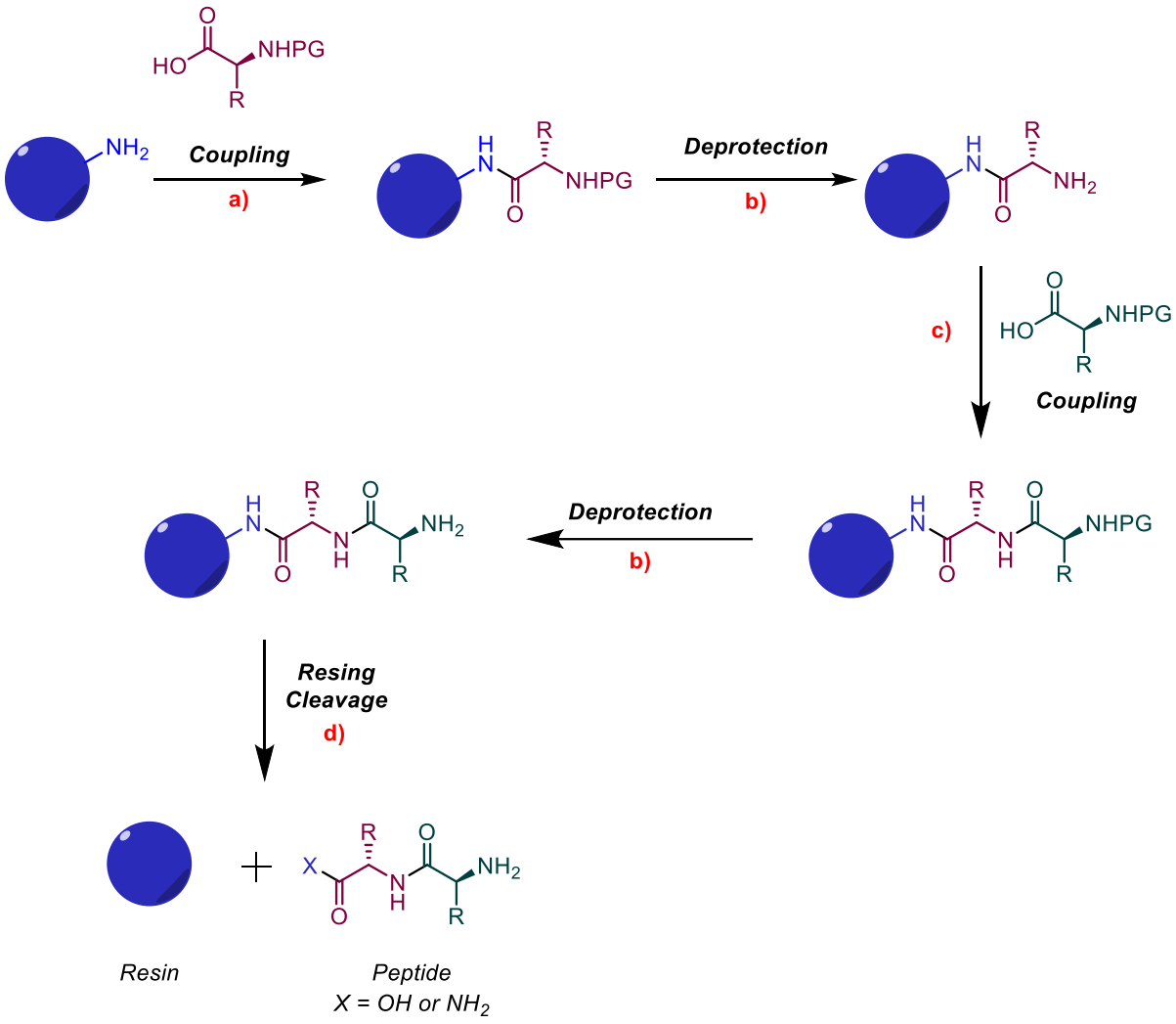

Figure 35: *Schematic representation of a solid phase peptide synthesis methodology, where PG stands for protecting group.*

A further consideration is the stereochemistry of the amino acid. An ideal building block would be a single enantiomer since different enantiomers have different spatial configurations which will impact the higher order structure of a peptide and/or protein. Considering that native proteins are made up primarily of L- residues, this configuration would be prefered.[143] L-Amino acid feedstocks are also more commonly available, more cost effective and thus widely adopted in peptide synthesis.

The final requirement for this amino acid scaffold is that the side chain of this amino acid must contain a moiety capable of binding the transition metal of interest to create a catalytic site in the peptide assembly. In the natural amino acid toolbox there are several oxygen, nitrogen and sulfur donors capable of coordinate to metals, in particular first row transition metals such as copper and zinc. However, is not possible to bind late-stage transition metals such as palladium and gold. Thus, in order to achieve my goal of creating catalytic centres with late-stage transition metals embedded in peptide scaffolds, ligands which feature commonly in small molecule catalysis are required. For this purpose, ligands, such as an NHC or phosphorous based ligands would be desirable. In both cases, these ligands are capable of binding different transition metals, this would allow for altering reactivity by simply swapping the metal, without having to redesign a completely different ligand system. In the following section the efforts to synthesize NHC containing amino acids that match these requirements will be discussed.

2.2 - Results and Discussion

Amino acids scaffolds bearing imidazolium functionality have been reported in the literature, however their chemistry in subsequent reactions has not been widely explored.[120-122, 124, 125, 128, 132, 134, 144, 145] Boc carbamates have been extensively used in these types of scaffolds which limits their use in Fmoc SPPS methodologies. In theory it is possible to remove the Boc group in these amino acids and subsequentially synthesize the Fmoc carbamate, but this process introduces two extra steps which will diminish the yield and atom economy of the overall synthesis.

One of the well-known routes to obtain an NHC precursor is through the alkylation of imidazole derivatives.[146] The natural amino acid histidine contains an imidazole side chain and therefore it was the obvious starting material. Utilizing the commercially available Fmoc-L-His(Trt)-OH **130**, means that the right stereogenic configuration, amino acid backbone and the Fmoc protecting group were already in place. Double alkylation of the imidazole nitrogen atoms would provide the imidazolium salt that could be subsequently coordinated to a range of different transition metals (Scheme 15).

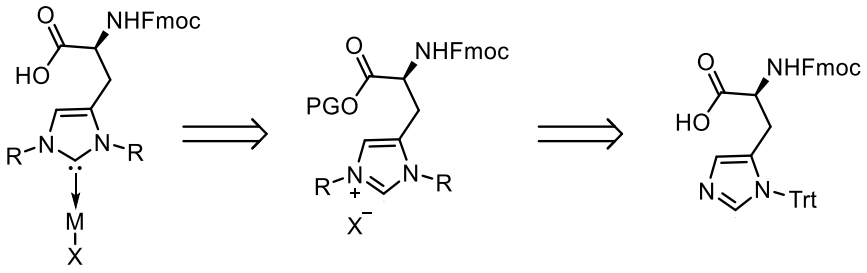

128 **129** **130**

Scheme 15: *Retrosynthetic analysis of an NHC metal complex containing an amino acid side chain, from a commercially available amino acid feedstock.*

It is well established that the groups attached to the nitrogen atoms of the imidazolium have an impact on the properties of the carbene.[147, 148] By modifying these groups, it is possible to tune the polarity and sterics of the molecule as well as altering the electronics of the carbene.[149] The ability to introduce two different groups on the NHC side chains provides greater scope to tune the carbene properties even more than a double alkylation. For example, an NHC containing an aromatic side chain can be electronically more stable, however also quite apolar and bulky. So, by combining an aromatic side chain on one nitrogen, whilst keeping the second side chain small and aliphatic can allow for a more stable carbene, but smaller than a double arylated system. In this work both double

alkylation and unsymmetrical alkylation of histidine to form imidazolium salts was explored.

As one of the main goals of this project is the incorporation of these amino acids in complex peptide superstructures, the sterics and polarity of the side chains is important. The supramolecular assembly of peptides into specific structures is partly dependent on the entropy associated with burying hydrophobic side chains whilst exposing hydrophilic sites in water. The placement of a highly hydrophobic functionality in locations that are designed to be solvent exposed can lead to a disruption of the intended structure. The superstructure compensates these high energy states, by burying of hydrophobic functionality into less solvent exposed areas. Therefore, by starting with less bulky groups the chance of successful incorporation into complex peptide scaffolds, without disturbing the desired quaternary structure, would be higher. Nevertheless, it is necessary to consider that steric bulk and electron density are commonly used to stabilize the carbene of the imidazole moiety.[149] Small substituents such as methyl groups can lead to dimerization of the NHC and prevent coordination to metal ions.[150] Consequently, it is likely that a compromise between steric bulk and stability of the carbene might be required for successful metal ion coordination and subsequent catalysis applications.

2.2.1 - Methylation of Histidine Benzyl Derivatives

As a starting point a double methylation functionalization was chosen due to the small size of methyl groups and high reactivity of methyl iodide as an alkylating agent. Unsymmetrical alkylations would also be expected to be possible, though in these initial studies that level of complexity was not

introduced.[128] All the double alkylation reactions described in the literature were performed on the ester form of histidine, indicating that protection of the carboxylic acid would be required prior to the formation of the imidazolium salt.[120-122, 125, 128, 130, 144]

Due to their often hygroscopic nature, imidazolium salts have a tendency to be soluble in water, making them harder to isolate thus increasing the complexity and cost associated with purification strategies (e.g. reverse phase chromatography). Therefore, protecting groups which provide simple reaction processing were first studied. A benzyl protecting group was chosen to protect the carboxylic acid as a starting point due to being orthogonal to the Fmoc carbamate. Benzyl esters can be cleaved by hydrogenation, which have simple workup procedures, often not requiring aqueous extractions. Using the Mitsunobo protocol described by Zhao *et al.,* commercially available **130** was protected to give histidine derivative **131** in 57% yield.[151] Subsequent selective cleavage of the trityl group using 50% TFA in dichloromethane gave the resulting free imidazole **132** in 61% yield (Scheme 16).

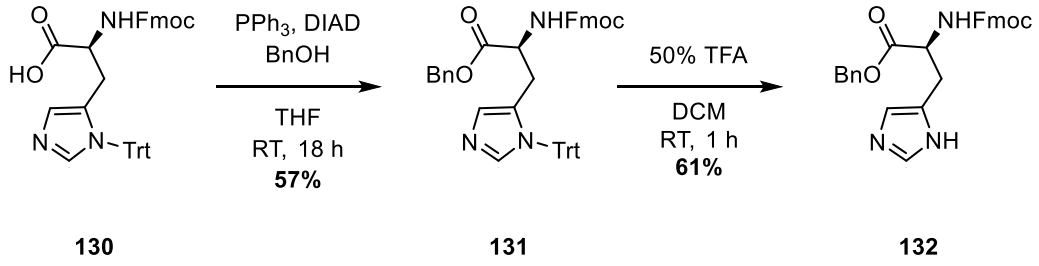

130 **131** **132**

Scheme 16: *Synthesis of free imidazole* ***132*** *from commercially available Fmoc-L-His(Trt)-OH 130.*

Upon reviewing the literature two procedures for the alkylation of histidine derivatives stood out.[120, 128] These procedures differed on the amount of

alkylation agent and length of reaction and both were tested to determine which one would provide the best yield. The conditions reported by Drost *et al*. for N,N'-dibenzyl systems utilized fewer equivalents of sodium bicarbonate and methyl iodide and higher temperature (80 °C).[128] The obtained crude reaction mixture was complex, nevertheless pure product **133** was isolated after normal phase silica gel column chromatography with a 31% yield (Scheme 17). Previous reports of similar molecules suggested that the counter ion comes from the alkylating agent halide and in the case of compound **133,** it would be a iodide as determined from the reported elemental analysis data.[145]

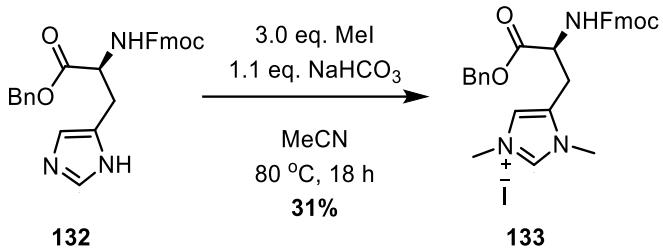

Scheme 17: *Synthesis of imidazolium salt **133** by alkylation of histidine derivative **132** using methyl iodide.*

Transmetallation of silver NHC complexes is a well-known method of preparing several different NHC complexes of metals such as Ru, Au and Pd.[152] In order to test reactivity and coordination chemistry, compound **133** was subjected to two different routes to form the NHCAu complex: silver transmetallation and direct carbene insertion (Scheme 18). Both gold NHC complexes **135** and **136** were successfully accessed with comparable yield (40 and 42%, Scheme 18).

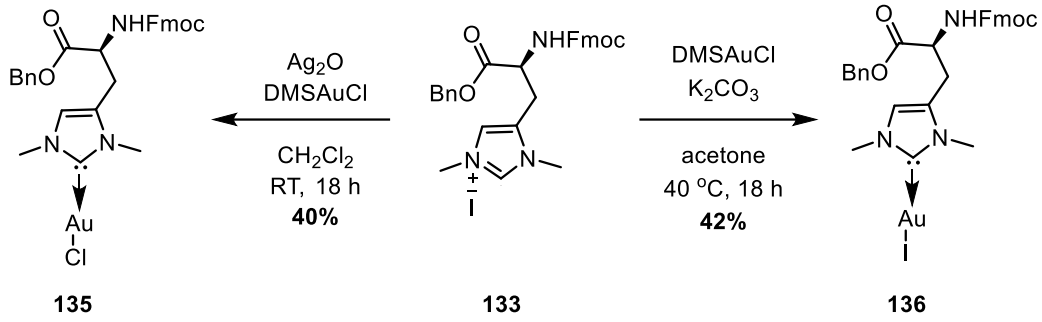

Scheme 18: *Synthesis of gold complexes of compound* ***133*** *via two routes.*

The conditions reported by Hannig *et al.* comprised of four equivalents of methyl iodide, in the presence of four equivalents of sodium bicarbonate as a base (Scheme 19).[120] The methylation reaction proceeded at 40 °C, providing the desired imidazolium salt **134,** after four days. Upon further analysis of the material **134**, it was noticed that while no impurities were observed in the ^{1}H and ^{13}C NMR spectra, the LCMS contained an extra unexpected peak corresponding to a mixture inorganic impurities (characterized by early retention time and salt adducts). Identification of single species was not possible due to a lack of resolution of this m/z cluster of peaks. Usually, an aqueous extraction would have been sufficient to remove inorganic impurities, however the compound **134** was also water soluble. Therefore, reverse phase preparative HPLC was utilized to remove this impurity. The HPLC purification provided **134** as a deliquescent yellow solid in 45% yield.

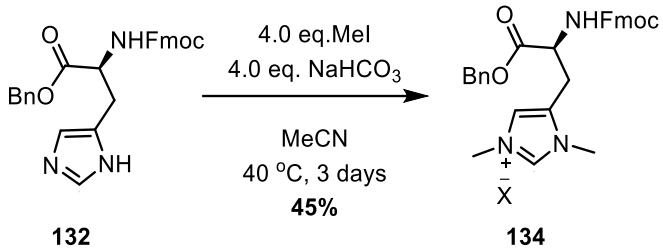

Scheme 19: *Synthesis of imidazolium salt **134** by alkylation of histidine derivative **132** using methyl iodide.*

The mass spectrum and ^{1}H NMR spectrum of **133** and **134** were identical however, their solubility was different**.** Compound **133** was easily solubilized in dichloromethane whilst compound **134** was not, which suggested that these molecules might not be the same. Since the above-mentioned spectra only characterize the cationic part of the salt, the difference was likely to reside the anionic part of the molecule. Different batches of both **133** and **134** were prepared to make sure this difference was not due to batch inconsistency.

2.2.2 - Determining the Counter Ion

The methods to determine halide counter ions are X-ray crystallography and elemental analysis. Growing good quality single crystals of a molecule can often prove challenging, with low or too high nucleation rate, spontaneous precipitation or chemical degradation in solution being some of the main problems.[153] On the other hand, elemental analysis requires circa 10 mg of non-recoverable material and cannot be applied to mixtures of compounds, and is hard to obtain for hygroscopic compounds. Combined it can make counterion determination challenging and time consuming. With imidazolium salts most counter ions are determined by the crystal structure or elemental analysis. Due to the previously

discussed hygroscopic properties of the salts, obtaining precise and correct determination of the elemental composition of these types of scaffold can prove challenging. A single crystal of the salt **134** was successfully grown from acetonitrile and diethyl ether. The counterion part of the molecule showed high level of disorder which made the solution of this part of the molecule hard, although it was very clear that it was not the expected halide. A first solution of the structure pointed out to the counter ion being an oxalic acid derivative. The two carbons of oxalic acid type counter ion should be visible in the ^{13}C NMR spectra however, these were not observed in the previously obtained spectra due to the low sample concentration (10 mg/mL). In contrast a longer ^{13}C NMR experiment combined with a more concentrated sample (20 mg/mL) was run. This experiment showed instead of the expected singlets, the presence of two distinct quartets in the ^{13}C NMR spectrum at 158 and 116 ppm, the latter resonance exhibiting a large coupling constant of 294 Hz characteristic of a $^{1}J_{C\text{-}F}$ coupling with fluorine (Figure 36 and *see* Appendix 7.1). This demonstrated that the counter ion was not an oxalate but instead a trifluoroacetate ion. Further solving of the crystal data was completed with a fit that agreed better with these findings (Figure 37). The trifluoroacetate is thought to originate from a counterion exchange with the iodide during the HPLC purification as the solvent used contained a TFA addictive.

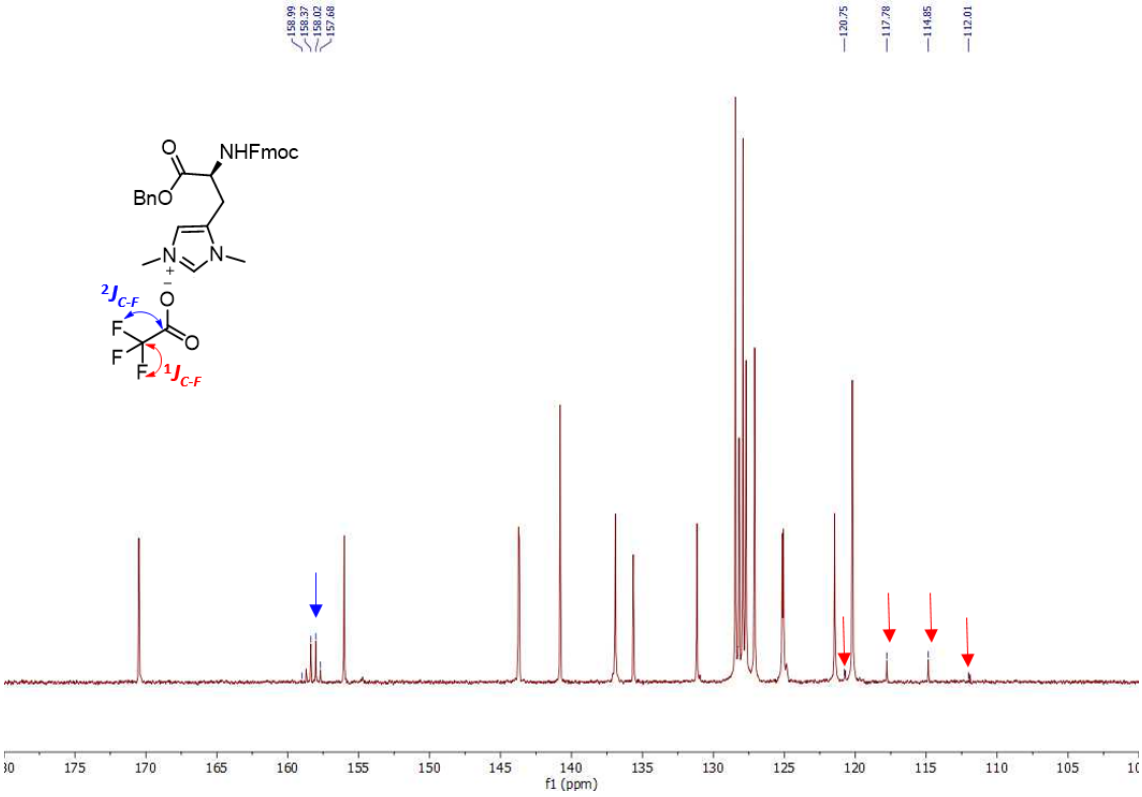

Figure 36: *Expansion of the ^{13}C NMR spectrum of derivative **134** in d_6-DMSO, the blue arrow indicates the quartet at 158 ppm corresponding to the carboxylate carbon and the red arrows indicate the quartet at 116 ppm corresponding to the CF_3 carbon of the trifluoroacetate counter ion.*

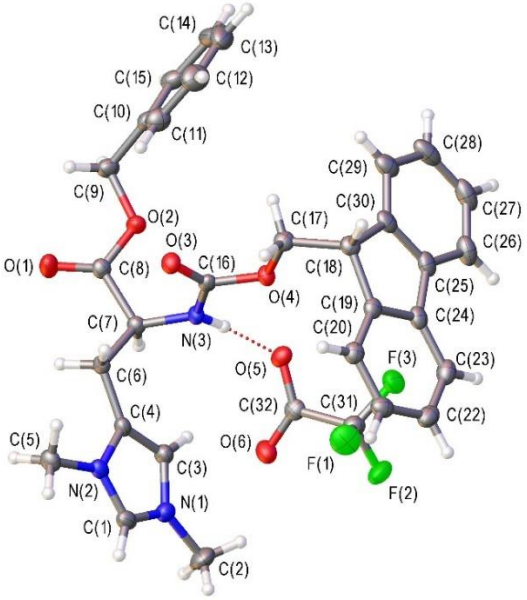

Figure 37: *Crystal structure of **134** with ellipsoids drawn at the 50 % probability level. The structure contains a trifluoroacetate anion which is disordered over two positions, of which only the major position is shown for clarity. Hydrogen bonding is shown using dotted lines. Crystal structure data solved by Louise Male.*

To further support that the halide counter ion could be exchanged by trifluoroacetate anion a sample of the amino acid **134** prepared by the 80 °C method was stirred with silver trifluoroacetate in acetonitrile for two hours (Scheme 20). After filtration, the imidazolium salt **133** was isolated and characterized. The ^{13}C NMR spectra confirmed the incorporation of trifluoroacetate counterion whilst the ^{1}H NMR of **134** completely overlaid with the starting material **133** and substrate **134** purified by HPLC.

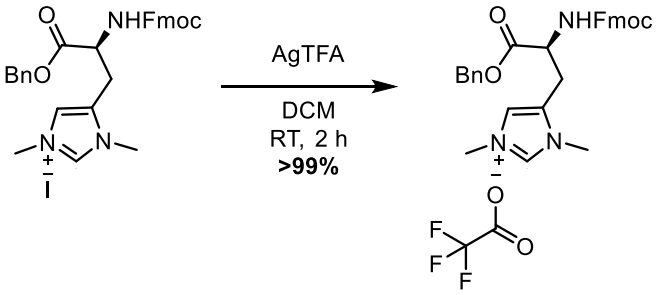

133 **134**

Scheme 20: *Anion exchange from iodide to trifluoroacetate using with silver salt.*

In order to evaluate the coordination chemistry of compound **134** coordination to different metals was attempted. Therefore, several one-pot approaches via silver transmetallation to gold and palladium, as well as direct carbene insertion of gold and copper procedures were attempted. None of these attempts were successful, in all cases starting material was recovered. (Scheme 21). This suggests that the lack of coordination is a result of an intrinsic property of this scaffold and not due to the coordination chemistry of a specific metal.

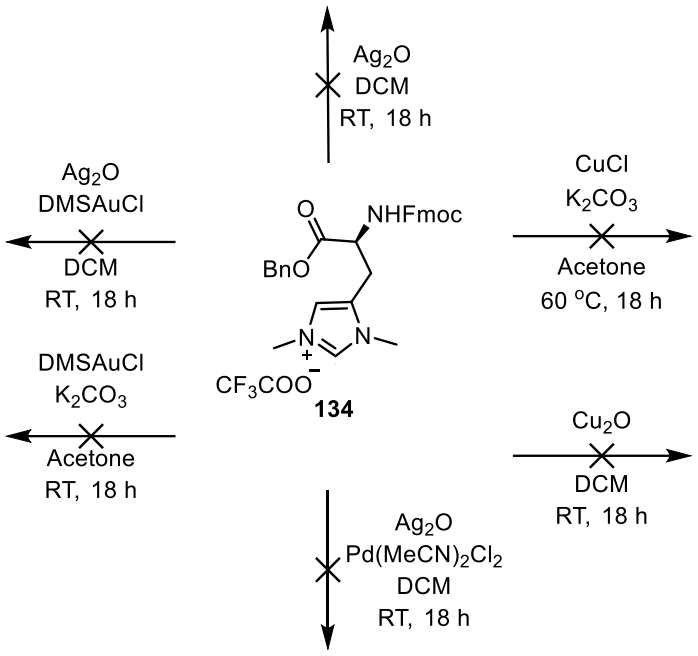

Scheme 21: *The different conditions of metal coordination attempted for imidazolium salt* ***134****.*

The trifluoroacetate counterion could be the reason why coordination of this NHC derivative to gold failed. The non-amino acid analogue 1,3-dimethylimidazolium iodide has been used in transmetallation reactions to yield several iridium, rhodium and ruthenium complexes.[154-156] Although the chloride derivative had been employed in direct coordination to palladium and gold, species with an iodide counterion have not.[157] The trifluoroacetate derivative is also known, and has been used as an ionic liquid, but no coordination chemistry has been reported (Scheme 22).[157] Other imidazolium trifluoroacetate salts bearing different substituents have been shown to be capable of coordination.[134]

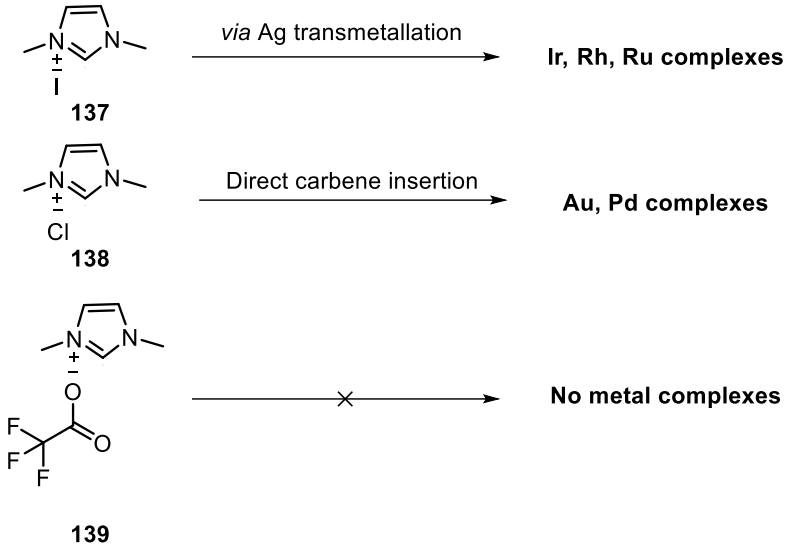

Scheme 22: *A Summary of the citations reports for coordination of imidazolium salts to different metals, illustrating the effect of the reported anions.*

2.2.3 - Different Protecting Group Strategies and its Impact on Coordination

In the case of substrates **133** and **134**, their unconventional behaviour during its synthesis, low yield and issues with removal of the benzyl group suggested that it was not a suitable candidate to explore further. Thus, a different combination of orthogonal protecting groups was explored. The Fmoc carbamate protecting group was maintained, given that is required for SPPS and the benzyl group was replaced by a methyl ester, as this had proved reliable with the previously reported Boc scaffold **83**.[128]

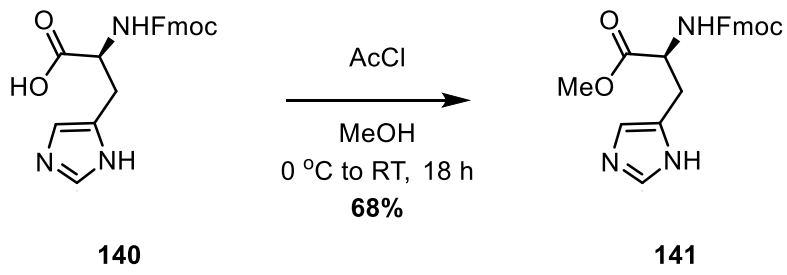

Scheme 23: *Protection of the free carboxylic acid of the Fmoc-L-histidine 140 via esterification using acetyl chloride and methanol.*

Fmoc protected histidine was esterified with methanol according to a described procedure (Scheme 23).[151] This moiety was then subject to the two previously employed methylation strategies to yield the dimethyl imidazolium salt **142** with comparable yields in both cases. The products were then subjected to the two different coordination strategies discussed above (Scheme 24). The same coordination behaviour, as well as the supporting analytical data shows that independently of the synthesis method, the same product is accessed. The yields for both syntheses are higher than the benzyl derivative **133** and are comparable between the two methodologies with product being made in 64% and 68% yield. Amino acid **142** is more soluble in less polar solvents, such as dichloromethane, and less hygroscopic than benzyl derivatives **133** and **134**. The reaction mixtures for the synthesis of **142** are cleaner than those for **133** and **134**. Filtration through celite and concentration under vacuum followed by flash silica gel column chromatography, using dichloromethane and methanol as solvents, yields a pure deliquescent solid. The ability to process material in this way avoids preparative HPLC and the counterion exchange with TFA previously mentioned. Compound **142** requires storage under argon in a desiccator to prevent it from becoming a dark brown oil, which upon analysis of the ^{1}H NMR spectra shows clear signs of degradation. The higher temperature route was preferred to prepare larger batches due to the shorter reaction time and higher atom economy.

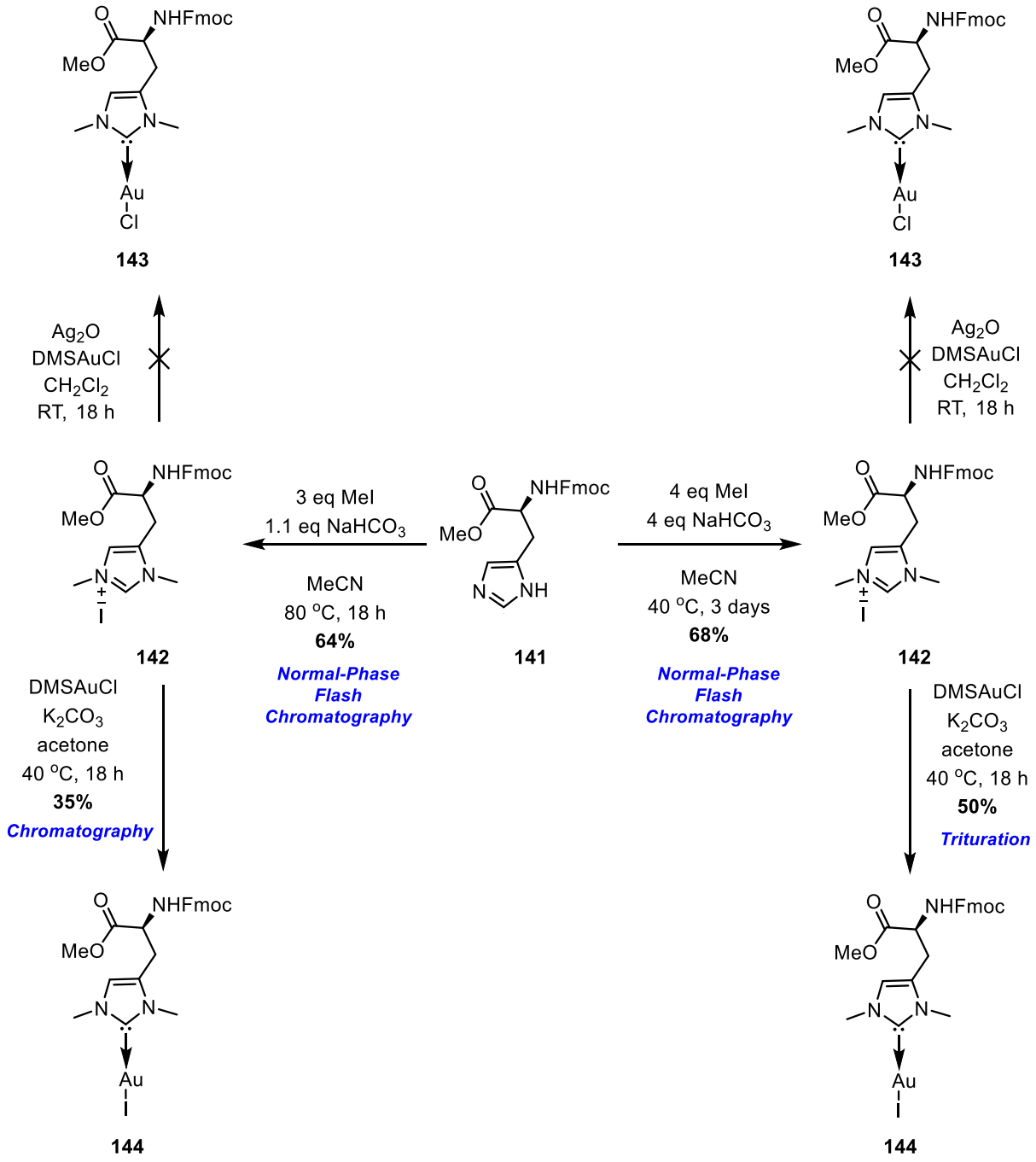

Scheme 24: *Relationship between synthetic methodology and the outcome of the product in two different metal coordination strategies for the protecting group combination Fmoc/Me ester.*

Surprisingly, although direct carbene insertion to gold was successful affording **144**, coordination via the silver transmetallation method was not achieved. These results have been repeated twice with a different purification for the gold complexation step. The 50% yields for **144** made via lower temperature

were accessed through trituration with diethyl ether. In the case of the higher temperature method a small unknown impurity needed to be removed via column chromatography, giving a lower yield. Hayes *et al.* theoretical study of the mechanism of silver NHCs formation has revealed that a deprotonation of the imidazolium by silver oxide and subsequent transfer of the silver to the free NHC, assisted by a second imidazolium was the viable mechanism.[158] In the case of direct coordination, Nolan's group has isolated the complex $[imidazolium]^{+}[AuClX]^{-}$, in which X is the halide anion of the starting material which in the presence of the base yields a single gold-NHC species.[159] In both mechanisms a deprotonation step is required for the formation of the carbene. However, the ligand sphere is different at this step for each of the mechanisms, which might explain the difference in reactivity. Another potential explanation is the difference in temperature. The one-pot transmetalation approach was carried out at room temperature, whilst the direct insertion was performed at 40 °C, and thus the increase in temperature could potentially facilitate the deprotonation step.

2.2.4 - Exploring Side Chain Scope

The combination of Fmoc/OMe protecting groups leads to the formation of more predictable and robust imidazolium containing amino acids and therefore will be used further. The ability to tune the nitrogen substituents in the carbene part of the molecule is a particularly desirable property. A single NHC amino acid is unlikely to be the solution to every protein/peptide or catalytic application, therefore a library of NHC containing amino acids suitable for routine peptide synthesis would be a valuable contribution to the field. A study of this combination

of protecting groups and how they would tolerate different side chains was carried out. The initial study focused on the viability of symmetric alkylations.

2.2.4.1 – Double Alkylation

It is well known that bulky and aromatic groups stabilize the carbene, preventing degradation pathways such as dimerization.[150] As a starting point the corresponding histidine derivative **141** with Fmoc protecting groups was alkylated with different benzyl type derivatives, utilizing the methodology mentioned above (Scheme 24). The bulkier benzyl groups facilitated easier handling of the salt, which is less hygroscopic and more soluble in dichloromethane than its corresponding methyl counterpart (Scheme 25).

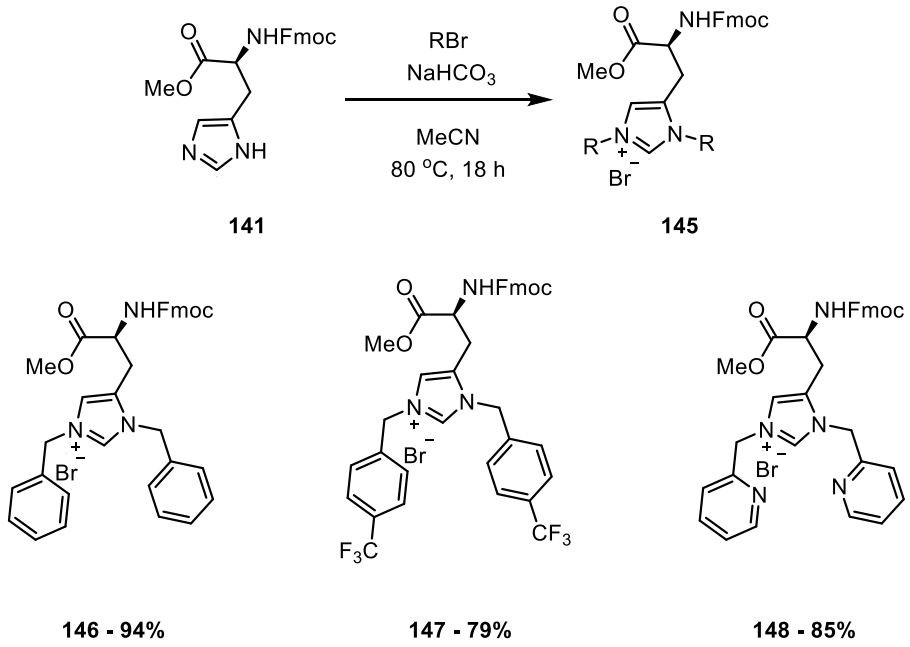

Scheme 25: *Substrate scope with aromatic residues.*

The alkylation reaction was caried out at 80 °C in acetonitrile in the presence of sodium bicarbonate as a base (Scheme 25). The benzyl derived **146**

was accessed with 94% yield and successfully crystallized from acetonitrile/diethyl ether (Figure 38).

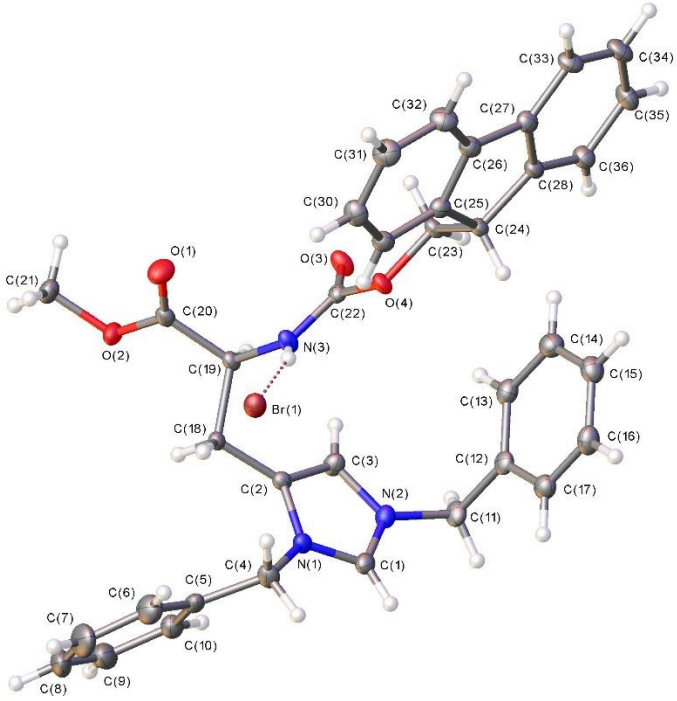

Figure 38: *Crystal structure of derivative* ***146*** *with ellipsoids drawn at the 50 % probability level. Hydrogen bonding is shown using dotted lines. Crystal structure data solved by Dr. Louise Male.*

Pyridine residues are known to coordinate to transition metals and are used often as ligands.[160, 161] Dichloro(2-pyridinecarboxylato)gold complex is a widely used gold (III) complex, in which one of the ligands is a pyridine ring.[162, 163] Direct alkylation with two methylpyridine groups strategy was chosen to explore the possibly providing potential second coordination sites for transition metals. Pyridine rings are electron deficient, so in order to distinguish whether potential differences in behaviour between pyridine derivative **148** and the corresponding benzyl **146** are related to a change in electron density or second coordination sites, the electron poor *para-(*trifluororomethyl)benzyl variant was introduced for comparation purposes. In order to the reaction to occur in the case

of both the *para*-(trifluororomethyl)benzyl bromide and 2-(bromomethyl)pyridine alkylations, the equivalents of sodium bicarbonate were increased from 1.1 to 4.0 equivalents. The trifluoro substituted benzyl imidazolium **147** was formed in 79% and the 2-pyridine derivative **148** was formed in 85% yield.

The introduction of large hydrophobic side chains on the nitrogens of the imidazolium ring might cause a problem at later stages of the project, potently disrupting the quaternary structure of certain peptides. As mentioned before, methyl derivative **142** is prone to decomposition and is highly hygroscopic. Therefore, a scope of smaller and diverse side chains was studied.

To optimize reaction conditions for these new types of functionalities, 1-bromopropane was chosen as the test alkylating agent because it was available (Scheme 26). Starting from the standard conditions (Table 1, entry 1). a very messy reaction mixture was obtained, with numerous compounds visible by TLC, with none being the desired product. Increasing the number of equivalents of alkylating agent did not result in any improvement (Table 1, entry 2). Hannig *et al.* reported the use of 25 equivalents of 1-bromopropane at 65 °C in the presence of 4 equivalents of sodium bicarbonate to generate a related imidazolium species.[120] These conditions yielded imidazolium **151** in 68% yield (Table 1, entry 3). Attempts to diminish the amount of alkylating agent used to 6 equivalents while maintaining the temperature and base stoichiometry were made, but incomplete conversion of starting materials was observed. Therefore, despite the lack of elegance, the methodology using 25 eq. of alkylating agent was employed to prepare other alkane containing derivatives.

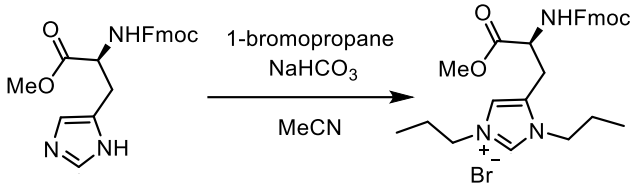

141 151

Scheme 26: *Alkylation of histidine derivative* ***141*** *with 1-bromopropane. Details about reaction conditions discussed in* ***Table*** *1,*

Table 1*: Optimization of alkylation of* ***141*** *reaction using 1-bromopropane, yields provided are isolated yield.*

Entry	***RX***	***Eq. of RX***	***Eq. of Base***	***T °C***	***Time***	***Yield***
1	1-bromopropane	3	1.1	80	24 h	0%
2	1-bromopropane	10	1.1	80	24 h	0%
3	1-bromopropane	25	4	65	3 days	68%
4	1-bromopropane	25	4	40	3 days	28%

Ethyl, propyl and butyl side chains were chosen for the progression of size. Isopropyl was chosen for increasing the bulk around the carbene in an attempt to access a more stabilized, but still small carbene. The yields for alkylation with 1-bromoethane and 2-iodopropane are similar at around 40%. In all cases the TLC of the reaction mixture showed several spots which were not characterized. Comparison between the effect of counterion on both yield and stability was made using the 1-propyl substrate. Histidine derivative **141** was alkylated with 1-bromopropane as well as 1-iodopropane. As expected, the alkyl iodide is more reactive, and the reaction proceeds at 40 °C with high yields. Whilst formed in

higher yield, the iodide salt **152** is much more hygroscopic and less soluble in dichloromethane.

Alkenes are known to be good coordination sites for metals like palladium.[164] Thus besides exploring the tolerance of the reaction conditions and scope for stability of side chains, in this particular case the allyl groups can also provide secondary coordination sites in metal complexes that can further impact reactivity. Of note is that palladium allyl NHC complexes can undergo reductive elimination leading to decomposition of the NHC.[165] Alkylation with allyl bromide was also tolerated, giving almost quantitative yield at 40 °C. Allyl imidazolium compounds can also decompose by allyl elimination pathways, though stability could in theory be an issue, no decomposition was observed when storing **153** as a solid in a desiccator for over one month.

In some cases, increasing the reaction temperature improved starting material conversion (isopropyl **154**), whereas reducing the reaction temperature for the ethyl substrate (**150**) yielded a cleaner reaction mixture (Scheme 27). Unfortunately using these conditions and increasing the temperature up to 80 °C did not result in the synthesis of the cyclopropyl and *tert*-butyl substituted imidazoliums **156** and **157**. The only reported cyclopropane on an imidazole nitrogen is reported with 3% yield.[166] In general all of the NHC derivatives prepared are hygroscopic but bench stable, not requiring storage under argon and retaining the same appearance over three months and purity which was confirmed by their NMR spectra. The iodine salts tend to decompose quicker by becoming dark brown sticky solids, showing several baseline impurities in the ^{1}H NMR spectra as soon as their appearance starts to change.

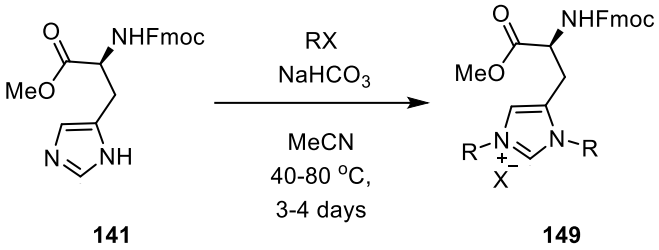

141 **149**

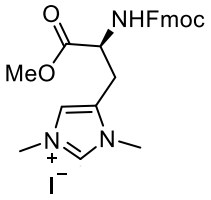

142

40 °C - **68%**[a]
80 °C - **64%**[a]

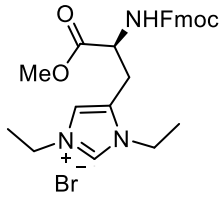

150

40 °C - **40%**

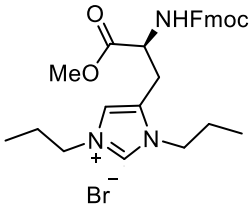

151

40 °C - **28%**
65 °C - **68%**

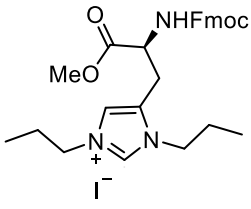

152

40 °C - **<99%**

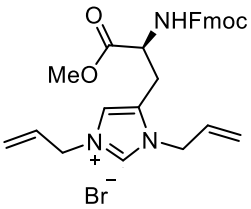

153

40 °C - **<99%**

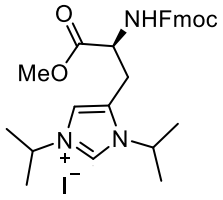

154

40 °C - **0%**
65 °C - **42%**

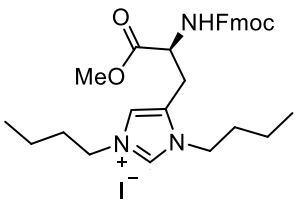

155

40 °C - **29%**
65 °C - **<99%**

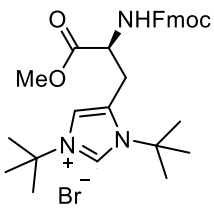

156

40 °C - **0%**
65 °C - **0%**
80 °C - **0%**

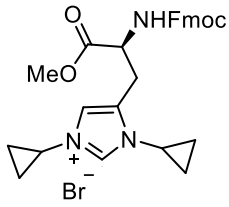

157

65 °C - **0%**
80 °C - **0%**

Scheme 27: *Side chain scope for aliphatic symmetric alkylation. Yields of reactions performed at different temperature for the methyl substrate* ***142****.* [a] *Compounds made by methods previously described in Scheme 24.*

The more widely used NHCs such as IPr and IMes have two aryl groups directly bound to the nitrogen atoms of the imidazole ring. These are synthesized

from acyclic precursors by condensation reactions.[146, 167] Double C-N arylation of imidazoles has not been described and therefore there is no precedent for double C-N arylation of histidine residues. In order to synthesize this type of bi-arylated NHC, one needs to start from acyclic precursors versus the readily available histidine amino acid. For this reason, this type of scaffold has not been exploited.

2.2.5.2 - Unsymmetrical alkylation

The incorporation of two different groups on the imidazole nitrogen can allow for fine tuning of the carbenes properties, by combining groups with different electronic and steric bulk. Unsymmetric aliphatic systems have been reported in the literature.[122, 123] Due to the two tautomeric forms of the histidine imidazole, sequential alkylation strategies yielded regioisomers as well as loss of enantiopurity via racemization of the α-carbon. Thus, in order to obtain regioselectivity and retain chiral information a new route was developed by Hodges and Chivikas.[168] This involved the formation of a cyclic urea which locks one of the tautomeric forms in a six membered ring with the amine of the amino acid backbone.[123, 168, 169] After functionalization of the free nitrogen, the cyclic urea can be opened using an alcohol in basic conditions to release the protected amino acid, which is ready to be alkylated once more to provide the imidazolium salt (Scheme 28*).* Despite success, this route starts from the less accessible free amine amino acids, the ring opening/protection step can be low yielding and it is less atom economical. This methodology also gives access to the Boc amino acids and to the best of our knowledge the ring opening, and protection step has not been described for the formation of the Fmoc derivatives.

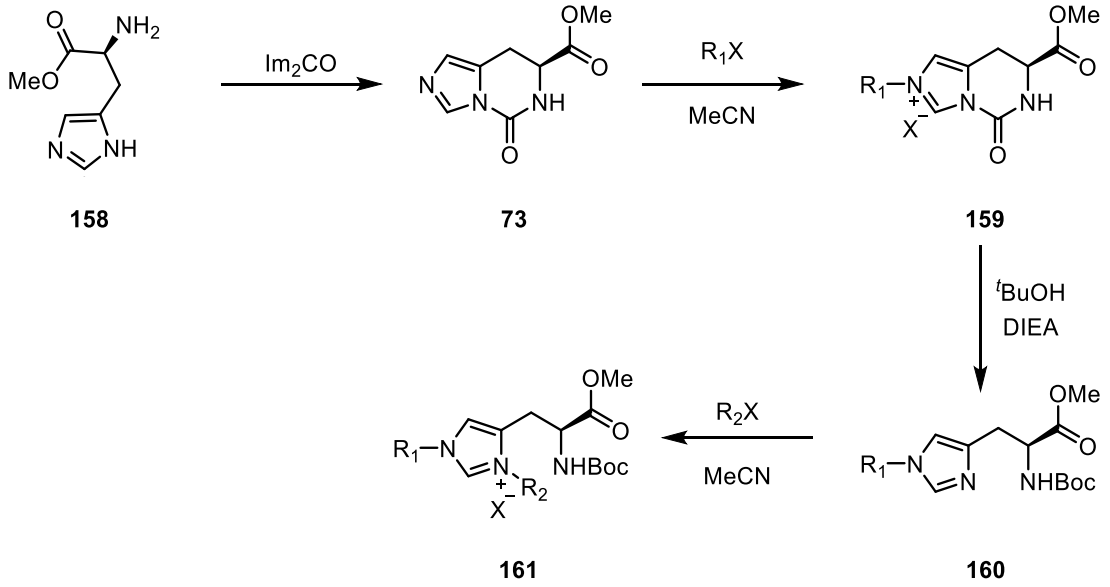

Scheme 28: *Synthesis of asymmetric aliphatic NHC* ***161*** *starting from methyl-histidine* ***158*** *via cyclic urea to prevent racemization*.[168]

As previously mentioned, a hybrid asymmetric NHC containing a stabilizing aromatic group and a small aliphatic side chain would be a versatile building block. Drost *et al.,* reported a similar substrate but for a Boc protected amino acid in 2015.[128] Their approach involved a Chan-Lam-Evans arylation followed by an alkylation yielding the desired imidazolium salt.

A similar approach to the one reported by Drost *et al.* was followed but starting from the Fmoc containing scaffold **141**. For the aryl side chains 4-methoxyphenyl boronic acid was chosen due to being widely available and being an affordable boronic acid. Despite being bulky and potentially causing problems in the arylation reaction, the mesityl group would introduce bulk and lock the aryl position perpendicular to the plane of the imidazole, diminishing the freedom of rotation. The Chan-Lam-Evans conditions used in this case differ from the original paper by being performed at room temperature and extending the reaction time. Following this new procedure compound **162** was synthesized with a reasonably

high yield of 68%.[170] In the case of the mesityl group the reaction is considerably slower, and after one week full consumption of starting material was still not achieved, yielding product **163** in a moderate 31% yield (Scheme 29). Heating the reaction to 60 °C in an attempt to increase conversion lead to an intractable reaction mixture. The resulting N-aryl histidine derivatives were then alkylated using methyl iodide and allyl bromide which were selected due to their high reactivity and suitable properties. Methyl is the smallest possible group to incorporate and allyl can potentially provide a second coordination site for metal complexes, such as palladium and impacting on the reactivity and selectivity of the subsequent catalysis reactions.

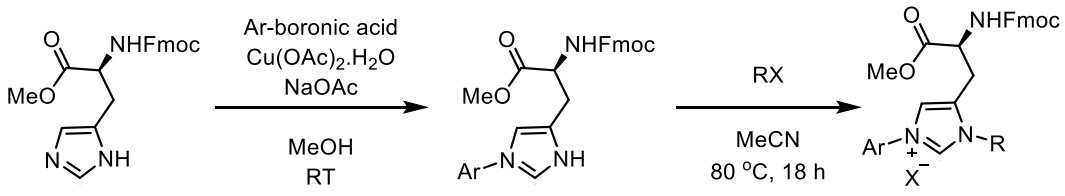

141

162 Ar = *p*-OMeOPh **68%**

163 Ar = Mesityl **31%**

164 R = Me; Ar = *p*-OMeOPh **80%**

165 R = allyl; Ar = *p*-OMeOPh **82%**

166 R = Me; Ar = Mesityl **80%**

Scheme 29: *Synthesis of unsymmetrical NHC via Chan-Lam-Evans coupling and subsequent alkylation.*

Alkylation reactions were performed at 80 °C in all cases giving the desired products (**164, 165** and **166**) in high yields after column chromatography. Three novel unsymmetrical NHC containing amino acids were successfully prepared and their reactivity will be further explored in the following chapter.

2.2.5 - Protecting group manipulation

In order to explore the versatility of the synthesized building blocks for peptide synthesis their protecting groups need to be removed in a selective

manner ahead of amide coupling. Cleaving protecting groups in amino acids containing an imidazolium functionality has not been widely exploited. Therefore, the reported hydrolysis of Boc and benzyl carbamates as well as removal of methyl esters in imidazolium containing amino acids will be discussed.

In the three reports of cleavage of Boc carbamate imidazolium bearing amino acids, HCl in dioxane at room temperature was used, and the amine HCl salts were accessed in very high yields.[125, 128, 132] Guillen *et al.* also utilize HCl, but in aqueous and access the corresponding salt in quantitative yield.[121] When using this procedure a counter ion exchange occurs and the isolated products are the chloride imidazolium salts (Scheme 30).

Proline derived imidazolium containing amino acids were reported by the Gilbertson group where a benzyl carbamate was removed by hydrogenation utilizing palladium on carbon as a catalyst and methanol as a solvent however, the major product was the methyl alkylated amine. Adjusting the conditions to palladium hydroxide on carbon in ethanol gave the desirable free amine in 86% yield.[134]

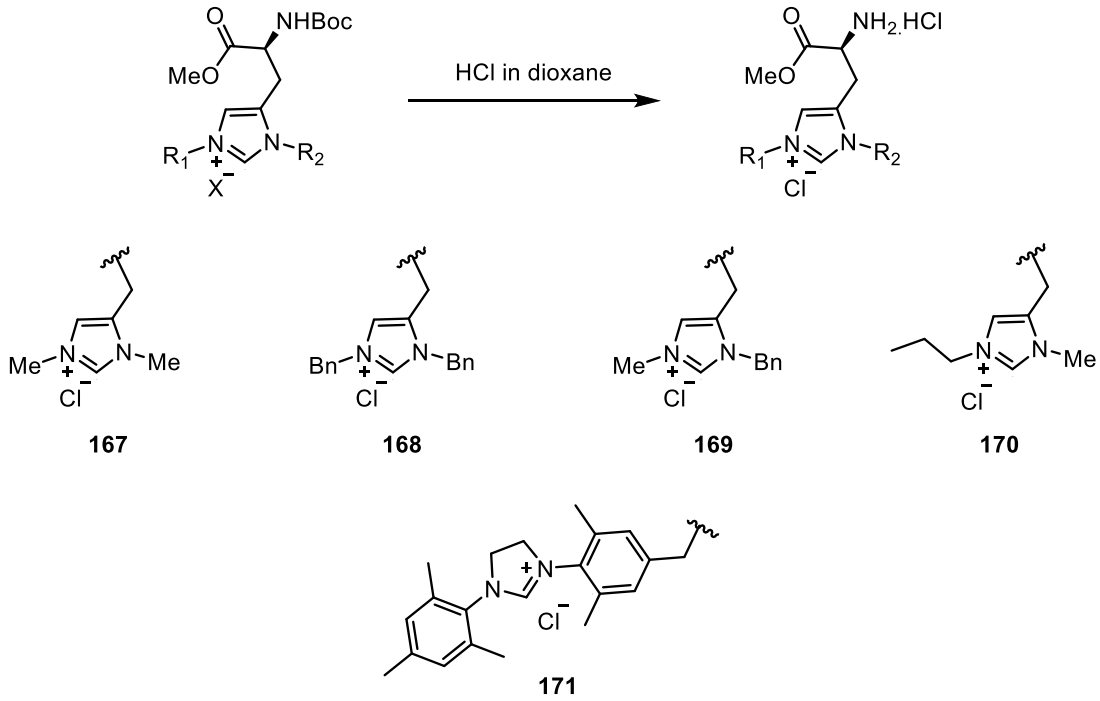

Scheme 30: *Removal of Boc carbamate in imidazolium containing amino acids. Selected side chain examples of reported scaffolds.*

Cleavage of methyl esters in the presence of Boc carbamates has been achieved taking advantage of the high tolerance to basic conditions of Boc groups. The Boc amino methyl esters containing NHC side chains were deprotected using large amounts of lithium hydroxide. Excess of 10 equivalents of lithium hydroxide in methanol were used by Drost *et al.* to provide the lithium carboxylate salt.[128] The Gilbertson group utilized excess lithium hydroxide in water/methanol or water/THF mixtures at 0 °C to access the free carboxylic acids (Scheme 31, A).[132, 134]

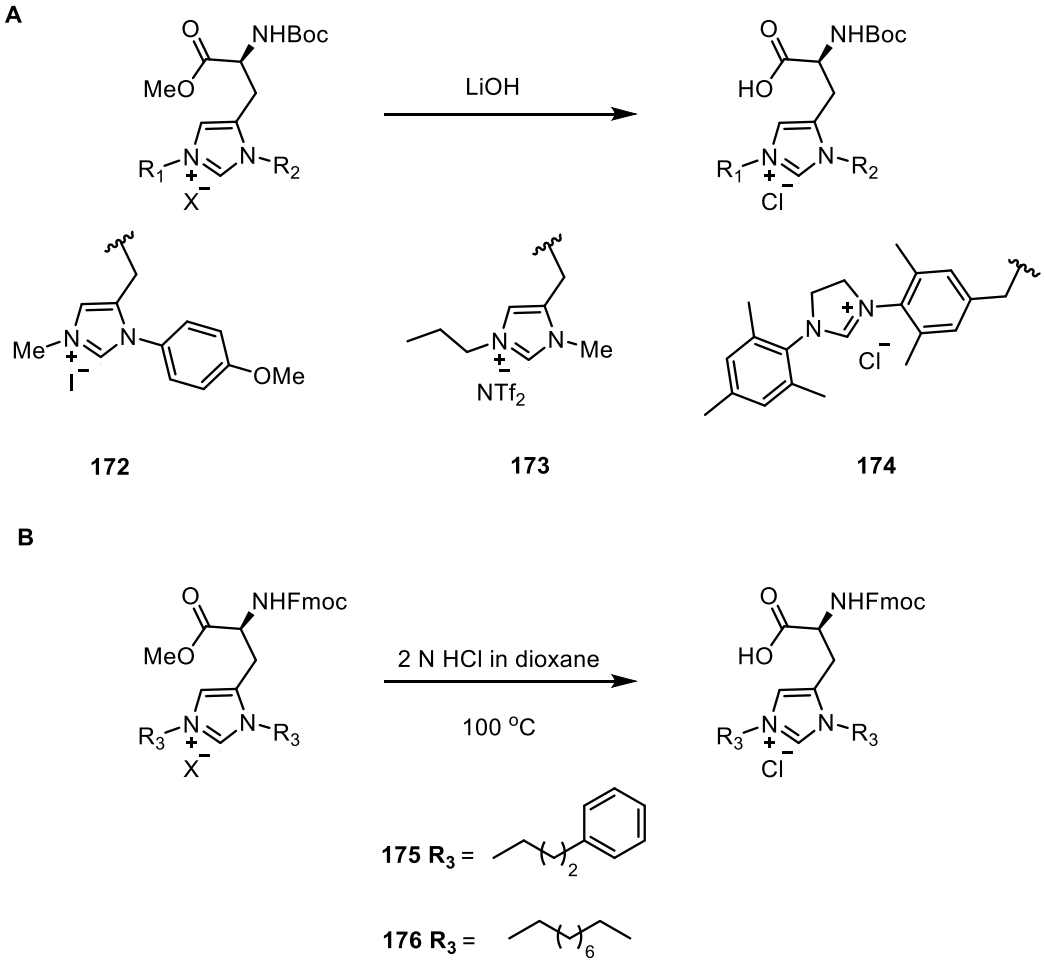

Scheme 31: *Removal of Boc carbamate in imidazolium containing amino acids. Selected side chain examples of reported scaffolds. A) Removal of methyl ester in the presence of Boc carbamate; B) removal of methyl ester in the presence of Fmoc carbamate.*

To the best of our knowledge the only example of the hydrolysis of a methyl ester in the presence of an Fmoc carbamate imidazolium containing amino acid moiety was reported by Shin and Bang in 2013. The amino acids were heated at 100 °C in 2 N HCl in dioxane for three hours, providing the corresponding carboxylic acids in 43-67% yield (Scheme 31**,** B). Despite the harsh conditions the hypothesis of racemization was not commented on.[130] Herein, protecting group manipulation of the new developed scaffolds will be discussed.

2.2.5.1 - Hydrolysis of Methyl Ester

In order to start this study, Boc derivative **177** was synthesized according to a literature procedure.[128] Since methyl esters are known to be base labile whilst *tert*-butyl carbamates are base stable and therefore acidic conditions are used in their removal. Reproducing the literature method using 10 equivalents of LiOH in methanol in the presence of water, selective cleavage of the ester in the presence of the *tert*-butyl carbamate was achieved yielding carboxylic acid **178** (Scheme 32).[128]

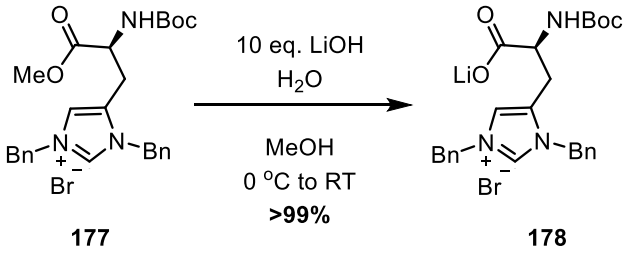

Scheme 32: *Methyl ester deprotection in the presence of LiOH in methanol resulting in the desired free carboxylic acid.*

The Fmoc group is also base labile, however selective cleavage has been previously reported in NHC containing scaffolds.[132] Using the conditions employed with Boc derivative **177** (10 eq. of LiOH) with the Fmoc equivalent **146** lead to double deprotection yielding the free carboxylic acid and free amine. Fmoc carbamates can be labile in solution at pH 12 or higher and can be removed by amine bases such as piperidine.[171] The large excess of LiOH in the reaction mixture lead to an increase in pH and the Fmoc group was cleaved, yielding compound **179**. Even though this was not the desired product it is noteworthy that with just one step, one may access the completely deprotected amino acid bearing an imidazolium side chain (Scheme 33).

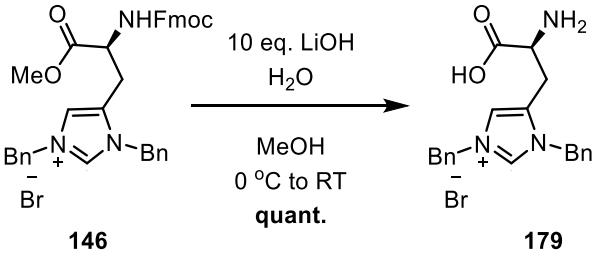

Scheme 33: *Synthesis of free amine from attempts to selectively remove methyl ester in the presence of Fmoc.*

In order to establish a methodology that would allow for selective cleavage one equivalent of LiOH was added to a solution of the amino acid in THF. The formation of a new compound was observed by TLC, however full conversion was not achieved. Full selective deprotection was achieved, as shown by ^{1}H NMR spectra, when a second equivalent of solid LiOH was added, yielding imidazolium salt **180** in 70% yield (Scheme 35). Optimization of the purification methods allowed for the preparation of the benzyl substituted imidazolium salt **180** from the commercially available Fmoc-*L*-His-OMe substrate in 3 steps with an overall yield of 43% on a 7 g scale without requiring column chromatography in any of the steps (Scheme 34). Change in the purification method lead to a decrease in yield for the synthesis of imidazolium **146** from the 94% obtained by flash chromatography (Scheme 25) to 70% obtained via precipitation from hot ethyl acetate. Scale up of the deprotection reaction lead to higher material recovery from trituration with hexane, increasing the yield of substrate **180** from 70% (2.0 mmol, Scheme 35) to 93% (Scheme 34). This free carboxylic acid, Fmoc protected imidazolium amino acid (**180**) will be tested under standard Fmoc SPPS conditions.

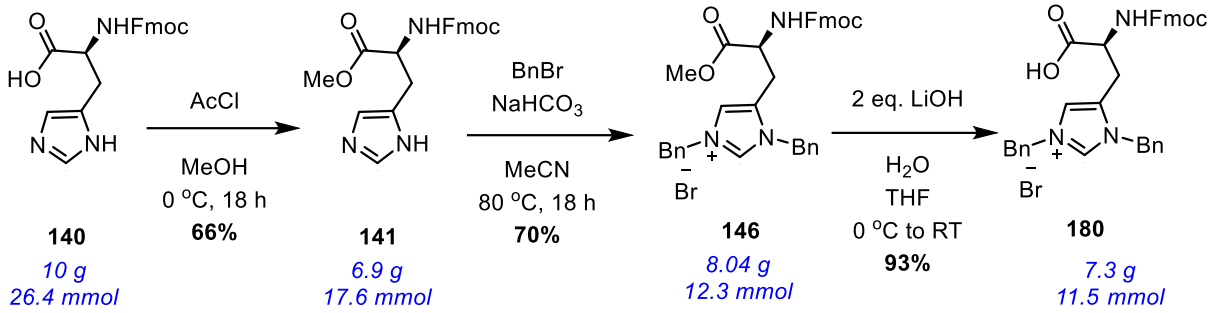

Scheme 34: *Scale up synthesis of derivative* ***180,*** *no column chromatography was required for purification.*

The same procedure was applied to the different imidazolium derivatives (Scheme 35). The methyl derivative **142** resulted in an intractable reaction mixture from which no product was isolated, albeit full starting material consumption was observed. The high polarity and low stabilizing effect of the methyl groups on the imidazolium may have contributed to this reaction outcome. For the smaller chain amino acid imidazolium salts, extracting the aqueous layer with a chloroform: isopropanol mixture (3:1) allowed an improved mass recovery. This method allowed for the deprotection of the methyl ester in all substrates prepared except the methyl scaffold **181**. A library of amino acids containing different imidazolium side chains in which the carboxylic acid is free, and the amine protected with an Fmoc carbamate was prepared in good yields (39%-70%; **182** – **190**) Elemental analysis data for derivatives **180** and **186** shows that the final product is the halide salt derived from the starting material. This data was used to deduced that no counter ion exchanged occur and thus, all the imidazolium salt products were the halide salts. The potential of some of these scaffolds was further exploited in both batch and SPPS methodologies (see section 2.2.7 and Chapter 4).

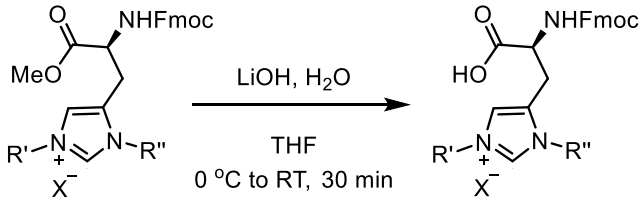

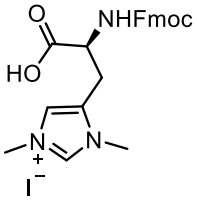

181 - 0%

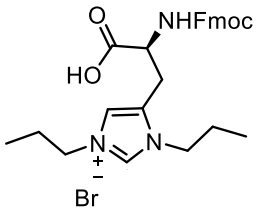

182 - 56%

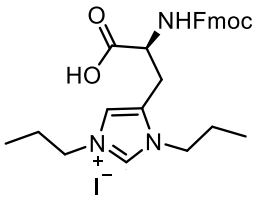

183 - 67%

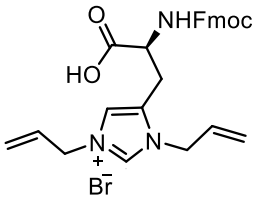

184 - 39%

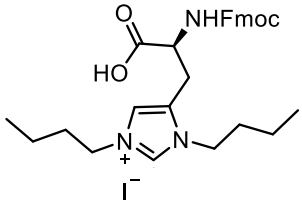

185 - 52%

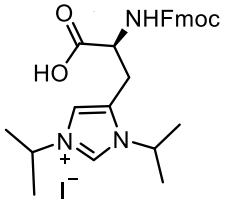

186 - 44%

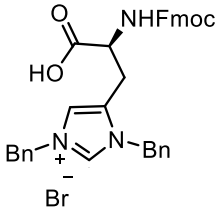

180 -70%

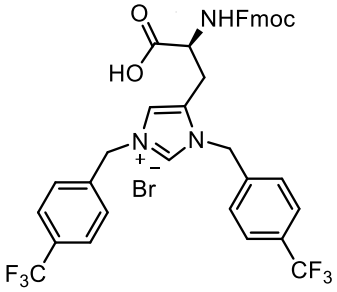

187 - 52%

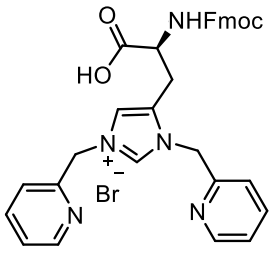

188 - 61%

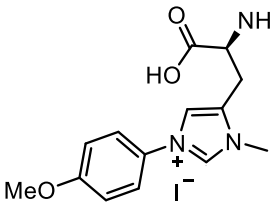

189 - 68%

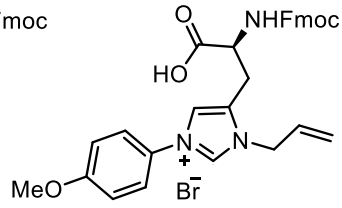

190 - 60%

Scheme 35: *Scope for methyl ester removal.*

2.2.5.2 - Fmoc Carbamate Removal

Shin and Bang have reported that the Fmoc group on an imidazolium salt bearing amino acid was removed with 20% piperidine in DMF at room

temperature.[130] Thus, showcasing that the standard SPPS procedure for Fmoc removal can be applied to this type of scaffold without causing degradation.

The most common method utilized to cleave of Fmoc groups in SPPS consists of 20% piperidine in DMF. DMF was replaced by DCM for ease of handling in these studies. This swap is common for small hydrophobic peptides.[172] DMF's high boiling point combined with its partial solubility in both organic solvents and water would result in difficult purification strategies for this batch process. The benzyl substituted imidazolium **146** were subjected to these conditions and the corresponding free amine was isolated with quantitative yield (Scheme 36). This demonstrates that this scaffold can tolerate the Fmoc removal conditions and thus is more likely to be compatible with SPPS and be successfully incorporated in the middle of peptide sequences.

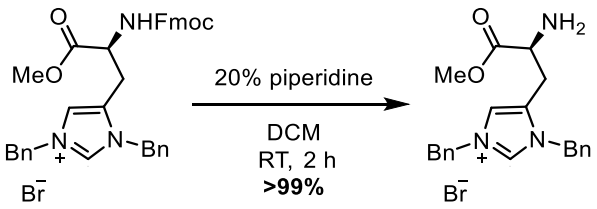

146 **191**

Scheme 36: *Removal of Fmoc carbamate on imidazolium* ***146****.*

2.2.6 - Solution Peptide Synthesis.

With free amines and carboxylic acids in hand their behaviour under amide coupling conditions was then studied. Initially batch solution synthesis was considered. Their use in SPPS will be considered in later work (see Chapter 4).

The NHC amino acids **178** and **191** were coupled to benzyl glycine or Fmoc-L-alanine protected amino acids, using HATU as a coupling agent, DIEA as an activator base and THF as solvent. Once again DMF was replaced by a

more volatile solvent (THF) to facilitate handling and product isolation.[172] For each of the attempted amino acids the coupling was successful and the correspondent dipeptides isolated with moderate yields (Scheme 37). The crude reaction mixtures were a combination of starting materials and various coupling side reactions which were difficult to separate using normal phase column chromatography.

The NHC functionality was not compromised during the coupling, however in all cases a counterion exchange occurred, where the PF_6^- counterion from HATU was isolated as the anionic part of the molecule, determined by both ^{19}F and ^{31}P NMR spectroscopy. Imidazolium salts containing a PF_6^- counterion have been widely used and reported for the formation of Bis(NHC) silver complexes.[173, 174] However, this can be overcome by employing a direct carbene insertion method which allows access to the mono NHC complexes.[159, 175, 176] This work has shown that we can successfully couple this non-natural amino acids both in C and N termini of a peptide.

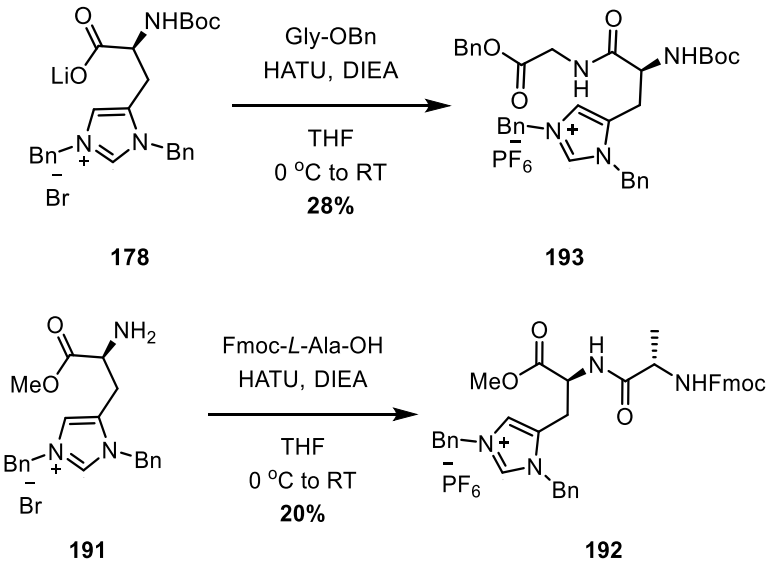

Scheme 37: *Solution synthesis of dipeptides using NHC amino acids.*

Applications of these non-natural amino acids in SPPS, in transition metal complex synthesis and their catalytic activity will be explored further in this thesis (see chapters 3 and 4).

2.2.7 - Thiazolium Amino Acid Synthesis

NHCs are a valuable tool to catalyse Umpolung chemistry. Umpolung chemistry transforms a functional group by reversing its polarity allowing the expansion of the toolbox of heteroatom substitution patterns. In nature this type of reactivity is exploited to generate carbonyl anions from the corresponding α-keto acids utilizing the cofactor of vitamin B1: thiamine pyrophosphate. Thiamine contains a thiazole ring in which the nitrogen is quaternized by attachment to a methylpyrimidine ring forming a thiazolium salt. Thiazolium salts have been widely employed as catalysts in Umpolung type reactions.[95] Metal complexes of thiazolium salts have also been reported, however these are not as widely explored as their imidazolium counterparts.

Amino acids containing a thiazole ring are commercially available and have been employed in peptide synthesis. Alkylation reactions have yielded the thiazolium salts and these have been used as catalysts in the Stetter reaction, whilst their corresponding metal complexes cytotoxic activity against cancer lines has been tested.[177-179] However, for the most part the Boc derivative of the thiazolium salts has been used and applied only to small peptide sequences which were synthesized in solution and not with SPPS procedures. To the best of our knowledge an Fmoc carbamate containing amino acid with a thiazolium side chain has not been explored. Due to their great performance in

organocatalysis as well as the potential to explore transition metal catalysis, a thiazolium containing amino acid **195** was synthesized.

Commercially available Fmoc-L-thiazolylalanine-OH was stirred at 90 °C in methyl iodide and acetonitrile in a high-pressure tube to yield salt **195** with 96% yield (Scheme 38).

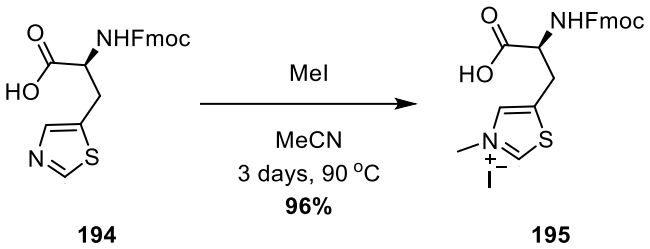

Scheme 38: *Synthesis of thiazolium **195** by methyl iodide alkylation for 3 days in a sealed tube.*

The alkylation reaction provided the free carboxylic amino acid directly, for inclusion in peptide synthesis. Activity of this amino acid, metal coordination and its inclusion in peptide scaffolds will be exploited further in this thesis (*see* Chapter 3 and 4).

2.3 - Conclusions

Herein, the synthesis of imidazolium salts containing amino acids has been explored, their tolerance to protecting group manipulation conditions and their application in solution phase peptide synthesis has also been studied.

When Fmoc-L-His-OBn derivative **132** was subjected to methylation reactions different reaction mixtures dependent on the amount of base and alkylating agent used were obtained. Higher equivalents of sodium bicarbonate and methyl iodide lead to a very complex crude reaction mixture, requiring

preparative HPLC to obtain the pure product. Due to the solvent system used for purification the isolated imidazolium salt **134** had trifluoroacetate as a counter ion. This counter ion identity was confirmed by both NMR and XRD data. Diminishing the equivalents of alkylating agent and base, while increasing the temperature of the reaction has allowed for the isolation of imidazolium salt **133** by normal phase silica gel chromatography with the iodide counter ion.

Attempts to coordinate gold, silver, palladium and copper to the trifluoroacetate salt **134** failed, yet the iodine salt **133** was able to be converted to the corresponding gold(I) complex with 40% yield.

Changing the protecting group combination from Fmoc/Bn to Fmoc/Me lead to that independently of the synthesis conditions the iodide imidazolium salt was obtained. This protecting group combination provided cleaner reactions mixtures and more predicable reactivities than its benzyl counterparts. Due to the goals of the project requiring an Fmoc containing amino acid, the Fmoc/Me combination was the one carried forward.

A novel library of different side chain NHC amino acids can be prepared by double alkylation of histidine. Methyl, propyl and butyl side chains, as well as isopropyl, allyl, benzyl and methylpyridine groups can be installed. Alkylation with cyclopropyl and tert-butyl bromide were not successful. Chan-Lam-Evans C-N arylation followed by alkylation gave access to unsymmetrical substrates. This demonstrates the versatility of Fmoc-*L*-His-OMe **141** as a substrate to install tuneable imidazolium functionality on to an amino acid backbone. This work is the largest reported library of different Fmoc- amino acids bearing imidazolium functionality.

Protecting group manipulation allowed for the deprotection of the whole library of methyl esters except for the methyl NHC derivative, which under the reaction conditions decomposed. This work has resulted in the synthesis of eleven novel building blocks ready for application in Fmoc peptide synthesis methodologies. The benzyl derivative can be prepared in a three-step synthesis with a 43% overall yield on a 7 g scale. This demonstrates the scalability of our synthetic route for accessing amino acids bearing imidazolium functionalities which can be used as SPPS building blocks.

In order to incorporate these amino acids into the middle of a peptide sequence, the Fmoc carbamate needs to be removed. Standard Fmoc deprotection conditions (20% piperidine in DCM) gave access to the free amine precursor **191**. Thus, showing that these standard conditions can be applied and tolerated by these types of scaffolds.

The benzyl derivative **191** was then employed in solution phase peptide synthesis to test the tolerance of these scaffolds to the standard conditions. This resulted in a complex crude reaction mixture, however the successfully coupled bispeptides were isolated with yields of circa 20%. Large scale preparation and the tolerability of this scaffold to coupling and deprotection conditions showcase that these compounds can be versatile building blocks in peptide synthesis.

Chapter 3:

3.Transition Metal Complexes of Amino Acid Derived Ligands

3.1 - Introduction

Catalysts reactivity and selectivity can be tuned by using various metals and ligands with different electronic and steric properties. Thus, to maximize the chemical space that can be accessed with metallopeptides, a variety of ligands and metal complexes are required.

NHC ligands have different electronics than phosphorous based ligands and consequently display different reactivities.[180, 181] NHCs are more electron rich and thus more readily donate electrons, however, they are poorer acceptors of backbonding than phosphines.[181] The introduction of oxygen atoms bound to the phosphorous atom affects the π-accepting properties, altering the electronics of the metal centre.[74]

Amino acids bearing phosphorous ligands have been described and reviewed in chapter 1 (*see* section 1.4.1). However, their synthesis is lengthy and has been poorly explored for Fmoc based derivatives. In this chapter new routes to access phosphorous based ligands and metal complexes on amino acid backbones will be discussed.

The coordination chemistry of the imidazolium amino acid derivatives will be explored with the synthesis of novel gold and palladium complexes. Whilst the use of gold catalysis in organic synthesis has increased largely over the last decade, the linear coordination environment of Au(I) remains a challenge for the

design and synthesis of successful asymmetric catalysts.[182, 183] Therefore, gold is a good example to study the effect of using structured metallopeptides versus the conventional small molecule catalysts in enantioselective catalysis. Palladium is ubiquitous in transition metal catalysis and thus a study of the effect of large peptide assemblies in palladium catalysis would be of value.

Phosphorous metal complexes are commonly accessed by reacting the ligand with halide metal salt.[184, 185] NHC metal complexes can be accessed by synthesis of the free carbene, followed by metal coordination, silver transmetallation or direct carbene insertion of gold or copper metals.[149, 186, 187] Silver transmetallation can lead to the formation of bisNHCAg type complexes.[152, 188] Generally with halides as coordinating anions mono-NHC silver(I) complexes are formed, whilst non coordinating anions such as PF_6^-, BF_4^- and OTf^- yield bisNHC silver(I) complexes.[149, 189] The mono NHC silver complexes are reported as having higher activity in transmetallation reactions than the corresponding bisNHC silver complexes and are thus preferred for their versatility.[152]

The transition metal complex amino acids synthesized are intended to be included in peptide scaffolds and their catalytic activity assessed. Determining if the activity and selectivity is due to the peptide scaffold or the amino acid is important. Therefore, the catalytic activity of the amino acids will initially be explored.

3.1.1- Considerations on gold catalysis and gold catalyst design

Gold(I) metal complexes have demonstrated immense versatility by catalysing diverse transformations of alkenes, alkynes and allenes.[182] In recent years gold has been used in the synthesis of complex heterocycles from simpler

starting materials in one step.[190-192] Due to its increasing importance as a tool in organic chemistry, gold catalysis has been extensively reviewed.[182, 193-195]

The linear two-coordinate geometry of gold(I) has made accessing asymmetric transformations challenging.[182] However, in order to take full advantage of gold(I) reactivity asymmetric transformations are required. In the past decade large amounts of research has been carried out to design and synthesize gold(I) catalysts capable of forming chiral products from achiral precursors.[195] Previously described chiral phosphine and phosphite ligands, such as SEGPHOS, BINAP and Josiphos have been employed with success in some gold catalysed reactions, such as enyne cycloisomerization (Figure 39).[196-198] However, several researchers have reported the design and synthesis of bespoke chiral ligands for gold catalysis.[182]

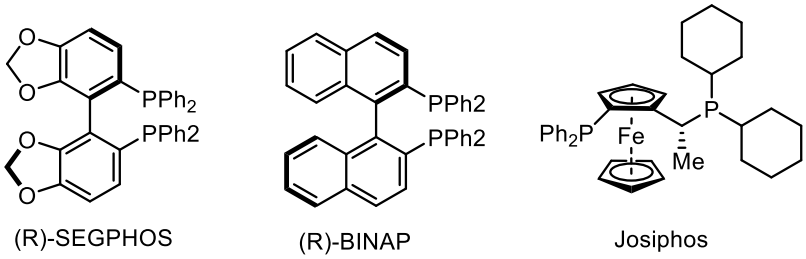

Figure 39: *Chiral ligands used in asymmetric catalysis.*

The design and synthesis of novel chiral ligands for gold catalysis has been extensively reviewed.[182, 195, 199] The successful use of supramolecular type chiral catalysts is a promising precedent for the successful use of synthetic peptides as ligands for gold catalysis. A supramolecular gold catalyst was synthesized by Sollogoub *et al.* in which a cyclodextrin was capped with an NHC gold complex (Figure 40, A).[200] This supramolecular catalyst was capable of catalysing alkoxycyclization reactions with high enantioselectivity (up to 94% *ee*).

Voituriez and Marinetti have reported the use of phosphahelicenes as chiral ligands for gold capable of catalysing enantioselective [4+2] cycloaddition of hept-6-en-1ynylbenzene derivatives with high enantioselectivity (up to 91% *ee*) (Figure 40, B).[201] Helicenes use nature's helices as inspiration for synthetic rigid three-dimensional structures. The success with helicenes demonstrates the potential in the use of helical peptides for catalysis.

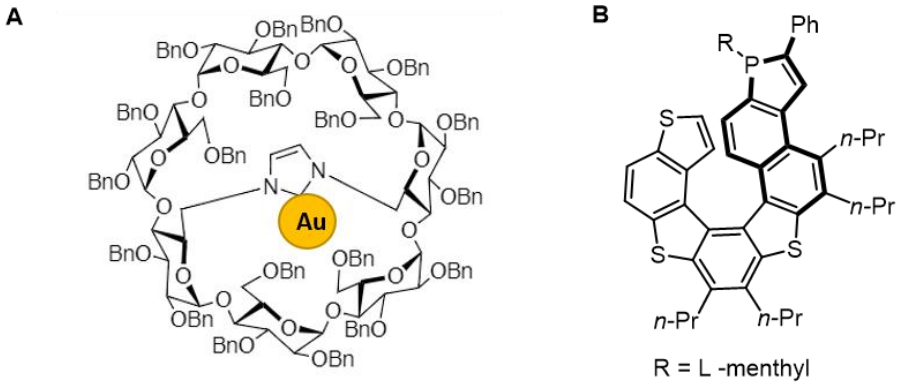

Figure 40: A) *Cyclodextrin based catalyst, with an NHC ligand;* ***B)*** *Helicene ligand for gold catalysts.*[200, 201]

The overall strategy of such efforts is to create a bulky chiral environment which blocks one of the faces of the gold(I) complex to force a preferential formation of one of the diasteriotopic transition states. Proteins and structural peptides are widely known to be able to create an active site in which the structure is used to favour the formation of one enantiomer, and thus the use of artificial metalloenzymes may benefit gold catalysis.

3.2 - Results and Discussion

3.2.1- Synthesis of NHC Gold Complexes

The coordination chemistry of the prepared imidazolium salt library was explored by studying their ability to coordinate to gold. Two of the main routes to access NHCAu complexes are silver transmetallation and direct carbene insertion of gold. Of note is that Albrech and co-workers reported racemization during a silver transmetallation reaction to form an iridium complex.[123] This was thought to be due to the basicity of silver oxide. Selected examples of the imidazolium library were subjected to direct carbene insertion to form gold complexes. This method was preferred to the silver transmetallation due to it not requiring dry conditions, as well as the solvent acetone being a safer and more sustainable choice than dichloromethane.

The reaction conditions used were the same as those reported by Collado *et al.,* requiring 1.1 equivalents of potassium carbonate as a base and 1 equivalent of DMSAuCl as a metal source in acetone at 40 °C (Scheme 39).[159]

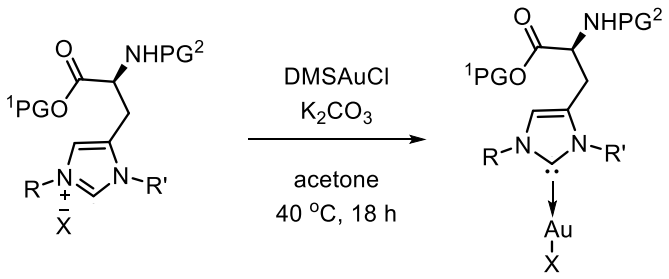

196 **197**

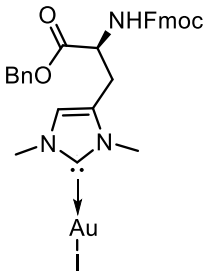

136 - 42%

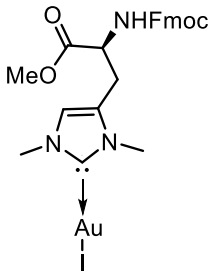

144 - 50%

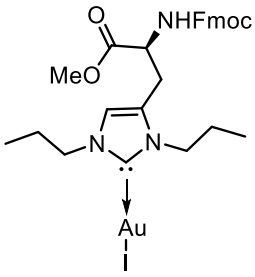

198 - 13%

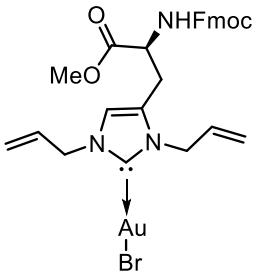

199 - 42%

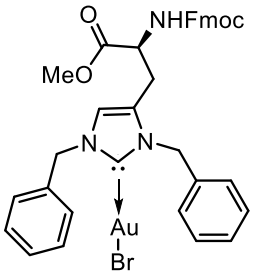

200 - 65%

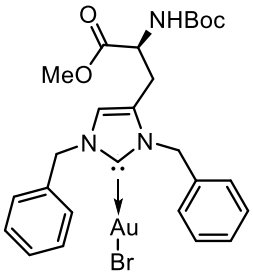

201 - 56%

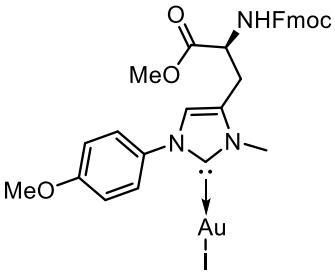

202 - 61%

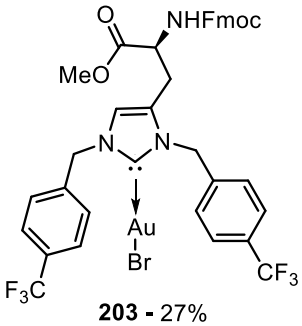

203 - 27%

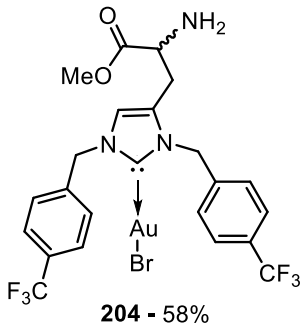

204 - 58%

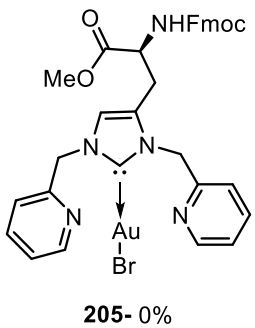

205- 0%

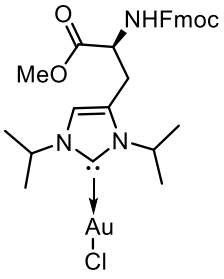

206 - 0%

Scheme 39: *Substrate scope for gold coordination to imidazolium bearing amino acids. In the case of compound **205** and **206** only starting material was recovered.*

The successful preparation of these gold complexes was readily determined using ^{1}H NMR spectroscopy through the absence of the

characteristic NCHN proton and a shift of the NCHCN proton. The appearance of a new resonance between 175 and 182 ppm, which in the ^{13}C NMR spectra corresponded to the carbene carbon. Of note is that in these conditions the iodide imidazolium salts yielded the gold-iodide complexes whilst the bromide imidazolium salts provided the gold-bromide complexes. This observation is supported by the obtained crystal structures, elemental analysis data and the chemical shift of the carbon bonded to the gold atom in the ^{13}C NMR spectra (Table 2).[202] Previous reports demonstrate that carbene carbon resonances shift according to the Lewis acidity of the metal.[203] In the case of gold(I) complexes the ligand of the NHCAu leads to different chemical shifts. In the case of the halides the higher the electronegativity, the more Lewis acidic is the gold and Therefore the resonances of the carbene carbon shift upfield. Thus, complexes of the type NHCAuCl have resonances between 165-175 ppm, whilst NHCAuBr type complexes have resonances between 167-180 ppm.[203] There are fewer reports of NHCAuI type complexes, however due to decrease of electronegativity of iodide versus bromide one would the carbene carbon resonances are expected to be between 178-190 ppm.[159, 204]

Table 2: *^{13}C NMR chemical shifts for the carbon atom bonded to the gold atom for each of the prepared gold complexes where R' and R'' represent the substituents of the nitrogen atoms of the ring..*

Compound no.	***R'***	***R''***	***NHCAuX***	***^{13}C NMR C-Au ppm***
136	Me	Me	I	182.6
144	Me	Me	I	179.7
198	propyl	propyl	I	181.8
199	allyl	allyl	Br	175.8
200	Bn	Bn	Br	176.0
201	Bn	Bn	Br	175.8
202	Me	*p*-PhOMe	I	181.5
203	*p*-PhCF$_3$	*p*-PhCF$_3$	Br	176.8
204	*p*-PhCF$_3$	*p*-PhCF$_3$	Br	176.2

In chapter 2 two different gold complexes were prepared using the direct gold coordination method in good yield (**136** and **144**, Scheme 39). Propyl derivative **198** was accessed in the lowest yield at 13%. This low yield is due to a loss of material by decomposition during the purification, in which a large purple deposit was observed on top of the column. The *N,N'*-bisallyl complex **199** was synthesized in 42% yield and it was stable for at least a month when stored in the dark. Even though allyl imidazolium salts have been described, this is the first example of an *N,N'*-allyl bearing NHC gold complex.[205] The Boc and Fmoc *N,N'* -bisbenzyl derivatives **201** and **200** were successfully synthesized and crystalised (Figure 41). In both cases only the single S enantiomer was obtained in the unit cell, and the ligand-gold and gold-bromide distances are 1.97 Å and 2.39 Å in both complexes. These distances are similar to the ones reported for the widely used catalysts: IMes-AuCl (1.99 Å) and IPr-AuCl (1.94 Å).[175] The angles between

ligand-gold and bromide are also similar in both cases (178 °), which are in good agreement to the angles reported for ligand-gold-chloride in IPrAuCl at 177°.[175] The difference in the carbamate used (Fmoc vs Boc) led to a different lattice packing of the benzyl groups. In the case of the Boc derivative **201** the benzyl groups are in similar positions at the same angle from the nitrogen in the imidazole ring whilst in the case of the Fmoc derivative **200**¸ each of the benzyl groups is in a different face of the imidazole. No intramolecular π-π stacking interactions were seen between the Fmoc and the benzyl aromatic systems. The position of the benzyl groups in the Fmoc derivative **200** is consistent to the positions of the corresponding imidazolium salt **146** (crystal structure of **146** in chapter 2, Figure 38)

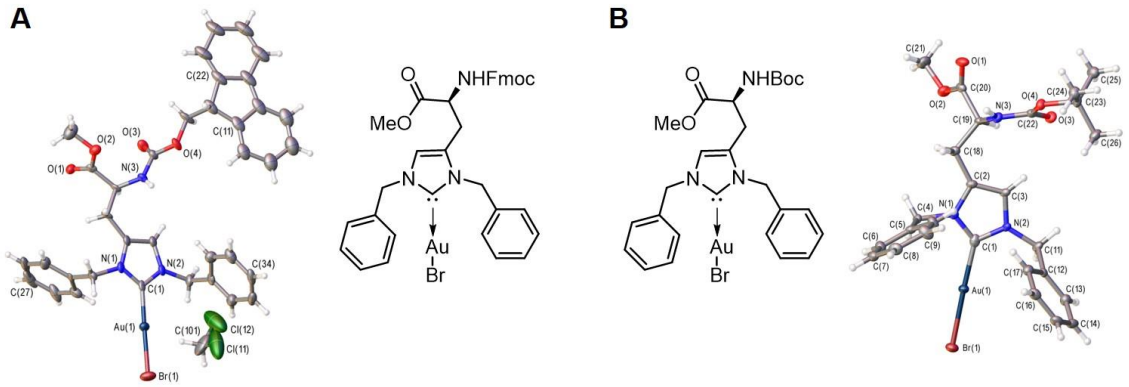

***Figure 41**: A) Crystal structure of **200** with ellipsoids drawn at the 50 % probability level. The structure contains a molecule of dichloromethane, which is present at 50% occupancy. All hydrogen atoms were fixed as riding models with the isotropic thermal parameters (U_{iso}) based on the U_{eq} of the parent atom. B) Crystal structure of **201** with ellipsoids drawn at the 50 % probability level. The position of the hydrogen atom bonded to N(3) was refined while all other hydrogen atoms were fixed as riding models. The isotropic thermal parameters (U_{iso}) of all hydrogen atoms were based on the U_{eq} of the parent atom. Carbon atoms are grey; hydrogen atoms are white; nitrogen atoms in blue; oxygen atoms in red and chlorine atoms in green. Crystal structure data solved by Dr. Louise Male.*

The gold complex of the scaffold **202** was also successfully synthesized in 61% yield. The *para*-CF_3 benzyl gold complex **203** was access in 27% yield. Decomposition of this scaffold was observed during the purification by flash chromatography on silica gel. When doing a repeat of the synthesis of *para*-CF_3 benzyl gold complex **203**, a calculation error lead to the use of 1.2 equivalents of potassium carbonate instead of 1.0 equivalents. This resulted in a loss of the Fmoc group and the free amine gold complex **204** was obtained in 58% yield. This reaction mixture also leads to loss of enantiopurity at the α-carbon as seen in the crystal structure of **204**, in which the space group is centrosymmetric such there is, by symmetry an exact 50:50 mixture of *R* and *S* chiral centres in the unit cell (Figure 42). There was not complete racemization as the optical rotation value is different from zero at +1.60 (c 0.2, $CHCl_3$). The dataset for this crystal structure was poor with smeared reflections and major disorder around the α-carbon however, it is possible to see that the benzyl groups have adopted a conformation more similar to the Fmoc derivative **200** than to the Boc derivative **201** (Figure 42).

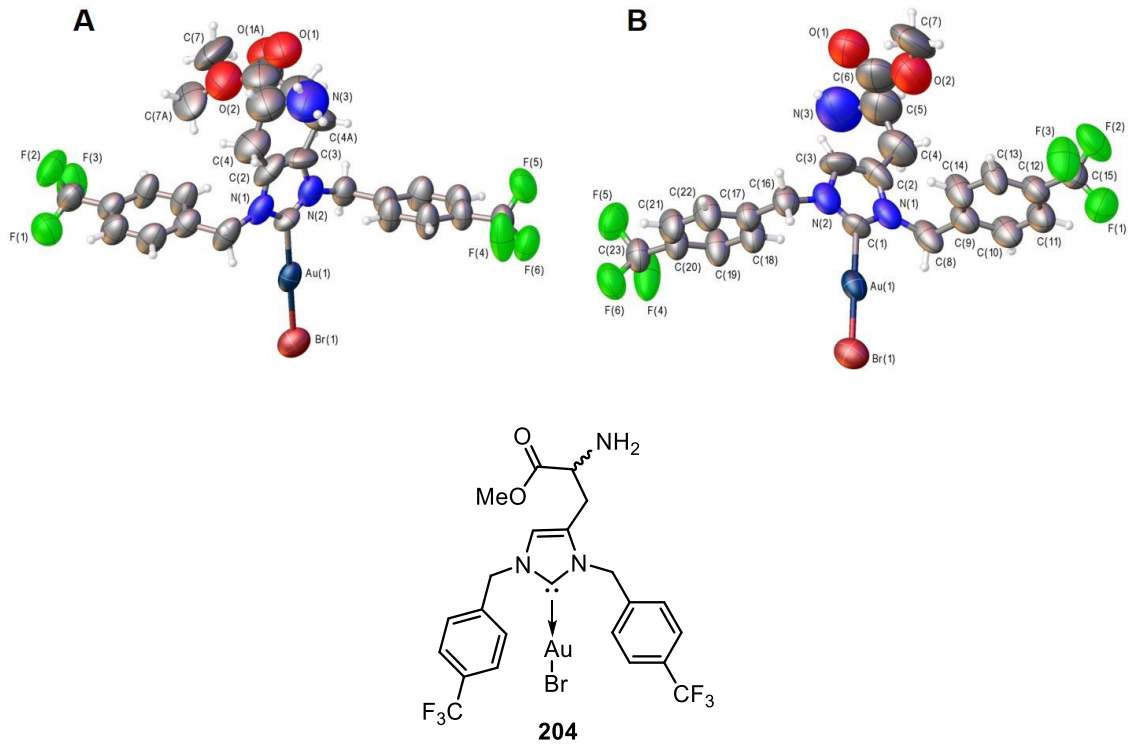

Figure 42: *A) Crystal structure of **204** with ellipsoids drawn at the 50 % probability level. The C-C(N)-C(O)-OMe group is disordered over two positions, C4-C(5)(N(3))-C(6)(O(1))-O(2)-C(7) and C(4A)-C(5A)(N(3))-C(6A)(O(1A))-O(2)-C(7A) at a refined percentage occupancy ratio of 69.4 (19) : 30.6 (19). Note how atoms N(3) and O(2) are present in the same positions in both disordered components. The major component is bonded to atom C(2) of the five-membered ring and the minor component is bonded to atom C(3). B) Crystal structure of **204** with ellipsoids drawn at the 50 % probability level. The C-C(N)-C(O)-OMe group is disordered over two positions, C4-C(5)(N(3))-C(6)(O(1))-O(2)-C(7) and C(4A)-C(5A)(N(3))-C(6A)(O(1A))-O(2)-C(7A) at a refined percentage occupancy ratio of 69.4 (19) : 30.6 (19). Only the major component has been shown for clarity. Note how atoms N(3) and O(2) are present in the same positions in both disordered components. The major component is bonded to atom C(2) of the five-membered ring and the minor component is bonded to atom C(3). Carbon atoms are grey; hydrogen atoms are white; nitrogen atoms in blue; oxygen atoms in red and fluorine atoms in green. Crystal structure data solved by Dr. Louise Male.*

Gold complexes of the pyridine and isopropyl derivatives **148** and **154** could not be prepared. In both cases the starting material was recovered and there was no sign of decomposition, which suggests that no carbene was formed. This could be due to sterics in the case of the isopropyl group, and potentially due to some coordination interactions between the pyridine and the gold moiety which prevent access to the imidazolium carbon.

The *N,N'*-methyl Boc/Me NHC **89** that has been previously described in the literature was also made for comparison purposes. This complex was prepared by transmetallation with silver as reported, in 54% yield (Scheme 40).[127] The yield reported in the literature was higher at 79%, this difference can be due to loss of material during the final filtration, as the formed solid was very fine.

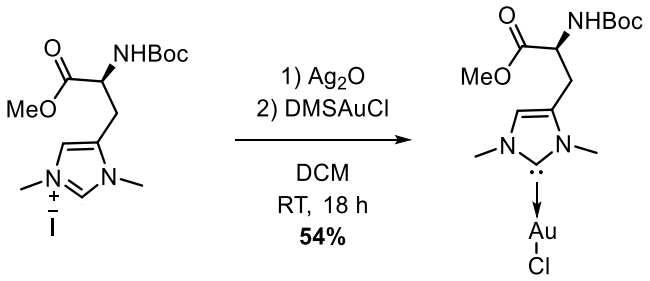

83 **89**

Scheme 40: *Synthesis of gold complex **89** as reported in the literature.*

An attempt to synthesize the gold complex of the imidazolium containing dipeptide **192** was made. The direct carbene insertion conditions were used, but after eighteen hours the starting material was recovered (Scheme 41). As the dipeptide was the PF_6^- salt, silver transmetallation was not used because it would yield the bisNHCAu complex, which are not as catalytically active as their monoNHC counterparts.[149, 152, 189] This results demonstrates that gold coordination to a PF_6^- salt of an imidazolium bearing peptide is not a viable route for the formation of artificial metallopeptides. Counter ion exchange from PF_6^- to a halide counterion could be an alternative route in which using silver transmetallation to gold could be possible. This result does indicate that there might be issues with gold coordination to peptide scaffolds and might require optimization of the methodologies available.

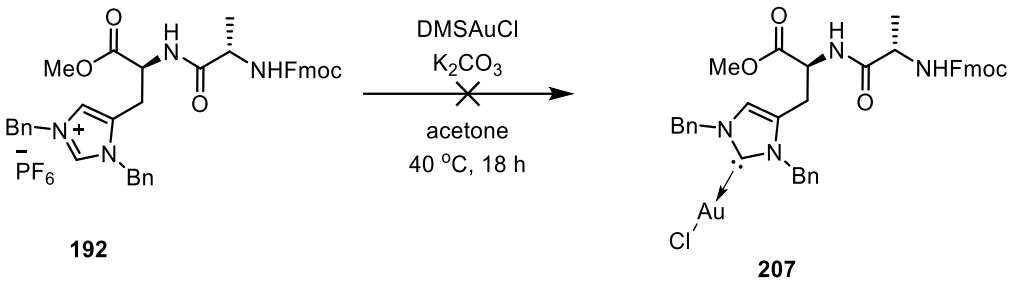

192 **207**

Scheme 41: *Unsuccessful attempt to form the dipeptide gold(I) complex.*

The formation of a gold complex using the free carboxylic acid derivative **180** was unsuccessful. The reaction mixture showed extreme degradation by TLC as well as the formation of a purple mirror in the flask which indicated reduction of Au(I) to Au(0).

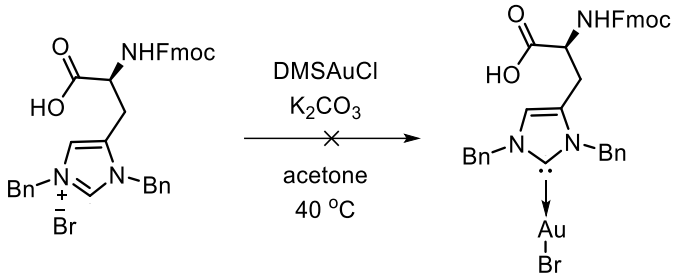

180 **208**

Scheme 42: *Unsuccessful attempt to form the gold complex on carboxylic acid **180**.*

3.2.2 – Synthesis of NHC Palladium Complexes

Palladium is one of the most widely used metals in catalysis in organic chemistry, from hydrogenations and aminations to the highly used cross-coupling reactions.[206, 207] The ability to introduce palladium in a protein is thus a massive advantage to the field of enzyme mimetics. Therefore, the potential of forming palladium complexes of the previously described imidazolium amino acids was explored by preparing analogues of [Pd^{II}(NHC)(η^3- allyl)Cl] complexes (Scheme 43). Reported [Pd^{II}(NHC)(η^3- allyl)Cl] complexes are highly stable, readily

synthesized and are used as efficient precatalysts for several reactions such as cross-couplings, cyclopropanations as well as semihydrogenation of alkynes.[207-211] The examples chosen to make novel palladium complexes were ones where there was a potential for second coordination sites for palladium.[205] Allyl groups and pyridine are hemilabile groups which coordinate to palladium and have been reported to increase catalytic efficiency of palladium complexes.[128, 209, 210] A reported one-pot silver transmetallation route was used to prepare the novel palladium complexes from the imidazolium salts (Scheme 43).***[128]*** As in the case of the gold complexes, ^{1}H NMR spectroscopic analysis showed the absence of the imidazolium proton and the shift of the NCHCN proton. The ^{13}C NMR spectra revealed the appearance of a new peak between 179 and 182 ppm (Scheme 43). The ^{1}H and ^{13}C NMR spectra also showed the presence of new peaks corresponding to incorporation of an extra allyl group.

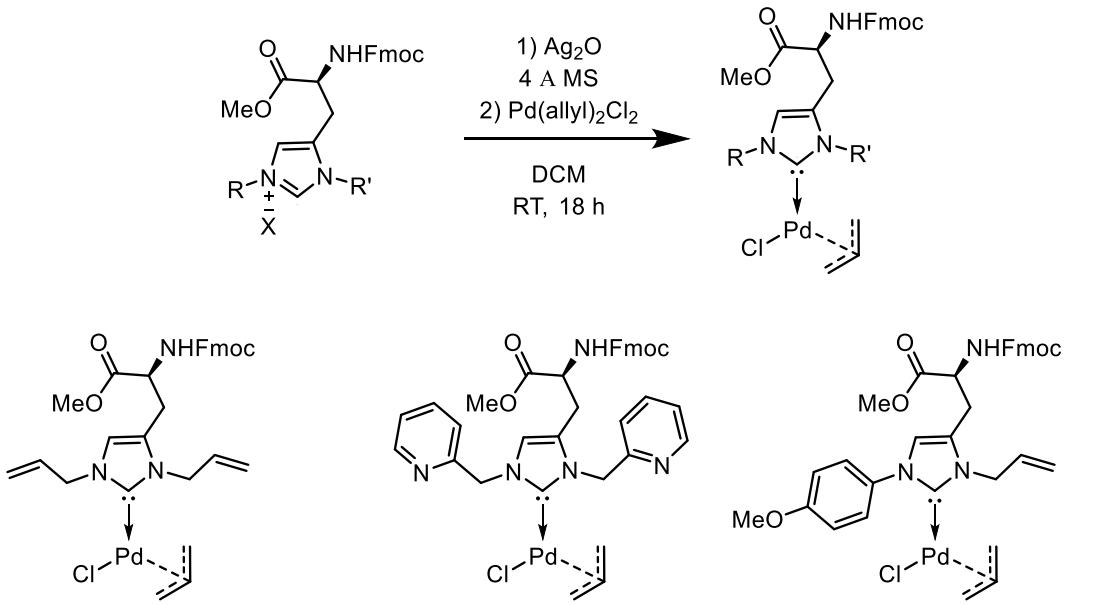

209- 49%
^{13}C NMR C-Pd δ 181.7 ppm

210 - 46%
^{13}C NMR C-Pd δ 179.8ppm

211- 24%
^{13}C NMR C-Pd δ 181.8 ppm

Scheme 43: *Substrate scope for the synthesis of novel palladium amino acid complexes.*

The bisallyl and bismethyl pyridine derivatives **209** and **210** were successfully synthesized with similar yields (49% and 46% respectively) (Scheme 43). These compounds were stable when stored as solids in the dark for months. The Boc equivalent of the pyridine containing complex **210** has been reported with quantitative yield.[128] The lower yield for the novel Fmoc derivative can be due to the different carbamate sterics. It is notable that this complex was obtained despite the direct insertion of gold failed. This suggests that transmetallation of the silver carbene onto gold could be a successful way of accessing the corresponding gold complex. The unsymmetrical allyl/*para*-methoxyphenyl complex **211** was prepared with 24% yield. Decomposition during column chromatography purification lead to low mass recovery, and thus low yield. (Scheme 43). This was surprising as aromatic groups are known to stabilize the metal carbene. A reason for this decomposition could be the presence of the allyl group which is known to undergo palladium insertion and subsequent reductive elimination that leads to decomposition.[165] However, that the bisallyl complex **209** proved stable to chromatographic purification, suggests that this pathway is unlikely. Drost *et al.* have reported that a similar palladium allyl complex of an unsymmetrical NHC substituted with a methyl group and a *para*-methoxy phenyl group could not be isolated because it fully decomposed during column chromatography, whilst other complexes containing hemilabile groups were successful isolated.[128] This supports our observation that the mono arylated scaffold has intrinsic stability problems.

These palladium allyl complexes can have different isomers dependent on the arrangement of the ligands on the square planar coordination sphere of palladium.[212] The unsymmetrical derivative **211** has more possible isomers due to the asymmetry on the imidazole ring. In all reported cases, the ^{1}H NMR spectra

shows no obvious signs of the presence of more than one diastereomer. However, the broadness of some peaks makes it hard to conclude for sure that only a single diastereomer was isolated. Trace amounts of different compounds were observed on the TLC of the reaction mixture. These compounds were not isolate and characterized but they could potentially be some of the other diastereomers.

3.2.3 - Protecting Group Manipulation in NHC Metal Complexes

A strategy to access artificial metalloenzymes is the incorporation of the metal complex directly in the peptide sequence. For this to occur the metal complex must tolerate the same SPPS conditions described for their ligand counterparts. The most challenging of these conditions was the stability of the complexes to the high concentrations of trifluoracetic acid commonly used for resin cleavage and side chain protecting group deprotection. The stability of these type of scaffolds to TFA will be discussed in Chapter 4. Protecting group manipulation to obtain the carboxylic acid for coupling is also required and it will be assessed in the next section.

3.2.3.1 – Methyl Ester Hydrolysis.

Since the coordination of gold to an acid amino acid with a free carboxylic acid resulted in degradation (Scheme 42), an alternative approach to access the free carboxylic acid was explored here. The same conditions used to cleave the methyl ester in the imidazolium salts were applied to gold complex **202** (Scheme 44). The free carboxylic acid was isolated with 49% yield and the reaction was readily scaled up to yield 1.11 g of the SPPS building block. TLC analysis showed

full conversion from the starting material to product, however during the purification process (flash chromatography silica gel) there was significant decomposition which lead to lower mass recovery. Attempts to purify the product via recrystallization or trituration failed to yield pure product due to a small unknown impurity which was visible in the ^{1}H NMR spectra.

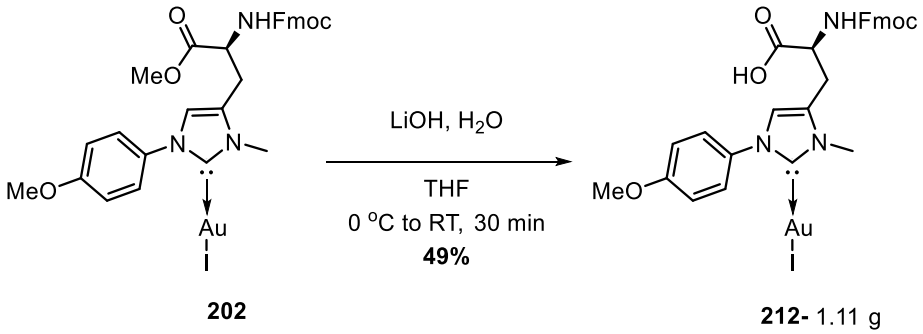

202 **212-** 1.11 g

Scheme 44: *Hydrolysis of the methyl ester on gold complex* ***196****.*

The same conditions were applied to the bisbenzyl complex **200**, however signs of decomposition in the reaction mixture were noticed in the TLC (Scheme 45). Attempts to purify and isolate the desired product resulted in less than 5% yield which rapidly decomposed within hours as seen by the ^{1}H NMR spectra and change of appearance of the product (from a white solid into purple). This result combined with the failed coordination to gold of the free carboxylic acid shows that this substrate is highly prone to decomposition. On the other hand, the unsymmetrical gold complex **212** was stable which suggests that NHCs with different nitrogen substituents will behave differently in their reactivity and stability and thus, each complex should be evaluated independently.

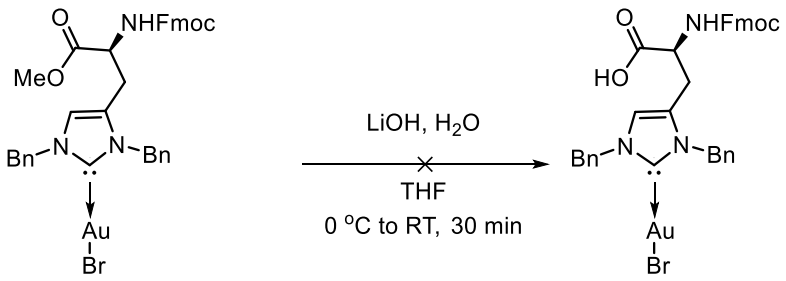

200 **213**

Scheme 45: *Attempts to hydrolyse the methyl ester in gold complex* ***200****.*

The tolerance of building block **212** in SPPS procedures will be explored in chapter 4.

3.2.3.2 – Fmoc removal

In order to introduce the gold complexes in the middle of a peptide sequence using SPPS, the Fmoc group needs to be removed. The most common conditions used for Fmoc removal are 20% piperidine in DMF. In order to test the tolerance of gold complexes to these conditions, gold complex **200** was subjected to 20% piperidine in dichloromethane for eighteen hours. Dichloromethane was used due to its low boiling point, which makes it easier to remove from the reaction mixture than DMF. The free amine gold complex **214** was successfully isolated in 99% yield (Scheme 46). This demonstrates that the gold complexes can tolerate these conditions and can potentially be used in the middle of a peptide sequence. These findings were further supported by experiments described in chapter 4 (*see* Scheme 64).

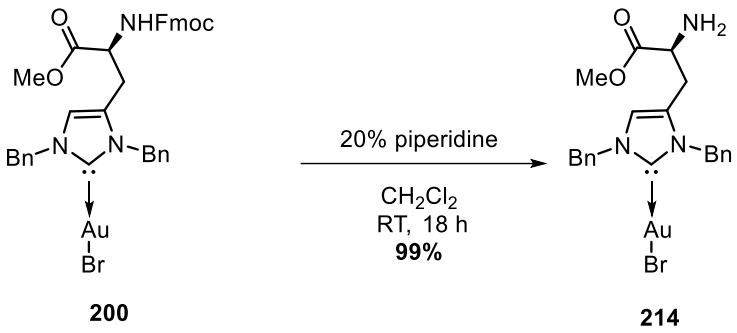

Scheme 46: *Successful cleavage of the Fmoc group of gold complex* ***200****.*

3.2.4 - Synthesis of Phosphorous-Based Ligands and Complexes

Phosphorous based ligands are ubiquitous in transition metal catalysis and thus it would be useful to have these ligands available in an amino acid building block that could be used in SPPS.

3.2.4.1 - Synthesis of Phosphine Bearing Amino Acids

At the beginning of 2018, Arribat *et al.* reported the synthesis of phospholyl(borane) amino acids for use in fluorescent labelling of peptides. Their approach used iodoalanine derivatives to react with a phospholide ion which was then protected with a borane species. One of the borane species was shown to be able to be converted into either the sulfide equivalent or a gold(I) complex. The amino acids used were protected with a combination of Boc, allyl and benzyl groups, which are not useful as building blocks for conventional SPPS. They have shown that it is possible to convert the sulfide derivative into an Fmoc building block, but this adds two steps to the route diminishing the overall efficiency of the process. The substituents on the phosphorous are large rigid aromatic systems intended for their luminescent applications. In our pursuit of making an artificial metalloenzyme, these substrates are rigid, sterically large and highly hydrophobic

which can lead to disruption of designed peptide superstructure and as such are not ideal.

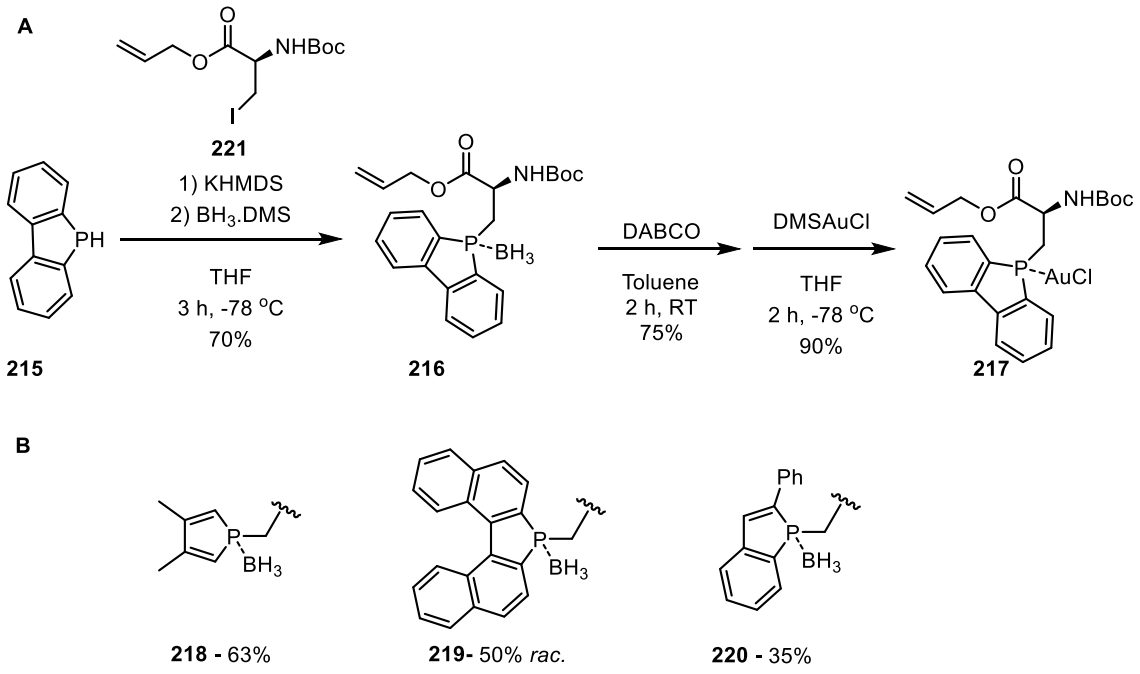

***Scheme 47**: Example of explored chemical space for phospholyl amino acids in the literature.*[213]

The potential of using the methodology reported by Arribat *et al.* on Fmoc containing scaffolds was explored. Diphenylphosphine was used as the phosphorous precursor due to being commercially available and less rigid than the systems explored in the aforementioned paper. To test if the reaction conditions would be tolerated by diphenylphosphine, the reported Boc/allyl derivative **221** was used as a starting material. The corresponding phospholyl(borane) amino acid **223** was successfully isolated with 18% yield (Scheme 48). The iodoalanine starting material is prone to elimination and thus large amount of the alkene side-product was recovered from the reaction mixture. Other impurities were seen in the reaction mixture, mostly phosphorous containing side products making purification challenging.

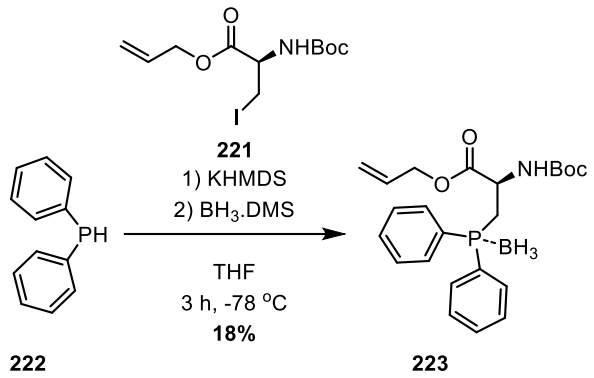

Scheme 48: *Synthesis of novel phospholyl(borane)* ***223.***

After this positive result, the methodology was used in a Fmoc containing building block. The carboxylic acid of the commercially available Fmoc-L-Serine was protected with a tert-butyl group which is acid labile and can be orthogonally deprotected in the presence of the Fmoc carbamate. A known synthetic procedure using *N, N'*–dicyclohexylcarbodiimide, copper chloride (I) and tert-butanol yielded the desired product with 65% yield (Scheme 49).[214] The hydroxyl group was then substituted by an iodide using a described methodology, to access the desirable iodoalanine derivative **226** with 70% yield (Scheme 49).

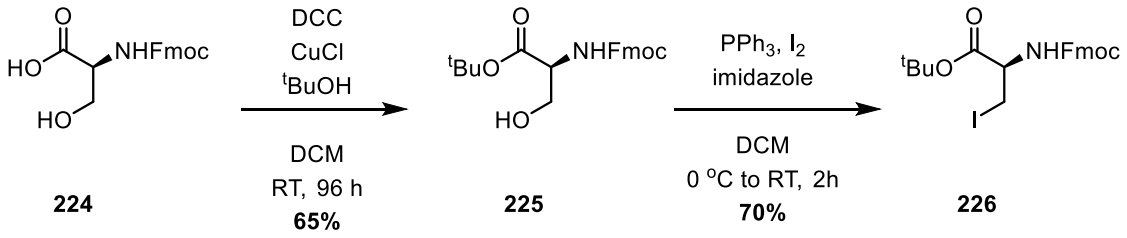

Scheme 49*: Synthesis of iodoalanine* ***226.***

Reaction of amino acid **226** with diphenylphosphine yielded the novel Fmoc derivative **228** with 20% yield (Scheme 50). Changing the protecting groups did not impact the yield of the transformation. The previously described alkene and phosphorous side-products were also observed in this reaction. This

has shown that the methodology can be applied to Fmoc substrates and thus allow easy access to Fmoc derived building blocks. Attempts to convert product **228** to the gold(I) complex using a one-pot approach were unsuccessful (Scheme 50).

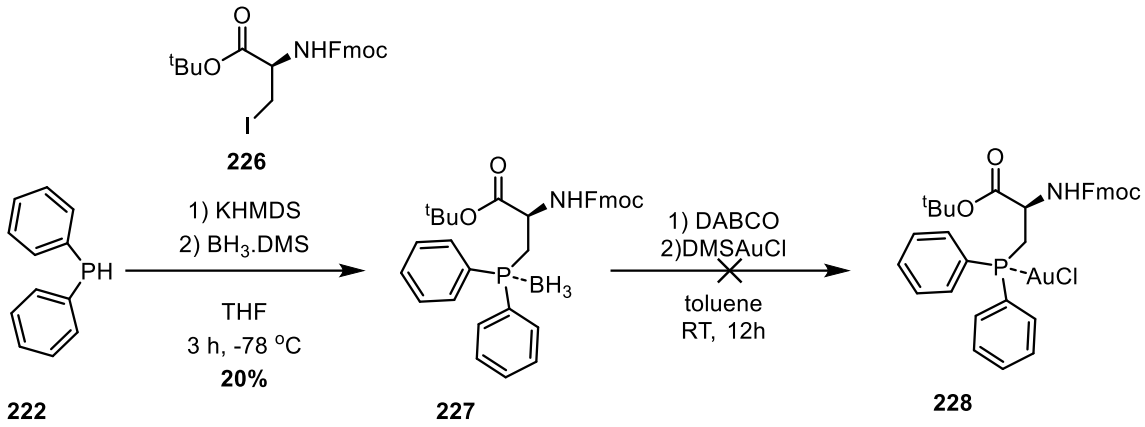

Scheme 50: *Synthesis of Fmoc phosphorous containing building block* ***228*** *and unsuccessful gold coordination.*

3.2.4.2- Synthesis of Phosphinite Bearing Amino Acids

Oxygen containing phosphorous ligands can have a different reactivity profile than the phosphine.[74] Therefore, a strategy to synthesize this type of scaffolds was envisioned. This would involve the reaction between a phosphochloridite with a hydroxyl group in an amino acid backbone (Scheme 51). There are two natural amino acids which contain hydroxyl groups (serine and threonine) and one that contains a phenol group (tyrosine). All these three amino acids could provide easy access to three different types of phosphorous containing building blocks. A larger substrate scope would also be possible by varying the phosphochloridite substituents.

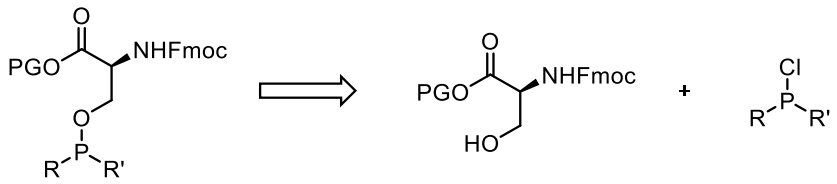

Scheme 51: *Retrosynthetic analysis of the synthesis of phosphorous ligands amino acids.*

The previously used Fmoc-L-Serine-O^{t}Bu derivative **225** was used as a starting material. The carboxylic acid was protected with tert-butyl group to avoid any potential side reactions with the highly reactive phosphochloridite reagents.

Phosphochloridite motifs have been described since the 1950's and are known to be highly sensitive to oxygen and water, being easily hydrolysed to release HCl.[215] Phosphochloridites are synthesized by reacting an alcohol with phosphorous trichloride under inert atmospheres. Following the thorough procedure described by Lucas *et al*. for the synthesis of 2-choro-1,3,2-dioxaphospholane, isolation of the chloridite intermediate was possible.[***215***] The use of freshly distilled reagents, inert atmosphere and rapid distillation were proven to be essential for the isolation of the product **230** (Scheme 52). The amino acid **225** was stirred with pyridine in dry dichloromethane at 0 °C, and the phosphochloridite **230** was added dropwise. Pyridine was chosen as a base to neutralize the hydrochloric acid formed in the reaction as it should not cleave the Fmoc carbamate. The reaction was allowed to warm up to room temperature and full consumption of the amino acid **225** was observed by TLC after twenty-four hours. The ^{31}P NMR spectra of the crude reaction mixture showed resonances at 135 and 121 ppm which are consistent with two phosphite moieties being present. It was hypothesized that one of the resonances was the desired product

and the second resonance a product of the substitution of the chloride atom of the phosphochloridite **230** with water. Attempts to purify the reaction mixture using flash chromatography on silica gel failed. The starting material Fmoc-serine **225** was recovered, even though it had been consumed in the reaction mixture. Attempts to purify the product by recrystallization and by deactivated silica column were unsuccessful as only decomposition products were recovered. Decomposition of similar systems has been reported in the literature.[83, 216, 217]

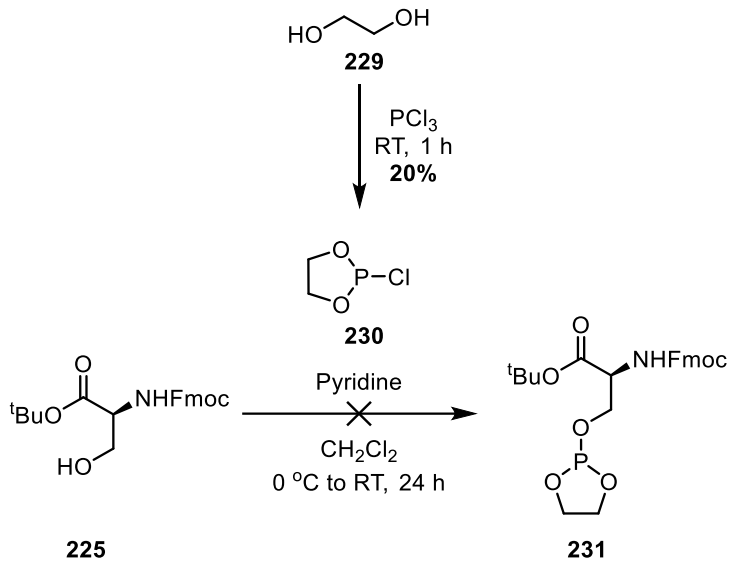

Scheme 52: *Attempted synthesis route for the preparation of a novel phosphine bearing amino acid.*

Considering the positive results achieved for the synthesis of phosphine scaffolds a new strategy was tested. Firstly, a more stable and commercially available phosphochloridite such as diphenylphosphochloridite would be used. This would prevent some of the degradation pathways present for the diaxophospholane type structures. Secondly, a borane reagent would be used to protect the phosphinite moiety in order to allow the use of column chromatography in purification. As a starting point pyridine was kept as a base in

degassed tetrahydrofuran which is commonly used in temperature sensitive phosphorous chemistry (Scheme 53, Table 3, entry 1).[218]

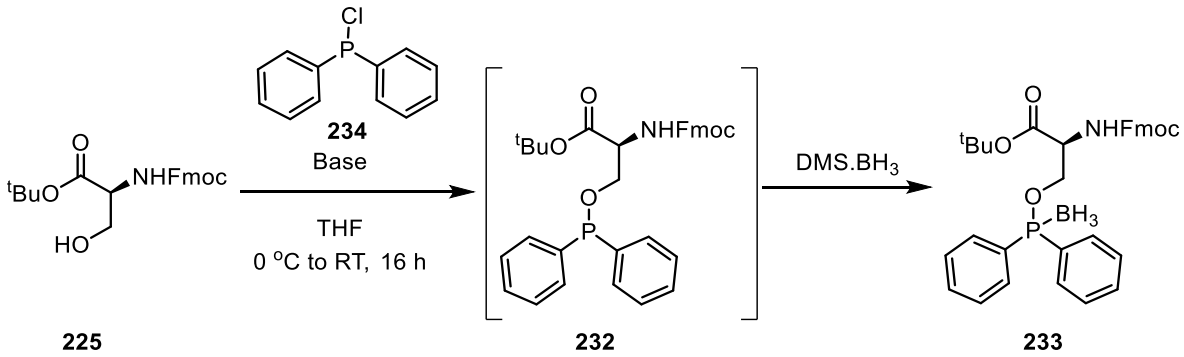

Scheme 53: *Synthesis of phosphorylborane amino acid* ***233*** *from serine building block* ***225.***

Table 3: *Base optimization table for the reaction of serine with diphenylphosphochloridite Scheme 53.*

Entry	Base	Yield of 233
1	Pyridine	0%
2	Triethylamine	36%
3	DIEA	80%

Addition of the chloridite **234** to the amino acid and pyridine solution was performed at 0 °C. After 1 hour there was no conversion of the starting material, so the reaction was allowed to warm up to room temperature. After 24 hours there was only starting material (Table 3, entry 1). This lack of reactivity was surprising so the reaction was performed with two other bases that would not cleave the Fmoc group and had different steric bulk than the pyridine. Diisopropylethyleneamine (DIEA) and triethylamine were chosen as they should be compatible with Fmoc groups. In both cases product was formed after 1 hour and the borane reagent was then added and left to stir over night. Column

chromatography and yielded the desired product in both instances. The yield was higher for the reaction using DIEA at 80% whilst the triethylamine reaction provided the product in 36% yield (Table 3, entries 2 and 3). When comparing the pK_a of the three used bases, pyridine has the lowest pK_a at 5.2. DIEA and triethylamine have similar pK_a at 10.5 and 10.2 respectively. DIEA is the more basic and thus is the best at deprotonation of the hydroxyl group of serine. Recrystallization of the product **233** from hot ethanol yielded needle like crystals from which an x-ray structure was obtained (Figure 43). The structure revealed four crystallographic independent motifs in the unit cell which interact with each other via hydrogen bonding (*see* appendix Figure 84). All molecules in the unit cell are chiral and all are the S enantiomer.

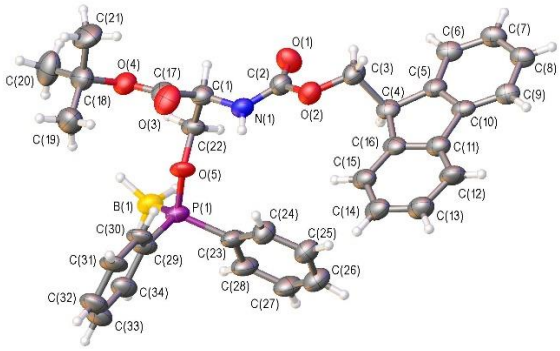

Figure 43: *Crystal structure of **233** with ellipsoids drawn at the 50 % probability level. The structure contains four crystallographically-independent molecules of which only molecule 1 is shown for clarity. The hydrogen atoms bonded to B(1), B(101), B(201) and B(301) were all located in the electron density and refined, with the geometry (B-H distances, H-B-H and P-B-H angles) restrained in all cases. All remaining hydrogen atoms were fixed as riding models. The isotropic thermal parameters (U_{iso}) of all hydrogen atoms were based on the U_{eq} of the parent atom. Crystal structure data solved by Dr. Louise Male.*

Considering the success of the previous strategy, it was hypothesized that the phosphinite intermediate could be directly trapped with a metal salt. This would allow for direct access of phosphinite gold complexes amino acids in one step from amino acid feedstocks. After the first stage of the reaction was

completed, (dimethylsulfide)gold(I) chloride was used instead of the previously used borane as a metal source. After 1 hour at room temperature, full conversion of the phosphinite intermediate was observed by TLC. Purification via column chromatography resulted in the desired gold complex **235** being isolated in 63% yield (Scheme 54).

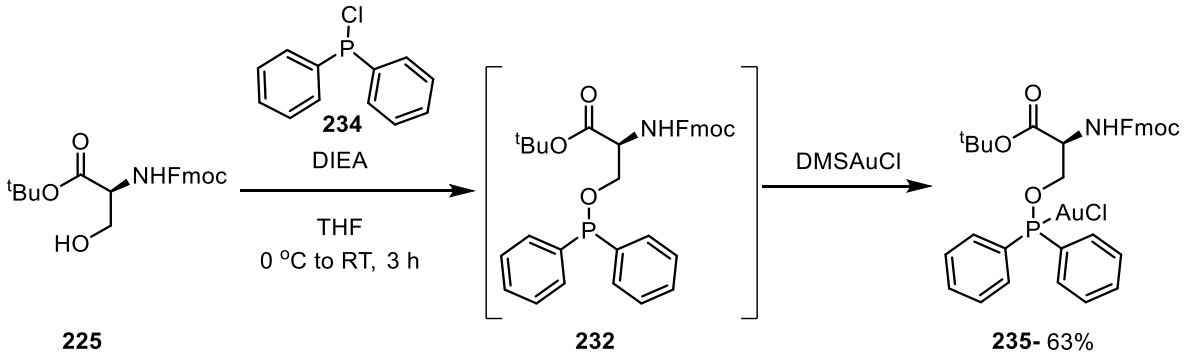

Scheme 54: *Synthesis of the gold complex **235** via in situ gold(I) trapping of **232** using DMSAuCl.*

It is notable that attempts to recrystalise compound **235** from the reaction mixture using hot ethanol lead to decomposition via a replacement of the amino acid backbone by an ethoxy group (Scheme 55). Similar recrystallization conditions were used for the borane derivative and resulted in sharp colourless needles of product **233**. However, this type of ligand exchange for the synthesis of phosphorous gold complexes has been previously reported in the literature.[219]

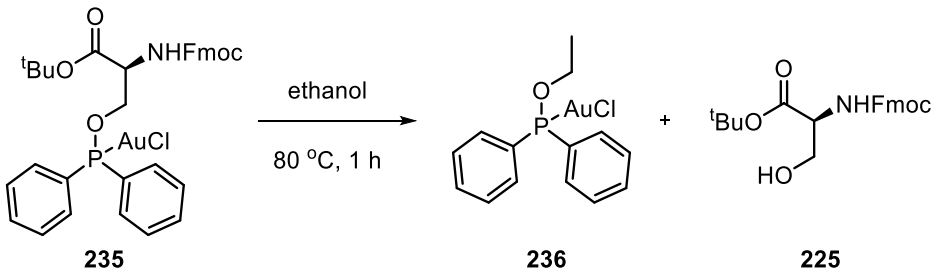

Scheme 55*: Ligand exchange when heating the product **235** in ethanol.*

3.2.5 - Study of Catalytic Activity of the Gold Complexes

3.2.5.1 - Enyne Cycloisomerization

Enyne cycloisomerization is an intramolecular rearrangement of enynes which gives access to a cyclic isomer. This type of rearrangement can be thermodynamically promoted but is more often enabled by transition metal catalysts.[220] Alkyne activation using gold(I) catalysts can be used in the construction of rings with stereogenic centres.[220-224] Different catalysts can induce different reactivity pathways and therefore yield different products (Scheme 56).[184, 220, 225] These processes are highly versatile, as they can generate different products and stereogenic centres in one step. Thus, these reactions are suitable to assess the reactivity profile of our library of complexes and evaluate the impact of including these species in peptide scaffolds. The chiral environment of peptide ligands can lead to selective formation of one preferential product and/or enantiomer.

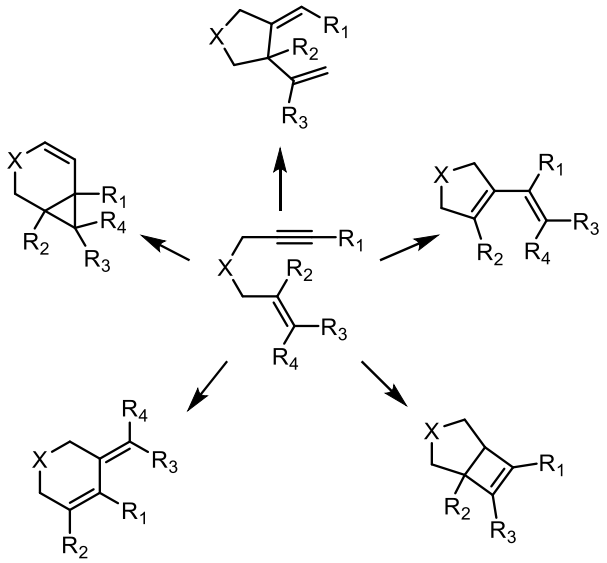

Scheme 56: *Example of potential outcomes of a metal catalysed enyne cycloisomerization reaction.*

The 6-endo-dig cyclization of *N*-tethered 1,6 enynes was chosen as test reaction due to being widely studied and the easy access to starting materials.[184] A silver salt, solvent and temperature screen was performed to try and find optimal conditions for the catalysis using our type of complex. Gold complex **202** was used as the benchmark catalyst. The choice of this specific catalyst was based on the fact that it was readily available in larger quantities. Due to the *N*-arylated groups in the NHC ring this catalyst was the most similar to widely used and commercially available NHC gold(I) catalysts. Initially, phenylacetylene enyne **237** was used in toluene at 40 °C as reported in the literature and starting material was fully recovered (Table 4, entries 1 and 3). Increasing the temperature to reflux resulted in no change and once again all the starting material was recovered (Table 4, entries 2 and 4).

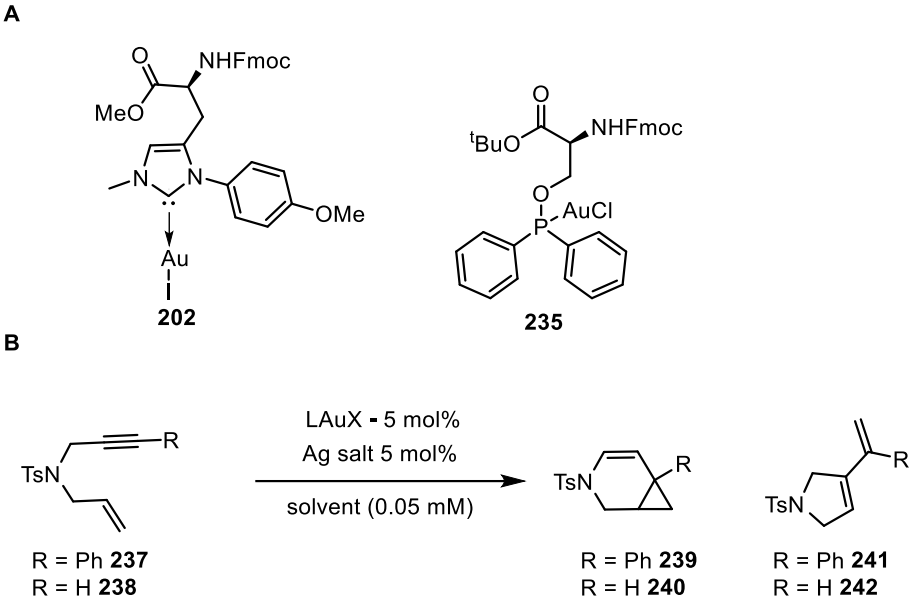

Scheme 57: *Cycloisomerization of N-tethered 1,6 enynes.* ***A)*** *Catalysts tested.* ***B)*** *Reaction conditions.*

Table 4: *Reaction conditions tested for the cycloisomerization of enynes using catalyst* ***202*** *and* ***235****. The yields shown are calculated using quantitative ^{1}H NMR spectroscopy.*

Entry	*R*	*Catalyst*	*Silver salt*	*Solvent*	*T (°C)*	*Time (h)*	*Yield of 239 or 240 (%)*	*Yield of 241 or 242 (%)*
1	Ph	**202**	AgOTf	toluene	40	17	0	0
2	Ph	**202**	AgOTf	toluene	110	17	0	0
3	Ph	**202**	$AgSbF_6$	toluene	40	22	0	0
4	Ph	**202**	$AgNTf_2$	toluene	110	22	0	0
5	H	**202**	AgOTf	toluene	110	22	0	0
6	H	**202**	$AgNTf_2$	toluene	110	22	0	0
7	H	**202**	AgOTf	CH_2Cl_2	40	24	0	0
8	H	**202**	AgSbF	CH_2Cl_2	40	24	0	0
9	H	**235**	$AgNTf_2$	CH_2Cl_2	40	24	33	7

Phenylacetylene enyne **237** is known to be less reactive than **238**, so in an effort to obtain some catalysis the terminal alkyne **238** was tested. Reaction in toluene at reflux once again resulted in no product formation (Table 4, entries 5 and 6). The lack of reactivity could be due to low of solubility of the catalyst in toluene and thus the reaction was tested in dichloromethane. The change in solvent did not improve reactivity and once again there was full recovery of starting material (Table 4, entries 7 and 8). One particular observation was that whilst in the reactions in toluene started to form a purple mirror in the reaction vessel, the reaction using dichloromethane remained clear. Different silver salts did not alter the outcome of the reaction. Thus, the tested catalyst **202** has not shown any reactivity using the above conditions.

The previously prepared phosphinite gold complex **235** was also tested as a catalyst for the cycloisomerization of enyne **238** (Table 4, entry 9). The solvent used was dichloromethane as it is more polar and thus more likely to dissolve the catalyst and the silver salt chosen was $AgNTf_2$. After twenty-four hours there was still starting material left but there was formation of both products **240** and **242** in 33% and 7% yield, respectively. As catalyst **235** was shown to decompose under ethanol heating (*see* Scheme 55), the catalyst stability in dichloromethane was tested. Refluxing the catalyst **235** in dry dichloromethane under inert atmosphere for twenty-four hours did not result in any decomposition.

3.2.5.2 - Regioselective Hydration of Alkynes

Hydration of alkynes is one of the most atom economical ways of accessing novel carbonyl compounds.[226] Gold catalysts have been used to facilitate this transformation since 1976, however, in recent years several reports

have shown that NHC(Au) type catalysts are extremely efficient for this transformation even at very low catalyst loading.[227, 228] Hydration of unsymmetrical alkynes leads to the potential formation of regioisomers. In the case of alkyne **243** literature reports demonstrate that different ligands can have large differences in their catalytic activity and thus was a good test reaction to benchmark our library of catalysts (Scheme 58).[186, 228] The study by Nolan and co-workers demonstrates that whilst IPrAuCl is successful in product formation, IMesAuCl shows no reaction.[228] Xu and co-workers demonstrate that steric hindrance of ligands is more influential in the reaction than electronic effects.[229]

There are several conditions reported for the gold catalysed hydrations of alkynes.[228, 229] Considering the overall goal of the project is to include these ligands in large peptide scaffolds, methanol was chosen as a solvent due to its high polarity and miscibility with water (Scheme 58). The yields were determined using quantitative GC and for five examples the yield calculated from quantitative 1H NMR analysis was also determined and found to be comparable to the GC results.

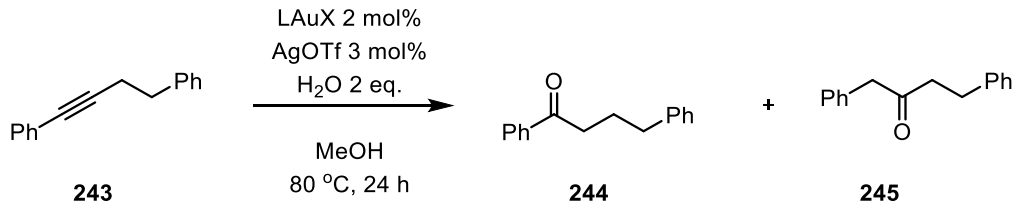

Scheme 58: *Hydration of alkyne model reaction, using unsymmetrical alkyne* ***243*** *as a starting material.*

Table 5: *Catalytic outcome of testing the prepared gold complex library. The yields are an average of two repeats. Reactions were performed at 0.1 mM and yields were determined via GC.*

Entry	***Catalyst***	***AuX***	***Overall yield (%)***	***Yield of 224 (%)***	***Yield of 245 (%)***
1	IPrAuCl	Cl	100	55	45
2	Ph_3PAuCl	Cl	93	65	28
3	AgOTf control	-	0	0	0
4	**201**	Br	19	11	8
5	**202**	I	6	3	3
6	**200**	Br	22	11	11
7	**204**	Br	64	37	27
8	**199**	Br	48	23	24
9	**235**	Cl	89	58	32

Absence of gold catalyst in the reaction lead to no product formation (Table 5, entry 3). Commercially available and widely used gold catalysts IPrAuCl and

PPh_3AuCl were tested under the same conditions for comparison purposes. As expected, both commercial catalysts resulted in high conversion, as reported.[186, 228] The commercial NHC catalysts demonstrated no regioselectivity and the phosphine favoured the Markovnikov product in a 2.3:1 ratio (Table 5, entries 1 and 2). Overall, the NHC ligands tested showed very little regioselectivity with variable degrees of conversion (Table 5, entries 4 to 8). The type of carbamate chosen does not seem to impact the reaction as both the Boc and Fmoc bisbenzyl derivatives **201** and **202** show similar conversions at 19% and 22% yield respectively (Table 5, entries 4 and 6). The bis-allyl derivative **199** shows moderate conversion at 48% yield, but no regioselectivity (Table 5, entry 8). The free amine **204**, shows the highest conversion and regioselectivity at 64% yield and 1.4:1 ratio of product **224** (Table 5, entry 8). All the aforementioned catalysts with the exception of the free amine have similar electronic properties. The allyl derivative **199** has smaller substituents in the nitrogen atoms of the imidazolidene and higher conversion is observed. The free amine **204** albeit having the same substituents in the nitrogen atoms of imidazolidine ring, lacks the large and bulky Fmoc group. This could possibly facilitate the access of the substrates to the metal centre and thus achieve higher conversions. In order to test the effect of different substituents on the imidazolidine ring, gold complex **212** was tested (Table 5, entry 5). Of note is that this substrate has an iodide instead of bromide counter ion. This derivative showed only trace amounts of product with a 6% yield and no regioselectivity (Table 5, entry 5). This lack of reactivity for catalyst **212** supports the results obtained for the cycloisomerization of alkynes in which no product was observed (Table 4). The phosphinite **235** was also tested, displaying the highest conversion in the library with 89% conversion and a slight preference for product **244** at a 1.8 :1 ratio (Table 5, entry 9). Considering that when heated

in ethanol this species has undergone a ligand exchange is possible that under the reaction conditions the same would have occurred. The gold catalyst **235** was subjected to the reaction conditions in the absence of the alkyne for twenty-four hours (Scheme 59). The reaction mixture showed conversion of amino acid derived catalyst **235**, to a mixture of products. The main products were the serine derived amino acid **225** and the methoxy diphenylphosphinite gold chloride **246** (Scheme 59). A small amount of the oxidation product **247** was also visible in the ^{1}H and ^{31}P NMR spectra. Thus, the catalysis results under these conditions are likely to be a result of the activity of catalyst **246**.

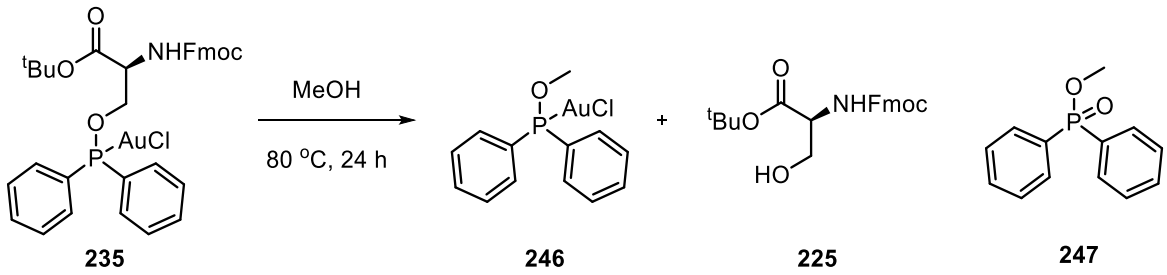

Scheme 59: *Stability test of gold complex **235** under the hydration reaction conditions. After twenty-four hours three different products were observed.*

3.3 - Conclusions

A library of novel amino acids metal complexes was prepared, and their catalytic activity was explored. Nine novel NHC gold(I) complexes were prepared via direct carbene insertion. The allyl derivative **199** was the first *N*-allyl NHC gold complex reported and has been shown to be stable. Three novel palladium allyl complexes were successfully synthesized. A gold amino acid scaffold ready for SPPS was prepared at gram scale. The tolerance of this building block to SPPS will be explored in chapter 4.

The synthesis of these NHC metal complexes and the study of protecting group manipulation has demonstrated that different nitrogen-substituents on the imidazolium and NHC ring have a distinct impact in their stability and reactivity. Thus, it is not possible to fully extrapolate behaviour based on one independent scaffold. Therefore, further studies into the coordination and ester hydrolysis of individual scaffolds is required.

Novel phosphorous bearing ligands were successful prepared. Protecting the phosphorous moiety with borane and the use of degassed solvent was essential for the successful synthesis and purification of the ligands. In situ trapping with gold has proven to be an effective strategy to access the gold complex amino acids. This strategy yielded the first reports of a phosphinite gold complex on an amino acid backbone.

The catalytic activity of some of the complexes was explored. In general, the NHC derived gold complexes displayed modest activities. As the aim of this project is not to design new small molecule catalysts, this result is important but not discouraging. The novel phosphinite catalyst **235** displayed catalytic activity despite, the stability issues in alcohol solvents

Chapter 4:

4.Incorporation of Non-Natural Amino Acids Through Solid-Phase Peptide Synthesis

4.1 - Introduction

Solid phase peptide synthesis has allowed for easy access of peptide sequences and consequently different three-dimensional structures. Some of the most commonly accessed three-dimensional peptide structures are α-helical based motifs, however loops and β-sheet structures have also been synthesized (Figure 44).[18, 20, 230]

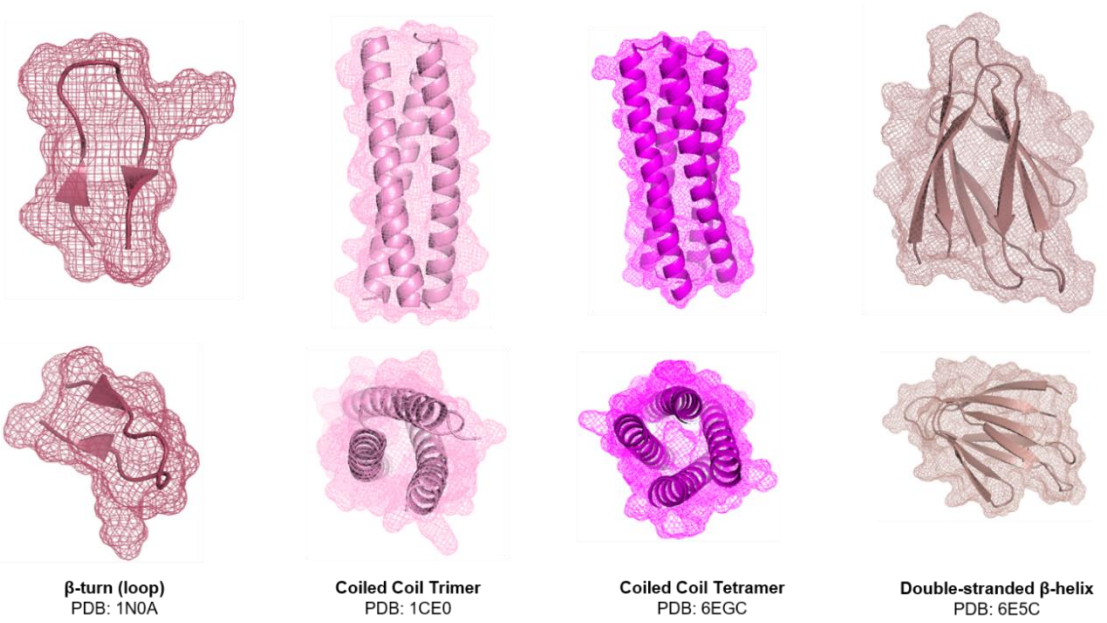

Figure 44: *Crystal structure images for different 3D structures of peptides derived from PDB IDs.*

Non-natural amino acids can be included in protein scaffolds in three ways: expression, bespoke synthesis procedures and SPPS. There have been reports

of non-natural amino acids being encoded by DNA and successfully expressed in a protein sequence within a cell.[231] However, this process is challenging, very time consuming and specific for each amino acid. Bespoke synthesis involves the use of tailored conditions to attach an amino acid into a peptide. This usually means that the particular scaffold cannot tolerate standard SPPS conditions and therefore may have restricted use and applications. Thus, the synthesis of amino acids which tolerate standard Fmoc-based SPPS are more likely to be widely used as building blocks for peptide synthesis and can potentially even find commercial value.

Two of the strategies for introducing metal catalyst activity in a peptide scaffold via SPPS are to introduce a ligand amino acid in the sequence and then perform metal coordination with the peptide scaffold or introduce the metal complex directly in the peptide sequence (Figure 45).

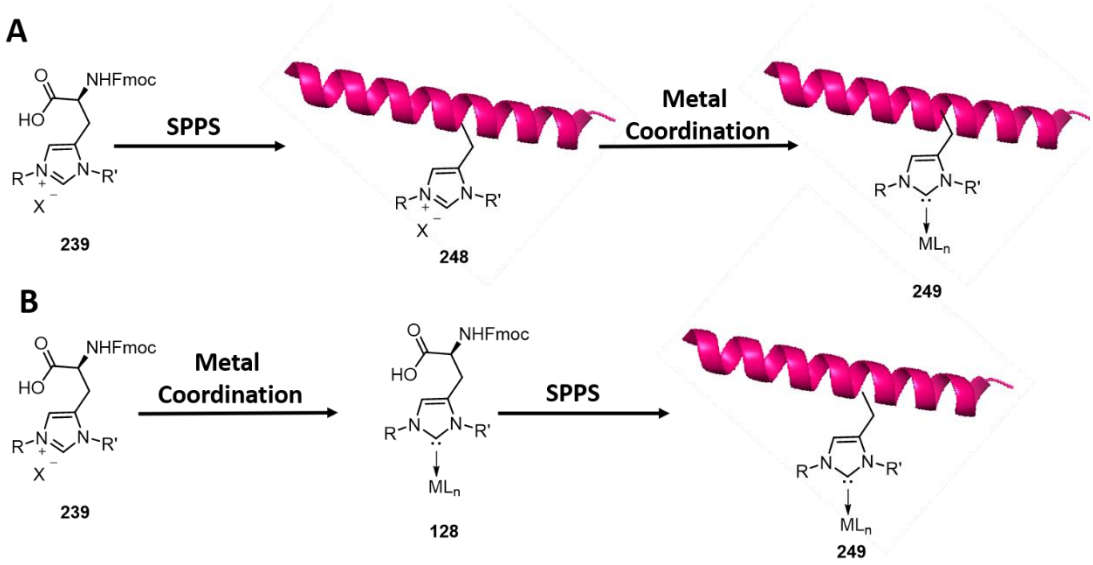

Figure 45: *Schematic representation of two strategies to access artificial metalloenzymes using synthetic peptides and non-natural amino acids.* ***A)*** *In this strategy an amino acid bearing a ligand side chain is incorporated in a sequence using SPPS, subsequent metal coordination yields the metallopeptide.* ***B)*** *In this strategy the ligand is converted to its metal complex which is then incorporated in the peptide sequence using SPPS to yield the desired metallopeptide.*

In the first instance the ligand needs to tolerate SPPS conditions and then metal coordination procedures need to be established. This route allows for the synthesis of a ligand peptide scaffold which can then be derivatized with different metals for different reactivity. Some issues with this approach are the establishment of viable coordination routes and the potential for incomplete coordination.

The second route requires the metal complex to be stable during the SPPS procedure, in particular resin cleavage conditions using TFA. This route can prevent issues such as incomplete coordination but limits the versatility as each catalyst needs to be synthesized individually instead of having one ligand with the potential to bind different metals.

The majority of examples of peptides bearing imidazolium salts and NHC metal complexes reported are of small sequences, with simple non-reactive amino acids and no complex superstructure.[121, 124, 132, 232, 233] The amino acids were often included at the *N*-terminus of peptides using solution coupling methods.[121, 124, 125] Medal and co-workers reported the use of NHC palladium bearing peptides as heterogeneous on-resin catalysts and thus were not exposed to the large quantities of TFA required for resin cleavage.[133]

The only reported study of the use of imidazolium ligands and the corresponding rhodium and ruthenium NHC complex in SPPS was performed in 2008 by Nolte and co-workers.[232] However, this study does not use imidazolium or NHC amino acids but end tethers, which were used to cap the *N*-terminus of a peptide containing four residues. Imidazolium salt **250** tolerated 2% TFA in dichloromethane resin conditions (Scheme 60, A). Coordination to the imidazolium salt using a silver transmetallation route failed. The rhodium carbene was not stable even at 1% TFA in dichloromethane.

The ruthenium complex survived up to 2% TFA in dichloromethane showing 30% degradation after four hours (Scheme 60, B). Further optimization of the resin cleavage conditions included a two-hour long cleavage with 10% TFA in methanol, followed by a second cleavage with 20%TFA in methanol for one hours. With these conditions it was possible to isolate ruthenium complex **253** in 30% yield. This study highlights potential stability problems of metal complexes to high concentrations of TFA. The residues used had no protecting group side chains, and there was no testing of the stability of the scaffolds to Fmoc removal conditions, capping procedures, or tolerance to coupling of challenging residues such as proline.

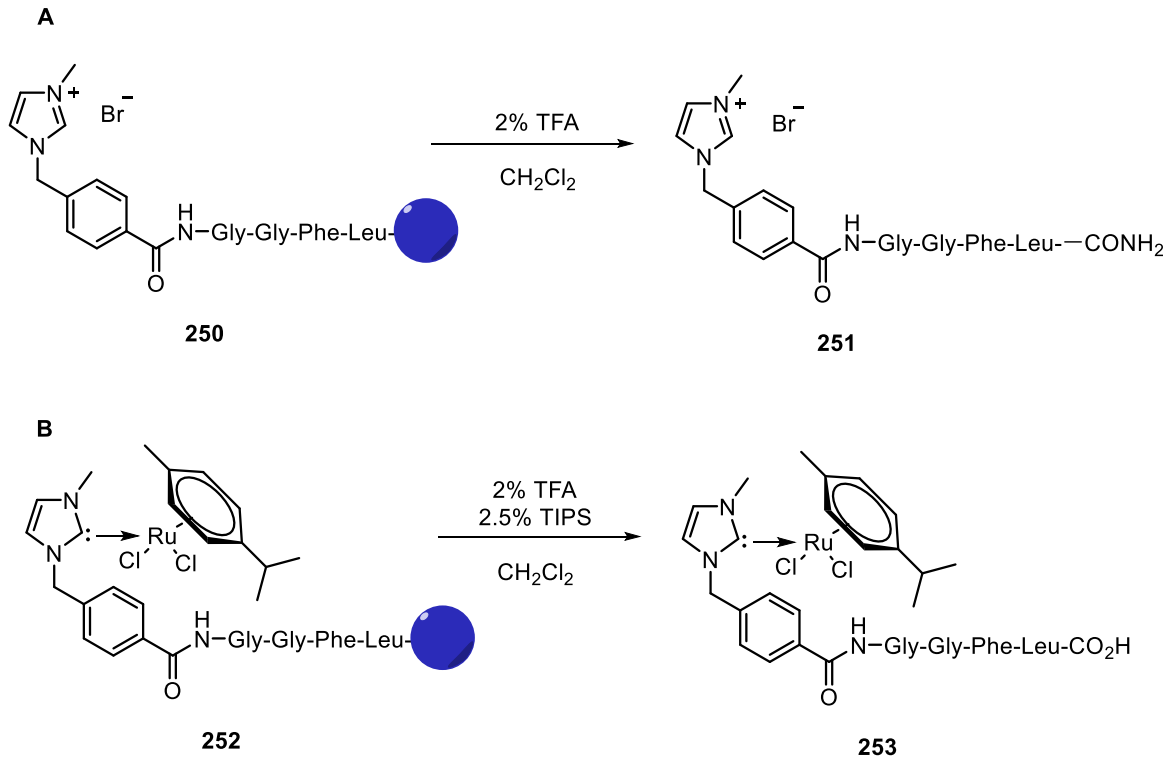

Scheme 60: A) *Resin cleavage conditions of an imidazolium bearing peptide, silver transmetallation to rhodium or ruthenium of peptide* ***251*** *failed. The resin used in this case was Sieber amide resin.* ***B)*** *Initial resin cleavage conditions used for ruthenium complex* ***252.*** *The resin used in this case was 2-Clr-Trt resin.*

There is a need for further investigation of the stability of Fmoc-amino acids bearing imidazolium and metal complexes to SPPS conditions. There are no reports of the inclusion of imidazolium amino acids in complex long sequences such as coiled coil sequences, or the use of gold NHC bearing amino acids in SPPS. In this chapter the tolerance of previously synthesized scaffolds to SPPS will be tested. *De novo* peptides will be designed for the inclusion of such amino acids and their structure characterized. Studies of potential metal coordination to imidazolium bearing peptides will also be discussed.

4.2 - Results and Discussion

4.2.1 – Stability of Non-Natural Amino Acid to Trifluoracetic Acid.

Trifluoroacetic acid is a very common reagent in SPPS for the cleavage of peptides from the solid support, as well as cleave acid-labile side chain protecting groups. In order to effectively incorporate the designed amino acids into a peptide using standard SPPS procedures, their tolerance to trifluoroacetic acid needs to be tested.

Drost *et al.* have reported that attempts to cleave a Boc carbamate on an amino acid allyl palladium complex **91** using trifluoracetic acid led to decomposition (Scheme 61)[128] This highlights a potential instability of such complexes to resin cleavage conditions. However, the starting material tested in the paper contained a *N,N'*-bisbenzyl group which was shown to be less stable than the complexes containing hemilabile groups such as pyridine in processes such as column chromatography. Therefore, some of the other substituent combinations such as the bipyridyl scaffold

210 might tolerate cleavage conditions. The study of the stability and deprotection of the gold amino acids was therefore prioritized due to no instability precedent.

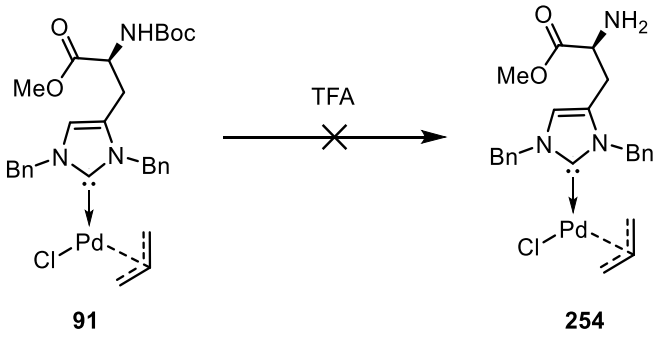

91 **254**

Scheme 61*: Deprotection of the Boc carbamate on palladium allyl complex* ***91*** *resulted in decomposition.*[128]

The stability of the imidazolium salts **180** and **146** and the gold complex **200** to trifluoroacetic acid was studied by ^{1}H NMR spectrometry. Imidazolium salts **180** and **146** allow for testing the stability of the ligand in an ester and carboxylic acid form. The tolerance of gold complex **200** to TFA allows insight into the potential of including a gold complex directly into the peptide scaffold.

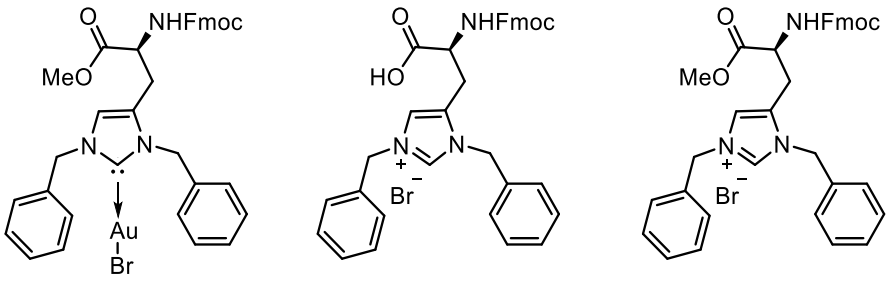

200 **180** **146**

Scheme 62: *Scaffolds used in the trifluoracetic acid stability study.*

Commonly used resin cleavage conditions use TFA in different concentrations (from 1% to 99% TFA) dependent on the resin used and side chain protecting groups.

The milder but still widely used resin cleavage conditions consist of 1% TFA in dichloromethane, thus these conditions were used a starting point. A potential issue with these conditions is that they are not compatible with the removal of side chain protecting groups of some amino acids. If the amino acids were not able to tolerate these conditions, it was unlikely that they would be able to tolerate the standard over 90% TFA type conditions. The gold complex **200** was placed in a 1% trifluoroacetic acid (6.5 equivalents compared to amino acid **200**) solution in deuterated chloroform and the ^{1}H NMR spectra monitored over time. After thirty minutes in solution there was the appearance of a new set of resonances (Figure 46). These resonances all appeared to be a duplication of a previous signals but at a lower chemical shift. The integration of all the peaks in the spectra integrated to double the number of protons in compound **200,** when the integration of the doublet of doublets corresponding to a βCH_2 proton at 2.94 ppm of the starting material was set to one. The ratio between duplicated peaks was approximately 1:1. After three days there was significant broadening of peaks, but the overall integration remained the same. Small baseline resonances appeared at in the three-day spectrum which could be due to a small level of decomposition.

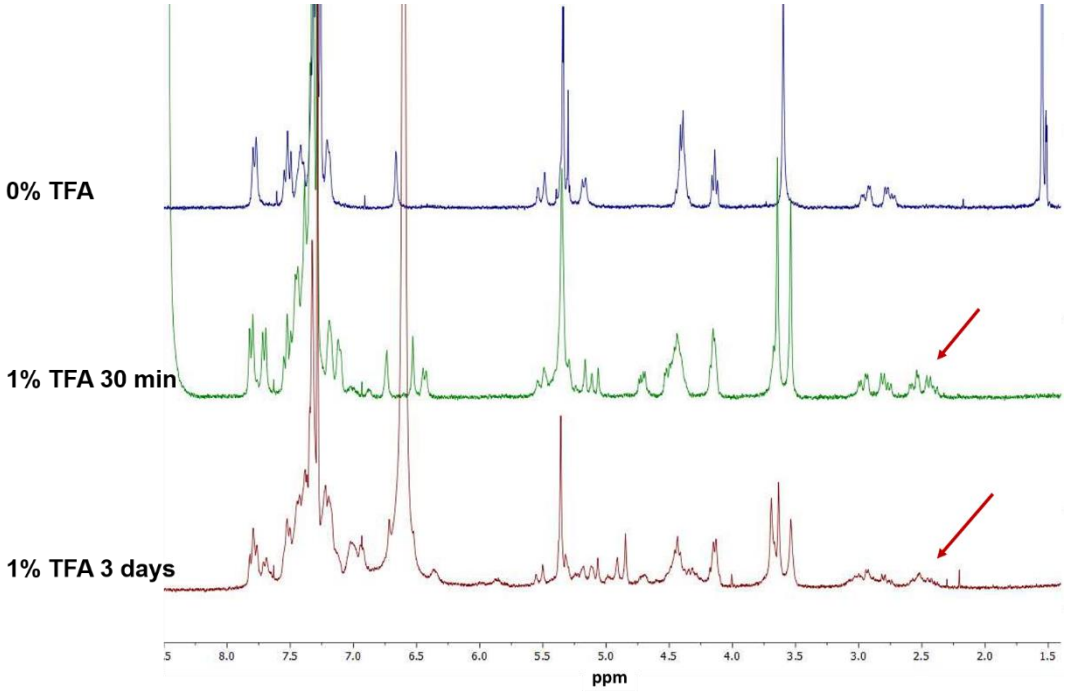

Figure 46: *^{1}H NMR (300 MHz) spectra of gold complex **200** in $CDCl_3$, and in 1% (6.5 equivalents)TFA initially over 30 minutes and after 3 days. The arrows in red highlight the new set of doublet of doublets as an example of the signals which appeared in the presence of TFA.*

The fact of the new resonances were similar to the product resonances combined with the overall integration being double of the number of expected environments for the starting material indicated that there was a new species formed that was chemically very similar to the initial gold complex **200**. Carbamates are known to cause restricted rotation around the amide bond which can lead to the formation of different rotamers.[234] Restricted rotation of different rotamers is characterized by the broadening of signals or appearance of double the number of similar peaks on the ^{1}H NMR spectra.[235] If there is no restricted rotation, the rotamers are free to interconvert faster than the NMR time scale and thus would be indistinguishable. This results in a simpler spectrum with one signal for each proton environment. When there is a restriction of this rotation the rotamers are no longer easily interchangeable and thus

the NMR experiment shows the different proton environments for each rotamer. This results in two different sets of peaks for each proton environment, one for each rotamer.

It was hypothesized that the trifluoracetic acid could be protonating different sites of the molecule which lead to restriction of rotation. Following these observations, a titration of trifluoroacetic acid into the gold complex **200** in deuterated chloroform was carried out. This would demonstrate how many equivalents are required for the formation of the new peaks and how many equivalents are necessary to achieve the 1:1 peak ratio. This would give us an indication of how many equivalents of TFA per molecule of starting material are necessary for at least 50% of the material to convert into the new peaks, potentially providing insight into protonation sites. At 0.5 equivalents of trifluoroacetic acid a broad resonance in the baseline where the new peaks are expected to appear was visible. At 1.5 equivalents the new peaks are clearly visible but lack definition (Figure 47). At 1 equivalent there is the appearance of a new resonance at 5.9 ppm which shifts downfield towards the last spectrum. These resonances integrate to one proton and supports the hypothesis of protonation occurring at 1 equivalent of TFA and causing restricted rotation. At 7 equivalents the new peaks are now at a 1:1 ratio and are much more defined (Figure 47). Twenty-four hours after the last addition the spectrum is more resolved and no signs of decomposition were observed (Figure 47).

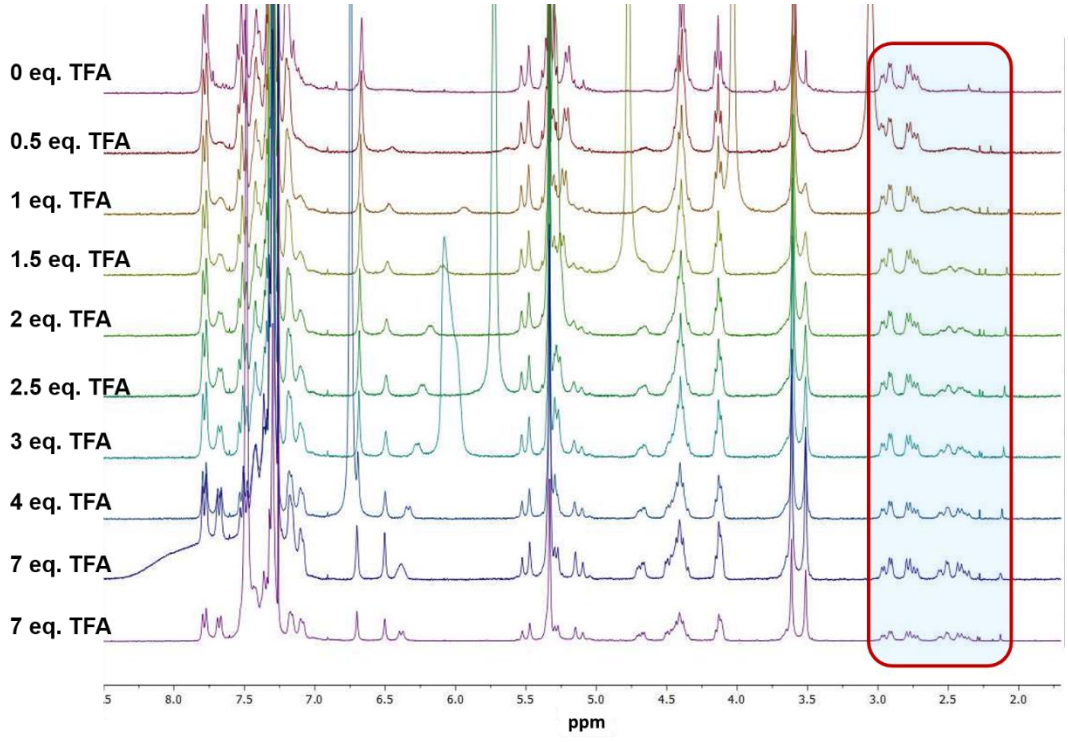

Figure 47: *^{1}H NMR (300 MHz) titration of TFA into gold amino acid **200** in $CDCl_3$. The box highlights the behaviour of the protons corresponding to the βCH_2 of the starting material and the new similar resonances which appeared at a lower chemical shift.*

At an excess of 450 equivalents of trifluoracetic acid (50% TFA in $CDCl_3$) the ratio was still 1:1, and after 3 days there were no signs of decomposition on the ^{1}H NMR spectrum.

In order to fully prove that the new peaks forming were a result of restricted rotation, a variable temperature ^{1}H NMR study was carried out.[235] If the new peaks formed in the presence of trifluoracetic acid belonged to a completely different species, increasing the temperature should not lead to any changes in the ^{1}H NMR spectra. However, if these new peaks were caused by restricted rotation, increasing the temperature should lead to firstly broadening and eventually full merging of the peaks into one set of defined peaks, as providing thermal energy can allow for free rotation to occur. The study was carried out by adding 7 equivalents of TFA to a solution of

compound **200** in deuterated trichloroethylene. The previous TFA titration showed that 7 equivalents of TFA were required to achieve a 1:1 ratio and that addition of extra equivalents did not cause any change in the ratio. Deuterated trichloroethylene was used because of its high boiling point and similar polarity to chloroform. Upon addition of the trifluoracetic acid the new peaks appeared (B, Figure 48). As the temperature increased these new peaks broadened and merged with those of the starting material ones broadening them (D to F, Figure 48). These new resonances resolved at 100 °C into a single set of well-defined peaks (G, Figure 48). This supports the hypothesis that the addition of TFA causes restricted rotation, locking rotamers into place. The mechanism of locking of rotamers for this case is unknown, I hypothesize that protonation of the amide nitrogen and/or one of the carbonyl groups of molecule, leads to the formation of hydrogen bonding interactions with one of the hydrogen bond donors present in the molecule. This interaction will favour a specific conformation locking one of the rotamers in place.

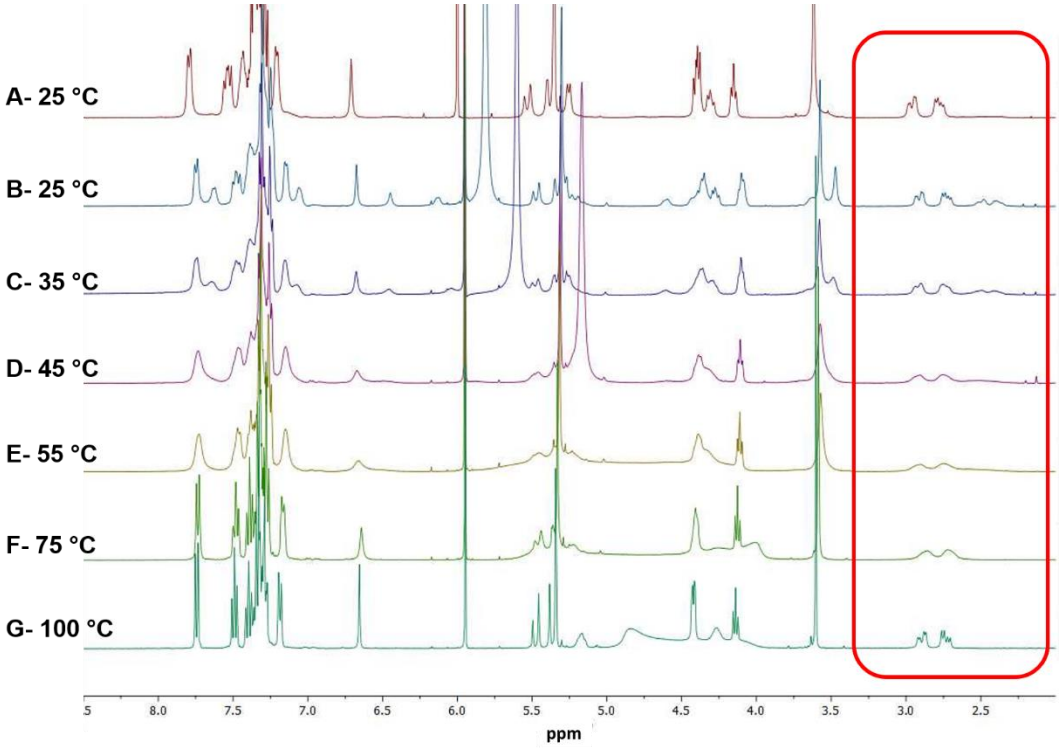

Figure 48: *Variable temperature ^{1}H NMR (400 MHZ) studies of compound **200** in the presence of trifluoroacetic acid. A) ^{1}H NMR spectrum of **200** with 0 equivalents of TFA. B-G) ^{1}H NMR spectrum of 194 with 7 equivalents of TFA at different temperatures. The red box highlights the behaviour of the βCH$_2$ protons.*

Of note is that heating compound **200** with 7 equivalents of trifluoracetic acid did not result in degradation. This combined with the previous experiments have showed that scaffold 194 can tolerate up to 450 equivalents of trifluoroacetic acid.

The stability of the corresponding imidazolium salt **180** was also tested. This ligand was to be included in a peptide scaffold via SPPS. The imidazolium salt **180** was placed in a 1% trifluoroacetic acid solution in deuterated chloroform approximately 9 equivalents trifluoracetic acid) and the ^{1}H NMR spectrum monitored over time (Figure 49). After thirty minutes in solution there was no signs of degradation however, the imidazolium peak shifted from 9.75 ppm to 8.22 ppm and there was visible broadening of other signals. This broadening was most noticeable for the case of the βCH$_2$ protons,

which change from two broad doublet of doublets into a broad singlet. After six days the spectrum was similar to the spectrum run at thirty minutes and there was no sign of decomposition or restricted rotation at 1% trifluoracetic acid.

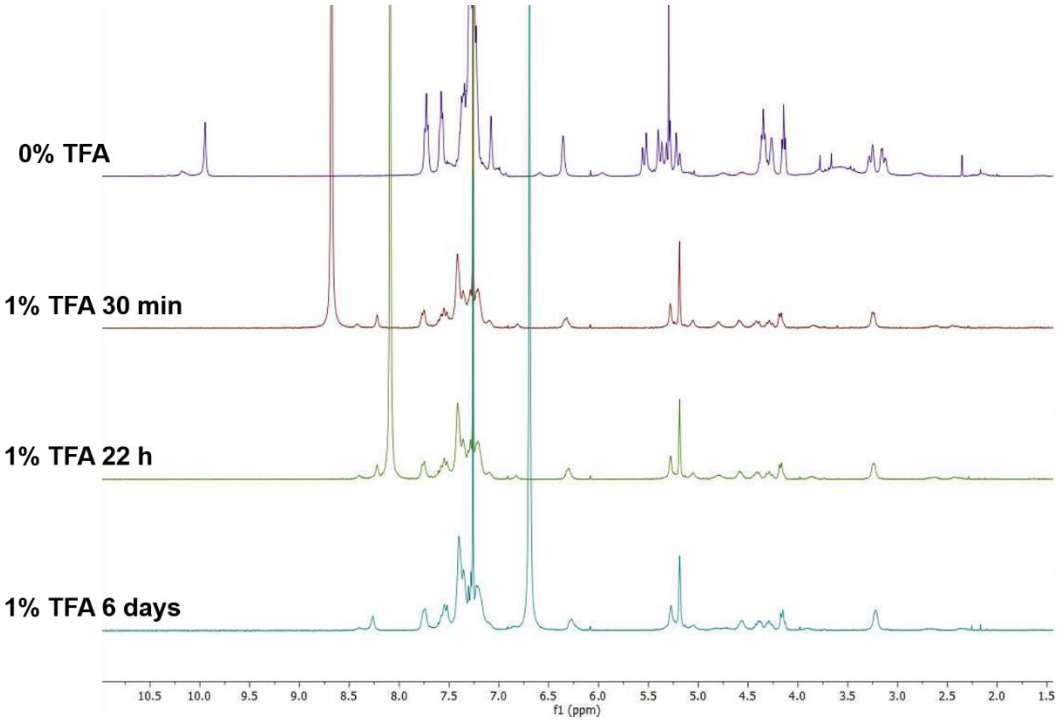

Figure 49: *^{1}H NMR (300 MHz) spectra of imidazolium salt **180** in $CDCl_3$, and in 1% TFA in $CDCl_3$ over 30 minutes, twenty-two hours and six days.*

A 4-fold excess of trifluoroacetic acid was added to imidazolium **180** and the ^{1}H NMR spectra monitored. The same shift of the imidazolium proton was observed as well as formation of new peaks which are consistent to the locking of rotamers observed for the gold complex **200**. After six days the signals had broadened but no signs of decomposition were observed (see appendix Figure 70 for spectrum).

As a last stability test for this scaffold the corresponding methyl ester **146** was dissolved in deuterated trifluoroacetic acid and the ^{1}H NMR spectra was recorded after four hours. The presence of rotamers was visible from the formation of new peaks after

thirty minutes in solution (Figure 50). After four hours the ^{1}H NMR spectrum was the same as the one obtained at thirty minutes (Figure 50). This showed that four hours in concentrated trifluoroacetic acid did not result in decomposition of scaffold **146**. The usual procedure of resin cleavage consists of only two hours in a solution of trifluoracetic acid and scavengers (19:1 ratio), and thus our study shows that our scaffolds can tolerate these harsh conditions.

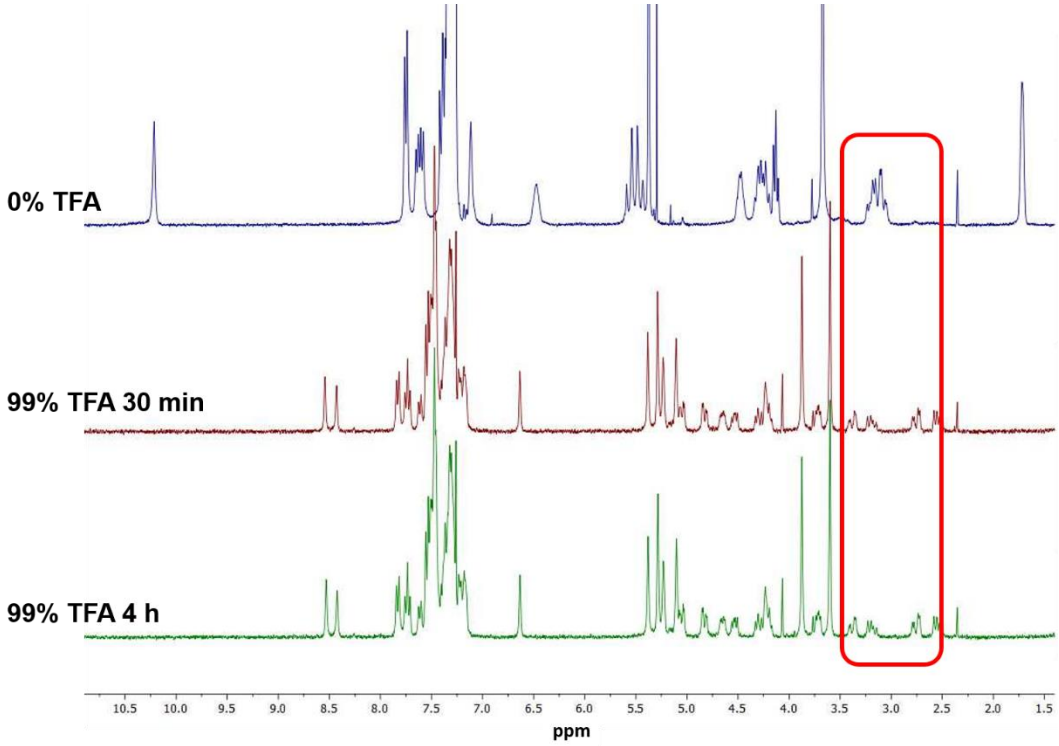

Figure 50: *^{1}H NMR (300 MHz) spectra of imidazolium salt **146** in deuterated trifluoracetic acid overtime. The red box highlights the behaviour of the βCH_2 protons.*

4.2.2 – Solid-Phase Synthesis of Test Dipeptides.

The tolerance of imidazolium **180** to coupling, deprotection and capping conditions was tested, using a mild-cleavage resin preloaded with glycine (Scheme 63). Wang resin loaded with glycine was used due its convenience, affordability and widespread use in SPPS. HATU was used as an activator and DIEA was used as the

activator base in DMF as this is one the most common SPPS procedures.[236] After two hours a Kaiser test was performed to check if the coupling (2 eq. of amino acid) had been successful.[237]. The performed Kaiser test resulted in colourless beads whilst the control was dark purple, which meant no free amine was present, and thus successful coupling had occurred. The peptide was cleaved from the resin using trifluoroacetic acid and dichloromethane in a 1:1 ratio. Attempts to precipitate the product using cold diethyl ether failed, so the trifluoracetic acid was removed under reduced pressure as an azeotrope with dichloromethane. Mass spectrometry analysis of the crude reaction mixture did not show a peak corresponding to the successful coupling, but instead an intractable mixture was observed. Most products had higher mass than glycine and a lower mass than the desired product. This combined with the Kaiser test result suggests that some coupling to the amine of the resin occurred but was potentially followed by degradation pathways yielding a complex mixture.

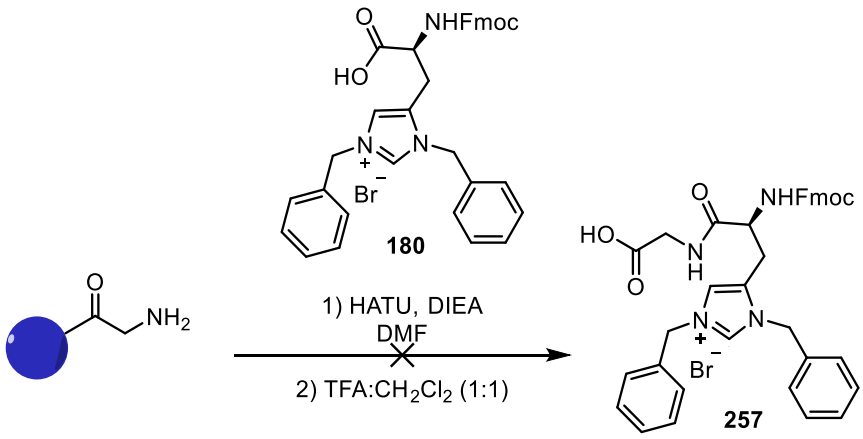

Scheme 63: *Peptide coupling attempt on glycine loaded Wang resin using HATU, DIEA in DMF, followed by resin cleavage using TFA:CH_2Cl_2 (1:1). Coupling performed on a 0.06 mmol scale.*

The coupling conditions were modified to a different combination using HBTU and HOBt in DMF, as used in the reported procedure by Shin and Bang.[130] The resin

chosen for this experiment was 2-chlorotrityl resin, pre-loaded with a glycine residue. This resin allows for mild cleavage conditions at 1% trifluoracetic acid in dichloromethane for thirty minutes, which should minimize any potential degradation from the cleavage conditions. The previous ^{1}H NMR studies demonstrated that this residue can tolerate these conditions. In order to assess if any of the stages of the complete SPPS procedures would not tolerate the new residue **180**, a new experiment was designed. After the coupling step, a third of the resin would be cleaved whilst the other two thirds would be carried forward to the Fmoc deprotection step. After the Fmoc cleavage step the resin would be split in half and one half would be cleaved and the other half would be capped with acetic anhydride. After the capping, that last portion of resin would also be cleaved. This experiment would allow for monitoring the tolerance of the residue to each step and should yield three different dipeptides (Scheme 64).

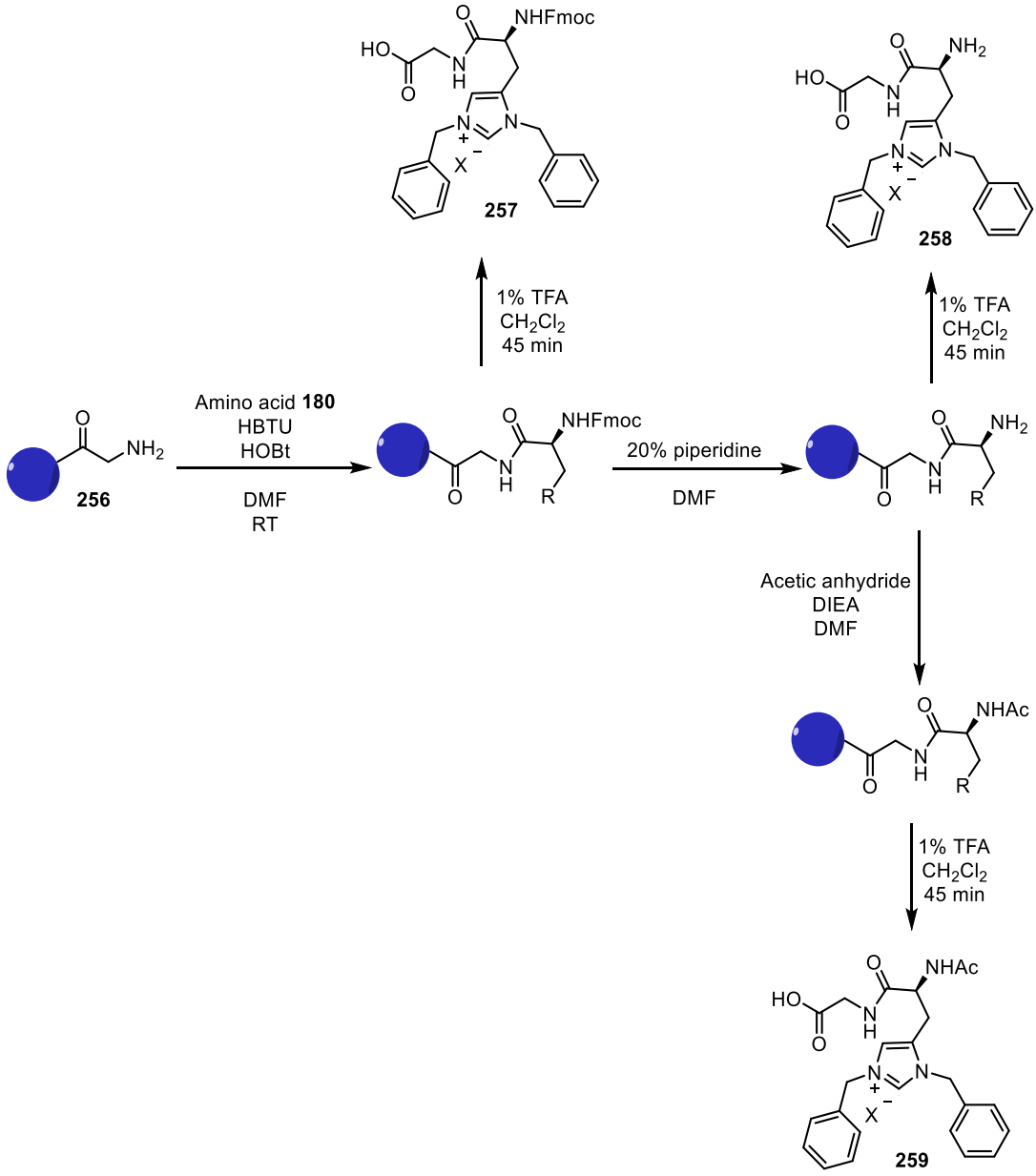

Scheme 64: *Synthesis of 3 different peptides showcasing the tolerance of building block* ***180*** *to this standard SPPS. The scale of reaction was 1 mmol of resin. After each cleavage the presence of product was confirmed by mass spectrometry and crude* ^{1}H *NMR spectra.*

The three different crude mixtures were subjected to mass spectrometry and ^{1}H NMR. This analysis showed that in all cases the desired product was formed (Scheme 64). Thus, this procedure could be applied to building block **180**.

After establishing that the ligand could be included in a peptide scaffold a similar experiment was performed, using gold complex **212**. The successful conditions employed the imidazolium salt **180** were used however, no coupling of the gold complex **212** to the glycine residue was observed, as indicated by the mass spectrum in which only glycine was visible. Therefore, the coupling conditions were altered to more reactive conditions in which DIEA was used as an activator base and PyBOP as a coupling agent.[238] The same resin splitting experiment as previously reported was used and the three different dipeptides **260**, **261** and **262** were the expected products (Scheme 65). The mass spectra of the three different crude reaction mixtures showed a peak corresponding to bisNHCAu type complexes in which both NHC ligands of this molecule were dipeptides (Scheme 65). This type of adduct is also visible in the MS spectrum of the single amino acid gold complex, even though the rest of the characterization data (such as crystal structure) shows that it is a single NHCAuX type complex. The ^{1}H NMR spectra of the crude mixture is not conclusive as which type of complex is being formed. Therefore, it remains to be explored whether the bisNHCAu complexes are an artifact of the MS experiment or if they do represent the true molecular structure. These results have shown that under the conditions applied for SPPS the gold containing amino acid is tolerated using the appropriate coupling agents. This opens a novel strategy to design and synthesize artificial gold-based metallopeptides that was previously unknown.

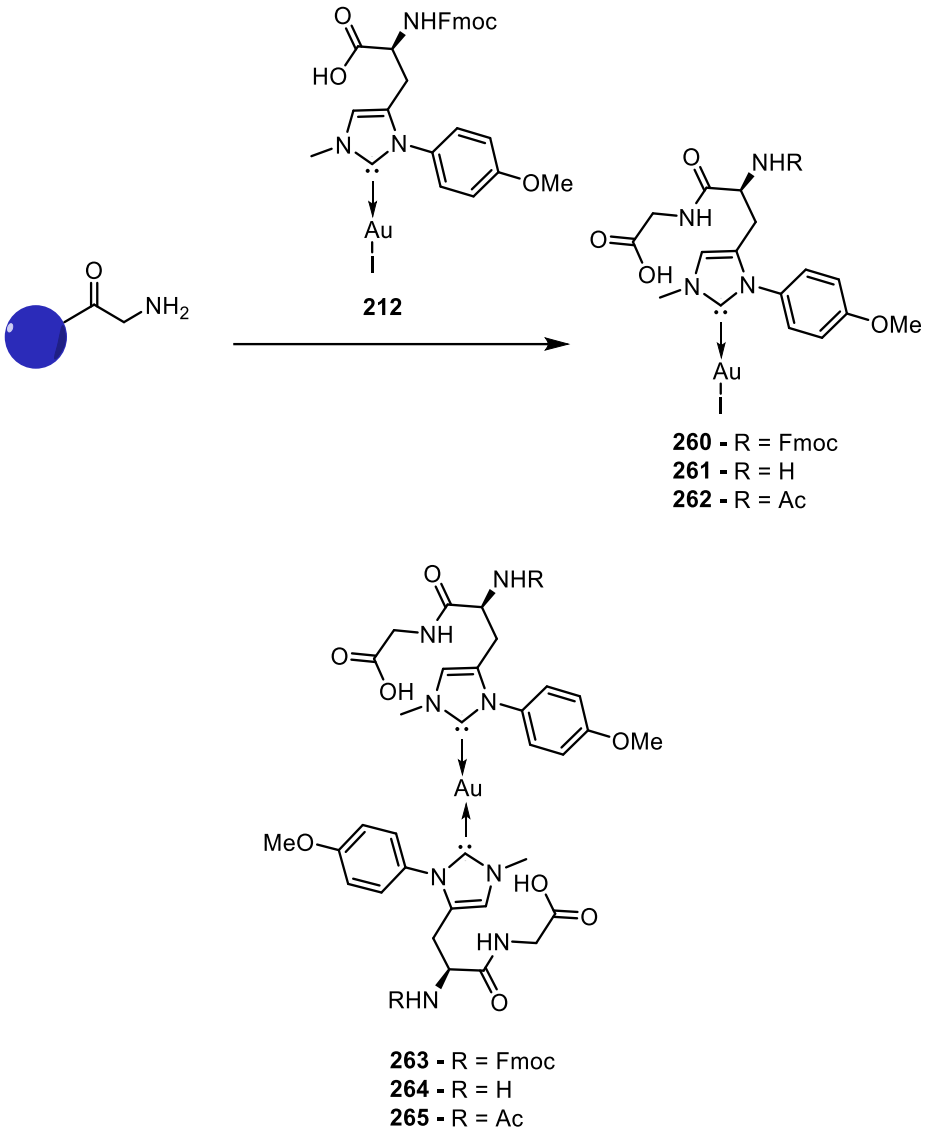

Scheme 65: *Dipeptides synthesized using gold amino acid **212** using the resin splitting method employed in Scheme 64, with PyBOP and DIEA as coupling reagents. Product formation determined by mass spectrometry (see Appendix Figure 82).*

In Chapter 2, a thiazolium amino acid was prepared and thus its compatibility with SPPS procedures was also studied. Firstly, the same conditions used for the imidazolium salt **195** were employed. As seen for the gold complex, the HBTU, HOBt conditions resulted in no coupling of the thiazolium amino acid onto the glycine. Thus, the PyBOP, DIEA conditions were used for the coupling and the resin once again was

split after each reaction. In all three cases the corresponding masses of the three desired dipeptides were visible in the MS spectra (Scheme 66).

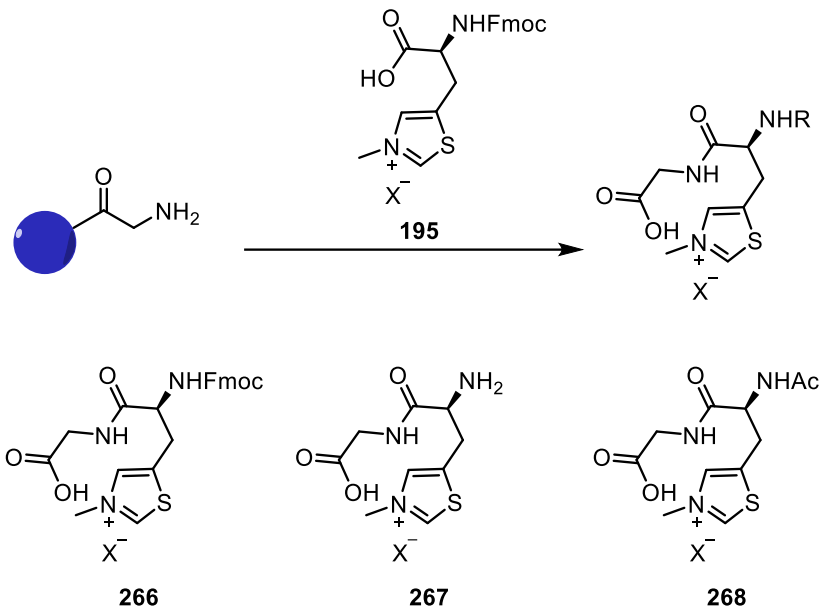

Scheme 66: *Dipeptides synthesized using a thiazolium amino acid* ***195****. Product formation determined by mass spectrometry (see Appendix Figure 83).*

The only product of the cleavage straight after the coupling was the desired dipeptide **266**. The two cleavages after the Fmoc deprotection and capping of the peptides resulted in a mixture containing a second major product. This product m/z was, in both cases, an additional 84 mass units greater than the desired product. Considering that this side product is only visible after the resin mixture was exposed to 20% piperidine in DMF deprotection conditions, and that the molecular weight of piperidine is 85.15 g mol^{-1} it was hypothesized that an addition of piperidine is involved. Under the basic conditions the carbene can be formed via deprotonation of the thiazolium, subsequent oxidative addition of piperidine can occur, as the deprotection step was performed under air (Scheme 67). These type of adducts have been previously reported.[239]

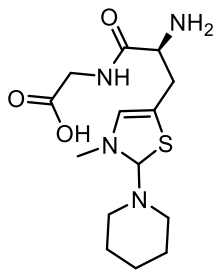

269

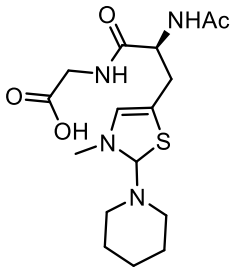

270

Scheme 67: *Side products from the SPPS procedure. These products are a result of addition of piperidine to the carbene.*

This study has identified that the thiazolium amino acid is susceptible to some unwanted reactivity during the standard SPPS employed. However, the desired products were still isolated, showing that there is no full decomposition. Literature reports suggest that for this transformation to occur a large excess of piperidine is required.[239] Thus, by diminishing the equivalents of piperidine or using different Fmoc deprotection conditions this side reaction might be avoidable. Nevertheless, inclusion of this thiazolium amino acid at the beginning of a long sequence might be challenging. If piperidine is still used for the Fmoc deprotection of the following amino acid residues, the thiazolium will be exposed to large amounts of piperidine, resulting in degradation.

4.2.3 – Incorporation of Non-Natural Amino Acid in Structured Peptides.

4.2.3.1 – Coiled Coil Design Principles

Coiled coils are a type of peptide fold in which multiple α-helices supercoil around one another. This particular type of motif is very common in nature, being present in the proteins of eukaryotic cells, as well as in some viruses.[240] Coiled coils possess a well-structured three dimension environment and have been used in enzyme mimetics before.[16, 31] The oligomeric state of a coiled coil is defined by the

number of helices coming together, the most common motifs are dimers, trimers and tetramers (Figure 51).[241,18] These assemblies can be parallel or antiparallel depending on the orientation of each strand. Coiled coils can be homo-structures in which all the helices are the same peptide sequence, or heterostructures in which different helices come together.[18]

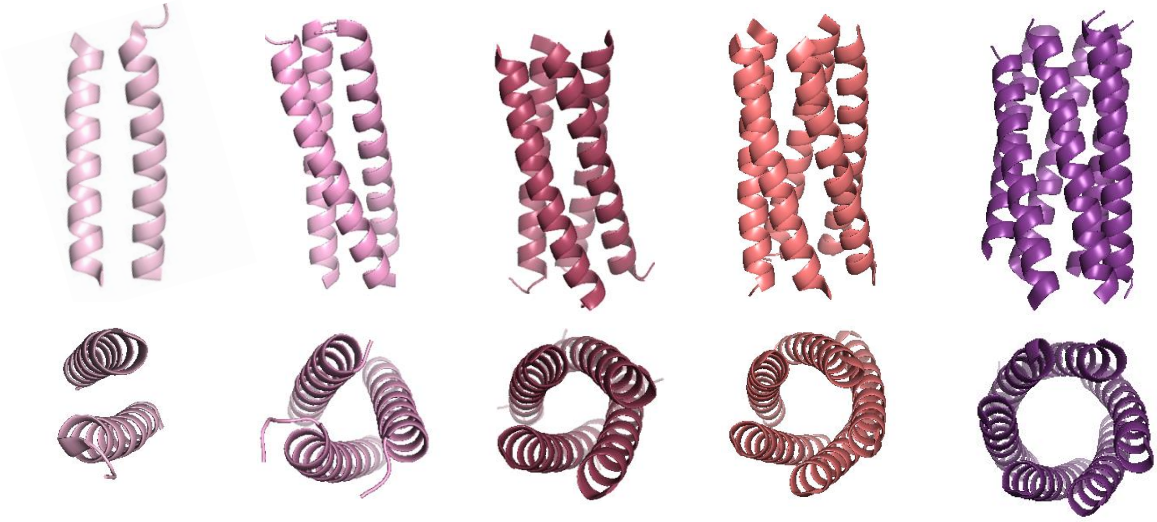

Figure 51: *Schematic representation of different oligomeric states of the coiled coils,side-on and top-down views are shown.*

α-Helices and coiled coils have well defined design rules when compared to other types of protein superstructures such as β-sheets, and thus are widely used by researchers.[230, 242-246] The design of coiled coils is based on the heptad repeat abcdefg approach, in which hydrophobic residues occupy the a and d positions in order to achieve a hydrophobic core (Figure 52). Residues in positions e and g are important in the establishment of salt bridges that promotes supercoiling.[247] Together with formation of the hydrophobic core, these interactions lead to the formation of a left-handed super-coil.[248] The folding is driven by the entropically favourable release of water molecules that were sequestered around the hydrophobic residues.[249, 250]

Typical hydrophobic core residues are leucine (Leu), isoleucine (Ile) and valine (Val).[251] The preference for aliphatic side chains, is due to the greater steric bulk of the aromatic residues. Positions b, c, e, f and g tend to be more tolerant to a variety of amino acids. Therefore, these are the main positions in which non-natural amino acids are more easily included with less chance of disrupting the superstructure. The non-covalent interactions can control the alignment of the coil in a parallel or anti-parallel fashion.

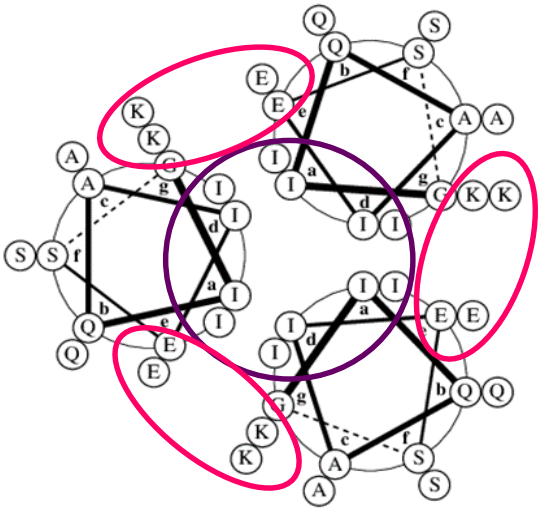

Figure 52: *Helical wheel diagram (DrawCoil) of a trimeric coiled coil. The hydrophobic core is shown in purple and salt bridge interactions between e and g are highlighted in pink.*

Glycine (Gly) and proline (Pro) are residues well known to disrupt the α-helix motif, so these residues tend to be avoided in the design of the coiled coil. Nevertheless, Gly is usually included at either terminus in order to provide some flexibility at the ends, facilitating the first coupling onto the resin.

Although several de novo metallocoiled coils have been described, most of the previous work described tends to be based on biomimetic approaches, rather than offering new function.[18]

4.2.3.2 – Design of a De Novo Coiled Coil for Ligand Incorporation

Several metallocoiled coils with applications in catalysis have been described, however, most of them make use of natural amino acid side chains for metal chelation. Sequences which contain designed metal binding sites are not ideal for including the previously described ligands because they can create competiting sites. Some of the sequences described such as CoilSer and its derivatives have complex surfaces which could lead to undesirable coordination. Therefore, a new coiled coil sequence was designed for the incorporation of the non-natural amino acids previously synthesised. For initial studies, it was necessary to select which oligomeric state would be the best model. Trimers are well described in the literature, they allow for the possibility of burying binding sites in non-solvent exposed areas (not achievable in dimers) but are simpler and better understood than higher oligomeric states.[16]

Using the heptad repeat approach a parallel trimer with five heptads was designed.[252] Stable coiled coils with a only four heptads are described however, it has been shown that when including destabilizing binding sites in the middle of the sequence an extra heptad can stabilize the superstructure.[53] The hydrophobic core was comprised of trimeric inducing isoleucine residues (position a and d), combined with a small helical inducing alanine on the c position.[253] Salt bridging was achieved by incorporating Glutamate (e position) and Lysine (g position) residues.[254] Polar residues such as Glutamine in the b position and serine (f position) enhanced aqueous solubility. On the penultimate heptad, the serine was replaced by a tryptophan for ease of concentration determination (Table 8).[255] The coiling propensity of the designed sequence was analysed using a Markov model base software called MARCOIL (Figure 53).[256] The programme evaluates the peptide or protein primary sequence predicting

helical coil structure based on a statistical evaluation of described protein structures. The AA1C sequence shows very high helical propensity between the third and the thirty fourth residue and the termini as being flexible and less structured, this is consistent with the literature reports of coiled coil structures (Figure 53).[257]

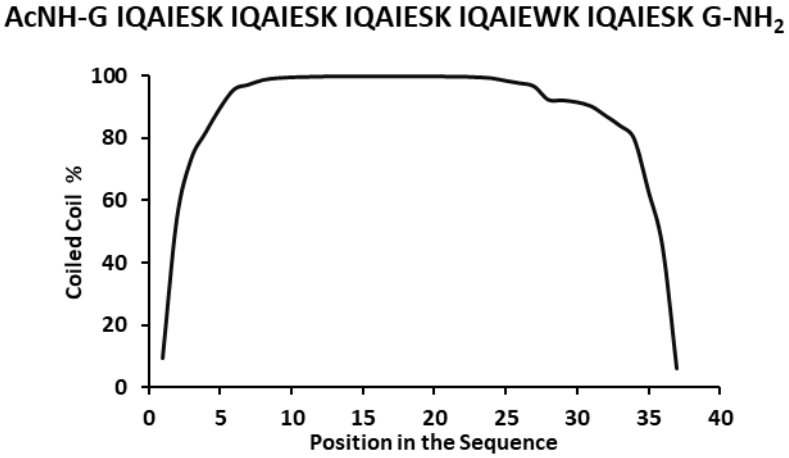

Figure 53: *Design sequence of AA1C peptide and the MARCOIL profile of AA1C which shows the coiling propensity at each residue according to their position in the sequence.*

After evaluating the propensity to the sequence to form coiled structures, a different programme LOGICOIL was used to model the oligomeric state of the AA1C sequence.[258] The output represents the probability of forming a particular oligomeric state and values within less than 0.3 of each other indicate that multiple oligomeric states might be present in equilibrium. For comparison purposes the sequence of well characterized CoilSer peptide was also analysed, this peptide is known to form trimeric species which have been characterized by X-ray crystallography.[259] AA1C sequence shows a very high probability to be a coiled coil trimer as designed, and very low probability of any of the other analysed oligomeric states (Table 6). When compared to the probabilities of CoilSer, AA1C shows a higher probability of forming a trimer, similar values of probability of being a antiparallel dimer and tetramer and a much lower

probability value of forming a parallel dimer (Table 6). This modelling data is consistent with the sequence of AA1C being likely to form a coiled coil trimer in solution (Table 6, Figure 53). However, due to the non-covalent nature of the supramolecular coiled coil assembly it is likely that other oligomeric states will still be present in solution albeit at very low concentrations.[18, 260]

Table 6: *LOGICOIL output for the oligomeric propensity of the designed sequence AA1C and the literature reported CoilSer peptide.*

Peptide	Antiparallel Dimer	Parallel Dimer	Trimer	Tetramer
AA1C	0.92	0.64	2.89	0.83
CoilSer	0.93	1.03	1.58	0.85

The AA1C peptide was successfully synthesized using automated SPPS and purified by reverse-phase preparative HPLC. The secondary structure of AA1C peptide was determined by circular dichroism which revealed a molar ellipticity minimum at 222 nm (θ_{222}) and 208 nm (θ_{208}) which are characteristic of α- helical domains.[261] Furthermore, if the ratio of $\theta_{222/}\ \theta_{208}$ is greater than one indicates formation of a superstructure such as a coiled coil.[261] In the case of AA1C the ratio of $\theta_{222/}\ \theta_{208}$ is 1.08 which combined with the circular dichroism profile is consistent with the presence of coiled coil assemblies (Figure 54).[262, 263] Using the molar ellipticity at 222 nm and the peptide concentration it is possible to calculate a percentage of the peptide that is helical in solution. At room temperature 83 ± 3% of AA1C peptide is in a helical form which suggest that the core is well structured whilst the termini remain flexible (consistent with the MARCOIL prediction, Figure 53). Heating is known to cause disruption of covalent superstructures of proteins known as the denaturing process.[264]

As the design system will be utilized in catalysis application, a thermal denaturation experiment would provide insight into a temperature range at which structural integrity is maintained. At 80 °C over 55% of AA1C peptide was in a helical form, demonstrating that the superstructure is still present at higher temperatures (Figure 54).

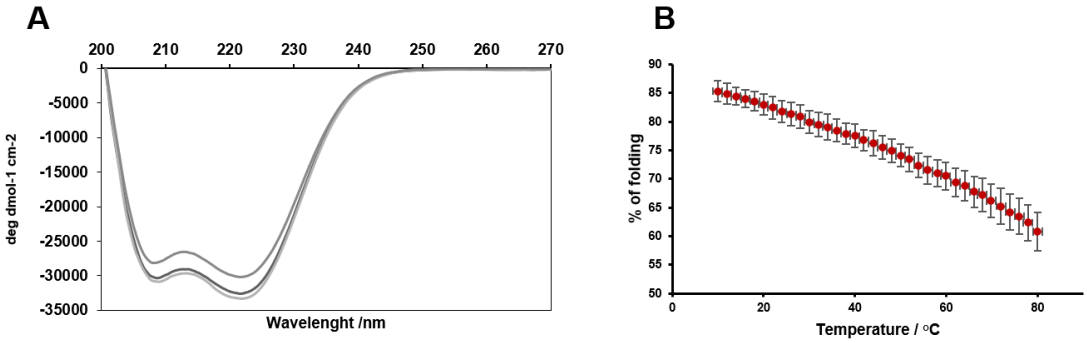

Figure 54: *A) Three repeats of the CD profile of AA1C peptide on a 90 μM peptide and 10 mM HEPES buffer (pH 7.0) sample; B) thermal unfolding of a sample of peptide AA1C; measure by CD spectroscopy on a 90 μM peptide and 100 mM HEPES buffer (pH 7.0) sample. Error bars represent the standard deviation of two repeats.*

Intact coiled coils superstructures have been observed by mass spectrometry within the Peacock group.[265] This technique has allowed for the determination of oligomeric states of coiled coils as well as providing information about the number of metal ions bound to a coiled coil structure. The AA1C peptide was subjected to this technique by O. Daubney in which the spectra showed a five charged peak at 2473.48 amu. consistent with a trimeric assembly (Figure 55). The mass spectrum also shows the present of a two charged peak at 2061.47 amu and a three charge peak at 2747.97 amu consistent with monomer and dimer species respectively. These lower oligomeric states are the result of fragmentation from the trimer species as shown by the reported analysis of ion counts for this type of experiment.[265]

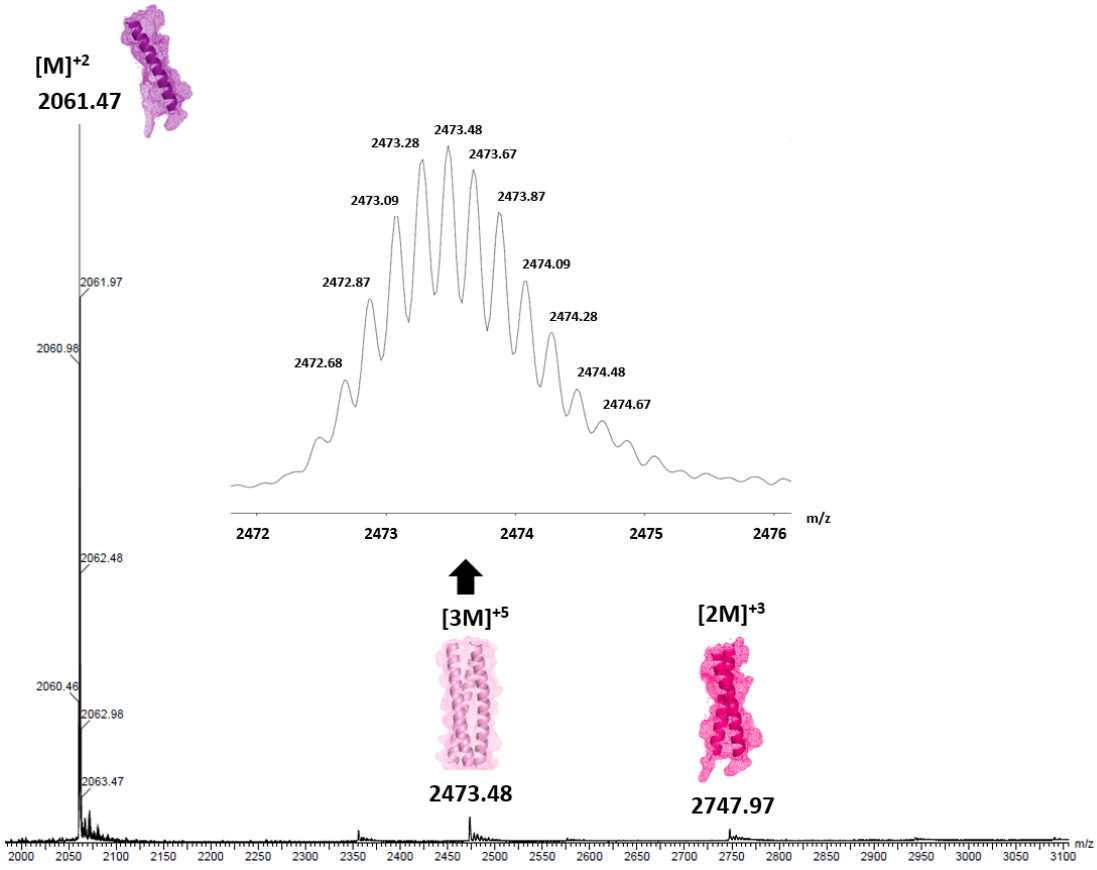

Figure 55: *Electrospray ionization mass spectrum of AA1C peptide in which M represents one single strand. Insert of a zoom of the* $[3M]^{+5}$ *peaks showcasing the isotopic pattern and charge distribution for the trimeric species.*

Analytical ultracentrifugation data was collected by S. Harding's group at the national centre for molecular hydrodynamics and is reported in Table 7. AA1C peptide data shows that the major species in solution is a trimeric species. However, there is also a small percentage of peptide present in a dimer state. This data supports the obtained results from the native mass spectrometry experiment as well as the LOGICOIL prediction for the AA1C sequence to preferentially form trimeric coiled coil structures.

Table 7: *Analytical ultracentrifugation data for peptide AA1C. Data collected by Harding's group at the national center of molecular hydrodynamics.*

Monomer molar mass	Theoretical molar mass dimer (d), trimer (t), tetramer (tet) (kDa)	M_w, weight average molar mass over the whole distribution (kDa) +/- 5%	Oligomeric state
4119	t 12.36 d 8.2	11.0	Trimer (with some dimer)

Determining if a coiled coil is parallel or antiparallel can be challenging, the most common method is by crystal structure. However, examples where the solid state showed an anti-parallel structure, whilst solution state studies showed a parallel assembly, are reported.[266] This reinforced that solid state is not always representative of solution state especially when non-covalent bonding is involved. From the data collected it is not possible to determine if AA1C forms a parallel or antiparallel coiled coil. Nevertheless, the sequence design suggests it is likely to be a parallel assembly.

4.2.3.3 – Inclusion of Non-Natural Amino Acid in the AA1 System

The AA1C peptide was successfully prepared and its characterization has shown that it is a well-structured, moderately thermal stable peptide coiled coil. Thus, the ability to incorporate our ligands in this system was explored.

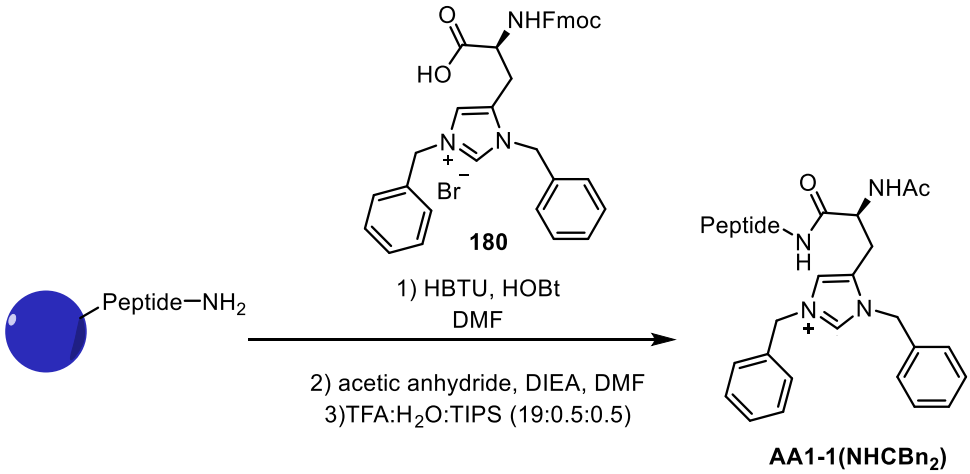

Peptide = $(IQAIESK)_3$ IQAIEWK IQAIESK G

Scheme 68: *Manual coupling of the amino acid **180** to complete the synthesis of peptide AA1-1(NHCBn$_2$) via SPPS.*

The amino acid **180** was included at the 1 position of the sequence replacing the glycine at the *N*-terminus (Table 8). This position was chosen because it was the least likely to cause structural disruption and did not involve any subsequent couplings. This would test the compatibility of residue **180** with complex peptide sequences whilst minimizing exposure to excess coupling agents in the first instance. The peptide AA1-1(NHCBn$_2$) was successfully synthesized by manually coupling the residue onto the resin using the previously established conditions with HBTU and HOBt. The coupling had a low efficiency (~50%) as determined by preparative HPLC when monitored at 210 and 280 nm. The presence of the non-coupled peptide made purification very difficult. The incorporation of the amino acid was confirmed by mass spectrometry and ^{1}H NMR spectra of pure sample (*see* appendix 7.3). At 9.09 ppm a new peak correspondent to the imidazolium proton appeared, as well as a peak at 5.40 ppm correspondent to the benzylic CH_2 protons. An extra 11 protons were present in the aromatic region (Figure 56). The α and β protons from the amino acid chain were not

visible as this was indistinguishable from other resonances belonging to all the other amino acid in the sequence. Of note is that the anion of the imidazolium salt is unknown. Due to the large quantities of TFA used during the resin cleavage procedure it is likely that a counterion exchange occurred and thus trifluoroacetate could be the anion.

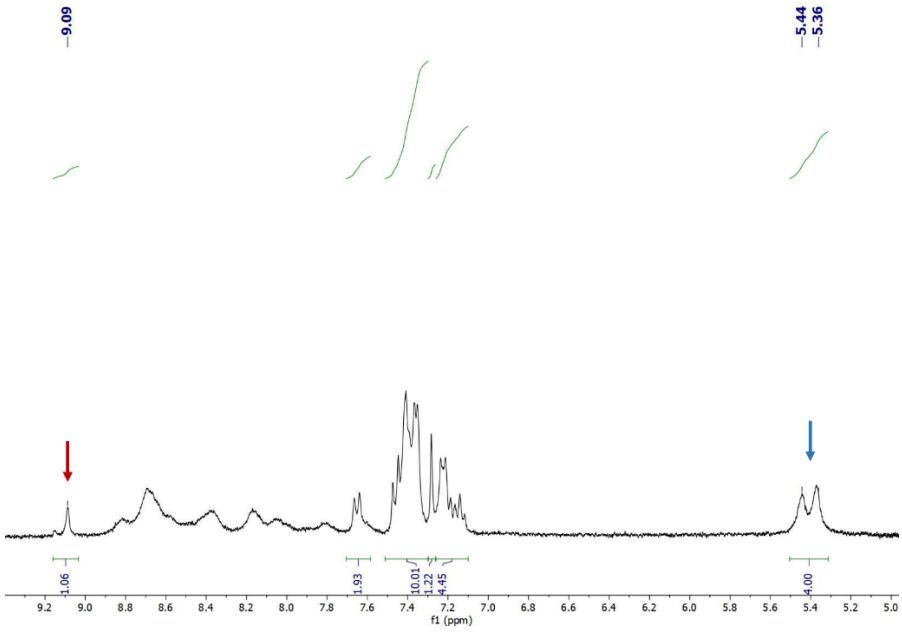

Figure 56: *Zoom of the aromatic region of the ^{1}H NMR (300 MHz)spectra of pure AA1-1(NHCBn$_2$) in D_2O, referenced to 1,4-dioxane. Arrow in red indicates the imidazolium proton and arrow in blue indicates the benzylic CH_2 protons of the imidazolium salt residue.*

The circular dichroism data showed that AA1-1(NHCBn$_2$) peptide has a $\theta_{222}/\theta_{208}$ ratio of 1.12 which shows the presence of coiled coil assemblies. Using the peptide concentration and molar ellipticity at 222 nm the calculated percentage of peptide in a helical structure was 73 ± 2% (Figure 57). As expected, the placement of the amino acid **180** at position 1 had little impact on the ability to form a coiled coil, because there is flexibility at the top of the helices and the middle three heptads are the most important for structure.[256] However, there is a 10% drop in the percentage of helical

structure when compared with the peptide AA1C which shows that not surprisingly the bulky residue **180** destabilizes the end termini more than a glycine residue. This could be due to the hydrophobic benzylic side chains wanting to be in a less solvent exposed position thus trying to accommodate in the core causing disruption of the first heptad.

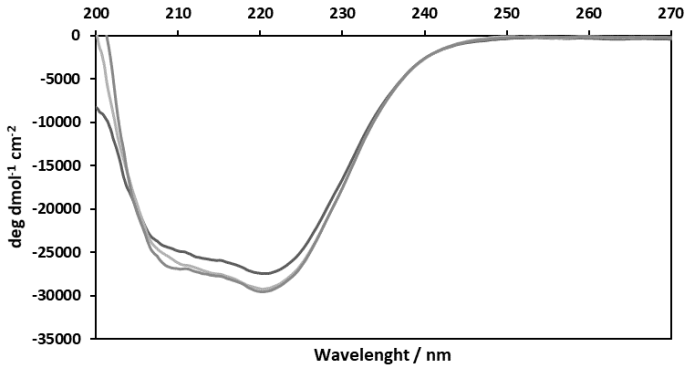

Figure 57: *Three independent repeats of the CD profile of AA1-1(NHCBn$_2$) peptide on a 90 μM peptide and 10 mM HEPES buffer (pH 7.0) sample*

The AA1-1(NHCBn$_2$) peptide was subjected to the native mass spectrometry technique which showed a seven charged peak at 1878.92 amu correspondent to the trimeric assembly (Figure 58). Confirming the oligomeric state of this coiled coil featuring residue **180**, as a trimer. As seen for AA1C spectra, the monomer and dimer species resulting from trimer dissociation under the ionization conditions were also observed.

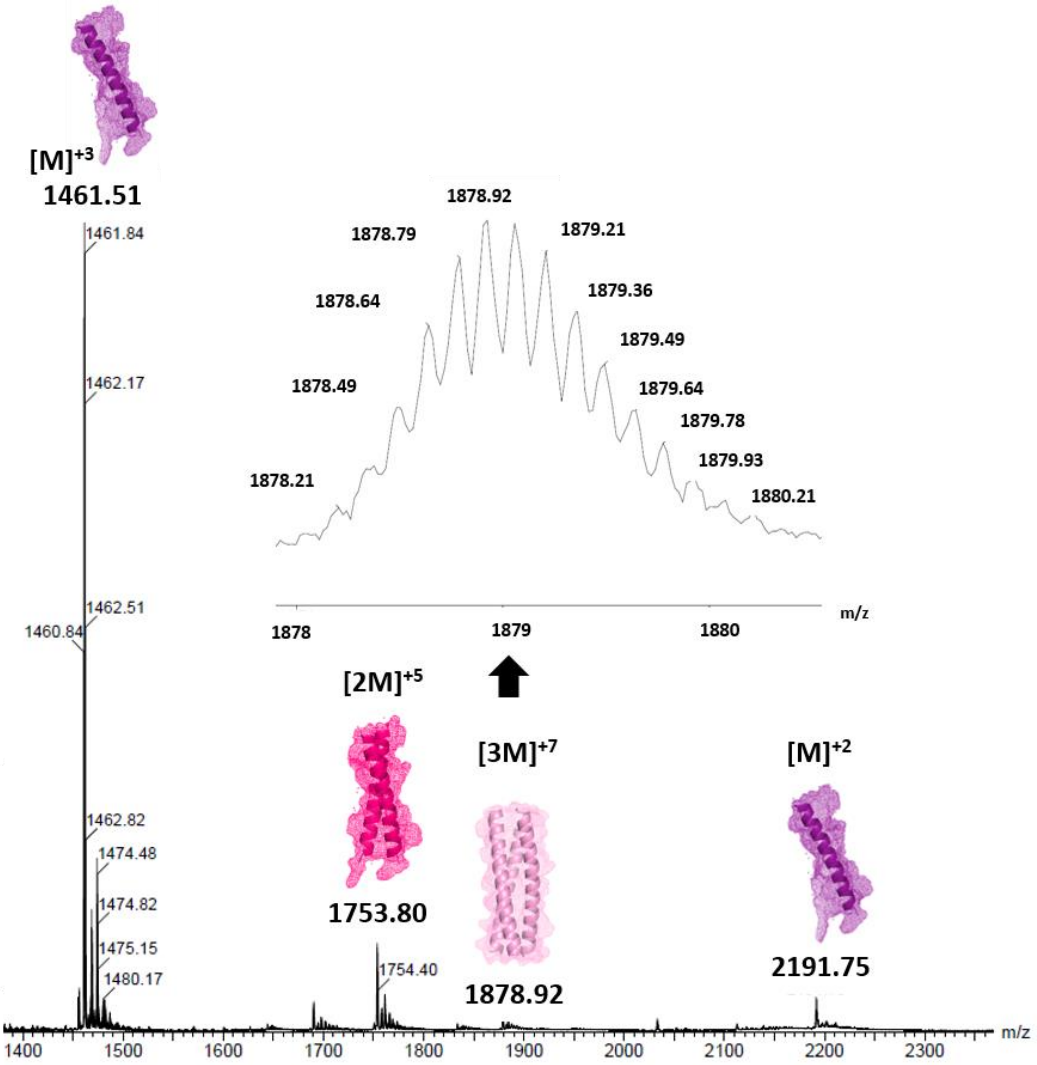

Figure 58: *Electrospray ionization mass spectrum of AA1-1(NHCBn$_2$) peptide in which M represents one single strand. Insert of a zoom of the [3M]$^{+7}$ peaks showcasing the isotopic pattern and charge distribution for the trimeric species.*

In order to explore if other NHC side chains could be tolerated at that position, the unsymmetrical amino acid **189** was coupled at the same position 1, yielding the peptide AA1-1(NHCMe/pOMe) (Scheme 69, Table 8). Of note is the higher efficiency of coupling for this amino acid as no uncoupled side product was visible in the MS spectra or in the preparative HPLC. The absence of this side product greatly facilitated the purification process.

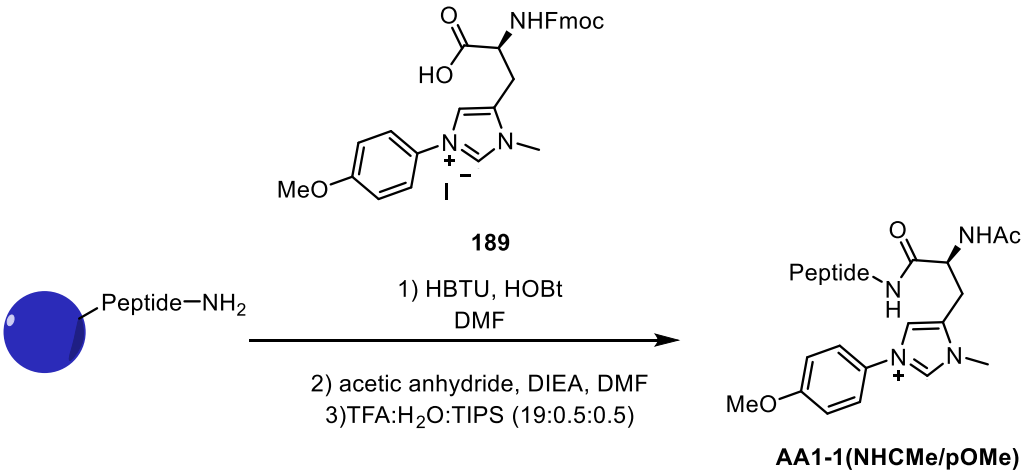

Peptide = $(IQAIESK)_3$ IQAIEWK IQAIESK G

Scheme 69: *Manual coupling of the amino acid* ***189*** *to complete the synthesis of peptide AA1-1(NHCBn$_2$) via SPPS.*

The 1H NMR spectrum of this peptide was obtained following deuteration process, in which the peptide NH resonances are not visible. The imidazolium proton integration is not reliable as this proton is also exchangeable with deuterium.[267] The ^{1}H NMR spectra showed the appearance of the characteristic imidazolium peak at 9.08 ppm and an extra five aromatic protons correspondent to residue **189** side chain (Figure 59).

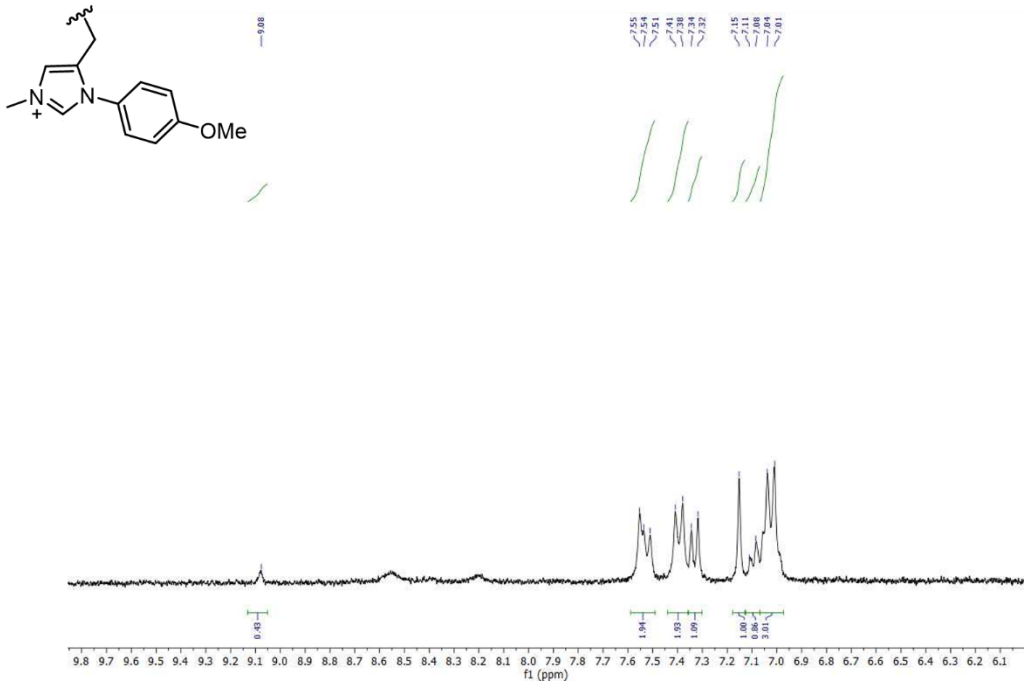

Figure 59: *Zoom of the aromatic region of the ^{1}H NMR (300 MHz) spectra of AA1-1(NHCMe/pMeO) in D_2O referenced to dioxane. The imidazolium side chain in shown in the picture.*

Circular dichroism analysis of peptide AA1-1(NHCMe/pMeO) showed a coiled coil profile with a $\theta_{222/}$ θ_{208} ratio of 1.09 consistent with the formation of a coiled coil assembly. Analysis of the molar ellipticity at 222 nm and peptide concentration showed that 49 ± 3% of the peptide is in an organized helical form. This value is significantly less than the AA1-1($NHCBn_2$) peptide showing that the side chain of amino acid **189** has a larger structural impact than its benzylic counterpart **180**. Crystal structures of well-known imidazolium ligands such as IPr **271** have shown that the aryl rings are on a perpendicular position to the plain of the imidazolium ring (Scheme 70). Thus, the para-methoxyphenyl ring on amino acid **189** could adopt a similar perpendicular conformation which is more sterically demanding than the benzyl side chains which have full freedom of rotation on the methylene bridge (Scheme 70). The oligomeric state of peptide AA1-1(NHCMe/pMeO) was not determined. However, due to less than

50% of the peptide being helical, the peptide in solution is likely to be a mixture of helical structures in different oligomeric states as well as other less organized peptide structures.

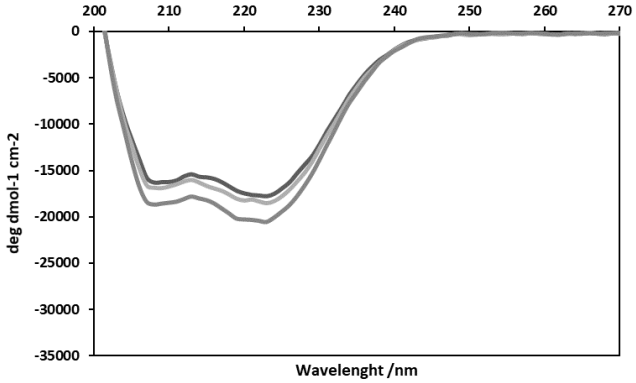

Figure 60: *Three independent repeats of the CD profile of AA1-1(NHCMe/pMeO) peptide on a 90 μM peptide and 10 mM HEPES buffer (pH 7.0) sample.*

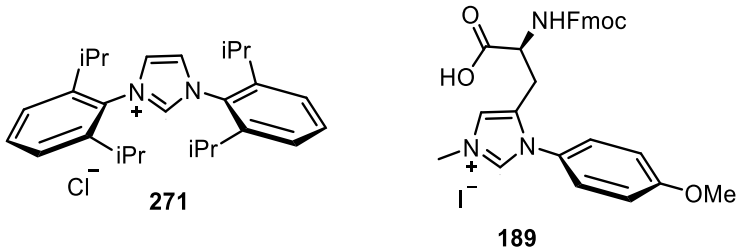

Scheme 70: *Conformation scheme of IPr ligand **271** and proposed conformation of aryl ring in amino acid **189**.*

As inclusion at the termini of the coil was well established for two different side chains, the ability to include these types of residues in the middle of a complex sequence was studied. The amino acid **180** was introduced at position 19 of the AA1C sequence replacing a serine residue (Table 8). Position 19 corresponds to an f position of the third heptad, which is known to be solvent exposed and tolerant of the inclusion of larger residues.[18] The first sixteen amino acids were coupled to the resin using microwave assisted automated SPPS. The sixteenth residue was manually

deprotected and the amino acid **180** was manually coupled as well as the subsequent glutamate. By manually coupling these residues fewer equivalents of the amino acid were required than for automated synthesiser (5 equivalents instead of 10) and the success of the coupling could be established directly. After the glutamate, the completion of the sequence was carried out using microwave assisted automated SPPS (Scheme 71).

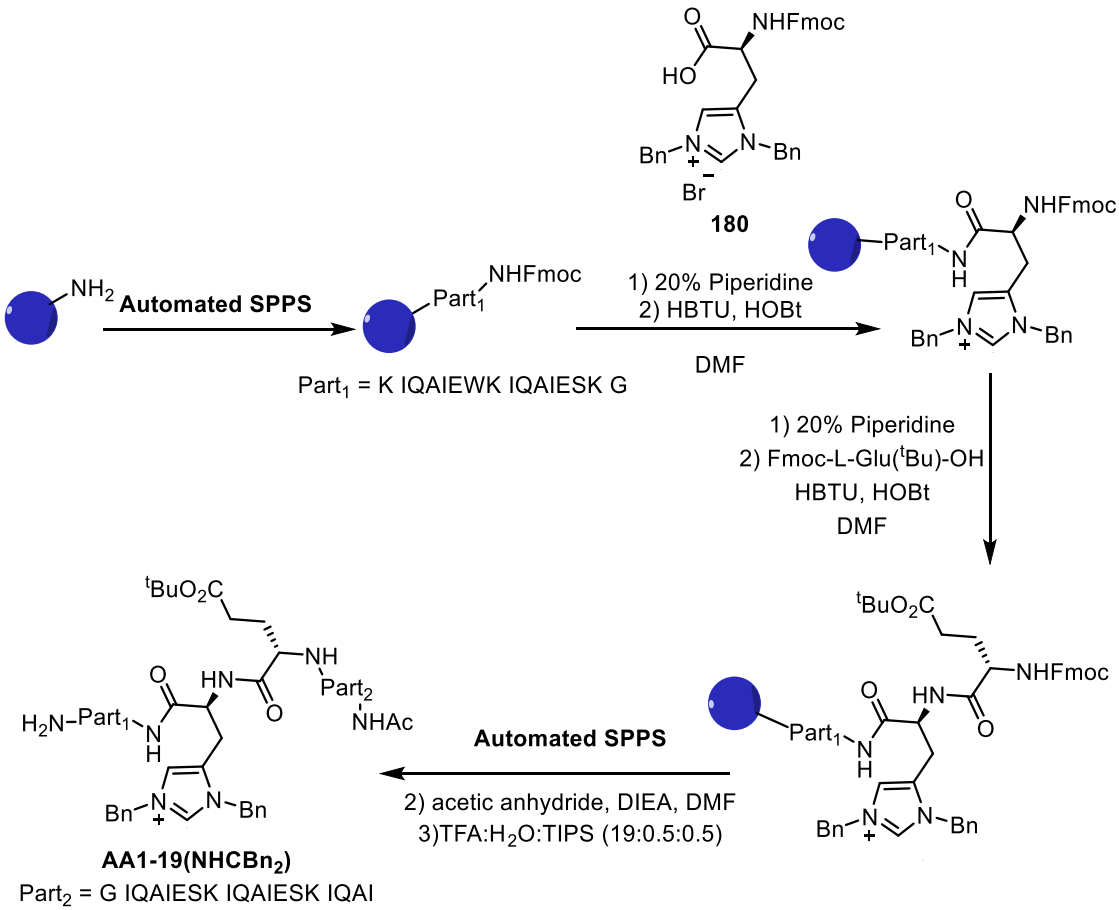

Scheme 71: *Synthetic route of peptide AA1-19(NHCBn$_2$), first part sequence was made via microwave assisted automated SPPS, manual deprotection and manual coupling of amino acid **180** and the subsequent glutamate residue, followed by the part 2 of the sequence via microwave assisted automated SPPS.*

The peptide AA1-19($NHCBn_2$) was successfully isolated as evidenced by the presence of the correct mass in the mass spectrum and ^1H NMR spectrum which shows the resonances at 8.43 ppm characteristic of the imidazolium NCHN protons (*see* appendix Figure 71). These findings demonstrate the tolerance of residue **180** to microwave irradiation, inclusion in the middle of a complex sequence and being coupled to residues such as lysine and glutamate which have reactive side chains. A large amount of the non-coupled product was present in the crude reaction mixture, highlighting the lower coupling efficiency for this particular residue **180** when compared to residue **189**.

Circular dichroism analysis of peptide AA1-19($NHCBn_2$) showed a coiled coil profile with a $\theta_{222/}\ \theta_{208}$ ratio of 1.03 consistent with the formation of a coiled coil assembly. Analysis of the molar ellipticity at 222 nm and peptide concentration showed that 62 ± 1% of the peptide is in an organized helical form. This percentage is lower than the one for peptide AA1-1($NHCBn_2$) and AA1C, however is 13% higher than AA1-1(NHCMe/pMeO). This highlights that residue **180** is less steric demanding on the structure even in the middle of the sequence than residue **189** at the top positions. Position 19 is a f position of a heptad as is known to be very tolerant of larger residues, however it is still encouraging to see that two benzylic side chains on an imidazolium are well tolerated. Unfortunately, we were not able to collect any information regarding the oligomeric state of this peptide at the time of submission of this thesis.

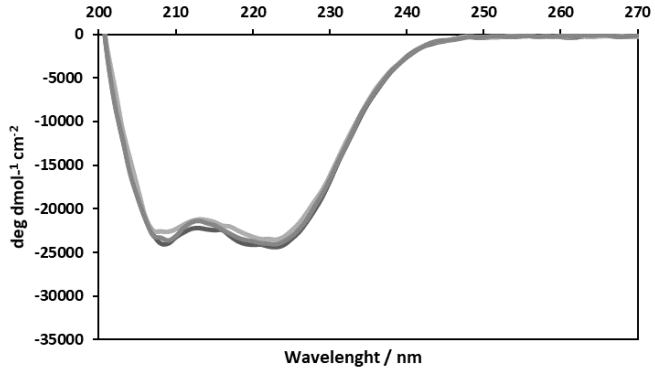

Figure 61: *Three independent repeats of the CD profile of AA1-19(NHCBn$_2$) peptide on a 90 μM peptide and 10 mM HEPES buffer (pH 7.0) sample.*

In total four new peptide sequences which form supramolecular assemblies of helices were successfully synthesized (Table 8). Three of these sequences contained non-natural amino acids, which have for the first time been successfully incorporated into structured peptides.

Table 8: *Sequences of synthesized peptides in which the numbers **180** and **189** represent the non-natural amino acids included.*

Peptide	Sequence
AA1C	AcNH G (IQAIESK)$_3$ IQAIEWK IQAIESK G NH_2
AA1-1(NHCBn$_2$)	AcNH **180** (IQAIESK)$_3$ IQAIEWK IQAIESK G NH_2
AA1-1(NHCMe/pMeO)	AcNH **189**(IQAIESK)$_3$ IQAIEWK IQAIESK G NH_2
AA1-19(NHCBn$_2$)	AcNH G (IQAIESK) IQAIE**180**K IQAIWK IQAIESK G NH_2

4.2.3.4 – Inclusion of Non-Natural Amino Acid in the AA2 System

Coiled coils are large peptide assemblies which are soluble in water or mixture of water and highly polar systems such as methanol and acetonitrile. A peptide scaffold which was smaller and more soluble in less polar solvents would allow for a comparison study and to access reactions and substrates that might not be available in aqueous environments. β-Turns have been used successfully in catalysis.[268] The Gilbertson group reported the use of non-natural phosphine amino acids in a β-turn motif for asymmetric palladium-catalysed addition to cyclic allyl acetates and in the desymmetrization of 2,4-cyclopentenediol.[25, 80, 81] These studies revealed that a small peptide with defined secondary structure could provide a chiral environment to achieve asymmetric catalysis.

A β-turn inducing sequence, was designed to incorporate the non-natural amino acid residues previously synthesized. The sequence was comprised of six amino acids with a proline and a D-Alanine residue inducing the turn motif.[***19***] Phenylalanine and tyrosine residues were introduced for their π-stacking interactions, and an alanine residue was placed at the C-terminus due to being the smallest chiral amino acid. The final sequence for the β-turn was Ac-Tyr-XX-Pro-$_D$Ala-Phe-Ala-NH_2 in which XX represents the site of inclusion of the non-natural amino acid. This placement of the catalytic residue was shown to result in the best enantiomeric excess in the Gilbertson studies.[25, 80, 81]

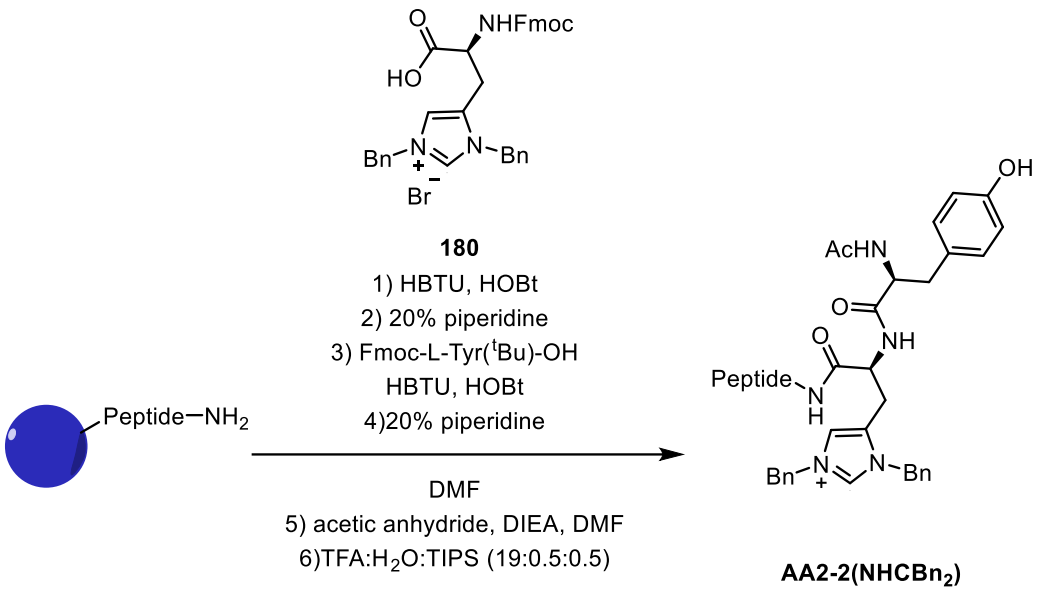

Scheme 72: *Synthesis of peptide AA2-2(NHCBn$_2$), represented are the conditions of manual coupling of the amino acid180 and the subsequent tyrosine residue. The peptide was then capped and cleaved of the resin to yield peptide AA2-2(NHCBn$_2$).*

The peptide AA2-2(NHCBn$_2$) was successfully synthesized, the first four amino acids were coupled using microwave assisted automated SPPS, and residue 180 and subsequent tyrosine residue were coupled manually (Scheme 72). The ^{1}H NMR spectrum of this peptide showed the characteristic resonances at 8.81 ppm correspondent to the imidazolium proton and, and at 5.19 and 5.21 ppm two resonances corresponding to the benzylic CH$_2$ protons.

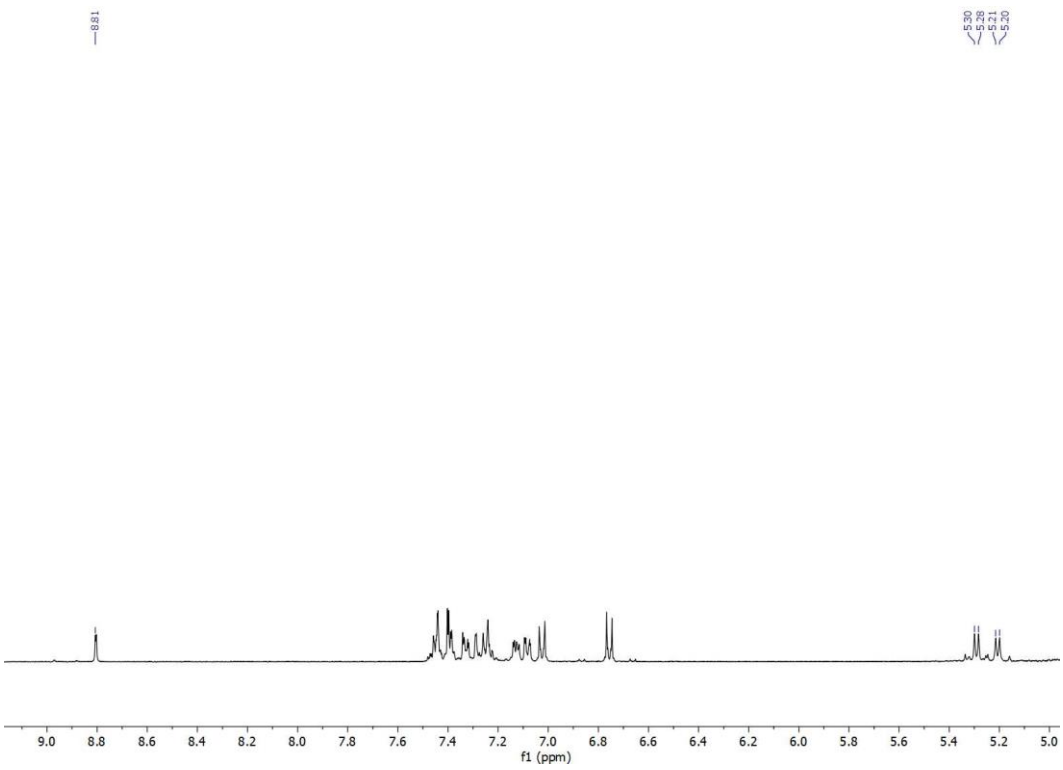

Figure 62: *Zoom of the aromatic region of the ^{1}H NMR (400 MHz) spectra of AA2-2(NHCBn$_2$) in D_2O, referenced to dioxane.*

The secondary structure of peptide AA2-2(NHCBn$_2$) was analysed using circular dichroism (Figure 63). This peptide did not show a β-turn profile as expected from the design, or any other recognizable protein secondary structure. β-turns and sheets are known to be harder to design than helical structures.[230] A redesign would be required in order to obtain a β-turn with residue **180**, which would potentially include an extension of the sequence in order to have other residues stabilize the secondary structure.

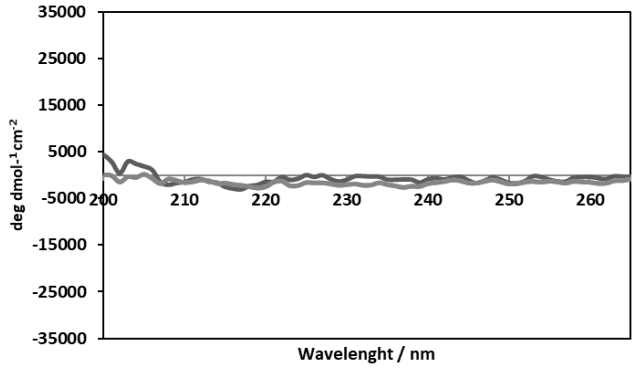

Figure 63: *Three repeats of the CD profile of AA2-2(NHCBn$_2$) peptide on a 90 μM peptide and 10 mM HEPES buffer (pH 7.0) sample.*

4.2.4 – Studies of Metal Coordination

Having prepared a series of peptides containing imidazolium ligands, the ability to coordinate metals to form catalytic species was studied. In order to determine if the metal complex was forming, ^{1}H NMR spectroscopy and mass spectrometry were used. Upon formation of the metal complex the resonance corresponding to the imidazolium proton should disappear as well as the resonance corresponding to the imidazole NCHCN proton should shift in the ^{1}H NMR spectra. Of note is the fact that the imidazolium proton can be exchanged with deuterium.[267] Due to the solubility of the peptide, the NMR spectra was run in D_2O which can lead to proton exchange and thus, a change in integration or disappearance of the imidazolium proton is not sufficient evidence of coordination. The MS spectra should report a mass of the peptide minus a proton and plus a metal atom.

As a starting point $KAuCl_4$ was titrated into a solution of AA1-1(NHCBn$_2$) peptide in D_2O and monitored by ^{1}H NMR spectrometry. The first data point was collected at 0.3 eq of $KAuCl_4$ per peptide monomer in which broadening of the aromatic region was visible (Figure 64). A second addition of 0.3 equivalents lead to disappearance of all

peptide signals from the ^{1}H NMR spectra and the formation of a precipitate was observed (Figure 64). The addition of $KAuCl_4$ salt caused aggregation of the peptide into insoluble particulates. Aggregation was further promoted by the high concentrations of peptide required for the NMR experiment.

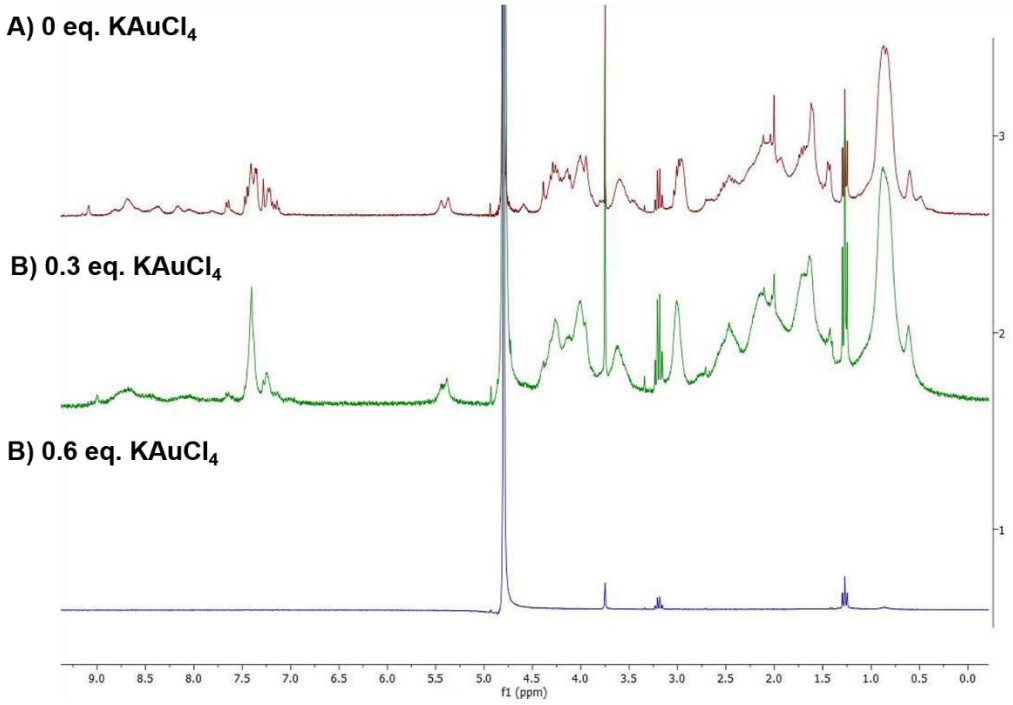

Figure 64: *The ^{1}H NMR (300 MHz) spectra for the titration of $KAuCl_4$ into a solution of peptide AA1-37(NHCBn$_2$) in D_2O referenced to 1,4-dioxane.*

Since the titration with $KAuCl_4$ did not yield any successful results, several different reaction conditions were tested in an effort to successfully form metal complexes of the peptide. A change in peptide from AA1-37(NHCBn$_2$) to AA1-1(NHCMe/pMeO) was carried out due to the coupling efficiency being higher for this NHC side chain which meant it was easier to process larger amounts of peptide than its benzyl counterpart. The conditions of gold coordination used for the small molecule amino acids were attempted, and yielded only starting material (Table 9, entry 1). The peptide showed poor solubility in acetone even at 40 °C. A change of solvent to

tetrahydrofuran and use of potassium bis(trimethylsilyl)amide (KHMDS) as a base lead to the appearance of a new resonance at 5.55 ppm as a doublet of doublets with J couplings of 5.9 and 2.0 Hz corresponding to 4 times the integration of the imidazolium proton in the ^{1}H NMR spectrum (Table 9, entry 2). This identity of this new resonance was not established but combined with no change in the aromatic region excluded this route to gold coordination. Attempts to form the palladium allyl complex through a silver transmetallation route were performed. The conditions used for the small amino acid complexes were employed however, the peptide showed no solubility in dichloromethane and all the starting material was recovered (Table 9, entry 3).

Table 9: *Reaction conditions used to attempt metal coordination to AA1-1(NHCMe/pMeO) peptide.*

Entry	Metal source	Additives	Solvent	Temperature (°C)	Time (h)
1	DMSAuCl	K_2CO_3	acetone	40	24
2	DMSAuCl	KHMDS	THF	25	2
3	1) Ag_2O 2)Pd(allyl)Cl_2	4 Å MS	CH_2Cl_2	25	18
4	Ag_2O	none	water	25	24

Reports of formation of NHC silver complexes in aqueous media suggested that coordination should occur if the water was degassed and the reaction carried out under an inert atmosphere.[269, 270] After subjecting peptide AA1-1(NHCMe/pMeO) to silver oxide in degassed water for twenty-four hours the ^{1}H NMR showed several new peaks

(Figure 65). A new peak at 10.12 ppm with an integration of 0.8 when normalized to the imidazolium peak at 9.21 ppm was observed. The starting material spectrum was obtained from a thorough deuteration process and thus the NH peaks of the peptide backbone, and the imidazolium proton are not visible. Comparing the starting material spectra with the crude reaction mixture spectrum it is noticeable that there are sixteen new proton resonances (Figure 65). Of note are the references at 10.1 and 9.20 ppm which are likely to be two different NCHN protons. The identity of these products is unknown. If a coiled coil trimer is present in solution with three NHC ligands each, coordination of the silver to one of these ligands will cause loss of symmetry in the trimer and thus some of the aromatic peaks could desymmetrize appearing now at different chemical shifts.

The MS spectra of the crude reaction mixture showed a peak at m/z 4324 corresponding to the starting material and a new peak with a m/z of 4432 corresponding to starting material plus a silver atom. Of note is that the peak corresponding of an addition of a silver atom was only visible when the samples were run without the use of an acid additive. An additive of 0.1% TFA in the acetonitrile and water solvents used to run the MS sample lead to only starting material being visible in the spectra. This silver adduct could be due to coordination to the carbene, but it could also be a salt adduct in which no dative bond was formed. A MS/MS experiment was carried out by C. Williams in which the peptide was fragmented. If the NHCAg complex had formed, it was expected to see peptide fragments which differ from the fragmentation pattern of the starting material by a silver atom. In every instance, this experiment resulted in the loss of the silver atom upon fragmentation suggesting that there was no dative bond forming. However, it is possible that the energy required to

fragment peptide was greater than that required to break the dative bond between the carbene and silver. The data collected does not conclusively demonstrate that coordination occurred.

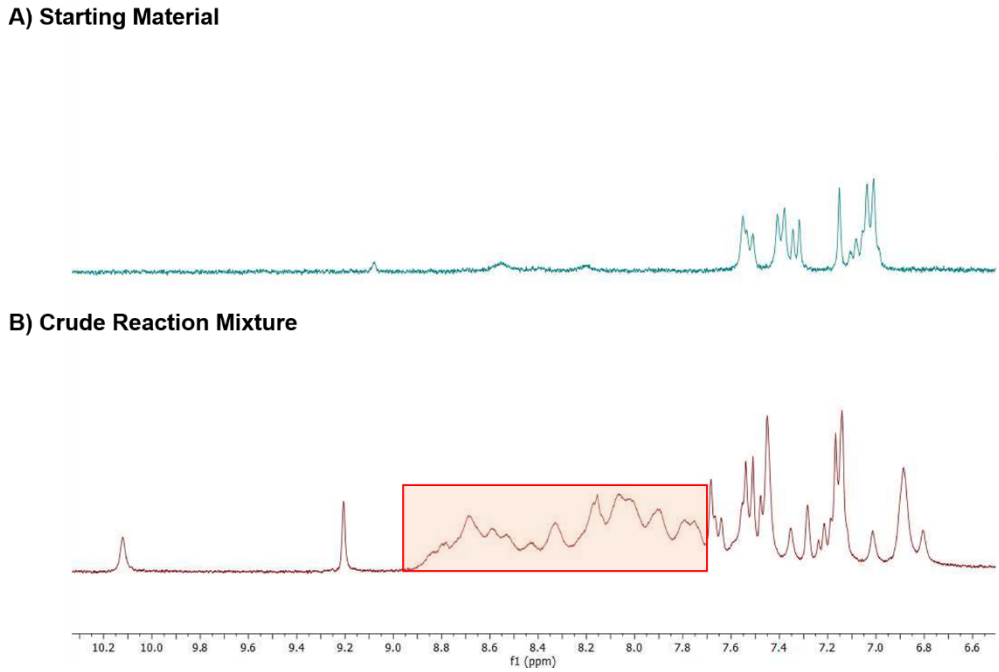

Figure 65: *A) ^{1}H NMR (300 MHz) spectra of the peptide AA1-1(NHCMe/pOMe) in D_2O, after deuteration of the peptide; B) ^{1}H NMR spectra of crude reaction mixture obtained by reacting the peptide AA1-1(NHCMe/pOMe) with silver oxide in water; the red box indicates the protons correspondent to the NH of the peptide backbone. The spectrum were referenced with 1,4-dioxane.*

4.3 – Conclusions

In this chapter, the potential to use new sets of imidazolium, thiazolium and NHCAu amino acids to design novel peptide scaffolds with potential for catalytic applications was demonstrated.

The previously synthesized imidazolium bearing amino acids **146** and **180** proved to be stable to harsh resin cleavage conditions (99% TFA) and were successfully incorporated in complex peptide sequences. The amino acid **180** showed

tolerance to be coupled to different amino acids such as proline, isoleucine and glutamate residues, which have bulky and/or reactive side chains. These were the first reports on introducing imidazolium salt amino acids in complex peptide structures in particular in coiled coil assemblies. The amino acid **180** was compatible with the removal of the Fmoc group on resin and subsequent coupling of eighteen other residues under microwave conditions.

This demonstrates that these types of scaffolds can be incorporated as ligands or as potential organocatalysts in protein supra structures, thus being a useful building block for routine use in SPPS and consequently artificial metalloenzyme synthesis.

Work towards the formation of metal complexes from the peptides bearing imidazolium salts is reported. The lack of solubility of these peptides to traditional organic solvents has invalidated the use of traditional coordination conditions. Silver oxide in water were some of the conditions which lead to significant changes in the ^{1}H NMR spectrum of the peptide and thus are a good starting point for future studies.

For the first time the structural implications, in solution, of introducing bulky imidazolium salt amino acids in coiled coil scaffolds was studied. Although inclusion of the amino acid **180** in the middle of the sequence resulted in a decrease in folding, the resulting peptide is still over 60% in a coiled coil structure.

The thiazolium amino acid **195** show tolerance to SPPS albeit seeing the formation of a side product in the Fmoc deprotection reaction. Further optimization of the deprotection conditions could lead to a viable route for incorporation of these scaffolds in highly structured peptides.

The tolerance of gold amino acid **212** to SPPS conditions demonstrates that this molecule is also a versatile building block to incorporate in protein moieties. This is the first report of a gold NHC amino acid in SPPS. Of note is the tolerance of this amino acid to high concentrations of TFA. This can open a new avenue in using peptides as gold catalysts or even peptide mediated drug delivery of gold complexes since these have been shown to possess interesting biological activity.[103, 271]

Chapter 5:

5.Conclusions and Future work

Artificial metalloenzymes are a promising way to access new catalyst reactivity and selectivity. The field of artificial metalloenzymes has received large interest from the research community in the past decades. However, most of the work is carried out on large native proteins or synthetic peptides are used to mimic native enzyme activity. There is therefore a need to investigate the use of synthetic peptides in organic chemistry transformations which are not present in nature. This work describes my efforts towards establishing the tools required to create such catalysts.

Late transition metals can allow access to reactivity not present in biology, however, the natural amino acid toolbox does not have the required ligands to bind such metals. Thus, the synthesis of amino acids bearing imidazolium and phosphorous based ligands was explored in this work.

In this work a library of novel amino acids bearing imidazolium and thiazolium functionality was prepared. These amino acids contain an Fmoc carbamate protecting group which is the state-of the art protecting group for SPPS. Prior to this work there were few reports of amino acids bearing imidazolium or metal NHC functionality and most of these reports did not include Fmoc protecting groups. This work offers routes towards the incorporation of several different substituents on the nitrogen atoms of the imidazole ring, varying from small alkyl groups such as methyl, to allyl, benzyl or mesityl groups. This vast range of functional groups allows the properties of the amino

acid side chains to be tuned, such as steric bulk and polarity. The potential scalability of this work was demonstrated by the synthesis of 7 grams of derivative **180**, in 3 steps, no column chromatography was required and the overall yield was 43%. This result suggests that these routes can be optimized to produce the large quantities of material often required for SPPS.

Novel gold and palladium metal complexes of the imidazolium amino acids were also successfully prepared, which can have applications not only in catalysis but also as potential metallo-drugs.

New routes to access amino acids bearing phosphorous ligands and metal complexes were explored. Novel Fmoc derivatives of these ligands were successfully synthesized. A two-step synthesis of a phosphinite gold complex on an amino acid backbone was reported in high yields. This opens a quick route into more amino acid-based gold complexes. The use of this route to prepare other metal complexes will be explored in future work.

The catalytic activity of the gold complexes on the regioselective hydration of alkenes was tested. Despite the low conversions obtain for some of the NHC complexes, the poor regioselectivity was comparable to the widely used gold (I) NHC catalysts (IPr and IMes). The phosphinite gold catalyst activity and regioselectivity was high and demonstrates the potential of these types of metal complexes.

The literature also lacked examples of the tolerance of imidazolium substrates to SPPS conditions. In particular demanding conditions including large quantities of trifluoracetic acid, microwave radiation and reactive or sterically demanding amino acid side chains such as proline, glutamate, lysine, or tryptophan. This work has shown that

imidazolium and thiazolium functionality was tolerated in standard SPPS conditions. Indeed this work contains the first report of an amino acid bearing a gold NHC successfully tolerating SPPS and thus providing a new route into peptide base gold catalysts.

A coiled coil structure was designed from scratch to include the novel synthesized amino acids as a test system. This work made successful use of the design principles as well as software available to predict the oligomeric state of the coiled coil. In this work is described the first-time imidazolium amino acids were included in coiled coil type scaffolds. Three different novel coiled coils were successfully accessed containing imidazolium functionality, including one example of the inclusion of the imidazolium in the centre of a 37 amino acid sequence. The quaternary structure of the novel coiled coils was analysed using circular dichroism which demonstrate that the bis-benzyl derivative **180** was tolerated better than the aryl derivative **189**.

The work carried out in this research has established the knowledge required to access diverse amino acids bearing ligands, their tolerance of SPPS conditions. The design of a coiled coil structure as a model system to test the novel building blocks has also been demonstrated. The activity of the gold amino acid complexes was tested which will serve as a benchmark of activity that will be compared to the supramolecular systems. This will allow for the nature of reactivity and activity of those complexes to be studied.

Future work will be investigating the inclusion of the gold amino acid in a coiled coil system. The activity will be characterized using the reactions previously studied for the small amino acids. This will be the first example of a gold artificial metalloenzyme.

Studies will continue regarding the use of the prepared peptide/imidazolium ligands as potential organocatalysts and their coordination to different metals such as gold and palladium.

The impact of the ligands and metal complexes on the structure of coiled coils will be studied by placing the different amino acid building blocks at different positions of the coiled coil sequence. This structural information will be helpful in future catalyst design.

The routes established for the synthesis of phosphorous based ligands will be utilized to access a library of ligands for metal coordination and catalytic activity. The tolerance of these types of ligands and metal complexes to SPPS conditions will be evaluated, to study potential routes to access different artificial metalloenzymes.

CHAPTER 6:

6.Experimental:

6.1 - General Information

Commercially available chemicals/reagents were purchased from major suppliers and used without further purification except where stated. Peptide synthesis resins and reagents (natural amino acids, coupling agents and *N,N*'-dimethyl formamide (DMF) were purchased from Pepceuticals or Cambridge Reagents Ltd. All water used in the preparation of peptide samples was ultrapure grade obtained from a Millipore-Elix-Gradient A10 system. Centrifugation of peptides was performed using an Eppendorf centrifuge 5702 with A-4-38 and rotational speed of 4400 rpm for 10 minutes. For reactions performed under inert atmosphere the glassware was pre-dried using a heat gun under high vacuum. Activation of 4 Å Linde type molecular sieves was performed by heating the sieves in heating mantel up to 300 °C under vacuum for a minimum of 5 hours, the sieves were then allowed to cool to room temperature and stored under an argon atmosphere. When dry solvents were used these were dried over activated 4 Å Linde type molecular sieves in dry glassware; in the case of tetrahydrofuran and dichloromethane were obtained from a Pure Solv-Md solvent purification system and dried further over activated 4 Å Linde type molecular sieves. Degassing of solvents was performed by either bubbling argon through the solution whilst sonicating it for a minimum of 20 minutes or in the case of tetrahydrofuran for the synthesis of phosphorous compound **227** using the freeze-thaw method. All reactions were stirred using Teflon coated magnetic stirrer bars. For reactions bellow room temperature, the following cooling baths were used: 0 °C (ice/water) -78 °C (dry ice/acetone or a Julabo

FT902 immersion cooler). For reactions above room temperature pre-heated paraffin oil baths or heating blocks on stirrer hotplates equipped with temperature controlling external probes. Reactions were monitored by thin layer chromatography (TLC) using Merk silica gel 60 F254 (aluminium support) TLC plates which were developed using standards visualising agents: UV fluorescence (254 nm), potassium permanganate/ Δ or anisaldehyde/Δ. Flash chromatography was carried out on silica gel manually unless stated otherwise. Automated flash chromatography was performed on a Teledyne CombiFlash Nextgen 300+ and 4 g columns were pre-packed from Interchim and 12 g, 24 g and 40 g columns were manually packed using Sigma 60 Å pore, with a 40-63 μM particle size silica. Polarimetry was carried out on a Bellingham and Stanley ADP450 series Peltier polarimeter (25 °C). Melting points were measured in open capillaries using Stuart scientific melting point apparatus and were uncorrected. Infra-red spectra were recorded using a Perkin-Elmer Spectrum 100 FTIR spectrometer using an ATR attachment; only selected absorbencies ($\nu_{(max)}$) are reported. NMR spectra were recorded using Bruker AVIII300 (^{1}H NMR = 300 MHz, ^{31}P NMR = 121 MHz, ^{19}F NMR = 282 MHz), AVIII400 (^{1}H NMR = 400 MHz, ^{13}C NMR = 101 MHz) or a Bruker AVANCE NEO400 (^{1}H NMR = 400 MHz, ^{13}C NMR = 101 MHz, ^{31}P NMR = 162 MHz, ^{19}F NMR = 376 MHz and ^{11}B NMR = 128 MHz) in commercially deuterated solvents with or without TMS). Chemical shifts (δ) are given in relationship to TMS and are calibrated using residual peak solvents for small molecules and for peptide samples using a 1,4-dioxane standard. ^{13}C Jmod and 2D COSY, HSQC and HMBC spectra were recorded when necessary to assist NMR assignment. Assignments were performed using a combination of chemical shift, multiplicity, 2D experiments and assignment of previous derivatives. Spectra were processed using MestReNova

software. Mass spectra of small molecules were obtained using Micromass LCT (ESI), Bruker MicrOTOF QII (ESI) and Waters Xevo-G2-XS (ESI). High resolution spectra used a lock-mass. Peptide mass spectra were obtained using Waters Xevo-G2-XS (ESI) and MS/MS and native mass spectrometry experiments obtained using a Waters Synapt G2-S spectrometer. Elemental analysis was carried out on a thermo scientific flash smart elemental analyser using a CHNS method. Analytical gas chromatography GC was performed using a Shimadzu GC-2010 gas chromatograph equipped with a flame ionization detector (H_2 carrier gas, 1 mL/min). The column used was a Zebron ZB-5 (30 meter) capillary column. The detector temperature was 300 °C with a split ratio of 100:1. Retention times (t_R) and integrations were obtained using Chromeleon software. Crystals were grown by A. Almeida. In the case of the crystals of molecules **134, 146** and **201**, the data set was collected and solved by L. Male. In the case of the structures of compounds **200**, **204**and **233** the data set was collected by A. Almeida in collaboration with L. Male and the final structure was solved by L.Male.

6.2 - Synthesis of Histidine Derivatives:

Benzyl Nα-(((9H-fluoren-9-yl)methoxy)carbonyl)-Nπ-trityl-L-histidinate ***130:***

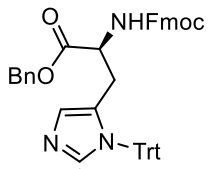

Synthesised according to literature procedure.[151] In a dried multi-neck flask under argon was added triphenylphosphine (0.840 g, 3.20 mmol) and dry THF (10.0 mL). The mixture was cooled down to 0 ºC and DIAD (0.330 mL, 3.20 mmol) was added dropwise. Upon addition of DIAD a white suspension was formed, and it was left to stir at 0 °C for 10 minutes. Then, still at 0 °C, benzyl alcohol (0.640 mL, 3.20 mmol) was added dropwise and the suspension was stirred for 90 minutes at 0 ºC. A solution of Fmoc-L-His(Trt)-OH (1.00 g, 1.60 mmol) in

dry THF (10.0mL) was added slowly. The reaction mixture was stirred for 2 hours at 0 °C and then left to slowly warm up to room temperature and stirred for 14 hours. The reaction mixture was concentrated under reduce pressure to give the crude material as a yellow oil. The crude residue was purified by flash chromatography on silica gel [hexane:ethyl acetate (2:1)] to afford the product **130** as a white solid (1.30 g, 1.80 mmol) with 57% yield. **$[\alpha]_D$ =** + 6.11 (c 1, $CHCl_3$); **Mp.:** 65-66 °C**; IR (neat) $\nu_{(max)}$ cm^{-1}:** 3373 w, 1737 s, 1679 s, 1538 s, 1447 m, 1386 m, 1370 m, 1338 s, 1259 s, 1153 s, 1056 s, 842 m, 763 s, 739 s; **^{1}H NMR (400 MHz, Chloroform-*d*)** δ 7.75 (d, *J* = 7.5 Hz, 2H, arom. Fmoc), 7.62 (t, *J* = 6.9 Hz, 2H, arom. Fmoc), 7.42 – 7.30 (m, 18H, CH arom.), 7.17 – 7.10 (m, 7H, arom.), 6.60 (d, *J* = 8.2 Hz, 1H, NH), 6.50 (s, 1H, NCHCN), 5.05 (AB, *J* = 12.3 Hz, 2H, CH_2 Bn), 4.72 – 4.63 (m, 1H, αCH), 4.36 (dd, *J* = 10.0, 7.2 Hz, 1H, CH_2 Fmoc), 4.32 – 4.26 (m, 1H, CH_2 Fmoc), 4.26 – 4.18 (m, 1H, CH Fmoc), 3.14 – 3.02 (m, 2H, βCH_2); **^{13}C NMR (101 MHz, Chloroform-d)** δ 171.6 (CO_2 Bn), 156.4 (CO_2 Fmoc), 144.3 (C arom), 144.1 (C arom), 142.4 (C arom), 141.4 (C arom), 139.0 (C arom), 136.5 (C arom), 135.6 (CH NCHN), 129.9 (2CH arom.), 128.6 (3CH arom.), 128.4 (4CH arom.), 128.2 (2CH arom. overlapping resonances), 127.7 (2CH arom.), 127.2 (2CH arom.), 125.6 (CH arom. Fmoc), 125.4 (CH arom. Fmoc), 120.0 (CH arom. Fmoc), 119.8 (CH NCHCN), 75.4 (C Trt), 67.4 (CH_2 Bn), 67.0 (CH_2 Fmoc), 54.5 (αCH), 47.3 (CH Fmoc), 30.2 (βCH_2); **HRMS (ESI):** *m/z* calculated for $C_{47}H_{40}N_3O_4$: 798.8381, found 710.3033 [M+H].

Benzyl (((9H-fluoren-9-yl)methoxy)carbonyl)-L-histidinate ***131*****:**

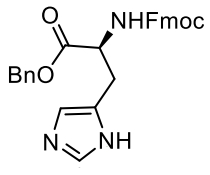

The compound **130** (0.660 g, 0.930 mmol) was dissolved in DCM (1.00 mL) and TFA (1.00 mL) was added dropwise to the solution. The reaction mixture was left to stir at room temperature for 1 h. DCM was removed under reduced pressure and Et_2O was added, causing a white precipitate to form. Filtration afforded the product as a white solid (0.270g, 0.570 mmol) with 61% yield. **$[\alpha]_D$ =** -13.4 (c 1 MeOH); **Mp.:** 170-171 °C; **IR (neat)** $\nu_{(max)}$ cm^{-1}: 3321 w, 3149 w, 2594 w br, 1732 m, 1684 s, 1543 s, 1176 s, 722 s, 737 s; **^{1}H NMR (400 MHz, DMSO-d_6)** δ 14.34 (s, 1H, NH), 8.95 (d, *J* = 1.2 Hz, 1H, NCHNH), 7.99 (d, *J* = 8.2 Hz, 1H, NCHCNH), 7.89 (d, *J* = 7.5 Hz, 2H, arom. Fmoc), 7.63 (d, *J* = 7.4 Hz, 2H, arom. Fmoc), 7.41 (t, *J* = 7.4 Hz, 2H, arom. Fmoc), 7.36 – 7.26 (m, 7H, CH arom.), 5.14 (s, 2H, CH_2 Bn), 4.53 – 4.44 (m, 1H, αCH), 4.35 – 4.24 (m, 2H, CH_2 Fmoc), 4.19 (t, *J* = 6.8 Hz, 1H, CH Fmoc), 3.18 (dd, *J* = 15.1, 5.5 Hz, 1H, βCH_2), 3.06 (dd, *J* = 15.1, 9.8 Hz, 1H, βCH_2); **^{13}C NMR (101 MHz, DMSO-d_6)** δ 170.7 (CO_2 Bn), 155.9 (CO_2 Fmoc), 143.7 (C arom. Fmoc), 140.7 (C arom. Fmoc), 135.6 (C arom. Bn), 134.0 (C NCN), 129.2 (C NCHCN), 128.4 (CH arom. Bn), 128.1 (CH arom. Bn), 127.8 (CH arom. Bn), 127.6 (CH arom. Fmoc), 127.1 (CH arom. Fmoc), 125.1 (CH arom. Fmoc), 120.2 (CH arom. Fmoc), 117.2 (NCHCN) 66.4 (CH_2 Bn), 65.7 (CH_2 Fmoc), 53.1 (αCH), 46.5 (CH Fmoc), 26.0 (βCH_2); **HRMS (ESI):** *m/z* calculated for $C_{28}H_{26}N_3O_4$: 468.1923, found 468.1924 [M^+].

Methyl (((9H-fluoren-9-yl)methoxy)carbonyl)-L-histidinate ***141*****:**

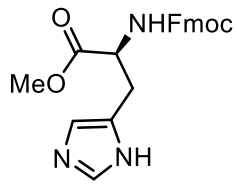

Synthesized according to literature procedure.[2] In a round bottom flask, methanol (40.0 mL) was cooled down to 0 °C with an ice bath. Acetyl chloride (1.20 mL, 16.0 mmol) was then added dropwise over 3 minutes and the reaction mixture was stirred for 10 min at 0 °C. Fmoc-L-His-OH (2.00 g, 5.30 mmol) was then added and the ice bath removed allowing the mixture to warm up to room temperature. After 24 hours of stirring, the mixture was neutralized by pouring carefully, portion wise, onto a saturated solution of sodium bicarbonate. The methanol was removed under reduced pressure and the residue extracted with dichloromethane. The organic layers were combined and dried over sodium sulfate and concentrated under vacuum. The crude material was purified by recrystallization in hot ethyl acetate to afford the product as a white solid (1.30 g, 3.40 mmol) with 64% yield. **Mp.:** 130-131 °C (EtOAc). **IR (neat):** $\nu_{(max)}$ cm^{-1} 3397 w br, 3182 w br, 2970 m br, 2950 m br, 1727 s, 1692 s, 1278 s, 1234 s, 1049, s, 756 s, 742 s, 731 s. **^{1}H NMR (400 MHz, Chloroform-*d*)** 7.76 (d, *J* = 7.5 Hz, 2H, arom. Fmoc), 7.66-7.55 (m, 3H, arom. Fmoc and NCHN), 7.40 (t, *J* = 7.4 Hz, 2H, arom. Fmoc), 7.31 (td, *J* = 7.5, 1.1 Hz, 2H, arom. Fmoc), 6.81 (s, 1H, NCHCN), 6.19 (s, 1H, NH), 4.72-4.56 (m, 1H, αCH), 4.39 (d, *J* = 7.2, 2H, CH_2 Fmoc), 4.24 (t, *J* = 7.1 Hz, 1 H, CH Fmoc), 3.73 (s, 3H, OCH_3), 3.25-3.07 (m, 2H, βCH_2). **HRMS (ESI):** *m/z* calculated for $C_{22}H_{22}N_3O_4$: 392.1604, found 392.1618 $[M+2H]^+$.

6.3 - Synthesis of Imidazolium Salts:

General Procedure 1 for the synthesis of NHC salts (GP1):

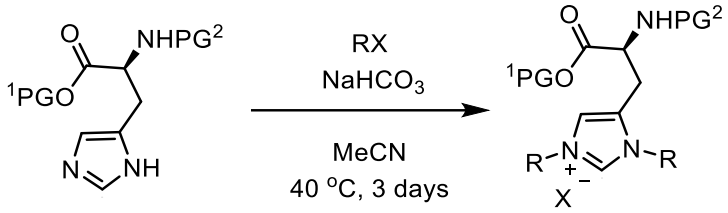

In a heat gun dried Schlenk tube under argon amino acid (1.0 eq) was dissolved in dry acetonitrile (0.1 M in respect to the amino acid). $NaHCO_3$ (4.0 eq.) was added and the mixture was stirred at room temperature for 10 minutes. Halide (4.0 eq.) was added dropwise to the heterogeneous solution. The reaction mixture was warmed up to 40 ºC and left to stir for 3 to 4 days. The reaction mixture was allowed to cool down to room temperature and was filtrate through celite. The filtrate was concentrated under reduced pressure and, where necessary, purified by flash column chromatography or recrystallization.

General Procedure 2 for the synthesis of NHC salts (GP2):

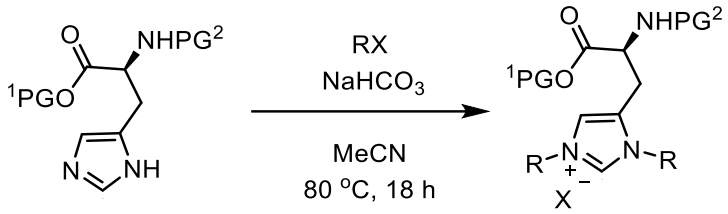

In a dried reflux apparatus under argon amino acid (1.0 eq.) was dissolved in dry acetonitrile (0.1 M in respect to the amino acid). Halide (3.0 eq.) was added followed by the addition of $NaHCO_3$ (1.1 eq.). The reaction mixture was warmed up to 80 ºC and left to stir for 16 to 19 hours. The reaction mixture was allowed to cool down to room temperature and was filtered through celite. The filtrate was concentrated under

reduced pressure and, where necessary, purified by flash column chromatography or recrystallization.

General Procedure 3 for the synthesis of NHC salts (GP3):

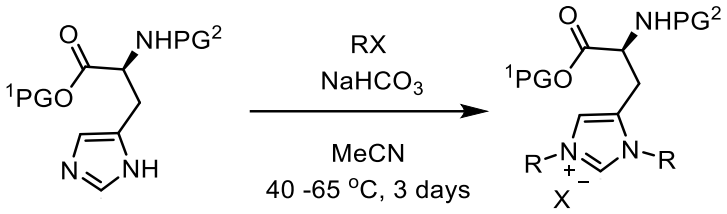

In a heat gun dried Schlenk tube under argon amino acid (1.0 eq) was dissolved in dry acetonitrile (0.1 M in respect to the amino acid). $NaHCO_3$ (4.0 eq.) was added and the mixture was stirrer at room temperature for 10 minutes. Halide (25 eq.) was added dropwise to the heterogeneous solution. The reaction mixture was warmed up to 40 °C or 65 °C and left to stir for 3 to 4 days. The reaction mixture was allowed to cool down to room temperature and was filtrate through celite. The filtrate was concentrated under reduced pressure and, where necessary, purified by flash column chromatography or recrystallization.

(S)-5-(2-((((9H-Fluoren-9-yl)methoxy)carbonyl)amino)-3-(benzyloxy)-3-oxopropyl)-1,3-dimethyl-1H-imidazol-3-ium 2,2,2-trifluoroacetate ***134:***

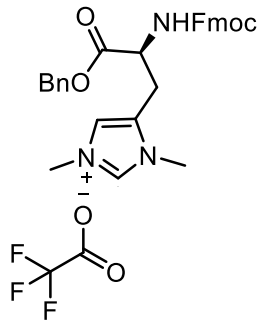

Following GP1 using histidine derivative **132** (0.400 g, 0.700 mmol), acetonitrile (8.00 mL), $NaHCO_3$ (0.231 g, 2.80 mmol) and methyl iodide (0.170 mL, 2.80 mmol). The crude material was dissolved in a small quantity of acetonitrile and precipitated with diethyl ether. The solid was purified by reverse-phase preparative HPLC (water 0.05% TFA to 100% acetonitrile 0.05% TFA)

liophylization gave **134** as a yellow solid (0.190 g, 0.312 mmol) with 45% yield. **Mp.:** 46-47 °C; **IR (neat)** $\nu_{(max)}$ cm^{-1}: 3066 w, 2956 w, 1672 br s, 1609 w, 1574 w, 1534 m, 1449 m, 1252 m, 1173 s, 1126 s, 1081 w, 1047 w, 827 w, 760 m, 717 s, 709 m; **^{1}H NMR (400 MHz, DMSO-d_6)** δ 8.99 (s, 1H, NCHN), 8.02 (d, *J* = 8.3 Hz, 1H, NH), 7.90 (d, *J* = 7.5 Hz, 2H, arom. Fmoc), 7.66 (t, *J* = 6.6 Hz, 2H, arom. Fmoc), 7.45 – 7.39 (m, 3H, arom. Fmoc and NCHCN), 7.33 (d, *J* = 12.1 Hz, 5H, arom. Bn), 5.17 (s, 1H, CH_2 Bn), 4.49 (m, 1H, αCH), 4.39 (dd, *J* = 10.0, 6.8 Hz, 1H CH_2 Fmoc), 4.29 (dd, *J* = 10.5, 6.8 Hz, 1H, CH_2 Fmoc), 4.20 (t, *J* = 6.7 Hz, 1H, CH Fmoc), 3.78 (s, 3H, CH_3),3.72 (s, 3H, CH_3), 3.21 (dd, *J* = 15.8, 5.1 Hz, 1H, βCH_2), 3.07 (dd, *J* = 15.8, 9.6 Hz, 1H, βCH_2). **^{13}C NMR (101 MHz, DMSO-d_6) δ** 170.5 (CO_2Bn), 158.2 (q, *J* = 34.3 Hz, COO^- TFA), 156.0 (CO_2 Fmoc), 143.7 (C arom. Fmoc), 143.7 (C arom. Fmoc), 140.8 (NCN imidazole), 136.9 (C arom. Bn), 135.6 (C NCHCN), 131.2 (CH arom. Bn), 128.4 (CH arom. Bn), 128.2 CH arom. Bn), 127.9 (CH arom. Fmoc), 127.7 (CH arom. Fmoc), 127.1 (CH arom. Fmoc), 121.4 (CH NCHCN), 120.2 (CH arom. Fmoc), 116.3 (q, *J* = 294 Hz, CF_3), 66.5 (CH_2 Bn), 65.8 (CH_2 Fmoc), 52.3 (αCH), 46.6 (CH Fmoc), 35.6 (CH_3 imidazole), 33.3 (CH_3 imidazole), 24.6 (βCH_2);**^{19}F NMR (282 MHz, DMSO-d_6)** δ -74.35 (CF_3). **HRMS (ESI):** *m/z* calculated for $C_{30}H_{30}N_3O_4^+$: 496.2231, found 496.2233 $[M\text{-}TFA]^+$.

(S)-5-(2-((((9H-Fluoren-9-yl)methoxy)carbonyl)amino)-3-(benzyloxy)-3-oxopropyl)-1,3-dimethyl-1H-imidazol-3-ium iodide ***133:***

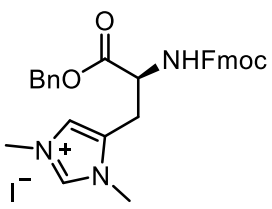

Following GP2 using histidine derivative **132** (0.100 g, 0.210 mmol), acetonitrile (2.10 mL), $NaHCO_3$ (0.0190 g, 0.230 mmol) and methyl iodide (0.0400 mL, 0.64 mmol).

Purification using flash silica gel column chromatography (CH_2Cl_2 9:1 MeOH) gave access to product **133** as a yellow foam (41.0 mg, 0.066 mmol) in 31% yield.

[α] = -12.6 (c 1, $CHCl_3$); **Mp.**: 131-133 °C; **IR (neat)** $\nu_{(max)}$ cm^{-1}: 2970 w, 2848 w, 1737 s, 1696 w, 1574 m, 1448 m, 1228 s, 1216 s, 1054 m, 760 s, 740 s, 618 s; **^{1}H NMR (400 MHz, DMSO-d_6)** δ 9.01 (s, 1H, NC*H*N), 8.01 (d, *J* = 8.2 Hz, 1H, NH), 7.90 (d, *J* = 7.5 Hz, 2H, arom. Fmoc), 7.66 (t, *J* = 6.7 Hz, 2H, arom. Fmoc), 7.45 – 7.39 (m, 3H, arom. Fmoc and NCHCNH), 7.38 – 7.26 (m, 7H, CH arom.), 5.16 (s, 2H, CH_2 Bn), 4.48 (td, *J* = 9.4, 5.2 Hz, 1H, αCH), 4.37 (dd, *J* = 10.5, 6.8 Hz, 1H, CH_2 Fmoc), 4.28 (dd, *J* = 10.5, 6.8 Hz, 1H, CH_2 Fmoc), 4.20 (t, *J* = 6.7 Hz, 1H, CH Fmoc), 3.74 (s, 3H, NCH_3), 3.73 (s, 3H, NC*H*$_3$), 3.20 (dd, *J* = 15.8, 5.1 Hz, 1H, βCH_2), 3.07 (dd, *J* = 15.8, 9.6 Hz, 1H, βCH_2); **^{13}C NMR (101 MHz, DMSO-d_6)** δ 170.5 (CO_2 Me), 156.0 (CO_2 Fmoc), 143.7 (C arom.), 143.6 (C arom.), 140.8 (C arom.), 136.8 (NCHN), 135.6 (C arom), 131.1(C NCHCNH), 128.4 (CH arom), 128.2 (CH arom.), 127.9 (CH arom.), 127.7 (CH arom.), 127.7 (CH arom.), 125.1 (CH arom.), 125.4 (CH arom.), 121.4 (CH arom.), 120.2 (CH NCHCNH), 66.5 (CH2), 65.8 (CH2), 52.3 (αCH), 46.5 (CH Fmoc), 35.7 (NCH_3), 33.3 (NCH_3), 24.6 (βCH_2); **HRMS (ESI):** *m/z* calculated for $C_{30}H_{30}N_3O_4^+$:496.2231, found 496.2239 $[M\text{-}I]^+$.

(S)-5-(2-((((9H-Fluoren-9-yl)methoxy)carbonyl)amino)-3-methoxy-3-oxopropyl)-1,3-dimethyl-1H-imidazol-3-ium iodide ***142:***

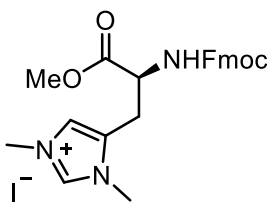

Following GP2 using histidine derivative **141** (0.100 g, 0.250 mmol), acetonitrile (2.50 mL), $NaHCO_3$ (0.0230 g, 0.270 mmol) and methyl iodide (0.0480 mL, 0.760 mmol).

Purification using flash silica gel column chromatography (CH_2Cl_2 9:1 MeOH) gave access to product **142** as a yellow foam (0.087 g, 0.160 mmol) in 64% yield.

$[\alpha]_D$ = -15.3 (c 1, $CHCl_3$); **Mp.**: 131-133 °C; **IR (neat)** $\nu_{(max)}$ cm^{-1}: 2970 w, 1738 s, 1523 w, 1446 w, 1365 m, 1228 m, 1217 m, 763 w, 742 w, 619 w; **^{1}H NMR (300 MHz, Chloroform-d)** δ 9.72 (s, 1H, NCHN), 7.76 (d, *J* = 7.4 Hz, 2H, CH Fmoc), 7.63 (t, *J* = 7.8 Hz, 2H, CH Fmoc), 7.41 (t, *J* = 7.4 Hz, 2H, CH Fmoc), 7.33 (t, *J* = 7.9 Hz, 2H, CH Fmoc), 7.01 (s, 1H, CH NCHCNH), 6.16 (d, *J* = 6.0 Hz, 1H, NH), 4.61 (br s, 1H, αCH), 4.42 (m, 2H, CH_2 Fmoc), 4.20 (t, *J* = 6.5 Hz, 1H, CH Fmoc), 3.88 (s, 6H, 2 NCH_3), 3.80 (s, 3H, OCH_3), 3.25 (br d, *J* = 3.3 Hz, 2H, βCH_2);**^{13}C NMR (101 MHz, Chloroform-d)** δ 170.8 (CO_2 Me), 156.6 (CO_2 Fmoc), 143.9 (C Fmoc), 143.7 (C Fmoc), 141.3, 138.0 (CH NCHN), 131.8 (C NCH*C*NH), 128.0 (CH Fmoc), 127.3 (CH Fmoc), 125.5 (CH Fmoc), 125.4 (CH Fmoc), 121.5 (CH Fmoc), 120.1 (CH NCHCNH), 67.3 (CH_2 Fmoc), 53.2 (OCH_3), 52.5 (αCH), 46.9 (CH Fmoc), 36.1 (NCH_3), 33.7 (NCH_3), 25.7 (βCH_2); **HRMS (ESI):** *m/z* calculated for $C_{24}H_{26}N_3O_4^+$:420.1918, found 420.1924 $[M-I]^+$.

(S)-4-(2-((((9H-Fluoren-9-yl)methoxy)carbonyl)amino)-3-methoxy-3-oxopropyl)-1,3-dibenzyl-1H-imidazol-3-ium bromide ***146:***

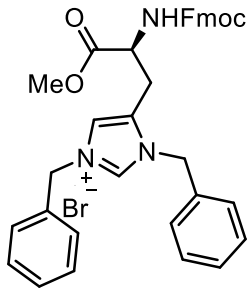

Following GP2 using histidine derivative **141** (6.9 g, 17.6 mmol), acetonitrile (175 mL), $NaHCO_3$ (1.62 g, 19.4 mmol) and benzyl bromide (6.33 mL, 52.8 mmol). Recrystallization from hot EtOAc gave access to **146** as white solid with 70% yield (8.03 g,12.3 mmol). **$[\alpha]_D$ =** -9.28 (c 1, $CHCl_3$); **Mp.:** 115-116 °C; **IR (neat)** $\nu_{(max)}$ cm^{-1}: 3035 w, 2950 m, 1704 s, 1605 w, 1498 m, 1252 m, 1159 s, 1031 m, 706 s, 739 s, 702 s; **^{1}H NMR (400 MHz, Chloroform-d)** δ 10.08 (s, 1H, NCN), 7.76 (d, *J* = 7.4 Hz,

2H, arom. Fmoc), 7.61 (dd, *J* = 13.3, 7.5 Hz, 2H, arom. Fmoc), 7.45 – 7.27 (m, 14H, CH arom.), 7.08 (s, 1H, NCHCN), 6.38 (d, *J* = 7.5 Hz, 1H, NH), 5.50 (AB, *J* = 15.3 Hz, 2H, CH_2 Bn), 5.38 (s, 2H, CH_2 Bn), 4.53 – 4.44 (m, 1H, αCH), 4.32 (m, 1H, CH_2 Fmoc), 4.25 (m, 1H, CH_2 Fmoc), 4.15 (t, *J* = 7.2 Hz, 1H, CH Fmoc), 3.69 (s, 3H, OMe), 3.27-2.91 (m, 2H, βCH_2);**^{13}C NMR (101 MHz, Chloroform-d)** δ 170.7 (CO_2 Me), 156.3 (CO_2 Fmoc), 143.8 (C arom. Fmoc), 143.6 (C arom. Fmoc), 141.4 (C arom. Fmoc), 137.0 (CH NCHN), 132.7 (C arom. Bn), 132.6 (C arom. Bn), 131.8 (C NCHCN.), 129.63 (CH arom. Bn), 129.59 (CH arom. Bn), 129.53 (CH arom. Bn), 129.45 (CH arom. Bn), 128.9 (CH arom. Bn), 128.3 (CH arom. Fmoc), 127.9 (CH arom. Bn), 127.3 (CH arom. Fmoc), 125.5 (CH arom. Fmoc), 125.4 (CH arom. Fmoc), 120.7 (CH arom. Fmoc), 120.1 (CH NCHCN), 67.4 (CH_2 Fmoc), 53.6 (CH_2 Bn), 53.2 (OCH_3), 52.5 (αCH), 51.5 (CH_2 Bn), 47.0 (CH Fmoc), 26.4 (βCH_2); **HRMS (ESI):** *m/z* calculated for $C_{36}H_{34}N_3O_4^+$: 572.2549, found 572.2552 $[M\text{-}Br]^+$; **Elemental analysis** calculated for: $C_{36}H_{34}N_3O_4Br$: C, 66.26; H, 5.25; N, 6.44. Found: C, 66.32; H, 5.07; N, 6.33.

(S)-5-(2-((((9H-Fluoren-9-yl)methoxy)carbonyl)amino)-3-methoxy-3-oxopropyl)-1,3-bis(4-(trifluoromethyl)benzyl)-1H-imidazol-3-ium bromide ***147***:

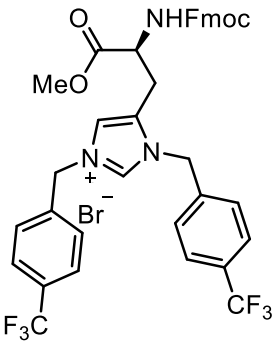

Following GP2 using histidine derivative **141** (0.500 g, 1.30 mmol), acetonitrile (13.0 mL), $NaHCO_3$ (0.437 g, 5.20 mmol) and 4-(Trifluoromethyl)benzyl bromide (0.726 mL, 3.80 mmol). Automated flash chromatography on silica gel (EtOAc 100% → 20% MeOH) gave access to **147** as white foam (0.812 mg, 1.03 mmol) with 79% yield. **$[\alpha]_D$ =** -20.9 (c 1, $CHCl_3$); **Mp.:** 105-106 °C; **IR (neat)$\nu_{(max)}$** cm^{-1}: 2957 w, 1714 m, 1621 w, 1556 w, 1530 w, 1450 w, 1421 w, 1322 s, 1162 s, 1113 s,

1066 s, 760 s, 740 s; **^{1}H NMR (400 MHz, Chloroform-d)** δ 10.51 (s, 1H, NCHN), 7.74 (d, *J* = 7.5 Hz, 2H, arom. Fmoc), 7.66 – 7.53 (m, 6H, CH arom.), 7.53 – 7.44 (m, 4H, CH arom.), 7.39 (t, *J* = 7.4 Hz, 2H, arom. Fmoc), 7.35 – 7.27 (m, 2H, arom. Fmoc), 7.08 (s, 1H, NCHCNH), 6.46 (d, J = 7.7 Hz, 1H, NH), 5.77 – 5.46 (m, 4H, CH_2 *p*CF_3Bn), 4.54 – 4.40 (m, 1H, αCH), 4.34 (app t, *J* = 8.9 Hz, 1H, CH_2 Fmoc), 4.25 (app t, *J* = 8.9 Hz, 1H, CH_2 Fmoc), 4.14 (t, *J* = 7.1 Hz, 1H, CH Fmoc), 3.71 (s, 3H, OMe), 3.22 – 2.95 (m, 2H, βCH_2); **^{13}C NMR (101 MHz, Chloroform-d)** δ 170.4 (CO_2 Me), 156.3 (CO_2 Fmoc), 143.7 (C_0 Fmoc), 143.5 (C arom. Fmoc), 141.4 (C arom. *p*CF_3Bn), 138.1 (NCHN), 136.5 (C arom. *p*CF_3Bn), 132.0 (C NCHCNH), 131.6 (q, *J* = 35.4 Hz, CCF_3), 131.5 (q, *J* = 34.1 Hz, CCF_3), 129.3 (CH arom.), 128.7 (CH arom.), 128.1 (CH arom.), 127.3 (CH arom.), 126.6 (br q, *J* = 3.7 Hz, 4 X $CHCCF_3$), 125.4 (CH arom.), 125.2 (CH arom.), 123.7 (q, *J* = 270 Hz, CF_3), 123.6 (q, *J* = 269 Hz, CF_3), 120.2 (CH NCHCNH), 67.5 (CH_2 Fmoc), 53.3 (αCH), 53.0 (OMe), 52.6 (CH_2 *p*CF_3Bn), 52.5 (CH_2 *p*CF_3Bn), 47.0 (CH Fmoc), 26.7 (βCH_2); **^{19}F NMR (282 MHz, Chloroform-d)** δ -62.89 (s, 3F), -62.92 (s, 3F); **HRMS (ESI):** *m/z* calculated for $C_{38}H_{32}N_3O_4F_6$ 708.2292, found 708.2296 $[M\text{-}Br]^+$; **Elemental analysis** calculated for: $C_{38}H_{32}N_3O_4F_6Br$: C, 57.88; H, 4.09; N, 5.33; found: C, 57.77; H, 4.13; N, 5.58.

(S)-5-(2-((((9H-Fluoren-9-yl)methoxy)carbonyl)amino)-3-methoxy-3-oxopropyl)-1,3-bis(pyridin-2-ylmethyl)-1H-imidazol-3-ium bromide ***148****:*

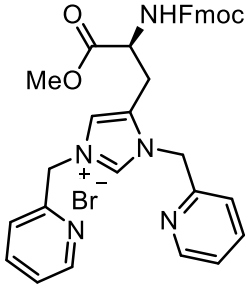

Following GP2 using histidine derivative **141** (0.500 g, 1.30 mmol), acetonitrile (13.0 mL), $NaHCO_3$ (0.437 g, 5.20 mmol) and 2-(bromomethyl)pyridine (0.961 g, 3.80 mmol). Automated flash chromatography on silica gel (EtOAc 100% → 20% MeOH) gave

access to **148** as yellow solid (0.726 g, 1.11 mmol) with 85% yield. **$[\alpha]_D$ =** +16.4 (c 1, $CHCl_3$); **Mp.:** 58-60 °C; **IR(neat):$\nu_{(max)}$** cm^{-1}: 3041 w, 1713 s, 1593 m, 1531 m, 1435 s, 1218 s, 1155 s, 759 s, 740 s; **^{1}H NMR (400 MHz, Chloroform-d)** δ 10.38 (s, 1H, CH NCHN), 8.42 (dd, *J* = 17.8, 4.4 Hz, 2H, NCH pyridine), 7.79 – 7.70 (m, 4H, CH arom.), 7.67 – 7.54 (m, 3H, CH arom.),7.50 (d, *J* = 7.5 Hz, 1H, CH arom.), 7.45 (s, 1H, C HNCHCN), 7.38 (q, *J* = 7.2 Hz, 2H, CH arom.), 7.32 – 7.26 (m, 1H, CH arom.), 7.26 – 7.20 (m, 1H, CH arom.), 7.20 – 7.17 (m, 2H, CH Py), 6.85 (d, *J* = 7.6 Hz, 1H, NH), 5.76 (d, *J* = 15.5 Hz, 1H, CH_2 Py), 5.61 – 5.43 (m, 3H, CH_2 Py), 4.69 – 4.58 (m, 1H, αCH), 4.41 – 4.25 (m, 2H, CH_2 Fmoc), 4.13 (t, *J* = 6.8 Hz, 1H, CH Fmoc), 3.72 (s, 3H, OMe), 3.35 (dd, *J* = 15.9, 8.4 Hz, 1H, βCH_2), 3.27 (dd, *J* = 15.9, 4.8 Hz, 1H, βCH_2); **^{13}C NMR (101 MHz, Chloroform-d)** δ 170.8 (CO_2 Me) 156.3 (CO_2 Fmoc), 152.3 (C Py), 152.2 (C Py), 149.9 (CH arom.), 143.7 (C Fmoc) , 143.7 (C Fmoc), 141.4 (C Fmoc), 138.1 (CH arom.), 138.0 (NCHN), 138.0 (CH arom.), 131.7 (C NCHCN), 127.9 (CH arom.), 127.3 (CH arom.), 127.3 (CH arom.), 125.3 (CH arom.), 125.1(CH arom.), 124.2 (CH arom.), 124.2 (CH arom.), 124.0 (CH arom.), 124.0 (CH arom.), 121.0 (CH arom.), 120.1 (CH NCHCN), 67.2 (CH_2 Fmoc), 54.3 (CH_2 Py), 53.2 (αCH), 53.0 (OMe), 52.0 (CH_2 Py), 47.1 (CH Fmoc), 26.3 (βCH_2); **HRMS (ESI):** *m/z* calculated for $C_{34}H_{32}N_5O_4$: 574.2454, found 574.2451 $[M\text{-}Br]^+$.

(S)-5-(2-((((9H-Fluoren-9-yl)methoxy)carbonyl)amino)-3-methoxy-3-oxopropyl)-1,3-diethyl-1H-imidazol-3-ium bromide ***150****:*

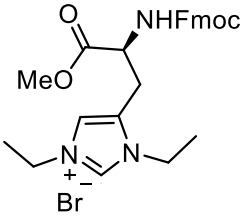

Following GP3 using histidine derivative **141** (0.500 g, 1.28 mmol), acetonitrile (12.0 mL), $NaHCO_3$ (0.430 g, 5.12 mmol) and 1-bromoethane (2.30 mL, 32.0 mmol) at 40 °C. Automated flash

chromatography on silica gel (EtOAc 100% → 20% MeOH) gave access to **150** as white solid (0.265 g, 0.502 mmol) with 40% yield. **$[\alpha]_D$ =** -28.5 (c 1, MeCN);

Mp.: 71-72 °C; **IR(neat)** $\nu_{(max)}$ cm^{-1}: 2980 w, 1733 m, 1715 m, 1639 w, 1560 m, 1447 m, 1166 m, 1020 w, 728 s, 689 w, 668 w; **^{1}H NMR (400 MHz, Chloroform-*d*)** δ 10.10 (s, 1H, NCHN), 7.74 (d, *J* = 7.5 Hz, 2H, arom. Fmoc), 7.63 (dd, *J* = 13.2, 7.5 Hz, 2H, arom. Fmoc), 7.38 (m, 3H, arom. Fmoc and NCHCN), 7.29 (tdd, *J* = 7.5, 2.9, 1.1 Hz, 2H, CH arom. Fmoc), 6.77 (d, *J* = 7.6 Hz, 1H, NH), 4.81 – 4.46 (m, 1H, αCH), 4.44 – 4.04 (m, 7H, CH_2 ethyl, CH Fmoc and CH_2 Fmoc), 3.77 (s, 3H, OCH_3), 3.36 (dd, *J* = 15.7, 8.7 Hz, 1H, βCH_2), 3.29 – 3.18 (dd, *J* = 15.7, 3.8 Hz, 1H, βCH_2) 1.56 (t, *J* = 7.0 Hz, 3H, CH_3 ethyl), 1.47 (t, *J* = 7.4 Hz, 3H, CH_3 ethyl); **^{13}C NMR (101 MHz, Chloroform-*d*)** δ 170.8 (CO_2 Me), 156.4 (CO_2 Fmoc), 143.8 (C arom. Fmoc), 143.6 (C arom Fmoc), 141.4 (C NCHCN), 131.2 (NCHN), 128.0 (CH arom. Fmoc), 127.3 (CH arom. Fmoc), 125.5 (CH arom. Fmoc), 125.4 (CH arom. Fmoc), 120.2 (CH NCHCN), 67.5 (CH_2 Fmoc), 53.4 (OCH_3) , 52.5(αCH), 47.1 (Fmoc CH), 45.3 (CH_2 ethane), 42.9 (CH_2 ethane), 26.2 (βCH_2), 15.7 (CH_3 ethane), 15.6 (CH_3 ethane); **HRMS (ESI):** *m/z* calculated for $C_{28}H_{34}N_3O_4$: 476.2549, found 476.2552 $[M\text{-}Br]^+$; **Elemental analysis** calculated for: $C_{26}H_{30}N_3O_4Br$: C, 59.10; H, 5.72; N, 7.95; found: C, 59.04; H, 5.64; N, 7.82.

(S)-5-(2-((((9H-Fluoren-9-yl)methoxy)carbonyl)amino)-3-methoxy-3-oxopropyl)-1,3-dipropyl-1H-imidazol-3-ium bromide ***151****:*

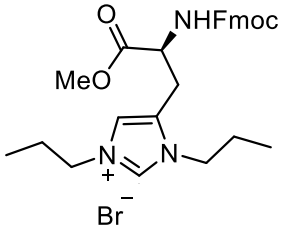

Following GP3 using histidine derivative **141** (1.00 g, 2.60 mmol), acetonitrile (29.0 mL), $NaHCO_3$ (0.873 g, 10.4 mmol) and 1-bromopropane (6.00 mL, 63.8 mmol) reacted at 65 °C.

Automated flash chromatography on silica gel (EtOAc 100% → 20% MeOH) gave access to product **151** as a beige foam (0.991 g, 1.78 mmol) in 68% yield. **$[\alpha]_D$ =** +19.9 (c 1, $CHCl_3$); **Mp.:** 40-42 °C ; **IR (neat)** $\nu_{(max)}$ cm^{-1}: 2964 m, 1712 s, 1529 m, 1448 m, 1251 s, 1219 s, 1045 s, 761 s, 741 s; **^{1}H NMR (400 MHz, Chloroform-d)** δ 10.16 (s, 1H, NCN), 7.75 (d, *J* = 7.5 Hz, 2H, arom. Fmoc), 7.63 (dd, *J* = 14.5, 7.4 Hz, 2H, arom. Fmoc), 7.39 (t, *J* = 7.5 Hz, 2H, arom. Fmoc), 7.34 – 7.26 (m, 3H, arom. Fmoc and CH imidazole), 6.56 (d, *J* = 7.5 Hz 1H, NH), 4.69 – 4.54 (m, 1H,αCH), 4.46 – 4.26 (m, 2H, CH_2 Fmoc), 4.17 (dt, *J* = 14.6, 7.2 Hz, 5H, CH Fmoc and 2CH_2 propyl), 3.78 (s, 3H, OMe), 3.32 (dd, *J* = 15.9, 8.3, 1H, βCH_2), 3.24 (dd, *J* = 15.7, 4.4 Hz, 1H, βCH_2) 1.99 – 1.88 (m,2H, CH_2 propyl), 1.88 – 1.80 (m, 2H, CH_2 propyl), 0.97 (t, *J* = 7.3 Hz, 3H CH_3 propyl), 0.89 (t, *J* = 7.4 Hz, 3H, CH_3 propyl);**^{13}C NMR (101 MHz, Chloroform-d)** δ 170.7 (CO_2Me), 156.3 (CO_2 Fmoc), 143.8 (C, arom. Fmoc), 143.6 (C, arom. Fmoc), 141.4 (C arom. NCHCN), 131.0 (NCHN), 127.9 (CH arom. Fmoc), 127.3 (CH arom. Fmoc), 125.49 (CH arom. Fmoc), 125.39 (CH arom. Fmoc), 120.2 (CH NCHCN), 67.5 (CH_2 Fmoc), 53.3 (OCH_3), 52.5 (αCH), 51.5 (CH_2 propyl), 48.91 (CH_2 propyl), 47.1 (Fmoc CH), 26.3 (βCH_2), 23.6 (CH_2 propyl), 23.6 (CH_2 propyl), 10.9 (CH_3 propyl), 10.8 (CH_3 propyl); **HRMS (ESI):** *m/z* calculated for $C_{26}H_{30}N_3O_4$: 448.2231, found 448.2225 $[M\text{-}Br]^+$.

(S)-5-(2-((((9H-Fluoren-9-yl)methoxy)carbonyl)amino)-3-methoxy-3-oxopropyl)-1,3-dipropyl-1H-imidazol-3-ium iodide ***152****:*

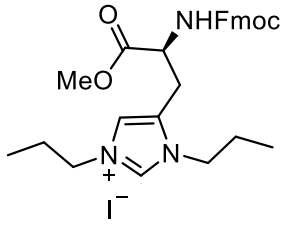

Following GP3 using histidine derivative **141** (0.150 g, 0.380 mmol), acetonitrile (3.80 mL), $NaHCO_3$ (0.128 g, 1.50 mmol) and 1-iodopropane (0.926 mL, 9.50 mmol) reacted at 40 °C.

Automated flash chromatography on silica gel (EtOAc 100% → 20% MeOH) gave access to product **152** as a white foam (0.229 g, 0.380 mmol) in 99% yield. **$[\alpha]_D$ =** -17.4 (c 1, MeCN); **Mp.:** 61-63 °C; **IR(neat):$\nu_{(max)}$** cm^{-1}: 2963 w, 1713 s, 1503 w, 1561 w, 1516 m, 1448 m, 1249 s, 1218 s, 1048 m, 762 s, 741 s, 620 s; **^{1}H NMR (300 MHz, Chloroform-d)** δ 9.84 (s, 1H, NCHN), 7.76 (d, *J* = 7.4 Hz, 2H, arom. Fmoc), 7.62 (t, *J* = 7.5 Hz, 2H, arom. Fmoc), 7.41 (t, *J* = 7.4 Hz, 2H, arom. Fmoc), 7.33 (tt, *J* = 7.4, 1.4 Hz, 2H, arom. Fmoc), 7.11 (s, 1H, NCHCN), 6.14 (d, *J* = 6.1 Hz, 1H, NH), 4.62 (m, 1H, αCH), 4.49 – 4.29 (m, 2H, CH_2 Fmoc), 4.26 – 4.05 (m, 5H, CH Fmoc and 2 CH_2 propyl), 3.81 (s, 3H, OCH_3), 3.24 (br s, 2H, βCH_2), 2.01 – 1.81 (m, 4H, 2 CH_2 propyl), 0.99 (t, *J* = 7.4 Hz, 3H, CH_3 propyl), 0.93 (t, *J* = 7.4 Hz, 3H, CH_3 propyl); **^{13}C NMR (101 MHz, Chloroform-d)** δ 170.6 (CO_2 Me), 156.2 (CO_2 Fmoc), 143.7 (C arom. Fmoc), 143.5 (C arom. Fmoc), 141.4 (C NCHCN), 136.3 (CH NCHN), 128.0 (CH arom. Fmoc), 127.3 (CH arom. Fmoc), 125.5 (CH arom. Fmoc), 125.3 (CH arom. Fmoc), 120.3 (CH arom. Fmoc), 120.2 (CH NCHCN and CH arom. Fmoc), 67.5 (CH_2 Fmoc), 53.5 (OCH_3), 52.5 (αCH), 51.7 (CH_2 propyl), 49.1 (CH_2 propyl), 47.0 (CH Fmoc), 26.4 (βCH_2), 23.6 (2 X CH_2 propyl, overlapping resonances), 11.0 (CH_3 propyl), 10.8 (CH_3 propyl); **HRMS (ESI):** *m/z* calculated for $C_{28}H_{34}N_3O_4^+$: 476.2544, found 476.2561 $[M-I]^+$.

(S)-5-(2-((((9H-Fluoren-9-yl)methoxy)carbonyl)amino)-3-methoxy-3-oxopropyl)-1,3-diallyl-1H-imidazol-3-ium bromide ***153****:*

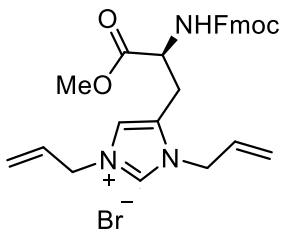

Following GP4 using histidine derivative **141** (0.200 g, 0.510 mmol), acetonitrile (5.00 mL), $NaHCO_3$ (0.171 g, 2.00 mmol) and allyl bromide (5.00 mL, 2.50 mmol). Automated flash chromatography on silica gel (EtOAc 100% → 20% MeOH) gave

access to product **153** as a yellow solid (0.278 g, 0.510 mmol) in 99% yield. **$[\alpha]_D$ =** +1.3 (c 1, $CHCl_3$); **Mp.:** 65-66 °C ; **IR(neat):$\nu_{(max)}$** cm^{-1}: 3023 w, 1709 s, 1645 w, 1605 w, 1556 m, 1448 m, 1528 m, 1324 s, 1162 s, 761 s, 741 s; **^{1}H NMR (300 MHz, Chloroform-d)** δ 10.06 (s, 1H, NCHN), 7.76 (d, *J* = 7.4 Hz, 2H, arom. Fmoc),7.62 (t, *J* = 8.1 Hz, 2H, arom. Fmoc) 7.41 (t, *J* = 7.4 Hz, 2H, arom. Fmoc), 7.32 (t, *J* = 6.9 Hz, 2H, CH Fmoc), 7.16 (br s, 1H, NCHCN), 6.42 (d, *J* = 7.3 Hz, 1H, NH), 6.10 – 5.82 (m, 2H, CH allyl), 5.41 (br d, *J* = 12.8 Hz, 2H, CH_2 alkene), 5.31 (br d, *J* = 15.3 Hz, 2H, CH_2 alkene), 4.97 (b s, 2H, NCH_2), 4.84 (d, *J* = 6.3 Hz, 2H, NCH_2), 4.72 – 4.52 (m, 1H, αCH), 4.44 – 4.29 (m, 2H, CH_2 Fmoc), 4.19 (t, *J* = 6.8 Hz, 1H, CH Fmoc), 3.79 (s, 3H, OCH_3), 3.25 (br d, *J* = 4.7 Hz, 2H, βCH_2); **13C NMR (101 MHz, Chloroform-d)** δ 170.6 (CO_2 Me), 156.3 (CO_2 Fmoc), 143.8 (C arom. Fmoc), 143.6 (C arom. Fmoc), 141.4 (C arom. Fmoc), 137.2 (C NCHCN), 130.0 (NCHN), 129.6 (CH allyl), 128.0 (CH arom. Fmoc), 127.3 (CH arom. Fmoc), 125.4 (CH arom. Fmoc), 125.3 (CH arom. Fmoc), 122.9 (CH_2 allyl), 121.9 (CH_2 allyl), 120.3 (CH arom. Fmoc), 120.2 (CH NCHCN), 67.5 (CH_2 Fmoc), 53.4 (OCH_3), 52.6 (CH_2 allyl), 52.3 (αCH), 50.1 (CH_2 allyl), 47.1 (CH Fmoc), 26.5 (βCH_2); **HRMS (ESI):** *m/z* calculated for $C_{28}H_{30}N_3O_4^+$: 472.2236, found 472.2240 $[M\text{-}Br]^+$*;* **Elemental analysis** calculated for: $C_{28}H_{30}N_3O_4Br$: C, 60.87; H, 5.47; N, 7.61; found: C, 60.94; H, 5.81; N, 7.61.

(S)-5-(2-((((9H-Fluoren-9-yl)methoxy)carbonyl)amino)-3-methoxy-3-oxopropyl)-1,3-diisopropyl-1H-imidazol-3-ium iodide ***154****:*

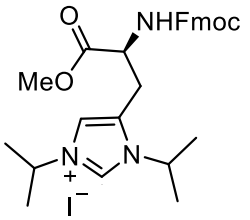

Following GP3 using histidine derivative **141** (1.00 g, 2.60 mmol), acetonitrile (26.0 mL), $NaHCO_3$ (0.873 g, 10.4 mmol) and 2-iodopropane (6.00 mL, 63.8 mmol) reacted at 65 °C. Automated

flash chromatography on silica gel (EtOAc 100% → 20% MeOH) gave access to product **154** as a beige foam (0.660 g, 1.10 mmol) in 42% yield. **$[\alpha]_D$ =** -12.6 (c 1, MeCN); **Mp.:** 67-70 °C; **IR (neat)** $\nu_{(max)}$ cm^{-1}: 2968 m, 1709 s, 1448 m, 1248 m, 1050 m, 761 s, 741 s*;* **^{1}H NMR (400 MHz, Chloroform-d)** δ 9.89 (s, 1H, NCHN), 7.74 (d, *J* = 7.5 Hz, 2H, arom. Fmoc), 7.65 (d, *J* = 7.4 Hz, 1H, arom. Fmoc), 7.61 (d, *J* = 7.4 Hz, 1H, arom. Fmoc), 7.47 (s, 1H, NCHCN), 7.38 (t, *J* = 7.5 Hz, 2H, arom. Fmoc), 7.34 – 7.27 (m, 2H, arom. Fmoc), 6.48 (d, *J* = 7.8 Hz, 1H, NH), 4.89 (hept, *J* = 6.7 Hz, 1H, CH iPr), 4.68 – 4.60 (m, 1H, αCH), 4.60 – 4.52 (m, 1H, CH iPr), 4.34 (ap t, *J* = 10.6, 7.4 Hz, 1H, CH_2 Fmoc), 4.26 (app t, *J* = 9.5, 7.5 Hz, 1H, CH_2 Fmoc), 4.18 (t, *J* = 7.0 Hz, 1H, CH Fmoc), 3.79 (s, 3H, OCH_3), 3.39 (dd, *J* = 15.9, 8.8 Hz, 1H, βCH_2), 3.30 (dd, *J* = 15.8, 4.5 Hz, 1H, βCH_2), 1.68 (d, *J* = 6.8 Hz, 3H, CH_3 iPr), 1.65 (d, *J* = 6.7 Hz, 3H, CH_3 iPr), 1.53 (d, *J* = 2.0 Hz, 3H, CH_3 iPr), 1.51 (d, *J* = 2.0 Hz, 3H, CH_3 iPr). **^{13}C NMR (101 MHz, Chloroform-*d*)** δ 170.6 (CO_2 Me), 156.3 (CO_2 Fmoc), 143.7 (C arom. Fmoc), 143.5 (C arom. Fmoc), 141.4 (C arom. Fmoc), 133.7 (NCHN), 130.7 (C NCHCN), 128.0 (CH arom. Fmoc), 127.3 (CH arom. Fmoc), 125.5 (CH arom.), 125.4 (CH arom. Fmoc), 120.1 (CH NCHCN), 67.5 (CH_2 Fmoc), 53.5 (OCH_3), 53.4 (αCH), 52.6 (CH iPr), 51.2 (CH iPr), 47,0 (CH Fmoc), 26.6 (βCH_2), 23.7 (CH_3 iPr), 23.4 (CH_3 iPr), 23.3 (CH_3 iPr), 23.2 (CH_3 iPr); **HRMS (ESI):** *m/z* calculated for $C_{28}H_{34}N_3O_4$: 476.2549, found. 476.2556 $[M\text{-}I]^+$.

(S)-5-(2-((((9H-fluoren-9-yl)methoxy)carbonyl)amino)-3-methoxy-3-oxopropyl)-1,3-dibutyl-1H-imidazol-3-ium iodide ***155****:*

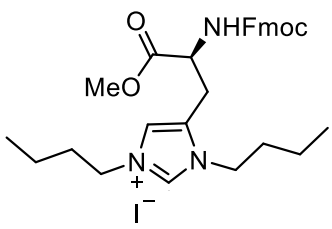

Following GP3 using histidine derivative **141** (0.300 g, 0.770 mmol), acetonitrile (7.70 mL), $NaHCO_3$ (0.258 g, 3.10 mmol)

and 2-iodobutane (2.20 mL, 19.1 mmol) reacted at 65 °C. Automated flash chromatography on silica gel (EtOAc 100% → 20% MeOH) gave access to product **155** as a white foam (0.575 g, 10.910 mmol) in >99% yield. **$[\alpha]_D$ =** -16.9 (c 1, MeCN); **Mp.:** 111-113 °C ; **IR (neat)** $\nu_{(max)}$ cm^{-1}: 2933 m, 1712 s, 1523 m, 1449 m, 1247 s, 1218 s, 1050 m, 761 s, 740 s; **^{1}H NMR (400 MHz, Chloroform-d)** δ 9.82 (s, 1H, NCHN), 7.75 (d, *J* = 7.5 Hz, 2H, arom. Fmoc), 7.66 (d, *J* = 7.4 Hz, 1H, arom. Fmoc), 7.62 (d, *J* = 7.4 Hz, 1H, arom. Fmoc), 7.40 (t, *J* = 7.5 Hz, 2H, arom. Fmoc), 7.32 (tdd, *J* = 7.4, 2.6, 1.1 Hz, 2H, arom. Fmoc), 7.23 (s, 1H, NCHCN), 6.33 (d, *J* = 7.5 Hz, 1H, NH), 4.62 (app q, *J* = 6.8 Hz, 1H, αCH), 4.37 (app t, *J* = 7.4 Hz, 1H, CH Fmoc), 4.31 (app. t, *J* = 7.3 Hz, 1H. CH Fmoc), 4.24 – 4.14 (m, 5H, CH Fmoc and 2 NCH_2 Bu), 3.80 (s, 3H, OCH_3), 3.28 (m, 2H, βCH_2), 1.93 – 1.83 (m, 2 H, NCH_2CH_2 Bu), 1.79 (q, *J* = 7.6 Hz, 2H, CH_2 Bu), 1.45 – 1.22 (m, 4H, CH_2 Bu), 0.95 (t, *J* = 7.4 Hz, 3H, CH_3 Bu), 0.89 (t, *J* = 7.2 Hz, 3H, CH_3 Bu); **^{13}C NMR (101 MHz, Chloroform-d)** δ 170.6 (CO_2 Me), 156.2 (CO_2 Fmoc), 143.7 (C Fmoc), 143.5 (C Fmoc), 141.4 (2C Fmoc), 136.1 (CH NCHN), 131.1 (C NCHCN), 127.8 (CH arom. Fmoc), 127.3 (CH arom. Fmoc), 125.5 (CH arom, Fmoc), 125.3 (CH arom. Fmoc), 120.1 (CH, NCHCN), 67.5 (CH_2 Fmoc), 53.4 (OCH_3), 52.5 (αCH), 50.0 (CH_2 Bu), 47.5 (CH_2 Bu), 47.0 (CH Fmoc), 32.1(CH_2 Bu), 32.0 (CH_2 Bu), 26.4 (βCH_2), 19.8 (CH_2 Bu), 19.6 (CH_2 Bu), 13.64 (CH_3 Bu), 13.55 (CH_3 Bu). **HRMS (ESI):** *m/z* calculated for $C_{30}H_{38}N_3O_4^+$: 504.2855, found 504.2857 $[M-I]^+$.

Methyl Nα-(((9H-fluoren-9-yl)methoxy)carbonyl)-Np-(4-methoxyphenyl)-L-histidinate

162:

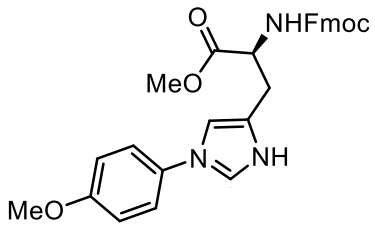

Histidine derivative **141** (1.12 g, 3.10 mmol) was dissolved in MeOH (19.0 mL). Sodium acetate (0.762 g, 9.30 mmol) and copper (II) acetate monohydrate (0.062 g, 0.310 mmol) were added, and the mixture stirred at room temperature for 10 minutes. 4-Methoxyphenylboronic acid (1.42 g, 9.30 mmol) was added and the mixture stirred at room temperature for 24 hours. The reaction mixture was concentrated, and the residue dissolved in EtOAc and washed with water (2 x 25 mL). The organic layer was collected and dried over sodium sulfate. The organic layer was concentrated under vacuum. The crude residue was purified using automated flash column chromatography on silica gel (EtOAc) yielding product **162** as a beige solid (1.05 g, 2.10 mmol) in 68% yield. **$[\alpha]_D$ =** +27.5 (c 1, $CHCl_3$); **Mp.:** 52-53 °C; **IR (neat) $\nu_{(max)}$** cm^{-1}: 2953 w, 1715 s, 1602 m, 1516 s, 1449 m, 1245 s, 1029 m, 1072 m, 828 s, 759 s, 739 s, 646 w, 621 m; **^{1}H NMR (400 MHz, Chloroform-d)** δ 7.75 (d, *J* = 7.6 Hz, 2H, arom. Fmoc), 7.62 (app. t, *J* = 7.8 Hz, 2H, arom. Fmoc), 7.38 (t, *J* = 7.4 Hz, 2H, arom. Fmoc), 7.29 (t, *J* = 7.5 Hz, 2H, arom. Fmoc), 7.27 – 7.23 (m, 3H, CH arom. *p*OMePh and NCHCN), 6.97 (d, *J* = 8.9 Hz, 2H, CH arom. *p*OMePh), 6.37 (*d*, J = 6.7 Hz, 1H, NH), 4.69 (br s, 1H, αCH), 4.37 (ABX, ^3J = 7.2 Hz and ^2J = 4.8 Hz, 2H, CH_2 Fmoc), 4.25 (app. t, *J* = 7.3 Hz, 1H, CH Fmoc), 3.85 (s, 3H, CO_2CH_3), 3.76 (s, 3H, OCH_3), 3.30 – 3.08 (br s, 2H, βCH_2); **^{13}C NMR (101 MHz, Chloroform-d) δ** 172.4 (CO_2 Me), 159.1 (CO_2 Fmoc), 156.3 (C arom.), 144.2 (C arom.), 144.1 (C. arom), 141.4 (C arom Fmoc), 127.8 (CH arom. Fmoc), 127.2 (CH arom. Fmoc), 125.43 (CH arom. Fmoc), 125.39 (CH arom. Fmoc), 123.2 (CH NCHCN), 120.1 (CH arom. Fmoc), 115.1

(CH arom pOMePh), 67.3 (CH_2 Fmoc), 55.8 (CO_2CH_3), 54.1 (αCH), 52.6 ($PhOCH_3$), 47.3 (CH Fmoc), 30.3 (βCH_2);**HRMS (ESI):** *m/z* calculated for $C_{29}H_{28}N_3O5$: 498.2029, found 498.2032 $[M-H]^+$.

Methyl Nα-(((9H-fluoren-9-yl)methoxy)carbonyl)-Np-mesityl-L-histidinate ***163****:*

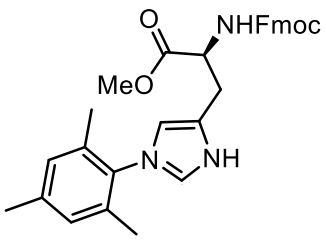

Histidine derivative **141** (0.893 g, 2.28 mmol) was dissolved in MeOH (12.0 mL). Sodium acetate (0.561 g, 6.84 mmol) and copper (II) acetate monohydrate (0.046 g, 0.228 mmol) were added, and the mixture stirred at room temperature for 10 minutes. 2,4,6-Trimethylphenylboronic acid (1.12 g, 6.84 mmol) was added and the mixture stirred at room temperature for 7 days. The reaction mixture was concentrated, and the residue dissolved in EtOAc and washed with water (2 X 25 mL). The organic layer was collected and dried over sodium sulfate. The organic layer was concentrated under vacuum. The crude residue was purified using automated flash column chromatography on silica gel (EtOAc) yielding product **163** as a beige solid (0.359 g, 0.700 mmol) in 31% yield. **$[\alpha]_D$ =** +18.2 (c 1, $CHCl_3$); **Mp.:** 55-56 °C ; **IR (neat) $\nu_{(max)}$** cm^{-1}: 2951 w, 1719 s, 1609 w, 1498 s, 1449 m, 1204 s, 1048 s, 852 w, 759 s, 739 s, 662 m; **^{1}H NMR (400 MHz, Chloroform-d)** δ 7.73 (t, *J* = 9.1, 8.3 Hz, 2H, arom. Fmoc), 7.63 (t, *J* = 7.7 Hz, 2H, arom. Fmoc), 7.42 – 7.33 (m, 4H, arom. Fmoc and NCHN), 7.29 (t, *J* = 7.5 Hz, 2H, arom. Fmoc), 6.96 (s, 2H, arom. Mes), 6.81 (s, 1H, NCHCN), 6.41 (d, *J* = 7.5 Hz, 1H, NH), 4.69 (br s, 1H, αCH), 4.43 – 4.34 (m, 2H, CH_2 Fmoc), 4.25 (t, *J* = 7.1 Hz, 1H, CH Fmoc), 3.71 (s, 3H, OCH_3), 3.18 (br s, 2H, βCH_2), 2.34 (s, 3H, CH_3), 1.96 (s, 6H, CH_3); **^{13}C NMR (101 MHz, Chloroform-d)** δ 172.3 (CO_2 Me), 156.3 (CO_2 Fmoc), 144.2 (C arom.), 144.0 (C arom.), 141.41 (C arom.), 141.38 (C

arom.), 139.8 (C arom.), 139.1 (C arom.), 138.7 (CH NCHN), 135.5 (C arom.), 135.4 (C arom.), 129.1 (CH arom, Mes), 127.8 (CH NCHCN), 127.4 (CH arom. Fmoc), 127.2 (CH arom. Fmoc), 125.42 (CH arom. Fmoc), 125.38 (CH arom. Fmoc), 120.05 (CH arom. Fmoc), 67.2 (CH_2 Fmoc), 54.3 (OCH_3), 52.4 (αCH), 47.3 (CH Fmoc), 30.4 (βCH_2), 21.2 (CH_3), 17.4 (CH_3), 17.3 (CH_3); **HRMS (ESI):** *m/z* calculated for $C_{31}H_{32}N_3O_4$: 510.2388, found 510.2387 $[M+H]^+$.

(S)-5-(2-((((9H-Fluoren-9-yl)methoxy)carbonyl)amino)-3-methoxy-3-oxopropyl)-1-(4-methoxyphenyl)-3-methyl-1H-imidazol-3-ium iodide ***164***:

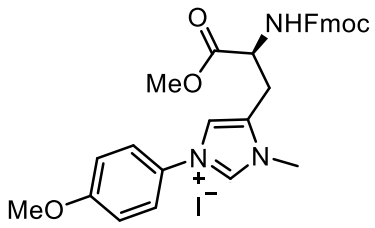

Histidine derivative **162** (0.812 g, 1.63 mmol) was dissolved in acetonitrile (16.3 mL) and methyl iodide (0.507 mL, 8.20 mmol) was added. The reaction mixture was refluxed at 80 °C for 18 hours. The reaction mixture was concentrated and purified by automated column chromatography on silica gel (100% EtOAc → 20% MeOH). Product **164** was obtained as a beige foam (0.834 g, 1.30 mmol) in 80% yield. **$[\alpha]_D$ =** -73.2 (c 1, $CHCl_3$); **Mp.:** 65-69 °C; **IR(neat):$\nu_{(max)}$** cm^{-1}: 3431 b w, 1708 s, 1608 m, 1562 m, 1513 s, 1253 s, 1214 s, 761 s, 740 s; **^{1}H NMR (400 MHz, Chloroform-d)** δ 9.91 (s, 1H, NCHN), 7.70 (d, *J* = 7.4 Hz, 2H. arom. Fmoc), 7.62 (br t, *J* = 7.7 Hz, 2H, arom. Fmoc), 7.50 (d, *J* = 8.9 Hz, 2H, arom. Ph), 7.40 (s, 1H, NCHCN), 7.35 (dt, *J* = 8.9, 4.6 Hz, 2H, arom. Fmoc), 7.29 – 7.22 (m, 2H, arom. Fmoc), 6.90 (d, *J* = 8.8 Hz, 2H, CH arom.), 6.55 (d, *J* = 7.6 Hz, 1H, NH), 4.77 – 4.60 (br m, 1H, αCH), 4.33 (br d, *J* = 6.9 Hz, 2H, CH_2 Fmoc), 4.14 (br t, J = 6.7 Hz, 1H, CH Fmoc), 4.04 (s, 3H, NCH_3), 3.79 (s, 3H, OCH), 3.78 (s, 3H, OCH_3), 3.40 (dd, *J* = 15.6, 8.6 Hz, 1H, βCH_2), 3.31 (dd, *J* = 15.1, 3.6 Hz, 1H, βCH_2); **^{13}C NMR (101 MHz,**

Chloroform-d) δ 170.6 (CO_2 Me), 160.8 (CO_2 Fmoc), 156.3 (C arom.), 143.64 (C arom. Fmoc), 143.55 (C arom Fmoc), 141.3 (C arom), 135.2 (CH NCHN), 132.4 (C NCHCN), 127.9 (CH arom. Fmoc), 127.4 (CH arom Ph), 127.3 (CH arom Fmoc), 125.5 (CH arom Fmoc), 125.4 (CH arom. Fmoc), 123.7 (CH arom. Ph.), 120.1 (CH arom. Fmoc), 119.6 (CH NCHCN), 115.5 (CH arom. Ph), 67.3 (CH_2 Fmoc), 55.8 (OCH3), 53.4 (OCH3), 52.3 (αCH), 47.0 (CH Fmoc), 35.0 (NCH_3), 26.2 (βCH_2); **HRMS (ESI):** *m/z* calculated for $C_{30}H_{30}N_3O_5^+$: 512.2180, found 512.2177 $[M-I]^+$; **Elemental analysis:** calculated for: $C_{30}H_{30}N_3O_5I.H_2O$: C, 54.89; H, 4.76; N, 6.40. Found: C, 55.24; H, 4.88; N, 6.31.

(S)-5-(2-((((9H-Fluoren-9-yl)methoxy)carbonyl)amino)-3-methoxy-3-oxopropyl)-1-mesityl-3-methyl-1H-imidazol-3-ium iodide ***166****:*

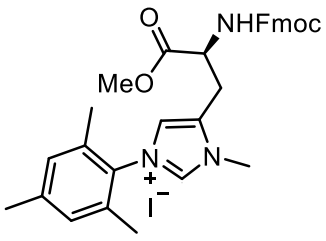

Histidine derivative **163** (0.990 g, 0.200 mmol) was dissolved in acetonitrile (2.00 mL) and methyl iodide (0.067 mL, 1.00 mmol) was added. The reaction mixture was refluxed at 80 °C for 18 hours. The reaction mixture was concentrated and purified by automated column chromatography on silica gel (100% EtOAc → 20% MeOH). Product **166** was obtained as a beige foam (0.106 g, 0.160 mmol) in 80% yield. **$[\alpha]_D$ =** +2.49 (c 1, MeCN); **Mp.:** 81-83 °C; **IR (neat)** $\nu_{(max)}$ cm^{-1}: 2952 w, 1713 s, 1607 w, 1557 w, 1447 m, 1206 s, 761 s, 741 s; **^{1}H NMR (400 MHz, Chloroform-d)** δ 9.45 (s, 1H, NCHN), 7.74 – 7.52 (m, 4H, CH arom.), 7.37 – 7.20 (m, 4H, CH arom.), 6.97 – 6.82 (br m, 3H, CH arom. and NCHCN), 6.50 (d, *J* = 7.5 Hz, 1H, NH), 4.68 (br s, 1H, αCH), 4.38 (ABX, *J* = 10.2, 7.1 Hz, 1H, CH_2 Fmoc), 4.24 (ABX, *J* = 9.7, 7.5 Hz,1H, CH_2 Fmoc), 4.16 (s, 3H, CH_3), 4.11 (app t, *J* = 6.6 Hz, 1H), 3.75 (s, 3H, CH_3),

3.45 (dd, *J* = 15.5, 9.7 Hz, 1H, βCH$_2$), 3.36 (dd, *J* = 15.0, 3.7 Hz, 1H, βCH$_2$), 2.30 (s, 3H, CCH$_3$), 1.98 (s, 3H, CCH$_3$), 1.93 (s, 3H, CCH$_3$); **^{13}C NMR (101 MHz, Chloroform-d)** δ 170.6 (CO$_2$ Me), 156.2 (CO$_2$ Fmoc), 143.7 (C arom.), 143.5 (C. arom.), 141.2 (C arom.), 141.1 (C arom), 139.8 (C arom.) 137.0 (NCHN), 134.44 (C arom.), 134.35 (C arom.), 132.4 (C NCHCN), 130.6 (C arom.), 129.84 (CH arom. Fmoc), 129.81 (CH arom. Fmoc), 127.82 (CH arom. Fmoc), 127.75 (CH arom. Fmoc), 127.23 (CH arom. Fmoc), 127.21 (CH arom. Fmoc), 125.5 (CH arom. Fmoc), 125.2 (CH arom. Fmoc), 122.0 (CH NCHCN), 120.0 (CH arom. Ph), 119.92(CH arom. Ph), 67.0 (CH$_2$ Fmoc), 53.3 (OCH$_3$), 52.0 (αCH), 47.1 (CH Fmoc), 35.5 (NCH$_3$), 26.3 (βCH$_2$), 22.7 (CCH$_3$), 21.2 (CCH$_3$), 18.1 (CCH$_3$); **HRMS (ESI):** *m/z* calculated for $C_{32}H_{34}N_3O_4$: 524.2544, found 524.2545 $[M\text{-}I]^+$.

(S)-5-(2-((((9H-Fluoren-9-yl)methoxy)carbonyl)amino)-3-methoxy-3-oxopropyl)-3-allyl-1-(4-methoxyphenyl)-1H-imidazol-3-ium bromide ***165****:*

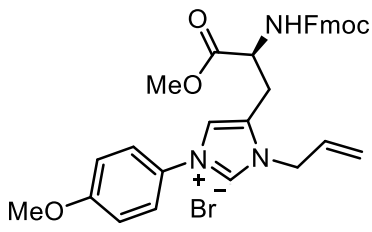

Histidine derivative **162** (0.400 g, 0.800 mmol) was dissolved in acetonitrile (9.00 mL) and allyl bromide (0.347 mL, 4.00 mmol) was added. The reaction mixture was refluxed at 80 °C for 18 hours. The reaction mixture was concentrated and purified by automated column chromatography on silica gel (100% EtOAc → 20% MeOH). Product **165** was obtained as a beige foam (0.408 g, 0.660 mmol) in 82% yield. **$[\alpha]_D$ =** -3.3 (c 1, $CHCl_3$); **Mp.:** 93–95 °C; **IR (neat) $\nu_{(max)}$** cm^{-1}: 2952 w, 1713 s, 1608 w, 1556 m, 1514 s, 1448 m, 1254 s, 1216 s, 1182 s, 1025 m, 1025 m, 832 s, 761 s, 741 s, 619 m; **^{1}H NMR (400 MHz, Chloroform-d)** δ 10.19 (s, 1H, NCHN), 7.70 (d, *J* = 3.8 Hz, 1H, arom. Fmoc), 7.68 (d, *J* = 3.7 Hz, 1H, arom.

Fmoc), 7.66 (s, 1H, NCHCN), 7.63 (t, *J* = 9.3 Hz, 2H), 7.54 (d, *J* = 8.8 Hz, 2H, arom Ph), 7.34 (td, *J* = 7.4, 4.2 Hz, 2H, arom. Fmoc), 7.24 (t, *J* = 7.5 Hz, 2H, arom. Fmoc), 7.03 (d, *J* = 8.0 Hz, 1H, NH), 6.88 (d, *J* = 8.8 Hz, 2H, arom. Ph), 6.04 (ddt, *J* = 16.2, 11.0, 5.8 Hz, 1H, CH allyl), 5.44 – 5.32 (m, 2H, CH_2 allyl), 5.16 (d, *J* = 5.0 Hz, 2H, CH_2 allyl), 4.76 – 4.64 (m, 1H, αCH), 4.29 (d, *J* = 7.2 Hz, 2H, CH_2 Fmoc), 4.12 (t, *J* = 7.1 Hz, 1H, CH Fmoc), 3.77 (s, 3H, OCH_3), 3.76 (s, 3H, OCH_3), 3.44 (dd, *J* = 15.9, 9.2 Hz, 1H, βCH_2), 3.30 (dd, *J* = 16.0, 3.6 Hz, 1H, βCH_2); **^{13}C NMR (101 MHz, Chloroform-d)** δ 170.9 (CO_2 Me), 160.7 (CO_2 Me), 156.5 (C arom), 143.8 (C arom.), 143.7 (C arom.), 141.3 (C arom.), 135.1 (CH NCHN), 132.4 (C NCHCN), 130.3 (CH allyl), 127.9 (CH arom. Fmoc), 127.5 (CH arom. Fmoc), 127.3 (CH arom. Fmoc), 125.5 (CH arom. Fmoc), 125.4 (CH arom. Fmoc), 123.4 (CH arom. Ph), 121.7 (CH_2 allyl), 120.0 (CH arom. Fmoc), 119.7 (CH NCHCN), 115.5 (CH arom. Ph), 67.4 (CH_2 Fmoc), 55.8 (OCH_3), 53.3 (OCH_3), 52.3 (αCH), 50.2 (NCH_2 allyl), 47.0 (CH Fmoc), 26.1 (βCH_2)*;* **HRMS (ESI):** *m/z* calculated for $C_{32}H_{32}N_3O5^+$, 538.2326 found 538.2326 $[M\text{-}Br]^+$.

(S)-1,3-Dibenzyl-5-(2-((tert-butoxycarbonyl)amino)-3-methoxy-3-oxopropyl)-1H-imidazol-3-ium bromide ***177***:

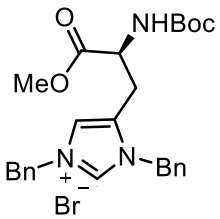

Following GP2 using Boc-*L*-His-OMe (0.050 g, 0.190 mmol), acetonitrile (1.00 mL), $NaHCO_3$ (0.018 g, 0.210 mmol), benzyl bromide (0.068 mL, 0.570 mmol). The crude material was dissolved in a small quantity of acetonitrile and precipitated with diethyl ether. Filtration afforded the product as a hygroscopic white solid (0.074 g, 0.140 mmol) in 74% yield. **$[\alpha]_D$ =** +13.7 (c 1, $CHCl_3$); **Mp:** 75-79 °C; **IR (neat)** $\nu_{(max)}$ cm^{-1}: 3225 w, 2977 w, 1741 m, 1698 s, 1557 m, 1157 s, 735 m, 700 s. **^{1}H NMR (300 MHz, Chloroform-d)**

δ 10.73 (s, 1H, NCHN), 7.58 – 7.31 (m, 8H, CH Bn), 7.02 (s, 1H, NCHCN), 5.61 (d, *J* = 15.2 Hz, 1H, NH), 5.55 – 5.39 (m, 4H, CH_2 Bn), 4.43 (br s, 1H, αCH), 3.65 (s, 3H, OCH_3), 3.09 (dd, *J* = 16.1, 5.3 Hz, 1H, βCH_2), 2.99 (dd, *J* = 15.8, 7.4 Hz, 1H, βCH_2), 1.38 (s, 9H, CH_3 Boc);**^{13}C NMR (101 MHz, Chloroform-d)** δ 170.8 (CO_2 Me), 155.5 (CO_2 Boc), 137.6 (CH NCHN), 132.8 (C arom. Bn), 132.7 (C arom. Bn), 131.7 (C NCHCN), 129.7 (CH arom. Bn), 129.6 (CH arom. Bn), 129.6 (CH arom. Bn), 129.4 (CH arom. Bn), 129.1 (CH arom. Bn), 128.3 (CH arom. Bn), 120.3 (CH NCHCN), 80.9 (C Boc), 53.6(CH_2 Bn), 53.1 (OCH_3), 52.3 (αCH), 51.4 (CH_2 Bn), 28.3 (CH_3 Boc), 26.9 (βCH_2); **HRMS (ESI):** *m/z* calculated for $C_{26}H_{32}N_3O_4^+$: 450.2393, found 450.2390 [M-Br]$^+$.

6.4 – Protecting Group Manipulation:

(S)-1,3-Dibenzyl-5-(2-((tert-butoxycarbonyl)amino)-2-carboxyethyl)-1H-imidazol-3-ium bromide ***178:***

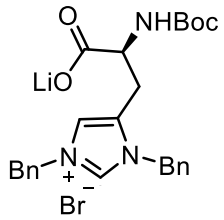

Imidazolium salt **177** (0.050 g, 0.090 mmol) was dissolved in MeOH (7.50 mL), then water (0.750 mL) and LiOH (0.023 g, 0.900 mmol) were added at 0 °C. The reaction mixture was allowed to warm up to room temperature and after 1 hours TLC analysis (CH_2Cl_2 9:1 MeOH) showed complete consumption of starting material. The reaction mixture was concentrated under vacuum. The crude material was purified by trituration with cold diethyl ether to yield product **177** as a white solid (0.047 g, 0.090 mmol) in quantitative yield. **$[\alpha]_D$ =** +8.86 (c 0.5, MeCN); **Mp.:** 158–159 °C; **IR (neat)** $\nu_{(max)}$ cm^{-1}: 3371 w, 3056 w, 1695 s, 1680 s, 16909 w, 1561 m, 1520 s, 1498 m, 1455 m, 1364 w, 1324 w, 1252 m, 1161 s, 1141 s, 1030 m, 723 m, 740 m, 698 s, 666 s; **^{1}H NMR (400 MHz, Methanol-**

d_4) δ 7.48 – 7.31 (m, 11H, arom. Ph and NCHCN), 5.47 (d, *J* = 15.2 Hz, 1H, CH_2 Bn), 5.40 (d, *J* = 15.2 Hz, 1H, CH_2 Bn), 5.35 (br s, 2H, CH_2 Bn), 4.18 (app. t, *J* = 5.6 Hz, 1H, αCH), 3.17 (dd, *J* = 15.4, 5.1 Hz, 1H, βCH_2), 2.,99 (dd, *J* = 15.5, 6.5 Hz, 1H, βCH_2), 1.38 (s, 9H, $C(CH_3)_3$);**^{13}C NMR (101 MHz, Methanol-d_4)** δ 176.2 (CO_2Li), 156.8 (CO_2 Boc), 135.2 (C NCHCN), 134.8 (C arom), 134.6 (C arom.), 130.5 (CH arom Bn), 130.4 (CH arom Bn), 130.3 (CH arom Bn), 130.2 (CH arom Bn), 129.6 (CH arom Bn), 129.3 (CH arom Bn), 122.3 (CH NCHCN), 80.5 (C $C(CH_3)_3$), 55.8 (αCH), 54.1 (CH_2 Bn), 52.0 (CH_2 Bn), 28.7 (CH_3 $C(CH_3)_3$), 28.6 (βCH_2), CH NCHN not visible in MeOD; **HRMS (ESI):** *m/z* calculated for $C_{25}H_{30}N_3O_4^+$: 436.2236, found 436.2238 $[M\text{-}Br]^+$.

General Procedure 4 for the removal of methyl ester (GP4):

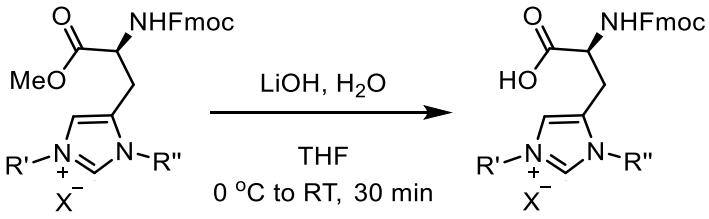

In a round bottom flask, amino acid (1 eq.) was dissolved in THF (0.06 M) and the mixture was cooled down to 0 °C. LiOH (2 eq.) and H_2O (304 eq.) were added and the mixture stirred at 0 °C until full starting material consumption was observed by TLC. The reaction mixture was acidified to pH 3 using 1 M HCl. The mixture was concentrated under reduced pressure and the residue dissolved in $CHCl_3$. Organic layer was extracted twice with $CHCl_3$ and once with CH_2Cl_3 3:1 isopropanol. The organic layer was dried over sodium sulfate and the mixture concentrated. The crude material was purified by trituration with hexane or diethyl ether.

(S)-5-(2-((((9H-Fluoren-9-yl)methoxy)carbonyl)amino)-2-carboxyethyl)-1,3-dipropyl-1H-imidazol-3-ium bromide ***182***:

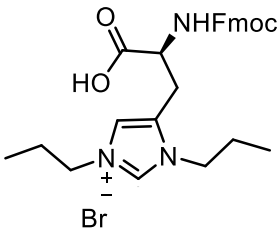

Following GP4 using imidazolium salt **151** (0.100 g, 0.180 mmol), THF (3.00 mL), LiOH (9.00 mg, 0.360 mmol) and H_2O (1.01 mL). Full consumption observed by TLC (CH_2Cl_2 9:1 MeOH) 30 min after the start of reaction. Trituration of crude material with hexane gave access to **182** as a white solid (0.0520 g, 0.100 mmol) with 56% yield. **Mp.:** 72-75 °C; **IR (neat)** $\nu_{(max)}$ cm^{-1}: 3386 w, 2964 w, 1706 s, 1605 w, 1559 w, 1530 w, 1449 m, 1248 s, 1158 m, 1047 s, 859 w, 760 s, 740 s; **^{1}H NMR (300 MHz, Chloroform-d)** δ 10.12 (br s, 1H, CO_2H), 9.74 (s, 1H, NCHN), 7.75 (d, *J* = 7.4 Hz, 2H, arom. Fmoc), .7.60 (d, *J* = 5.4 Hz, 1H, arom. Fmoc), 7.58 (d, *J* = 5.0 Hz, 1H, arom. Fmoc) 7.39 (t, *J* = 7.2 Hz, 2H, arom. Fmoc), 7.36 – 7.28 (m, 3H, arom. Fmoc and NC*H*CN), 6.11 (br s, 1H, NH), 4.44 – 4.36 (m, 1H, αCH), 4.25 – 4.09 (m, 3H, CH and CH_2 Fmoc), 4.06-3.94 (m, 4H, 2 CH_2 propyl), 3.30 (br s, 2H, βCH_2), 1.81 (m, 4 H, 2 CH_2 propyl), 0.89 (t, *J* = 4.9 Hz, 3H, CH_3 propyl), 0.86 (t *J* = 4.6 Hz, 3H, CH_3); **^{13}C NMR (101 MHz, Chloroform-d)** δ 172.8 (CO_2H), 156.2 (CO_2 Fmoc), 144.0 (C arom Fmoc), 143.7 (C arom Fmoc), 141.5 (C arom. Fmoc,) 141.4 (C arom. Fmoc), 135.6 (CH NCHN), 131.9 (C NCHCN), 128.0(CH arom. Fmoc), 127.3 (CH arom. Fmoc), 125.2 (CH arom. Fmoc), 125.1 (CH arom. Fmoc), 121.1 (CH NCHCN), 120.17 (CH arom Fmoc), 120.15 (CH arom. Fmoc), 66.8 (CH_2 Fmoc), 54.4 (αCH), 51.2 (CH_2 propyl), 48.6 (CH_2 propyl), 47.3 (CH Fmoc), 23.8 (CH_2 propyl), 23.6 (CH_2 propyl), 22.8 (βCH_2), 10.88 (CH_3 propyl), 10.81 (CH_3 propyl); **HRMS (ESI):** *m/z* calculated for $C_{27}H_{32}N_3O_4^+$: 462.2392, found 462.2387 $[M\text{-}Br]^+$.

(S)-5-(2-((((9H-Fluoren-9-yl)methoxy)carbonyl)amino)-2-carboxyethyl)-1,3-dipropyl-1H-imidazol-3-ium iodide ***183***:

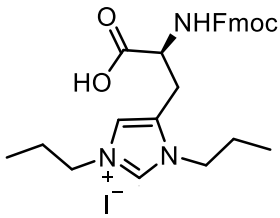

Following GP4 using imidazolium salt **152** (0.100 g, 0.160 mmol), THF (2.60 mL), LiOH (8.00 mg, 0.330 mmol) and H_2O (0.890 mL). Full consumption observed by TLC (CH_2Cl_2 9:1 MeOH) 30 min after the start of reaction. Trituration of crude material with hexane gave access to **183** as a white solid yield (0.063 g, 0.110 mmol) in 67%. **$[\alpha]_D$ =** +3.60 (c 1, MeCN); **Mp.:** 60-62 °C; **IR (neat)** $\nu_{(max)}$ cm^{-1}: 3388 w, 2966 w, 1705 s, 1606 m, 1558 m, 1449 s, 1246 m, 1157 m, 1047 s, 916 w, 760 s, 738 s, 620 m; **^{1}H NMR (300 MHz, Chloroform-d)** δ 9.45 (s, 1H, NCHN), 7.76 (d, *J* = 7.4 Hz, 2H, arom. Fmoc), 7.61 (d, *J* = 5.8 Hz, 1H, arom. Fmoc), 7.59 (d, *J* = 5.6 Hz, 1H, arom. Fmoc), 7.40 (t, *J* = 7.2 Hz, 2H, arom Fmoc), 7.36 – 7.27 (m, 3H, arom. Fmoc and NCHCN), 6.11 (s, 1H, NH), 4.51 – 4.39 (m, 1H, αCH), 4.37 (br. d, *J* = 8.0 Hz, 2H, CH_2 Fmoc), 4.16 (m, 3H, CH Fmoc and CH_2 Propyl), 4.08 – 3.92 (m, 2H, CH_2 propyl), 3.31 (s, 2H, βCH_2), 1.83 (m, 4H, CH_2 propyl), 0.98 – 0.81 (m, 6H, CH_3 propyl); **^{13}C NMR (101 MHz, Chloroform-d)** δ 172.9 (CO_2H), 156.3 (CO_2 Fmoc), 144.0 (C arom. Fmoc), 143.7(C arom. Fmoc), 141.5 (C arom. Fmoc), 141.4 (C arom. Fmoc), 135.1 (CH NCHN), 132.1 (C NCHCN), 127.92 (CH arom. Fmoc), 127.24 (CH arom. Fmoc), 125.2 (CH arom. Fmoc), 125.08(CH arom. Fmoc), 120.2 (CH NCHCN), 66.9 (CH_2 Fmoc), 54.5 (αCH), 51.3 (CH_2 propyl), 48.6 (CH_2 propyl), 47.2 (CH Fmoc), 29.8 (βCH_2), 26.1 (CH_2 propyl), 23.7(CH_2 propyl), 23.6(CH_2 propyl),10.9 (CH_3 propyl), 10.8(CH_3 propyl); **HRMS (ESI):** *m/z* calculated for $C_{27}H_{32}N_3O_4^+$: 462.2392, found 462.2404 $[M-I]^+$.

(S)-5-(2-((((9H-Fluoren-9-yl)methoxy)carbonyl)amino)-2-carboxyethyl)-1,3-diallyl-1H-imidazol-3-ium bromide ***184****:*

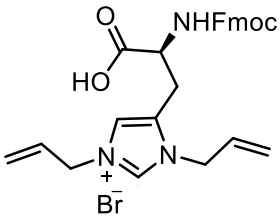

Following GP4 using imidazolium salt **153** (0.060 g, 0.110mmol), THF (1.8 mL), LiOH (0.005 g, 0.210 mmol) and H_2O (0.611 mL). Full consumption observed by TLC (CH_2Cl_2 9:1 MeOH) 30 min after the start of reaction. Trituration with hexane gave access to **184** as a beige solid (0.023 g, 0.043 mmol) in 39% yield. **Mp.:** 94-95 °C; **IR (neat)** $\nu_{(max)}$ cm^{-1}: 3359 br w, 3039 w, 1714 s, 1590 s, 1559 s, 1448 m, 1379 m, 1297 w, 1152 s, 937 m, 917 m, 728 s, 669 w; **^{1}H NMR (400 MHz, Chloroform-d)** δ 9.76 (s, 1H, NCHN), 7.74 (d, *J* = 7.3 Hz, 2H, arom. Fmoc), 7.59 (t, *J* = 7.2 Hz, 2H, arom. Fmoc), 7.37 (t, *J* = 7.3 Hz, 2H, arom. Fmoc), 7.28 (t, *J* = 7.6 Hz, 2H, arom. Fmoc), 7.06 (s, 1H, NCHCN), 6.37 (d, *J* = 3.6 Hz, 1H, NH), 5.97 – 5.79 (m, 2H, CH allyl), 5.30 (d, *J* = 11.4 Hz, 2H, CH_2 allyl), 5.26 (d, *J* = 4.4 Hz, 1H, CH_2 allyl), 5.14 (d, *J* = 17.1 Hz, 1H, CH_2 allyl), 5.01 – 4.91 (m, 1H, CH_2 allyl), 4.89 – 4.80 (m, 1H, CH_2 allyl), 4.78 – 4.70 (m, 2H, CH_2 allyl), 4.36 (d, *J* = 6.8 Hz, 2H, CH_2 allyl), 4.26 – 4.21 (m, 1H, αCH), 4.17 (t, *J* = 6.8 Hz, 1H, CH Fmoc), 3.23 (br s, 2H, βCH_2); **^{13}C NMR (101 MHz, Chloroform-d)** δ 172.9 (CO_2 Me), 156.2 (CO_2 Fmoc), 144.1 (C arom. Fmoc), 143.9 (C arom. Fmoc), 141.4 (C arom. Fmoc), 141.3 (C arom. Fmoc), 136.5 (CH NCHN), 133.1 (C NCHCN), 130.8 (CH allyl), 130.2 (CH allyl) 127.8 (CH arom. Fmoc), 127.2 (CH arom. Fmoc), 125.22 (CH arom. Fmoc), 125.18 (CH arom. Fmoc), 121.9 (CH_2 allyl), 120.5 (CH_2 allyl), 120.1 (CH NCHCN), 66.6 (CH_2 Fmoc), 54.7 (αCH), 49.3 (CH_2 allyl), 47.347.1 (CH Fmoc), 26.5 (βCH_2); **HRMS (ESI):** *m/z* calculated for $C_{27}H_{28}N_3O_4^+$: 458.2096, found 458.2088 [M-Br]$^+$.

(S)-5-(2-((((9H-Fluoren-9-yl)methoxy)carbonyl)amino)-2-carboxyethyl)-1,3-dibutyl-1H-imidazol-3-ium iodide ***185****:*

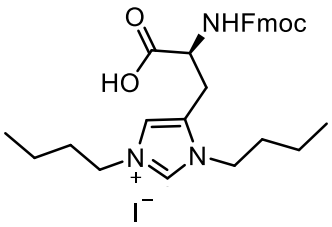

Following GP4 using imidazolium salt **155** (0.100 g, 0.160 mmol), THF (0.890 mL), LiOH (0.007 g, 0.310 mmol) and H_2O (2.70 mL). Full consumption observed by TLC (CH_2Cl_2 9:1 MeOH) 30 min after the start of reaction. Trituration with diethyl ether gave access to **185** as yellow solid (0.051 g, 0.083 mmol) with 52% yield. **$[\alpha]_D$ =** + 3.50 (c 0.7, MeCN); **Mp.:** 55-57°C; **IR (neat)** $\nu_{(max)}$ cm^{-1}: 3376 w, 2958 w, 1705 s, 1606 m, 1448 m, 1156 s, 1046 s, 739 s; **^{1}H NMR (300 MHz, Chloroform-d)** δ 9.33 (s, 1H, NCHN), 7.74 (d, *J* = 7.4 Hz, 2H, arom. Fmoc), 7.60 (t, *J* = 8.3 Hz, 2H, arom. Fmoc), 7.41 (s, 1H, NCHCN), 7.39 (t, *J* = 7.5 Hz, 2H, arom. Fmoc), 7.35 – 7.27 (m, 2H, arom. Fmoc), 6.29 (d, *J* = 4.6 Hz, 1H, NH), 4.54 – 4.39 (m, 1H, αCH), 4.39 – 4.24 (m, 2H, CH_2 Fmoc), 4.24 – 4.00 (m, 5H, CH Fmoc and CH_2 butyl), 3.45 – 3.20 (m, 2H, βCH_2), 1.90 – 1.67 (m, 4H, CH_2 butyl), 1.28 (tt, *J* = 14.5, 6.1 Hz, 4H, CH_2 butyl), 0.98 – 0.82 (m, 6H, CH_3 butyl); **^{13}C NMR (101 MHz, Chloroform-d)** δ 172.9 (CO_2 H), 156.2 (CO_2 Fmoc), 144.0 (C arom. Fmoc), 143.6 (C arom. Fmoc), 141.40 (C arom. Fmoc), 141,35 (C arom. Fmoc), 135.0 (CH NCHN), 131.8 (C NCHCN), 128.0 (CH arom. Fmoc), 127.3 (CH arom. Fmoc), 125.3 (CH arom. Fmoc), 125.2 (CH arom. Fmoc), 120.2 (CH NCHCN), 67.2 (CH_2 Fmoc), 54.0 (αCH), 49.9 (CH_2 Bu), 47.3 (CH_2 Bu), 47.1 (CH Fmoc), 32.2 (CH_2 Bu), 32.1 (CH_2 Bu), 26.3 (βCH_2), 19.7 (CH_2 Bu), 19.6 (CH_2 Bu), 13.61 (CH_3 Bu), 13.59 (CH_3 Bu); **HRMS (ESI):** *m/z* calculated for $C_{29}H_{36}N_3O_4^+$: 490.2697, found 490.2700 $[M\text{-}I]^+$.

*(S)-5-(2-((((9H-Fluoren-9-yl)methoxy)carbonyl)amino)-2-carboxyethyl)-1,3-diisopropyl-1H-imidazol-3-ium iodide **186**:*

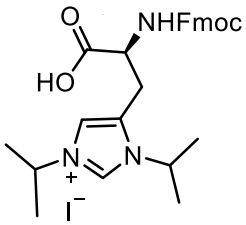

Following GP4 using imidazolium salt **154** (0.100 g, 0.170 mmol), THF (0.950 mL), LiOH (0.008 g, 0.330 mmol) and H_2O (2.80 mL). Full consumption observed by TLC (CH_2Cl_2 9:1 MeOH) 30 min after the start of reaction. Trituration with hexane gave access to **186** as a white solid (0.044 g, 0.075 mmol) in 44% yield. **$[\alpha]_D$ =** +4.84 (c 1, MeCN); **Mp.:** 140-143 °C; **IR (neat)** $\nu_{(max)}$ cm^{-1}: 2980 w, 2970 w, 1710 m, 1599 w, 1448 m, 1244 m,1048 m, 761 s, 739 s; **^{1}H NMR (400 MHz, Chloroform-d)** δ 9.58 (s, 1H, NCHN), 7.73 (d, *J* = 7.5 Hz, 2H, CH arom. Fmoc), 7.59 (d, *J* = 7.5 Hz, 1H, CH arom. Fmoc), 7.56 (d, *J* = 7.6 Hz, 1H, CH arom. Fmoc), 7.45 (s, 1H, NCHCN), 7.38 (t, *J* = 7.4 Hz, 2H, CH arom. Fmoc), 7.32 – 7.25 (m, 2H, CH arom. Fmoc), 6.23 (d, *J* = 4.8 Hz, 1H, NH), 4.80 (m, 1H, CH isopropyl), 4.65 – 4.55 (br. m, 1H, αCH), 4.45 – 4.34 (m, 2H, CH_2 Fmoc), 4.25 (t, *J* = 6.8 Hz, 1H, CH Fmoc), 4.15 (m, 1H, CH isopropyl), 3.31 (br. s, 2H, βCH_2), 1.55 (br. s, 6H, CH_3 isopropyl), 1.50 (d, *J* = 6.7 Hz, 3H, CH_3 isopropyl), 1.47 (d, *J* = 6.7 Hz, 3H, CH_3 isopropyl); **^{13}C NMR (101 MHz, Chloroform-d)** δ 172.9 (CO_2H), 156.3 (CO_2 Fmoc), 143.9 (C arom. Fmoc), 143.6 (C arom. Fmoc), 141.4 (C arom. Fmoc) 141.3 (C arom. Fmoc), 132.6 (CH NCHN), 131.3 (C NCHCN), 128.0 (CH arom. Fmoc), 127.2 (CH arom. Fmoc), 125.3 (CH arom. Fmoc), 125.1 (CH arom. Fmoc), 120.2 (CH NCHCN), 67.1 (CH_2 Fmoc), 54.0 (αCH), 53.4 (CH isopropyl), 50.7 (CH isopropyl), 47.1 (CH Fmoc), 26.6 (βCH_2), 23.7 (CH_3 isopropyl), 23.5 (CH_3 isopropyl), 23.1 (CH_3 isopropyl), 23.0 (CH_3 isopropyl); **HRMS (ESI):** *m/z* calculated for $C_{27}H_{32}N_3O_4^+$: 462.2392, found 462.2404 $[M-I]^+$; **Elemental analysis** calculated for: $C_{27}H_{32}N_3O_4I$: C, 55.01; H, 5.47; N, 7.13. Found: C, 55.25; H, 5.29; N, 7.42.

(S)-5-(2-((((9H-Fluoren-9-yl)methoxy)carbonyl)amino)-2-carboxyethyl)-1,3-dibenzyl-1H-imidazol-3-ium bromide ***180***:

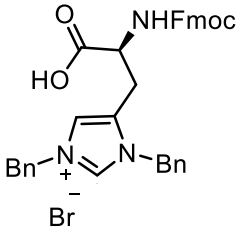

Following GP4 using imidazolium salt **146** (8.04 g, 12.3 mmol), THF (208 mL), LiOH (0.590 g, 24.6 mmol) and H_2O (69.0 mL). Full consumption observed by TLC (CH_2Cl_2 9:1 MeOH) 30 min after he start of reaction. Trituration with hexane gave access to **180** as a white solid (7.35 g, 11.5 mmol) in 93% yield. **$[\alpha]_D$ =** +17.3 (c 1, $CHCl_3$); **Mp.:** 86-88 °C; **IR (neat)** $\nu_{(max)}$ cm^{-1}: 3360 w, 2918 w, 1707 m, 1603 m, 450 m, 1365 m, 1049 m, 759 m, 735 s, 701 s; **^{1}H NMR (400 MHz, Chloroform-d)** δ 9.95 (s, 1H, NCHN), 7.73 (app. t, *J* = 6.7 Hz, 2H, arom. Fmoc), 7.58 (t, *J* = 6.6 Hz, 2H, arom. Fmoc), 7.42 – 7.18 (m, 14H, arom Fmoc and arom. Bn), 7.08 (s, 1H, NCHCN), 6.44 – 6.28 (br. s, 1H, NH), 5.54 (d, *J* = 15.0 Hz, 1H, Bn CH_2), 5.43 – 5.26 (m, 2H, Bn CH_2), 5.20 (d, *J* = 14.3 Hz, 1H, Bn CH_2), 4.43 – 4.29 (m, 2H, Fmoc CH_2), 4.27 (br. s, 1H, αCH), 4.14 (t, *J* = 6.7 Hz, 1H, CH Fmoc), 3.27 (br. d, *J* = 13.4 Hz, 1H, βCH_2), 3.14 (dd, *J* = 14.6, 4.4 Hz, 1H, βCH_2); **^{13}C NMR (101 MHz, Chloroform-d)** δ 173.0 (CO_2H), 156.2 (CO_2 Fmoc), 144.2 (C arom. Fmoc), 144.0 (C arom. Fmoc), 141.5 (C arom. Fmoc), 141.4 (C arom. Fmoc), 136.4 (CH NCHN), 133.5 (C Bn), 133.4 (C Bn), 133.2 (C, NCHCN), 129.6 (CH arom.), 129.5 (CH arom.), 129.2 (CH arom.), 128.5 (CH arom.), 127.8 (CH arom.), 127.2 (CH arom.), 125.3 (CH arom.), 120.1 (CH NCHCN), 66.5 (CH_2 Fmoc), 54.8 (αCH), 53.2 (CH_2 Bn), 50.8 (CH_2 Bn), 47.4 (CH Fmoc), 26.5 (βCH_2); **HRMS (ESI):** *m/z* calculated for $C_{35}H_{32}N_3O_4^+$: 558.2393, found 558.2392 $[M\text{-}Br]^+$; **Elemental analysis** calculated for: $C_{35}H_{32}N_3O_4Br$: C, 65.83; H, 5.05; N, 6.58; found: C, 65.66; H, 5.08; N, 6.86.

(S)-5-(2-((((9H-Fluoren-9-yl)methoxy)carbonyl)amino)-2-carboxyethyl)-1,3-bis(4-(trifluoromethyl)benzyl)-1H-imidazol-3-ium bromide ***187****:*

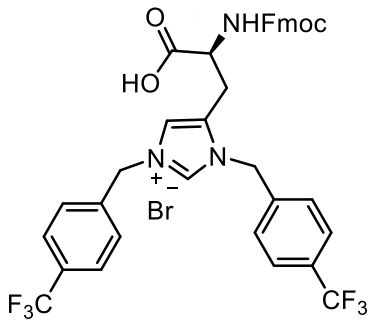

Following GP4 using imidazolium salt **147** (0.100 g, 0.130 mmol), THF (2.00 mL), LiOH (6.00 mg, 0.250 mmol) and H_2O (0.723 mL). Full consumption observed by TLC (CH_2Cl_2 9:1 MeOH) 30 min after the start of the reaction. Trituration with hexane gave access to **187** as a white foam (0.0520 g, 0.0670 mmol) in 52% yield. **$[\alpha]_D$ =** +1.66 (c 0.5, MeCN); **Mp.:** 130-131 °C; **IR (neat)** $\nu_{(max)}$ cm^{-1}: 2956 w br, 1709 m, 1619 w, 1450 w, 1323 s, 1163 m, 1114 s, 1067 s, 1018 m, 822 w, 740 m, 614 w; **^{1}H NMR (400 MHz, Chloroform-d)** δ 10.04 (s, 1H, NCHN), 7.74 – 7.67 (m, 2H, arom. Fmoc), 7.61 – 7.47 (m, 8H, arom. Ph), 7.40 (br. d, *J* = 7.9 Hz, 2H, arom. Fmoc), 7.34 (m, 3H, arom. Fmoc and NCHCN), 6.30 (br. s, 1H, NH), 5.66 (d, *J* = 14.9 Hz, 1H, Bn CH_2), 5.42 (m, 3H, Bn CH_2), 4.42 – 4.27 (m, 3H, αCH and Fmoc CH_2), 4.12 (t, *J* = 6.4 Hz, 1H, CH Fmoc), 3.18 (br. d, *J* = 13.8 Hz, 1H, βCH_2), 3.10 (br. d, *J* = 15.5 Hz, 1H, βCH_2); **^{13}C NMR (101 MHz, Chloroform-d)** δ 173.1 (CO_2H), 156.1 (CO_2 Fmoc), 144.0 (C arom.), 143.6 (C arom.), 141.5 (C arom.), 137.1 (C arom.), 137.0 (C arom.), 136.6 (CH NCHN), 132.9 (C arom.), 131.8 (q, *J* = 32.9 Hz, C CCF_3), 131.5 (q, *J* = 33.0 Hz, C CCF_3), 129.1 (CH arom.), 128.8 (CH arom.), 128.4 (CH arom.), 128.0 (CH arom.), 127.2 (CH arom.), 126.5 (q, *J* = 4.9 Hz, $CHCCF_3$), 125.1 (q, *J* = 4.6 Hz, $CHCCF_3$), 123.7 (q, *J* = 277 Hz CF3), 123.6 (q, *J* = 278 Hz, CF_3), 120.2 (CH NCHCN), 66.8 (CH_2 Fmoc), 54.4 (αCH), 52.6 (CH_2 pCF_3Bn), 50.3 (CH_2 pCF_3Bn), 47.3 (CH Fmoc), 26.5 (βCH_2); **HRMS (ESI):** *m/z* calculated for $C_{75}H_{30}F_6N_3O_4^+$: 694.2135, found 694.2148 $[M\text{-}Br]^+$.

(S)-5-(2-((((9H-Fluoren-9-yl)methoxy)carbonyl)amino)-2-carboxyethyl)-1,3-bis(pyridin-2-ylmethyl)-1H-imidazol-3-ium bromide ***188****:*

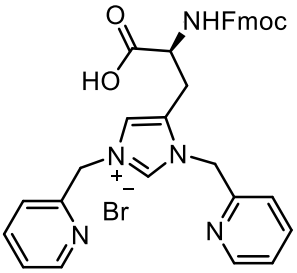

Following GP4 using imidazolium salt **148** (0.050 g, 0.063 mmol), THF (1.00 mL), LiOH (3.00 mg, 0.126 mmol) and H_2O (0.350 mL). Full consumption observed by TLC (CH_2Cl_2 9:1 MeOH) 30 min after he start of reaction. Trituration with hexane gave access to **188** as a beige solid (0.0300 g, 0.0390 mmol) in 61% yield. **$[\alpha]_D$ =** + 45.7 (c 0.11, MeCN); **Mp.:** 120-111 °C; **IR (neat)** $\nu_{(max)}$ cm^{-1}: 3044 br w, 2961 w, 1708 s, 1593 m, 1572 m, 1557 w, 1477 w, 1436 s, 1247 s, 1152 s, 1049 s, 996 m, 834 w, 758 s, 740 s; **^{1}H NMR (300 MHz, Chloroform-*d*)** δ 9.64 (s, 1H, NCHN), 8.45 (t, *J* = 5.7 Hz, 2H, arom. Py), 7.79 – 7.69 (m, 2H, arom.), 7.67 – 7.59 (m, 4H, arom.), 7.47 – 7.40 (m, 3 H, arom.), 7.33 – 7.29 (m, 3H, arom.), 7.25 – 7.15 (m, 2H, arom.), 6.34 (br. s, 1H, NH), 5.61 (dd, *J* = 31.0, 15.4 Hz, 2H, CH_2 Py), 5.40 (app. t, *J* = 15.7 Hz, 2H, CH_2 Py), 4.51 – 4.30 (m, 3H, CH_2 Fmoc and αCH), 4.18 (t, *J* = 6.4 Hz, 1H, Ch Fmoc), 3.44 – 3.10 (br. m, 2H, βCH_2); **^{13}C NMR (101 MHz, Chloroform-d)** δ 173.1 8 (CO_2 H), 156.2 8 (CO_2 Fmoc), 152.8 (C arom.), 152.6 (C arom.), 150.02 (C arom.), 149.98 (CH Py), 144.1 (C arom.), 143.8 (C arom.), 141.43 (C arom.), 141.36 (C. arom.), 137.7 (CH NCHN), 137.9 (CH Py), 137.2 (CH Py), 132.4 (C NCHCN), 127.9 (CH arom.), 127.3(CH arom.), 125.3(CH arom.), 125.2(CH arom.), 123.9 (CH arom.), 123.8(CH arom.), 123.2 (CH arom.), 123.0 (CH arom.), 120.1, (CH NCHCN) 66.7 (CH Fmoc), 54.5 (αCH), 54.1 (CH_2 Py), 51.6 (CH_2 Py), 47.4 (CH Fmoc), 26.6 (βCH_2); **HRMS (ESI):** *m/z* calculated for $C_{33}H_{30}N5O_4^+$: 560.2292, found 560.2307 $[M]^+$.

(S)-5-(2-((((9H-Fluoren-9-yl)methoxy)carbonyl)amino)-2-carboxyethyl)-1-(4-methoxyphenyl)-3-methyl-1H-imidazol-3-ium iodide ***189****:*

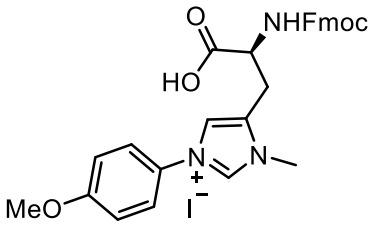

Following GP4 using imidazolium salt **174** (2.00 g, 3.10 mmol), THF (52.0 mL), LiOH (0.150 g, 6.20 mmol) and H_2O (17.0 mL). Full consumption was observed by TLC (CH_2Cl_2 9:1 MeOH) 30 min after the start of reaction. Trituration with hexane gave **189** as a yellow solid (1.30 g, 2.07 mmol) in 67% yield. **$[\alpha]_D$ =** +30.3 (c 1, $CHCl_3$); **Mp.:** 80-81 °C; **IR (neat) $\nu_{(max)}$** cm^{-1}: 2957 b w, 1705 m, 1603 m, 1514 s, 1386 m, 1253 s, 1180 m, 1104 w, 1180 s, 1029 m, 831 m, 760 s, 739 s, 649 w, 620 m; **^{1}H NMR (400 MHz, Chloroform-d**) δ 9.50 (s, 1H, NCHN), 7.73 – 7.62 (m, 2H, arom. Fmoc), 7.55 (t, *J* = 8.1 Hz, 2H, arom. Fmoc), 7.39 – 7.28 (m, 4H, arom. Fmoc), 7.23-7.19 (m, 2H, arom.), 6.78 (dd, *J* = 21.7, 8.1 Hz, 2H, arom.), 6.50 (s, 1H, NCHCN), 4.38 – 4.23 (m, 2H, CH_2 Fmoc), 4.09 (br s, 1H, αCH), 3.89 (br s, 1H, CH Fmoc), 3.71 (br. s, 6H, CH_3), 3.35 – 3.19 (m, 2H, βCH_2);**^{13}C NMR (101 MHz, Chloroform-d)** δ 160.6 (CO_2H), 156.3 (CO_2Fmoc), 144.0 (C arom.), 143.7 (C arom.), 141.3 (C arom.), 136.1 (CH NCHN), 133.7(C NCHCN),127.9 (CH arom. Fmoc), 127.4 (CH arom. Fmoc), 127.2 (CH arom. Fmoc), 125.2(CH arom. Fmoc), 123.2 (CH arom. Fmoc), 120.1 (CH arom. Fmoc), 119.4 (CH NCHCN), 115.4 (CH arom. Ph), 66.8 (CH_2 Fmoc), 55.8 (OCH_3), 55.1 (αCH), 47.2 (CH Fmoc), 34.4 (NCH_3), 26.7 (βCH_2); **HRMS (ESI):** *m/z* calculated for $C_{29}H_{328}N_3O_5$: 498.2014, found 498.2023 $[M-I]^+$.

(S)-5-(2-((((9H-Fluoren-9-yl)methoxy)carbonyl)amino)-2-carboxyethyl)-3-allyl-1-(4-methoxyphenyl)-1H-imidazol-3-ium bromide ***190***:

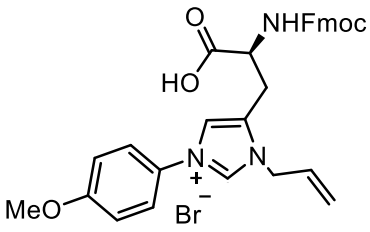

Following GP4 using NHC salt **165** (0.050 g, 0.080 mmol), THF (1.30mL), LiOH (4.00 mg, 0.160 mmol) and H_2O (0.429 mL). Full consumption observed by TLC (CH_2Cl_2 9:1 MeOH) 30 min after the start of reaction. Trituration with hexane gave **190** as a beige solid (0.029 g, 0.048 mmol) in 60% yield. **Mp.:** 118-119 °C; **IR (neat)** $\nu_{(max)}$ cm^{-1}: 2950 w, 1709 s, 1606 s, 1557 s, 1514 s, 1449 m, 1255 s, 1031 m, 833 m, 761 s, 741 s; **^{1}H NMR (400 MHz, Chloroform-d)** δ 9.95 (s, 1H, NCHN), 7.70 (t, *J* = 7.1 Hz, 2H, arom. Fmoc), 7.64 – 7.54 (m, 2H, arom. Fmoc), 7.45 (br s, 3H, arom. Fmoc and NCHCN), 7.39 – 7.29 (m, 2H, arom. Fmoc), 7.25 – 7.18 (m, 2H, arom. Ph), 6.89 (d, *J* = 6.5 Hz, 2H, arom. Ph), 6.51 (br. s, 1H, NH), 5.92 (br. s, 1H, CH allyl), 5.28 – 4.86 (m, 4H, 2 CH_2 allyl), 4.34 (m, 3H, CH_2 Fmoc and αCH), 4.15 (t, *J* = 7.0 Hz, 1H, CH Fmoc), 3.32 (br s, 2H, βCH_2); **^{13}C NMR (101 MHz, Chloroform-d)** δ 160.6 (CO_2 H), 156.4 (CO_2 Fmoc), 144.1 (C arom.), 143.8 (C arom.), 141.4 (C arom.), 134.4 (CH NCHN), 133.5 (C NCHCN), 130.7 (CH allyl), 127.8 (CH arom), 127.6 (C arom.), 127.2 (CH arom), 125.3 (CH arom.), 125.2 (CH arom.), 123.1 (CH arom), 120.9 (CH_2 allyl), 120.1 (CH arom. Fmoc), 119.4 (CH NCHCN), 115.3 (CH arom. Ph) 66.8 (CH_2 Fmoc), 55.78 (αCH), 49.7 (NCH_2 allyl), 47.3 (CH Fmoc), 26.5 (βCH_2); **HRMS (ESI):** *m/z* calculated for $C_{31}H_{30}N_3O_5^+$: 524.2180, found 524.2192 $[M]^+$.

(S)-5-(2-Amino-3-methoxy-3-oxopropyl)-1,3-dibenzyl-1H-imidazol-3-ium bromide ***191***:

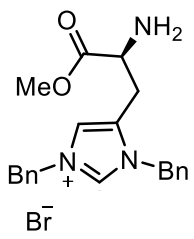

Imidazolium salt **146** (0.200 g, 0.310 mmol) was dissolved in dichloromethane (6.20 mL) and piperidine (0.105 mL, 1,10 mmol) was added. The mixture was stirred at room temperature for 18 hours until TLC showed complete conversion (CH_2Cl_2 9:1 MeOH). The mixture was concentrated and triturated with hexane. The precipitate was then purified by automated flash chromatography on alumina 20% MeOH in dichloromethane to yield product **191** as a sticky beige solid (0.133 g, 0.310 mmol) with quantitative yield. **$[\alpha]_D$ =** + 20.7 (c 0.2, MeCN); **IR (neat)** $\nu_{(max)}$ cm^{-1}: 3370 br w, 2949 m, 1734, s, 1601 w. 1557 s, 1497 m, 1455 s, 1206 s, 1157 s, 1029 m, 924 m, 704 br s; **^{1}H NMR (400 MHz, Chloroform-d)** δ 10.74 (s, 1H, NCHN), 7.50 – 7.27 (m, 10H, arom. Bn), 7.09 (s, 1H, NCHCN), 5.65 (s, 2H, CH_2 Bn), 5.54 (s, 2H CH_2 Bn), 3.65 (s, 3H, OCH_3), 3.59 – 3.56 (m, 1H, αCH), 2.93 (dd, *J* = 15.6, 4.5 Hz, 1H, βCH_2), 2.70 (dd, *J* = 15.4, 8.3 Hz, 1H, βCH_2); **^{13}C NMR (101 MHz, Chloroform-d)** δ 173.8 (CO_2 Me), 138.1 (NCHN), 133.2 (C Bn), 133.0 (C Bn), 132.2 (C NCHCN), 129.6(CH arom. Bn), 129.3(CH arom. Bn), 129.1(CH arom. Bn), 128.0 (CH arom. Bn), 120.3 (CH NCHCN), 53.7 (CH_2 Bn), 53.3 (αCH), 52.8 (OCH_3), 51.5 (CH_2 Bn), 28.7 (βCH_2); **HRMS (ESI):** *m/z* calculated for $C_{21}H_{24}N_3O_2^+$: 350.1863, found 350.1869 $[M+H]^+$.

6.5 – Solution Peptide Coupling:

General Procedure 5 for the amide coupling of NHC amino acids in solution (GP5):

A heat gun dried Schlenk tube under argon was charged with imidazolium salt (1 eq.), Glycine benzyl ester or Fmoc-L-Ala-OH (1 eq.), and HATU (1 eq). The solids were

dissolved in dry THF (0.1 M) and then DIEA (3 eq) was added. The reaction mixture was stirred at room temperature until complete consumption of imidazolium salt was visible by TLC. The mixture was concentrated and purified by flash silica gel column chromatography.

*Dipeptide **193:***

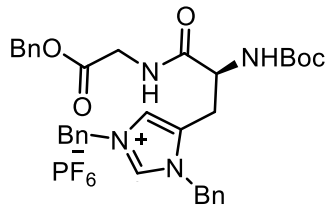

Following GP5 glycine benzyl ester (8.00 mg, 0.039 mmol), imidazolium **178** (0.0200 g, 0.039 mmol), HATU (0.0150 g, 0.039 mmol) and DIEA (0.0200 mL, 0.120 mmol) were dissolved in THF (1.00 mL). Flash chromatography on silica gel (CH_2Cl_2 9:2 MeOH) yielded product **193** as a beige solid (0.008 g, 0.011 mmol) in 28% yield. **IR (neat)** $\nu_{(max)}$ cm^{-1}: 3311 w, 2919 w, 1742 m, 1677 m, 1639 m, 1561 m, 1489 m, 1405 w, 1366 w, 1253 m, 1192 m, 1162 s, 828 s, 777 w, 737 m, 698 s, 659 m; **^{1}H NMR (400 MHz, Chloroform-d)** δ 8.33 (s, 1H, NCHN), 7.45 – 7.28 (m, 16H, arom. and NCHCN), 6.74 (t, *J* = 5.2 Hz, 1H, NH), 5.55 (d, *J* = 15.6 Hz, 2H, NH and CH_2 Bn), 5.35 (d, *J* = 15.2 Hz, 1H, CH_2 Bn), 5.26 – 5.11 (m, 4H, CH_2 Bn), *4*.27 (dd, *J* = 12.9, 3.7 Hz, 1H, αCH), 4.21 (dd, *J* = 17.8, 6.5 Hz, 1H, CH_2 Gly), 3.80 (dd, *J* = 17.7, 5.4 Hz, 1H, CH_2 Gly), 3.06 (dd, *J* = 15.2, 3.6 Hz, 1H, βCH_2), 2.91 (dd, *J* = 15.0, 9.4 Hz, 1H, βCH_2), 1.44 (s, 9H, $C(CH_3)_3$); **^{13}C NMR (101 MHz, Chloroform-d)** δ 169.9 (CO_2R), 169.5 (CO_2R), 155.1(CO_2Boc), 135.5 (C arom), 135.1 (C arom), 132.7 (C arom), 132.3 (C arom), 130.7 (NCHN), 129.7 (CH arom.), 129.6 (2CH arom.), 129.5 (CH arom.), 129.3 (CH arom.), 128.8 (CH arom.), 128.6 (CH arom.), 128.5, 128.2 (CH arom.), 122.5 (CH NCHCN), 80.7 (C $C(CH_3)_3$), 67.2 (CH_2 Bn), 53.8 (CH_2 Bn), 53.4 (αCH), 51.2 (CH_2 Bn), 29.8 (βCH_2), 28.4 (CH_3 $C(CH_3)_3$), 28.0 (βCH_2); **^{31}P NMR (121 MHz,**

Chloroform-d) δ -144.42 (hept, $J_{P,\ F}$ = 713.5 Hz); **HRMS (ESI):** *m/z* calculated for $C_{34}H_{39}N_4O_5^+$: 583.2937, found 583.2923 $[M]^+$.

*Dipeptide **192:***

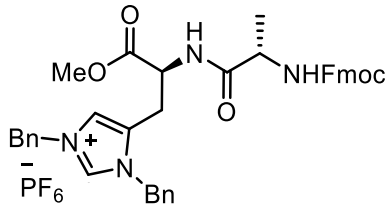

Following GP5 Fmoc-L-Ala-OH (0.040 g, 0.130 mmol), imidazolium **191** (0.0600 g, 0.130 mmol), HATU (0.0490 g, 0.0130 mmol) and DIEA (0.068 mL, 0.390 mmol) were dissolved in THF (5 mL). Flash chromatography on silica gel (CH_2Cl_2 9:2 MeOH) gave access to product **192** as a sticky white solid (0.020 g, 0.026 mmol) in 20% yield.**^{1}H NMR (400 MHz, Chloroform-d)** δ 8.04 (s, 1H, NCHN), 7.75 (d, *J* = 7.6 Hz, 2H, arom. Fmoc), 7.60 (d, *J* = 8.4 Hz, 2H, arom. Fmoc), 7.38 (m, 5H, arom.), 7.34 – 7.28 (m, 5H, arom.), 7.25 – 7.21 (m, 4H, arom.), 7.18 (s, 1H, NCHCN), 6.98 (d, *J* = 10.0 Hz, 1H, NH), 5.29 – 5.13 (m, 4H, CH_2 Bn), 4.84 – 4.65 (m, 1H, αCH), 4.37 (dd, *J* = 10.7, 7.4 Hz, 1H, CH_2 Fmoc), 4.29 (dd, *J* = 10.4, 7.1 Hz, 1H, CH_2 Fmoc), 4.24 – 4.14 (m, 2H, CH Fmoc and αCH), 3.70 (s, 3H, OCH_3), 3.26 – 3.08 (m, 2H, β CH_2), 1.34 (d, *J* = 7.2 Hz, 3H, CH_3); **^{13}C NMR (101 MHz, Chloroform-d)** δ 173.6 (CO_2Me), 170.2 (CONH), 156.3 (CO_2Fmoc), 144.1 (C arom.), 143.9 (C arom.), 141.4 (C arom.), 134.9 (NCHN), 132.3 (C arom.), 132.2 (C arom.), 131.4 (C NCHCN), 129.8 (CH arom.), 129.6 (CH arom.), 129.0 (CH arom.), 128.3 (CH arom.), 127.9 (CH arom.), 127.3 (CH arom.), 125.4 (CH arom.), 121.9 (CH arom.), 120.1 (CH NCHCN), 67.3 (CH_2 Fmoc), 53.7 (CH_2 Bn), 53.2 (αCH), 51.4 (CH_2 Bn), 50.9 (αCH), 50.6 (OCH_3), 47.1 (CH Fmoc), 25.6 (βCH_2), 17.7 (CH_3 Ala); **HRMS (ESI):** *m/z* calculated for for $C_{39}H_{39}N_4O_5^+$: 643.2920, found 643.2921 $[M]^+$

6.6-Synthesis of thiazolium amino acids:

(S)-5-(2-((((9H-Fluoren-9-yl)methoxy)carbonyl)amino)-2-carboxyethyl)-3-methylthiazol-3-ium iodide ***195****:*

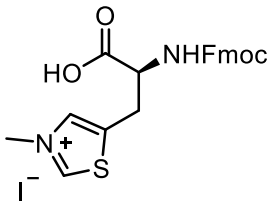

In a pressure tube Fmoc-L-thiazolylalanine (0.60 mg, 1.52 mmol) was dissolved in acetonitrile (3.00 mL), methyl iodide (5 mL, 9.63 mmol) was added. The tube was sealed and heated up to 90 °C and the reaction mixture was stirred for 3 days. The tube was allowed to slowly cool down to room temperature and the reaction mixture concentrated. Trituration with diethyl ether yielded the product **195** as a yellow solid (782 mg, 1.46 mmol) in 96% yield. **$[\alpha]_D$ =** -31.5 (c 1, MeCN); **Mp.:** 110-113 °C; **IR (neat)** $\nu_{(max)}$ cm^{-1}: 3110 w, 2955 w, 1704 s, 1602 s, 1563 m, 1514 s, 1372 w, 1252 s, 1179 m, 1080 w, 1029 m, 830 m, 760 s, 739 s, 620 s; **^{1}H NMR (400 MHz, DMSO-d_6)** δ 13.19 (s, 1H, OH), 10.08 (s, 1H, NCHN), 7.93 (d, *J* = 2.5 Hz, 1H, NCHCN), 7.89 (d, *J* = 7.5 Hz, 2H. arom. Fmoc), 7.84 (d, *J* = 8.5 Hz, 1H, NH), 7.66 (d, *J* = 4.3 Hz, 1H, arom. Fmoc), 7.64 (d, *J* = 4.2 Hz, 1H, arom. Fmoc), 7.42 (t, *J* = 7.4 Hz, 2H, arom. Fmoc), 7.33 (td, *J* = 7.5, 1.2 Hz, 2H, CH arom. Fmoc), 4.48 (ddd, *J* = 10.4, 8.7, 4.4 Hz, 1H, αCH), 4.32 (dd, *J* = 10.4, 7.2 Hz 1H, CH_2 Fmoc), 4.28 (dd, *J* = 9.9, 5.9 Hz, 1H, CH_2 Fmoc), 4.20 (app t, *J* = 6.8 Hz, 1H, CH Fmoc), 4.13 (s, 3H, NCH_3), 3.40 (dd, *J* = 15.7, 5.5 Hz, 1H, βCH_2), 3.25 – 3.13 (m, 1H, βCH_2); **^{13}C NMR (101 MHz, DMSO-d_6)** δ 171.9 (CO_2H), 160.0 (NCHS), 156.0 (CO_2 Fmoc), 146.1 (C Fmoc), 143.7 (C Fmoc), 140.8 (C NCHCS), 127.7 (CH arom. Fmoc), 127.1 (CH arom. Fmoc), 125.1 (CH arom. Fmoc), 123.0 (CH arom.), 120.2 (CH NCHCS), 66.0 (CH_2 Fmoc), 51.7 (αCH), 46.6 (CH Fmoc), 40.0 (NCH_3)28.3 (βCH_2); **HRMS (ESI):** *m/z* calculated for $C_{22}H_{21}N_2O_4S^+$: 409.1217, found 409.1228 $[M]^+$;

Elemental analysis calculated for: $C_{22}H_{21}N_2O_4SI$: C, 49.26; H, 3.95; N, 5.22, S, 5.98; found: C, 49.20; H, 3.98, N, 5.34, S, 5.61.

6.7 - Synthesis of NHC Metal Complexes:

General Procedure 7 for the synthesis of NHC gold complexes (GP7):

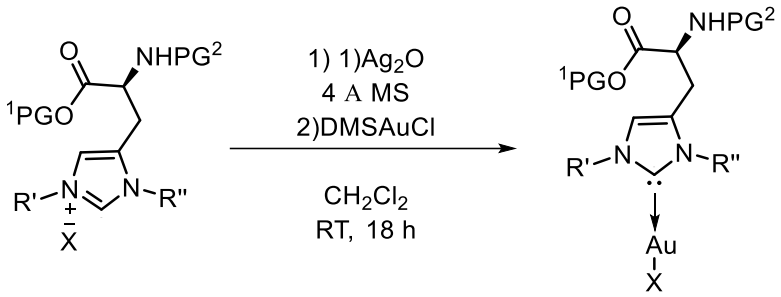

A heat gun dried Schlenk tube under argon was charged with amino acid (1.0 eq.) and Ag_2O (0.5 eq.). The charged Schlenk tube was evacuated under vacuum and backfilled with argon. Dichloromethane (0.03 M) was added, and the reaction mixture stirred in the dark for 1 hour. DMSAuCl (1 eq.) was added and the reaction mixture left to stir at RT, in the dark for up to 24 hours. The reaction mixture was filtered through celite and the filtrate was concentrated under reduced pressure. The crude material was purified by flash column chromatography or recrystallization.

General Procedure 8 for the synthesis of NHC gold complexes (GP8):

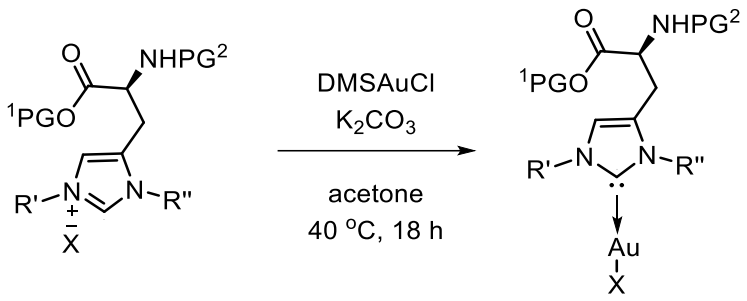

In a round bottom flask equipped with a reflux condenser, amino acid (1 eq.), potassium carbonate (1 eq.) and DMSAuCl (1eq.) were dissolved in acetone (0.03 M). The reaction mixture was heated to 40 °C and left to stir for up to 24 hours. After completion (verified by TLC), the reaction mixture was allowed to cool down to RT and the acetone removed under vacuum. The residue was dissolved in dichloromethane and filtered through celite and the filtrate was concentrated under reduced pressure. The crude material was purified by flash column chromatography or trituration.

General Procedure 9 for the synthesis of NHC palladium allyl complexes (GP9):

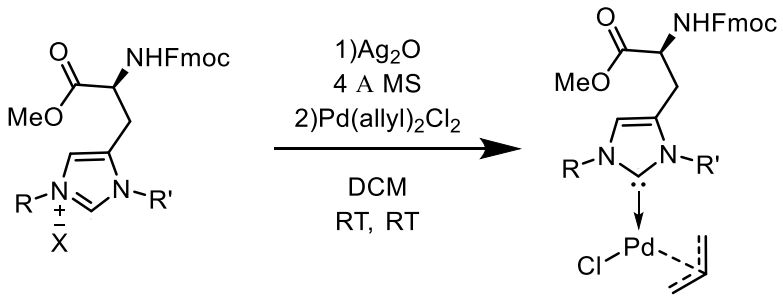

A heat gun dried Schlenk tube under argon was charged with amino acid (1.0 eq.) and Ag_2O (0.5 eq.). The charged Schlenk tube was back flushed/back purged under vacuum with argon. Dichloromethane (0.03 M) was added, and the reaction mixture stirred in the dark for 1 hour. $[Pd(allyl)Cl]_2$ (0.5 eq.) was added, and the reaction mixture left to stir at RT, in the dark for up to 24 hours. The reaction mixture was filtered through

celite and the filtrate was concentrated under reduced pressure. The crude material was purified by automated flash column chromatography.

(R)-(4-(2-((tert-Butoxycarbonyl)amino)-3-methoxy-3-oxopropyl)-1,3-dimethyl-1,3-dihydro-2H-imidazol-2-ylidene)gold chloride ***89****:*

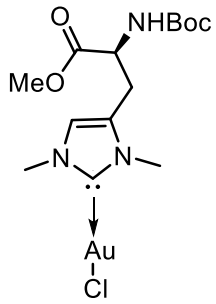

Following GP7 using imidazolium salt **83** (0.030 g, 0.070 mmol), Ag_2O (8.00 mg, 0.035 mmol), DMSAuCl (0.0210 g, 0.0700 mmol) and dichloromethane (1.00 mL). Trituration with diethyl ether yielded the product **89** as a yellow solid (0.0200 g,0.0380 mmol) in 54% yield. **Mp.:** 81-82 °C; **IR (neat)** $\nu_{(max)}$ cm^{-1}: 2970 w, 1738 s, 1446 w, 1365 s, 1228 s, 1217 s, 763 m, 742 m, 619 m; **^{1}H NMR (300 MHz, Chloroform-d)** δ 6.72 (s, 1H, NCHCN), 5.17 (d, *J* = 7.1 Hz, 1H, NH), 4.57 (q, *J* = 5.8 Hz, 1H, αCH), 3.79 (s, 3H, OCH_3), 3.76 (s, 6H, NCH_3), 3.18 (dd, *J* = 15.7, 5.1 Hz, 1H, βCH_2), 2.96 (dd, *J* = 15.7, 6.7 Hz, 1H, βCH_2), 1.42 (s, 9H, $C(CH_3)_3$); **Elemental analysis** calculated for: $C_{14}H_{23}N_3O_4AuCl$: C, 31.74; H, 4.38; N, 7.93; found: C, 31.67; H, 4.23, N, 7.93. Spectroscopic data are consistent with those described in the literature.[126]

(S)-(4-(2-((((9H-Fluoren-9-yl)methoxy)carbonyl)amino)-3-(benzyloxy)-3-oxopropyl)-1,3-dimethyl-1,3-dihydro-2H-imidazol-2-ylidene)gold chloride ***136***:

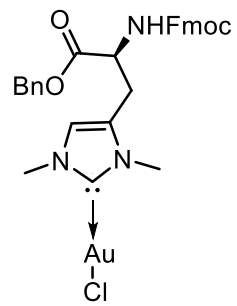

Following GP8 using imidazolium salt **133** (0.0380 g, 0.0600 mmol), acetone (2.00 mL), K_2CO_3 (0.008 g, 0.060 mmol) and DMSAuCl (0.0180 g, 0.0600 mmol). Full consumption observed by TLC (CH_2Cl_2 9:1 MeOH) 18 h after the start of reaction. Automated flash chromatography (100% EtOAc to 30% MeOH) gave access to **136**

as a yellow solid (0.0180 g, 0.0250 mmol) with 42% yield. **$[\alpha]_D$ =** + 4.15 (c 0.1, $CHCl_3$); **Mp.:** 89-92 °C; **IR (neat):$\nu_{(max)}$** cm^{-1}: 3331 w br, 2949 w, 1712 m, 1449 m, 1195 m, 1049 m, 758 s, 739 s, 698 s; **^{1}H NMR (400 MHz, Chloroform-d)** δ 7.78 (d, *J* = 7.3 Hz, 2H, arom. Fmoc), 7.55 (d, *J* = 7.4 Hz, 2H, arom. Fmoc), 7.46 – 7.37 (m, 5H, arom. Bn), 7.36 – 7.29 (m, 4H, arom. Fmoc), 6.12 (s, 1H, NCHCN), 5.41 (d, *J* = 6.7 Hz, 1H, NH), 5.30 (d, *J* = 11.8 Hz, 1H, CH_2 Bn), 5.08 (d, *J* = 11.8 Hz, 1H, CH_2 Bn), 4.60 (q, *J* = 5.6 Hz, 1H, αCH), 4.52 (app t, *J* = 8.5 Hz 1H, CH_2 Fmoc), 4.46 (app t, *J* = 8.3 Hz 1H, CH_2 Fmoc), 4.18 (t, *J* = 6.1 Hz, 1H, CH Fmoc), 3.56 (s, 3H, NCH_3), 3.54 (s, 3H, NCH_3), 3.10 (dd, *J* = 15.5, 5.2 Hz, 2H, βCH_2), 2.99 (dd, *J* = 15.6, 4.7 Hz, 2H, βCH_2); **^{13}C NMR (101 MHz, Chloroform-d)** δ 182.6 (NCAuN), 170.2 (CO_2Bn), 155.7 (CO_2 Fmoc), 143. (C arom.), 143.4 (C arom.), 141.6 (C arom.), 141.5 (C arom.), 134.6 (C NCHCN), 129.4 (CH arom. Bn), 129.2 (CH arom. Bn), 129.0 (CH arom. Bn), 128.2 (CH arom. Bn), 128.1 (CH arom. Fmoc), 127.3 (CH arom. Fmoc), 124.9 (CH arom. Fmoc), 120.3 (CH arom. Fmoc), 119.8 (CH NCHCN) 68.2 (CH_2), 67.1 (CH_2), 53.0 (αCH), 47.2 (CH Fmoc), 37.8 (NCH_3), 35.1 (NCH_3), 27.3 (βCH_2); **HRMS (ESI):** *m/z* calculated for $C_{30}H_{29}N_3O_4Au^+$: 692.1824, found 692.1824 $[M\text{-}Cl]^+$;

*(S)-(4-(2-((((9H-Fluoren-9-yl)methoxy)carbonyl)amino)-3-methoxy-3-oxopropyl)-1,3-dimethyl-1,3-dihydro-2H-imidazol-2-ylidene)gold chloride **144**:*

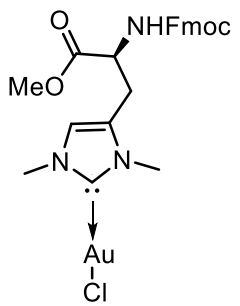

Following GP8 using imidazolium salt **142** (0.100 g, 0.180 mmol), acetone (6.00 mL), K_2CO_3 (0.0250 g, 0.180 mmol) and DMSAuCl (0.0540 g, 0.180 mmol). Full consumption observed by TLC (CH_2Cl_2 9:1 MeOH) 18 h after the start of reaction. Automated flash chromatography (100% EtOAc to 30% MeOH) gave access to **144**

as a yellow solid (0.0580 g, 0.0900 mmol) in 50% yield. **$[\alpha]_D$ =** + 12.5 (c 0.2, $CHCl_3$); **Mp.:** 110-112 °C; **IR (neat)** $\nu_{(max)}$ cm^{-1}: 3354 b w, 2950 w, 1710 s, 1607 m, 1498 w, 1559 s, 1379 w, 1212 m, 1104 w, 1049 m, 759 s, 739 s, 699 m; **^{1}H NMR (400 MHz, Chloroform-d)** δ 7.78 (d, *J* = 7.5 Hz, 2H, arom. Fmoc), 7.57 (d, *J* = 2.8 Hz, 1H, arom. Fmoc), 7.55 (d, *J* = 3.2 Hz, 1H, arom. Fmoc), 7.43 (t, *J* = 7.4 Hz, 2H, arom. Fmoc), 7.37 – 7.30 (m, 2H, arom. Fmoc), 6.59 (s, 1H, NCHCN), 5.38 (d, *J* = 7.2 Hz, 1H, NH), 4.60 (q, *J* = 5.9 Hz, 1H, αCH), 4.55 – 4.41 (b m, 2H, CH_2 Fmoc), 4.19 (t, *J* = 6.2 Hz, 1H, CH Fmoc), 3.78 (s, 3H, CH_3), 3.72 (s, 3H, CH_3), 3.66 (s, 3H, CH_3), 3.15 (dd, *J* = 15.6, 5.1 Hz, 1H, βCH_2), 3.00 (dd, *J* = 15.7, 6.2 Hz, 1H, βCH_2); **^{13}C NMR (101 MHz, Chloroform-d)** δ 179.7 (NCAuN), 170.8 (CO_2Me), 155.8 (CO_2Fmoc), 143.7, (C arom.) 143.5 (C arom.)., 141.5 (C arom.), 141.5 (C arom.), 128.1 (C NCHCN), 128.1 (CH arom. Fmoc), 127.3 (CH arom. Fmoc), 124.9 (CH arom. Fmoc), 120.3 (CH arom. Fmoc), 119.8 (CH NCHCN), 67.1 (CH_2 Fmoc), 53.3 (αCH), 52.8 (OCH_3), 47.2 (CH Fmoc), 38.0 (NCH_3), 35.2 (NCH_3), 27.5 (βCH_2); **HRMS (ESI):** *m/z* calculated for $C_{24}H_{25}N_3O_4Au^+$: 616.1505, found 616.1516 $[M\text{-}Cl]^+$

(S)-(1,3-Dibenzyl-5-(2-((tert-butoxycarbonyl)amino)-3-methoxy-3-oxopropyl)-1H-2l6-imidazol-3-ium-2-ylidene)gold bromide ***201:***

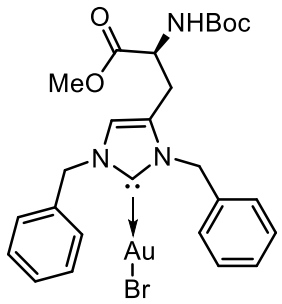

Following GP8 using imidazolium salt **177** (0.124 g, 0.340 mmol), acetone (6.00 mL), K_2CO_3 (0.0320 g, 0.340 mmol) and DMSAuCl (0.0690 g, 0.340 mmol). Full consumption observed by TLC (CH_2Cl_2 9:1 MeOH) 18 h after the start of reaction. Automated flash chromatography (100% EtOAc →20% MeOH) gave access to **201** as a yellow solid (0.129 g, 0.190 mmol) with 56% yield.

$[\alpha]_D$ = +27.9 (c 0.5, $CHCl_3$); **Mp.:** 97-103 °C; **IR (neat)** $\nu_{(max)}$ cm^{-1}: 3320 br w, 2950 w, 1721 s, 1607 w, 1515 m, 1496 m, 1449 s, 1351 m, 1216 s, 1104 w, 1051 m, 840 w, 759 s, 738 s, 101, s, 620 m; **^{1}H NMR (400 MHz, Chloroform-*d*)** δ 7.35 (m, 8H, arom. Bn), 7.23 (m, 2H, arom. Bn), 6.70 (s, 1H, NCHCN), 5.59 (d, *J* = 15.7 Hz, 1H, NH), 5.44 – 5.30 (m, 3H, CH_2 Bn), 5.02 (d, *J* = 7.3 Hz, 1H, CH_2 Bn), 4.40 (m, 1H, αCH), 3.59 (s, 3H, OCH_3), 2.94 (dd, *J* = 15.9, 5.4 Hz, 1H, βCH_2), 2.74 (dd, *J* = 15.9, 6.9 Hz, 1H, βCH_2), 1.40 (s, 9H, $C(CH_3)_3$); **^{13}C NMR (101 MHz, Chloroform-d)** δ 175.8 (NCAuN), 171.2 (CO_2Me), 155.2 (CO_2Fmoc), 135.1 (C arom. Bn), 130.0 (C NCHCN),129.3 (CH arom. Bn), 129.2 (CH arom. Bn), 128.9 (CH arom. Bn), 128.6 (CH arom. Bn), 128.1 (CH arom. Bn), 127.1 (CH arom. Bn), 119.3 (CH NCHCN), 80.9 (C $C(CH_3)_3$), 55.3 (CH_2 Bn), 52.9 (αCH), 52.7 (CH_2 Bn), 52.5 (OCH_3), 28.4 (CH_3 $C(CH_3)_3$), 28.0 (βCH_2); **HRMS (ESI):** *m/z* calculated for $C_{26}H_{31}N_3O_4AuBrNa$: 748.1061, found 748.1059 $[M+Na]^+$; **Elemental analysis** calculated for: $C_{26}H_{31}N_3O_4AuBr$: C, 42.99; H, 4.30; N, 5.78; found: C, 42.95; H, 4.39, N, 5.89.

(S)-(4-(2-((((9H-Fluoren-9-yl)methoxy)carbonyl)amino)-3-methoxy-3-oxopropyl)-1,3-dibenzyl-1,3-dihydro-2H-imidazol-2-ylidene)gold bromide ***200:***

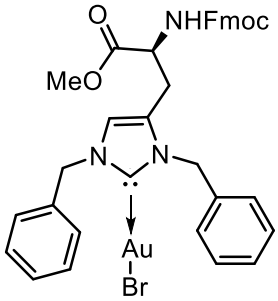

Following GP8 using imidazolium salt **146** (0.150 g, 0.230 mmol), acetone (7.60 mL), K_2CO_3 (0.0320 g, 0.237 mmol) and DMSAuCl (0.068 g, 0.230 mmol). Full consumption observed by TLC (CH_2Cl_2 9:1 MeOH) 18 h after the start of reaction. Automated flash chromatography (100% EtOAc →20% MeOH) gave access to **200** as a yellow solid (0.128 g, 0.150 mmol) in 65% yield.

$[\alpha]_D$ = +16.6 (c 1, $CHCl_3$); **Mp.:** 86-88 °C; **IR (neat)** $\nu_{(max)}$ cm^{-1}: 2960w, 1715 m, 1496 w, 1449 m, 1211 m, 1030 m, 759 s, 732 s; **^{1}H NMR (300 MHz, Chloroform-d)** δ 7.78 (d, *J* = 7.3 Hz, 2H, arom. Fmoc), 7.52 (t, *J* = 8.2 Hz, 2H, arom. Fmoc), 7.46 – 7.38 (m, 2H, arom. Fmoc), 7.31 (m, 10H, arom. Bn and Fmoc), 7.20 (m, 2H, arom. Bn), 6.66 (s, 1H, NCHCN), 5.51 (d, *J* = 16.4 Hz, 1H, CH_2 Bn), 5.44 – 5.27 (m, 3H, CH_2 Bn), 5.17 (bd, *J* = 7.0 Hz, 1H, NH), 4.53 – 4.33 (m, 3H, αCH and CH_2 Fmoc), 4.14 (t, *J* = 6.5 Hz, 1H, CH Fmoc), 3.60 (s, 3H, OCH_3), 2.94 (dd, J = 14.8, 4.9 Hz, 1H, βCH_2), 2.75 (dd, *J* = 14.8, 4.9 Hz, 1H, βCH_2); **^{13}C NMR (101 MHz, Chloroform-d)** δ 176.0 (NCN), 170.9 (CO_2Me), 155.8 (CO_2Fmoc), 143.7 (C arom. Fmoc), 143.6 (C arom. Fmoc), 141.5 (C arom. Fmoc), 135.1 (C arom. Bn), 135.0 (C arom. Bn), 129.7 (C NCHCN), 129.2 (CH arom. Bn), 128.9 (CH arom. Bn), 128.7 (CH arom. Bn), 128.1 (CH arom. Bn), 127.3(CH arom.), 127.0 (CH arom.), 125.0 (CH arom. Fmoc), 124.9 (CH arom. Fmoc), 120.3 (CH arom. Fmoc), 119.3 (CH NCHCN),67.3 (CH_2 Fmoc), 55.4 (CH_2 Bn), 53.07 (αCH), 52.8 (OCH_3), 47.2 (CH Fmoc), 28.0 (βCH_2); **HRMS (ESI):** m/z calculated for $C_{36}H_{33}N_3O_4AuBr$: 870.1218, found 870.1221 $[M]^+$.

*(S)-(4-(2-((((9H-Fluoren-9-yl)methoxy)carbonyl)amino)-3-methoxy-3-oxopropyl)-1,3-bis(4-(trifluoromethyl)benzyl)-1,3-dihydro-2H-imidazol-2-ylidene)gold(III) bromide **203**:*

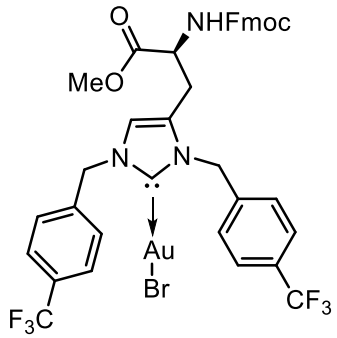

Following GP8 using imidazolium salt **147** (0.100 g, 0.130 mmol), acetone (4.00 mL), K_2CO_3 (0.0180 g, 0.130 mmol) and DMSAuCl (0.0370 g, 0.130 mmol). Full consumption observed by TLC (CH_2Cl_2 9:1 MeOH) 20 h after the start of reaction. Automated flash chromatography (100% EtOAc →30% MeOH) gave access to **203** as a white foam (0.0340 g,

0.0350 mmol) in 27% yield. **$[\alpha]_D$ =** + 11.7 (c 0.2, $CHCl_3$) **Mp.:** 103-104 °C; **IR (neat)** $\nu_{(max)}$ cm^{-1}: 2943 w, 1682 s, 1325 s, 1166 s, 1122 s, 1067 m, 739 s; **^{1}H NMR (300 MHz, Chloroform-d)** δ 7.78 (d, *J* = 7.1 Hz, 2H, arom. Fmoc), 7.60 (d, *J* = 8.0 Hz, 4H, arom.), 7.53 (t, *J* = 7.9 Hz, 2H, arom. Fmoc), 7.46 – 7.36 (m, 4H, arom.), 7.34 – 7.29 (m, 4H, arom.), 6.71 (s, 1H, NCHCN), 5.61 – 5.24 (m, 4H, CH_2 Bn), 4.49 – 4.37 (m, 3H, CH_2 Fmoc and αCH), 4.16 (t, *J* = 6.2 Hz, 1H, CH Fmoc), 3.62 (s, 3H, OCH_3), 2.94 (dd, *J* = 15.9, 4.1 Hz, 1H, βCH_2), 2.74 (dd, *J* = 14.4, 7.4 Hz, 1H, βCH_2); **^{13}C NMR (101 MHz, Chloroform-d)** δ 176.8 (NCN), 170.6 (CO_2 Me),161.7 (CO_2 Fmoc) 143.6 (C arom.), 143.4 (C arom.), 141.5 (C arom.), 138.80 (C arom.), 138.77 (C arom.), 131.18 (q, *J* = 32.8 Hz, C CCF_3), 127.3 (CH arom.), 126.3 (q, *J* = 4.3 Hz, CH $CHCCF_3$), 124.9 (CH arom.), 124.8 (CH arom.), 123.8 (q, *J* = 269 Hz, CF_3), 123.7 (q, *J* = 270 Hz, CF_3), 120.4 (CH arom.), 119.6 (CH NCHCN), 67.2 (CH_2 Fmoc), 54.7 (CH_2 Bn), 53.1 (OCH_3), 52.8 (αCH), 52.1 (CH_2 Bn), 47.2 (CH Fmoc), 28.0 (βCH_2). **^{19}F NMR (282 MHz, Chloroform-d)** δ -62.70; **HRMS (ESI):** *m/z* calculated for $C_{38}H_{31}N_3O_4F_6Au^+$: 904.1884, found 904.1896 $[M]^+$.

*(S)-(4-(2-((((9H-Fluoren-9-yl)methoxy)carbonyl)amino)-3-methoxy-3-oxopropyl)-1,3-dipropyl-1H-2l6-imidazol-3-ium-2-ylidene)gold chloride **198**:*

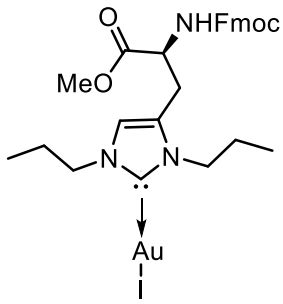

Following GP8 using imidazolium salt **152** (0.100 g, 0.170 mmol), acetone (5.60 mL), K_2CO_3 (0.0230 g, 0.170 mmol) and DMSAuCl (0.049 g, 0.170 mmol). Full consumption observed by TLC (CH_2Cl_2 9:1 MeOH) 18 h after the start of reaction. Automated flash chromatography (100% EtOAc →30% MeOH) gave access to **198** as a yellow solid (0.0160 g, 0.0220 mmol) in 13% yield.

Mp.: 72-73 °C; **IR (neat)** $\nu_{(max)}$ cm^{-1}: 3049 b w, 2956 w, 1705 s, 1602s, 1563 m, 1514 s, 1448 m, 1253 s, 1029 s, 830 s, 759 s, 739 s, 620 s; **^{1}H NMR (400 MHz, Chloroform-d)** δ 7.77 (d, *J* = 7.5 Hz, 2H, arom. Fmoc), 7.57 (d, *J* = 3.8 Hz, 1H, arom. Fmoc), 7.55 (d, *J* = 3.8 Hz, 1H, arom. Fmoc), 7.42 (t, *J* = 7.4 Hz, 2H, arom. Fmoc), 7.32 (tt, *J* = 7.6, 1.1 Hz, 2H, arom. Fmoc), 6.67 (s, 1H, NCHCN), 5.41 (d, *J* = 7.6 Hz, 1H, NH), 4.61 (q, *J* = 6.3 Hz, 1H, αCH), 4.45 (m, 2H, CH_2 Fmoc), 4.20 (t, *J* = 6.5 Hz, 1H, CH Fmoc), 4.05 (t, *J* = 7.1 Hz, 4H, NCH_2), 3.77 (s, 3H, OCH_3), 3.15 (dd, *J* = 15.8, 5.1 Hz, 1H, βCH_2), 2.98 (dd, *J* = 15.9, 6.6 Hz, 1H, βCH_2), 1.88 – 1.75 (m, 4H, CH_2 propyl), 0.95 (t, *J* = 7.4 Hz, 3H, CH_3 propyl), 0.89 (t, *J* = 7.4 Hz, 3H, CH_3 propyl); **^{13}C NMR (101 MHz, Chloroform-d)** δ 181.8 (NCN), 171.0 (CO_2Me), 155.8 (CO_2Fmoc), 143.7 (C arom. Fmoc), 143.5 (C arom. Fmoc), 141.5 (2C arom. Fmoc), 128.2 (C NCHCN), 128.1 (CH arom. Fmoc), 127.3 (CH arom. Fmoc), 125.0 (CH arom. Fmoc), 120.3 (CH arom. Fmoc), 118.2 (CH NCHCN), 67.3 (CH_2 Fmoc), 53.2 (αCH), 52.9 (OCH_3), 49.8 ($2CH_2$ propyl), 47.2 (CH Fmoc), 27.7 (βCH_2), 24.8 (CH_2 propyl), 24.4 (CH_2 propyl), 11.3 (CH_3 propyl), 11.1 (CH_3 propyl); **HRMS (ESI):** *m/z* calculated for $C_{28}H_{33}N_3O_4Au$: 672.2137, found 672.2130 $[M]^+$.

*(S)-(4-(2-((((9H-Fluoren-9-yl)methoxy)carbonyl)amino)-3-methoxy-3-oxopropyl)-1,3-diallyl-1H-2l6-imidazol-3-ium-2-ylidene)gold bromide **199**:*

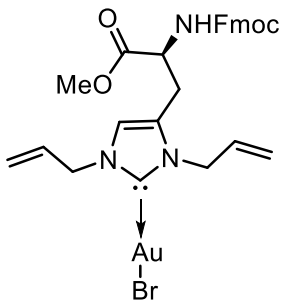

Following GP8 using imidazolium salt **153** (0.100 g, 0.180 mmol), acetone (6.00 mL), K_2CO_3 (0.0250 g, 0.180 mmol) and DMSAuCl (0.0530 g, 0.180 mmol). Full consumption observed by TLC (CH_2Cl_2 9:1 MeOH) 18 h after the start of reaction. Automated flash chromatography (100% EtOAc →30%

MeOH) gave access to **199** as a white foam (0.0570 g, 0.0760 mmol) in 41% yield. **$[\alpha]_D$ =** +15.9 (c 0.3, $CHCl_3$); **Mp.:** 65-67°C; **IR (neat)** $\nu_{(max)}$ cm^{-1}: 3330 b w, 2952 w, 1718 s, 1644 w, 1513 m, 1449 s, 1409 m, 1327 m, 1213 s, 1178 m, 1050 m, 991 m, 924 m, 760 s, 738 s, 620 m; **^{1}H NMR (400 MHz, Chloroform-d)** δ 7.78 (d, *J* = 7.5 Hz, 2H, arom. Fmoc), 7.55 (t, *J* = 6.5 Hz, 2H, arom. Fmoc), 7.42 (t, *J* = 7.4 Hz, 2H, arom. Fmoc), 7.32 (td, *J* = 7.5, 1.0 Hz, 2H, arom. Fmoc), 6.72 (s, 1H, NCHCN), 5.85 (m, 2H, CH allyl), 5.39 (d, *J* = 7.7 Hz, 1H, NH), 5.24 (d, *J* = 10.0 Hz, 2H, CH_2 allyl), 5.16 (d, *J* = 17.1 Hz, 1H, CH_2 allyl), 5.01 (d, *J* = 17.2 Hz, 1H, CH_2 allyl), 4.83 (d, *J* = 16.9 Hz, 1H, CH_2 allyl), 4.79 – 4.69 (m, 3H, CH_2 allyl), 4.59 (q, *J* = 6.9 Hz, 1H, αCH), 4.45 (*d*, J = 6.5 Hz, 2H, CH_2 Fmoc), 4.19 (t, *J* = 6.4 Hz, 1H, CH Fmoc), 3.76 (s, 3H, OCH_3), 3.12 (dd, *J* = 15.9, 5.2 Hz, 1H, βCH_2), 2.95 (dd, *J* = 15.8, 6.9 Hz, 1H, βCH_2); **^{13}C NMR (101 MHz, Chloroform-d)** δ 175.8 (NCN), 171.0 (CO_2 Me), 155.8 (CO_2 Fmoc), 143.7 (C arom. Fmoc), 143.5 (C arom. Fmoc), 141.5 (C arom. Fmoc), 132.5 (CH arom. Fmoc), 132.1 (CH arom. Fmoc), 129.2 (C NCHCN), 128.08 (CH arom. Fmoc), 128.06 (CH arom. Fmoc), 127.28 (CH arom. Fmoc), 125.0 (CH arom. Fmoc), 124.9 (CH arom. Fmoc), 120.3 (CH NCHCN), 119.8 (CH_2 allyl), 118.79 (CH allyl), 118,73 (CH allyl), 118.5 (CH_2 allyl), 67.3 (CH_2 Fmoc), 54.00 (CH_2 allyl), 53.90 (CH_2 allyl), 53.2 (αCH), 52.8 (OCH_3), 51.10, 47.2 (CH Fmoc), 27.8. (βCH_2)*;* **HRMS (ESI):** *m/z* calculated for $C_{28}H_{29}N_3O_4Au$: 668.1824, found 668.1837 $[M]^+$.

(S)-(5-(2-((((9H-Fluoren-9-yl)methoxy)carbonyl)amino)-3-methoxy-3-oxopropyl)-1-(4-methoxyphenyl)-3-methyl-1H-2l6-imidazol-3-ium-2-ylidene)gold chloride ***202****:*

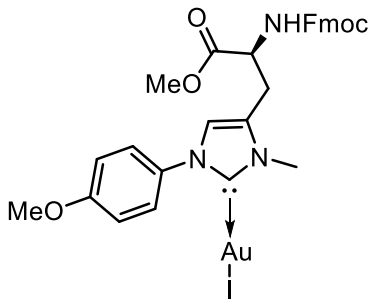

Following GP8 using imidazolium salt **164** (0.150 g, 0.230 mmol), acetone (8.00 mL), K_2CO_3 (0.0320 g, 0.230 mmol) and DMSAuCl (0.0690 g, 0.230 mmol). Full consumption observed by TLC (CH_2Cl_2 9:1 MeOH) 18 h after the start of reaction. Automated flash chromatography (100% EtOAc→ 30% MeOH) gave access to **202** as a yellow solid (0.101 g, 0.140 mmol) in 61% yield. **$[\alpha]_D$ =** +4.90 (c 0.5, $CHCl_3$); **Mp.:** 103-105 °C; **IR (neat)** $\nu_{(max)}$ cm^{-1}: 3331 w, 2925 w, 1716 s, 1513 s, 1448 m, 1250 s, 1214 s, 1027 s, 833 m, 759 s, 738 s; **^{1}H NMR (300 MHz, Chloroform-d)** δ 7.76 (d, *J* = 3.1 Hz, 1H, arom. Fmoc), 7.73 (d, *J* = 3.0 Hz, 1H, arom. Fmoc), 7.55 (t, *J* = 6.9 Hz, 2H, arom. Fmoc), 7.47 – 7.36 (m, 4H, arom. Fmoc and Ph), 7.33 – 7.27 (m, 2H, arom. Fmoc), 6.92 (d, *J* = 8.9 Hz, 2H, arom. Ph), 6.85 (s, 1H, NCHCN), 5.47 (d, *J* = 7.4 Hz, 1H, NH), 4.65 (q, *J* = 6.2 Hz, 1H, αCH), 4.52 (dd, *J* = 13.8, 9.4 Hz, 1H, CH_2 Fmoc), 4.45 (dd, *J* = 13.8, 8.4 Hz, 1H, CH_2 Fmoc), 4.17 (t, *J* = 6.2 Hz, 1H, CH Fmoc), 3.84 (s, 3H, OCH_3), 3.79 (s, 3H, OCH_3), 3.76 (s, 3H, NCH_3), 3.22 (dd, *J* = 15.0, 4.0 Hz, 1H, βCH_2), 3.06 (dd, *J* = 15.8, 6.0 Hz, 1H, βCH_2); **^{13}C NMR (101 MHz, Chloroform-d)** δ 181.5 (NCN), 170.8 (CO_2 Me), 160.0 (CO_2 Fmoc), 143.6 (C arom), 143.4 (C arom), 141.5(C arom), 141.5 (C arom), 132.0 (C NCHCN), 128.09 (CH arom.), 128.05 (CH arom.), 127.28 (CH arom.), 127.25 (CH arom.), 125.8 (CH arom.), 124.9 (CH arom.), 120.3 (CH arom.), 119.9 (CH NCHCN), 114.8 (CH arom. Ph), 67.1 (CH_2 Fmoc), 55.8 (OCH_3), 53.3 (αCH), 52.8 (OCH_3), 47.2 (CH Fmoc), 35.7 (NCH_3), 27.7 (βCH_2); **HRMS (ESI):** *m/z* calculated for $C_{30}H_{29}N_3O_5AuI$: 708.1773, found 708.1753 $[M]^+$; **Elemental**

analysis calculated for: $C_{30}H_{29}N_3O_5AuI$: C, 43.13; H, 3.50; N, 5.03; found: C, 43.08; H, 3.53, N, 4.71.

*(4-(2-Amino-3-methoxy-3-oxopropyl)-1,3-bis(4-(trifluoromethyl)benzyl)-1H-2l6-imidazol-3-ium-2-ylidene)gold bromide **204**:*

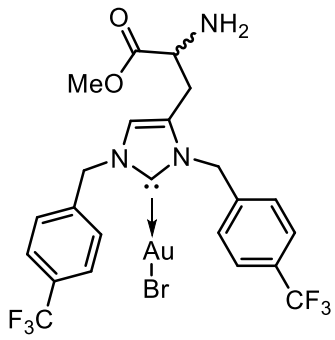

Following GP8 using imidazolium salt **147** (0.100 g, 0.130 mmol), acetone (4.00 mL), K_2CO_3 (0.0190 g, 0.143 mmol) and DMSAuCl (0.0370 g, 0.130 mmol). Full consumption observed by TLC (CH_2Cl_2 9:1 MeOH) 18 h after the start of reaction. Automated flash chromatography (100% EtOAc→ 20% MeOH) gave access to **204** as a yellow solid (0.0580 g, 0.0760 mmol) in 58% yield. **$[\alpha]_D$ =** +1.60 (c 0.2, $CHCl_3$); **Mp.:** decomposed at 170 °C; **IR (neat) $\nu_{(max)}$** cm^{-1}: 3345 w, 3001 w, 1737 m, 1620 m, 1417 m, 1324 s, 1163 s, 1112 s, 1065 s, 1016 m, 943 w, 820 m, 754 w, 716 w; **^{1}H NMR (400 MHz, Chloroform-d)** δ 7.65 (d, *J* = 8.1 Hz, 2H, arom. Ph), 7.62 (d, *J* = 8.1 Hz, 2H, arom. Ph), 7.46 (d, *J* = 8.0 Hz, 2H, arom. Ph), 7.32 (d, *J* = 8.1 Hz, 2H, arom. Ph), 6.88 (s, 1H, NCHCN), 5.63 (s, 2H, CH_2), 5.46 (s, 2H, CH_2), 3.62 (s, 3H, OCH_3), 3.49 (dd, *J* = 7.8, 4.9 Hz, 1H, αCH), 2.80 (dd, *J* = 15.7, 4.9 Hz, 1H, βCH_2), 2.58 (dd, *J* = 15.3, 8.1 Hz, 1H, βCH_2); **^{13}C NMR (101 MHz, Chloroform-d)** δ 176.2 (NCN), 174.2 (CO_2Me), 139.1 (C arom.), 138.9 (C arom.), 131.5 (C NCHCN), 130.95 (q, *J* = 32.4 Hz, C CCF_3), 128.3 (CH arom.), 127.2 (CH arom.), 126.3 (q, *J* = 3.6 Hz, CH $CHCCF_3$), 123.87 (q, *J* = 274.1 Hz, CF_3), 119.6 (CH NCHCN), 54.7 (CH_2), 53.5 (αCH), 52.7 (OCH_3), 52.2 (CH_2), 29.6 (βCH_2); **^{19}F NMR (282 MHz, Chloroform-d)** δ -62.7 (s, 6F); **HRMS (ESI):** *m/z* calculated for $C_{46}H_{42}AuF_{12}N_6O_4$: 1167.2741 found 1167.2753 $[2M-Br]^+$.

*(S)-(4-(2-((((9H-Fluoren-9-yl)methoxy)carbonyl)amino)-3-methoxy-3-oxopropyl)-1,3-diallyl-1H-2l6-imidazol-3-ium-2-ylidene)(prop-1-en-2-yl)palladium chloride **209**:*

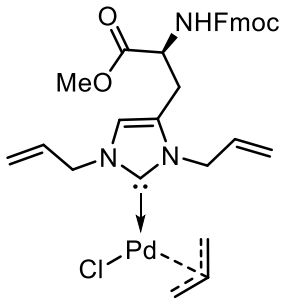

Following GP9 using imidazolium salt **153** (0.050 g, 0.0900 mmol), Ag_2O (0.0100 g, 0.0450 mmol), $[Pd(allyl)Cl]_2$ (0.0160 g, 0.0450 mmol) and dichloromethane (2.00 mL). Full consumption observed by TLC (CH_2Cl_2 9:1 MeOH) 18 h after the start of reaction. Automated flash chromatography (100% EtOAc →20% MeOH) gave access to **209** as a yellow solid (0.0290 g, 0.0440 mmol) with 49% yield. **$[\alpha]_D$ =** +13.2 (c 0.5, $CHCl_3$); **Mp.:** 68-69 °C; **IR (neat) $\nu_{(max)}$** cm^{-1}: 3039 b w, 2922 w, 1715 s, 1644 w, 1524 m, 1448 m, 1406 m, 1326 w, 1213 s, 177 m, 1055 m, 93398 s, 760 s, 739 s, 620 w; **^{1}H NMR (400 MHz, Chloroform-d)** δ 7.77 (d, *J* = 7.5 Hz, 2H, arom. Fmoc), 7.57 (t, *J* = 6.6 Hz, 2H, arom. Fmoc), 7.41 (t, *J* = 7.5 Hz, 2H, arom. Fmoc), 7.32 (tt, *J* = 7.4, 1.4 Hz, 2H, arom. Fmoc), 6.74 (s, 1H, NCHCN), 6.05 – 5.83 (m, 2H, CH N-allyl), 5.44 (d, *J* = 7.7 Hz, 1H, NH), 5.27 (br s, 1H, CH_2 Pd-allyl), 5.19 (t, *J* = 10.1 Hz, 2H, CH_2 N-allyl), 5.08 (d, *J* = 17.1 Hz, 1H, CH_2 N-allyl), 4.95 (d, *J* = 17.3 Hz, 2H, CH_2 N-allyl), 4.88 – 4.67 (m, 3H, CH_2 N-allyl), 4.63 (q, *J* = 7.2 Hz, 1H, αCH), 4.41 (d, *J* = 6.9 Hz, 2H, CH_2 Fmoc), 4.27 (d, *J* = 7.4 Hz, 1H, CH_2 Pd-allyl), 4.21 (t, *J* = 6.7 Hz, 1H, CH Fmoc), 3.77 (s, 3H, OCH_3), 3.37 (br s, 1H, CH_2 Pd-allyl), 3.26 (br d, *J* = 13.2 Hz, 1H, CH_2 Pd-allyl), 3.09 (dd, *J* = 15.9, 5.2 Hz, 1H, βCH_2), 2.96 (dd, *J* = 15.9, 7.0 Hz, 1H, βCH_2), 2.45 – 2.29 (m, 1H CH Pd-allyl); **^{13}C NMR (101 MHz, Chloroform-d)** δ 181.7 (NCN), 171.4 (CO_2 Me), 155.9 (CO_2 Fmoc), 143.8 (C arom. Fmoc), 143.7 (C arom. Fmoc), 141.5 (C arom. Fmoc), 133.8 (CH arom. Fmoc), 133.6 (CH arom. Fmoc), 129.6 (C NCHCN), 128.0 (CH arom. Fmoc), 127.27 (CH arom. Fmoc), 127.26 (CH arom. Fmoc), 125.13 (CH arom. Fmoc), 125.10 (CH arom. Fmoc), 120.2 (CH

NCHCN), 119.3 (CH allyl), 118.4 (CH_2 allyl), 117.3 (CH_2 allyl), 115.1 (CH_2, Pd allyl), 73.2 (CH, Pd allyl) 67.4 (CH_2 Fmoc), 53.8 (CH_2 allyl), 53.2 (αCH), 52.7 (OCH_3), 51,0 (CH_2 allyl), 49.1 (CH_2, Pd allyl), 47.2 (CH Fmoc), 27.7 (βCH_2)*;* **HRMS (ESI):** *m/z* calculated for $C_{31}H_{34}N_3O_4PdCl$: 653.1273, found 616.1581 $[M\text{-}Cl]^+$; **Elemental analysis** calculated for: $C_{31}H_{34}N_3O_4PdCl$: C, 56.89; H, 5.24; N, 6.42; found: C, 56.59; H, 5.37, N, 6.36.

*((S)-(4-(2-((((9H-Fluoren-9-yl)methoxy)carbonyl)amino)-3-methoxy-3-oxopropyl)-1,3-bis(pyridin-2-ylmethyl)-1H-2l6-imidazol-3-ium-2-ylidene)(prop-1-en-2-yl)palladium chloride **210**:*

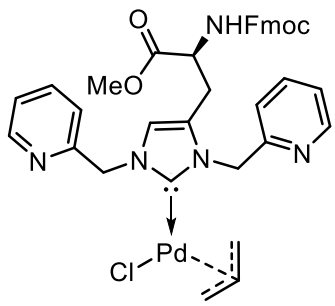

Following GP9 using imidazolium salt **148** (0.0700 g, 0.110 mmol), Ag_2O (0.0120 g, 0.0530 mmol), $[Pd(allyl)Cl]_2$ (0.0190 g, 0.0530 mmol) and dichloromethane (2.70 mL). Full consumption observed by TLC (CH_2Cl_2 9:1 MeOH) 18 h after the start of reaction. Automated flash chromatography (100% EtOAc →20% MeOH) gave access to **210** as a yellow solid (0.0380 g, 0.0500 mmol) in 46% yield. **$[\alpha]_D$ =** +5.80 (c 0.5, $CHCl_3$); **Mp.:** 106-108 °C **IR (neat) $\nu_{(max)}$** cm^{-1}: 3120 w, 2952 w, 1713 s, 1593 w, 1571 w, 1537 m, 1477 m, 1436 s, 1256 b s, 1214 s, 1105 w, 1049 s, 760 s, 741 s, 645 w, 620 w; **^{1}H NMR (400 MHz, Chloroform-d)** δ 8.54 (d, *J* = 4.7 Hz, 1H, arom. Py), 8.52 (d, *J* = 4.9 Hz, 1H, arom. Py), 7.73 (d, *J* = 7.5 Hz, 2H, arom. Fmoc), 7.71 – 7.65 (m, 1H, arom Py), 7.62 (t, *J* = 7.3 Hz, 2H, arom. Fmoc), 7.56 (d, *J* = 7.5 Hz, 1H, arom. Py), 7.36 (t, *J* = 7.5 Hz, 3H, arom. Fmoc and Py), 7.30 – 7.23 (m, 3H, arom. Fmoc and Py), 7.23 – 7.15 (m, 3H, arom. Py and NCHCN), 5.59 (br s, 2H, CH_2 Py), 5.40 (br s, 2H, CH_2 Py), 5.19 (m, 1H, CH allyl), 4.53

(q, *J* = 7.9 Hz, 1H, αCH), 4.34 (dd, *J* = 10.2, 7.0 Hz, 1H, CH_2 Fmoc), 4.21 (m, 2H, CH_2 Fmoc and allyl CH_2), 4.14 (t, *J* = 7.1 Hz, 1H, CH Fmoc), 3.73 (s, 3H, OCH_3), 3.37 (dd, *J* = 15.6, 8.4 Hz, 1H, βCH_2), 3.29 – 3.15 (m, 2H, βCH_2 and allyl CH_2), 2.03 (d, *J* = 3.7 Hz, 2H, allyl CH_2); **^{13}C NMR (101 MHz, Chloroform-d)** δ 179.8 (NCN), 171.4 (CO_2 Me), 156.6 (CO_2 Fmoc), 155.6 (C Py), 151.2 (CH arom.), 150.7 (CH arom.), 144.0 (CH arom.), 143.9 (CH arom.), 141.33 (CH arom.), 141.30 (CH arom.), 138.1 (CH arom.), 138.0 (CH arom.), 131.5 (C NCHCN), 127.8 (CH arom.), 127.3 (CH arom.), 125.6 (CH arom.), 125.3 (CH arom.), 124.4 (CH arom.), 123.7 (CH arom.), 123.6 (CH arom.), 120.51 (CH arom.), 120.0 (CH NCHCN), 117.5 (CH allyl), 73.3 (CH_2 allyl), 67.1 (CH_2 Fmoc), 56.3 (CH_2 Py), 54.1 (αCH), 52.9 (OCH_3), 52.6 (CH_2 Py), 48.9 (CH_2 allyl), 47.2 (CH Fmoc), 26.6 (βCH_2);. **HRMS (ESI):** *m/z* calculated for $C_{37}H_{36}N_5O_4PdCl$: 755.1491, found 718.1797s $[M-Cl]^+$; **Elemental analysis** calculated for: $C_{37}H_{36}N_5O_4PdCl$: C, 58.74; H, 4.80; N, 9.26; found: C, 58.77; H, 4.95, N, 9.10.

*(S)-(4-(2-((((9H-Fluoren-9-yl)methoxy)carbonyl)amino)-3-methoxy-3-oxopropyl)-3-allyl-1-(4-methoxyphenyl)-1H-2l6-imidazol-3-ium-2-ylidene)(prop-1-en-2-yl)palladium chloride **211**:*

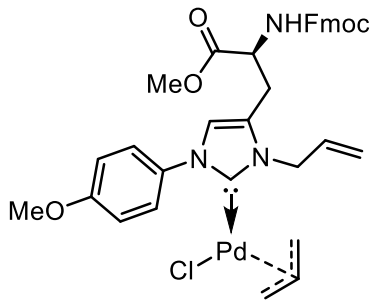

Following GP9 using imidazolium salt **165** (0.0700 g, 0.110 mmol), Ag_2O (0.0130 g, 0.0600 mmol), $[Pd(allyl)Cl]_2$ (0.0220 g, 0.0600 mmol) and dichloromethane (2.70 mL). Full consumption observed by TLC (CH_2Cl_2 9:1 MeOH) 18 h after the start of reaction. Automated flash chromatography (100% EtOAc→ 20% MeOH) gave access to **211** as a yellow solid (0.0190 g, 0.0260 mmol) in 24% yield. **$[\alpha]_D$ =** + 48.4 (c 0.1, $CHCl_3$); **Mp.:** 98-99 °C **IR**

(neat) $\nu_{(max)}$ cm^{-1}: 3335 br w, 2924 w, 1716 s, 1602 s, 1515 s, 1449 m, 1410 m, 1338 m, 1246 s, 1169 s, 1028 s, 919 w, 834 m, 760 s, 740 s, 677 w; **^{1}H NMR (400 MHz, Chloroform-d)** δ 7.75 (d, *J* = 7.5 Hz, 2H, arom. Fmoc), 7.63 (dd, *J* = 8.9, 4.0 Hz, 2H, arom. Fmoc), 7.57 (t, *J* = 8.1 Hz, 2H, arom. Fmoc), 7.42 – 7.35 (m, 2H, arom.), 7.31 – 7.27 (m, 2H, arom. Fmoc), 7.00 (s, 1H, NCHCN), 6.90 (d, *J* = 8.8 Hz, 2H, arom.), 6.07 – 5.92 (m, 1H, CH allyl), 5.58 – 5.50 (m, 1H, allyl), 5.20 (d, *J* = 10.4 Hz, 1H, allyl), 5.12 – 4.90 (m, 2H, allyl), 4.71 – 4.58 (m, 1H, αCH), 4.43 (d, *J* = 6.7 Hz, 2H, CH_2 Fmoc), 4.21 (t, *J* = 6.7 Hz, 1H, CH Fmoc), 4.16 (d, *J* = 7.4 Hz, 1H, allyl), 3.83 (s, 3H, OCH_3), 3.80 (s, 3H, OCH_3), 3.19 (dd, *J* = 16.0, 3.9 Hz, 1H, βCH_2), 3.14 – 3.01 (m, 2H, allyl), 2.97 (br s, 1H, βCH_2), 1.86 (dd, *J* = 18.5, 11.4 Hz, 2H, allyl); **^{13}C NMR (101 MHz, Chloroform-d)** δ 181.8 (NCN), 171.4 (CO_2 Me), 156.0 (CO_2 Fmoc), 143.8 (C arom.), 143.6 (C arom.), 141.5 (C arom.), 133.9 (CH arom.), 133.7 (CH arom.), 130.1 (CH arom.), 129.6 (C NCHCN), 129.2 (CH arom.), 128.0 (CH arom.), 127.3 (CH arom.), 125.9 (CH arom.), 125.1 (CH arom.), 125.1 (CH arom.), 120.2 (CH NCHCN), 119.7 (CH allyl), 117.4 (CH_2 allyl), 114.6 (CH_2 allyl), 71.6 (CH allyl), 67.4 (CH_2 Fmoc), 55.7 (OCH_3), 53.3 (OCH_3), 52.7 (αCH), 51.1 (CH_2 allyl), 47.2 (CH Fmoc), 44.7 (CH_2 allyl), 27.5 (βCH_2), 22.7 (CH_2 allyl); **HRMS (ESI):** *m/z* calculated for $C_{35}H_{36}N_3O_5Pd$: 682.1695, found 628.1696 $[M]^+$.

(S)-(4-(2-((((9H-Fluoren-9-yl)methoxy)carbonyl)amino)-2-carboxyethyl)-1-(4-methoxyphenyl)-3-methyl-1H-2l6-imidazol-3-ium-2-ylidene)gold chloride ***212****:*

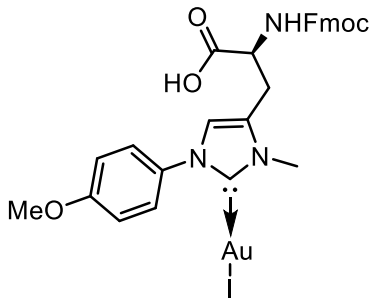

Following GP4 using NHCAuI **202** (0.609 g, 0.820 mmol), THF (13.0 mL), LiOH (0.039 g, 1.63 mmol) and H_2O (4.00 mL). Full consumption observed by TLC (CH_2Cl_2 9:1 MeOH) 30 min after he start of reaction. Trituration with hexane gave access to **212** as a beige solid (0.292 g, 0.401 mmol) with 49% yield. **$[\alpha]_D$ =** +11.1 (c 1, $CHCl_3$); **Mp.:** 144-145 °C; **IR (neat)** $\nu_{(max)}$ cm^{-1}: 3442 br w, 2920 m, 1714 s, 1608 w, 1514 s, 1448 s, 1326 w, 1250 s, 1179 w, 1105 w, 1029 m, 823 s, 759 s, 738 s; **^{1}H NMR (400 MHz, Chloroform-d)** δ 7.78 – 7.63 (m, 2H, arom. Fmoc), 7.59 – 7.47 (m, 2H, arom. Fmoc), 7.41 (d, *J* = 8.9 Hz, 2H, arom. Ph), 7.37 (t, *J* = 7.6 Hz, 2H, arom. Fmoc), 7.33 – 7.27 (m, 2H, arom. Fmoc), 6.91 (s, 1H, NCHCN), 6.89 – 6.83 (m, 2H, arom. Ph), 5.73 (d, *J* = 6.9 Hz, 1H, NH), 4.65 – 4.56 (m, 1H, αCH), 4.51 – 4.44 (m, 1H, CH_2 Fmoc), 4.41 – 4.33 (m, 1H, CH_2 Fmoc), 4.13 (t, *J* = 6.2 Hz, 1H, CH Fmoc), 3.87 – 3.65 (m, 6H, CH_3), 3.27 – 3.17 (m, 1H, βCH_2), 3.10 (dd, *J* = 15.5, 5.9 Hz, 1H, βCH_2); **^{13}C NMR (101 MHz, Chloroform-d**) δ 181.1 (NCN), 159.9 (CO_2 H), 156.0 (CO_2 Fmoc), 143.7 (C arom), 143.4 (C arom), 141.5 (C arom), 141.4 (C arom), 132.0 (C NCHCN), 129.3(CH arom.), 128.1 (CH arom.), 127.3 (CH arom.), 125.7 (CH arom.), 125.0 (CH arom.), 120.3 (CH arom.), 120.2 (CH NCHCN), 114.7 (CH arom. Ph), 67.2 (CH_2 Fmoc), 55.8 (OCH_3), 53.0 (αCH), 47.2 (CH Fmoc), 35.8 (NCH_3), 29.9. (βCH_2); **HRMS (ESI):** *m/z* calculated for $C_{29}H_{27}N_3O_5Au$: 694.1616, found 694.1610 $[M+H]^+$.

(R)-(4-(2-amino-3-methoxy-3-oxopropyl)-1,3-dibenzyl-1,3-dihydro-2H-imidazol-2-ylidene)gold(III) bromide ***214:***

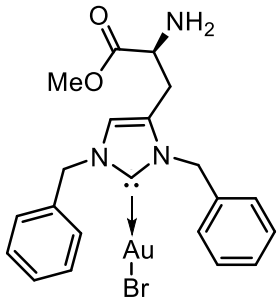

Piperidine (0.018 mL, 0.184 mmol) was added to a solution of NHCAuBr **200** (0.0600 g, 0.0920 mmol) in dichloromethane (2.00 mL). The reaction mixture was stirred at room temperature for 18 hours. The reaction mixture was concentrated under vacuum. Automated flash chromatography on alumina (100% EtOAc →30% MeOH) gave access to **214** as a beige solid (0.0570 g, 0.0920 mmol) in 99% yield. **Mp.:** 98-99 °C; **IR (neat)** $\nu_{(max)}$ cm^{-1}: 2921 m, 1851 m, 1735 s, 1676 m, 1606 w, 1451 s, 1441 m, 1204 s, 1172 m, 1079 w, 1028 w, 701 br s; **^{1}H NMR (400 MHz, Chloroform-d)** δ 7.44 – 7.28 (m, 8H. arom.), 7.23 – 7.16 (m, 2H, arom.), 6.80 (s, 1H, NCHCN), 5.54 (d, *J* = 3.1 Hz, 2H, CH_2 Bn), 5.38 (d, *J* = 2.9 Hz, 2H, CH_2 Bn), 3.60 (s, 3H, OCH_3), 3.40 (dd, *J* = 7.8, 5.2 Hz, 1H, αCH), 2.82 (dd, *J* = 15.9, 5.4 Hz, 1H, βCH_2), 2.58 (dd, *J* = 15.9, 7.5 Hz, 1H, βCH_2); **^{13}C NMR (101 MHz, Chloroform-d)** δ 174.3 (NCN), 172.0 (CO_2 Me), 135.1 (C arom.), 130.9 (C arom.), 129.14 (CH arom.), 129.09 (CH arom.), 128.8 (CH arom.), 128.4 (CH arom.), 128.0 (CH arom.), 126.9 (CH arom.), 126.8 (CH arom.), 119.3 (CH NCHCN), 55.3 (CH_2 Bn), 53.3 (αCH), 52.7 (OCH_3), 52.4 (CH_2 Bn), 29.7 (βCH_2)*;* **HRMS (ESI):** m/z calculated for $C_{21}H_{24}N_3O_2AuBr$: 626.0712, found 626.0720 $[M+H]^+$.

6.8 - Synthesis of Phosphorous Based ligands:

Allyl (tert-butoxycarbonyl)-L-serinate:

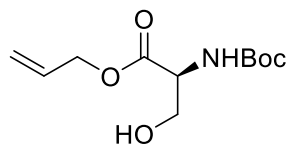

Synthesized according to literature procedure.[272] **IR (neat)** $\nu_{(max)}$ cm^{-1}: 3426 br m, 2978 m, 1739 m, 1714 m, 1693 s, 1505 m, 1367 s, 1157 s, 1057 m, 929 w; **^{1}H NMR (300 MHz, Chloroform-d)** δ 5.92 (ddt, *J* = 17.2, 10.4, 5.7 Hz, 1H, CH allyl), 5.43 (br s, 1H, NH), 5.35 (dd, *J* = 17.2, 1.5 Hz, 1H, CH_2 allyl), 5.27 (dd, *J* = 10.4, 1.2 Hz, 1H, CH_2 allyl), 4.68 (dt, *J* = 5.7, 1.4 Hz, 2H, CH_2 allyl), 4.49-4.26 (m, 1H, αCH), 4.00 (dd, *J* = 11.1, 3.8 Hz, 1H, βCH_2), 3.93 (dd, *J* = 11.1, 3.6 Hz, 1H, βCH_2), 1.46 (s, 9H, $C(CH_3)_3$); **MS (ESI):** m/z calculated for $C_{11}H_{19}NO_5$: 245.12, found 268.12 $[M+Na]^+$. Spectroscopic data are consistent with those reported.[272, 273]

*Allyl (R)-2-((tert-butoxycarbonyl)amino)-3-iodopropanoate **221:***

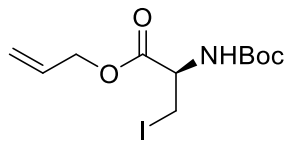

Synthesized according to literature procedure.[213 272] **^{1}H NMR (300 MHz, Chloroform-d)** δ 5.93 (ddt, *J* = 16.3, 10.4, 5.9 Hz, 1H, CH allyl), 5.42 – 5.25 (m, 2H, NH and CH_2 allyl), 4.72 – 4.65 (m, 2H, CH_2 allyl), 4.53 (dt, *J* = 7.5, 3.7 Hz, 1H, αCH), 3.62 (dd, *J* = 10.4, 3.7 Hz, 1H, βCH_2), 3.56 (dd, *J* = 10.4, 4.0 Hz, 1H, βCH_2), 1.46 (s, 9H, $C(CH_3)_3$); **^{13}C NMR (101 MHz, Chloroform-d)** δ 168.8 , 154.2, 132.3, 131.0, 119.3, 117.9, 66.7, 65.9, 53.9, 7.20; **MS (ESI):** m/z calculated for $C_{11}H_{18}NO_4I$: 355.03, found 378.02 $[M+Na]^+$. Spectroscopic data are consistent with those reported.[274]

tert-butyl (((9H-fluoren-9-yl)methoxy)carbonyl)-L-serinate ***225:***

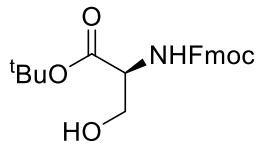

Synthesized according to literature procedure.[214] **IR (neat)** $\nu_{(max)}$ cm^{-1}: 3425 w, 3066 w, 3007 w, 2978 w, 2889 w, 1720 s, 1518 s, 1450 w, 1259 m, 1152 s, 980 m, 842 m, 763 s, 739 s; **^{1}H NMR (300 MHz, Chloroform-d)** δ 7.77 (d, *J* = 7.4 Hz, 2H, arom. Fmoc), 7.61 (d, *J* = 7.4 Hz, 2H, arom. Fmoc), 7.44 – 7.37 (m, 2H, arom. Fmoc), 7.32 (tt, *J* = 7.4, 1.1 Hz, 2H, arom. Fmoc), 5.67 (d, *J* = 7.1 Hz, 1H, NH), 4.42 (d, *J* = 7.0 Hz, 2H, CH_2 Fmoc), 4.38 – 4.28 (m, 1H, αCH), 4.23 (t, *J* = 6.9 Hz, 1H, CH Fmoc), 4.00 – 3.85 (m, 2H, βCH_2), 1.49 (s, 9H, $C(CH_3)_3$); **MS (ESI):** m/z calculated for $C_{22}H_{25}NO_5Na$: 406.16, found 406.16 $[M+Na]^+$. Spectroscopic data are consistent with those reported.[275]

tert-Butyl(R)-2-((((9H-fluoren-9-yl)methoxy)carbonyl)amino)-3-iodopropanoate ***226:***

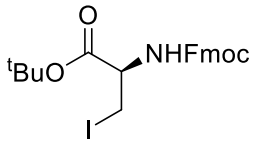

Synthesized according to literature procedure.[276] **IR (neat)** $\nu_{(max)}$ cm^{-1}: 3386 m, 3011 w, 2978 m, 1720 br s, 1513 s, 1242 m; **^{1}H NMR (400 MHz, Chloroform-d)** δ 7.77 (d, *J* = 7.5 Hz, 2H, arom. Fmoc), 7.62 (d, *J* = 7.4 Hz, 2H, arom. Fmoc), 7.40 (td, *J* = 7.4, 4.0 Hz, 2H, arom. Fmoc), 7.36 – 7.29 (m, 2H, arom. Fmoc), 5.68 (d, *J* = 7.0 Hz, 1H, NH), 4.46 – 4.31 (m, 3H, αCH and CH_2 Fmoc), 4.25 (t, *J* = 7.2 Hz, 1H, CH Fmoc), 3.65 – 3.55 (m, 2H, βCH_2), 1.52 (s, 9H, $C(CH_3)_3$). **MS (ESI):** m/z calculated for $C_{22}H_{24}NO_4INa$: 516.0642, found 516.0658 $[M+Na]^+$. Spectroscopic data are consistent with those reported.[276]

*2-Chloro-1,3,2-dioxaphospholane **230:***

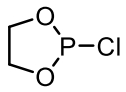

Synthesized according to literature procedure.[215] **Bp.:** 79 – 80 °C; **^{1}H NMR (400 MHz, Chloroform-d)** δ 4.42 (dt, *J* = 8.4, 1.5 Hz, 2H, CH_2), 4.26 – 4.17 (m, 2H, CH_2); **^{13}C NMR (101 MHz, Chloroform-d)** δ 65.28 (d, $J_{C,P}$ = 8.8 Hz); **^{31}P NMR (122 MHz, Chloroform-d)** δ 167.51. Spectroscopic data are consistent with those reported.[215]

*Phosphino borane **223:***

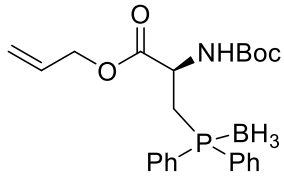

A solution of KHMDS 0.5 M in toluene (3.00mL) was added dropwise over 10 minutes to a solution of Ph_2PH (0.348 mL, 2.00 mmol) in anhydrous THF (7.00 mL) at -78 °C. The reaction mixture was stirred at -78 °C for 45 minutes. A cold (-78 °C) solution of Boc-iodoalanine-OAll (0.520 g, 1.50 mmol) in anhydrous THF (7.00 mL) was added dropwise to the reaction mixture. After 1 hour stirring DMS.BH_3 2.0 M in THF (0.750 mL) was added to the reaction mixture which was stirred for 1 hour at -78 °C. The reaction mixture was quenched with saturated ammonium chloride and allowed to slowly warm up to room temperature. The reaction mixture was concentrated under vacuum and the residue was dissolved in EtOAc and washed with water (3 X 15 mL). The organic layers were dried over sodium sulfate and concentrated under reduced pressure. The crude oil was purified via automated flash chromatography (100% hexane → 80% EtOAc) yielding **223** as a sticky white solid (0.114 g, 0.267 mmol) in 18% yield. **$[\alpha]_D$ =** + 18.8 (c 0.5, $CHCl_3$); **IR (neat) $\nu_{(max)}$** cm^{-1}: 3431 w, 2979 w, 2385 m, 2332 m, 1736 s, 1695 s, 1520 m, 1487 m, 1344 w, 1253 s, 1232 s, 1155 s, 1065 s, 917 s, 856 w, 808 w, 740 s, 692 s; **^{1}H NMR (400 MHz, Chloroform-d)** δ 7.75 – 7.62

(m, 5H. arom. Ph), 7.46 (m, 5H, arom. Ph), 5.97 – 5.76 (m, 1H, CH allyl), 5.29 (dd, *J* = 17.2, 1.4 Hz, 1H, CH_2 allyl), 5.22 (br d, J = 11.3 Hz, 2H, NH and CH_2 allyl), 4.57 (dd, *J* = 13.7, 6.1 Hz, 1H, CH_2 allyl), 4.50 (dd, *J* = 13.6, 5.6 Hz, 1H, αCH), 4.43 (dd, *J* = 13.7, 6.4 Hz, 1H, CH_2 allyl), 3.01 (dt, *J* = 14.9, 9.8 Hz, 1H, βCH_2), 2.91 (dt, *J* = 14.8, 7.5 Hz, 1H, βCH_2), 1.54 – 1.44 (m, 3H, BH_3), 1.31 (s, 9H, $C(CH_3)_3$); **^{13}C NMR (101 MHz, Chloroform-d**) δ 170.7 (CO_2 allyl), 154.9 (CO_2 Fmoc), 132.3 (d, $J_{C,P}$ = 9.5 Hz, Ph), 132.2 (d, $J_{C,P}$ = 9.4 Hz, Ph), 131.5 (d, $J_{C,P}$ = 4.6 Hz, Ph), 129.1 (app. t, $J_{C,P}$ = 8.9 Hz, Ph), 118.9 (allyl), 80.2 (C $C(CH_3)_3$), 66.5 (allyl), 50.6 (αCH), 28.3 (allyl), 28.02 (d, $J_{C,P}$ = 7.4 Hz, βCH_2), 27.6 ($C(CH_3)_3$); **^{31}P NMR (162 MHz, Chloroform-d)** δ 12.81; **^{11}B NMR (128 MHz, Chloroform-d)** δ -39.63 **HRMS (ESI):** m/z calculated for $C_{23}H_{31}BNO_4PNa$: 450.1975, found 450.2023 $[M+H]^+$.

*Phosphino borane **227:***

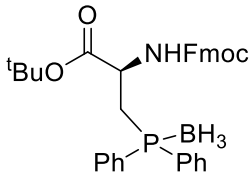

A solution of KHMDS 0.5 M in toluene (1.60 mL) was added dropwise over 10 minutes to a solution of Ph_2PH (0.190 mL, 1.09 mmol) in anhydrous THF (8.40 mL) at -78 °C. The reaction mixture was stirred at -78 °C for 45 minutes. A cold (-78 °C) solution of Fmoc-iodoalanine-O^{t}Bu **228** (0.416 g, 0.840 mmol) in anhydrous THF (4.20 mL) was added dropwise to the reaction mixture. After 1 hour stirring DMS.BH_3 2.0 M in THF (0.527 mL) was added to the reaction mixture which was stirred for 1 hour at -78 °C. The reaction mixture was quenched with saturated ammonium chloride and allowed to slowly warm up to room temperature. The reaction mixture was concentrated under vacuum and the residue was dissolved in EtOAc and washed with water (3 X 15 mL). The organic layers were dried over sodium sulfate and concentrated under reduced

pressure. The crude oil was purified via automated flash chromatography (100% hexane → 80% EtOAc) yielding **227** as a sticky white solid (0.095 g, 0.168 mmol) in 20% yield; **IR (neat)** $\nu_{(max)}$ cm^{-1}: 3358 w, 2929 w, 2387 m, 1722 s, 1506 s, 1450 m, 1437 m, 1394 w, 1368 m, 1319 w, 1223 s, 1148 s, 1105 m, 990 w, 840 w, 758 m, 736 s, 692 s; ^{1}H NMR (400 MHz, Chloroform-d) δ 7.81 – 7.64 (m, 6 H, CH arom.), 7.50 (dd, *J* = 7.4, 2.9 Hz, 2H, CH arom. Fmoc), 7.46 – 7.36 (m, 8H, CH arom.), 7.34 – 7.27 (m, 2H, CH arom.), *5.43* (d, *J* = 7.5 Hz, 1H, NH), 4.48 – 4.37 (m, 1H, αCH), 4.12 (dd, *J* = 9.4, 6.9 Hz, 1, CH_2 Fmoc), 4.03 (app. t, *J* = 7.1 Hz, 1H, CH Fmoc), 3.97 (dd, *J* = 9.3, 7.3 Hz, 1H, CH_2 Fmoc), 3.06 (dt, *J* = 15.0, 9.9 Hz, 1H, βCH_2), 2.91 (ddd, *J* = 15.1, 11.2, 4.2 Hz, 1H, CH_2 Fmoc), 1.44 (s, 9H, $C(CH_3)_3$), 1.32 – 1.19 (m, 3H, BH_3); **^{13}C NMR (101 MHz, Chloroform-d)** δ 169.6 (CO_2 ^{t}Bu), 155.3 (CO_2 Fmoc), 143.89 (d, $J_{C,P}$ = 4.4 Hz, C Ph), 141.3 (C arom. Fmoc), 132.33 (d, $J_{C,P}$ = 9.5 Hz, CH arom.), 132.19 (d, $J_{C,P}$ = 9.4 Hz, CH arom.), 131.49 (d, $J_{C,P}$ = 6.4 Hz, CH arom.), 129.02 (app t, $J_{C,P}$ = 11.4 Hz, CH arom.), 127.8 (CH arom. Fmoc), 127.2 (CH arom. Fmoc), 125.4 (CH arom. Fmoc), 120.1 (CH arom. Fmoc), 83.0 (C $C(CH_3)_3$), 67.9 (CH_2 Fmoc), 51.4 (αCH), 47.1 (CH Fmoc), 28.0 ($C(CH_3)_3$), 27.6 (d, $J_{C,P}$ = 37.6 Hz, βCH_2); **^{31}P NMR (121 MHz, Chloroform-d) δ** 12.60; **^{11}B NMR (128 MHz, Chloroform-d)** δ -39.52; **HRMS (ESI):** m/z calculated for $C_{34}H_{35}BNO_4P$: 563.2391, found 563.2421 $[M+H]^+$.

*Phosphino borane **233:***

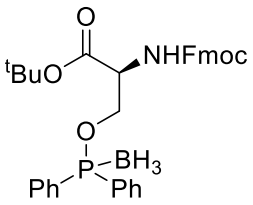

Fmoc-Ser-O^{t}Bu **225** (0.150 g, 0.390 mmol) was dissolved in THF (2.00 mL) in a dry Schlenk flask under argon. The solution was cooled down to 0 °C and stirred for 10 minutes. DIEA (0.077 mL, 0.470 mmol) was added and the reaction mixture stirred for 5

minutes. Ph_2PCl (0.105 mL, 0.590 mmol) was added dropwise for 5 minutes and the reaction mixture left to stir at 0 °C for 1 hour until all starting material was consumed by TLC (hexane 2:1 EtOAc). $DMS.BH_3$ 2M in THF (0.295 mL) was added dropwise for 5 minutes and the reaction allowed to slowly warm up to room temperature and left to stir for 16 hours. A couple of drops of methanol were added to the reaction mixture and the mixture was concentrated under vacuum to yield a sticky white solid. Automated flash chromatography (100%hexane →40% EtOAc→100% EtOAc) gave access to **225** as a sticky white solid (0.182 g, 0.310 mmol) in 80% yield. **$[\alpha]_D$ =** +52.7(c 1, $CHCl_3$); **Mp.:** 91-92 °C, **IR (neat) $\nu_{(max)}$** cm^{-1}: 3333 br w, 2980 w, 2385 m, 2339 m, 1742 m, 1724 m, 1689 s, 1536 m, 1477 m, 1437 s, 1340 m, 1368 m, 1218 m, 1156 s, 1061 s, 1024 m, 943 w, 747 m, 732 s, 695 s; **^{1}H NMR (400 MHz, Chloroform-d)** δ 7.77 (d, *J* = 7.4 Hz, 2H, arom. Fmoc), 7.74 – 7.64 (m, 4H, arom. Ph), 7.59 (br t, *J* = 6.9 Hz, 2H, arom. Fmoc), 7.53 – 7.47 (m, 2H, arom. Fmoc), 7.46 – 7.37 (m, 6H, arom. Ph), 7.30 (t, *J* = 7.4 Hz, 3H, arom. Fmoc), 5.62 (d, *J* = 7.9 Hz, 1H, NH), 4.56 – 4.47 (m, 1H, αCH), 4.44 – 4.37 (m, 1H, CH Fmoc), 4.34 (d, *J* = 7.9 Hz, 2H, CH_2 Fmoc), 4.27 – 4.18 (m, 2H, βCH_2), 1.46 (s, 9H, $C(CH_3)_3$); **^{13}C NMR (101 MHz, Chloroform-d)** δ 168.4 (CO_2 ^{t}Bu), 155.8 (CO_2 Fmoc), 143.92 (d, $J_{C,P}$ = 4.6 Hz, C arom. Ph), 141.4 (C arom. Fmoc), 132.26 (d, $J_{C,P}$ = 21.2 Hz, CH arom.), 131.51 (d, $J_{C,P}$ = 11.5 Hz, CH arom.), 131.22 (d, $J_{C,P}$ = 11.4 Hz, CH arom.), 128.87 (app t, $J_{C,P}$ = 11.0 Hz, CH arom.). 127.9 (CH arom. Fmoc), 127.2 (CH arom. Fmoc), 125.3 (CH arom. Fmoc), 120.1 (CH arom. Fmoc), 83.4 (C $C(CH_3)_3$), 67.5 (βCH_2), 67.4 (CH_2 Fmoc), 55.2 (αCH), 47.2 (CH Fmoc), 28.1 (CH_3 $C(CH_3)_3$) .**^{31}P NMR (162 MHz, Chloroform-d)** δ 107.39; **^{11}B NMR (128 MHz, Chloroform-d)** δ -40.83; **HRMS (ESI):** m/z calculated for $C_{34}H_{37}NO_5PB$: 581.2502, found 604.2394 $[M+Na]^+$.

*Phosphino **235:***

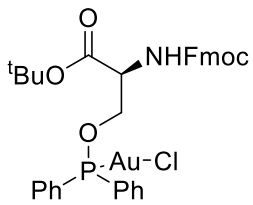

Fmoc-Ser-O^{t}Bu **225** (0.100 g, 0.260 mmol) was dissolved in THF (21.50 mL) in a dry Schlenk flask under argon. The solution was cooled down to 0 °C and stirred for 10 minutes. DIEA (0.054mL, 0.310 mmol) was added and the reaction mixture stirred for 5 minutes. Ph_2PCl (0.070 mL, 0.390 mmol) was added dropwise for 5 minutes and the reaction mixture left to stir at 0 °C for 1 hour until all starting material was consumed by TLC (hexane 2:1 EtOAc). DMSAuCl (0.114 g, 0.390 mmol) was added reaction allowed to slowly warm up to room temperature and left to stir for 1 hours. The reaction mixture was concentrated under vacuum to yield a sticky white solid. Automated flash chromatography (100%hexane 100% EtOAc) gave access to **235** as a white solid with 63% yield (0.132 g, 0.164 mmol). **$[\alpha]_D$ =** + 19.3 (c 0.3, $CHCl_3$); **Mp.:** 83-85 °C; **IR (neat) $\nu_{(max)}$** cm^{-1}: 3324 w, 2976 w, 1720 s, 1505 m, 1478 w, 1437 s, 1247 s, 1152 s, 1108 s, 1056 s, 1022 s, 975 m, 942 w, 842 w, 740 s, 704 s, 690 s, 645 w; **^{1}H NMR (400 MHz, Chloroform-d)** δ 7.77 (d, *J* = 7.1 Hz, 2H, arom. Fmoc), 7.68 (m, 4H, arom. Ph), 7.60 (d, *J* = 7.5 Hz, 2H, arom. Fmoc), 7.55 (m, 3H, arom. Ph), 7.47 (m, 3H, arom. Ph), 7.41 (t, *J* = 7.5 Hz, 2H, arom. Fmoc), 7.31 (td, *J* = 7.5, 1.1 Hz, 2H, arom. Fmoc), 5.56 (d, *J* = 7.2 Hz, 1H, NH), 4.52 (dd, *J* = 5.1, 2.2 Hz, 1H, αCH), 4.49 – 4.43 (m, 1H, βCH_2), 4.42 – 4.35 (m, 2H, CH_2 Fmoc), 4.33 (dd, *J* = 7.0, 2.7 Hz, 1H, βCH_2) 4.21 (t, *J* = 7.1 Hz, 1H, CH Fmoc), 1.47 (s, 9H, $C(CH_3)_3$); **^{13}C NMR (101 MHz, Chloroform-d)** δ 168.0 (CO_2 ^{t}Bu), 155.7 (CO_2 Fmoc), 143.9 (C arom.), 141.4 (C arom.), 133.23 (CH arom.), 133.0 (CH arom.), 132.50 (d, $J_{C,P}$ = 16.5 Hz, CH arom. Ph), 131.9 (d, $J_{C,P}$ = 15.8 Hz, CH arom. Ph), 129.35 (app t, $J_{C,P}$ = 12.6 Hz, CH arom. Ph), 127.9 (CH arom. Fmoc), 127.3 (Ch arom. Fmoc), 125.3 (CH arom. Fmoc), 120.2 (CH arom. Fmoc), 84.0 (C

$C(CH_3)_3$), 71.0 (βCH_2), 67.5 (CH_2 Fmoc), 55.1 (αCH), 47.2 (CH Fmoc), 28.2 ($C(CH_3)_3$); **^{31}P NMR (121 MHz, Chloroform-d)** δ 114.03; **HRMS (ESI):** m/z calculated for $C_{21}H_{24}N_3O_2AuBr$: 626.0712, found 626.0720 $[M+H]^+$.

6.9 – Catalytic Activity Studies

*N-allyl-4-methyl-N-(prop-2-yn-1-yl)benzenesulfonamide **238:***

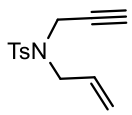

Synthesized according to literature procedure[277]. White solid. **IR (neat)** $\nu_{(max)}$ cm^{-1}: 3277 w, 2982 w, 2923 w, 2120 w, 1644 w, 1598 w, 1495 w, 1431 w, 1345 s, 1328 s, 1259 w, 1156 s, 1120 m, 1091 s, 1061 m, 1018 m; **^{1}H NMR (400 MHz, Chloroform-d)** δ 7.79-7.70 (m, 2H), 7.30 (d, *J* = 8.0 Hz, 2H), 5.84-5.63 (m, 1H), 5.39-5.18 (m, 2H), 4.15-4.06 (m, 2H), 3.87 (dd, *J* = 7.2, 5.6, 2H), 2.43 (s, 3H), 2.02 (t, *J* = 2.5 Hz, 1H); **MS (ESI):** m/z calculated for $C_{13}H_{15}NO_2S$: 249.08, found 250.09 $[M+H]^+$. Data are consistent with those described in the literature.[277]

*N-allyl-4-methyl-N-(3-phenylprop-2-yn-1-yl)benzenesulfonamide **237:***

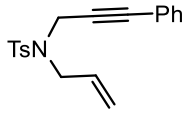

Synthesized according to literature procedure.[278] . **IR (neat)** $\nu_{(max)}$ cm^{-1}: 2910 w, 1460 m, 1378 m, 1161 s, 723 m; 693 s; **^{1}H NMR (400 MHz, Chloroform-d)** δ 7.78 (d, *J* = 8.0 Hz, 2H), 7.28–7.21 (m, 5H), 7.06 (d, *J* = 7.0 Hz, 2H), 5.83–5.77 (m, 1H), 5.33 (d, *J* = 17.4 Hz, 1H), 5.26 (d, *J* = 10.0 Hz, 1H), 4.32 (s, 2H), 3.89 (d, *J* = 6.0 Hz, 2H), 2.34 (s, 3H); **MS (ESI):** m/z calculated for $C_{19}H_{19}NO_2S$: 325,42 found 326.12 $[M+H]^+$. Data are consistent with those described in the literature.[278]

Quantification of Reaction Yields using Gas Chromatography:

But-1-yne-1,4-diyldibenzene (1.00 eq) was added to a screw cap glass vial equipped with a magnetic stirrer. Methanol (0.1 mM), water (2.00 eq.), AgOTf (3 mmol%) and the gold catalyst (2 mmol%) were added and the reaction stirred at 80 °C for 24 hours. After the 24 hours the heating was switched off and the reaction allowed to cool down to 30 °C. The reaction mixture was stirred with sodium sulfate and filtered through cotton wool. The mixture was concentrated under vacuum until no solvent was visible and left on less than 10 mbar pressure for 10 minutes. The oily residue was dissolved in 4.00 mL of methanol and 0.020 mL of this solution was added to a sample vial containing 0.500 mL of MeOH and 0.010 mL of a solution of 1,2,4,5-tetramethylbenzene in methanol (0.103 mM). The sample (0.005 mL) was injected in the GC. The column oven temperature was programmed as follows: 50 °C for 2 minutes, 50 °C to 300 °C for 25 minutes and then 10 minutes at 300 °C.

GC response factors were established by the following equation using 1,2,4,5-tetramethylbenzene as the internal standard:

$$Response\ factor = \frac{(mmols\ of\ compound)}{(area\ of\ compound)} \times \frac{(area\ of\ internal\ standard)}{(mmols\ of\ internal\ standard)}$$

Eight samples containing known amounts of the product and internal standard were prepared in 0.500 mL of MeOH. An aliquot of each sample was injected into the GC and the average of 8 response factors was used to monitor the hydration reactions.

Compound	Response Factor	T_R (min)
1,4-diphenylbutan-1-one	0.770	21.3
1,4-diphenylbutan-2-one	1.53	20.6
1,2,4,5-tetramethyl benzene	-	9.9

*But-1-yne-1,4-diyldibenzene **243**:*

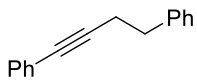

Following the literature procedure[279] using triphenylphosphine)palladium(II) dichloride (0.373 g, 0.530 mmol), copper(I) iodide (0.203 g, 1.06 mmol), degassed THF (216 mL), iodobenzene (2.98 mL, 26.5 mmol), degassed triethylamine (42.0 mL) and 4-phenyl-1-butyne (4.00 mL, 29.2 mmol). Purification by automated flash chromatography (100% hexane) to give alkyne **243** as a colourless oil with 69% yield (3.77 g, 18.3 mmol). **IR (neat)** $\nu_{(max)}$ cm^{-1}: 3027 w, 2927 w, 1599m, 1490 s; 752 s, 714 w, 690 s; **^{1}H NMR (400 MHz, Chloroform-d)** δ 7.39-7.19 (m, 10H, arom. CH), 2.92 (t, *J* = 7.5 Hz, 2H, CH_2), 2.69 (t, *J* = 7.5 Hz, 2H, CH_2); **^{13}C NMR (101 MHz, Chloroform-d)** δ 140.9, 131.7, 128.7, 128.5, 128.3, 127.8, 126.5, 124.0, 89.6 81.5, 35.3, 21.8. Spectroscopic data are consistent with those reported.[279]

*1,4-Diphenylbutan-1-one **244**:*

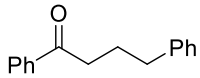

White solid. **IR (neat)** $\nu_{(max)}$ cm^{-1}: 3062 w, 3027 w, 2936 w, 1682 s, 1598 s, 1448 s, 1367 s, 1000 m, 750 a, 686 s, 608 s; **^{1}H NMR (400 MHz, Chloroform-d)** δ 7.97-7.89 (m, 2H, arom. CH), 7.59-7.52 (m, 1H, arom. CH), 7.49-7.41 (m, 2H, arom. CH), 7.34-7.26 (m, 2H, arom. CH), 7.25-7.17 (m,3H), 2.99 (t, *J* = 7.3 Hz, 2H, CH_2), 2.73 (t, *J* = 7.5 Hz, 2H, CH_2), 2.09 (app. quint, *J* = 7.4 Hz, 2H, CH_2); **^{13}C NMR (101 MHz, Chloroform-d)** δ 200.3, 141.8, 137.1, 133.1, 128.7, 128.7, 128.5, 128.2, 126.1, 37.8, 35.3, 25.8. Data are consistent with those described in the literature.[279]

*1,4-Diphenylbutan-2-one **245**:*

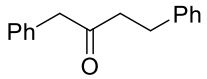

White solid. **IR (neat)** $\nu_{(max)}$ cm^{-1}: 3028 w, 2926 w, 1708 s, 1602 m, 1496 m, 1454m; 1958 s, 753 s, 700 s, 675 s; **^{1}H NMR (400 MHz, Chloroform-d)** δ 7.37-7.22 (m, 5H, arom. CH), 7.22-7.08 (m, 5H, arom. CH), 3.67 (s, 2H, CH_2), 2.87 (m, 2H, CH_2), 2.77 (m, 2H, CH_2); **^{13}C NMR (101 MHz, Chloroform-d)** δ 207.6 , 141.0, 134.2, 129.5, 128.9, 128.6, 128.5, 127.2, 126.2, 50.5, 43.6, 29.9. Data are consistent with those described in the literature.[279]

6.10 - Solid-Phase Peptide Synthesis:

6.10.1- Automated SPPS:

Peptide synthesis was facilitated by standard solid phase peptide synthesis protocols utilising a CEM Liberty Blue Automated Peptide Synthesiser.[280] The protected amino acids used were *N*-(9-fluorenylmethyloxycarbonyl)-*L*-alanine, *N*-(9-fluorenylmethyloxycarbonyl)-*D*-alanine N_α-(9-fluorenylmethoxycarbonyl)-N_γ-trityl-*L*-asparagine, *N*-(9-fluorenylmethyloxycarbonyl) -*L*-aspartic acid 4-^{t}butyl ester, N_α-(9-fluorenylmethoxycarbonyl)-N_δ-trityl-*L*-glutamine, *N*-(9-fluorenylmethyloxycarbonyl)-*L*-glutamic acid 5-^{t}butyl ester, *N*-(9-fluorenylmethyloxycarbonyl)-glycine, N_α-(9-fluorenylmethoxycarbonyl)-*N*-trityl-*L*-histidine, *N*-(9-fluorenylmethyloxycarbonyl)-*L*-isoleucine, N_α-(9-fluorenylmethoxycarbonyl)-N_ε-^{t}butyloxycarbonyl-*L*-lysine, *N*-(9-fluorenylmethyloxycarbonyl)-*O*-^{t}butyl-*L*-serine, N_α-(9-fluorenylmethoxycarbonyl)-*N*-^{t}butyloxycarbonyl-*L*-tryptophan, *N*-(9-fluorenylmethyloxycarbonyl)-*O*-^{t}butyl-*L*-tyrosine. These species were dissolved in *N,N*-dimethylformamide (DMF) to give 0.2 M solutions. Rink amide 4-methylhydrylamine resin (0.368 g, 0.68 meq g^{-1}) was agitated

in *DMF* (10 mL) for 20 minutes to swell the resin. The swollen resin was then loaded into the automated synthesiser reaction vessel. All methods on the automated synthesiser were carried out under an inert nitrogen atmosphere. The *N*-fluorenylmethyloxycarbonyl protecting groups were removed using 20% piperidine in DMF, facilitated by microwave methods (60 W, 75 °C, 180 s or 30 s). Following deprotection, the next amino acid in the sequence was coupled in the presence of an activator such as *O*-(benzotriazol-1-yl)-*N*,*N*,*N'*,*N'*-tetramethyluronium hexafluorophosphate (HBTU, 0.5 M) in DMF and an activator base such as *N,N*-diisopropylethylamine (DIEA, 2 M) in *N*-methyl-2-pyrrolidone. The couplings were facilitated by microwave methods, typically 10 minutes coupling time (30 W, 75 °C, 600 s). The first residue to be attached to the resin was double coupled and the final three heptads were also double coupled. Following any reaction, either deprotection or coupling, the vessel was washed with DMF (3 x 5 mL, 5 s drain time). After couplings the manifold was also washed with DMF (2 x 4 mL, 5 s drain time).

Upon completion of the sequence synthesis, the final residue was left deprotected ready for capping in the case of peptide AA1C and the second part of AA1-19NHCBn$_2$). The resin was removed from the automated synthesiser and swollen in DMF (10.0 mL) for 20 minutes before the addition of a capping mixture consisting of DIEA (5.00 mL) and acetic anhydride (5.00 mL). The mixture was agitated for 30 minutes, then filtered and the resin washed with dichloromethane (3 x 7.00 mL) and diethyl ether (3 x 7.00 mL) before air drying for 2 hours. In the case of the synthesis of peptides AA1-1(NHCBn$_2$), AA1-1(NHCMe/pMeO), AA1-2(NHCBn$_2$) and the first part of AA1-19(NHCBn$_2$) the synthesis was stopped before the last deprotection and the Fmoc protected peptide on resin was manually manipulated.

The dry capped peptides on resin was placed in a falcon tube prior to the addition of a cleavage cocktail consisting of trifluoroacetic acid (18.0 mL), water (1.00 mL) and triisopropylsilane (1.00 mL). The tube was agitated for 3 hours before filtering and washing the solids with trifluoroacetic acid (2-3.00 mL). The filtrate was triturated in ice-cold diethyl ether (4 x 40.0 mL) and placed in the freezer for 30 minutes. The solid crude peptide was isolated by centrifugation (Eppendorf centrifuge 5702 with A-4-38 and rotational speed of 4400 rpm for 10 minutes), the diethyl ether was decanted and a further addition of ice-cold diethyl ether was added (4 x 20 mL). The tubes were agitated for 20 minutes and placed in the freezer for 30 minutes prior to centrifugation and decanting of the diethyl ether. This yielded the crude peptide as a white/cream solid. The crude peptide was dissolved in aqueous acetonitrile (1:1), typically requiring 25-30 mL before filtering through a Millex syringe-driven filter unit (0.45 μm pore size) in preparation for high pressure liquid chromatography purification.

6.10.2 - Manual SPPS:

6.10.2.1 – Incorporation of imidazolium salts

The resin (0.100 mmol) was swelled in DMF (8.00 mL) for one hour. The DMF was filtered and HOBt (5.00 eq.), HBTU (5.00 eq), the imidazolium salt amino acid **180** or **189** (5.00 eq.) and DMF (3.00 mL) were added to the resin and shaken for 2 hours. The resin was filtered and washed with DMF (3 X 5.00 mL). A second coupling was carried out with HOBt (5.00 eq.), HBTU (5.00 eq), the imidazolium salt amino acid **180** or **189**(5.00 eq.) and DMF (3.00 mL) and the resin shaken for 16 hours. The resin filtered and washed with DMF (3 X 5.00 mL). A solution of 20% piperidine in DMF (4.00

mL) was added to the resin and shaken for 30 minutes. The resin was filtered, and the same procedure repeated. The resin was filtered and washed with DMF (5 X 5 mL).

In the case of AA1-1NHC(Bn_2) and AA1-1NHC(Me/pMeO) the resin was capped and cleave according to the previously described procedures. In the case of AA1-19(Bn_2) and AA2-5(Bn_2) the next amino acid was coupled and deprotected using the same procedure. AA1-19(Bn_2) resin was then placed back on the automated synthesizer for the rest of the sequence.

In the case of dipeptides **257, 258** and **259,** the resin (0.100 mmol) was swelled in DMF (8.00 mL) for one hour. The DMF was filtered and HOBt (5.00 eq.), HBTU (5.00 eq), the imidazolium salt amino acid **180** (5.00 eq.) and DMF (3.00 mL) were added to the resin and shaken for 2 hours. The resin was filtered and washed with DMF (3 X 5.00 mL). A second coupling was carried out with HOBt (5.00 eq.), HBTU (5.00 eq), the imidazolium salt amino acid (5.00 eq.) and DMF (3.00 mL) and the resin shaken for 16 hours. The resin filtered and washed with DMF (3 X 5.00 mL). A third of the resin was dried and cleaved using a 50% solution of TFA in dichloromethane (5.00 mL) which was shaken for 45 minutes. The leftover two thirds were deprotected using a solution of 20% piperidine in DMF (4.00 mL) and shaken for 30 minutes. The resin was filtered, and the same procedure repeated. The resin was filtered and washed with DMF (5 X 5.00 mL). The resin was split in half, half was cleaved using the above-mentioned procedure and the other half was capped. The capping procedure used acetic anhydride (2.00 mL), DIEA (2.00 mL) and DMF (6.00 mL) and shaken for 30 minutes. The resin was filtered and washed with DMF (5 X 5.00 mL), dichloromethane (5 X 5.00 mL) and diethyl ether (5 X 5.00 mL) and left to dry for 1 hours. The resin was cleaved using a 50% solution of TFA in dichloromethane (5.00 mL) which was shaken

for 45 minutes. The dipeptides were precipitated with cold diethyl ether (30.0 mL) and cooled in the freezer for a minimum of 1 hour. The suspension was centrifuged for 10 minutes and the diethyl ether decanted yielding the crude peptide as a white sticky solid.

6.10.2.2 – Incorporation of thiazolium 195

The resin (0.100 mmol) was swelled in DMF (8.00 mL) for one hour. The DMF was filtered and DIEA (5.00 eq.), HBTU (5.00 eq), the thiazolium amino acid **195** (5.00 eq.) and DMF (3.00 mL) were added to the resin and shaken for 2 hours. The resin was filtered and washed with DMF (3 X 5.00 mL). A second coupling was carried out with HOBt (5.00 eq.), HBTU (5.00 eq), the thiazolium amino acid **195** (5.00 eq.) and DMF (3.00 mL) and the resin shaken for 16 hours. The resin filtered and washed with DMF (3 X 5.00 mL). A third of the resin was dried and cleaved using a 50% solution of TFA in dichloromethane (5.00 mL) which was shaken for 45 minutes. The leftover two thirds were deprotected using a solution of 20% piperidine in DMF (4.00 mL) and shaken for 30 minutes. The resin was filtered, and the same procedure repeated. The resin was filtered and washed with DMF (5 X 5.00 mL). The resin was split in half, half was cleaved using the above-mentioned procedure and the other half was capped. The capping procedure used acetic anhydride (2.00 mL), DIEA (2.00 mL) and DMF (6.00 mL) and shaken for 30 minutes. The resin was filtered and washed with DMF (5 X 5.00 mL), dichloromethane (5 X 5.00 mL) and diethyl ether (5 X 5.00 mL) and left to dry for 1 hours. The resin was cleaved using a 50% solution of TFA in dichloromethane (5.00 mL) which was shaken for 45 minutes. The suspension was centrifuged for 10

minutes and the diethyl ether decanted yielding the crude peptide as a beige sticky solid.

6.10.2.2 – Incorporation of NHCAu Amino Acid 212

The resin (0.100 mmol) was swelled in DMF (8.00 mL) for one hour. The DMF was filtered and DIEA (5.00 eq.), HBTU (5.00 eq.), the NHCAu amino acid **212** (2.00 eq.) and DMF (3.00 mL) were added to the resin and shaken for 2 hours. The resin was filtered and washed with DMF (3 X 5.00 mL). A second coupling was carried out with HOBt (5.00 eq.), HBTU (5.00 eq.), the NHCAu amino acid **212** (2.00 eq.) and DMF (3.00 mL) and the resin shaken for 16 hours. The resin filtered and washed with DMF (3 X 5.00 mL). A third of the resin was dried and cleaved using a 50% solution of TFA in dichloromethane (5.00 mL) which was shaken for 45 minutes. The leftover two thirds were deprotected using a solution of 20% piperidine in DMF (4.00 mL) and shaken for 30 minutes. The resin was filtered, and the same procedure repeated. The resin was filtered and washed with DMF (5 X 5.00 mL). The resin was split in half, half was cleaved using the above-mentioned procedure and the other half was capped. The capping procedure used acetic anhydride (2.00 mL), DIEA (2.00 mL) and DMF (6.00 mL) and shaken for 30 minutes. The resin was filtered and washed with DMF (5 X 5.00 mL), dichloromethane (5 X 5.00 mL) and diethyl ether (5 X 5.00 mL) and left to dry for 1 hours. The resin was cleaved using a 50% solution of TFA in dichloromethane (5.00 mL) which was shaken for 45 minutes. The suspension was centrifuged for 10 minutes and the diethyl ether decanted yielding the crude peptide as a beige sticky solid.

6.11 - High Pressure Liquid Chromatography (HPLC)

6.11.1 - Preparative HPLC:

The crude peptide was purified by reverse phase high pressure liquid chromatography on a preparative Waters XBridge C_{18} column. The eluent A consisted of water and trifluoroacetic acid (0.05% v/v) and the eluent B consisted of acetonitrile and trifluoroacetic acid (0.05% v/v). The method involved going from 0 – 100% eluent B over 40 minutes followed by a wash cycle. Flow rate was maintained at 10 mL min^{-1} throughout the method and the observed detector wavelengths were set at 210 and 280 nm. The resultant pure fractions were rotary evaporated to remove the acetonitrile and lyophilised on a freeze dryer overnight to yield the pure peptide as fluffy white powder.

6.11.2 - Analytical HPLC:

A sample of the purified peptide in aqueous acetonitrile (50% v/v) was placed into the auto sampler for analysis by reverse phase high pressure liquid chromatography on an analytical Waters XBridge C_{18} column. The eluent A consisted of water and trifluoroacetic acid (0.05% v/v) and the eluent B consisted of acetonitrile and trifluoroacetic acid (0.05% v/v). The method involved going from 0 – 100% eluent B over 40 minutes followed by a wash cycle. Flow rate was maintained at 1 mL min^{-1} throughout the method and the observed detector wavelengths were set at 210 and 280 nm. Note that the signals present between 5 and 10 are instrumental artefacts and were present in water blanks as well as the sample. The typical retention times for all peptides in this thesis were between 25 and 32 minutes and the purities were found to

be >95%.The analytical chromatograms for each peptide can be found in the supporting information (*see* Appendix).

6.12 - Sample Preparation

6.12.1 - Peptide Concentration Determination:

Peptide stock solutions were prepared in ultrapure water, typically 1 mg mL^{-1}. The peptide concentration was determined by taking an aliquot of the stock (20 µL) and placing it in a 1.5 mL eppendorf with an aqueous solution of urea (680 µL, 7 M) to give a total volume of 700 µL. The solution was appropriately mixed by using a vortex mixer for 45 seconds. The solution was left to stand for 10 minutes before 600 µL were placed in a quartz cuvette prior to UV-vis characterisation to determine the peptide concentration via the Beer-Lambert law.

Ultraviolet and visual spectrum absorption profiles were recorded on a Carey 50 UV Spectrophotometer, using single beam mode and a medium scan speed. The slit width was set at 1.0 nm and the data interval was set at 1.0 nm. All samples were placed in a quartz UV-vis cuvette (pathlength of 1 cm).

Peptide samples were scanned from 500 - 200 nm with a baseline of urea (680 µL, 7 M) and water (20 µL). The baseline was removed from the sample absorption profile and the peptide concentrations were determined based on tryptophan absorbance at 280 nm (5690 M^{-1} cm^{-1}), and tyrosine absorbance at 274 nm (1405 M^{-1} cm^{-1}).[255] The concentration of the sample was calculated utilising the molar absorptivity of the chromophore present on the peptide, this in turn was used to calculate the original stock concentration.

6.12.2 - Circular Dichroism Spectroscopy:

The circular dichroism spectra were recorded using a JASCO J-715 Spectropolarimeter which required the optical chamber to be purged with nitrogen for ~20 minutes prior to use. The optics were kept under a nitrogen atmosphere throughout the experiment. For each sample measurement there were three scans recorded from 350-190 nm using a 100 nm min^{-1} scan rate, 1 nm bandwidth and 1 s response time. The sample chamber temperature was maintained at 20 °C throughout the experiment.

The samples consisted of the aqueous peptide (90 µM) and 2-[4-(2-hydroxyethyl)piperazin-1-yl]ethanesulfonic acid (HEPES) buffer (10 mM, pH 7.0) with the baseline sample being just the HEPES buffer (10 mM, pH 7.0). The 300 µL samples were placed in a 1 mm pathlength quartz cuvettes.

The observed ellipticity, θ_{obs} (mdeg) was converted into molar ellipticity, (θ), and is reported in units of deg $dmol^{-1}$ cm^2. The helical content was determined following the method reported by Y. Chen *et al.* and using the minimum molar ellipticity determined by J. Myers *et al.*[261, 281]The change in molar ellipticity was analysed as an isotherm.

6.12.3 - Native Mass Spectrometry:

Samples were prepared by A. Almeida and the experiment run by O. Daubney. Mass spectrometry of the trimer complexes was carried out on a Synapt G2S mass spectrometer fitted with a TirVersa NanoMate chip-based spray controller and Nanoflow+. Samples of peptide (9 µM) in ammonium acetate buffer (10 mM, pH 6.4) were added in 5 - 10 µL sprays, with a gas pressure of 0.15 psi and a voltage of 1.75

- 1.80 kV. It was essential to maintain the backing vacuum at 6.5 x 10^{-6} torr and the valve temperature at 100 °C. Detected ionisation parameters were carried out utilising a local method, file identity – OJD_2017. Stepwave Offsets were varied between 11 - 25 and the TrapCE and TransferCD were generally set to 20, though these were not always applied. Gas controls were particularly important for larger oligomeric states with trimers generally visible between 3.0 - 5.0 gas flow but tetramers requiring >5.0. The capture range was set to 2000 - 3000 m/z;

7.Appendix

7.1 - NMR spectra for derivative 134

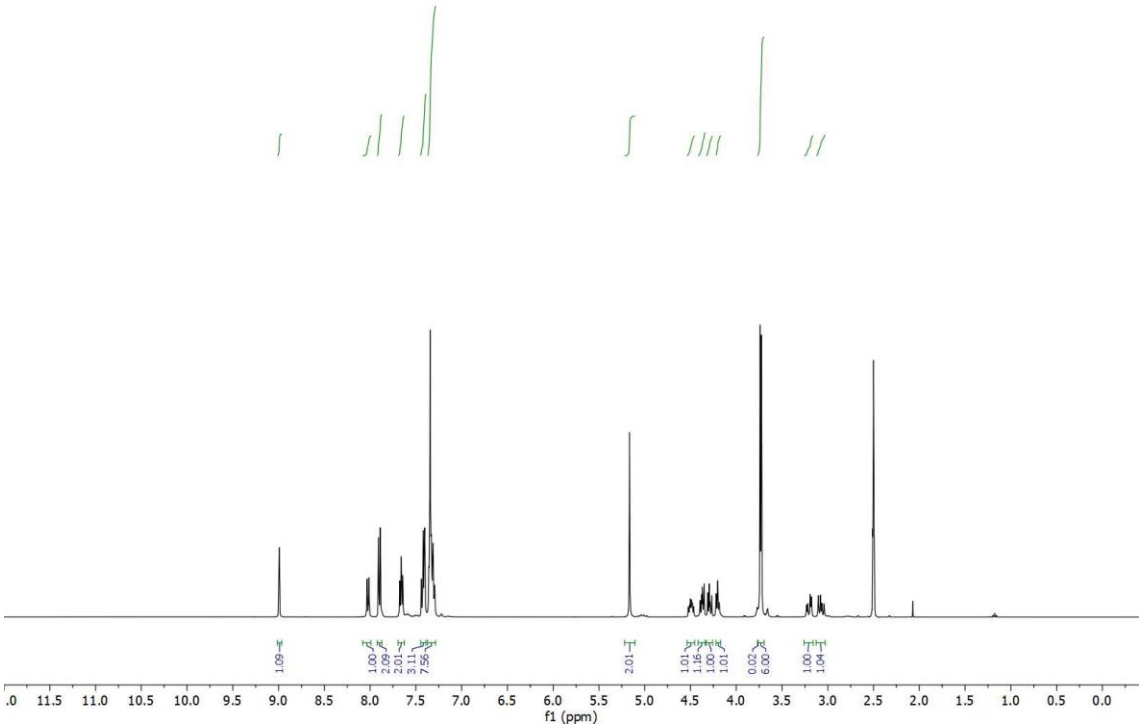

Figure 66: *^{1}H NMR spectrum of 134 at 400 MHz in DMSO-d_6*

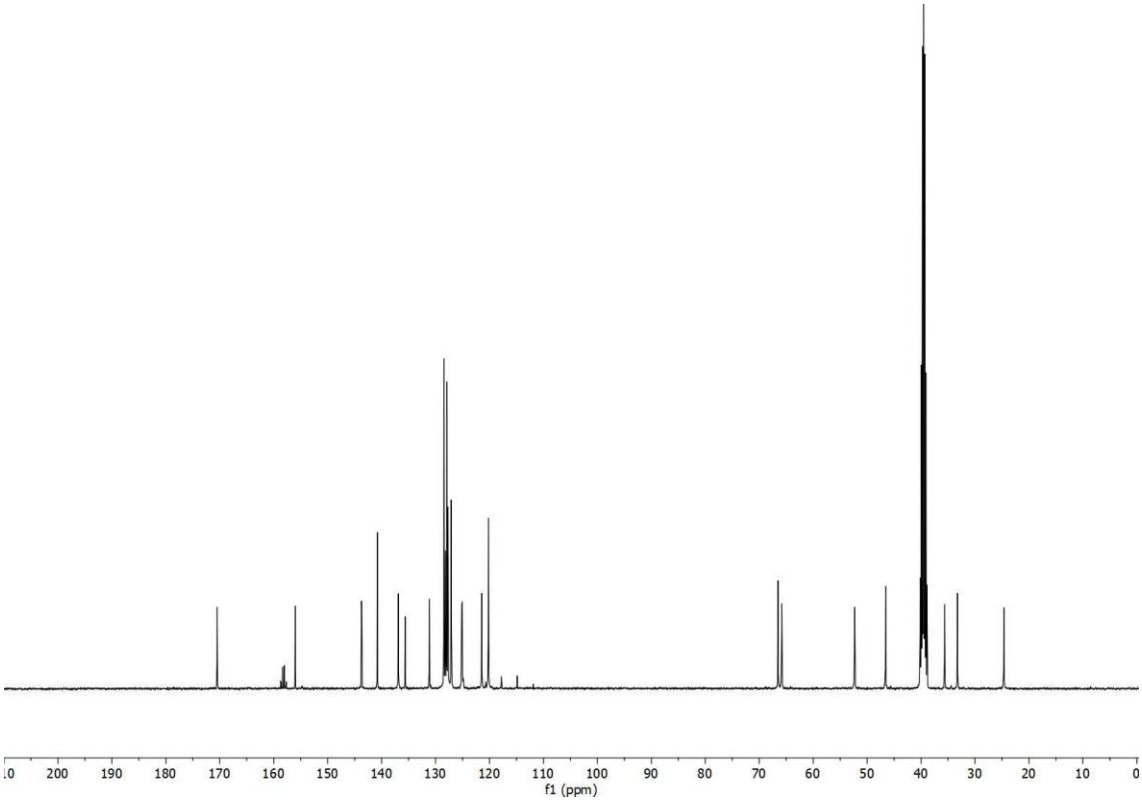

Figure 67: *^{13}C NMR spectrum of 134 at 400 MHz in DMSO-d_6.*

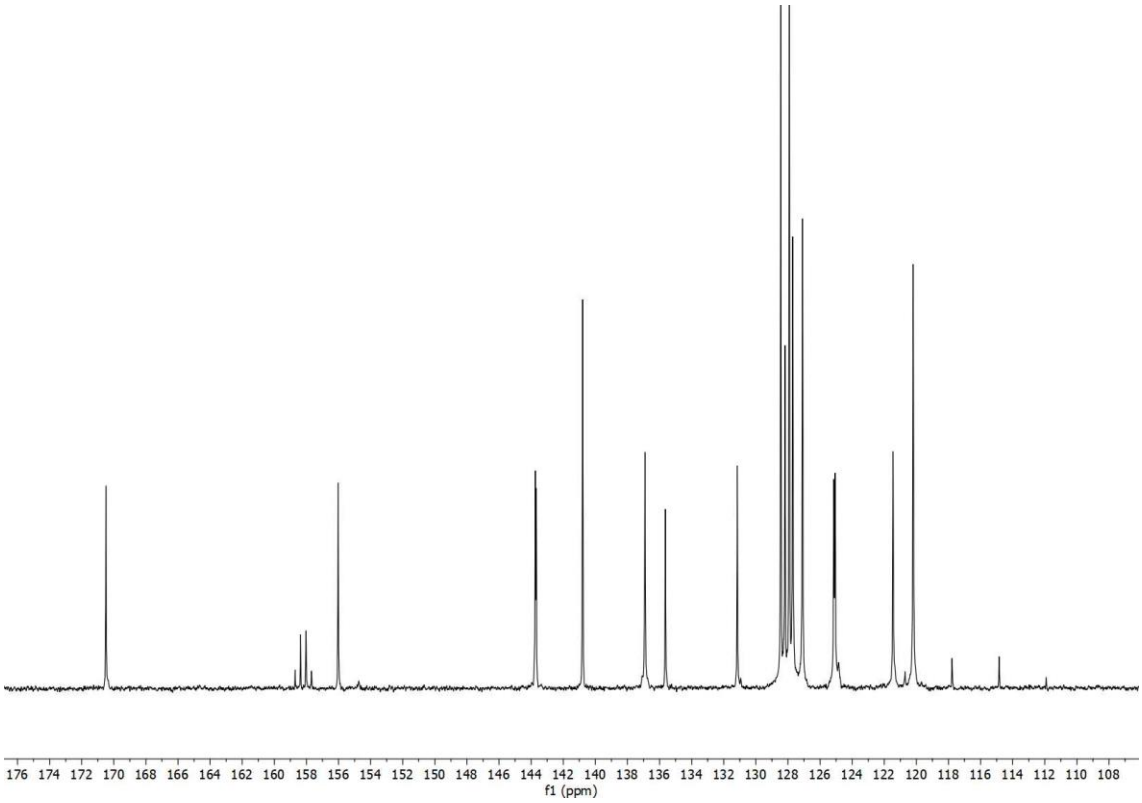

Figure 68: *Zoom of the^{13}C NMR spectrum of 134 at 400 MHz in DMSO-d_6.*

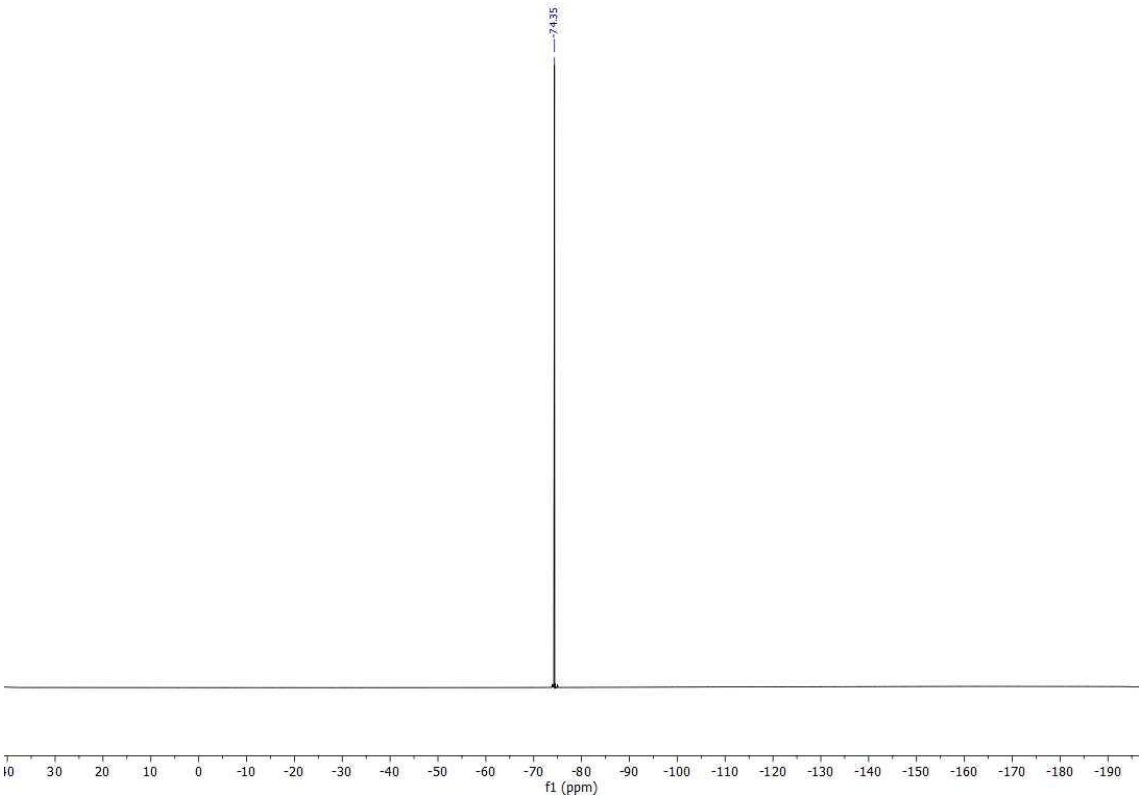

Figure 69: *^{19}F NMR spectrum of 134 at 300 MHz in DMSO-d_6.*

7.2 - Tolerance test of 180 to TFA:

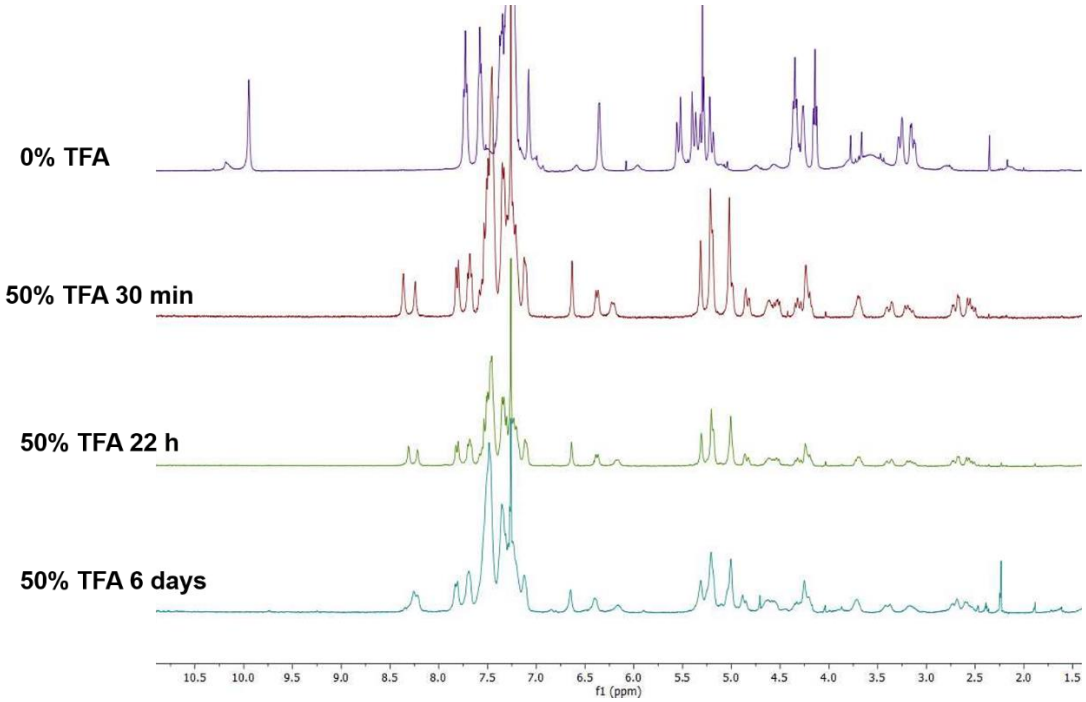

Figure 70: *^{1}H NMR (300 MHz) spectra of imidazolium salt **180** in $CDCl_3$, and in 50% TFA in $CDCl_3$ over 30 minutes, twenty two hours and six days.*

7.3 - Peptide Characterization:

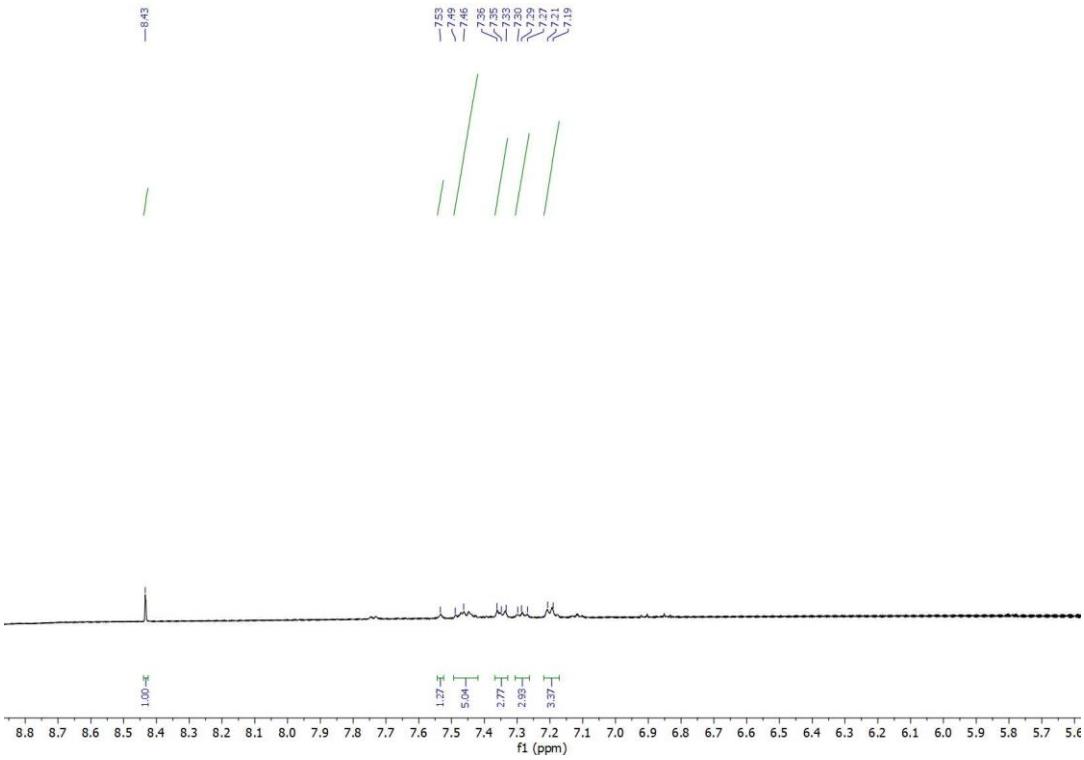

Figure 71: *Zoom of the aromatic region of the ^{1}H NMR (500 MHz) spectra of AA1-19(NHCBn$_2$) in D_2O referenced to dioxane.*

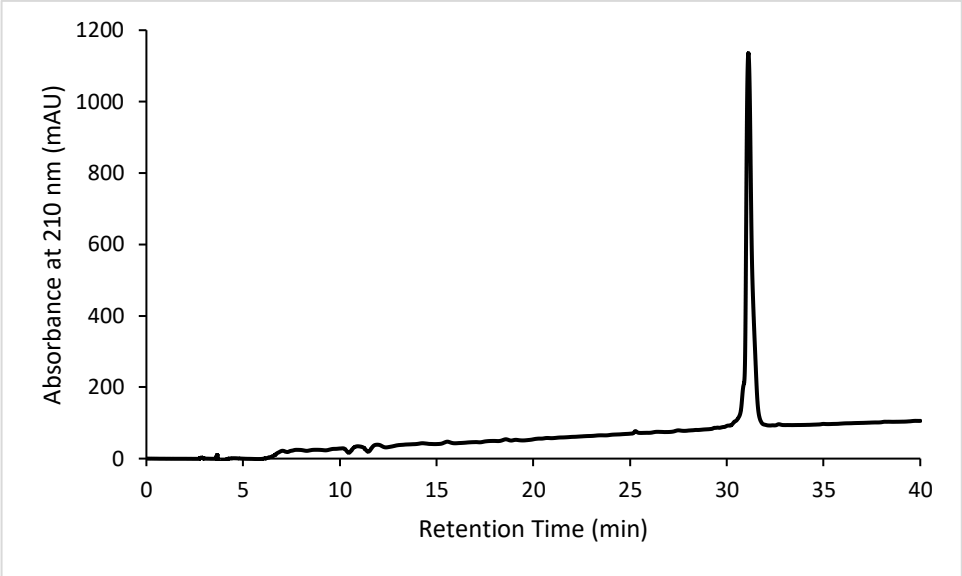

Figure 72: *The C_{18} reverse phase analytical HPLC chromatogram for pure AA1C. The absorbance was monitored at 210 nm and the solvent system went from 100% water with 0.05% TFA to 100% acetonitrile with 0.05% TFA over 40 minutes.*

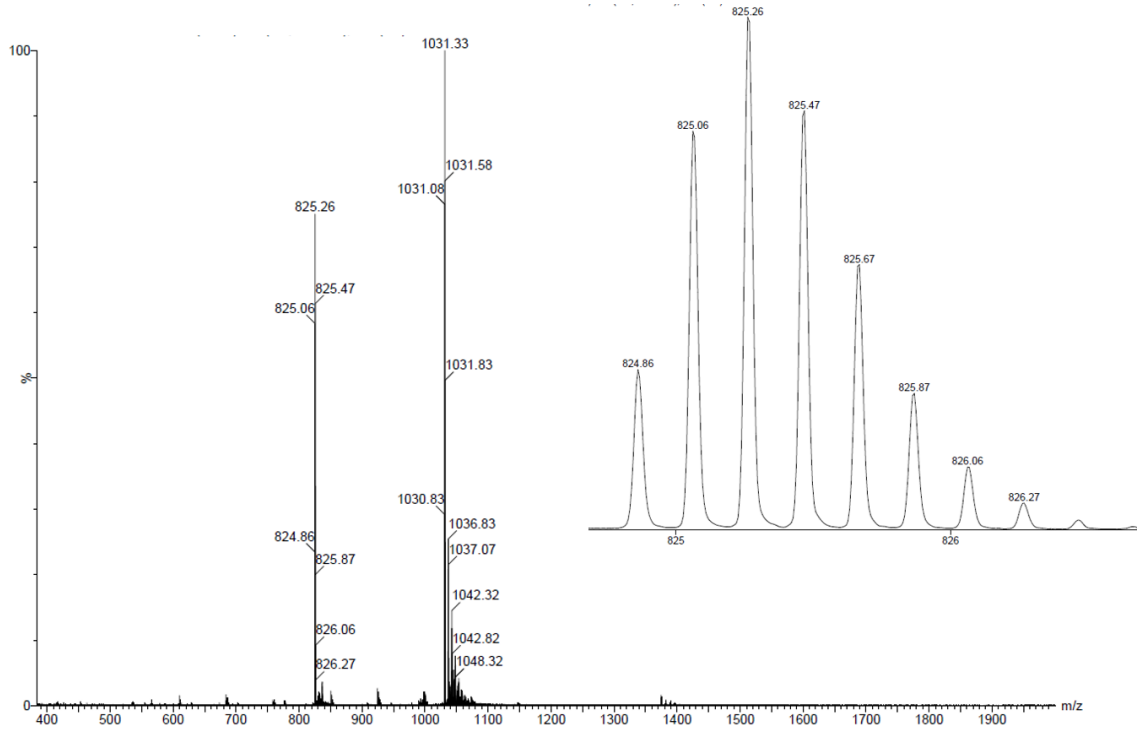

Figure 73: *The ESI spectrum for pure AA1C. The insert shows the isotope distribution of the M^{+4} peak.*

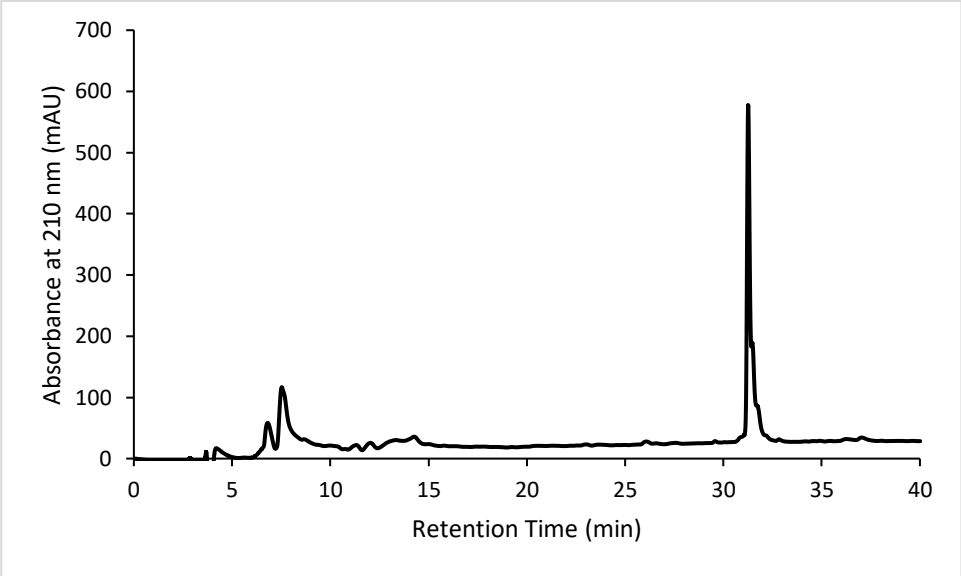

Figure 74: *The C_{18} reverse phase analytical HPLC chromatogram for pure AA1-1(NHCBn$_2$). The absorbance was monitored at 210 nm and the solvent system went from 100% water with 0.05% TFA to 100% acetonitrile with 0.05% TFA over 40 minutes. Peaks between 5 and 10 minutes were present in the blank.*

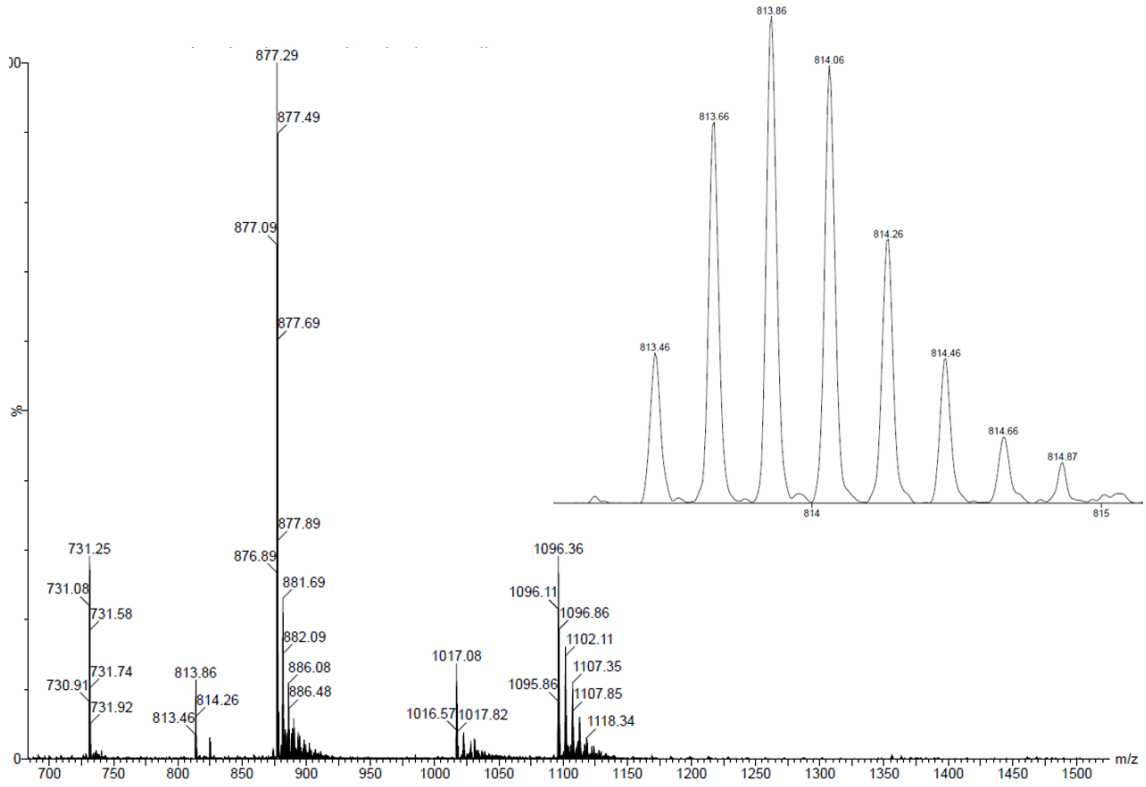

Figure 75: *The ESI spectrum for pure AA1-1(NHCBn$_2$). The insert shows the isotope distribution of the M^{+4} peak.*

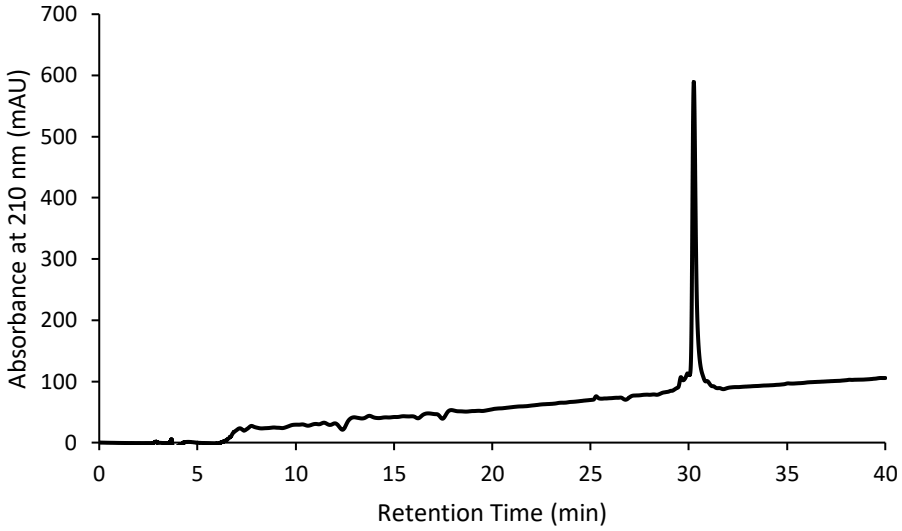

Figure 76: *The C_{18} reverse phase analytical HPLC chromatogram for pure AA1-1(NHCMe/pOMe). The absorbance was monitored at 210 nm and the solvent system went from 100% water with 0.05% TFA to 100% acetonitrile with 0.05% TFA over 40 minutes.*

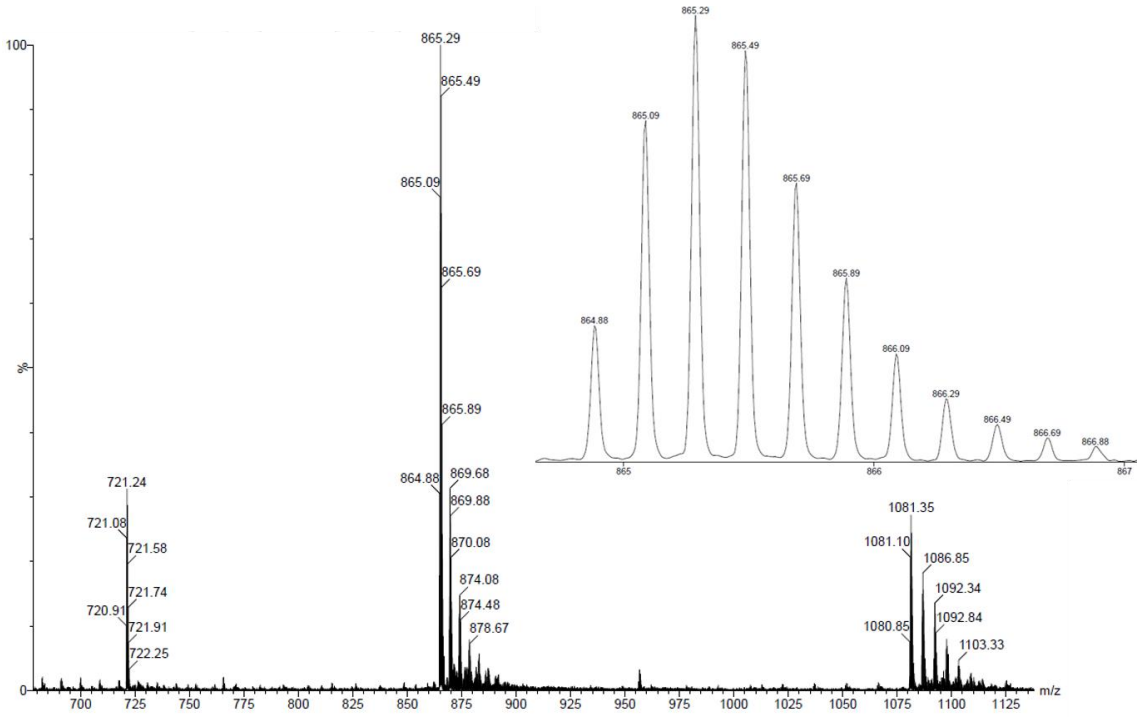

Figure 77: *The ESI spectrum for pure AA1-1(NHCMe/pOMe). The insert shows the isotope distribution of the M^{+4} peak.*

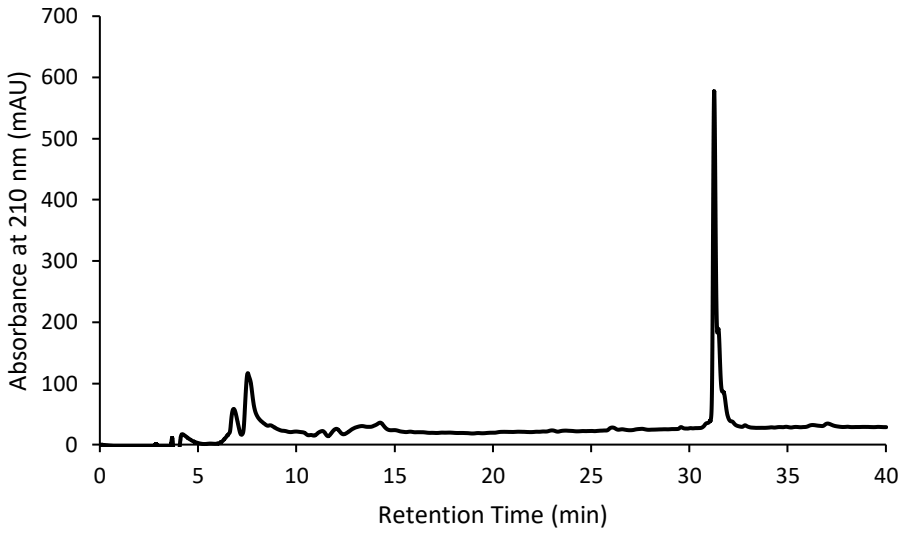

Figure 78: *The C_{18} reverse phase analytical HPLC chromatogram for pure AA1-19(NHCBn$_2$). The absorbance was monitored at 210 nm and the solvent system went from 100% water with 0.05% TFA to 100% acetonitrile with 0.05% TFA over 40 minutes. Peaks between 5 and 10 minutes were present in the blank.*

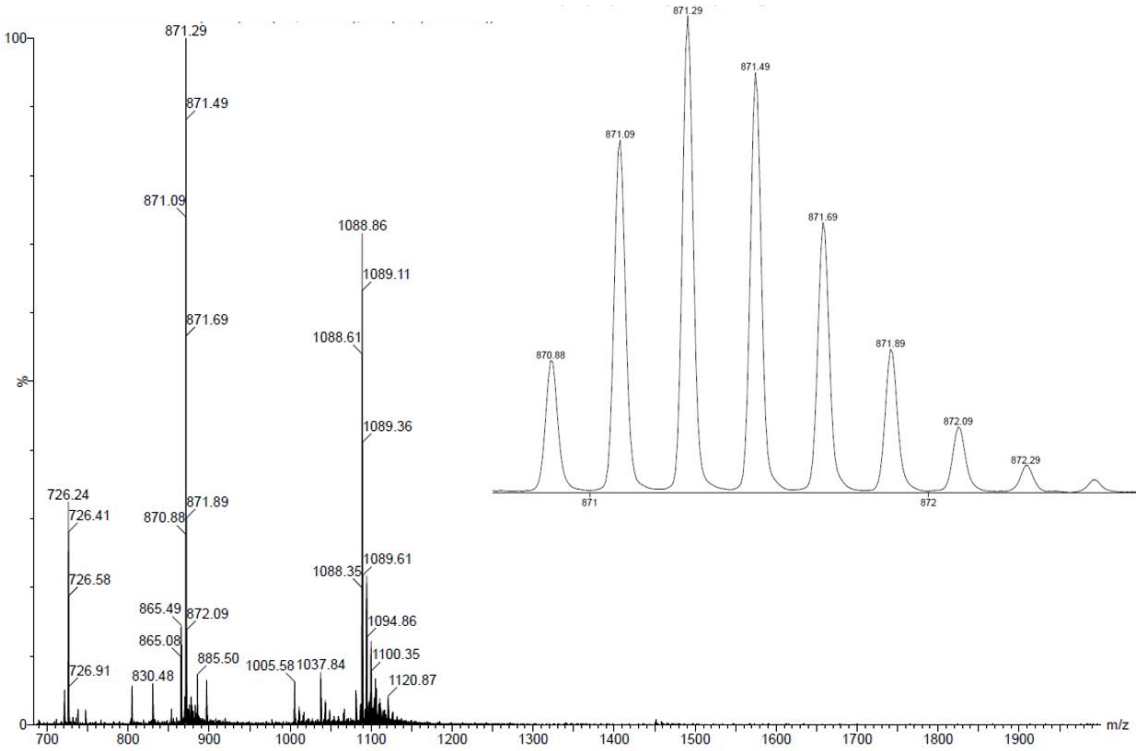

Figure 79: *The ESI spectrum for pure AA1-19(NHCBn$_2$). The insert shows the isotope distribution of the M^{+4} peak.*

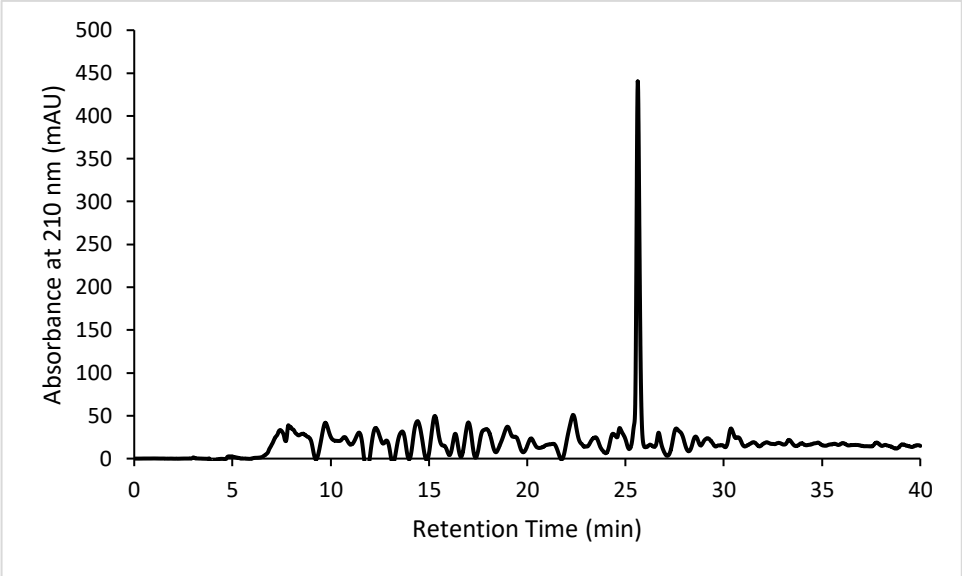

Figure 80: *The C_{18} reverse phase analytical HPLC chromatogram for pure AA2-2(NHCBn$_2$). The absorbance was monitored at 210 nm and the solvent system went from 100% water with 0.05% TFA to 100% acetonitrile with 0.05% TFA over 40 minutes.*

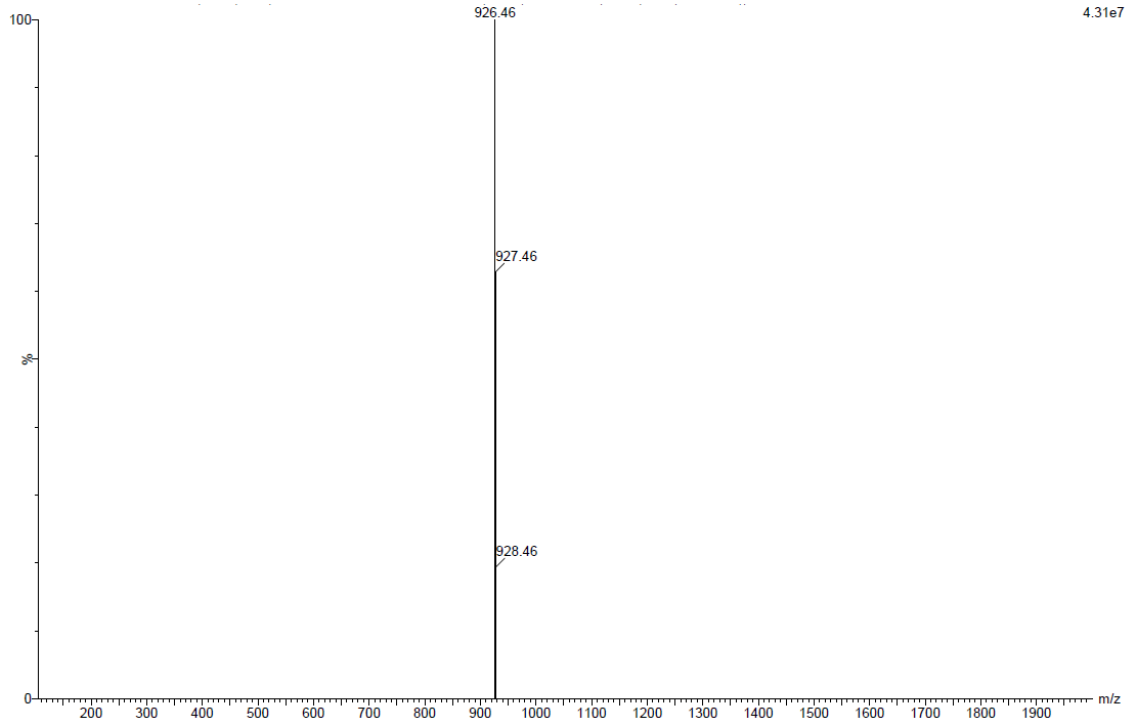

Figure 81: *The ESI spectrum for pure AA2-2(NHCBn$_2$).*

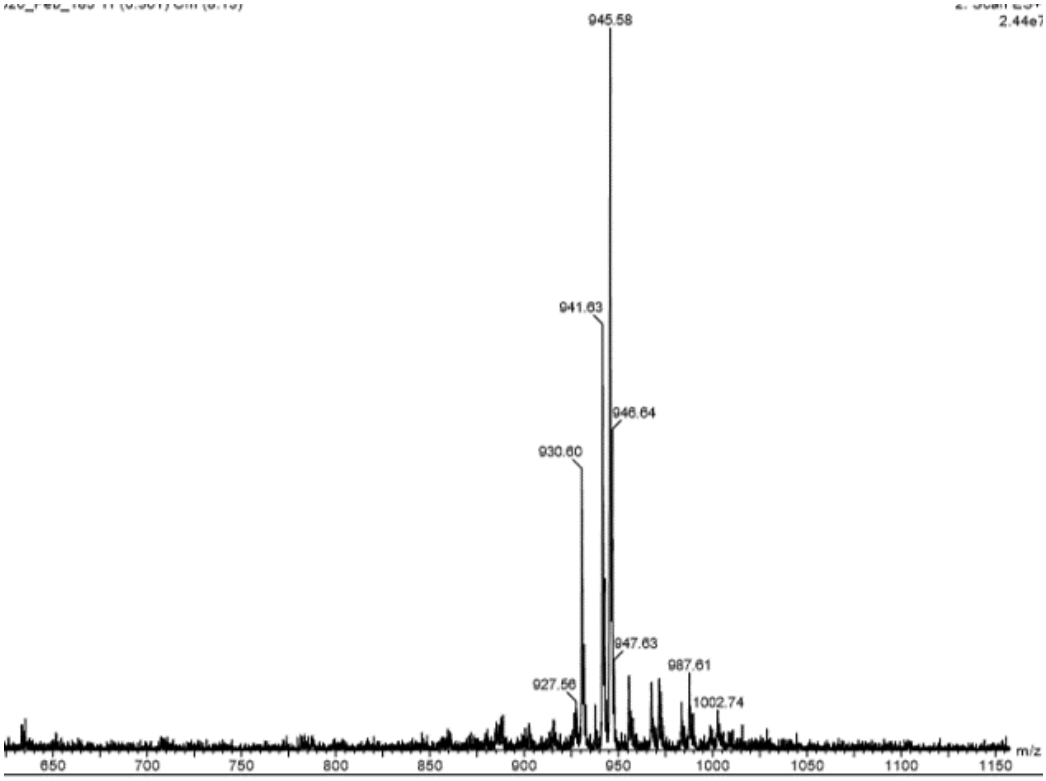

Figure 82: *Mass spectrum (ESI) of crude reaction mixture of compound* ***265****.*

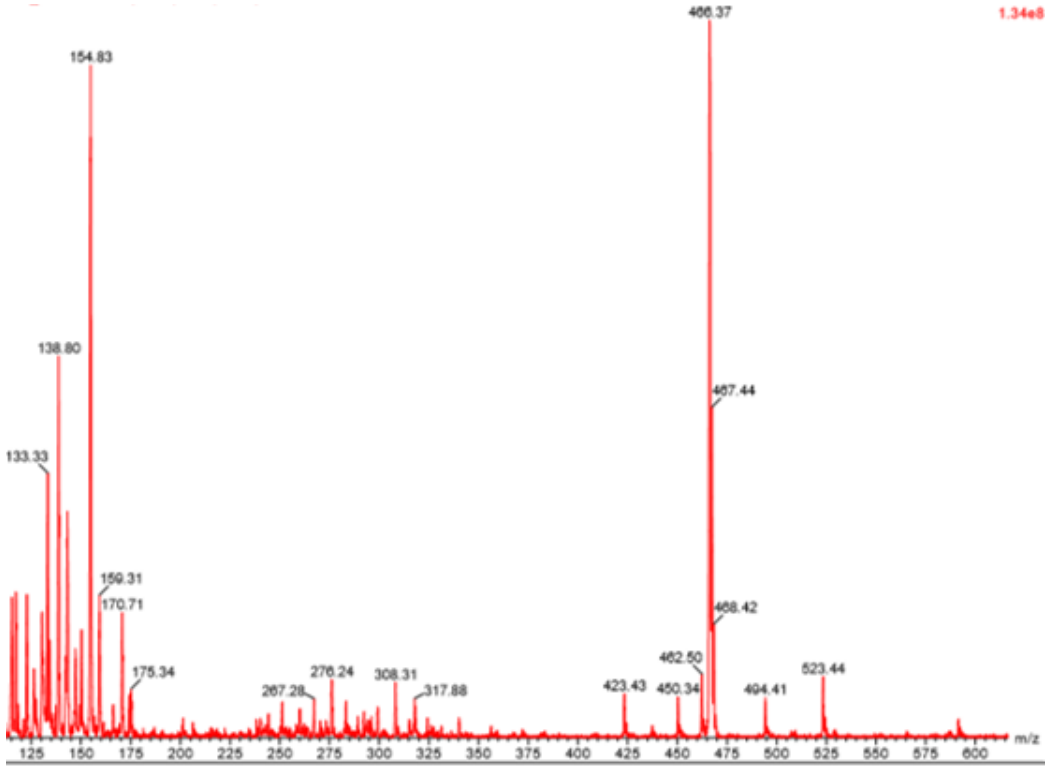

Figure 83: *Mass spectrum (ESI) for crude reaction mixture of compound* ***266****.*

7.4 - Crystal structure of imidazolium 134:

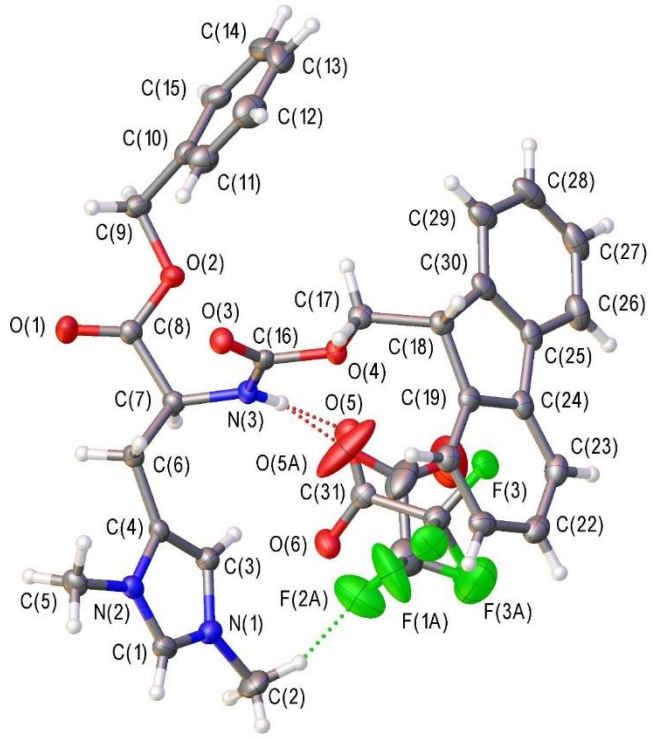

Table 1 Crystal data and structure refinement for 134.

Identification code	*AIA-111P*
Empirical formula	*$C_{32}H_{30}F_3N_3O_6$*
Formula weight	*609.59*
Temperature/K	*100.01(10)*
Crystal system	*orthorhombic*
Space group	*$P2_12_12_1$*
a/Å	*8.84920(10)*
b/Å	*14.81730(10)*
c/Å	*22.1637(2)*
α/°	*90*
1	*90*
γ/°	*90*
Volume/Å^3	*2906.13(5)*
Z	*4*

$\rho_{calc}g/cm^3$	1.393
μ/mm^{-1}	0.927
F(000)	1272.0
Crystal size/mm^3	0.224 × 0.126 × 0.062
Radiation	CuKα (λ = 1.54184)
2Θ range for data collection/°	7.176 to 147.886
Index ranges	-10 ≤ h ≤ 11, -18 ≤ k ≤ 18, -27 ≤ l ≤ 27
Reflections collected	55435
Independent reflections	5854 [R_{int} = 0.0402, R_{sigma} = 0.0161]
Data/restraints/parameters	5854/21/467
Goodness-of-fit on F^2	1.048
Final R indexes [I>=2σ (I)]	R_1 = 0.0279, wR_2 = 0.0723
Final R indexes [all data]	R_1 = 0.0291, wR_2 = 0.0736
Largest diff. peak/hole / e $Å^{-3}$	0.36/-0.18
Flack parameter	-0.04(3)

Table 2 Fractional Atomic Coordinates (×10⁴) and Equivalent Isotropic Displacement Parameters (Å²×10³) for 134. U_{eq} is defined as 1/3 of of the trace of the orthogonalised U_{IJ} tensor.

Atom	x	y	z	U(eq)
C1	-2731(2)	4464.7(13)	3007.4(8)	25.6(4)
C2	-1526(3)	3703.6(17)	3885.8(9)	39.3(5)
C3	-347(2)	4089.1(13)	2873.6(8)	25.2(4)
C4	-833(2)	4480.2(12)	2354.0(8)	20.7(3)
C5	-3366(2)	5075.8(13)	1995.4(9)	25.6(4)
C6	-72(2)	4672.6(12)	1768.6(8)	20.6(3)
C7	1611(2)	4436.1(12)	1782.9(8)	19.4(3)
C8	2205(2)	4366.9(12)	1134.1(8)	21.6(3)
C9	4399(2)	4444.5(13)	513.4(9)	27.3(4)
C10	5567(2)	5174.3(13)	478.4(8)	24.0(4)
C11	5121(3)	6075.2(14)	527.5(10)	32.7(4)

C12	6181(3)	6756.5(16)	514.7(11)	43.7(6)
C13	7698(3)	6552.6(18)	458.3(11)	45.4(6)
C14	8162(3)	5665.1(19)	405.9(10)	42.1(6)
C15	7087(2)	4970.8(15)	413.9(9)	30.8(4)
C16	2719(2)	5899.2(12)	2009.6(7)	18.5(3)
C17	4033(2)	7226.7(12)	2286.2(8)	23.5(4)
C18	4883(2)	7602.8(12)	2825.0(8)	22.3(4)
C19	4066(2)	7497.7(12)	3421.7(8)	22.0(4)
C20	2592(2)	7720.2(12)	3566.8(8)	24.3(4)
C21	2081(2)	7580.4(13)	4154.8(9)	28.1(4)
C22	3033(3)	7214.1(13)	4588.0(9)	30.4(4)
C23	4501(3)	6962.7(13)	4441.0(9)	29.4(4)
C24	5018(2)	7105.6(12)	3855.8(9)	24.4(4)
C25	6472(2)	6907.7(12)	3569.0(9)	27.2(4)
C26	7792(3)	6525.9(14)	3804.9(11)	34.8(5)
C27	9037(3)	6434.6(15)	3429.0(12)	39.6(5)
C28	8982(2)	6716.5(14)	2833.5(12)	38.3(5)
C29	7660(2)	7097.7(13)	2591.9(10)	31.3(4)
C30	6410(2)	7182.3(12)	2965.1(9)	25.6(4)
N1	-1545.9(19)	4089.2(12)	3272.4(7)	26.6(3)
N2	-2337.9(17)	4701.4(10)	2448.7(7)	21.8(3)
N3	2492.2(17)	5027.1(10)	2164.2(7)	19.0(3)
O1	1414.6(17)	4184.3(12)	711.9(6)	35.7(4)
O2	3695.1(15)	4488.0(9)	1109.4(5)	23.9(3)
O3	2162.7(15)	6281.7(9)	1579.9(6)	24.0(3)
O4	3677.3(14)	6293.6(8)	2409.5(5)	20.5(3)
C31	3182(3)	3924.5(15)	3606.3(12)	22.7(5)
C32	3485(3)	4524.7(16)	4159.1(10)	27.6(5)
F1	2500(2)	5217.7(11)	4160.7(8)	43.8(5)
F2	3317(4)	4096.8(17)	4687.6(11)	39.1(5)
F3	4898.5(17)	4877.6(10)	4162.4(7)	36.1(4)

O5	3898(3)	4132(2)	3141.7(11)	25.6(5)
O6	2193(2)	3350.1(11)	3683.6(8)	32.8(4)
C31A	3880(30)	4157(18)	3755(9)	62(6)
C32A	2560(20)	4246(13)	4189(9)	55(6)
F1A	1610(19)	4942(11)	4091(10)	84(6)
F2A	1652(17)	3539(10)	4155(9)	75(5)
F3A	3110(40)	4370(30)	4760(11)	109(14)
O5A	3550(50)	4180(30)	3216(11)	101(15)
O6A	5070(20)	3850(30)	4014(12)	158(19)

Table 3 Anisotropic Displacement Parameters ($Å^2×10^3$) for 134. The Anisotropic displacement factor exponent takes the form: $-2π^2[h^2a^{*2}U_{11}+2hka^*b^*U_{12}+…]$.

Atom	U_{11}	U_{22}	U_{33}	U_{23}	U_{13}	U_{12}
C1	23.6(9)	27.0(9)	26.1(9)	-7.1(7)	4.5(7)	-4.9(8)
C2	43.7(13)	52.9(13)	21.3(9)	5.2(9)	2.1(9)	-7.5(11)
C3	21.1(9)	31.5(9)	23.1(8)	-0.7(7)	-0.7(7)	-2.3(8)
C4	16.2(8)	23.7(8)	22.3(8)	-3.7(7)	-1.9(6)	-0.9(7)
C5	18.5(8)	27.5(9)	30.8(9)	-2.0(7)	-1.9(7)	2.9(7)
C6	16.0(8)	25.4(8)	20.4(8)	0.5(7)	-1.9(6)	0.2(7)
C7	17.2(8)	19.8(8)	21.2(8)	-0.6(6)	0.4(6)	0.3(7)
C8	21.3(8)	19.8(8)	23.7(8)	-3.2(7)	0.0(7)	0.4(7)
C9	27.7(10)	29.3(9)	24.7(9)	-4.1(7)	6.9(8)	-1.9(8)
C10	26.4(9)	27.1(9)	18.4(8)	-1.5(7)	1.2(7)	-1.1(7)
C11	37.3(11)	28.5(10)	32.4(10)	-2.9(8)	4.6(9)	0.7(9)
C12	58.0(16)	30.9(11)	42.2(12)	-5.4(9)	5.9(12)	-9.9(11)
C13	51.3(15)	49.0(13)	35.8(11)	-0.9(10)	-2.1(11)	-26.1(12)
C14	24.8(11)	73.9(17)	27.6(10)	6.2(11)	2.6(8)	-7.5(11)
C15	30.0(10)	39.1(10)	23.3(9)	4.3(8)	5.0(8)	3.9(9)
C16	15.5(8)	23.0(8)	17.0(7)	-3.0(6)	1.6(6)	2.3(7)
C17	27.4(9)	18.7(8)	24.3(9)	1.3(7)	0.2(7)	-2.0(7)

C18	23.4(9)	17.2(7)	26.2(8)	-1.0(7)	0.5(7)	-2.0(7)
C19	26.2(9)	16.3(7)	23.5(8)	-2.2(6)	-2.3(7)	-2.6(7)
C20	27.9(10)	18.7(8)	26.4(9)	-0.9(7)	-1.8(8)	-0.5(7)
C21	28.7(10)	23.5(9)	32.1(10)	-3.7(8)	4.7(8)	-4.3(8)
C22	41.8(12)	26.0(9)	23.5(9)	0.3(7)	1.1(8)	-8.4(8)
C23	37.9(11)	23.7(9)	26.5(9)	2.1(7)	-9.2(8)	-2.9(8)
C24	25.9(9)	17.8(8)	29.6(9)	-2.4(7)	-6.2(8)	-3.3(7)
C25	25.9(10)	21.7(9)	34.0(10)	-6.1(7)	-7.3(8)	-3.3(7)
C26	29.2(10)	30.5(10)	44.6(12)	-7.2(9)	-12.8(9)	1.7(9)
C27	24.9(11)	33.2(11)	60.8(14)	-12.6(11)	-12.4(10)	0.6(9)
C28	22.5(10)	28.8(10)	63.6(14)	-15.7(10)	5.1(10)	-4.4(8)
C29	26.3(10)	24.4(9)	43.2(11)	-9.0(8)	3.9(9)	-5.6(8)
C30	21.7(9)	18.6(8)	36.6(10)	-7.0(7)	-1.1(8)	-5.0(7)
N1	27.3(8)	31.8(8)	20.7(7)	-1.8(6)	1.1(6)	-5.3(7)
N2	17.6(7)	23.2(7)	24.7(7)	-5.0(6)	0.4(6)	-1.4(6)
N3	17.5(7)	21.5(7)	18.1(6)	1.0(6)	-3.1(6)	-0.1(5)
O1	25.9(7)	54.7(9)	26.6(7)	-14.9(6)	-0.2(6)	-5.1(7)
O2	19.0(6)	31.8(7)	21.1(6)	-1.5(5)	2.0(5)	-0.5(5)
O3	24.4(7)	24.8(6)	22.8(6)	2.4(5)	-3.6(5)	0.3(5)
O4	20.5(6)	18.4(5)	22.7(6)	-1.5(5)	-3.6(5)	-1.0(5)
C31	22.9(12)	21.0(10)	24.2(13)	2.8(9)	-2.4(9)	5.6(9)
C32	28.6(13)	27.5(12)	26.8(12)	-1.9(9)	3.0(9)	-0.5(10)
F1	44.4(11)	32.2(8)	54.7(9)	-10.8(7)	5.3(8)	11.9(8)
F2	53.1(14)	44.3(9)	19.7(8)	0.3(7)	2.5(8)	-10.0(9)
F3	34.2(8)	38.4(8)	35.7(8)	-7.6(6)	0.8(6)	-12.5(6)
O5	24.3(9)	32.0(11)	20.5(10)	1.8(9)	-0.9(7)	5.3(8)
O6	30.8(9)	36.7(9)	30.8(9)	4.6(7)	-6.0(7)	-9.2(8)
C31A	100(18)	58(15)	27(10)	8(10)	-6(10)	-26(15)
C32A	64(14)	45(12)	58(12)	-7(10)	3(11)	-14(12)
F1A	45(9)	61(9)	146(18)	-3(10)	-47(11)	-8(8)
F2A	49(8)	59(9)	116(15)	18(9)	2(9)	-4(7)

F3A	74(16)	190(40)	59(14)	-21(17)	-4(11)	10(20)
O5A	190(40)	90(20)	21(9)	8(11)	9(12)	80(20)
O6A	36(10)	340(60)	99(17)	-70(20)	-16(11)	-7(17)

Table 4 Bond Lengths for 134.

Atom	Atom	Length/Å	Atom	Atom	Length/Å
C1	N1	1.325(3)	C18	C30	1.521(3)
C1	N2	1.333(2)	C19	C20	1.383(3)
C2	N1	1.475(2)	C19	C24	1.405(3)
C3	C4	1.359(3)	C20	C21	1.395(3)
C3	N1	1.381(2)	C21	C22	1.388(3)
C4	C6	1.489(2)	C22	C23	1.390(3)
C4	N2	1.387(2)	C23	C24	1.391(3)
C5	N2	1.464(2)	C24	C25	1.465(3)
C6	C7	1.531(2)	C25	C26	1.399(3)
C7	C8	1.534(2)	C25	C30	1.400(3)
C7	N3	1.445(2)	C26	C27	1.388(3)
C8	O1	1.199(2)	C27	C28	1.385(4)
C8	O2	1.332(2)	C28	C29	1.405(3)
C9	C10	1.498(3)	C29	C30	1.387(3)
C9	O2	1.462(2)	C31	C32	1.537(3)
C10	C11	1.396(3)	C31	O5	1.248(3)
C10	C15	1.386(3)	C31	O6	1.233(3)
C11	C12	1.378(3)	C32	F1	1.347(3)
C12	C13	1.381(4)	C32	F2	1.340(3)
C13	C14	1.383(4)	C32	F3	1.356(3)
C14	C15	1.401(3)	C31A	C32A	1.52(2)
C16	N3	1.352(2)	C31A	O5A	1.23(2)
C16	O3	1.212(2)	C31A	O6A	1.28(2)
C16	O4	1.359(2)	C32A	F1A	1.35(2)

C17	C18	1.517(3)	C32A	F2A	1.32(2)
C17	O4	1.444(2)	C32A	F3A	1.37(2)
C18	C19	1.515(3)			

Table 5 Bond Angles for 134.

Atom	Atom	Atom	Angle/˚	Atom	Atom	Atom	Angle/˚
N1	C1	N2	108.41(17)	C26	C25	C24	130.7(2)
C4	C3	N1	107.42(17)	C26	C25	C30	120.5(2)
C3	C4	C6	132.59(17)	C30	C25	C24	108.79(17)
C3	C4	N2	106.03(16)	C27	C26	C25	118.5(2)
N2	C4	C6	121.37(16)	C28	C27	C26	121.0(2)
C4	C6	C7	112.23(15)	C27	C28	C29	120.9(2)
C6	C7	C8	109.23(14)	C30	C29	C28	118.2(2)
N3	C7	C6	113.47(14)	C25	C30	C18	110.43(17)
N3	C7	C8	113.81(14)	C29	C30	C18	128.64(19)
O1	C8	C7	123.11(17)	C29	C30	C25	120.8(2)
O1	C8	O2	125.17(17)	C1	N1	C2	125.53(18)
O2	C8	C7	111.63(15)	C1	N1	C3	108.93(15)
O2	C9	C10	108.00(15)	C3	N1	C2	125.50(18)
C11	C10	C9	119.44(19)	C1	N2	C4	109.20(16)
C15	C10	C9	121.19(18)	C1	N2	C5	125.09(16)
C15	C10	C11	119.35(19)	C4	N2	C5	125.58(15)
C12	C11	C10	120.4(2)	C16	N3	C7	120.72(15)
C11	C12	C13	120.2(2)	C8	O2	C9	116.94(14)
C12	C13	C14	120.3(2)	C16	O4	C17	115.12(13)
C13	C14	C15	119.7(2)	O5	C31	C32	115.2(2)
C10	C15	C14	120.0(2)	O6	C31	C32	114.4(2)
N3	C16	O4	109.76(14)	O6	C31	O5	130.2(3)
O3	C16	N3	125.86(17)	F1	C32	C31	109.28(19)
O3	C16	O4	124.37(16)	F1	C32	F3	107.6(2)

O4	C17	C18	108.11(14)	F2	C32	C31	113.8(2)
C17	C18	C30	116.78(15)	F2	C32	F1	106.7(2)
C19	C18	C17	114.39(15)	F2	C32	F3	106.3(2)
C19	C18	C30	101.77(15)	F3	C32	C31	112.86(19)
C20	C19	C18	128.93(17)	O5A	C31A	C32A	116(3)
C20	C19	C24	120.32(17)	O5A	C31A	O6A	130(3)
C24	C19	C18	110.75(17)	O6A	C31A	C32A	112.3(18)
C19	C20	C21	119.18(18)	F1A	C32A	C31A	116.2(19)
C22	C21	C20	120.5(2)	F1A	C32A	F3A	105(2)
C21	C22	C23	120.67(19)	F2A	C32A	C31A	111.1(18)
C22	C23	C24	118.98(19)	F2A	C32A	F1A	102.7(17)
C19	C24	C25	108.21(17)	F2A	C32A	F3A	112(2)
C23	C24	C19	120.30(19)	F3A	C32A	C31A	109(2)
C23	C24	C25	131.48(19)				

Table 6 Hydrogen Bonds for AIA-134.

D	H	A	d(D-H)/Å	d(H-A)/Å	d(D-A)/Å	D-H-A/°
N3	H3A	O5	0.83(3)	2.00(3)	2.828(3)	170(2)
N3	H3A	O5A	0.83(3)	1.99(4)	2.81(3)	167(3)

Table 7 Torsion Angles for AIA-134.

A	B	C	D	Angle/˚	A	B	C	D	Angle/˚
C3	C4	C6	C7	-4.9(3)	C24	C19	C20	C21	2.3(3)
C3	C4	N2	C1	0.9(2)	C24	C25	C26	C27	-178.43(19)
C3	C4	N2	C5	-175.04(17)	C24	C25	C30	C18	1.2(2)
C4	C3	N1	C1	0.2(2)	C24	C25	C30	C29	178.03(16)
C4	C3	N1	C2	178.12(19)	C25	C26	C27	C28	0.2(3)
C4	C6	C7	C8	162.56(15)	C26	C25	C30	C18	-178.05(17)
C4	C6	C7	N3	-69.29(19)	C26	C25	C30	C29	-1.2(3)

C6	C4	N2	C1	-179.53(16)	C26	C27	C28	C29	-0.4(3)
C6	C4	N2	C5	4.5(3)	C27	C28	C29	C30	-0.1(3)
C6	C7	C8	O1	-25.8(2)	C28	C29	C30	C18	177.16(17)
C6	C7	C8	O2	157.42(15)	C28	C29	C30	C25	1.0(3)
C6	C7	N3	C16	-68.9(2)	C30	C18	C19	C20	-176.80(17)
C7	C8	O2	C9	-179.57(14)	C30	C18	C19	C24	2.33(18)
C8	C7	N3	C16	56.8(2)	C30	C25	C26	C27	0.6(3)
C9	C10	C11	C12	178.1(2)	N1	C1	N2	C4	-0.9(2)
C9	C10	C15	C14	-177.51(18)	N1	C1	N2	C5	175.16(16)
C10	C9	O2	C8	139.27(17)	N1	C3	C4	C6	179.88(18)
C10	C11	C12	C13	-0.6(4)	N1	C3	C4	N2	-0.7(2)
C11	C10	C15	C14	0.8(3)	N2	C1	N1	C2	-177.52(18)
C11	C12	C13	C14	0.9(4)	N2	C1	N1	C3	0.4(2)
C12	C13	C14	C15	-0.4(3)	N2	C4	C6	C7	175.74(15)
C13	C14	C15	C10	-0.5(3)	N3	C7	C8	O1	-153.72(18)
C15	C10	C11	C12	-0.3(3)	N3	C7	C8	O2	29.5(2)
C17	C18	C19	C20	-49.9(2)	N3	C16	O4	C17	178.88(14)
C17	C18	C19	C24	129.18(16)	O1	C8	O2	C9	3.7(3)
C17	C18	C30	C25	-127.38(17)	O2	C9	C10	C11	-62.3(2)
C17	C18	C30	C29	56.1(3)	O2	C9	C10	C15	115.98(19)
C18	C17	O4	C16	170.46(14)	O3	C16	N3	C7	4.9(3)
C18	C19	C20	C21	-178.66(17)	O3	C16	O4	C17	-0.9(2)
C18	C19	C24	C23	178.82(16)	O4	C16	N3	C7	-174.96(14)
C18	C19	C24	C25	-1.8(2)	O4	C17	C18	C19	-55.0(2)
C19	C18	C30	C25	-2.10(18)	O4	C17	C18	C30	63.6(2)
C19	C18	C30	C29	-178.62(18)	O5	C31	C32	F1	90.1(3)
C19	C20	C21	C22	-0.6(3)	O5	C31	C32	F2	-150.8(3)
C19	C24	C25	C26	179.48(19)	O5	C31	C32	F3	-29.6(3)
C19	C24	C25	C30	0.3(2)	O6	C31	C32	F1	-85.4(2)
C20	C19	C24	C23	-2.0(3)	O6	C31	C32	F2	33.7(3)
C20	C19	C24	C25	177.46(16)	O6	C31	C32	F3	154.9(2)

C20	C21	C22	C23	-1.4(3)	
C21	C22	C23	C24	1.7(3)	
C22	C23	C24	C19	0.0(3)	
C22	C23	C24	C25	-179.31(19)	
C23	C24	C25	C26	-1.2(3)	
C23	C24	C25	C30	179.68(19)	
O5A	C31A	C32A	F1A	-50(4)	
O5A	C31A	C32A	F2A	67(4)	
O5A	C31A	C32A	F3A	-169(3)	
O6A	C31A	C32A	F1A	146(3)	
O6A	C31A	C32A	F2A	-97(3)	
O6A	C31A	C32A	F3A	27(4)	

Table 8 Hydrogen Atom Coordinates (Å×10⁴) and Isotropic Displacement Parameters (Å²×10³) for AIA-134.

Atom	x	y	z	U(eq)
H1	-3676.81	4548.87	3181.46	31
H2A	-1711.22	3066.02	3864.21	59
H2B	-2296.82	3984.9	4125.47	59
H2C	-556.18	3808.75	4066.86	59
H3	615.77	3863.04	2947.11	30
H5A	-2878.61	5566.5	1790.09	38
H5B	-4265.59	5291.15	2189.77	38
H5C	-3626.59	4615.08	1709.23	38
H6A	-186.84	5307.88	1673.36	25
H6B	-561.03	4327.83	1451.86	25
H7	1688.54	3830.5	1957.85	23
H9A	3643.11	4530.79	201.81	33
H9B	4867.37	3859.28	454.23	33
H11	4102.43	6216.47	569.13	39
H12	5873.91	7355.16	544.05	52
H13	8409.4	7014.35	455.64	54
H14	9182.82	5529.52	365.59	51
H15	7393.62	4373.22	375.85	37
H17A	3112.01	7567.45	2220.55	28
H17B	4652.06	7270.81	1926.14	28

H18	5040.44	8249.15	2755.41	27
H20	1949.8	7960.03	3275.91	29
H21	1094.72	7733.74	4257.31	34
H22	2685.94	7136.1	4980.51	37
H23	5128.59	6702.96	4729.39	35
H26	7834.13	6337.39	4204.77	42
H27	9921.48	6180.33	3579.21	48
H28	9832.18	6652.66	2590.29	46
H29	7624.53	7288.21	2192.36	38
H3A	2930(30)	4824(17)	2466(12)	34(6)

Table 9 Atomic Occupancy for 134.

Atom	Occupancy	Atom	Occupancy	Atom	Occupancy
C31	0.878(3)	C32	0.878(3)	F1	0.878(3)
F2	0.878(3)	F3	0.878(3)	O5	0.878(3)
O6	0.878(3)	C31A	0.122(3)	C32A	0.122(3)
F1A	0.122(3)	F2A	0.122(3)	F3A	0.122(3)
O5A	0.122(3)	O6A	0.122(3)		

Crystal structure determination of 134

Crystal Data for $C_{32}H_{30}F_3N_3O_6$ (M =609.59 g/mol): orthorhombic, space group $P2_12_12_1$ (no. 19), a = 8.84920(10) Å, b = 14.81730(10) Å, c = 22.1637(2) Å, V = 2906.13(5) $Å^3$, Z = 4, T = 100.01(10) K, μ(CuKα) = 0.927 mm^{-1}, Dcalc = 1.393 g/cm^3, 55435 reflections measured (7.176° ≤ 2Θ ≤ 147.886°), 5854 unique (R_{int} = 0.0402, R_{sigma} = 0.0161) which were used in all calculations. The final R_1 was 0.0279 ($I > 2\sigma(I)$) and wR_2 was 0.0736 (all data).

Refinement model description

Number of restraints - 21, number of constraints - unknown.

Details:

1. Fixed Uiso At 1.2 times of: All C(H) groups, All C(H,H) groups At 1.5 times of: *All C(H,H,H) groups. 2. Restrained distances C31-C32 ≈ C31A-C32A with sigma of 0.02 C31-O5 ≈ C31A-O5A with sigma of 0.02 C31-O6 ≈ C31A-O6A with sigma of 0.02 C32-F1 ≈ C32A-F1A with sigma of 0.02 C32-F2 ≈ C32A-F2A with sigma of 0.02 C32-F3 ≈ C32A-F3A with sigma of 0.02 C31-F1 ≈ C31A-F1A with sigma of 0.04 C31-F2 ≈ C31A-F2A with sigma of 0.04 C31-F3 ≈ C31A-F3A with sigma of 0.04 C32-O5 ≈ C32A-O5A with sigma of 0.04 C32-O6 ≈ C32A-O6A with sigma of 0.04 F1-F2 ≈ F1A-F2A with sigma of 0.04 F1-F3 ≈ F1A-F3A with sigma of 0.04 F2-F3 ≈ F2A-F3A with sigma of 0.04 O5-O6 ≈ O5A-O6A with sigma of 0.04. 3. Rigid bond restraints C31A, C32A, O5A, O6A with sigma for 1-2 distances of 0.01 and sigma for 1-3 distances of 0.01. 4. Others*

Sof(C31A)=Sof(C32A)=Sof(F1A)=Sof(F2A)=Sof(F3A)=Sof(O5A)=Sof(O6A)=1-FVAR(1)Sof(C31)=Sof(C32)=Sof(F1)=Sof(F2)=Sof(F3)=Sof(O5)=Sof(O6)=FVAR(1)5. a Ternary CH refined with riding coordinates: C7(H7),C18(H18). 5.b Secondary CH2 refined with riding coordinates: C6(H6A,H6B), C9(H9A,H9B), C17(H17A,H17B). 5.c Aromatic/amide H refined with riding coordinates: C1(H1), C3(H3), C11(H11), C12(H12), C13(H13), C14(H14), C15(H15), C20(H20), C21(H21), C22(H22), C23(H23), C26(H26), C27(H27), C28(H28), C29(H29). 5.d Idealised Me refined as rotating group: C2(H2A,H2B,H2C), C5(H5A,H5B,H5C)

7.5 - Crystal structure of 146:

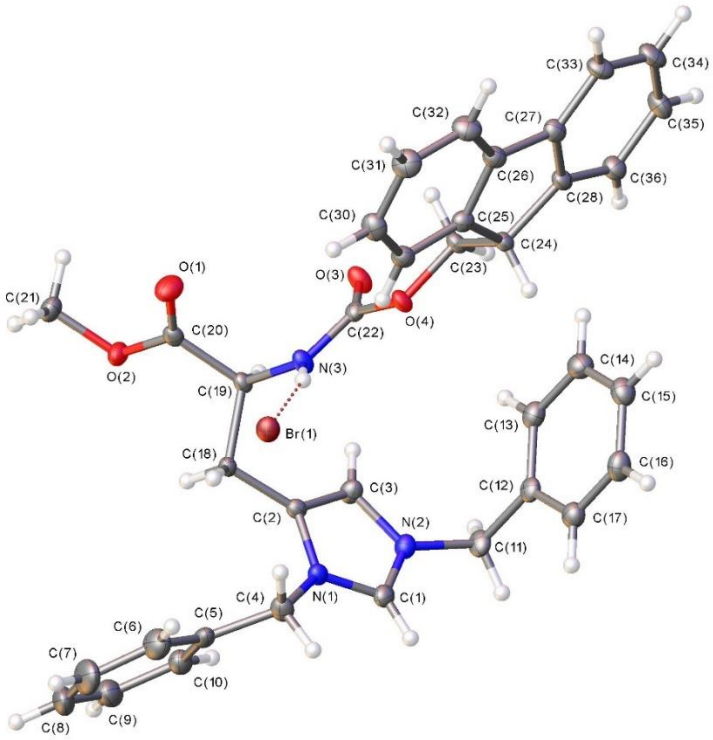

Table 1 Crystal data and structure refinement for 146

Identification code	*AIA-224C*
Empirical formula	$C_{36}H_{34}BrN_3O_4$
Formula weight	*652.57*
Temperature/K	*100.01(10)*
Crystal system	*monoclinic*
Space group	$P2_1$
a/Å	*8.46590(10)*
b/Å	*13.59270(10)*
c/Å	*13.96530(10)*
α/°	*90*
β/°	*97.2940(10)*
γ/°	*90*
Volume/Å³	*1594.04(3)*

Z	*2*
ρ_{calc}g/cm^3	*1.360*
μ/mm^{-1}	*2.107*
F(000)	*676.0*
Crystal size/mm^3	*0.206 × 0.16 × 0.062*
Radiation	*CuKα (λ = 1.54184)*
2Θ range for data collection/°	*9.116 to 149.164*
Index ranges	*-10 ≤ h ≤ 10, -16 ≤ k ≤ 16, -17 ≤ l ≤ 17*
Reflections collected	*30515*
Independent reflections	*6444 [R_{int} = 0.0284, R_{sigma} = 0.0190]*
Data/restraints/parameters	*6444/1/402*
Goodness-of-fit on F^2	*1.059*
Final R indexes [I>=2σ (I)]	*R_1 = 0.0197, wR_2 = 0.0507*
Final R indexes [all data]	*R_1 = 0.0199, wR_2 = 0.0510*
Largest diff. peak/hole / e Å^{-3}	*0.20/-0.33*
Flack parameter	*-0.038(4)*

Table 2 Fractional Atomic Coordinates (×10^4) and Equivalent Isotropic Displacement Parameters (Å^2×10^3) for 146. U_{eq} is defined as 1/3 of of the trace of the orthogonalised U_{IJ} tensor.

Atom	x	y	z	U(eq)
Br1	*2370.1(2)*	*4814.2(2)*	*4995.5(2)*	*19.67(6)*
C1	*7209(3)*	*2484.4(16)*	*4179.7(15)*	*18.0(4)*
C2	*6902(3)*	*4087.6(15)*	*3926.7(15)*	*14.8(4)*
C3	*8344(3)*	*3932.8(16)*	*4443.7(16)*	*19.0(4)*
C4	*4555(3)*	*2969.3(17)*	*3365.0(16)*	*21.1(4)*
C5	*4137(3)*	*3266.0(16)*	*2319.8(16)*	*21.4(5)*
C6	*2545(3)*	*3459(2)*	*1997(2)*	*34.9(6)*
C7	*2076(4)*	*3641(2)*	*1021(2)*	*46.7(8)*
C8	*3187(4)*	*3665(2)*	*379(2)*	*43.2(8)*
C9	*4763(4)*	*3490(2)*	*699.7(18)*	*35.6(6)*

C10	5248(3)	3284.0(17)	1667.7(17)	25.6(5)
C11	9794(3)	2457.5(17)	5249.4(16)	21.4(5)
C12	9527(3)	2593.8(16)	6294.1(16)	18.7(4)
C13	10168(3)	3400.7(17)	6819.3(16)	21.7(5)
C14	9917(3)	3522.2(19)	7778.9(17)	25.4(5)
C15	9012(3)	2838.2(19)	8213.3(17)	25.1(5)
C16	8365(3)	2037.0(18)	7688.5(17)	24.8(5)
C17	8623(3)	1908.5(18)	6735.4(16)	22.1(4)
C18	6079(2)	5024.7(13)	3617.5(14)	15.0(4)
C19	6580(3)	5826.8(15)	4373.0(14)	14.2(4)
C20	5852(3)	6825.3(16)	4075.4(15)	16.2(4)
C21	5702(3)	8086.1(16)	2916.9(17)	23.2(5)
C22	7072(2)	5705.9(15)	6123.9(14)	14.1(4)
C23	7110(2)	5611.5(16)	7818.6(14)	15.0(4)
C24	6117(2)	5162.5(16)	8538.9(14)	15.9(4)
C25	4449(3)	5587.6(16)	8514.0(15)	17.0(4)
C26	4253(3)	5995.1(16)	9415.1(15)	18.5(4)
C27	5750(3)	5897.2(16)	10057.6(15)	18.5(4)
C28	6858(3)	5403.1(16)	9562.9(14)	17.1(4)
C29	3209(3)	5604.5(16)	7760.2(15)	18.8(4)
C30	1765(3)	6040.9(18)	7911.5(17)	23.0(5)
C31	1571(3)	6433.8(19)	8815.2(18)	25.9(5)
C32	2806(3)	6410.6(19)	9571.3(17)	24.8(5)
C33	6190(3)	6222.1(17)	10998.9(15)	21.9(5)
C34	7734(3)	6047.5(19)	11430.0(16)	24.9(5)
C35	8822(3)	5550.7(19)	10940.5(16)	24.5(5)
C36	8379(3)	5219.1(17)	9996.6(16)	20.7(4)
N1	6212(2)	3169.2(13)	3766.4(13)	16.1(4)
N2	8512(2)	2930.6(14)	4593.9(13)	17.8(4)
N3	6143(2)	5527.2(14)	5291.8(12)	16.5(3)
O1	5031(2)	7299.4(12)	4539.7(12)	26.9(4)

O2	6275(2)	7116.1(11)	3230.7(11)	20.5(3)
O3	8366.3(18)	6100.1(13)	6218.0(10)	20.5(3)
O4	6326.9(18)	5379.5(11)	6870.4(10)	16.2(3)

Table 3 Anisotropic Displacement Parameters ($Å^2×10^3$) for 146. The Anisotropic displacement factor exponent takes the form: $-2π^2[h^2a^{*2}U_{11}+2hka^*b^*U_{12}+…]$.

Atom	U_{11}	U_{22}	U_{33}	U_{23}	U_{13}	U_{12}
Br1	15.36(10)	21.62(10)	21.72(10)	1.88(9)	1.13(7)	-2.87(10)
C1	22.1(11)	17.3(10)	15.2(10)	1.7(8)	4.3(8)	0.5(8)
C2	16.3(10)	15.0(10)	13.2(9)	0.0(7)	2.3(8)	-2.7(8)
C3	16.0(10)	17.4(10)	23.1(11)	1.8(8)	0.3(8)	-2.2(8)
C4	18.7(11)	21.7(11)	21.6(10)	1.9(9)	-2.7(9)	-6.3(9)
C5	27.5(12)	13.1(10)	21.4(11)	-0.1(8)	-5.4(9)	-2.0(8)
C6	32.4(15)	32.2(14)	37.3(14)	1.1(11)	-5.9(11)	6.8(11)
C7	47.6(19)	40.6(17)	44.5(17)	4.6(14)	-22.3(14)	10.8(14)
C8	70(2)	29.1(14)	24.9(13)	3.8(11)	-15.4(14)	5.6(14)
C9	56.4(19)	27.7(13)	21.4(12)	1.8(10)	-0.3(12)	-2.9(12)
C10	32.3(14)	21.4(12)	21.9(11)	1.6(9)	-1.7(10)	-2.1(9)
C11	18.1(11)	23.7(12)	22.3(11)	2.2(9)	2.4(9)	8.5(9)
C12	15.0(10)	19.5(11)	21.0(11)	2.8(8)	0.2(8)	6.1(8)
C13	19.7(11)	20.9(11)	24.6(11)	4.4(9)	2.8(9)	2.5(9)
C14	26.9(13)	23.3(11)	25.7(11)	-1.3(9)	2.2(9)	2.3(9)
C15	24.6(12)	30.1(13)	20.9(11)	2.1(9)	4.2(9)	4.1(10)
C16	21.5(12)	27.3(12)	25.7(11)	7.9(9)	2.9(9)	-0.7(9)
C17	20.2(11)	22.2(11)	23.1(11)	1.7(9)	-0.5(8)	1.3(9)
C18	18.2(10)	13.8(11)	12.3(8)	0.8(7)	-1.0(7)	-0.8(7)
C19	15.2(10)	16.5(10)	10.8(9)	0.8(7)	1.5(7)	-2.7(8)
C20	15.7(10)	17.5(10)	14.5(9)	-0.1(8)	-1.2(8)	-5.4(8)
C21	28.4(13)	16.5(11)	24.0(11)	4.1(9)	0.0(9)	0.7(9)
C22	15.0(10)	13.3(10)	14.1(9)	0.4(7)	2.6(7)	3.0(7)

C23	14.4(10)	19.5(10)	10.6(8)	-1.3(8)	-0.4(7)	-1.5(8)
C24	19.8(11)	16.6(9)	11.1(9)	-0.4(7)	0.6(8)	-0.5(7)
C25	17.9(11)	16.0(10)	17.5(9)	0.2(8)	4.0(8)	-2.1(8)
C26	19.6(11)	19.7(11)	16.6(10)	-0.9(8)	3.8(8)	-2.6(8)
C27	19.8(11)	20.1(10)	16.0(10)	1.3(8)	4.4(8)	-2.3(8)
C28	21.8(11)	17.3(10)	12.4(9)	-0.1(8)	2.5(8)	-1.8(8)
C29	19.8(11)	18.6(10)	17.9(9)	-1.2(8)	2.3(8)	-2.5(8)
C30	16.6(11)	28.5(12)	23.3(11)	1.4(9)	0.1(9)	-3.7(9)
C31	16.6(11)	30.3(13)	31.6(12)	-1.0(10)	6.0(9)	0.0(9)
C32	23.4(12)	28.7(12)	23.5(11)	-4.7(9)	8.5(9)	-0.3(9)
C33	25.2(12)	25.9(12)	15.5(10)	-4.9(9)	6.0(9)	-2.4(9)
C34	29.9(13)	31.5(13)	13.3(10)	-4.3(9)	3.3(9)	-5.2(10)
C35	22.3(12)	33.0(13)	17.0(10)	0.0(9)	-2.5(8)	-0.8(10)
C36	21.7(12)	23.5(11)	17.1(10)	-0.6(8)	2.8(8)	-0.1(9)
N1	17.6(9)	15.5(9)	14.8(8)	1.4(7)	1.1(7)	-2.6(7)
N2	16.3(9)	19.0(9)	18.3(8)	2.6(7)	3.6(7)	2.4(7)
N3	14.2(9)	22.2(9)	13.2(8)	2.0(7)	1.6(7)	-5.1(7)
O1	33.7(10)	22.5(9)	27.0(8)	-0.1(7)	13.1(7)	4.4(7)
O2	29.2(9)	16.5(8)	16.4(7)	3.5(6)	5.5(6)	2.7(6)
O3	15.5(8)	30.9(9)	14.9(7)	0.4(6)	0.8(6)	-4.9(6)
O4	17.4(7)	21.4(8)	9.9(6)	0.0(6)	1.5(5)	-3.0(6)

Table 4 Bond Lengths for 146

Atom	Atom	Length/Å	Atom	Atom	Length/Å
C1	N1	1.337(3)	C19	N3	1.439(3)
C1	N2	1.325(3)	C20	O1	1.197(3)
C2	C3	1.354(3)	C20	O2	1.335(3)
C2	C18	1.489(3)	C21	O2	1.453(3)
C2	N1	1.384(3)	C22	N3	1.340(3)
C3	N2	1.383(3)	C22	O3	1.212(3)

C4	C5	1.512(3)	C22	O4	1.360(2)
C4	N1	1.469(3)	C23	C24	1.518(3)
C5	C6	1.390(4)	C23	O4	1.439(2)
C5	C10	1.390(4)	C24	C25	1.522(3)
C6	C7	1.393(4)	C24	C28	1.522(3)
C7	C8	1.380(5)	C25	C26	1.404(3)
C8	C9	1.374(5)	C25	C29	1.389(3)
C9	C10	1.390(3)	C26	C27	1.463(3)
C11	C12	1.516(3)	C26	C32	1.391(3)
C11	N2	1.476(3)	C27	C28	1.405(3)
C12	C13	1.391(3)	C27	C33	1.392(3)
C12	C17	1.398(3)	C28	C36	1.375(3)
C13	C14	1.393(3)	C29	C30	1.398(3)
C14	C15	1.392(4)	C30	C31	1.399(3)
C15	C16	1.386(4)	C31	C32	1.389(3)
C16	C17	1.387(3)	C33	C34	1.388(3)
C18	C19	1.539(3)	C34	C35	1.390(3)
C19	C20	1.526(3)	C35	C36	1.399(3)

Table 5 Bond Angles for 146.

Atom	Atom	Atom	Angle/˚	Atom	Atom	Atom	Angle/˚
N2	C1	N1	108.32(19)	O4	C23	C24	106.99(16)
C3	C2	C18	130.13(19)	C23	C24	C25	114.99(17)
C3	C2	N1	106.24(19)	C23	C24	C28	109.83(17)
N1	C2	C18	123.52(18)	C25	C24	C28	102.13(16)
C2	C3	N2	107.58(19)	C26	C25	C24	110.15(18)
N1	C4	C5	114.45(19)	C29	C25	C24	129.28(19)
C6	C5	C4	117.4(2)	C29	C25	C26	120.6(2)
C10	C5	C4	122.8(2)	C25	C26	C27	108.78(19)
C10	C5	C6	119.5(2)	C32	C26	C25	120.5(2)

C5	C6	C7	119.6(3)	C32	C26	C27	130.7(2)
C8	C7	C6	120.5(3)	C28	C27	C26	108.82(19)
C9	C8	C7	119.8(3)	C33	C27	C26	131.1(2)
C8	C9	C10	120.5(3)	C33	C27	C28	120.0(2)
C5	C10	C9	120.0(2)	C27	C28	C24	110.09(19)
N2	C11	C12	110.85(17)	C36	C28	C24	128.74(19)
C13	C12	C11	120.5(2)	C36	C28	C27	121.14(19)
C13	C12	C17	119.5(2)	C25	C29	C30	118.9(2)
C17	C12	C11	120.0(2)	C29	C30	C31	120.2(2)
C12	C13	C14	120.2(2)	C32	C31	C30	120.9(2)
C15	C14	C13	120.0(2)	C31	C32	C26	118.9(2)
C16	C15	C14	119.8(2)	C34	C33	C27	118.7(2)
C15	C16	C17	120.4(2)	C33	C34	C35	121.1(2)
C16	C17	C12	120.1(2)	C34	C35	C36	120.3(2)
C2	C18	C19	109.22(16)	C28	C36	C35	118.7(2)
C20	C19	C18	112.13(16)	C1	N1	C2	109.12(18)
N3	C19	C18	109.35(17)	C1	N1	C4	123.78(19)
N3	C19	C20	110.72(17)	C2	N1	C4	126.27(19)
O1	C20	C19	124.99(19)	C1	N2	C3	108.74(18)
O1	C20	O2	123.9(2)	C1	N2	C11	125.24(19)
O2	C20	C19	111.06(18)	C3	N2	C11	125.20(19)
N3	C22	O4	109.12(18)	C22	N3	C19	122.21(18)
O3	C22	N3	126.68(19)	C20	O2	C21	114.72(17)
O3	C22	O4	124.21(18)	C22	O4	C23	115.45(16)

Table 6 Hydrogen Bonds for 146

D	H	A	d(D-H)/Å	d(H-A)/Å	d(D-A)/Å	D-H-A/°
N3	H3A	Br1	0.82(3)	2.51(3)	3.3132(19)	165(2)

Table 7 Torsion Angles for 146

A	B	C	D	Angle/˚	A	B	C	D	Angle/˚
C2	C3	N2	C1	0.1(2)	C25	C24	C28	C36	-178.1(2)
C2	C3	N2	C11	-170.01(19)	C25	C26	C27	C28	-1.7(2)
C2	C18	C19	C20	176.84(16)	C25	C26	C27	C33	176.5(2)
C2	C18	C19	N3	-60.0(2)	C25	C26	C32	C31	-1.3(4)
C3	C2	C18	C19	-31.0(3)	C25	C29	C30	C31	-1.3(3)
C3	C2	N1	C1	0.3(2)	C26	C25	C29	C30	0.5(3)
C3	C2	N1	C4	170.16(19)	C26	C27	C28	C24	0.8(2)
C4	C5	C6	C7	-173.8(3)	C26	C27	C28	C36	179.4(2)
C4	C5	C10	C9	175.0(2)	C26	C27	C33	C34	-178.1(2)
C5	C4	N1	C1	-124.6(2)	C27	C26	C32	C31	178.0(2)
C5	C4	N1	C2	67.0(3)	C27	C28	C36	C35	-1.2(3)
C5	C6	C7	C8	-2.3(5)	C27	C33	C34	C35	-0.6(4)
C6	C5	C10	C9	-0.3(4)	C28	C24	C25	C26	-1.3(2)
C6	C7	C8	C9	1.3(5)	C28	C24	C25	C29	179.2(2)
C7	C8	C9	C10	0.2(4)	C28	C27	C33	C34	0.0(3)
C8	C9	C10	C5	-0.7(4)	C29	C25	C26	C27	-178.6(2)
C10	C5	C6	C7	1.8(4)	C29	C25	C26	C32	0.9(3)
C11	C12	C13	C14	179.9(2)	C29	C30	C31	C32	0.9(4)
C11	C12	C17	C16	-179.4(2)	C30	C31	C32	C26	0.5(4)
C12	C11	N2	C1	-94.0(3)	C32	C26	C27	C28	178.9(2)
C12	C11	N2	C3	74.5(3)	C32	C26	C27	C33	-2.8(4)
C12	C13	C14	C15	-0.5(4)	C33	C27	C28	C24	-177.63(19)
C13	C12	C17	C16	0.2(3)	C33	C27	C28	C36	0.9(3)
C13	C14	C15	C16	0.1(4)	C33	C34	C35	C36	0.3(4)
C14	C15	C16	C17	0.5(4)	C34	C35	C36	C28	0.7(4)
C15	C16	C17	C12	-0.6(4)	N1	C1	N2	C3	0.1(2)
C17	C12	C13	C14	0.3(3)	N1	C1	N2	C11	170.19(18)
C18	C2	C3	N2	175.9(2)	N1	C2	C3	N2	-0.2(2)
C18	C2	N1	C1	-176.17(18)	N1	C2	C18	C19	144.62(19)

C18	C2	N1	C4	-6.3(3)	N1	C4	C5	C6	-155.9(2)
C18	C19	C20	O1	122.6(2)	N1	C4	C5	C10	28.7(3)
C18	C19	C20	O2	-58.7(2)	N2	C1	N1	C2	-0.3(2)
C18	C19	N3	C22	141.7(2)	N2	C1	N1	C4	-170.43(19)
C19	C20	O2	C21	-176.88(17)	N2	C11	C12	C13	-90.7(3)
C20	C19	N3	C22	-94.3(2)	N2	C11	C12	C17	88.9(2)
C23	C24	C25	C26	-120.2(2)	N3	C19	C20	O1	0.1(3)
C23	C24	C25	C29	60.3(3)	N3	C19	C20	O2	178.93(17)
C23	C24	C28	C27	122.73(19)	N3	C22	O4	C23	-173.91(17)
C23	C24	C28	C36	-55.7(3)	O1	C20	O2	C21	1.9(3)
C24	C23	O4	C22	-178.55(17)	O3	C22	N3	C19	-2.1(3)
C24	C25	C26	C27	1.9(2)	O3	C22	O4	C23	5.6(3)
C24	C25	C26	C32	-178.7(2)	O4	C22	N3	C19	177.38(18)
C24	C25	C29	C30	179.9(2)	O4	C23	C24	C25	-64.1(2)
C24	C28	C36	C35	177.0(2)	O4	C23	C24	C28	-178.56(16)
C25	C24	C28	C27	0.3(2)					

Table 8 Hydrogen Atom Coordinates (Å×10⁴) and Isotropic Displacement Parameters (Å²×10³) for 146

Atom	x	y	z	U(eq)
H1	7020.82	1810.26	4177	22
H3	9087.99	4413.22	4658.82	23
H4A	3855.33	3315.92	3749.09	25
H4B	4352.03	2270.81	3423.27	25
H6	1797.89	3465.95	2431.28	42
H7	1006.4	3746.27	801.02	56
H8	2868.68	3800.32	-270.06	52
H9	5511.23	3508.67	266.6	43
H10	6315.19	3158.41	1878.77	31
H11A	10810.86	2742.06	5149.39	26

H11B	9826.26	1760.63	5103.46	26
H13	10767.01	3860.84	6528.78	26
H14	10354.24	4060.12	8129.13	30
H15	8842.66	2918.56	8853.61	30
H16	7753.3	1582.73	7977.43	30
H17	8193.24	1365.78	6389.61	27
H18A	4934.89	4931.51	3555.16	18
H18B	6362.19	5224.02	2994.42	18
H19	7741.87	5890.86	4437.49	17
H21A	6100.2	8252.44	2323.91	35
H21B	6067.59	8562.38	3402.48	35
H21C	4558.73	8084.18	2816.97	35
H23A	7183.53	6318.79	7905.68	18
H23B	8178.02	5339.31	7907.48	18
H24	6056.58	4447.68	8450.64	19
H29	3336.71	5330.08	7164.83	23
H30	931.86	6070.05	7409.79	28
H31	601.55	6714.49	8910.85	31
H32	2667.59	6668.4	10171.91	30
H33	5464.64	6549.64	11332.3	26
H34	8045.17	6266.38	12056.55	30
H35	9850.26	5438.32	11242.18	29
H36	9100.07	4880.53	9668.51	25
H3A	5270(40)	5270(20)	5296(19)	18(7)

Crystal structure determination of 146

Crystal Data *for* $C_{36}H_{34}BrN_3O_4$ *(*M =652.57 *g/mol): monoclinic, space group* $P2_1$ *(no. 4),* a = *8.46590(10) Å,* b = *13.59270(10) Å,* c = *13.96530(10) Å,* β = *97.2940(10)°,* V = *1594.04(3) Å*^{3}*,* Z = *2,* T = *100.01(10) K, μ(CuKα) = 2.107 mm*$^{-1}$, Dcalc = *1.360 g/cm*^{3}*, 30515 reflections measured (9.116° ≤ 2Θ ≤ 149.164°), 6444*

unique (R_{int} *= 0.0284,* R_{sigma} *= 0.0190) which were used in all calculations. The final* R_1 *was 0.0197 (I > 2σ(I)) and* wR_2 *was 0.0510 (all data).*

Refinement model description

Number of restraints - 1, number of constraints - unknown.

Details:

1. Fixed Uiso At 1.2 times of: All C(H) groups, All C(H,H) groups At 1.5 times of: All C(H,H,H) groups. 2.a Ternary CH refined with riding coordinates: C19(H19), C24(H24). 2.b Secondary CH2 refined with riding coordinates: C4(H4A,H4B), C11(H11A,H11B), C18(H18A,H18B), C23(H23A,H23B). 2.c Aromatic/amide H refined with riding coordinates: C1(H1), C3(H3), C6(H6), C7(H7), C8(H8), C9(H9), C10(H10), C13(H13), C14(H14), C15(H15), C16(H16), C17(H17), C29(H29), C30(H30), C31(H31), C32(H32), C33(H33), C34(H34), C35(H35), C36(H36). 2.d Idealised Me refined as rotating group: C21(H21A,H21B,H21C)

7.6 - Crystal structure of 201:

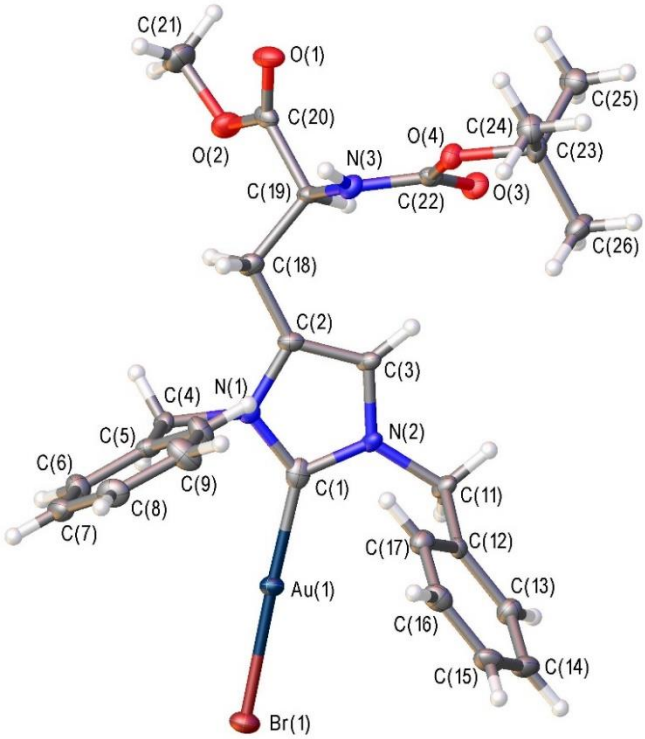

Table 1 Crystal data and structure refinement for 201.

Identification code	*AIA-215-01*
Empirical formula	*$C_{26}H_{31}AuBrN_3O_4$*
Formula weight	*726.41*
Temperature/K	*100.01(10)*
Crystal system	*monoclinic*
Space group	*$P2_1$*
a/Å	*11.1514(3)*
b/Å	*9.7618(2)*
c/Å	*13.0862(3)*
α/°	*90*
β/°	*112.000(3)*
γ/°	*90*
Volume/$Å^3$	*1320.80(6)*
Z	*2*
$\rho_{calc}g/cm^3$	*1.827*

μ/mm^{-1}	*12.537*
F(000)	*708.0*
Crystal size/mm^3	*0.152 × 0.045 × 0.036*
Radiation	*CuKα (λ = 1.54184)*
2Θ range for data collection/°	*7.286 to 136.476*
Index ranges	*-13 ≤ h ≤ 13, -11 ≤ k ≤ 11, -15 ≤ l ≤ 14*
Reflections collected	*23339*
Independent reflections	*4685 [R_{int} = 0.0507, R_{sigma} = 0.0332]*
Data/restraints/parameters	*4685/2/323*
Goodness-of-fit on F^2	*1.066*
Final R indexes [I>=2σ (I)]	*R_1 = 0.0258, wR_2 = 0.0621*
Final R indexes [all data]	*R_1 = 0.0267, wR_2 = 0.0628*
Largest diff. peak/hole / e Å^{-3}	*1.39/-1.01*
Flack parameter	*-0.050(8)*

Table 2 Fractional Atomic Coordinates (×10^4) and Equivalent Isotropic Displacement Parameters (Å^2×10^3) for 201. U_{eq} is defined as 1/3 of of the trace of the orthogonalised U_{IJ} tensor.

Atom	x	y	z	U(eq)
C1	4525(8)	4589(9)	7943(6)	20.0(16)
C2	2600(7)	5723(9)	7281(6)	16.6(16)
C3	2576(7)	4729(8)	6552(6)	15.7(15)
C4	4356(7)	6622(8)	9022(6)	16.4(15)
C5	5074(7)	7763(9)	8712(6)	17.5(16)
C6	6016(8)	8492(9)	9539(7)	21.9(19)
C7	6672(8)	9558(9)	9295(7)	24.0(18)
C8	6403(8)	9924(10)	8209(7)	25.2(18)
C9	5473(8)	9182(13)	7371(7)	30(2)
C10	4807(8)	8121(10)	7626(7)	24.0(18)
C11	4132(7)	2930(9)	6418(7)	19.2(16)
C12	5237(7)	3328(11)	6055(7)	15.8(18)

C13	5980(8)	2315(10)	5836(7)	21.8(17)
C14	6961(8)	2647(11)	5474(7)	25(2)
C15	7238(6)	4002(16)	5348(6)	25.3(15)
C16	6509(8)	5021(11)	5567(7)	24(2)
C17	5519(8)	4689(12)	5926(7)	21.2(19)
C18	1597(7)	6686(9)	7332(7)	18.8(17)
C19	282(7)	6458(10)	6402(6)	15.3(17)
C20	-820(7)	7010(9)	6701(6)	17.8(16)
C21	-1700(8)	6933(11)	8096(8)	32(2)
C22	-216(8)	6347(10)	4411(7)	17.3(19)
C23	-751(8)	6711(9)	2423(6)	20.8(17)
C24	-755(8)	8026(10)	1799(7)	24.6(18)
C25	-2081(8)	6083(10)	2040(8)	26.5(19)
C26	271(8)	5733(10)	2344(7)	25.5(19)
Au1	6297.8(2)	3979.8(4)	8852.7(2)	16.04(9)
Br1	8427.0(7)	3168.4(10)	9919.4(7)	23.38(19)
N1	3818(6)	5622(7)	8130(5)	16.1(13)
N2	3751(5)	4033(11)	6976(4)	15.6(11)
N3	237(7)	7054(9)	5371(6)	17.9(16)
O1	-1635(5)	7809(6)	6156(5)	24.3(13)
O2	-757(5)	6469(7)	7664(5)	25.1(13)
O3	-427(6)	5114(6)	4341(5)	20.5(13)
O4	-379(5)	7214(6)	3571(4)	17.9(12)

Table 3 Anisotropic Displacement Parameters ($Å^2×10^3$) for 201. The Anisotropic displacement factor exponent takes the form: $-2π^2[h^2a^{*2}U_{11}+2hka^*b^*U_{12}+…]$.

Atom	U_{11}	U_{22}	U_{33}	U_{23}	U_{13}	U_{12}
C1	30(4)	16(4)	19(4)	1(3)	14(3)	-4(3)
C2	13(3)	17(4)	21(4)	3(3)	7(3)	1(3)

C3	12(3)	11(4)	24(4)	0(3)	8(3)	0(3)
C4	17(3)	13(4)	18(4)	-3(3)	6(3)	1(3)
C5	13(3)	18(5)	22(4)	1(3)	8(3)	2(3)
C6	21(4)	23(5)	19(4)	-1(3)	4(3)	-1(3)
C7	16(3)	23(5)	31(4)	-7(4)	7(3)	-1(3)
C8	23(4)	19(5)	36(5)	3(4)	13(3)	-5(3)
C9	28(4)	30(7)	26(4)	8(4)	5(3)	-7(4)
C10	23(4)	26(5)	18(4)	-1(3)	1(3)	-6(4)
C11	17(3)	13(4)	30(4)	-4(3)	12(3)	0(3)
C12	13(3)	20(5)	14(3)	-5(3)	4(3)	-3(3)
C13	22(4)	22(5)	23(4)	-2(3)	10(3)	-1(3)
C14	15(4)	34(6)	25(4)	-1(4)	8(3)	3(4)
C15	14(3)	36(5)	26(3)	0(6)	9(3)	-3(6)
C16	20(4)	26(6)	23(4)	2(4)	7(3)	-6(4)
C17	21(4)	23(5)	19(4)	1(4)	7(3)	3(4)
C18	15(4)	18(5)	25(4)	0(3)	10(3)	-2(3)
C19	11(3)	15(5)	19(4)	0(3)	4(3)	2(3)
C20	15(3)	13(4)	22(4)	-1(3)	3(3)	-2(3)
C21	27(4)	44(7)	33(5)	-6(4)	18(4)	2(4)
C22	12(3)	19(5)	21(4)	-1(3)	6(3)	0(3)
C23	26(4)	19(5)	17(4)	-5(3)	8(3)	0(3)
C24	28(4)	22(5)	23(4)	1(3)	9(3)	0(4)
C25	23(4)	22(5)	33(5)	-2(4)	9(4)	0(4)
C26	28(4)	24(5)	27(4)	1(4)	14(3)	8(4)
Au1	13.02(13)	15.86(16)	18.77(13)	0.70(17)	5.41(9)	0.46(16)
Br1	14.7(3)	27.3(5)	25.0(4)	2.4(3)	3.8(3)	2.7(3)
N1	15(3)	14(4)	19(3)	-1(3)	7(2)	-2(3)
N2	12(2)	13(3)	23(3)	-5(4)	9(2)	-2(4)
N3	20(3)	13(4)	23(4)	-1(3)	10(3)	1(3)
O1	15(2)	19(4)	36(3)	1(2)	6(2)	2(2)
O2	21(3)	30(4)	29(3)	0(3)	14(2)	0(3)

O3	24(3)	11(3)	27(3)	2(2)	10(2)	1(2)
O4	23(3)	15(3)	17(3)	1(2)	9(2)	1(2)

Table 4 Bond Lengths for 201.

Atom	Atom	Length/Å	Atom	Atom	Length/Å
C1	Au1	1.979(8)	C13	C14	1.384(12)
C1	N1	1.357(11)	C14	C15	1.382(18)
C1	N2	1.351(10)	C15	C16	1.380(16)
C2	C3	1.355(11)	C16	C17	1.391(13)
C2	C18	1.481(11)	C18	C19	1.531(10)
C2	N1	1.399(9)	C19	C20	1.521(11)
C3	N2	1.394(10)	C19	N3	1.453(11)
C4	C5	1.513(11)	C20	O1	1.207(10)
C4	N1	1.467(10)	C20	O2	1.343(10)
C5	C6	1.389(11)	C21	O2	1.441(10)
C5	C10	1.384(11)	C22	N3	1.354(10)
C6	C7	1.376(12)	C22	O3	1.223(11)
C7	C8	1.384(13)	C22	O4	1.345(11)
C8	C9	1.397(13)	C23	C24	1.520(12)
C9	C10	1.385(14)	C23	C25	1.506(11)
C11	C12	1.528(11)	C23	C26	1.520(11)
C11	N2	1.451(11)	C23	O4	1.485(9)
C12	C13	1.388(12)	Au1	Br1	2.3938(8)
C12	C17	1.390(12)			

Table 5 Bond Angles for 201.

Atom	Atom	Atom	Angle/˚	Atom	Atom	Atom	Angle/˚
N1	C1	Au1	129.2(6)	C20	C19	C18	111.7(6)
N2	C1	Au1	125.9(7)	N3	C19	C18	111.7(7)

N2	C1	N1	104.9(7)	N3	C19	C20	110.3(7)
C3	C2	C18	132.1(7)	O1	C20	C19	125.3(7)
C3	C2	N1	105.4(7)	O1	C20	O2	124.9(8)
N1	C2	C18	122.3(7)	O2	C20	C19	109.8(7)
C2	C3	N2	107.6(7)	O3	C22	N3	124.5(9)
N1	C4	C5	112.1(6)	O3	C22	O4	126.5(8)
C6	C5	C4	119.4(7)	O4	C22	N3	109.1(9)
C10	C5	C4	122.0(7)	C25	C23	C24	111.1(7)
C10	C5	C6	118.6(8)	C25	C23	C26	113.0(8)
C7	C6	C5	121.3(8)	C26	C23	C24	110.2(7)
C6	C7	C8	120.2(8)	O4	C23	C24	102.0(7)
C7	C8	C9	118.9(8)	O4	C23	C25	109.8(7)
C10	C9	C8	120.4(8)	O4	C23	C26	110.1(6)
C5	C10	C9	120.5(8)	C1	Au1	Br1	178.0(3)
N2	C11	C12	112.9(7)	C1	N1	C2	111.5(7)
C13	C12	C11	119.7(9)	C1	N1	C4	123.1(6)
C13	C12	C17	118.5(8)	C2	N1	C4	124.8(7)
C17	C12	C11	121.8(7)	C1	N2	C3	110.6(8)
C14	C13	C12	120.9(9)	C1	N2	C11	124.5(7)
C15	C14	C13	120.4(9)	C3	N2	C11	124.8(6)
C16	C15	C14	119.3(8)	C22	N3	C19	121.9(9)
C15	C16	C17	120.4(10)	C20	O2	C21	117.1(7)
C12	C17	C16	120.5(9)	C22	O4	C23	121.4(7)
C2	C18	C19	112.8(7)				

Table 6 Hydrogen Bonds for AIA-201

D	H	A	d(D-H)/Å	d(H-A)/Å	d(D-A)/Å	D-H-A/°
N3	H3A	O3[1]	0.86(3)	2.17(4)	3.008(12)	163(9)

Table 7 Torsion Angles for 201.

A	B	C	D	Angle/˚	A	B	C	D	Angle/˚
C2	C3	N2	C1	-1.4(10)	C18	C19	C20	O1	126.1(9)
C2	C3	N2	C11	-177.2(8)	C18	C19	C20	O2	-54.2(9)
C2	C18	C19	C20	157.1(7)	C18	C19	N3	C22	132.1(7)
C2	C18	C19	N3	-78.8(9)	C19	C20	O2	C21	177.2(7)
C3	C2	C18	C19	2.7(13)	C20	C19	N3	C22	-103.0(8)
C3	C2	N1	C1	-0.7(9)	C24	C23	O4	C22	-177.6(7)
C3	C2	N1	C4	170.3(7)	C25	C23	O4	C22	64.5(9)
C4	C5	C6	C7	-178.5(7)	C26	C23	O4	C22	-60.6(10)
C4	C5	C10	C9	179.2(8)	Au1	C1	N1	C2	179.8(6)
C5	C4	N1	C1	81.9(9)	Au1	C1	N1	C4	8.7(11)
C5	C4	N1	C2	-88.0(8)	Au1	C1	N2	C3	-179.1(6)
C5	C6	C7	C8	-0.1(13)	Au1	C1	N2	C11	-3.3(12)
C6	C5	C10	C9	0.3(13)	N1	C1	N2	C3	1.0(9)
C6	C7	C8	C9	-1.0(13)	N1	C1	N2	C11	176.7(8)
C7	C8	C9	C10	1.8(15)	N1	C2	C3	N2	1.2(9)
C8	C9	C10	C5	-1.5(15)	N1	C2	C18	C19	-170.9(7)
C10	C5	C6	C7	0.5(12)	N1	C4	C5	C6	-156.6(7)
C11	C12	C13	C14	178.0(8)	N1	C4	C5	C10	24.5(10)
C11	C12	C17	C16	-178.3(7)	N2	C1	N1	C2	-0.2(9)
C12	C11	N2	C1	-63.6(11)	N2	C1	N1	C4	-171.4(7)
C12	C11	N2	C3	111.5(9)	N2	C11	C12	C13	159.7(7)
C12	C13	C14	C15	1.5(13)	N2	C11	C12	C17	-20.9(12)
C13	C12	C17	C16	1.1(14)	N3	C19	C20	O1	1.2(12)
C13	C14	C15	C16	-1.2(11)	N3	C19	C20	O2	-179.0(7)

C14	C15	C16	C17	0.9(11)	N3	C22	O4	C23	174.3(6)
C15	C16	C17	C12	-0.9(14)	O1	C20	O2	C21	-3.1(12)
C17	C12	C13	C14	-1.4(13)	O3	C22	N3	C19	-12.1(11)
C18	C2	C3	N2	-173.2(9)	O3	C22	O4	C23	-5.3(12)
C18	C2	N1	C1	174.5(7)	O4	C22	N3	C19	168.3(7)
C18	C2	N1	C4	-14.5(12)					

Table 8 Hydrogen Atom Coordinates (Å×10^4) and Isotropic Displacement Parameters (Å^2×10^3) for 201

Atom	x	y	z	U(eq)
H3	1898.35	4544.73	5889.01	19
H4A	4941.73	6158.32	9673.26	20
H4B	3659.01	7011.97	9202.06	20
H6	6207.77	8255.75	10271.46	26
H7	7298.41	10033.51	9861.22	29
H8	6834.06	10652.93	8040.68	30
H9	5299.5	9400.56	6638.1	36
H10	4176.07	7646.95	7062.41	29
H11A	3391	2655.57	5775.67	23
H11B	4396.89	2147.06	6908.57	23
H13	5816.03	1399.57	5933.8	26
H14	7437.02	1954.58	5314.92	30
H15	7907.59	4225.11	5117.7	30
H16	6682.2	5934.16	5473.56	28
H17	5041.08	5383.73	6080.5	25
H18A	1878.84	7617.51	7290.51	23
H18B	1502.38	6579.67	8034.64	23
H19	155.64	5467.91	6290	18
H21A	-1608.2	7902.62	8224.61	49
H21B	-1566.47	6468.82	8776.51	49
H21C	-2553.63	6737.22	7574.44	49

H24A	*-1371.6*	*8654.84*	*1887.58*	*37*
H24B	*-988.12*	*7823.5*	*1030.86*	*37*
H24C	*90.52*	*8431.1*	*2084.67*	*37*
H25A	*-2054.22*	*5263*	*2452.56*	*40*
H25B	*-2361.19*	*5863.45*	*1270.3*	*40*
H25C	*-2673.99*	*6722.16*	*2152.13*	*40*
H26A	*1091.1*	*6193.15*	*2578.2*	*38*
H26B	*33.86*	*5435.11*	*1594.49*	*38*
H26C	*333.86*	*4953.96*	*2808.34*	*38*
H3A	*210(100)*	*7940(30)*	*5300(80)*	*22*

Crystal structure determination of 201

Crystal Data *for* $C_{26}H_{31}AuBrN_3O_4$ *(*M *=726.41 g/mol): monoclinic, space group* $P2_1$ *(no. 4),* a *=* $11.1514(3)$ *Å,* b *=* $9.7618(2)$ *Å,* c *=* $13.0862(3)$ *Å,* β *=* $112.000(3)°$*,* V *=* $1320.80(6)$ $Å^3$*,* Z *= 2,* T *=* $100.01(10)$ *K,* $\mu(CuK\alpha) = 12.537$ mm^{-1}*,* Dcalc *=* 1.827 g/cm^3*, 23339 reflections measured (7.286° ≤ 2Θ ≤ 136.476°), 4685 unique (*$R_{int} = 0.0507$*,* $R_{sigma} = 0.0332$*) which were used in all calculations. The final* R_1 *was 0.0258 (I > 2σ(I)) and* wR_2 *was 0.0628 (all data).*

Refinement model description

Number of restraints - 2, number of constraints - unknown.

Details:

1. Fixed Uiso At 1.2 times of: All C(H) groups, All C(H,H) groups, All N(H) groups At 1.5 times of: All C(H,H,H) groups. 2. Restrained distances N3-H3A 0.87 with sigma of 0.023.a Ternary CH refined with riding coordinates: C19(H19). 3.b Secondary CH2 refined with riding coordinates: C4(H4A,H4B), C11(H11A,H11B), C18(H18A,H18B). 3.c Aromatic/amide H refined with riding coordinates: C3(H3), C6(H6), C7(H7), C8(H8), C9(H9), C10(H10), C13(H13), C14(H14), C15(H15), C16(H16), C17(H17). 3.d Idealised Me refined as rotating group: C21(H21A,H21B,H21C), C24(H24A,H24B,H24C), C25(H25A,H25B,H25C), C26(H26A,H26B, H26C)

7.7 - Crystal structure of 200

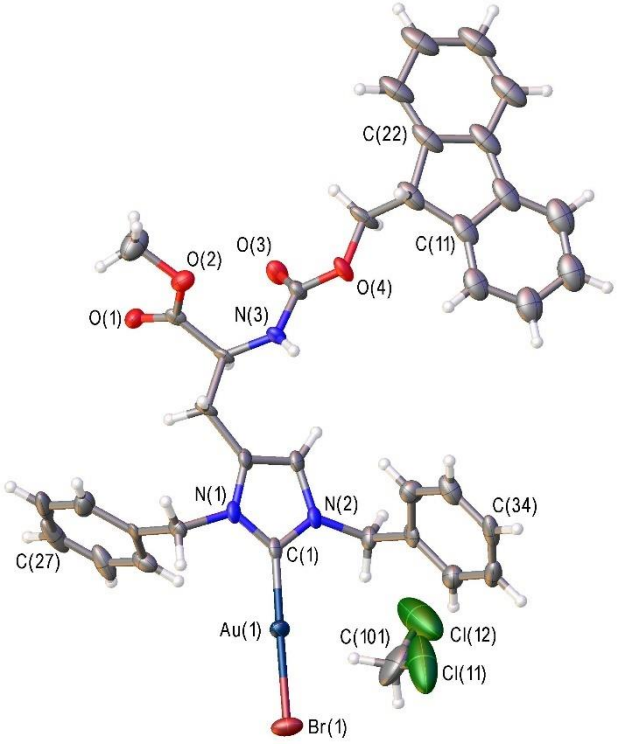

Table 1 Crystal data and structure refinement for 200.

Identification code	*AIA-457-01*
Empirical formula	$C_{36.5}H_{34}AuBrClN_3O_4$
Formula weight	*890.99*
Temperature/K	*100.01(10)*
Crystal system	*monoclinic*
Space group	$P2_1$
a/Å	*5.0196(2)*
b/Å	*26.0116(9)*
c/Å	*13.4087(6)*
α/°	*90*
β/°	*97.278(4)*
γ/°	*90*
Volume/Å³	*1736.63(13)*
Z	*2*

ρ_{calc}g/cm^3	1.704
μ/mm^{-1}	10.362
F(000)	874.0
Crystal size/mm^3	0.302 × 0.084 × 0.029
Radiation	CuKα (λ = 1.54184)
2Θ range for data collection/°	7.466 to 148.958
Index ranges	-6 ≤ h ≤ 6, -32 ≤ k ≤ 31, -16 ≤ l ≤ 16
Reflections collected	13472
Independent reflections	13472 [R_{int} = ?, R_{sigma} = 0.0321]
Data/restraints/parameters	13472/150/435
Goodness-of-fit on F^2	1.038
Final R indexes [I>=2σ (I)]	R_1 = 0.0829, wR_2 = 0.2324
Final R indexes [all data]	R_1 = 0.0895, wR_2 = 0.2422
Largest diff. peak/hole / e Å^{-3}	6.15/-2.65
Flack parameter	-0.029(19)

Table 2 Fractional Atomic Coordinates (×10^4) and Equivalent Isotropic Displacement Parameters (Å^2×10^3) for 200. U_{eq} is defined as 1/3 of of the trace of the orthogonalised U_{IJ} tensor.

Atom	x	y	z	U(eq)
C1	12910(50)	3439(8)	4943(15)	21(2)
C2	9890(50)	3467(8)	3534(16)	24(2)
C3	9360(50)	3034(9)	4029(15)	24(2)
C4	8530(40)	3675(10)	2523(14)	25(4)
C5	6030(40)	3393(9)	2065(15)	21(3)
C6	4900(40)	3709(8)	1194(14)	21(4)
C7	4550(80)	3857(16)	-520(20)	56(9)
C8	4370(50)	2573(9)	1522(17)	25(4)
C9	2740(60)	1798(12)	780(30)	40(7)
C10	3800(60)	1310(12)	380(20)	43(5)
C11	4870(60)	926(11)	1200(20)	43(5)

C12	7030(60)	968(12)	1940(20)	45(5)
C13	7600(80)	562(14)	2590(30)	54(6)
C14	6100(80)	118(15)	2510(30)	60(6)
C15	3870(80)	77(15)	1770(30)	58(6)
C16	3230(70)	482(13)	1090(30)	50(5)
C17	1220(70)	529(13)	240(30)	51(5)
C18	-850(80)	202(16)	-170(30)	60(6)
C19	-2650(90)	357(19)	-1000(40)	64(7)
C20	-2370(80)	846(17)	-1450(30)	62(6)
C21	-240(70)	1169(16)	-1050(30)	55(6)
C22	1470(60)	1023(13)	-210(30)	47(5)
C23	12980(50)	4228(9)	3874(16)	24(4)
C24	11000(50)	4639(8)	4114(17)	24(4)
C25	10060(60)	4651(11)	5020(20)	36(6)
C26	8120(60)	5033(12)	5220(30)	53(8)
C27	7320(60)	5389(13)	4510(40)	59(11)
C28	8270(70)	5379(12)	3600(30)	56(10)
C29	10110(60)	5002(12)	3400(20)	42(6)
C30	11540(50)	2608(9)	5619(17)	28(5)
C31	13580(50)	2202(9)	5379(18)	26(4)
C32	15170(60)	1950(12)	6160(20)	39(6)
C33	17030(60)	1566(11)	5930(20)	42(7)
C34	17280(50)	1451(10)	4950(30)	41(7)
C35	15710(70)	1702(11)	4180(20)	43(6)
C36	13890(50)	2071(12)	4380(20)	35(6)
Au1	15832.7(14)	3604.4(5)	6012.7(5)	24.3(3)
Br1	19433(5)	3788.9(13)	7315.2(18)	40.5(7)
N1	11990(40)	3702(6)	4102(12)	24(2)
N2	11290(40)	3022(7)	4892(13)	23(2)
N3	6560(40)	2868(8)	1852(13)	23(3)
O1	3490(40)	4090(7)	1280(12)	34(4)

O2	5570(30)	3531(9)	322(11)	32(4)
O3	2100(40)	2728(7)	1530(15)	34(4)
O4	5020(40)	2103(7)	1230(14)	31(4)
C101	9280(90)	2800(30)	8990(50)	95(18)
Cl11	11970(100)	2517(11)	8550(20)	131(13)
Cl12	6320(100)	2471(14)	8850(20)	137(14)

Table 3 Anisotropic Displacement Parameters ($Å^2×10^3$) for 200 The Anisotropic displacement factor exponent takes the form: $-2π^2[h^2a^{*2}U_{11}+2hka^*b^*U_{12}+…]$.

Atom	U_{11}	U_{22}	U_{33}	U_{23}	U_{13}	U_{12}
C1	27(5)	11(5)	28(5)	0(4)	12(4)	6(4)
C2	28(5)	12(5)	31(5)	-2(4)	4(4)	5(4)
C3	28(5)	13(5)	31(5)	-2(4)	6(4)	4(4)
C4	22(7)	25(9)	27(6)	-11(7)	-1(6)	-11(7)
C5	15(6)	21(7)	26(5)	-10(5)	1(5)	-9(5)
C6	12(7)	25(9)	25(6)	-6(6)	4(5)	-7(6)
C7	60(20)	60(20)	43(15)	9(15)	11(14)	24(18)
C8	24(12)	18(11)	32(10)	-7(8)	1(8)	-1(8)
C9	24(14)	33(16)	62(18)	-29(13)	4(12)	-9(11)
C10	42(11)	33(10)	58(10)	-19(9)	23(9)	-12(9)
C11	44(10)	31(9)	59(10)	-18(8)	27(8)	-2(8)
C12	46(12)	34(10)	61(11)	-10(9)	26(9)	4(9)
C13	58(13)	42(11)	69(12)	-4(10)	29(10)	8(10)
C14	62(13)	43(12)	81(13)	-4(11)	33(11)	4(11)
C15	58(13)	42(11)	81(13)	-11(11)	35(10)	0(10)
C16	50(10)	34(9)	71(10)	-23(9)	33(9)	-5(9)
C17	49(10)	40(10)	71(10)	-31(9)	30(9)	-13(9)
C18	55(12)	53(12)	78(12)	-36(11)	32(10)	-19(11)
C19	57(13)	61(13)	78(13)	-42(12)	25(11)	-25(11)
C20	57(13)	62(13)	71(12)	-43(11)	22(10)	-21(11)

C21	49(12)	53(12)	65(12)	-37(10)	18(10)	-17(10)
C22	44(10)	40(10)	63(10)	-30(9)	24(8)	-16(8)
C23	24(12)	19(11)	29(10)	-1(8)	2(8)	-7(8)
C24	22(11)	9(10)	38(11)	-2(8)	-9(8)	-6(8)
C25	39(15)	33(15)	36(13)	-9(11)	6(10)	-13(11)
C26	39(17)	24(15)	100(30)	-13(16)	22(16)	-7(12)
C27	21(15)	29(16)	130(30)	-30(19)	2(16)	1(12)
C28	40(18)	16(13)	100(30)	-2(15)	-23(18)	2(11)
C29	37(15)	30(15)	56(16)	4(12)	-8(12)	5(11)
C30	35(13)	18(11)	30(11)	6(9)	8(9)	2(9)
C31	23(11)	15(10)	40(12)	5(9)	8(9)	-6(8)
C32	44(16)	30(15)	42(13)	4(11)	-3(11)	-2(11)
C33	29(14)	25(13)	67(18)	15(13)	-12(12)	-4(10)
C34	25(14)	17(12)	80(20)	6(12)	7(12)	0(9)
C35	43(18)	27(14)	62(17)	-8(12)	17(13)	-4(12)
C36	30(14)	35(15)	40(13)	-2(11)	0(10)	4(10)
Au1	21.4(4)	24.4(4)	26.1(4)	-1.7(4)	-1.7(2)	1.8(5)
Br1	27.9(13)	62.8(19)	28.8(11)	-6.5(10)	-4.1(9)	-1.9(11)
N1	29(5)	13(5)	30(4)	0(4)	7(4)	6(4)
N2	28(5)	12(5)	29(5)	-1(4)	7(4)	4(4)
N3	18(7)	20(7)	31(7)	-6(6)	-2(6)	-4(6)
O1	44(11)	26(10)	29(8)	1(7)	-9(7)	5(8)
O2	29(8)	37(13)	28(6)	4(8)	0(5)	-1(8)
O3	21(9)	26(9)	53(10)	-6(8)	0(7)	2(7)
O4	27(9)	16(8)	51(10)	-11(7)	5(7)	-1(7)
C101	120(30)	90(40)	70(30)	50(30)	0(30)	20(20)
Cl11	260(40)	55(15)	102(18)	11(13)	100(20)	20(20)
Cl12	240(30)	100(20)	81(15)	-25(16)	50(20)	-80(30)

Table 4 Bond Lengths for 200.

Atom	Atom	Length/Å	Atom	Atom	Length/Å
C1	Au1	1.97(2)	C17	C18	1.40(5)
C1	N1	1.35(3)	C17	C22	1.43(5)
C1	N2	1.35(3)	C18	C19	1.40(7)
C2	C3	1.35(3)	C19	C20	1.43(7)
C2	C4	1.54(3)	C20	C21	1.41(4)
C2	N1	1.36(3)	C21	C22	1.38(5)
C3	N2	1.41(3)	C23	C24	1.52(3)
C4	C5	1.51(3)	C23	N1	1.50(3)
C5	C6	1.48(3)	C24	C25	1.35(4)
C5	N3	1.43(3)	C24	C29	1.38(4)
C6	O1	1.23(3)	C25	C26	1.44(4)
C6	O2	1.34(3)	C26	C27	1.35(6)
C7	O2	1.45(4)	C27	C28	1.37(6)
C8	N3	1.37(3)	C28	C29	1.40(4)
C8	O3	1.21(3)	C30	C31	1.53(3)
C8	O4	1.34(3)	C30	N2	1.45(3)
C9	C10	1.50(4)	C31	C32	1.40(4)
C9	O4	1.46(3)	C31	C36	1.41(4)
C10	C11	1.53(5)	C32	C33	1.42(4)
C10	C22	1.52(4)	C33	C34	1.37(5)
C11	C12	1.38(5)	C34	C35	1.38(4)
C11	C16	1.41(4)	C35	C36	1.37(4)
C12	C13	1.38(5)	Au1	Br1	2.397(2)
C13	C14	1.38(5)	C101	Cl11	1.71(4)
C14	C15	1.41(6)	C101	Cl12	1.70(4)
C15	C16	1.40(6)	Cl11	$Cl12^{1}$	2.17(7)
C16	C17	1.43(6)			

Table 5 Bond Angles for 200

Atom	Atom	Atom	Angle/°	Atom	Atom	Atom	Angle/°
N1	C1	Au1	130.0(16)	C21	C20	C19	119(4)
N1	C1	N2	103.0(19)	C22	C21	C20	121(4)
N2	C1	Au1	127.0(15)	C17	C22	C10	109(3)
C3	C2	C4	129(2)	C21	C22	C10	130(3)
C3	C2	N1	106.6(19)	C21	C22	C17	121(3)
N1	C2	C4	124.1(19)	N1	C23	C24	110.8(18)
C2	C3	N2	105(2)	C25	C24	C23	121(2)
C5	C4	C2	116.1(19)	C25	C24	C29	119(3)
C6	C5	C4	105.4(18)	C29	C24	C23	120(2)
N3	C5	C4	112.3(19)	C24	C25	C26	120(3)
N3	C5	C6	115.8(17)	C27	C26	C25	119(3)
O1	C6	C5	122.6(18)	C26	C27	C28	121(3)
O1	C6	O2	125(2)	C27	C28	C29	120(3)
O2	C6	C5	112.7(19)	C24	C29	C28	120(3)
O3	C8	N3	122(2)	N2	C30	C31	112.0(18)
O3	C8	O4	125(2)	C32	C31	C30	120(2)
O4	C8	N3	113(2)	C32	C31	C36	118(2)
O4	C9	C10	108(2)	C36	C31	C30	122(2)
C9	C10	C11	114(3)	C31	C32	C33	120(3)
C9	C10	C22	109(3)	C34	C33	C32	120(2)
C22	C10	C11	103(3)	C33	C34	C35	120(3)
C12	C11	C10	130(3)	C36	C35	C34	121(3)
C12	C11	C16	122(3)	C35	C36	C31	121(3)
C16	C11	C10	108(3)	C1	Au1	Br1	178.8(6)
C13	C12	C11	119(3)	C1	N1	C2	113.4(18)
C14	C13	C12	122(4)	C1	N1	C23	123.2(18)
C13	C14	C15	120(4)	C2	N1	C23	123.1(17)
C16	C15	C14	120(4)	C1	N2	C3	111.6(19)

C11	C16	C17	111(3)	C1	N2	C30	124(2)
C15	C16	C11	118(4)	C3	N2	C30	124(2)
C15	C16	C17	131(3)	C8	N3	C5	116.1(19)
C16	C17	C22	109(3)	C6	O2	C7	112(2)
C18	C17	C16	133(4)	C8	O4	C9	114(2)
C18	C17	C22	118(4)	Cl12	C101	Cl11	117(5)
C19	C18	C17	121(4)	C101	Cl11	$Cl12^{1}$	141(3)
C18	C19	C20	121(4)	C101	Cl12	$Cl11^{2}$	146(4)

Table 6 Hydrogen Bonds for 200.

D	H	A	d(D-H)/Å	d(H-A)/Å	d(D-A)/Å	D-H-A/°
N3	H3A	$O3^{1}$	0.86	2.11	2.89(3)	150.3

Table 7 Torsion Angles for 200.

A	B	C	D	Angle/˚	A	B	C	D	Angle/˚
C2	C3	N2	C1	2(2)	C22	C10	C11	C16	-2(3)
C2	C3	N2	C30	-177(2)	C22	C17	C18	C19	-1(5)
C2	C4	C5	C6	171.8(17)	C23	C24	C25	C26	-178(2)
C2	C4	C5	N3	-61(2)	C23	C24	C29	C28	179(2)
C3	C2	C4	C5	8(3)	C24	C23	N1	C1	-101(2)
C3	C2	N1	C1	1(2)	C24	C23	N1	C2	72(2)
C3	C2	N1	C23	-172.4(19)	C24	C25	C26	C27	-2(4)
C4	C2	C3	N2	177(2)	C25	C24	C29	C28	0(4)
C4	C2	N1	C1	-177.8(19)	C25	C26	C27	C28	2(5)
C4	C2	N1	C23	9(3)	C26	C27	C28	C29	-1(5)
C4	C5	C6	O1	-82(2)	C27	C28	C29	C24	0(5)
C4	C5	C6	O2	99(2)	C29	C24	C25	C26	1(4)
C4	C5	N3	C8	174.3(18)	C30	C31	C32	C33	179(2)
C5	C6	O2	C7	-177(2)	C30	C31	C36	C35	-179(3)

C6	C5	N3	C8	-65(3)	C31	C30	N2	C1	-86(3)
C9	C10	C11	C12	-64(4)	C31	C30	N2	C3	93(3)
C9	C10	C11	C16	115(3)	C31	C32	C33	C34	1(4)
C9	C10	C22	C17	-120(3)	C32	C31	C36	C35	0(4)
C9	C10	C22	C21	60(4)	C32	C33	C34	C35	-1(4)
C10	C9	O4	C8	173(2)	C33	C34	C35	C36	0(4)
C10	C11	C12	C13	-180(3)	C34	C35	C36	C31	0(4)
C10	C11	C16	C15	180(3)	C36	C31	C32	C33	-1(4)
C10	C11	C16	C17	3(3)	Au1	C1	N1	C2	-179.5(15)
C11	C10	C22	C17	1(3)	Au1	C1	N1	C23	-6(3)
C11	C10	C22	C21	-178(3)	Au1	C1	N2	C3	178.4(15)
C11	C12	C13	C14	0(4)	Au1	C1	N2	C30	-3(3)
C11	C16	C17	C18	180(3)	N1	C1	N2	C3	-1(2)
C11	C16	C17	C22	-2(3)	N1	C1	N2	C30	177.8(19)
C12	C11	C16	C15	0(4)	N1	C2	C3	N2	-2(2)
C12	C11	C16	C17	-178(2)	N1	C2	C4	C5	-173.2(19)
C12	C13	C14	C15	-2(5)	N1	C23	C24	C25	51(3)
C13	C14	C15	C16	2(5)	N1	C23	C24	C29	-128(2)
C14	C15	C16	C11	-1(4)	N2	C1	N1	C2	0(2)
C14	C15	C16	C17	176(3)	N2	C1	N1	C23	173.4(18)
C15	C16	C17	C18	3(6)	N2	C30	C31	C32	145(2)
C15	C16	C17	C22	-179(3)	N2	C30	C31	C36	-35(3)
C16	C11	C12	C13	1(4)	N3	C5	C6	O1	153(2)
C16	C17	C18	C19	177(3)	N3	C5	C6	O2	-26(3)
C16	C17	C22	C10	0(3)	N3	C8	O4	C9	-174(2)
C16	C17	C22	C21	180(3)	O1	C6	O2	C7	3(3)
C17	C18	C19	C20	2(5)	O3	C8	N3	C5	-9(3)
C18	C17	C22	C10	179(3)	O3	C8	O4	C9	8(4)
C18	C17	C22	C21	-2(4)	O4	C8	N3	C5	173.0(19)
C18	C19	C20	C21	0(5)	O4	C9	C10	C11	73(3)
C19	C20	C21	C22	-3(5)	O4	C9	C10	C22	-173(3)

C20	C21	C22	C10	-177(3)	Cl11	C101	Cl12	Cl11[1]	-144(4)
C20	C21	C22	C17	4(5)	Cl12	C101	Cl11	Cl12[2]	-149(4)
C22	C10	C11	C12	178(3)					

Table 8 Hydrogen Atom Coordinates (Å×10⁴) and Isotropic Displacement Parameters (Å²×10³) for 200.

Atom	x	y	z	U(eq)
H3	8009.18	2795.44	3841.68	28
H4A	8063.91	4032.45	2613.86	30
H4B	9832.26	3666.82	2045.69	30
H5	4746.41	3398.87	2556.52	25
H7A	5460	3774.25	-1089.09	83
H7B	4869.54	4210.6	-341.01	83
H7C	2659.73	3800.14	-689.8	83
H9A	1722.92	1988.89	240.53	48
H9B	1566.52	1720.16	1282.7	48
H10	5179.44	1386.73	-49.79	52
H12	8071.71	1264.9	2006.41	54
H13	9044.6	587.83	3101.48	65
H14	6562.17	-154.99	2951.67	72
H15	2822.08	-219.19	1726.81	70
H18	-1018.9	-122.86	102.94	72
H19	-4042.67	139.44	-1250.14	77
H20	-3573.54	951.02	-1997.61	75
H21	24.79	1482.88	-1354.35	66
H23A	13219.66	4247.79	3168.26	29
H23B	14707.99	4288.5	4268.12	29
H25	10668.22	4411.22	5507.17	43
H26	7423.49	5034.57	5828	63
H27	6110.54	5642.73	4646.94	71

H28	*7688.14*	*5622.96*	*3116.19*	*67*
H29	*10745.92*	*4996.11*	*2776.63*	*50*
H30A	*9802.39*	*2446.39*	*5628.01*	*33*
H30B	*12100.08*	*2748.25*	*6282.39*	*33*
H32	*15020.38*	*2033.03*	*6822.15*	*47*
H33	*18067.89*	*1393.02*	*6451.91*	*50*
H34	*18502.45*	*1203.61*	*4803.8*	*50*
H35	*15891.31*	*1621.55*	*3515.43*	*51*
H36	*12853.31*	*2235.43*	*3854.08*	*42*
H3A	*8161.37*	*2743.87*	*1927.3*	*28*
H10A	*9760.6*	*2870.16*	*9704.94*	*115*
H10B	*8972.14*	*3132.26*	*8661*	*115*

Table 9 Atomic Occupancy for 200.

Atom	**Occupancy**	***Atom***	**Occupancy**	***Atom***	**Occupancy**
C101	*0.5*	*H10A*	*0.5*	*H10B*	*0.5*
Cl11	*0.5*	*Cl12*	*0.5*		

Crystal structure determination of 200

Crystal Data *for* $C_{36.5}H_{34}AuBrClN_3O_4$ *(*M *=890.99 g/mol): monoclinic, space group* $P2_1$ *(no. 4),* a = *5.0196(2) Å,* b = *26.0116(9) Å,* c = *13.4087(6) Å,* β = *97.278(4)°,* V = *1736.63(13) Å*^{3}*,* Z = *2,* T = *100.01(10) K, μ(CuKα) = 10.362 mm*$^{-1}$, Dcalc = *1.704 g/cm*^{3}*, 13472 reflections measured (7.466° ≤ 2Θ ≤ 148.958°), 13472 unique (*R_{int} *= ?,* R_{sigma} *= 0.0321) which were used in all calculations. The final* R_1 *was 0.0829 (I > 2σ(I)) and* wR_2 *was 0.2422 (all data).*

Refinement model description

Number of restraints - 150, number of constraints - unknown.

Details:

1. Twinned data refinement: Scales: 0.525(3); 0.475(3). 2. Fixed Uiso at 1.2 times of: all C(H) groups, all C(H,H) groups, all N(H) groups At 1.5 times of: All C(H,H,H) groups. 3. Restrained distances Cl11-C101 = Cl12-C101 1.7 with sigma of 0.02. 4. Rigid bond restraints C101, Cl11, Cl12 with sigma for 1-2 distances of 0.01 and sigma for 1-3 distances of 0.01. 5. Uiso/Uaniso restraints and constraints C4 ≈ C5 ≈ C6 ≈ N3: within 1.7A with sigma of 0.004 and sigma for terminal atoms of 0.008C1 ≈ C2 ≈ C3 ≈ N1 ≈ N2: within 1.7A with sigma of 0.002 and sigma for terminal atoms of 0.004 C10 ≈ C11 ≈ C12 ≈ C13 ≈ C14 ≈ C15 ≈ C16 ≈ C17 ≈C18 ≈ C19 ≈ C20 ≈ C21 ≈ C22: within 1.7A with sigma of 0.008 and sigma for terminal atoms of 0.016 Uanis(C101) ≈ Ueq: with sigma of 0.02 and sigma for terminal atoms of 0.046. Others Fixed Sof: C101(0.5) H10A(0.5) H10B(0.5) Cl11(0.5) Cl12(0.5). 7.a Ternary CH refined with riding coordinates: C5(H5), C10(H10) 7.b Secondary CH2 refined with riding coordinates C4(H4A,H4B), C9(H9A,H9B), C23(H23A,H23B), C30(H30A,H30B), C101(H10A,H10B) 7.c Aromatic/amide H refined with riding coordinates: C3(H3), C12(H12), C13(H13), C14(H14), C15(H15), C18(H18), C19(H19), C20(H20), C21(H21), C25(H25), C26(H26), C27(H27), C28(H28), C29(H29), C32(H32), C33(H33), C34(H34), C35(H35), C36(H36), N3(H3A). 7.d Idealised Me refined as rotating group: C7(H7A,H7B,H7C)

7.8 - Crystal structure of 204:

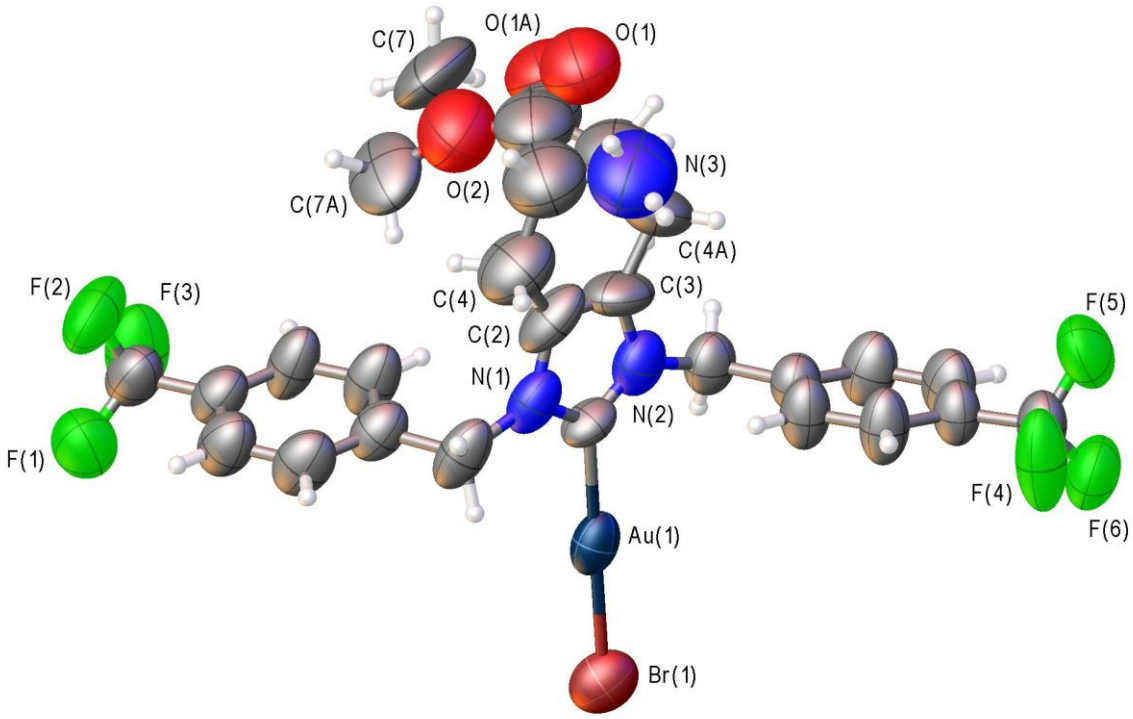

Table 1 Crystal data and structure refinement for 204

Identification code	*AIA-424*
Empirical formula	*$C_{23}H_{21}AuBrF_6N_3O_2$*
Formula weight	*762.30*
Temperature/K	*100.01(10)*
Crystal system	*triclinic*
Space group	*P-1*
a/Å	*7.5064(4)*
b/Å	*12.4524(10)*
c/Å	*13.9383(8)*
α/°	*77.166(6)*
β/°	*79.151(5)*
γ/°	*89.382(5)*
Volume/Å^3	*1246.94(14)*
Z	*2*

$\rho_{calc}g/cm^3$	2.030
μ/mm^{-1}	13.617
F(000)	728.0
Crystal size/mm^3	0.292 × 0.094 × 0.063
Radiation	CuKα (λ = 1.54184)
2Θ range for data collection/°	7.284 to 149.592
Index ranges	-9 ≤ h ≤ 7, -14 ≤ k ≤ 15, -16 ≤ l ≤ 17
Reflections collected	12785
Independent reflections	4915 [R_{int} = 0.0701, R_{sigma} = 0.0591]
Data/restraints/parameters	4915/172/371
Goodness-of-fit on F^2	1.044
Final R indexes [I>=2σ (I)]	R_1 = 0.0764, wR_2 = 0.2083
Final R indexes [all data]	R_1 = 0.0970, wR_2 = 0.2332
Largest diff. peak/hole / e $Å^{-3}$	4.13/-2.45

Table 2 Fractional Atomic Coordinates (×10⁴) and Equivalent Isotropic Displacement Parameters (Å²×10³) for 204. U_{eq} is defined as 1/3 of of the trace of the orthogonalised U_{IJ} tensor.

Atom	x	y	z	U(eq)
C1	7314(18)	6039(11)	5428(9)	72(3)
C2	7300(20)	7177(19)	6381(12)	107(5)
C3	6940(30)	7729(13)	5509(17)	114(6)
C4	7630(60)	7710(30)	7170(20)	153(9)
C5	7490(50)	8930(30)	7150(30)	192(10)
C6	5600(50)	9230(30)	7030(30)	177(10)
C7	2300(50)	8800(50)	7690(40)	230(20)
C4A	6740(120)	8910(20)	5300(50)	139(11)
C5A	6800(60)	9460(80)	6150(60)	178(10)
C6A	4890(100)	9210(90)	6750(50)	187(13)
C7A	3300(140)	7490(50)	8170(40)	170(30)
C8	7850(20)	5165(18)	7110(11)	103(5)
C9	6140(20)	4752(15)	7870(11)	91(4)
C10	6340(20)	4038(17)	8775(13)	107(5)

C11	4830(30)	3641(18)	9485(13)	109(6)
C12	3130(20)	3909(14)	9339(11)	91(4)
C13	2960(20)	4618(18)	8457(11)	110(6)
C14	4440(20)	5046(18)	7724(12)	107(6)
C15	1530(30)	3463(17)	10130(13)	110(6)
C16	6570(20)	7205(14)	3880(11)	89(4)
C17	8263(18)	7679(12)	3109(9)	80(3)
C18	9989(17)	7654(16)	3310(11)	101(5)
C19	11490(20)	8127(16)	2599(10)	102(5)
C20	11258(19)	8590(13)	1637(9)	86(4)
C21	9570(20)	8605(16)	1417(11)	105(5)
C22	8090(20)	8155(17)	2143(10)	108(5)
C23	12780(30)	9115(15)	858(11)	96(4)
Au1	7533.7(7)	4591.5(5)	4861.1(4)	79.6(3)
Br1	7871(3)	2954.8(19)	4218.8(17)	105.5(5)
F1	1663(19)	2407(10)	10528(10)	136(4)
F2	1250(19)	3989(12)	10858(10)	148(5)
F3	-11(17)	3517(14)	9791(11)	154(5)
F4	14358(16)	8959(14)	1132(9)	160(6)
F5	12631(18)	10208(9)	564(10)	132(4)
F6	12964(17)	8780(11)	12(8)	128(4)
N1	7487(17)	6083(13)	6298(9)	92(3)
N2	6928(17)	6950(13)	4921(10)	94(4)
N3	8590(50)	9600(20)	6300(30)	217(10)
O1	5120(60)	10080(30)	6550(30)	194(11)
O1A	3460(110)	9530(60)	6530(60)	198(18)
O2	4220(40)	8530(20)	7655(19)	209(8)

Table 3 Anisotropic Displacement Parameters ($Å^2×10^3$) for 204. The Anisotropic displacement factor exponent takes the form: $-2π^2[h^2a^{*2}U_{11}+2hka^*b^*U_{12}+…]$.

Atom	U_{11}	U_{22}	U_{33}	U_{23}	U_{13}	U_{12}
C1	77(8)	84(8)	67(7)	-45(6)	-10(6)	1(6)

C2	84(10)	183(16)	75(8)	-72(10)	-16(7)	17(10)
C3	137(14)	75(8)	138(14)	-54(9)	-12(12)	21(9)
C4	170(20)	176(15)	131(19)	-73(15)	-23(18)	9(15)
C5	243(18)	167(17)	170(20)	-69(16)	-25(19)	7(18)
C6	240(18)	125(15)	170(20)	-71(14)	-8(17)	6(14)
C7	250(20)	220(40)	190(40)	-100(30)	80(30)	40(20)
C4A	180(30)	80(20)	150(20)	-25(19)	-8(19)	40(20)
C5A	230(19)	123(19)	180(20)	-58(16)	-4(16)	10(20)
C6A	239(19)	150(20)	160(20)	-61(18)	10(19)	10(20)
C7A	270(70)	170(40)	90(30)	-70(30)	-30(40)	-20(40)
C8	64(8)	180(17)	70(8)	-37(9)	-13(6)	27(9)
C9	80(9)	125(12)	75(8)	-34(8)	-17(7)	16(8)
C10	82(10)	153(15)	90(10)	-28(10)	-27(9)	34(10)
C11	105(13)	141(15)	77(9)	-19(9)	-17(9)	31(11)
C12	87(10)	119(11)	71(7)	-31(7)	-13(7)	20(8)
C13	79(10)	179(17)	63(7)	-15(9)	-8(7)	27(10)
C14	68(9)	177(17)	72(8)	-19(9)	-17(7)	27(10)
C15	105(14)	130(14)	85(10)	-15(9)	-5(9)	36(11)
C16	69(8)	111(10)	78(8)	-9(7)	-6(6)	2(7)
C17	72(8)	92(8)	70(7)	-10(6)	-10(6)	2(6)
C18	73(9)	141(13)	74(8)	7(8)	-12(7)	2(9)
C19	66(9)	151(14)	73(8)	9(8)	-14(7)	-7(9)
C20	77(9)	108(10)	63(7)	2(6)	-13(6)	-3(7)
C21	104(13)	135(13)	68(8)	-1(8)	-25(8)	15(10)
C22	85(11)	161(16)	74(8)	-10(9)	-24(8)	10(10)
C23	100(12)	114(12)	66(7)	-2(7)	-13(7)	-5(9)
Au1	53.9(4)	119.5(5)	61.9(3)	-15.9(3)	-7.6(2)	0.3(3)
Br1	83.3(11)	133.6(14)	112.0(13)	-46.0(11)	-28.0(9)	15.0(9)
F1	133(10)	129(9)	130(9)	-7(7)	-12(8)	14(7)
F2	138(11)	178(11)	115(8)	-57(8)	39(8)	-22(9)
F3	88(8)	218(15)	130(10)	8(9)	-14(7)	-8(8)
F4	80(7)	246(16)	107(7)	57(9)	-15(6)	-23(8)
F5	133(10)	109(7)	125(8)	17(6)	-1(7)	-13(6)

F6	124(9)	155(9)	86(6)	-17(6)	12(6)	-2(7)
N1	67(7)	138(11)	71(6)	-32(7)	-3(5)	10(7)
N2	68(7)	126(10)	80(7)	-18(7)	0(6)	1(7)
N3	250(19)	182(17)	220(20)	-76(16)	-17(18)	-37(18)
O1	240(30)	162(18)	170(20)	-51(14)	-10(20)	13(17)
O1A	240(20)	160(40)	180(30)	-60(30)	20(30)	40(40)
O2	256(19)	179(15)	175(16)	-46(12)	8(15)	-2(15)

Table 4 Bond Lengths for 204.

Atom	Atom	Length/Å	Atom	Atom	Length/Å
C1	Au1	2.116(11)	C9	C14	1.36(2)
C1	N1	1.257(17)	C10	C11	1.37(3)
C1	N2	1.258(19)	C11	C12	1.36(2)
C2	C3	1.33(3)	C12	C13	1.37(2)
C2	C4	1.464(18)	C12	C15	1.49(2)
C2	N1	1.40(2)	C13	C14	1.38(2)
C3	C4A	1.44(2)	C15	F1	1.32(2)
C3	N2	1.40(2)	C15	F2	1.31(2)
C4	C5	1.51(2)	C15	F3	1.32(2)
C5	C6	1.50(2)	C16	C17	1.528(19)
C5	N3	1.412(19)	C16	N2	1.49(2)
C6	O1	1.21(2)	C17	C18	1.374(15)
C6	O2	1.394(19)	C17	C22	1.375(14)
C7	O2	1.47(2)	C18	C19	1.389(15)
C4A	C5A	1.51(2)	C19	C20	1.379(14)
C5A	C6A	1.51(2)	C20	C21	1.357(15)
C5A	N3	1.42(2)	C20	C23	1.46(2)
C6A	O1A	1.21(2)	C21	C22	1.382(16)
C6A	O2	1.37(2)	C23	F4	1.31(2)
C7A	O2	1.45(2)	C23	F5	1.34(2)
C8	C9	1.52(2)	C23	F6	1.32(2)
C8	N1	1.48(2)	Au1	Br1	2.395(2)

C9	C10	1.41(2)	

Table 5 Bond Angles for 204

Atom	Atom	Atom	Angle/˚	Atom	Atom	Atom	Angle/˚
N1	C1	Au1	124.7(12)	C9	C14	C13	119.3(16)
N1	C1	N2	113.0(13)	F1	C15	C12	112.2(15)
N2	C1	Au1	122.3(10)	F1	C15	F3	104(2)
C3	C2	C4	123(2)	F2	C15	C12	112.9(19)
C3	C2	N1	105.8(12)	F2	C15	F1	108.0(16)
N1	C2	C4	131(2)	F2	C15	F3	105.4(16)
C2	C3	C4A	122(3)	F3	C15	C12	113.3(15)
C2	C3	N2	106.0(15)	N2	C16	C17	111.9(12)
N2	C3	C4A	132(3)	C18	C17	C16	124.3(11)
C2	C4	C5	126(3)	C18	C17	C22	116.5(13)
C6	C5	C4	107(3)	C22	C17	C16	119.2(13)
N3	C5	C4	113(3)	C17	C18	C19	122.7(13)
N3	C5	C6	104(3)	C20	C19	C18	118.9(14)
O1	C6	C5	127(4)	C19	C20	C23	121.5(13)
O1	C6	O2	116(4)	C21	C20	C19	119.3(13)
O2	C6	C5	116(3)	C21	C20	C23	119.1(12)
C3	C4A	C5A	116(6)	C20	C21	C22	120.8(13)
C4A	C5A	C6A	101(7)	C17	C22	C21	121.7(14)
N3	C5A	C4A	113(6)	F4	C23	C20	113.3(12)
N3	C5A	C6A	140(7)	F4	C23	F5	106.6(16)
O1A	C6A	C5A	130(6)	F4	C23	F6	105.0(17)
O1A	C6A	O2	98(6)	F5	C23	C20	113.1(16)
O2	C6A	C5A	132(8)	F6	C23	C20	114.8(15)
N1	C8	C9	111.8(13)	F6	C23	F5	103.1(13)
C10	C9	C8	117.3(15)	C1	Au1	Br1	178.4(4)
C14	C9	C8	123.5(15)	C1	N1	C2	107.8(13)
C14	C9	C10	119.1(16)	C1	N1	C8	127.7(15)
C11	C10	C9	119.5(16)	C2	N1	C8	124.5(14)

C12	C11	C10	121.9(16)	C1	N2	C3	107.3(14)
C11	C12	C13	117.7(17)	C1	N2	C16	128.1(14)
C11	C12	C15	120.2(16)	C3	N2	C16	124.6(16)
C13	C12	C15	122.1(16)	C6	O2	C7	121(4)
C12	C13	C14	122.4(16)	C6A	O2	C7A	146(7)

Table 6 Torsion Angles for 204

A	B	C	D	Angle/˚	A	B	C	D	Angle/˚
C2	C3	C4A	C5A	-5(9)	C16	C17	C22	C21	179.5(18)
C2	C3	N2	C1	-2(2)	C17	C16	N2	C1	-96.5(19)
C2	C3	N2	C16	179.6(15)	C17	C16	N2	C3	81(2)
C2	C4	C5	C6	58(5)	C17	C18	C19	C20	-4(3)
C2	C4	C5	N3	-56(6)	C18	C17	C22	C21	-1(3)
C3	C2	C4	C5	5(5)	C18	C19	C20	C21	2(3)
C3	C2	N1	C1	2(2)	C18	C19	C20	C23	179.1(18)
C3	C2	N1	C8	-178.3(16)	C19	C20	C21	C22	-1(3)
C3	C4A	C5A	C6A	-80(8)	C19	C20	C23	F4	9(3)
C3	C4A	C5A	N3	78(9)	C19	C20	C23	F5	-113(2)
C4	C2	C3	N2	173(3)	C19	C20	C23	F6	129.6(19)
C4	C2	N1	C1	-170(3)	C20	C21	C22	C17	0(3)
C4	C2	N1	C8	9(4)	C21	C20	C23	F4	-174.1(19)
C4	C5	C6	O1	-143(5)	C21	C20	C23	F5	64(2)
C4	C5	C6	O2	47(5)	C21	C20	C23	F6	-53(2)
C5	C6	O2	C7	173(4)	C22	C17	C18	C19	3(3)
C4A	C3	N2	C1	175(5)	C23	C20	C21	C22	-177.6(19)
C4A	C3	N2	C16	-4(6)	Au1	C1	N1	C2	178.5(10)
C4A	C5A	C6A	O1A	-67(16)	Au1	C1	N1	C8	-1(2)
C4A	C5A	C6A	O2	109(13)	Au1	C1	N2	C3	-178.5(12)
C5A	C6A	O2	C7A	-102(15)	Au1	C1	N2	C16	0(2)
C8	C9	C10	C11	-179.8(19)	N1	C1	N2	C3	3.7(19)
C8	C9	C14	C13	179.4(19)	N1	C1	N2	C16	-178.1(14)
C9	C8	N1	C1	-100.8(18)	N1	C2	C3	C4A	-177(5)

C9	C8	N1	C2	80(2)	N1	C2	C3	N2	0(2)
C9	C10	C11	C12	1(3)	N1	C2	C4	C5	176(3)
C10	C9	C14	C13	-1(3)	N1	C8	C9	C10	-167.7(16)
C10	C11	C12	C13	-1(3)	N1	C8	C9	C14	12(3)
C10	C11	C12	C15	-180(2)	N2	C1	N1	C2	-3.7(18)
C11	C12	C13	C14	1(3)	N2	C1	N1	C8	176.8(14)
C11	C12	C15	F1	-43(3)	N2	C3	C4A	C5A	179(4)
C11	C12	C15	F2	79(2)	N2	C16	C17	C18	13(2)
C11	C12	C15	F3	-161.4(18)	N2	C16	C17	C22	-167.5(16)
C12	C13	C14	C9	0(3)	N3	C5	C6	O1	-23(7)
C13	C12	C15	F1	138(2)	N3	C5	C6	O2	167(3)
C13	C12	C15	F2	-99(2)	N3	C5A	C6A	O1A	147(12)
C13	C12	C15	F3	20(3)	N3	C5A	C6A	O2	-37(22)
C14	C9	C10	C11	1(3)	O1	C6	O2	C7	2(6)
C15	C12	C13	C14	179(2)	O1A	C6A	O2	C7A	74(15)
C16	C17	C18	C19	-177.8(18)					

Table 7 Hydrogen Atom Coordinates (Å×10^4) and Isotropic Displacement Parameters (Å^2×10^3) for 204.

Atom	x	y	z	U(eq)
H2	7396.71	7461.27	6932.15	128
H3	6740.9	8478.4	5326.14	137
H4A	8847.08	7522.88	7267.57	183
H4B	6815.98	7339.91	7775.03	183
H5	7756.13	9087.07	7767.14	230
H7A	1546.7	8224.5	8160.3	344
H7B	2082.5	9483.67	7898.58	344
H7C	2009.61	8870.51	7037.91	344
H4AA	5585.99	9061.12	5079.77	166
H4AB	7688.29	9236.69	4737.15	166
H5A	6625.45	10222.28	5797.74	214
H7AA	3145.67	7410.22	8877.02	260

H7AB	*2133.2*	*7456.86*	*7982.89*	*260*
H7AC	*4013.59*	*6895.34*	*7974.83*	*260*
H8A	*8732.22*	*5412.2*	*7445.74*	*124*
H8B	*8360.44*	*4563.31*	*6820.79*	*124*
H10	*7491.42*	*3837.27*	*8890.36*	*129*
H11	*4978.59*	*3173.87*	*10084.22*	*131*
H13	*1801.29*	*4819.11*	*8349.37*	*131*
H14	*4279.34*	*5529.93*	*7135.86*	*128*
H16A	*5611.25*	*7730.21*	*3832.46*	*107*
H16B	*6159.65*	*6536.56*	*3727.75*	*107*
H18	*10160.02*	*7305.39*	*3947.18*	*121*
H19	*12626.73*	*8130.74*	*2769.53*	*123*
H21	*9407.42*	*8922.04*	*771*	*126*
H22	*6946.88*	*8174.56*	*1973.77*	*130*
H3AA	*8093.92*	*10051.35*	*5867.35*	*260*
H3AB	*9750.64*	*9565.6*	*6209.55*	*260*
H3BC	*9490.07*	*9377.51*	*5921.62*	*260*
H3BD	*8773.8*	*9913.19*	*6765.06*	*260*

Table 8 Atomic Occupancy for 204.

Atom	**Occupancy**	***Atom***	**Occupancy**	***Atom***	**Occupancy**
H2	*0.306(19)*	*H3*	*0.694(19)*	*C4*	*0.694(19)*
H4A	*0.694(19)*	*H4B*	*0.694(19)*	*C5*	*0.694(19)*
H5	*0.694(19)*	*C6*	*0.694(19)*	*C7*	*0.694(19)*
H7A	*0.694(19)*	*H7B*	*0.694(19)*	*H7C*	*0.694(19)*
C4A	*0.306(19)*	*H4AA*	*0.306(19)*	*H4AB*	*0.306(19)*
C5A	*0.306(19)*	*H5A*	*0.306(19)*	*C6A*	*0.306(19)*
C7A	*0.306(19)*	*H7AA*	*0.306(19)*	*H7AB*	*0.306(19)*
H7AC	*0.306(19)*	*H3AA*	*0.694(19)*	*H3AB*	*0.694(19)*
H3BC	*0.306(19)*	*H3BD*	*0.306(19)*	*O1*	*0.694(19)*
O1A	*0.306(19)*				

Crystal structure determination of 204

Crystal Data *for $C_{23}H_{21}AuBrF_6N_3O_2$ (*M *=762.30 g/mol): triclinic, space group P-1 (no. 2),* a *= 7.5064(4) Å,* b *= 12.4524(10) Å,* c *= 13.9383(8) Å,* α *= 77.166(6)°,* β *= 79.151(5)°,* γ *= 89.382(5)°,* V *= 1246.94(14) Å^3, Z = 2,* T *= 100.01(10) K, μ(CuKα) = 13.617 mm^{-1},* Dcalc *= 2.030 g/cm^3, 12785 reflections measured (7.284° ≤ 2Θ ≤ 149.592°), 4915 unique (*R_{int} *= 0.0701,* R_{sigma} *= 0.0591) which were used in all calculations. The final* R_1 *was 0.0764 (I > 2σ(I)) and* wR_2 *was 0.2332 (all data).*

Refinement model description

Number of restraints - 172, number of constraints - unknown.

Details:

1. Fixed Uiso At 1.2 times of: All C(H) groups, All C(H,H) groups, All N(H,H,H,H) groups At 1.5 times of: All C(H,H,H) groups. 2. Restrained distances C4-C2 1.45 with sigma of 0.02 C5-C4 = C6-C5 1.5 with sigma of 0.02 O2-C6 1.35 with sigma of 0.02 O2-C7 1.45 with sigma of 0.02 O1-C6 1.2 with sigma of 0.02 N3-C5 1.4 with sigma of 0.02 C5A-C4A = C6A-C5A 1.5 with sigma of 0.02 C4A-C3 = O2-C7A 1.45 with sigma of 0.02 O2-C6A 1.35 with sigma of 0.02 O1A-C6A 1.2 with sigma of 0.02 N3-C5A 1.4 with sigma of 0.02 C18-C17 = C19-C18 = C20-C19 = C21-C20 = C22-C21 = C22-C17 1.39 with sigma of 0.02. 3. Rigid bond restraints C4, C5, C6, C7, N3, O1, O2, C4A, C5A, C6A, C7A, O1A with sigma for 1-2 distances of 0.01 and sigma for 1-3 distances of 0.014. Uiso/Uaniso restraints and constraintsC2 ≈ C3 ≈ C4 ≈ C5 ≈ C6 ≈ C7 ≈ N3 ≈ O1 ≈ O2≈ C4A ≈ C5A ≈ C6A ≈ C7A ≈ O1A: within 1.7A with sigma of0.04 and sigma for terminal atoms of 0.08. 5. Others Sof(H2)=Sof(C4A)=Sof(H4AA)=Sof(H4AB)=Sof(C5A)=Sof(H5A)=Sof(C6A) =Sof(C7A)= Sof(H7AA)=Sof(H7AB)=Sof(H7AC)=Sof(H3BC)=Sof(H3BD)=Sof(O1A)= 1-

FVAR(1) Sof(H3)=Sof(C4)=Sof(H4A)=Sof(H4B)=Sof(C5)=Sof(H5)=Sof(C6)=Sof(C7)= Sof(H7A)= Sof(H7B)=Sof(H7C)=Sof(H3AA)=Sof(H3AB)=Sof(O1)=FVAR(1). 6.a Ternary CH refined with riding coordinates: C5(H5), C5A(H5A). 6.b Secondary CH2 refined with riding coordinates: C4(H4A,H4B), C4A(H4AA,H4AB), C8(H8A,H8B), C16(H16A,H16B)6.c Me refined with riding coordinates: C7(H7A,H7B,H7C), C7A(H7AA,H7AB,H7AC)6.d Aromatic/amide H refined with riding coordinates: C2(H2), C3(H3), C10(H10), C11(H11), C13(H13), C14(H14), C18(H18), C19(H19),

C21(H21), C22(H22). 6.e X=CH2 refined with riding coordinates: N3(H3AA,H3AB), N3(H3BC,H3BD).

7.9 - Crystal structure of 233:

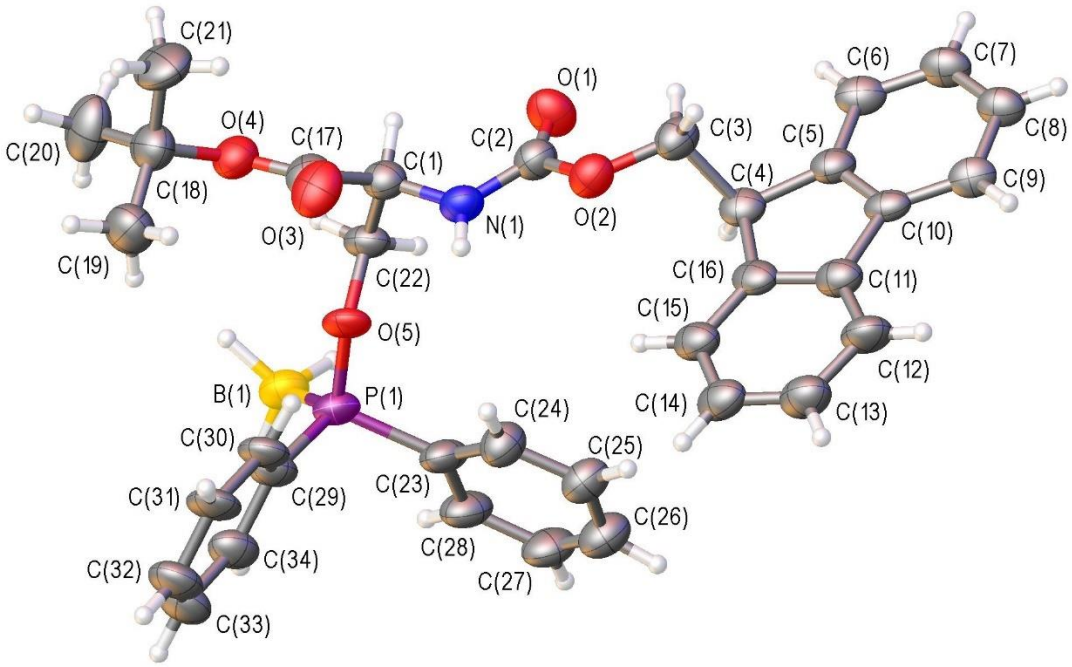

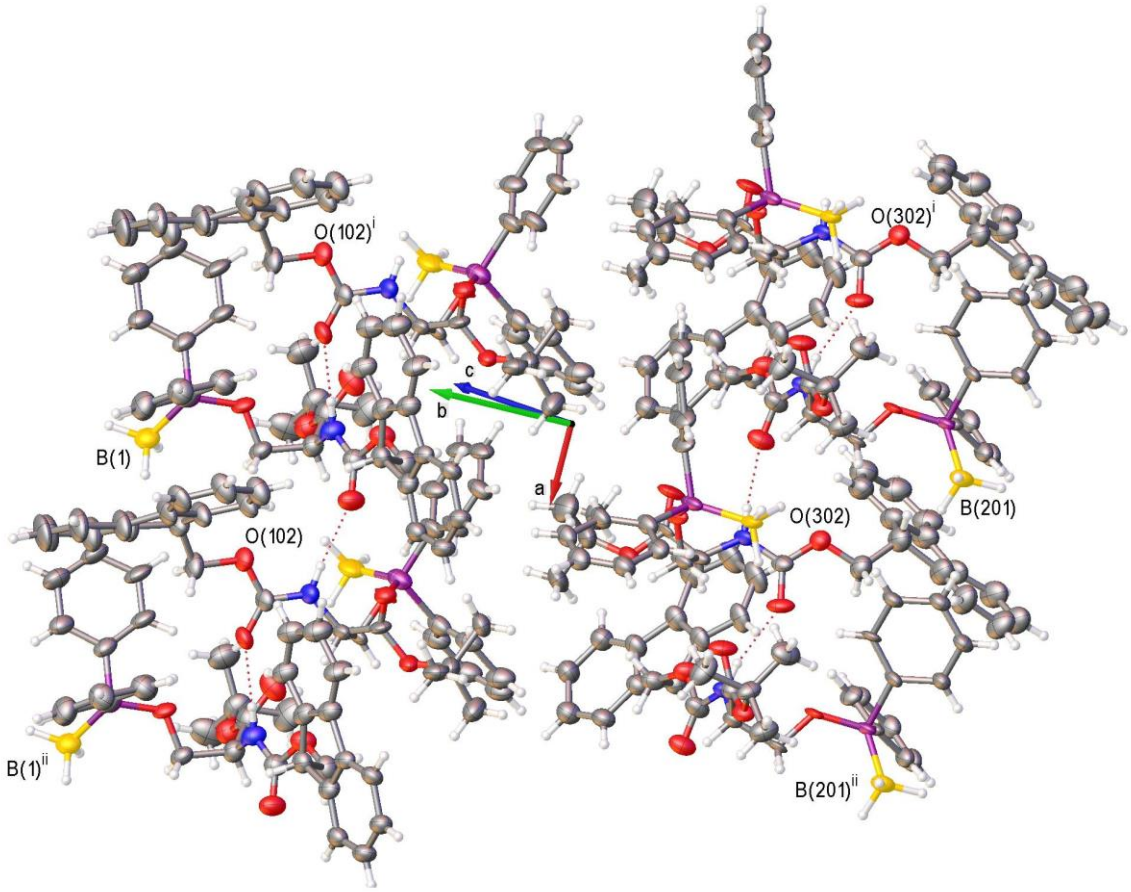

Figure 84: *Hydrogen bonding motifs in the crystal structure of 233 with ellipsoids drawn at the 50 % probability level. The structure contains four crystallographically-independent molecules. Molecules 1 and 2 and molecules 3 and 4 form ladders via N-H…O hydrogen bonding (shown as red dotted lines) in the a direction. Symmetry codes used for generating equivalent atoms, (i) -1+x, y, z and (ii) 1+x, y, z.*

Table 1 Crystal data and structure refinement for 233

Identification code	*AIA-495*
Empirical formula	*$C_{34}H_{37}BNO_5P$*
Formula weight	*581.42*
Temperature/K	*100.00(10)*
Crystal system	*monoclinic*
Space group	*$P2_1$*
a/Å	*9.1480(4)*
b/Å	*23.8115(7)*
c/Å	*29.7987(15)*
α/°	*90*

β/°	*91.526(4)*
γ/°	*90*
Volume/Å^3	*6488.7(5)*
Z	*8*
ρ_{calc}g/cm^3	*1.190*
μ/mm^{-1}	*1.072*
F(000)	*2464.0*
Crystal size/mm^3	*0.422 × 0.178 × 0.082*
Radiation	*CuKα (λ = 1.54184)*
2Θ range for data collection/°	*7 to 149.902*
Index ranges	*-8 ≤ h ≤ 11, -29 ≤ k ≤ 29, -37 ≤ l ≤ 37*
Reflections collected	*35635*
Independent reflections	*35635 [R_{int} = ?, R_{sigma} = 0.0349]*
Data/restraints/parameters	*35635/1638/1562*
Goodness-of-fit on F^2	*1.064*
Final R indexes [I>=2σ (I)]	*R_1 = 0.1100, wR_2 = 0.2978*
Final R indexes [all data]	*R_1 = 0.1248, wR_2 = 0.3087*
Largest diff. peak/hole / e Å^{-3}	*0.72/-0.68*
Flack parameter	*0.03(2)*

Table 2 Fractional Atomic Coordinates (×10^4) and Equivalent Isotropic Displacement Parameters (Å^2×10^3) for 233. U_{eq} is defined as 1/3 of of the trace of the orthogonalised U_{IJ} tensor.

Atom	x	y	z	U(eq)
C1	*5939(17)*	*7141(6)*	*9047(4)*	*46(2)*
C2	*5912(17)*	*7188(6)*	*8242(4)*	*46(2)*
C3	*5492(18)*	*7142(6)*	*7452(4)*	*51(3)*
C4	*5450(16)*	*7709(5)*	*7220(5)*	*44(2)*
C5	*5988(16)*	*7639(6)*	*6741(5)*	*44(2)*
C6	*7392(16)*	*7449(6)*	*6613(5)*	*47(2)*
C7	*7610(16)*	*7402(7)*	*6155(5)*	*50(3)*

C8	6540(16)	7546(6)	5840(5)	48(2)
C9	5138(15)	7737(6)	5974(5)	44(2)
C10	4925(14)	7788(5)	6432(4)	40(2)
C11	3581(17)	7975(6)	6674(5)	49(2)
C12	2252(19)	8155(7)	6505(6)	59(3)
C13	1220(20)	8318(8)	6824(6)	63(3)
C14	1538(18)	8291(7)	7284(5)	56(3)
C15	2853(18)	8098(6)	7435(5)	51(3)
C16	3939(17)	7933(5)	7133(5)	47(2)
C17	4949(18)	6813(6)	9340(5)	50(2)
C18	4720(20)	6364(8)	10071(5)	62(3)
C19	3300(20)	6638(9)	10191(6)	74(4)
C20	5800(20)	6356(11)	10465(6)	83(5)
C21	4550(30)	5770(8)	9880(7)	87(5)
C22	6514(16)	7669(6)	9282(5)	45(2)
C23	5346(18)	9072(6)	9122(5)	50(2)
C24	4583(19)	8916(7)	8734(5)	55(3)
C25	4529(18)	9273(7)	8365(5)	54(3)
C26	5140(20)	9806(7)	8406(6)	62(3)
C27	5910(20)	9969(7)	8778(6)	63(3)
C28	6010(20)	9610(6)	9147(5)	59(3)
C29	3836(17)	8653(7)	9881(5)	49(2)
C30	2677(17)	8284(7)	9800(5)	52(3)
C31	1358(19)	8333(7)	10021(5)	60(3)
C32	1120(20)	8777(8)	10313(6)	64(3)
C33	2190(20)	9159(8)	10395(5)	64(3)
C34	3526(17)	9103(7)	10179(5)	54(3)
B1	7110(20)	8732(8)	9987(6)	53(3)
N1	5233(13)	7275(5)	8628(4)	46(2)
O1	7182(12)	7124(5)	8198(3)	58(3)
O2	4906(11)	7182(4)	7894(3)	51(2)

O3	3693(14)	6678(5)	9209(4)	66(3)
O4	5503(12)	6699(4)	9733(3)	53(2)
O5	5268(10)	7981(4)	9403(3)	44.0(18)
P1	5456(4)	8611.5(15)	9604.0(12)	45.6(7)
C101	11286(14)	6891(6)	8058(5)	44(2)
C102	10950(16)	7767(5)	8462(4)	43(2)
C103	10470(20)	8668(6)	8735(5)	55(3)
C104	9283(19)	9074(6)	8706(5)	57(3)
C105	9770(20)	9643(6)	8871(6)	68(3)
C106	10360(30)	9783(8)	9290(7)	81(4)
C107	10660(30)	10327(8)	9383(8)	90(4)
C108	10640(30)	10728(8)	9020(7)	88(4)
C109	10060(20)	10617(7)	8587(7)	81(4)
C110	9730(20)	10054(6)	8514(6)	68(3)
C111	8925(19)	9800(6)	8119(6)	58(3)
C112	8345(19)	10017(7)	7719(6)	61(3)
C113	7640(20)	9687(7)	7412(6)	67(3)
C114	7470(20)	9104(7)	7499(6)	64(3)
C115	8033(18)	8865(6)	7901(6)	58(3)
C116	8740(18)	9208(6)	8222(6)	56(3)
C117	10773(14)	6763(6)	7590(5)	46(2)
C118	11365(17)	6165(7)	6944(6)	58(3)
C119	11580(17)	6648(8)	6609(6)	63(3)
C120	12480(20)	5705(9)	6900(6)	72(4)
C121	9825(18)	5913(7)	6903(6)	58(3)
C122	11344(14)	6380(6)	8366(5)	47(2)
C123	7489(15)	5615(7)	8472(5)	58(2)
C124	6320(15)	5491(7)	8742(6)	63(3)
C125	4868(16)	5447(7)	8553(6)	64(3)
C126	4674(16)	5510(7)	8108(6)	63(3)
C127	5813(15)	5638(7)	7824(6)	63(3)

C128	7174(16)	5699(7)	8005(6)	63(3)
C129	10440(17)	5070(6)	8566(5)	55(2)
C130	10646(17)	4956(6)	8136(6)	59(3)
C131	11510(19)	4452(7)	8040(6)	66(3)
C132	11945(18)	4116(8)	8393(6)	66(3)
C133	11709(18)	4266(7)	8836(6)	66(3)
C134	10922(18)	4750(7)	8922(6)	62(3)
B101	9460(20)	5900(9)	9304(7)	66(4)
N101	10381(13)	7335(4)	8242(4)	45(2)
O101	12288(11)	7842(4)	8552(3)	47(2)
O102	9866(11)	8128(4)	8566(3)	48.5(19)
O103	9719(10)	6971(4)	7404(3)	49(2)
O104	11637(10)	6373(5)	7410(3)	53(2)
O105	9881(9)	6153(4)	8336(4)	47.5(19)
P101	9339(4)	5704.4(17)	8689.4(15)	55.7(9)
C201	707(14)	2737(5)	5993(4)	36.1(19)
C202	726(16)	2601(7)	6791(5)	48(2)
C203	372(16)	2642(6)	7588(5)	47(2)
C204	326(17)	2091(6)	7839(5)	48(2)
C205	746(16)	2211(6)	8322(5)	46(2)
C206	2050(16)	2428(7)	8492(5)	51(3)
C207	2227(19)	2555(8)	8944(5)	59(3)
C208	1016(18)	2466(7)	9222(5)	58(3)
C209	-266(18)	2248(7)	9059(5)	55(3)
C210	-398(17)	2127(6)	8609(5)	49(2)
C211	-1593(18)	1893(6)	8331(5)	52(2)
C212	-3046(19)	1714(7)	8450(6)	61(3)
C213	-3910(20)	1504(8)	8131(6)	73(3)
C214	-3560(20)	1457(7)	7688(6)	69(3)
C215	-2217(19)	1645(6)	7562(5)	56(3)
C216	-1209(17)	1864(6)	7887(5)	48(2)

C217	-250(14)	3108(6)	5711(4)	40(2)
C218	-489(16)	3518(6)	4957(4)	46(2)
C219	-740(20)	4117(7)	5098(5)	65(4)
C220	570(19)	3480(7)	4580(5)	59(4)
C221	-1932(19)	3228(9)	4841(5)	65(4)
C222	1155(12)	2212(5)	5745(4)	35(2)
C223	-112(13)	847(5)	5773(5)	38.7(19)
C224	-894(16)	970(6)	6165(5)	47(2)
C225	-848(17)	561(6)	6508(5)	51(3)
C226	-176(18)	60(6)	6448(5)	53(3)
C227	616(17)	-48(6)	6061(5)	52(3)
C228	532(15)	348(5)	5732(5)	47(2)
C229	-1919(12)	1379(5)	5074(4)	37.6(19)
C230	-2269(14)	998(6)	4708(5)	43(2)
C231	-3646(14)	1007(6)	4497(5)	46(2)
C232	-4712(14)	1372(6)	4641(5)	47(2)
C233	-4373(14)	1754(6)	4991(5)	42(2)
C234	-3033(11)	1736(5)	5210(4)	35(2)
B201	1368(18)	1273(8)	4920(6)	55(4)
N201	-76(12)	2601(5)	6409(3)	42(2)
O201	2010(11)	2622(5)	6852(3)	55(2)
O202	-229(11)	2573(5)	7138(3)	54(2)
O203	-1456(10)	3290(5)	5829(3)	55(2)
O204	301(9)	3198(4)	5315(3)	40.1(17)
O205	-174(8)	1954(3)	5574(3)	35.9(16)
P201	-134(3)	1363.9(13)	5325.1(11)	36.8(6)
C301	6133(13)	2873(5)	7079(5)	44(2)
C302	5619(14)	2078(5)	6597(4)	40(2)
C303	5084(18)	1242(6)	6241(5)	51(3)
C304	3930(20)	822(6)	6201(6)	59(3)
C305	4580(20)	281(7)	5989(6)	65(3)

C306	5190(20)	224(7)	5568(6)	73(3)
C307	5680(20)	-294(7)	5451(7)	76(3)
C308	5470(20)	-742(8)	5723(7)	76(3)
C309	4910(20)	-695(7)	6153(7)	74(3)
C310	4537(19)	-183(6)	6295(6)	63(3)
C311	3749(19)	29(7)	6702(6)	63(3)
C312	3297(19)	-270(8)	7075(6)	65(3)
C313	2630(20)	11(9)	7411(6)	70(3)
C314	2330(20)	573(9)	7371(6)	68(3)
C315	2773(19)	884(7)	6987(6)	61(3)
C316	3422(18)	603(7)	6653(6)	59(3)
C317	5650(13)	3071(5)	7534(5)	43(2)
C318	6536(19)	3590(8)	8200(6)	67(3)
C319	8100(20)	3721(10)	8347(8)	86(5)
C320	5790(30)	4131(9)	8062(9)	95(5)
C321	5890(20)	3241(9)	8537(6)	73(4)
C322	6332(14)	3382(5)	6770(6)	48(2)
C323	2632(16)	4120(5)	6396(6)	52(2)
C324	1879(17)	3931(6)	6767(6)	57(3)
C325	479(18)	4085(7)	6840(6)	63(3)
C326	-269(18)	4399(7)	6536(6)	62(3)
C327	431(18)	4625(6)	6172(6)	61(3)
C328	1832(17)	4448(6)	6101(6)	56(3)
C329	5359(16)	4535(6)	6172(5)	49(2)
C330	5565(16)	4929(6)	6518(5)	49(3)
C331	6359(16)	5403(6)	6462(5)	51(3)
C332	6906(18)	5511(6)	6036(6)	55(3)
C333	6747(17)	5132(6)	5697(6)	54(3)
C334	5957(16)	4646(6)	5755(5)	50(2)
B301	4438(17)	3374(8)	5791(7)	58(4)
N301	5165(11)	2474(4)	6885(4)	40(2)

O301	6916(10)	2049(4)	6479(3)	49(2)
O302	4606(10)	1734(4)	6467(3)	44.9(18)
O303	4439(10)	3015(5)	7657(4)	62(3)
O304	6739(11)	3287(5)	7771(4)	56(2)
O305	4963(10)	3663(3)	6735(4)	49.0(18)
P301	4387(4)	3891.2(14)	6265.5(14)	49.0(8)

Table 3 Anisotropic Displacement Parameters ($Å^2×10^3$) for 233. The Anisotropic displacement factor exponent takes the form: $-2π^2[h^2a^{*2}U_{11}+2hka^*b^*U_{12}+…]$.

Atom	U_{11}	U_{22}	U_{33}	U_{23}	U_{13}	U_{12}
C1	48(5)	37(5)	54(4)	1(4)	6(4)	0(4)
C2	43(5)	44(6)	52(4)	6(5)	2(4)	2(5)
C3	57(6)	42(5)	53(4)	4(4)	-3(5)	-1(5)
C4	44(5)	30(5)	59(4)	0(4)	4(4)	-6(4)
C5	43(5)	30(5)	59(4)	2(4)	5(4)	1(4)
C6	36(5)	36(6)	70(5)	-3(5)	2(4)	-5(5)
C7	32(5)	47(6)	72(6)	-1(5)	10(4)	0(5)
C8	36(5)	43(6)	64(5)	-2(5)	10(4)	-1(5)
C9	30(5)	39(5)	63(5)	1(5)	1(4)	-6(4)
C10	33(4)	24(4)	63(4)	3(4)	7(4)	0(4)
C11	45(5)	38(5)	66(4)	6(5)	12(4)	2(4)
C12	51(6)	52(7)	76(6)	9(6)	10(5)	20(5)
C13	53(6)	57(7)	79(6)	13(6)	14(5)	12(6)
C14	51(6)	44(6)	75(5)	17(5)	16(5)	5(5)
C15	50(6)	39(6)	66(5)	10(5)	16(4)	5(5)
C16	51(5)	27(5)	63(4)	4(4)	15(4)	0(4)
C17	61(6)	33(5)	57(5)	2(4)	3(5)	-8(5)
C18	71(7)	55(6)	62(6)	10(5)	18(5)	2(6)
C19	72(9)	80(11)	72(9)	8(8)	21(7)	14(8)
C20	70(9)	107(13)	74(8)	35(8)	10(7)	-12(10)

C21	117(15)	40(6)	104(11)	16(6)	21(10)	3(7)
C22	40(6)	34(5)	61(5)	0(4)	12(4)	7(4)
C23	56(6)	35(4)	61(4)	1(4)	-1(4)	14(5)
C24	62(7)	46(5)	57(5)	5(4)	-2(5)	-2(5)
C25	50(7)	48(6)	64(5)	10(5)	-4(5)	0(5)
C26	65(8)	45(6)	75(6)	11(5)	-3(6)	0(6)
C27	75(8)	35(5)	78(6)	1(5)	-1(6)	6(5)
C28	72(8)	35(5)	70(6)	-5(4)	-4(6)	10(5)
C29	44(4)	44(5)	59(5)	-5(4)	4(4)	17(4)
C30	44(5)	43(6)	71(6)	-5(5)	16(5)	18(4)
C31	48(6)	53(6)	80(7)	-6(5)	19(5)	25(5)
C32	55(6)	64(7)	76(7)	-11(6)	20(6)	21(5)
C33	56(7)	69(7)	70(7)	-11(6)	18(5)	14(5)
C34	42(6)	57(6)	63(6)	-6(5)	1(5)	15(5)
B1	43(6)	48(9)	67(8)	3(6)	1(5)	9(6)
N1	40(5)	43(5)	55(4)	6(4)	6(4)	9(4)
O1	40(4)	73(7)	62(5)	-4(5)	7(4)	5(5)
O2	42(5)	52(5)	58(4)	10(4)	4(3)	2(4)
O3	65(6)	58(7)	74(6)	13(5)	-5(5)	-22(6)
O4	58(5)	43(4)	59(4)	7(4)	5(4)	1(4)
O5	31(4)	37(4)	65(4)	0(3)	9(3)	14(3)
P1	42.1(19)	35.1(16)	59.6(17)	0.4(13)	0.9(14)	10.1(14)
C101	22(5)	33(4)	77(5)	-9(4)	6(4)	-6(4)
C102	44(5)	22(4)	61(5)	3(4)	-1(5)	-6(4)
C103	67(7)	27(4)	71(6)	-6(5)	-13(5)	0(5)
C104	59(6)	30(4)	81(5)	-2(4)	-9(5)	1(4)
C105	79(7)	32(4)	92(6)	-7(4)	-19(6)	-2(5)
C106	101(9)	43(6)	98(7)	-8(5)	-25(7)	-8(7)
C107	110(10)	48(6)	110(8)	-14(6)	-25(8)	-24(7)
C108	109(10)	34(6)	120(8)	-12(5)	-28(8)	-28(7)
C109	97(9)	30(5)	115(8)	-12(5)	-28(7)	-8(6)

C110	76(7)	26(4)	100(6)	-5(4)	-23(6)	-12(5)
C111	53(6)	27(4)	93(6)	1(4)	-13(5)	-15(5)
C112	58(7)	38(6)	87(6)	11(5)	-4(6)	-23(5)
C113	72(8)	44(6)	85(7)	17(5)	-16(6)	-17(6)
C114	65(7)	40(6)	85(6)	10(5)	-16(6)	-13(6)
C115	52(7)	31(5)	90(6)	7(5)	-19(6)	-13(5)
C116	49(6)	26(4)	90(6)	1(4)	-17(5)	-6(4)
C117	22(5)	40(5)	77(5)	-11(4)	10(4)	10(4)
C118	38(6)	47(6)	88(6)	-28(5)	-3(6)	0(5)
C119	30(7)	64(8)	95(8)	-15(6)	13(7)	4(6)
C120	60(8)	67(9)	89(10)	-30(7)	-8(8)	18(8)
C121	45(7)	50(8)	80(9)	-22(6)	-5(6)	-11(6)
C122	23(5)	31(5)	87(6)	-5(5)	-5(5)	-11(4)
C123	29(4)	39(5)	105(6)	2(5)	-5(4)	-11(4)
C124	33(5)	45(6)	111(7)	1(6)	4(5)	10(5)
C125	29(5)	47(6)	115(7)	-9(6)	6(6)	17(5)
C126	27(5)	46(6)	115(7)	-11(6)	-1(5)	10(5)
C127	31(5)	50(6)	107(7)	-2(6)	-12(5)	-7(5)
C128	29(5)	53(7)	107(6)	4(6)	-10(5)	-13(5)
C129	36(5)	37(4)	91(5)	8(4)	-10(5)	-7(4)
C130	33(6)	47(6)	96(6)	13(5)	2(6)	-2(5)
C131	44(7)	55(7)	100(7)	13(5)	8(6)	8(5)
C132	42(7)	52(6)	104(7)	11(6)	0(6)	6(6)
C133	38(6)	58(6)	101(6)	19(6)	3(6)	5(5)
C134	40(6)	50(6)	96(6)	12(5)	-1(6)	-2(5)
B101	29(8)	69(11)	101(6)	-9(7)	-13(7)	10(8)
N101	36(5)	28(4)	73(5)	-8(4)	5(4)	-5(4)
O101	40(4)	35(5)	64(5)	-9(4)	-6(4)	-12(4)
O102	53(5)	26(4)	66(5)	-4(3)	-1(4)	-1(3)
O103	30(5)	44(5)	74(5)	-11(4)	3(4)	7(4)
O104	26(4)	46(5)	85(5)	-24(4)	-6(4)	8(4)

O105	11(3)	28(3)	103(5)	0(4)	-8(4)	-8(3)
P101	34.2(19)	43.6(18)	89(2)	4.9(17)	-3.8(16)	-4.6(15)
C201	22(4)	34(4)	53(4)	-1(3)	4(4)	-7(4)
C202	36(5)	55(6)	54(4)	4(5)	4(4)	-11(5)
C203	34(5)	49(6)	59(4)	5(4)	6(5)	0(5)
C204	43(5)	41(5)	60(4)	-1(4)	1(4)	-2(4)
C205	38(5)	39(5)	61(4)	2(4)	0(4)	-3(4)
C206	32(5)	51(6)	71(5)	-3(5)	-1(4)	0(5)
C207	45(6)	59(7)	71(6)	-6(6)	0(5)	-3(6)
C208	48(6)	56(7)	70(6)	-13(6)	3(4)	-8(6)
C209	46(6)	52(6)	67(5)	-7(5)	7(5)	-6(5)
C210	43(5)	40(5)	62(4)	3(4)	0(4)	-12(5)
C211	55(5)	40(5)	63(4)	5(5)	1(4)	-16(5)
C212	58(6)	51(7)	72(6)	12(5)	3(5)	-20(6)
C213	74(7)	58(7)	87(6)	13(6)	-4(5)	-36(6)
C214	76(7)	47(7)	83(6)	8(6)	-9(6)	-33(6)
C215	68(7)	35(6)	66(5)	5(5)	-6(5)	-25(5)
C216	52(5)	29(5)	62(4)	4(4)	0(4)	-15(4)
C217	32(5)	35(5)	54(4)	0(4)	0(4)	1(4)
C218	39(5)	48(6)	52(5)	1(4)	2(4)	16(5)
C219	91(11)	43(6)	59(7)	9(5)	10(7)	21(7)
C220	54(8)	61(9)	63(6)	9(6)	12(6)	16(7)
C221	48(7)	86(10)	59(8)	4(7)	-8(5)	4(7)
C222	9(4)	35(5)	61(5)	-2(4)	1(4)	-9(3)
C223	14(4)	29(4)	73(5)	-7(3)	0(4)	-1(4)
C224	41(6)	29(5)	70(5)	1(4)	4(5)	11(5)
C225	42(6)	34(5)	77(6)	5(4)	6(5)	4(5)
C226	49(7)	30(5)	80(6)	5(5)	-3(5)	-1(5)
C227	46(6)	29(5)	82(6)	-7(4)	-4(5)	-2(5)
C228	35(6)	28(4)	77(6)	-8(4)	-2(5)	-1(4)
C229	19(4)	24(4)	69(5)	-4(4)	-6(3)	-7(4)

C230	25(5)	36(5)	67(6)	-12(4)	0(4)	-5(4)
C231	26(5)	47(6)	64(6)	-10(5)	-5(4)	-6(4)
C232	25(5)	46(5)	70(6)	-6(5)	-5(4)	-3(5)
C233	19(4)	39(5)	69(6)	-3(4)	-4(4)	-5(4)
C234	8(4)	33(5)	64(5)	0(4)	1(4)	-5(4)
B201	26(6)	57(10)	83(9)	-10(7)	11(6)	-8(7)
N201	23(4)	50(5)	52(4)	3(4)	4(3)	-3(4)
O201	33(4)	69(7)	62(5)	6(5)	-5(4)	-4(5)
O202	39(4)	68(5)	56(4)	8(4)	11(3)	0(4)
O203	24(4)	73(7)	69(5)	7(5)	3(4)	11(4)
O204	28(4)	36(4)	56(4)	5(3)	2(3)	4(3)
O205	7(3)	31(3)	70(4)	-5(3)	-2(3)	-3(3)
P201	12.7(13)	27.9(13)	69.8(17)	-3.2(12)	1.9(12)	-4.3(11)
C301	18(5)	29(4)	86(5)	0(4)	-3(4)	-1(4)
C302	27(4)	29(4)	65(5)	5(4)	1(4)	5(4)
C303	55(6)	37(5)	63(6)	-2(4)	8(5)	1(4)
C304	60(6)	39(4)	78(5)	0(4)	9(5)	-5(4)
C305	68(7)	39(4)	89(6)	-2(4)	19(5)	-11(5)
C306	87(8)	42(5)	90(7)	1(5)	22(6)	-4(6)
C307	85(9)	44(6)	100(8)	3(5)	24(7)	8(6)
C308	75(8)	45(6)	109(8)	2(6)	27(7)	-6(6)
C309	70(8)	42(5)	111(7)	9(5)	23(7)	-7(6)
C310	54(6)	38(4)	98(6)	4(4)	19(5)	-13(5)
C311	52(6)	45(5)	92(6)	11(4)	13(5)	-5(5)
C312	48(7)	58(6)	88(7)	20(5)	5(5)	9(6)
C313	58(7)	70(7)	82(7)	19(6)	9(6)	8(6)
C314	57(8)	66(7)	80(6)	6(6)	8(6)	0(6)
C315	49(7)	50(6)	83(6)	0(5)	12(5)	-5(5)
C316	46(6)	45(5)	86(6)	4(4)	14(5)	-4(5)
C317	15(4)	27(5)	88(5)	-5(4)	-1(4)	-14(4)
C318	48(6)	48(6)	104(7)	-30(5)	1(6)	-11(5)

C319	49(8)	81(12)	128(12)	-49(10)	-1(7)	-22(7)
C320	83(12)	48(8)	155(15)	-24(8)	11(11)	5(8)
C321	62(10)	70(9)	86(8)	-29(7)	2(7)	-14(8)
C322	20(5)	26(5)	98(6)	1(5)	0(5)	-8(4)
C323	32(4)	22(4)	102(6)	-4(4)	4(4)	11(4)
C324	39(5)	29(5)	102(6)	-5(5)	9(5)	14(5)
C325	47(6)	43(6)	101(7)	-10(5)	13(5)	20(5)
C326	38(6)	41(6)	108(7)	-12(5)	-3(5)	9(5)
C327	44(6)	34(5)	104(7)	-13(5)	-2(5)	20(5)
C328	37(5)	34(5)	96(6)	-12(5)	-4(5)	15(4)
C329	34(5)	29(4)	86(5)	-2(4)	-3(4)	-5(4)
C330	34(6)	33(5)	78(6)	-2(4)	-5(5)	-11(4)
C331	42(6)	30(5)	81(6)	-2(5)	-8(5)	-5(5)
C332	47(6)	35(5)	83(6)	1(5)	-2(5)	-2(5)
C333	38(6)	43(6)	81(6)	-1(5)	0(5)	-6(5)
C334	37(6)	33(5)	78(6)	-4(4)	-3(5)	4(4)
B301	15(6)	47(8)	112(8)	-23(7)	10(7)	-2(6)
N301	21(4)	25(4)	75(5)	-2(3)	10(4)	-7(3)
O301	23(4)	55(6)	71(5)	10(4)	9(4)	11(4)
O302	40(4)	35(4)	60(4)	-2(3)	4(4)	2(3)
O303	14(4)	87(8)	86(6)	-7(6)	-3(4)	-8(5)
O304	28(4)	46(5)	93(5)	-18(4)	1(4)	-9(4)
O305	27(4)	19(3)	102(5)	8(3)	6(4)	-3(3)
P301	17.2(14)	26.4(14)	103(2)	-4.1(15)	1.9(15)	-3.2(12)

Table 4 Bond Lengths for 233.

Atom	Atom	Length/Å	Atom	Atom	Length/Å
C1	C17	1.49(2)	C201	C217	1.487(18)
C1	C22	1.52(2)	C201	C222	1.515(17)
C1	N1	1.428(18)	C201	N201	1.484(16)

C2	N1	1.336(18)	C202	N201	1.338(18)
C2	O1	1.182(18)	C202	O201	1.185(17)
C2	O2	1.368(18)	C202	O202	1.374(17)
C3	C4	1.517(19)	C203	C204	1.511(19)
C3	O2	1.441(17)	C203	O202	1.443(17)
C4	C5	1.531(19)	C204	C205	1.508(19)
C4	C16	1.50(2)	C204	C216	1.52(2)
C5	C6	1.42(2)	C205	C206	1.38(2)
C5	C10	1.37(2)	C205	C210	1.38(2)
C6	C7	1.39(2)	C206	C207	1.38(2)
C7	C8	1.38(2)	C207	C208	1.42(2)
C8	C9	1.43(2)	C208	C209	1.36(2)
C9	C10	1.388(19)	C209	C210	1.37(2)
C10	C11	1.509(19)	C210	C211	1.46(2)
C11	C12	1.37(2)	C211	C212	1.45(2)
C11	C16	1.40(2)	C211	C216	1.38(2)
C12	C13	1.41(2)	C212	C213	1.32(2)
C13	C14	1.40(2)	C213	C214	1.37(3)
C14	C15	1.35(2)	C214	C215	1.37(2)
C15	C16	1.41(2)	C215	C216	1.42(2)
C17	O3	1.246(19)	C217	O203	1.244(16)
C17	O4	1.292(17)	C217	O204	1.314(16)
C18	C19	1.50(3)	C218	C219	1.51(2)
C18	C20	1.52(3)	C218	C220	1.50(2)
C18	C21	1.53(3)	C218	C221	1.52(2)
C18	O4	1.486(18)	C218	O204	1.483(16)
C22	O5	1.415(15)	C222	O205	1.443(13)
C23	C24	1.38(2)	C223	C224	1.416(19)
C23	C28	1.42(2)	C223	C228	1.333(18)
C23	P1	1.808(14)	C223	P201	1.815(14)
C24	C25	1.39(2)	C224	C225	1.41(2)

C25	C26	1.39(2)	C225	C226	1.36(2)
C26	C27	1.35(2)	C226	C227	1.40(2)
C27	C28	1.40(2)	C227	C228	1.36(2)
C29	C30	1.39(2)	C229	C230	1.448(17)
C29	C34	1.43(2)	C229	C234	1.396(17)
C29	P1	1.719(15)	C229	P201	1.778(12)
C30	C31	1.39(2)	C230	C231	1.393(19)
C31	C32	1.39(2)	C231	C232	1.38(2)
C32	C33	1.35(3)	C232	C233	1.413(19)
C33	C34	1.40(2)	C233	C234	1.374(17)
B1	P1	1.895(18)	B201	P201	1.866(16)
O5	P1	1.625(10)	O205	P201	1.590(9)
C101	C117	1.49(2)	C301	C317	1.51(2)
C101	C122	1.52(2)	C301	C322	1.537(19)
C101	N101	1.459(17)	C301	N301	1.411(16)
C102	N101	1.318(17)	C302	N301	1.350(17)
C102	O101	1.259(17)	C302	O301	1.248(15)
C102	O102	1.355(17)	C302	O302	1.287(16)
C103	C104	1.45(2)	C303	C304	1.46(2)
C103	O102	1.482(16)	C303	O302	1.426(16)
C104	C105	1.51(2)	C304	C305	1.56(2)
C104	C116	1.54(2)	C304	C316	1.53(2)
C105	C106	1.39(3)	C305	C306	1.40(3)
C105	C110	1.44(2)	C305	C310	1.43(2)
C106	C107	1.35(3)	C306	C307	1.36(2)
C107	C108	1.44(3)	C307	C308	1.36(3)
C108	C109	1.41(3)	C308	C309	1.40(3)
C109	C110	1.39(2)	C309	C310	1.34(2)
C110	C111	1.50(2)	C310	C311	1.51(2)
C111	C112	1.39(2)	C311	C312	1.39(2)
C111	C116	1.453(19)	C311	C316	1.41(2)

C112 C113	1.36(2)	C312 C313	1.36(3)
C113 C114	1.42(2)	C313 C314	1.37(3)
C114 C115	1.41(2)	C314 C315	1.43(2)
C115 C116	1.40(2)	C315 C316	1.35(2)
C117 O103	1.207(17)	C317 O303	1.184(16)
C117 O104	1.341(15)	C317 O304	1.311(16)
C118 C119	1.54(3)	C318 C319	1.52(2)
C118 C120	1.51(2)	C318 C320	1.51(3)
C118 C121	1.53(2)	C318 C321	1.44(3)
C118 O104	1.491(18)	C318 O304	1.486(19)
C122 O105	1.444(14)	C322 O305	1.420(16)
C123 C124	1.39(2)	C323 C324	1.39(2)
C123 C128	1.43(2)	C323 C328	1.37(2)
C123 P101	1.808(15)	C323 P301	1.749(14)
C124 C125	1.432(19)	C324 C325	1.36(2)
C125 C126	1.34(2)	C325 C326	1.35(2)
C126 C127	1.39(2)	C326 C327	1.38(3)
C127 C128	1.351(18)	C327 C328	1.37(2)
C129 C130	1.328(19)	C329 C330	1.40(2)
C129 C134	1.370(19)	C329 C334	1.40(2)
C129 P101	1.857(16)	C329 P301	1.798(14)
C130 C131	1.47(2)	C330 C331	1.354(19)
C131 C132	1.37(2)	C331 C332	1.40(2)
C132 C133	1.39(2)	C332 C333	1.36(2)
C133 C134	1.39(2)	C333 C334	1.38(2)
B101 P101	1.89(2)	B301 P301	1.875(18)
O105 P101	1.590(10)	O305 P301	1.580(11)

Table 5 Bond Angles for 233.

Atom	Atom	Atom	Angle/˚	Atom	Atom	Atom	Angle/˚
C17	C1	C22	111.8(11)	C217	C201	C222	112.2(10)
N1	C1	C17	111.2(13)	N201	C201	C217	108.1(10)
N1	C1	C22	111.1(11)	N201	C201	C222	111.6(10)
N1	C2	O2	109.5(12)	N201	C202	O202	107.2(12)
O1	C2	N1	126.7(13)	O201	C202	N201	130.6(13)
O1	C2	O2	123.8(12)	O201	C202	O202	122.2(12)
O2	C3	C4	110.6(12)	O202	C203	C204	110.2(12)
C3	C4	C5	108.8(11)	C203	C204	C216	113.3(12)
C16	C4	C3	114.0(12)	C205	C204	C203	107.3(12)
C16	C4	C5	101.3(11)	C205	C204	C216	100.9(11)
C6	C5	C4	126.8(13)	C206	C205	C204	128.0(13)
C10	C5	C4	111.0(12)	C210	C205	C204	112.7(13)
C10	C5	C6	122.1(13)	C210	C205	C206	119.2(13)
C7	C6	C5	116.3(13)	C205	C206	C207	120.9(14)
C8	C7	C6	122.0(14)	C206	C207	C208	117.6(15)
C7	C8	C9	121.0(13)	C209	C208	C207	121.9(15)
C10	C9	C8	116.9(13)	C208	C209	C210	118.7(15)
C5	C10	C9	121.5(12)	C205	C210	C211	105.7(12)
C5	C10	C11	109.1(12)	C209	C210	C205	121.7(14)
C9	C10	C11	129.3(13)	C209	C210	C211	132.6(14)
C12	C11	C10	129.9(14)	C212	C211	C210	130.5(14)
C12	C11	C16	124.2(13)	C216	C211	C210	110.9(13)
C16	C11	C10	105.9(13)	C216	C211	C212	118.6(14)
C11	C12	C13	116.2(16)	C213	C212	C211	118.2(16)
C14	C13	C12	121.3(16)	C212	C213	C214	124.8(18)
C15	C14	C13	120.3(15)	C215	C214	C213	118.2(16)
C14	C15	C16	121.1(15)	C214	C215	C216	120.3(15)
C11	C16	C4	112.6(12)	C211	C216	C204	109.5(12)
C11	C16	C15	116.9(14)	C211	C216	C215	119.8(14)

C15	C16	C4	130.6(14)	C215	C216	C204	130.8(13)
O3	C17	C1	121.4(13)	O203	C217	C201	124.1(11)
O3	C17	O4	124.4(13)	O203	C217	O204	124.1(12)
O4	C17	C1	114.2(13)	O204	C217	C201	111.7(10)
C19	C18	C20	111.9(15)	C219	C218	C221	110.7(14)
C19	C18	C21	114.3(18)	C220	C218	C219	111.9(14)
C20	C18	C21	109.4(18)	C220	C218	C221	112.1(13)
O4	C18	C19	111.4(14)	O204	C218	C219	111.1(11)
O4	C18	C20	102.2(14)	O204	C218	C220	101.2(11)
O4	C18	C21	106.8(13)	O204	C218	C221	109.4(12)
O5	C22	C1	106.2(12)	O205	C222	C201	106.7(9)
C24	C23	C28	119.5(13)	C224	C223	P201	118.0(9)
C24	C23	P1	121.1(12)	C228	C223	C224	119.6(13)
C28	C23	P1	119.3(12)	C228	C223	P201	122.2(11)
C23	C24	C25	120.2(15)	C225	C224	C223	116.7(12)
C26	C25	C24	118.8(15)	C226	C225	C224	121.0(14)
C27	C26	C25	122.3(15)	C225	C226	C227	121.1(14)
C26	C27	C28	119.5(16)	C228	C227	C226	116.5(14)
C27	C28	C23	119.4(15)	C223	C228	C227	124.5(14)
C30	C29	C34	114.8(13)	C230	C229	P201	119.1(9)
C30	C29	P1	122.9(11)	C234	C229	C230	116.9(11)
C34	C29	P1	122.1(13)	C234	C229	P201	124.0(9)
C29	C30	C31	122.0(15)	C231	C230	C229	120.6(12)
C32	C31	C30	120.8(18)	C232	C231	C230	120.4(13)
C33	C32	C31	119.9(16)	C231	C232	C233	119.5(12)
C32	C33	C34	119.3(16)	C234	C233	C232	120.4(13)
C33	C34	C29	123.2(17)	C233	C234	C229	122.0(12)
C2	N1	C1	120.6(12)	C202	N201	C201	116.4(11)
C2	O2	C3	115.8(11)	C202	O202	C203	117.4(11)
C17	O4	C18	122.8(13)	C217	O204	C218	122.6(10)
C22	O5	P1	120.1(9)	C222	O205	P201	120.8(7)

C23	P1	B1	114.4(8)	C223	P201	B201	113.7(8)
C29	P1	C23	108.5(7)	C229	P201	C223	108.4(6)
C29	P1	B1	112.8(8)	C229	P201	B201	114.4(8)
O5	P1	C23	105.3(6)	O205	P201	C223	104.9(5)
O5	P1	C29	98.4(7)	O205	P201	C229	98.4(5)
O5	P1	B1	115.9(7)	O205	P201	B201	115.5(7)
C117	C101	C122	113.9(11)	C317	C301	C322	109.5(11)
N101	C101	C117	109.4(11)	N301	C301	C317	112.4(10)
N101	C101	C122	111.3(11)	N301	C301	C322	111.6(12)
N101	C102	O102	109.1(12)	O301	C302	N301	121.9(12)
O101	C102	N101	125.8(13)	O301	C302	O302	124.2(12)
O101	C102	O102	125.1(12)	O302	C302	N301	113.9(11)
C104	C103	O102	106.6(13)	O302	C303	C304	111.9(13)
C103	C104	C105	111.6(14)	C303	C304	C305	108.7(14)
C103	C104	C116	114.5(14)	C303	C304	C316	113.6(14)
C105	C104	C116	101.6(12)	C316	C304	C305	101.7(13)
C106	C105	C104	127.8(16)	C306	C305	C304	127.7(15)
C106	C105	C110	120.1(15)	C306	C305	C310	120.9(16)
C110	C105	C104	111.7(14)	C310	C305	C304	111.3(14)
C107	C106	C105	118.9(19)	C307	C306	C305	117.5(17)
C106	C107	C108	118.9(19)	C308	C307	C306	120.6(18)
C109	C108	C107	124.1(16)	C307	C308	C309	123.0(18)
C110	C109	C108	113.5(18)	C310	C309	C308	117.8(17)
C105	C110	C111	107.9(13)	C305	C310	C311	105.9(14)
C109	C110	C105	122.5(17)	C309	C310	C305	119.4(16)
C109	C110	C111	127.8(16)	C309	C310	C311	133.4(15)
C112	C111	C110	133.6(14)	C312	C311	C310	128.9(16)
C112	C111	C116	120.0(14)	C312	C311	C316	120.9(16)
C116	C111	C110	106.4(14)	C316	C311	C310	110.2(14)
C113	C112	C111	121.6(14)	C313	C312	C311	119.0(17)
C112	C113	C114	119.7(16)	C312	C313	C314	120.6(17)

C115 C114 C113	120.7(16)	C313 C314 C315	121.0(18)
C116 C115 C114	119.7(14)	C316 C315 C314	118.2(17)
C111 C116 C104	111.3(13)	C311 C316 C304	110.7(14)
C115 C116 C104	130.2(13)	C315 C316 C304	129.1(15)
C115 C116 C111	118.3(14)	C315 C316 C311	120.1(16)
O103 C117 C101	125.0(11)	O303 C317 C301	122.8(12)
O103 C117 O104	125.0(13)	O303 C317 O304	125.5(14)
O104 C117 C101	110.0(12)	O304 C317 C301	111.6(11)
C120 C118 C119	112.9(15)	C320 C318 C319	108.7(17)
C120 C118 C121	109.4(14)	C321 C318 C319	108.5(18)
C121 C118 C119	112.0(14)	C321 C318 C320	119.4(17)
O104 C118 C119	109.6(13)	C321 C318 O304	112.5(13)
O104 C118 C120	103.0(13)	O304 C318 C319	102.1(14)
O104 C118 C121	109.5(13)	O304 C318 C320	104.2(16)
O105 C122 C101	104.0(10)	O305 C322 C301	107.2(10)
C124 C123 C128	117.1(14)	C324 C323 P301	123.6(11)
C124 C123 P101	123.2(13)	C328 C323 C324	115.1(14)
C128 C123 P101	119.6(11)	C328 C323 P301	120.8(13)
C123 C124 C125	120.7(17)	C325 C324 C323	122.0(15)
C126 C125 C124	118.5(16)	C326 C325 C324	120.4(17)
C125 C126 C127	122.8(16)	C325 C326 C327	120.4(16)
C128 C127 C126	118.6(17)	C328 C327 C326	117.2(15)
C127 C128 C123	122.2(16)	C327 C328 C323	124.1(17)
C130 C129 C134	125.6(16)	C330 C329 P301	120.9(12)
C130 C129 P101	116.7(11)	C334 C329 C330	118.7(13)
C134 C129 P101	117.7(13)	C334 C329 P301	120.4(11)
C129 C130 C131	116.5(15)	C331 C330 C329	122.0(15)
C132 C131 C130	118.2(17)	C330 C331 C332	118.0(14)
C131 C132 C133	122.0(17)	C333 C332 C331	121.2(14)
C134 C133 C132	118.9(16)	C332 C333 C334	120.7(16)
C129 C134 C133	118.5(16)	C333 C334 C329	119.3(14)

C102	N101	C101	122.1(12)	C302	N301	C301	122.1(11)
C102	O102	C103	111.2(11)	C302	O302	C303	115.9(11)
C117	O104	C118	121.1(11)	C317	O304	C318	122.9(11)
C122	O105	P101	120.9(8)	C322	O305	P301	119.9(9)
C123	P101	C129	109.9(7)	C323	P301	C329	103.3(7)
C123	P101	B101	113.9(8)	C323	P301	B301	114.4(7)
C129	P101	B101	112.0(8)	C329	P301	B301	114.9(8)
O105	P101	C123	98.5(6)	O305	P301	C323	101.3(7)
O105	P101	C129	103.6(6)	O305	P301	C329	106.0(6)
O105	P101	B101	117.7(8)	O305	P301	B301	115.3(8)

Table 6 Hydrogen Bonds for 233.

D	H	A	d(D-H)/Å	d(H-A)/Å	d(D-A)/Å	D-H-A/°
N1	H1N	O101[1]	0.86	2.16	3.017(16)	172.4
N101	H11N	O1	0.86	2.12	2.969(16)	168.9
N201	H21N	O301[1]	0.86	2.24	3.062(15)	160.2
N301	H31N	O201	0.86	2.10	2.907(15)	156.8

Table 7 Torsion Angles for 233.

A	B	C	D	Angle/˚	A	B	C	D	Angle/˚
C1	C17	O4	C18	-178.4(13)	C201	C217	O204	C218	175.3(11)
C1	C22	O5	P1	-172.2(8)	C201	C222	O205	P201	-175.3(8)
C3	C4	C5	C6	-61.1(18)	C203	C204	C205	C206	-61.4(19)
C3	C4	C5	C10	119.2(13)	C203	C204	C205	C210	113.3(14)
C3	C4	C16	C11	-114.9(13)	C203	C204	C216	C211	-110.9(14)
C3	C4	C16	C15	64.5(19)	C203	C204	C216	C215	69(2)
C4	C3	O2	C2	-103.1(14)	C204	C203	O202	C202	-109.8(14)
C4	C5	C6	C7	177.9(13)	C204	C205	C206	C207	175.0(16)
C4	C5	C10	C9	-177.2(12)	C204	C205	C210	C209	-175.8(14)

C4	C5	C10	C11	0.4(15)	C204	C205	C210	C211	5.4(17)
C5	C4	C16	C11	1.9(14)	C205	C204	C216	C211	3.5(15)
C5	C4	C16	C15	-178.7(15)	C205	C204	C216	C215	-176.7(16)
C5	C6	C7	C8	2(2)	C205	C206	C207	C208	-1(2)
C5	C10	C11	C12	-179.2(16)	C205	C210	C211	C212	178.8(17)
C5	C10	C11	C16	0.8(15)	C205	C210	C211	C216	-2.9(18)
C6	C5	C10	C9	3(2)	C206	C205	C210	C209	-1(2)
C6	C5	C10	C11	-179.3(12)	C206	C205	C210	C211	-179.5(13)
C6	C7	C8	C9	-2(2)	C206	C207	C208	C209	2(3)
C7	C8	C9	C10	2(2)	C207	C208	C209	C210	-2(3)
C8	C9	C10	C5	-2.8(19)	C208	C209	C210	C205	1(2)
C8	C9	C10	C11	-179.8(13)	C208	C209	C210	C211	179.7(17)
C9	C10	C11	C12	-2(3)	C209	C210	C211	C212	0(3)
C9	C10	C11	C16	178.1(13)	C209	C210	C211	C216	178.4(17)
C10	C5	C6	C7	-2(2)	C210	C205	C206	C207	1(2)
C10	C11	C12	C13	-178.3(15)	C210	C211	C212	C213	-178.5(17)
C10	C11	C16	C4	-1.7(15)	C210	C211	C216	C204	-0.6(18)
C10	C11	C16	C15	178.8(12)	C210	C211	C216	C215	179.6(14)
C11	C12	C13	C14	-1(3)	C211	C212	C213	C214	-2(3)
C12	C11	C16	C4	178.3(15)	C212	C211	C216	C204	177.9(14)
C12	C11	C16	C15	-1(2)	C212	C211	C216	C215	-2(2)
C12	C13	C14	C15	-1(3)	C212	C213	C214	C215	-1(3)
C13	C14	C15	C16	2(2)	C213	C214	C215	C216	2(3)
C14	C15	C16	C4	-179.8(14)	C214	C215	C216	C204	179.5(16)
C14	C15	C16	C11	0(2)	C214	C215	C216	C211	-1(2)
C16	C4	C5	C6	178.4(13)	C216	C204	C205	C206	179.8(15)
C16	C4	C5	C10	-1.3(14)	C216	C204	C205	C210	-5.6(16)
C16	C11	C12	C13	2(2)	C216	C211	C212	C213	3(3)
C17	C1	C22	O5	-57.3(15)	C217	C201	C222	O205	-52.9(13)
C17	C1	N1	C2	-132.2(14)	C217	C201	N201	C202	-139.1(13)
C19	C18	O4	C17	-60(2)	C219	C218	O204	C217	62.9(17)

C20	C18	O4	C17	-179.5(15)	C220	C218	O204	C217	-178.1(12)
C21	C18	O4	C17	66(2)	C221	C218	O204	C217	-59.7(16)
C22	C1	C17	O3	126.1(15)	C222	C201	C217	O203	127.5(14)
C22	C1	C17	O4	-52.4(17)	C222	C201	C217	O204	-49.5(14)
C22	C1	N1	C2	102.6(15)	C222	C201	N201	C202	96.9(14)
C22	O5	P1	C23	90.8(11)	C222	O205	P201	C223	83.3(9)
C22	O5	P1	C29	-157.3(10)	C222	O205	P201	C229	-165.0(9)
C22	O5	P1	B1	-36.7(12)	C222	O205	P201	B201	-42.7(12)
C23	C24	C25	C26	-6(3)	C223	C224	C225	C226	-5(2)
C24	C23	C28	C27	-1(2)	C224	C223	C228	C227	-6(2)
C24	C23	P1	C29	-78.0(14)	C224	C223	P201	C229	-70.2(11)
C24	C23	P1	B1	155.0(13)	C224	C223	P201	B201	161.3(11)
C24	C23	P1	O5	26.6(15)	C224	C223	P201	O205	34.2(11)
C24	C25	C26	C27	7(3)	C224	C225	C226	C227	6(2)
C25	C26	C27	C28	-5(3)	C225	C226	C227	C228	-7(2)
C26	C27	C28	C23	2(3)	C226	C227	C228	C223	7(2)
C28	C23	C24	C25	3(2)	C228	C223	C224	C225	5(2)
C28	C23	P1	C29	99.8(14)	C228	C223	P201	C229	105.4(12)
C28	C23	P1	B1	-27.1(16)	C228	C223	P201	B201	-23.0(13)
C28	C23	P1	O5	-155.6(12)	C228	C223	P201	O205	-150.2(11)
C29	C30	C31	C32	4(3)	C229	C230	C231	C232	-2(2)
C30	C29	C34	C33	3(2)	C230	C229	C234	C233	-4.0(19)
C30	C29	P1	C23	93.3(14)	C230	C229	P201	C223	-88.2(11)
C30	C29	P1	B1	-138.8(13)	C230	C229	P201	B201	39.9(13)
C30	C29	P1	O5	-16.0(14)	C230	C229	P201	O205	163.0(10)
C30	C31	C32	C33	-2(3)	C230	C231	C232	C233	3(2)
C31	C32	C33	C34	1(3)	C231	C232	C233	C234	-5(2)
C32	C33	C34	C29	-2(3)	C232	C233	C234	C229	6(2)
C34	C29	C30	C31	-4(2)	C234	C229	C230	C231	2(2)
C34	C29	P1	C23	-80.2(13)	C234	C229	P201	C223	91.4(12)
C34	C29	P1	B1	47.7(14)	C234	C229	P201	B201	-140.6(12)

C34	C29	P1	O5	170.5(12)	C234	C229	P201	O205	-17.5(12)
N1	C1	C17	O3	1(2)	N201	C201	C217	O203	3.9(18)
N1	C1	C17	O4	-177.2(12)	N201	C201	C217	O204	-173.1(10)
N1	C1	C22	O5	67.5(14)	N201	C201	C222	O205	68.6(12)
N1	C2	O2	C3	174.8(12)	N201	C202	O202	C203	-172.0(12)
O1	C2	N1	C1	-18(2)	O201	C202	N201	C201	-11(2)
O1	C2	O2	C3	-5(2)	O201	C202	O202	C203	8(2)
O2	C2	N1	C1	161.8(12)	O202	C202	N201	C201	168.8(11)
O2	C3	C4	C5	-176.4(12)	O202	C203	C204	C205	-171.4(11)
O2	C3	C4	C16	-64.1(15)	O202	C203	C204	C216	-60.9(15)
O3	C17	O4	C18	3(2)	O203	C217	O204	C218	-2(2)
P1	C23	C24	C25	-179.1(13)	P201	C223	C224	C225	-179.6(11)
P1	C23	C28	C27	-179.1(13)	P201	C223	C228	C227	178.0(11)
P1	C29	C30	C31	-178.4(13)	P201	C229	C230	C231	-178.5(11)
P1	C29	C34	C33	177.3(13)	P201	C229	C234	C233	176.5(10)
C101	C117	O104	C118	179.8(12)	C301	C317	O304	C318	170.6(13)
C101	C122	O105	P101	-165.3(9)	C301	C322	O305	P301	-137.8(10)
C103	C104	C105	C106	-57(3)	C303	C304	C305	C306	-61(3)
C103	C104	C105	C110	114.9(18)	C303	C304	C305	C310	116.3(16)
C103	C104	C116	C111	-119.4(16)	C303	C304	C316	C311	-115.3(17)
C103	C104	C116	C115	66(2)	C303	C304	C316	C315	63(2)
C104	C103	O102	C102	163.0(12)	C304	C303	O302	C302	166.6(12)
C104	C105	C106	C107	-176(2)	C304	C305	C306	C307	-179(2)
C104	C105	C110	C109	177(2)	C304	C305	C310	C309	173.3(18)
C104	C105	C110	C111	11(2)	C304	C305	C310	C311	5(2)
C105	C104	C116	C111	1.0(19)	C305	C304	C316	C311	1.3(19)
C105	C104	C116	C115	-173.7(19)	C305	C304	C316	C315	179.7(18)
C105	C106	C107	C108	-13(4)	C305	C306	C307	C308	4(3)
C105	C110	C111	C112	167(2)	C305	C310	C311	C312	173.0(19)
C105	C110	C111	C116	-10(2)	C305	C310	C311	C316	-4(2)
C106	C105	C110	C109	-10(3)	C306	C305	C310	C309	-10(3)

C106 C105 C110 C111	-175.7(19)	C306 C305 C310 C311	-178.1(18)
C106 C107 C108 C109	13(4)	C306 C307 C308 C309	-7(4)
C107 C108 C109 C110	-11(4)	C307 C308 C309 C310	1(3)
C108 C109 C110 C105	9(3)	C308 C309 C310 C305	7(3)
C108 C109 C110 C111	172(2)	C308 C309 C310 C311	172(2)
C109 C110 C111 C112	3(4)	C309 C310 C311 C312	7(4)
C109 C110 C111 C116	-175(2)	C309 C310 C311 C316	-170(2)
C110 C105 C106 C107	12(4)	C310 C305 C306 C307	4(3)
C110 C111 C112 C113	-179(2)	C310 C311 C312 C313	178.5(19)
C110 C111 C116 C104	5(2)	C310 C311 C316 C304	1(2)
C110 C111 C116 C115	-179.1(17)	C310 C311 C316 C315	-177.1(16)
C111 C112 C113 C114	0(3)	C311 C312 C313 C314	4(3)
C112 C111 C116 C104	-172.4(16)	C312 C311 C316 C304	-175.7(17)
C112 C111 C116 C115	3(3)	C312 C311 C316 C315	6(3)
C112 C113 C114 C115	0(3)	C312 C313 C314 C315	-3(3)
C113 C114 C115 C116	1(3)	C313 C314 C315 C316	4(3)
C114 C115 C116 C104	171.9(18)	C314 C315 C316 C304	176.9(17)
C114 C115 C116 C111	-3(3)	C314 C315 C316 C311	-5(3)
C116 C104 C105 C106	-180(2)	C316 C304 C305 C306	179(2)
C116 C104 C105 C110	-8(2)	C316 C304 C305 C310	-4(2)
C116 C111 C112 C113	-2(3)	C316 C311 C312 C313	-5(3)
C117 C101 C122 O105	-55.5(14)	C317 C301 C322 O305	-59.4(14)
C117 C101 N101 C102	-134.2(13)	C317 C301 N301 C302	-151.6(12)
C119 C118 O104 C117	64.7(17)	C319 C318 O304 C317	176.9(16)
C120 C118 O104 C117	-174.9(15)	C320 C318 O304 C317	-70.0(19)
C121 C118 O104 C117	-58.6(18)	C321 C318 O304 C317	61(2)
C122 C101 C117 O103	121.2(16)	C322 C301 C317 O303	106.2(15)
C122 C101 C117 O104	-57.5(15)	C322 C301 C317 O304	-76.1(14)
C122 C101 N101 C102	99.0(14)	C322 C301 N301 C302	84.9(15)
C122 O105 P101 C123	178.9(11)	C322 O305 P301 C323	173.8(9)
C122 O105 P101 C129	-68.1(11)	C322 O305 P301 C329	-78.6(10)

C122 O105 P101 B101	56.1(12)	C322 O305 P301 B301	49.7(11)
C123 C124 C125 C126	2(2)	C323 C324 C325 C326	5(3)
C124 C123 C128 C127	-3(3)	C324 C323 C328 C327	5(2)
C124 C123 P101 C129	103.7(15)	C324 C323 P301 C329	-130.7(14)
C124 C123 P101 B101	-23.0(18)	C324 C323 P301 B301	103.7(15)
C124 C123 P101 O105	-148.5(14)	C324 C323 P301 O305	-21.0(14)
C124 C125 C126 C127	-3(3)	C324 C325 C326 C327	-8(3)
C125 C126 C127 C128	1(3)	C325 C326 C327 C328	9(2)
C126 C127 C128 C123	2(3)	C326 C327 C328 C323	-8(2)
C128 C123 C124 C125	0(2)	C328 C323 C324 C325	-3(2)
C128 C123 P101 C129	-79.2(15)	C328 C323 P301 C329	57.8(14)
C128 C123 P101 B101	154.1(14)	C328 C323 P301 B301	-67.8(15)
C128 C123 P101 O105	28.6(15)	C328 C323 P301 O305	167.5(12)
C129 C130 C131 C132	5(2)	C329 C330 C331 C332	4(2)
C130 C129 C134 C133	1(3)	C330 C329 C334 C333	1(2)
C130 C129 P101 C123	64.1(14)	C330 C329 P301 C323	62.6(14)
C130 C129 P101 B101	-168.2(13)	C330 C329 P301 B301	-172.1(12)
C130 C129 P101 O105	-40.3(13)	C330 C329 P301 O305	-43.5(13)
C130 C131 C132 C133	-6(3)	C330 C331 C332 C333	-5(2)
C131 C132 C133 C134	4(3)	C331 C332 C333 C334	4(2)
C132 C133 C134 C129	-2(2)	C332 C333 C334 C329	-2(2)
C134 C129 C130 C131	-2(2)	C334 C329 C330 C331	-2(2)
C134 C129 P101 C123	-113.5(13)	C334 C329 P301 C323	-119.0(13)
C134 C129 P101 B101	14.2(15)	C334 C329 P301 B301	6.3(15)
C134 C129 P101 O105	142.1(12)	C334 C329 P301 O305	134.9(12)
N101 C101 C117 O103	-4(2)	N301 C301 C317 O303	-18.4(19)
N101 C101 C117 O104	177.2(11)	N301 C301 C317 O304	159.2(11)
N101 C101 C122 O105	68.8(13)	N301 C301 C322 O305	65.7(14)
N101 C102 O102 C103	-169.3(11)	N301 C302 O302 C303	-167.2(11)
O101 C102 N101 C101	-2(2)	O301 C302 N301 C301	-1.2(19)
O101 C102 O102 C103	9.1(17)	O301 C302 O302 C303	11.1(18)

O102	C102	N101	C101	175.9(11)	O302	C302	N301	C301	177.2(11)
O102	C103	C104	C105	179.9(13)	O302	C303	C304	C305	-175.1(13)
O102	C103	C104	C116	-65.3(17)	O302	C303	C304	C316	-62.7(18)
O103	C117	O104	C118	1(2)	O303	C317	O304	C318	-12(2)
P101	C123	C124	C125	177.6(12)	P301	C323	C324	C325	-175.1(13)
P101	C123	C128	C127	-179.9(14)	P301	C323	C328	C327	177.3(12)
P101	C129	C130	C131	-179.6(12)	P301	C329	C330	C331	176.4(12)
P101	C129	C134	C133	178.1(13)	P301	C329	C334	C333	-177.4(12)

Table 8 Hydrogen Atom Coordinates (Å×10⁴) and Isotropic Displacement Parameters (Å²×10³) for 233.

Atom	x	y	z	U(eq)
H1	6782.15	6902.63	8984.13	55
H3A	4924.71	6872.58	7275.18	61
H3B	6493.11	7008.06	7473.3	61
H4	6052.73	7982.45	7386.19	53
H6	8122.63	7361.06	6823.88	57
H7	8504.22	7270.74	6057.31	60
H8	6735.48	7517.01	5536.41	57
H9	4400.85	7822.86	5764.28	53
H12	2043.66	8169.72	6197.78	71
H13	302.05	8445.96	6725.38	76
H14	845.28	8405.47	7487.97	68
H15	3045.05	8073.26	7742.56	62
H19A	2909.87	6454.16	10448.45	112
H19B	2613.56	6607.53	9942.56	112
H19C	3468.65	7027.06	10258.62	112
H20A	5909.1	6728.94	10584	125
H20B	6731.65	6224.83	10365.37	125
H20C	5453.57	6110.22	10693.36	125

H21A	3796.16	5575.09	10036.39	130
H21B	5455.55	5571.7	9917.91	130
H21C	4284.27	5791.15	9566.55	130
H22A	7099.48	7570.57	9546.17	54
H22B	7113.44	7885.33	9081.01	54
H24	4105.94	8571.11	8720.54	66
H25	4091.6	9157.82	8095	65
H26	5016.59	10058.3	8170.52	74
H27	6366.24	10317.72	8786.92	75
H28	6509.42	9721.95	9408.23	71
H30	2786.19	7996.36	9592.78	63
H31	630.45	8065.47	9972.56	72
H32	225.21	8811.59	10451.68	77
H33	2043.01	9454.33	10592.72	77
H34	4243.85	9373.15	10233.24	65
H1A	7350(110)	8340(30)	10220(30)	79
H1B	8210(60)	8800(60)	9790(30)	79
H1C	7030(110)	9130(30)	10210(30)	79
H1N	4364.19	7412.69	8622.88	55
H101	12283.11	7037.97	8041.97	53
H10A	10817.52	8628.13	9043.67	66
H10B	11275.97	8788.2	8554.06	66
H104	8462.53	8941.84	8882.53	68
H106	10559.08	9505.59	9503.58	97
H107	10861.91	10441.65	9676.15	108
H108	11039.97	11080.78	9075.2	106
H109	9915.83	10894.21	8370.34	98
H112	8443.63	10399.1	7661.07	74
H113	7265.64	9841	7146.6	81
H114	6990.53	8877.45	7288.54	76
H115	7933.12	8482.05	7953.5	70

H11A	12519.39	6817.74	6664.42	94
H11B	10827.52	6923.69	6645.72	94
H11C	11527.98	6503.23	6308.41	94
H12A	12383.55	5537.45	6607.29	108
H12B	12328.56	5424.04	7124.79	108
H12C	13446.33	5859.4	6938.79	108
H12D	9113.06	6208.54	6915.77	87
H12E	9683.19	5655.36	7145.73	87
H12F	9714.9	5717.97	6622.38	87
H12G	12053.65	6108.77	8265.32	57
H12H	11597.56	6489.14	8672.46	57
H124	6479.33	5436.17	9047.99	75
H125	4077.73	5376.42	8734.53	76
H126	3738.33	5464.83	7982.86	76
H127	5640.03	5682.23	7517.32	76
H128	7932.3	5797.9	7818.57	76
H130	10264.19	5183.14	7907.74	70
H131	11754.98	4362.53	7747.54	80
H132	12412.12	3777.98	8334.48	80
H133	12072.53	4044.69	9070.65	79
H134	10726.04	4855.08	9214.77	74
H1D	8840(140)	6310(40)	9390(30)	100
H1E	9110(160)	5540(30)	9540(20)	100
H1F	10700(60)	6000(60)	9400(30)	100
H11N	9446.82	7314.56	8206.27	55
H201	1594.65	2947.4	6076.54	43
H20D	-187.48	2922.39	7745.65	57
H20E	1374.5	2772.18	7574.74	57
H204	974.99	1811.46	7707.67	57
H206	2819.59	2488.53	8299.91	62
H207	3108.1	2693.14	9060.11	70

H208	1100.5	2559.17	9524.32	70
H209	-1038.7	2182.88	9249.02	66
H212	-3359.32	1746.23	8743.32	73
H213	-4831.39	1377.93	8212.78	87
H214	-4214.27	1301.98	7478.28	82
H215	-1963.38	1628.65	7262.31	68
H21D	180.69	4303.97	5138.72	97
H21E	-1254.07	4121.2	5375.12	97
H21F	-1316.41	4306.66	4870.19	97
H22C	196.34	3689.13	4326.67	89
H22D	692.46	3094.11	4496.62	89
H22E	1495.87	3633.25	4677.49	89
H22F	-2581.58	3268.5	5086.57	97
H22G	-1759.04	2836.67	4786.74	97
H22H	-2364.93	3396.45	4576.59	97
H22I	1789.42	2306.67	5500.54	42
H22J	1674.47	1957.29	5947.19	42
H224	-1411.93	1303.01	6194.06	56
H225	-1285.39	637.31	6779.91	61
H226	-242.97	-216.89	6666.94	64
H227	1170.05	-372.9	6031.5	63
H228	953.43	263.96	5459.01	56
H230	-1568.67	744.17	4612.95	51
H231	-3849.4	767.3	4256.72	55
H232	-5644.09	1365.34	4509.05	57
H233	-5060.78	2019.74	5073.9	51
H234	-2861.82	1969.42	5456.23	42
H1G	1320(120)	1590(40)	4620(30)	82
H1H	2510(50)	1290(60)	5100(30)	82
H1I	1340(120)	830(30)	4740(40)	82
H21N	-995.6	2526.24	6404.27	50

H301	7088.93	2692.01	7121.16	53
H30A	5916.42	1083.21	6404.41	62
H30B	5400.12	1343.96	5943.45	62
H304	3103.99	963.99	6018.82	71
H306	5273.75	528.95	5375.49	87
H307	6151.96	-341.15	5180.99	91
H308	5723.16	-1096.93	5619.42	91
H309	4795.33	-1009.46	6333.73	89
H312	3449.43	-655.11	7095.14	78
H313	2373.22	-179.91	7669.06	84
H314	1833.76	754.74	7597.11	81
H315	2617.27	1269.61	6967.58	73
H31A	8588.64	3907.51	8107.48	129
H31B	8604.77	3377.8	8419.99	129
H31C	8101.97	3960.42	8606.17	129
H32A	5979.88	4412.52	8286.08	143
H32B	4753.96	4068.78	8031.55	143
H32C	6157.57	4254.15	7779.81	143
H32D	6477.97	2910.17	8582.81	109
H32E	4922.21	3133.49	8439.8	109
H32F	5844.15	3445.5	8814.15	109
H32G	7074.19	3632.34	6895.04	57
H32H	6633.06	3260.5	6475.9	57
H324	2350.58	3691.45	6969.98	68
H325	32.23	3974.08	7102.3	76
H326	-1261.8	4464.67	6570.45	75
H327	-28.92	4885.35	5983.66	73
H328	2267.88	4558.23	5837.12	67
H330	5143.56	4863.18	6793.65	59
H331	6535.47	5649.3	6699.85	61
H332	7386.58	5848	5984.13	66

H333	*7175.55*	*5202.02*	*5422.66*	*65*
H334	*5823.78*	*4394.21*	*5518.42*	*59*
H1L	*3950(140)*	*3570(40)*	*5458(19)*	*87*
H1K	*5590(60)*	*3220(50)*	*5690(40)*	*87*
H1J	*3760(130)*	*2960(30)*	*5860(30)*	*87*
H31N	*4257.79*	*2484.02*	*6953.65*	*48*

Crystal structure determination of 233

Crystal Data *for* $C_{34}H_{37}BNO_5P$ *(*M *=581.42 g/mol): monoclinic, space group* $P2_1$ *(no. 4),* a = *9.1480(4) Å,* b = *23.8115(7) Å,* c = *29.7987(15) Å,* β = *91.526(4)°,* V = *6488.7(5) Å*^{3}*,* Z = *8,* T = *100.00(10) K, μ(CuKα) = 1.072 mm*$^{-1}$*,* Dcalc = *1.190 g/cm*^{3}*, 35635 reflections measured (7° ≤ 2Θ ≤ 149.902°), 35635 unique (*R_{int} *= ?,* R_{sigma} *= 0.0349) which were used in all calculations. The final* R_1 *was 0.1100 (I > 2σ(I)) and* wR_2 *was 0.3087 (all data).*

Refinement model description

Number of restraints - 1638, number of constraints - unknown.

Details:

1. Twinned data refinement Scales: 0.581(2) 0.419(2). 2. Fixed Uiso At 1.2 times of: All C(H) groups, All C(H,H) groups, All N(H) groups At 1.5 times of: All B(H,H,H) groups, All C(H,H,H) groups. 3. Restrained distances C123-C124 = C124-C125 = C125-C126 = C126-C127 = C127-C128 = C128-C123 1.39 with sigma of 0.02 C129-C130 = C130-C131 = C131-C132 = C132-C133 = C133-C134 = C134-C129 1.39 with sigma of 0.02 C310-C311 1.5 with sigma of 0.02 B1-H1A = B1-H1B = B1-H1C = B101-H1D = B101-H1E = B101-H1F 1.16 with sigma of 0.02 B201-H1G = B201-H1H = B201-H1I = B301-H1J = B301-H1K = B301-H1L 1.16 with sigma of 0.02 H1A-H1B 1.89 with sigma of 0.04 H1A-H1C 1.89 with sigma of 0.04 H1B-H1C 1.89 with sigma of 0.04 H1D-H1E 1.89 with sigma of 0.04 H1D-H1F 1.89 with sigma of 0.04 H1E-H1F 1.89 with sigma of 0.04 H1G-H1H 1.89 with sigma of 0.04 H1G-H1I 1.89 with sigma of 0.04 H1H-H1I 1.89 with sigma of 0.04 H1J-H1K 1.89 with sigma of 0.04 H1J-H1L 1.89 with sigma of 0.04 H1K-H1L 1.89 with sigma of 0.04 P1-H1A 2.6 with sigma of 0.04 P1-

H1B 2.6 with sigma of 0.04 P1-H1C 2.6 with sigma of 0.04 P101-H1D 2.6 with sigma of 0.04 P101-H1E 2.6 with sigma of 0.04 P101-H1F 2.6 with sigma of 0.04 P201-H1G 2.6 with sigma of 0.04 P201-H1H 2.6 with sigma of 0.04 P201-H1I 2.6 with sigma of 0.04 P301-H1J 2.6 with sigma of 0.04 P301-H1K 2.6 with sigma of 0.04 P301-H1L. 2.6 with sigma of 0.044. Rigid bond restraints All non-hydrogen atoms with sigma for 1-2 distances of 0.005 and sigma for 1-3 distances of 0.0055. Uiso/Uaniso restraints and constraints. All non-hydrogen atoms have similar U: within 2A with sigma of 0.007 and sigma for terminal atoms of 0.014 Uanis(C323) ≈ Ueq, Uanis(C324) ≈ Ueq, Uanis(C325) ≈ Ueq, Uanis(C326) ≈ Ueq, Uanis(C327) ≈ Ueq, Uanis(C328) ≈ Ueq: with sigma of 0.01 and sigma for terminal atoms of 0.01 6.a Ternary CH refined with riding coordinates: C1(H1), C4(H4), C101(H101), C104(H104), C201(H201), C204(H204), C301(H301), C304(H304)6.b Secondary CH2 refined with riding coordinates: C3(H3A,H3B), C22(H22A,H22B), C103(H10A,H10B), C122(H12G,H12H), C203(H20D, H20E), C222(H22I,H22J), C303(H30A,H30B), C322(H32G,H32H)6.c Aromatic/amide H refined with riding coordinates: C6(H6), C7(H7), C8(H8), C9(H9), C12(H12), C13(H13), C14(H14), C15(H15), C24(H24), C25(H25), C26(H26), C27(H27), C28(H28), C30(H30), C31(H31), C32(H32), C33(H33), C34(H34), N1(H1N), C106(H106), C107(H107), C108(H108), C109(H109), C112(H112), C113(H113), C114(H114), C115(H115), C124(H124), C125(H125), C126(H126), C127(H127), C128(H128), C130(H130), C131(H131), C132(H132), C133(H133), C134(H134), N101(H11N), C206(H206), C207(H207), C208(H208), C209(H209), C212(H212), C213(H213), C214(H214), C215(H215), C224(H224), C225(H225), C226(H226), C227(H227), C228(H228), C230(H230), C231(H231), C232(H232), C233(H233), C234(H234), N201(H21N), C306(H306), C307(H307), C308(H308), C309(H309), C312(H312), C313(H313), C314(H314), C315(H315), C324(H324), C325(H325), C326(H326), C327(H327), C328(H328), C330(H330), C331(H331), C332(H332), C333(H333), C334(H334), N301(H31N)6.d Idealised Me refined as rotating group: C19(H19A,H19B,H19C), C20(H20A,H20B,H20C), C21(H21A,H21B,H21C), C119(H11A,H11B, H11C), C120(H12A,H12B,H12C), C121(H12D,H12E,H12F), C219(H21D,H21E,H21F), C220(H22C,H22D,H22E), C221(H22F,H22G,H22H), C319(H31A,H31B,H31C), C320(H32A, H32B,H32C), C321(H32D,H32E,H32F).

8.References

1. C. R. Catlow, M. Davidson, C. Hardacre and G. J. Hutchings, *Philos. Trans. Royal Soc. A*, 2016, 374, 20150089.
2. F. Dumeignil, M. Guehl, A. Gimbernat, M. Capron, N. L. Ferreira, R. Froidevaux, J.-S. Girardon, R. Wojcieszak, P. Dhulster and D. Delcroix, *Catalysis Science & Technology*, 2018, 8, 5708-5734.
3. A. J. Thomson and H. B. Gray, *Curr Opin Chem Biol*, 1998, 2, 155-158.
4. R. A. Sheldon and D. Brady, *Chem. Commun.*, 2018, 54, 6088-6104.
5. A. Schmid, J. S. Dordick, B. Hauer, A. Kiener, M. Wubbolts and B. Witholt, *Nature*, 2001, 409, 258-268.
6. M. T. Reetz, *J. Am. Chem. Soc.*, 2013, 135, 12480-12496.
7. H. J. Davis and T. R. Ward, *ACS Cent. Sci.*, 2019, 5, 1120-1136.
8. E. P. Beaumier, A. J. Pearce, X. Y. See and I. A. Tonks, *Nat. Rev. Chem.*, 2019, 3, 15-34.
9. S. Díez-González, N. Marion and S. P. Nolan, *Chem. Rev.*, 2009, 109, 3612-3676.
10. K. Yamamura and E. T. Kaiser, *Chem. Commun.*, 1976, DOI: 10.1039/C39760000830, 830-831.
11. M. E. Wilson and G. M. Whitesides, *J. Am. Chem. Soc.*, 1978, 100, 306-307.

12. F. Schwizer, Y. Okamoto, T. Heinisch, Y. Gu, M. M. Pellizzoni, V. Lebrun, R. Reuter, V. Köhler, J. C. Lewis and T. R. Ward, *Chem. Rev.*, 2018, 118, 142-231.

13. T. Heinisch and T. R. Ward, *Accounts of Chemical Research*, 2016, 49, 1711-1721.

14. R. van Vught, R. J. Pieters and E. Breukink, *Comput. Struct. Biotechnol. J*, 2014, 9, e201402001.

15. D. F. Sauer, S. Gotzen and J. Okuda, *Org. Biomol. Chem.*, 2016, 14, 9174-9183.

16. F. Yu, V. M. Cangelosi, M. L. Zastrow, M. Tegoni, J. S. Plegaria, A. G. Tebo, C. S. Mocny, L. Ruckthong, H. Qayyum and V. L. Pecoraro, *Chem. Rev.*, 2014, 114, 3495-3578.

17. O. Zozulia, M. A. Dolan and I. V. Korendovych, *Chem. Soc. Rev.*, 2018, 47, 3621-3639.

18. D. Woolfson, *Adv. Protein Chem.*, 2005, 70, 79-112.

19. B. Imperiali, R. A. Moats, S. L. Fisher and T. J. Prins, *J. Am. Chem. Soc.*, 1992, 114, 3182-3188.

20. E. Marcos, T. M. Chidyausiku, A. C. McShan, T. Evangelidis, S. Nerli, L. Carter, L. G. Nivón, A. Davis, G. Oberdorfer, K. Tripsianes, N. G. Sgourakis and D. Baker, *Nat. Struct. Mol. Biol.*, 2018, 25, 1028-1034.

21. N. Habibi, N. Kamaly, A. Memic and H. Shafiee, *Nano Today*, 2016, 11, 41-60.

22. P. S. P. Wang, J. B. Nguyen and A. Schepartz, *J. Am. Chem. Soc.*, 2014, 136, 6810-6813.

23. H. F. Carvalho, R. J. F. Branco, F. A. S. Leite, M. Matzapetakis, A. C. A. Roque and O. Iranzo, *Catal. Sci. Technol.*, 2019, 9, 6723-6736.

24. N. Hartrampf, A. Saebi, M. Poskus, Z. P. Gates, A. J. Callahan, A. E. Cowfer, S. Hanna, S. Antilla, C. K. Schissel, A. J. Quartararo, X. Ye, A. J. Mijalis, M. D. Simon, A. Loas, S. Liu, C. Jessen, T. E. Nielsen and B. L. Pentelute, *Science*, 2020, 368, 980-987.

25. S. J. Greenfield, A. Agarkov and S. R. Gilbertson, *Org. Lett.*, 2003, 5, 3069-3072.

26. J. F. Jensen, K. Worm-Leonhard and M. Meldal, *Eur. J. Org. Chem.*, 2008, 2008, 3785-3797.

27. E. R. Jarvo and S. J. Miller, *Tetrahedron*, 2002, 58, 2481-2495.

28. I. V. Korendovych, A. Senes, Y. H. Kim, J. D. Lear, H. C. Fry, M. J. Therien, J. K. Blasie, F. A. Walker and W. F. DeGrado, *J. Am. Chem. Soc.*, 2010, 132, 15516-15518.

29. M. Mahajan and S. Bhattacharjya, *Angew. Chem. Int. Edit.*, 2013, 52, 6430-6434.

30. D. W. Watkins, J. M. X. Jenkins, K. J. Grayson, N. Wood, J. W. Steventon, K. K. Le Vay, M. I. Goodwin, A. S. Mullen, H. J. Bailey, M. P. Crump, F. MacMillan, A. J. Mulholland, G. Cameron, R. B. Sessions, S. Mann and J. L. R. Anderson, *Nat. Commun.*, 2017, 8, 358.

31. M. L. Zastrow, A. F. A. Peacock, J. A. Stuckey and V. L. Pecoraro, *Nat. Chem.*, 2012, 4, 118-123.

32. M. Tegoni, F. Yu, M. Bersellini, J. E. Penner-Hahn and V. L. Pecoraro, *Proc Natl Acad Sci USA*, 2012, 109, 21234-21239.

33. T. Tanaka, T. Mizuno, S. Fukui, H. Hiroaki, J.-i. Oku, K. Kanaori, K. Tajima and M. Shirakawa, *J. Am. Chem. Soc.*, 2004, 126, 14023-14028.

34. Z. Lengyel, C. M. Rufo, Y. S. Moroz, O. V. Makhlynets and I. V. Korendovych, *ACS Catal.*, 2018, 8, 59-62.

35. C. M. Rufo, Y. S. Moroz, O. V. Moroz, J. Stöhr, T. A. Smith, X. Hu, W. F. DeGrado and I. V. Korendovych, *Nature chemistry*, 2014, 6, 303-309.

36. O. V. Makhlynets, P. M. Gosavi and I. V. Korendovych, *Angew. Chem. Int. Edit.*, 2016, 55, 9017-9020.

37. C. M. Rufo, Y. S. Moroz, O. V. Moroz, J. Stöhr, T. A. Smith, X. Hu, W. F. DeGrado and I. V. Korendovych, *Nat. Chem.*, 2014, 6, 303-309.

38. J. L. Heier, D. J. Mikolajczak, C. Böttcher and B. Koksch, *Peptide Science*, 2017, 108, e23003.

39. M. A. Khalily, G. Gulseren, A. B. Tekinay and M. O. Guler, *Bioconjug. Chem.*, 2015, 26, 2371-2375.

40. W. J. Song and F. A. Tezcan, *Science*, 2014, 346, 1525-1528.

41. B. S. Der, D. R. Edwards and B. Kuhlman, *Biochemistry*, 2012, 51, 3933-3940.

42. D. Árus, N. V. Nagy, Á. Dancs, A. Jancsó, R. Berkecz and T. Gajda, *J. Inorg. Biochem*, 2013, 126, 61-69.

43. J. Fegler, *Nature*, 1944, 153, 137-138.

44. E. N. G. Marsh and W. F. DeGrado, *Proc. Natl. Acad. Sci. USA*, 2002, 99, 5150-5154.

45. J. Kaplan and W. F. DeGrado, *Proc Natl Acad Sci USA*, 2004, 101, 11566-11570.

46. A. J. Reig, M. M. Pires, R. A. Snyder, Y. Wu, H. Jo, D. W. Kulp, S. E. Butch, J. R. Calhoun, T. G. Szyperski, E. I. Solomon and W. F. DeGrado, *Nature chemistry*, 2012, 4, 900-906.

47. K. J. Koebke, F. Yu, E. Salerno, C. Van Stappen, A. G. Tebo, J. E. Penner-Hahn and V. L. Pecoraro, *Angew. Chem. Int. Edit.*, 2018, 57, 3954-3957.

48. Z. Yu and J. A. Cowan, in *Adv. Inorg. Chem.*, eds. P. J. Sadler and R. van Eldik, Academic Press, 2020, vol. 75, pp. 361-391.

49. M. J. Ross, S. S. Bradford and J. A. Cowan, *Dalton Trans.*, 2015, 44, 20972-20982.

50. Z. Yu and J. A. Cowan, *Angew .Chem. Int. Ed. Engl.*, 2017, 56, 2763-2766.

51. J. Li, H. Wu, J. Hong, X. Xu, H. Yang, B. Wu, Y. Wang, J. Zhu, R. Lai, X. Jiang, D. Lin, M. C. Prescott and H. H. Rees, *PLOS ONE*, 2008, 3, e2381.

52. Y. Guo, J. R. Stroka, B. Kandemir, C. E. Dickerson and K. L. Bren, *J. Am. Chem. Soc.*, 2018, 140, 16888-16892.

53. M. R. Berwick, D. J. Lewis, A. W. Jones, R. A. Parslow, T. R. Dafforn, H. J. Cooper, J. Wilkie, Z. Pikramenou, M. M. Britton and A. F. A. Peacock, *J. Am. Chem. Soc.*, 2014, 136, 1166-1169.

54. R. Sambasivan and Z. T. Ball, *J. Am. Chem. Soc.*, 2010, 132, 9289-9291.

55. B. V. Popp and Z. T. Ball, *J. Am. Chem. Soc.*, 2010, 132, 6660-6662.

56. S. C. Martin, F. Vohidov, H. Wang, S. E. Knudsen, A. A. Marzec and Z. T. Ball, *Bioconjug. Chem.*, 2017, 28, 659-665.

57. A. N. Zaykov, K. R. MacKenzie and Z. T. Ball, *Chem. Eur. J.*, 2009, 15, 8961-8965.

58. G. Duarah, P. P. Kaishap, T. Begum and S. Gogoi, *Adv. Synth. Catal*, 2019, 361, 654-672.

59. T. Naota, H. Takaya and S.-I. Murahashi, *Chem. Rev.*, 1998, 98, 2599-2660.

60. I. M. Pastor, P. Västilä and H. Adolfsson, *Chem. Eur. J.*, 2003, 9, 4031-4045.

61. M. A. Dolan, P. N. Basa, O. Zozulia, Z. Lengyel, R. Lebl, E. M. Kohn, S. Bhattacharya and I. V. Korendovych, *ACS Nano*, 2019, 13, 9292-9297.

62. Y. Iseki, M. Kudo, A. Mori and S. Inoue, *J. Org. Chem.*, 1992, 57, 6329-6331.

63. T. Katsuki and K. B. Sharpless, *J. Am. Chem. Soc.*, 1980, 102, 5974-5976.

64. H. Nitta, D. Yu, M. Kudo, A. Mori and S. Inoue, *J. Am. Chem. Soc.*, 1992, 114, 7969-7975.

65. A. Mori, H. Nitta, M. Kudo and S. Inoue, *Tetrahedron Lett.*, 1991, 32, 4333-4336.

66. M. B. Francis and E. N. Jacobsen, *Angew .Chem. Int. Ed.*, 1999, 38, 937-941.

67. Z. Zhang, H. Yang, C. Zhang and J. C. Lewis, *Organometallics*, 2012, 31, 7328-7331.

68. O. Cussó, M. W. Giuliano, X. Ribas, S. J. Miller and M. Costas, *Chem. Sci.*, 2017, 8, 3660-3667.

69. L. Vicens and M. Costas, *Dalton Trans.*, 2018, 47, 1755-1763.

70. M. N. Zafar, A. H. Atif, M. F. Nazar, S. H. Sumrra, E. S. Gul and R. Paracha, *Russ. J. Coord. Chem*+, 2016, 42, 1-18.

71. J. F. Miravet and B. Escuder, *Chem. Commun.*, 2005, DOI: 10.1039/B510874H, 5796-5798.

72. A. M. Embaby, L. P. W. M. Lelieveldt, F. Diness and M. Meldal, *Chem. Eur. J.*, 2018, 24, 17424-17428.

73. M. Karimiavargani, S. Tada, N. Minagawa, Y. Shimizu, T. Hirose, Y. Ito and T. Uzawa, *J. Pept. Sci.*, 2019, 25, e3158.

74. H. Fernández-Pérez, P. Etayo, A. Panossian and A. Vidal-Ferran, *Chem. Rev.*, 2011, 111, 2119-2176.

75. S. R. Gilbertson, X. Wang, G. S. Hoge, C. A. Klug and J. Schaefer, *Organometallics*, 1996, 15, 4678-4680.

76. S. R. Gilbertson, G. Chen and M. McLoughlin, *J. Am. Chem. Soc.*, 1994, 116, 4481-4482.

77. S. R. Gilbertson and X. Wang, *J. Org. Chem.*, 1996, 61, 434-435.

78. S. R. Gilbertson and X. Wang, *Tetrahedron Lett.*, 1996, 37, 6475-6478.

79. S. R. Gilbertson, G. Chen, J. Kao, A. Beatty and C. F. Campana, *J. Org. Chem.*, 1997, 62, 5557-5566.

80. S. R. Gilbertson, S. E. Collibee and A. Agarkov, *J. Am. Chem. Soc.*, 2000, 122, 6522-6523.

81. A. Agarkov, E. W. Uffman and S. R. Gilbertson, *Org. Lett.*, 2003, 5, 2091-2094.

82. S. R. Gilbertson and R. V. Pawlick, *Angew. Chem. Int. Edit.*, 1996, 35, 902-904.

83. A. Agarkov, S. Greenfield, D. Xie, R. Pawlick, G. Starkey and S. R. Gilbertson, *Peptide Science*, 2006, 84, 48-73.

84. D. Rageot, D. H. Woodmansee, B. Pugin and A. Pfaltz, *Angew. Chem. Int. Edit.*, 2011, 50, 9598-9601.

85. S. R. Gilbertson, D. Xie and Z. Fu, *J. Org. Chem.*, 2001, 66, 7240-7246.

86. S. R. Gilbertson and D. Xie, *Angew. Chem. Int. Edit.*, 1999, 38, 2750-2752.

87. S. J. Degrado, H. Mizutani and A. H. Hoveyda, *J. Am. Chem. Soc.*, 2001, 123, 755-756.

88. N. S. Josephsohn, K. W. Kuntz, M. L. Snapper and A. H. Hoveyda, *J. Am. Chem. Soc.*, 2001, 123, 11594-11599.

89. B. Breit and A. C. Laungani, *Tetrahedron-Asymmetr.*, 2003, 14, 3823-3826.

90. A. C. Laungani, J. M. Slattery, I. Krossing and B. Breit, *Chem. Eur. J.*, 2008, 14, 4488-4502.

91. A. C. Laungani and B. Breit, *Chem. Commun.*, 2008, DOI: 10.1039/B716529C, 844-846.

92. C. A. Christensen and M. Meldal, *Chem. Eur. J.*, 2005, 11, 4121-4131.

93. C. A. Christensen and M. Meldal, *J. Comb. Chem.*, 2007, 9, 79-85.

94. S. Roy, T.-A. D. Nguyen, L. Gan and A. K. Jones, *Dalton Trans.*, 2015, 44, 14865-14876.

95. D. M. Flanigan, F. Romanov-Michailidis, N. A. White and T. Rovis, *Chem. Rev.*, 2015, 115, 9307-9387.

96. A. Doddi, M. Peters and M. Tamm, *Chem. Rev.*, 2019, 119, 6994-7112.

97. E. Peris, *Chem. Rev.*, 2018, 118, 9988-10031.

98. E. Levin, E. Ivry, C. E. Diesendruck and N. G. Lemcoff, *Chem. Rev.*, 2015, 115, 4607-4692.

99. S. Lars-Arne, H. S. J., H. W. A. and K. F. E., *Angew. Chem. Int. Ed.*, 2013, 52, 270-289.

100. H. D. Velazquez and F. Verpoort, *Chem. Soc. Rev.*, 2012, 41, 7032-7060.

101. L. Mercs and M. Albrecht, *Chem. Soc. Rev.*, 2010, 39, 1903-1912.

102. A. Gautier and F. Cisnetti, *Metallomics*, 2012, 4, 23-32.

103. B. Albada and N. Metzler-Nolte, *Chem. Rev.*, 2016, 116, 11797-11839.

104. L. Oehninger, R. Rubbiani and I. Ott, *Dalton Trans.*, 2013, 42, 3269-3284.

105. D. F. Sauer, T. Himiyama, K. Tachikawa, K. Fukumoto, A. Onoda, E. Mizohata, T. Inoue, M. Bocola, U. Schwaneberg, T. Hayashi and J. Okuda, *ACS Catal.*, 2015, 5, 7519-7522.

106. M. Basauri-Molina, C. F. Riemersma, M. A. Wurdemann, H. Kleijn and R. J. M. Klein Gebbink, *Chem. Commun.*, 2015, 51, 6792-6795.

107. J. C. Lewis, *ACS Catalysis*, 2013, 3, 2954-2975.

108. R. Fiora and R. Gerard, *ChemCatChem*, 2010, 2, 916-927.

109. D. P. J., d. H. René, L. Wouter and K. P. C. J., *Chem. Eur. J.*, 2011, 17, 4680-4698.

110. F. Schwizer, Y. Okamoto, T. Heinisch, Y. Gu, M. M. Pellizzoni, V. Lebrun, R. Reuter, V. Köhler, J. C. Lewis and T. R. Ward, *Chemical Reviews*, 2018, 118, 142-231.

111. E. Ivry, A. Ben-Asuly, I. Goldberg and N. G. Lemcoff, *Chem.Commun.*, 2015, 51, 3870-3873.

112. E. Indrigo, J. Clavadetscher, S. V. Chankeshwara, A. Megia-Fernandez, A. Lilienkampf and M. Bradley, *Chem. Commun.*, 2017, 53, 6712-6715.

113. D. Kenta, K. Junko, Y. Haruka, A. Ryuichi and S. Satoshi, *Eur. J. Org. Chem.*, 2012, 2012, 7143-7152.

114. G. W. Nyce, T. Glauser, E. F. Connor, A. Möck, R. M. Waymouth and J. L. Hedrick, *J. Am. Chem. Soc.*, 2003, 125, 3046-3056.

115. D. J. Kim, K. H. Oh and J. K. Park, *Green Chem.*, 2014, 16, 4098-4101.

116. Z. Mao, J. Pan and T. I. Kalman, *J. Med. Chem.*, 1996, 39, 4340-4344.

117. A. Malanda Kimbonguila, S. Boucida, F. Guibé and A. Loffet, *Tetrahedron*, 1997, 53, 12525-12538.

118. R. L. Melo, R. C. Barbosa Pozzo, D. C. Pimenta, E. Perissutti, G. Caliendo, V. Santagada, L. Juliano and M. A. Juliano, *Biochemistry*, 2001, 40, 5226-5232.

119. R. L. Melo, R. C. Barbosa Pozzo, L. C. Alves, E. Perissutti, G. Caliendo, V. Santagada, L. Juliano and M. A. Juliano, *Biochimica et biophysica acta*, 2001, 1547, 82-94.

120. F. Hannig, G. Kehr, R. Fröhlich and G. Erker, *J. Organomet. Chem*, 2005, 690, 5959-5972.

121. F. Guillen, D. Brégeon and J.-C. Plaquevent, *Tetrahedron Lett.*, 2006, 47, 1245-1248.

122. A. Monney, G. Venkatachalam and M. Albrecht, *Dalton Trans.*, 2011, 40, 2716-2719.

123. A. Monney, E. Alberico, Y. Ortin, H. Müller-Bunz, S. Gladiali and M. Albrecht, *Dalton Trans.*, 2012, 41, 8813-8821.

124. A. Monney and M. Albrecht, *Chem. Commun.*, 2012, 48, 10960-10962.

125. A. Monney, F. Nastri and M. Albrecht, *Dalton Trans.*, 2013, 42, 5655-5660.

126. F. Schmitt, K. Donnelly, J. K. Muenzner, T. Rehm, V. Novohradsky, V. Brabec, J. Kasparkova, M. Albrecht, R. Schobert and T. Mueller, *J. Inorg. Biochem*, 2016, 163, 221-228.

127. A. J. Young, C. J. Serpell, J. M. Chin and M. R. Reithofer, *Chem. Commun.*, 2017, 53, 12426-12429.

128. R. M. Drost, D. L. J. Broere, J. Hoogenboom, S. N. de Baan, M. Lutz, B. de Bruin and C. J. Elsevier, *Eur. J. Inorg. Chem.*, 2015, 2015, 982-996.

129. C. Lu, D. VanDerveer and D. D. DesMarteau, *Org. Lett.*, 2008, 10, 5565-5568.

130. M. Ahn, R. N. Murugan, B. Jacob, J.-K. Hyun, C. Cheong, E. Hwang, H.-N. Park, J.-H. Seo, G. Srinivasrao, K. S. Lee, S. Y. Shin and J. K. Bang, *Eur. J. Med. Chem.*, 2013, 68, 10-18.

131. R. F. W. Jackson, N. Wishart, A. Wood, K. James and M. J. Wythes, *J. Org. Chem.*, 1992, 57, 3397-3404.

132. G. Xu and S. R. Gilbertson, *Org. Lett.*, 2005, 7, 4605-4608.

133. K. Worm-Leonhard and M. Meldal, *Eur. J. Org. Chem.*, 2008, 2008, 5244-5253.

134. Y. Zhao and S. R. Gilbertson, *Org. Lett.*, 2014, 16, 1033-1035.

135. Y. N. Belokon, A. V. Grachev, V. I. Maleev, V. N. Khrustalev, A. S. Peregudov and M. North, *Tetrahedron-Asymmetr.*, 2008, 19, 756-760.

136. T. Soeta, T. Ishizaka, Y. Tabatake and Y. Ukaji, *Chem. Eur. J.*, 2014, 20, 16773-16778.

137. C. Edith, P. G. Luigi, D. Georges, F. Sylvie, G. Gilles and B. L. Stéphane, *ChemPlusChem*, 2012, 77, 1028-1038.

138. R. B. Merrifield, *J. Am. Chem. Soc.*, 1963, 85, 2149-2154.

139. D. s. M. M. Jaradat, *Amino Acids*, 2018, 50, 39-68.

140. B. D. Larsen and A. Holm, *Int. J. Pept. Protein Res.*, 1994, 43, 1-9.

141. A. J. Mijalis, D. A. Thomas, M. D. Simon, A. Adamo, R. Beaumont, K. F. Jensen and B. L. Pentelute, *Nat. Chem.*, 2017, 13, 464-466.

142. S. L. Pedersen, A. P. Tofteng, L. Malik and K. J. Jensen, *Chem. Soc. Rev.*, 2012, 41, 1826-1844.

143. N. E. Shepherd, H. N. Hoang, G. Abbenante and D. P. Fairlie, *J. Am. Chem. Soc.*, 2009, 131, 15877-15886.

144. A. Monney, E. Alberico, Y. Ortin, H. Muller-Bunz, S. Gladiali and M. Albrecht, *Dalton Trans.*, 2012, 41, 8813-8821.

145. A. J. Young, C. J. Serpell, J. M. Chin and M. R. Reithofer, *Chemical Communications*, 2017, 53, 12426-12429.

146. L. Benhamou, E. Chardon, G. Lavigne, S. Bellemin-Laponnaz and V. César, *Chem. Rev.*, 2011, 111, 2705-2733.

147. A. Levens, F. An, M. Breugst, H. Mayr and D. W. Lupton, *Org. Lett.*, 2016, 18, 3566-3569.

148. R. Credendino, L. Falivene and L. Cavallo, *J. Am. Chem. Soc.*, 2012, 134, 8127-8135.

149. H. V. Huynh, *Chem. Rev.*, 2018, 118, 9457-9492.

150. A. Poater, F. Ragone, S. Giudice, C. Costabile, R. Dorta, S. P. Nolan and L. Cavallo, *Organometallics*, 2008, 27, 2679-2681.

151. X. Z. Zhao, D. Hymel and T. R. Burke, *Bioorg Med Chem Lett*, 2016, 26, 5009-5012.

152. J. C. Garrison and W. J. Youngs, *Chem. Rev.*, 2005, 105, 3978-4008.

153. D. A. Rychkov, S. G. Arkhipov and E. V. Boldyreva, *J. Appl. Crystallogr*, 2014, 47, 1435-1442.

154. D. G. H. Hetterscheid and J. N. H. Reek, *Chem. Commun.*, 2011, 47, 2712-2714.

155. J. C. Deaton, C. M. Taliaferro, C. L. Pitman, R. Czerwieniec, E. Jakubikova, A. J. M. Miller and F. N. Castellano, *Inorg. Chem.*, 2018, 57, 15445-15461.

156. R. Staehle, L. Tong, L. Wang, L. Duan, A. Fischer, M. S. G. Ahlquist, L. Sun and S. Rau, *Inorg. Chem.*, 2014, 53, 1307-1319.

157. A. Johnson and M. C. Gimeno, *Chem. Commun.*, 2016, 52, 9664-9667.

158. J. M. Hayes, M. Viciano, E. Peris, G. Ujaque and A. Lledós, *Organometallics*, 2007, 26, 6170-6183.

159. A. Collado, A. Gómez-Suárez, A. R. Martin, A. M. Z. Slawin and S. P. Nolan, *Chem. Commun.*, 2013, 49, 5541-5543.

160. C. Bianchini, G. Giambastiani, L. Luconi and A. Meli, *Coord. Chem. Rev.*, 2010, 254, 431-455.

161. S. Shi, P. Lei and M. Szostak, *Organometallics*, 2017, 36, 3784-3789.

162. Y. Zhang, B. Feng and C. Zhu, *Org. Biomol. Chem.*, 2012, 10, 9137-9141.

163. G. Annibale, L. Canovese, L. Cattalini, G. Marangoni, G. Michelon and M. L. Tobe, *Dalton Trans.*, 1984, DOI: 10.1039/DT9840001641, 1641-1646.

164. R. I. McDonald, G. Liu and S. S. Stahl, *Chem. Rev.*, 2011, 111, 2981-3019.

165. K. J. Cavell and A. T. Normand, in *N-Heterocyclic Carbenes in Transition Metal Catalysis and Organocatalysis*, ed. C. S. J. Cazin, Springer Netherlands, Dordrecht, 2011, DOI: 10.1007/978-90-481-2866-2_13, pp. 299-314.

166. D. S. Tromp, P. Hauwert and C. J. Elsevier, *Appl. Organomet.*, 2012, 26, 335-341.

167. M. Alcarazo, S. J. Roseblade, A. R. Cowley, R. Fernández, J. M. Brown and J. M. Lassaletta, *J. Am. Chem. Soc.*, 2005, 127, 3290-3291.

168. C. J. Chivikas and J. C. Hodges, *J. Org. Chem.*, 1987, 52, 3591-3594.

169. R. Jain, L. A. Cohen and M. M. King, *Tetrahedron*, 1997, 53, 4539-4548.

170. C. DalZotto, J. Michaux, E. Martinand-Lurin and J.-M. Campagne, *Eur. J. Org. Chem.* , 2010, 2010, 3811-3814.

171. T. Greene and P. G. M. Wuts, in *Greene's Protective Groups in Organic Synthesis*, John Wiley & Sons, Inc., 2007, DOI: 10.1002/9780470053485.ch7, pp. 696-926.

172. Y. E. Jad, G. A. Acosta, S. N. Khattab, B. G. de la Torre, T. Govender, H. G. Kruger, A. El-Faham and F. Albericio, *Org. Biomol. Chem.*, 2015, 13, 2393-2398.

173. V. Gierz, A. Seyboldt, C. Maichle-Mössmer, K. W. Törnroos, M. T. Speidel, B. Speiser, K. Eichele and D. Kunz, *Organometallics*, 2012, 31, 7893-7901.

174. C. Schulte to Brinke, T. Pape and F. E. Hahn, *Dalton Trans.*, 2013, 42, 7330-7337.

175. P. de Frémont, N. M. Scott, E. D. Stevens and S. P. Nolan, *Organometallics*, 2005, 24, 2411-2418.

176. in *PATAI'S Chemistry of Functional Groups*, DOI: 10.1002/9780470682531.pat0806, pp. 1-84.

177. A. Gutiérrez, M. C. Gimeno, I. Marzo and N. Metzler-Nolte, *Eur. J. Inorg. Chem.*, 2014, 2014, 2512-2519.

178. S. M. Mennen, J. T. Blank, M. B. Tran-Dubé, J. E. Imbriglio and S. J. Miller, *Chem. Commun.*, 2005, DOI: 10.1039/B414574G, 195-197.

179. J. Lemke and N. Metzler-Nolte, *J. Organomet. Chem*, 2011, 696, 1018-1022.

180. D. J. D. Wilson, S. A. Couchman and J. L. Dutton, *Inorg. Chem.*, 2012, 51, 7657-7668.

181. R. H. Crabtree, *J. Organomet. Chem*, 2005, 690, 5451-5457.

182. W. Zi and F. Dean Toste, *Chem. Soc. Rev.*, 2016, 45, 4567-4589.

183. J. Rodriguez and D. Bourissou, *Angew .Chem. Int. Ed.* , 2018, 57, 386-388.

184. G. Zuccarello, J. G. Mayans, I. Escofet, D. Scharnagel, M. S. Kirillova, A. H. Pérez-Jimeno, P. Calleja, J. R. Boothe and A. M. Echavarren, *J. Am. Chem. Soc.*, 2019, 141, 11858-11863.

185. D. W. Franco, *Inorg. Chim. Acta*, 1979, 32, 273-277.

186. M. Brill, A. Collado, D. B. Cordes, A. M. Z. Slawin, M. Vogt, H. Grützmacher and S. P. Nolan, *Organometallics*, 2015, 34, 263-274.

187. O. Santoro, A. Collado, A. M. Z. Slawin, S. P. Nolan and C. S. J. Cazin, *Chem. Commun.*, 2013, 49, 10483-10485.

188. U. Hintermair, U. Englert and W. Leitner, *Organometallics*, 2011, 30, 3726-3731.

189. I. J. B. Lin and C. S. Vasam, *Coord. Chem. Rev.*, 2007, 251, 642-670.

190. P. A. Rist, R. S. Grainger and P. W. Davies, *Org. Lett.*, 2021, 23, 642-646.

191. H. V. Adcock, E. Chatzopoulou and P. W. Davies, *Angew. Chem. Int. Ed.*, 2015, 54, 15525-15529.

192. A. S. K. Hashmi, W. Yang and F. Rominger, *Angew. Chem. Int. Ed.*, 2011, 50, 5762-5765.

193. A. Fürstner and P. W. Davies, *Angew. Chem. Int. Ed.*, 2007, 46, 3410-3449.

194. A. S. K. Hashmi, *Chem. Rev.*, 2007, 107, 3180-3211.

195. J.-J. Jiang and M.-K. Wong, *Chem. Asian J.*, 2021, 16, 364-377.

196. T. Koshikawa, M. Satoh, K. Masutomi, Y. Shibata and K. Tanaka, *Eur. J. Org.Chem.* , 2019, 2019, 1488-1492.

197. C. García-Morales, B. Ranieri, I. Escofet, L. López-Suarez, C. Obradors, A. I. Konovalov and A. M. Echavarren, *J. Am. Chem. Soc.*, 2017, 139, 13628-13631.

198. H. Kim, S. Y. Choi and S. Shin, *Angew .Chem. Int. Ed.*, 2018, 57, 13130-13134.

199. Y.-M. Wang, A. D. Lackner and F. D. Toste, *Acc. Chem. Res.*, 2014, 47, 889-901.

200. C. Tugny, N. del Rio, M. Koohgard, N. Vanthuyne, D. Lesage, K. Bijouard, P. Zhang, J. Meijide Suárez, S. Roland, E. Derat, O. Bistri-Aslanoff, M. Sollogoub, L. Fensterbank and V. Mouriès-Mansuy, *ACS Catal.*, 2020, 10, 5964-5972.

201. P. Aillard, D. Dova, V. Magné, P. Retailleau, S. Cauteruccio, E. Licandro, A. Voituriez and A. Marinetti, *Chem. Commun.*, 2016, 52, 10984-10987.

202. D. Marchione, M. A. Izquierdo, G. Bistoni, R. W. A. Havenith, A. Macchioni, D. Zuccaccia, F. Tarantelli and L. Belpassi, *Chem. Eur. J.*, 2017, 23, 2722-2728.

203. C. Hirtenlehner, C. Krims, J. Hölbling, M. List, M. Zabel, M. Fleck, R. J. F. Berger, W. Schoefberger and U. Monkowius, *Dalton Trans.*, 2011, 40, 9899-9910.

204. M. V. Baker, P. J. Barnard, S. K. Brayshaw, J. L. Hickey, B. W. Skelton and A. H. White, *Dalton Trans.*, 2005, DOI: 10.1039/B412540A, 37-43.

205. E. F. Hahn, B. Heidrich, A. Hepp and T. Pape, *J. Organomet. Chem*, 2007, 692, 4630-4638.

206. A. Biffis, P. Centomo, A. Del Zotto and M. Zecca, *Chem. Rev.*, 2018, 118, 2249-2295.

207. D. Wang and D. Astruc, *Chem. Rev.*, 2015, 115, 6621-6686.

208. R. A. Fernandes and J. L. Nallasivam, *Org. Biomol. Chem.*, 2019, 17, 8647-8672.

209. S. Warsink, R. M. Drost, M. Lutz, A. L. Spek and C. J. Elsevier, *Organometallics*, 2010, 29, 3109-3116.

210. N. Marion, O. Navarro, J. Mei, E. D. Stevens, N. M. Scott and S. P. Nolan, *J. Am. Chem. Soc.*, 2006, 128, 4101-4111.

211. C. Martín, F. Molina, E. Alvarez and T. R. Belderrain, *Chem. Eur. J.*, 2011, 17, 14885-14895.

212. B. Crociani, S. Antonaroli, M. Paci, F. Di Bianca and L. Canovese, *Organometallics*, 1997, 16, 384-391.

213. M. Arribat, E. Rémond, S. Clément, A. V. D. Lee and F. Cavelier, *J. Am. Chem. Soc.*, 2018, 140, 1028-1034.

214. D. Fillion, M. Deraët, B. J. Holleran and E. Escher, *J. Med. Chem.*, 2006, 49, 2200-2209.

215. H. J. Lucas, F. W. Mitchell and C. N. Scully, *J. Am. Chem. Soc.*, 1950, 72, 5491-5497.

216. D. M. Rothman, M. E. Vazquez, E. M. Vogel and B. Imperiali, *J. Org. Chem.*, 2003, 68, 6795-6798.

217. A. Aemissegger, C. N. Carrigan and B. Imperiali, *Tetrahedron*, 2007, 63, 6185-6190.

218. C. Schmitz, W. Leitner and G. Franciò, *Eur. J. Org. Chem.*, 2015, 2015, 6205-6230.

219. Y. Yang, V. Ramamoorthy and P. R. Sharp, *Inorg. Chem.*, 1993, 32, 1946-1950.

220. I. D. G. Watson and F. D. Toste, *Chem. Sci.*, 2012, 3, 2899-2919.

221. E. Jiménez-Núñez and A. M. Echavarren, *Chem. Rev.*, 2008, 108, 3326-3350.

222. L. Zhang and S. A. Kozmin, *J. Am. Chem. Soc.*, 2004, 126, 11806-11807.

223. J. C. H. Lee and D. G. Hall, *Tetrahedron Lett.*, 2011, 52, 321-324.

224. Y.-C. Lee and K. Kumar, *Isr. J. Chem.*, 2018, 58, 531-556.

225. V. Michelet, P. Y. Toullec and J.-P. Genêt, *Angew. Chem. Int. Edit.*, 2008, 47, 4268-4315.

226. L. Hintermann and A. Labonne, *Synthesis-Stuttgart*, 2007, 2007, 1121-1150.

227. R. O. C. Norman, W. J. E. Parr and C. B. Thomas, *J. Chem. Soc. Perkin Trans. I*, 1976, DOI: 10.1039/P19760001983, 1983-1987.

228. N. Marion, R. S. Ramón and S. P. Nolan, *J. Am. Chem. Soc.*, 2009, 131, 448-449.

229. R. E. Ebule, D. Malhotra, G. B. Hammond and B. Xu, *Adv. Synth. Catal*, 2016, 358, 1478-1481.

230. L. R. Whitby, Y. Ando, V. Setola, P. K. Vogt, B. L. Roth and D. L. Boger, *J. Am. Chem. Soc.*, 2011, 133, 10184-10194.

231. G. Roy, J. Reier, A. Garcia, T. Martin, M. Rice, J. Wang, M. Prophet, R. Christie, W. Dall'Acqua, S. Ahuja, M. A. Bowen and M. Marelli, *mAbs*, 2020, 12, 1684749.

232. L. Jessica and M. N. Nils, *Eur. J. Inorg. Chem.*, 2008, 2008, 3359-3366.

233. J. J. F., W. L. Kasper and M. Morten, *Eur. J. Org. Chem.*, 2008, 2008, 3785-3797.

234. M. J. Deetz, C. C. Forbes, M. Jonas, J. P. Malerich, B. D. Smith and O. Wiest, *J. Org. Chem.*, 2002, 67, 3949-3952.

235. M. T. Huggins, T. Kesharwani, J. Buttrick and C. Nicholson, *J. Chem. Educ.*, 2020, 97, 1425-1429.

236. J. M. Palomo, *RSC ADV*, 2014, 4, 32658-32672.

237. V. K. Sarin, S. B. H. Kent, J. P. Tam and R. B. Merrifield, *Anal. Biochem.*, 1981, 117, 147-157.

238. F. Albericio and A. El-Faham, *Org. Process Res. Dev.*, 2018, 22, 760-772.

239. F. G. Bordwell and A. V. Satish, *J. Am. Chem. Soc.*, 1991, 113, 985-990.

240. A. Lupas, M. Van Dyke and J. Stock, *Science*, 1991, 252, 1162-1164.

241. L. Truebestein and T. A. Leonard, *BioEssays*, 2016, 38, 903-916.

242. H. Robson Marsden and A. Kros, *Angew. Chem. Int. Edit.*, 2010, 49, 2988-3005.

243. G. Ghirlanda, J. D. Lear, A. Lombardi and W. F. DeGrado, *J. Mol. Biol*, 1998, 281, 379-391.

244. J. M. Fletcher, K. A. Horner, G. J. Bartlett, G. G. Rhys, A. J. Wilson and D. N. Woolfson, *Chem. Sci.*, 2018, 9, 7656-7665.

245. K. A. Scheib, N. A. Tavenor, M. J. Lawless, S. Saxena and W. S. Horne, *Chem. Commun.*, 2019, 55, 7752-7755.

246. A. J. Doerr and G. L. McLendon, *Inorg. Chem.*, 2004, 43, 7916-7925.

247. C. Cohen and D. A. D. Parry, *Proteins*, 1990, 7, 1-15.

248. A. F. A. Peacock, O. Iranzo and V. L. Pecoraro, *Dalton Trans.*, 2009, DOI: 10.1039/B818306F, 2271-2280.

249. A. E. Braunstein, in *Advances in Protein Chemistry*, eds. M. L. Anson and T. E. John, Academic Press, 1947, vol. Volume 3, pp. 1-52b.

250. L. Michaelis, in *Advances in Protein Chemistry*, eds. M. L. Anson and T. E. John, Academic Press, 1947, vol. Volume 3, pp. 53-66.

251. P. B. Harbury, T. Zhang, P. S. Kim and T. Alber, *Science*, 1993, 262, 1401.

252. D. N. Woolfson, *The Design of Coiled-Coil Structures and Assemblies*, Academic Press, 2005.

253. J. M. Fletcher, A. L. Boyle, M. Bruning, G. J. Bartlett, T. L. Vincent, N. R. Zaccai, C. T. Armstrong, E. H. C. Bromley, P. J. Booth, R. L. Brady, A. R. Thomson and D. N. Woolfson, *ACS Synthetic Biology*, 2012, 1, 240-250.

254. M. Meier, J. Stetefeld and P. Burkhard, *J. Struct. Biol.*, 2010, 170, 192-201.

255. H. Edelhoch, *Biochemistry*, 1967, 6, 1948-1954.

256. M. Delorenzi and T. Speed, *Bioinformatics (Oxford, England)*, 2002, 18, 617-625.

257. A. N. Lupas and M. Gruber, in *Adv. Protein Chem.*, Academic Press, 2005, vol. 70, pp. 37-38.

258. T. L. Vincent, P. J. Green and D. N. Woolfson, *Bioinformatics (Oxford, England)*, 2012, 29, 69-76.

259. B. Lovejoy, S. Choe, D. Cascio, D. McRorie, W. DeGrado and D. Eisenberg, *Science*, 1993, 259, 1288-1293.

260. J. P. Schneider, A. Lombardi and W. F. DeGrado, *Fold. Des.*, 1998, 3, R29-R40.

261. Y.-H. Chen, J. T. Yang and K. H. Chau, *Biochemistry*, 1974, 13, 3350-3359.

262. N. E. Zhou, C. M. Kay and R. S. Hodges, *J Biol Chem.*, 1992, 267, 2664-2670.

263. N. E. Zhou, C. M. Kay and R. S. Hodges, *Biochemistry*, 1992, 31, 5739-5746.

264. O. I. Povarova, I. M. Kuznetsova and K. K. Turoverov, *Cell Biol Int.*, 2007, 31, 405-412.

265. O. J. Daubney, PhD, University of Birmingham, 2019.

266. H. Wendt, C. Berger, A. Baici, R. M. Thomas and H. R. Bosshard, *Biochemistry*, 1995, 34, 4097-4107.

267. T. L. Amyes, S. T. Diver, J. P. Richard, F. M. Rivas and K. Toth, *J. Am. Chem. Soc.*, 2004, 126, 4366-4374.

268. H. Wennemers, *Chem. Commun.*, 2011, 47, 12036-12041.

269. J. Cure, R. Poteau, I. C. Gerber, H. Gornitzka and C. Hemmert, *Organometallics*, 2012, 31, 619-626.

270. E. A. Baquero, G. F. Silbestri, P. Gómez-Sal, J. C. Flores and E. de Jesús, *Organometallics*, 2013, 32, 2814-2826.

271. K. M. Hindi, M. J. Panzner, C. A. Tessier, C. L. Cannon and W. J. Youngs, *Chem. Rev.*, 2009, 109, 3859-3884.

272. J. Alsina, F. Rabanal, C. Chiva, E. Giralt and F. Albericio, *Tetrahedron*, 1998, 54, 10125-10152.

273. L. R. Malins, N. J. Mitchell, S. McGowan and R. J. Payne, *Angew. Chem. Int. Edit.*, 2015, 54, 12716-12721.

274. S. Bregant and A. B. Tabor, *J. Org. Chem.*, 2005, 70, 2430-2438.

275. H. Liu, V. R. Pattabiraman and J. C. Vederas, *Org. Lett.*, 2007, 9, 4211-4214.

276. H. J. C. Deboves, C. A. G. N. Montalbetti and R. F. W. Jackson, *J. Chem. Soc. Perkin Trans. I*, 2001, 1876-1884.

277. F. Kramm, J. Teske, F. Ullwer, W. Frey and B. Plietker, *Angew. Chem. Int. Edit.*, 2018, 57, 13335-13338.

278. H. W. Lee, L. N. Lee, A. S. C. Chan and F. Y. Kwong, *Eur. J. Org. Chem.*, 2008, 2008, 3403-3406.

279. Y. Zhao, M. G. Wakeling, F. Meloni, T. J. Sum, H. van Nguyen, B. R. Buckley, P. W. Davies and J. S. Fossey, *Eur. J. Org. Chem.*, 2019, 2019, 5540-5548.

280. A. F. Peacock, G. A. Bullen, L. A. Gethings, J. P. Williams, F. H. Kriel and J. Coates, *J. Inorg. Biochem.*, 2012, 117, 298-305.

281. J. K. Myers, C. N. Pace and J. M. Scholtz, *Proc Natl Acad Sci USA*, 1997, 94, 2833-2837.